NUREG-0260

# A SIMPLIFIED METHOD OF COMPUTING CLAD AND FUEL STRAIN AND STRESS DURING IRRADIATION



University of California at Los Angeles
for
U. S. Nuclear Regulatory Commission

Available from
National Technical Information Service
Springfield, Virginia 22161
Price: Printed Copy $9.75 ; Microfiche $3.00

The price of this document for requestors outside of the North American Continent can be obtained from the National Technical Information Service.

733 041

NUREG-0260
NRC-7

# A SIMPLIFIED METHOD OF COMPUTING CLAD AND FUEL STRAIN AND STRESS DURING IRRADIATION

Y-H Sun and D. Okrent

Principal Investigators
I. Catton
W. E. Kastenberg

Manuscript Completed: January 1977
Date Published: June 1977

School of Engineering and Applied Science
University of California
Los Angeles, CA 90024

Prepared for
Division of Reactor Safety Research
Office of Nuclear Regulatory Research
U. S. Nuclear Regulatory Commission
Under Contract No. AT(49-24)-0246

733 042

PREFACE

This report represents one aspect of the research program "Safety Considerations of Commercial Liquid Metal Fast Breeder Reactors" (AT(04-3) PA223 and AT(49-24)-0246) funded by the U.S. Nuclear Regulatory Commission, Division of Reactor Safety Research. The research program is divided into the following tasks; a) transient analysis of fuel elements, b) accident analysis, c) post accident heat removal, d) fuel-coolant interactions and e) thermodynamic effects.

Reports prepared previously under this grant include the following:

1. Post Accident Heat Removal with Advanced LMFBR Fuels, R.D. Gasser, UCLA-ENG-7518 (March 1975).
2. Dry-out of a Fluidized Particle Bed with Internal Heat Generation; R.S. Keowen and I. Catton, UCLA-ENG-7519 (March 1975).
3. Laminar Natural Convection From Blunt Bodies with Arbitrary Surface Heat Flux or Surface Temperature; G.M. Harpole, UCLA-ENG-7527 (April 1975).
4. Preliminary Assessments of Carbide Fuel Pins During Mild Overpower Transients; G.M. Nickerson, UCLA-ENG-7582 (October 1975).
5. A Simplified Method of Computing Clad and Fuel Strain and Stress During Irradiation; Y. Sun and D. Okrent, UCLA-ENG-7591 (Part I) (October 1975).
6. An Experimental Study of the Thermal Interaction for Molten Tin Dropped into Water; V.M. Arakeri, I. Catton, W.E. Kastenberg and M.S. Plesset, UCLA-ENG-7592 (December 1975).
7. A Mechanistic Study of Fuel Freezing and Channel Plugging During Fast Reactor Overpower Excursions; V.K. Dhir, K. Wong and W.E. Kastenberg, UCLA-ENG-7679 (July 1976).

8. A Simulation of Thermal Phenomenon Expected in Fuel Coolant Interactions In LMFBR's; J. Yasin, UCLA-ENG-76100, (September 1976).

9. On the Nonequilibrium Behavior of Fission Gas Bubbles With Emphasis on the Effects of Equation of State; W. G. Steele, UCLA-ENG-76118 (December 1976).

10. A Method for the Determination of the Equation of State of Advanced Fuels Based on the Properties of Normal Fluids; M. J. Hecht, UCLA-ENG-76122 (December 1976).

TABLE OF CONTENTS

TABLE OF CONTENTS (Cont'd.)



733 046

LIST OF FIGURES



733 047

LIST OF FIGURES (Cont'd.)



733 048

ACKNOWLEDGMENT

I would like to express my great appreciation to all members of my Ph.D. Committee for their support and interest. I would like to thank especially Professor D. Okrent for his continued help and his patience, and for providing me with the financial support necessary to develop my ideas and incorporate them into computer codes. I am also grateful to Professor R. A. Westmann for many useful discussions.

Mrs. V. Temes provided great help by editing the whole of this thesis. Mr. J. C. Cherng prepared the figures through many hours of effort. Their help is greatly appreciated.

## VITA

January 5, 1946--Born, Chen-Do, Republic of China

1968--B.S., National Tsing-Hua University (Taiwan, Republic of China)

1969-1970--Teaching Assistant, National Tsing-Hua University

1970-1971--Laboratory Assistant, National Tsing-Hua University

1971--M.S., National Tsing-Hua University

1972-1976--Research Assistant, School of Engineering and Applied Science, University of California at Los Angeles

## PUBLICATIONS

YANG-HO SUN, J. P. CHIEN
"Rossi-Alpha Experiments in ZPR-L," Tsing-Hua Nuclear News, 1, 25, 1971.

Y. SUN, D. OKRENT, A. WAZZAN
"Probabilistic Formulation of Fission Gas Release in Uranium Alloy Fuels," Trans. Amer. Nucl. Soc., 16, 81, June, 1973.

A. MADRID, Y. SUN, J. CERMAK, D. OKRENT
"On the Failure Modes of Irradiated LMFBR Fuel Pin During Transients," Trans. Amer. Nucl. Soc., 18, 203, June, 1974.

Y. SUN, D. OKRENT
"A Simplified Method of Computing Clad and Fuel Strain and Stress During Irradiation," UCLA-ENG-7591, Oct., 1975.

Y. SUN, D. OKRENT
"On the Fuel-Clad Stress-Strain State at the Beginning of a Transient," International Meeting Fast Reactor Safety and Related Physics, Chicago, Oct., 1976.

733 070

ABSTRACT OF THE DISSERTATION

A Simplified Method of Computing
Clad and Fuel Strain and Stress
During Irradiation

by

Yang-Ho Sun

Doctor of Philosophy in Engineering
University of California, Los Angeles, 1977
Professor David Okrent, Chairman

This dissertation develops a simplified, fast-running axisymmetric computer code, named KRASS (Kwik Running Analysis for Stress and Strain), intended for the prediction of fuel element conditions after long-term steady-state operation in a LMFBR. KRASS assumes that fuel restructuring has already occurred, and divides the fuel pellets into two zones, an inner, highly plastic hot region, and an outer, cooler region which together with the cladding can undergo creep.

This code allows for fission gas pressure, fuel swelling, hot pressing, and it also includes alternative correlations for stainless steel swelling. Fuel cracking is not included. The output of KRASS includes the radial and axial stress and strain distribution of the fuel and clad as a function of the burn-up. It takes KRASS $11 \times 10^2$ machine unit seconds on the IBM 360-91 to calculate the fuel element behavior to 15% burn-up, with seven axial sections in the fuel column.


733 051

The results of the calculations indicate that the axial variation of the fuel-clad mechanical interaction greatly depends on the fluence-to-burnup ratio, as well as on the applicable stainless steel swelling correlation. The results also show that transient fuel element behavior studies of the pre-irradiated fuel must make allowance for these differences. At higher linear power ratings the largest fuel-clad mechanical interaction generally occurs in the lower third of the fuel element while at low power ratings, this interaction is largest at the axial midsection.

At high fluence-to-burnup ratios, the central axial nodes frequently exhibit gap reopening tendencies.

THERE IS NO TEXT ON THIS PAGE

# CHAPTER I. INTRODUCTION

The study of steady-state fuel element behavior is important for long-term reactor operation; however, it is also important for transient accident analysis. The steady state behavior of fuel pins must be predicted with reasonable success if an acceptably accurate description of their behavior in transients is to be obtained. The ultimate course of a transient overpower accident depends on the mode of fuel pin failure. This, in turn, depends on the stress and strain conditions of the fuel and clad, due to fission gas release and retention, fuel and clad swelling, creep, loss of ductility, etc. Whether or not (and where) the fuel clad gap is open or closed prior to the transient, may be of major importance in predicting the time and location of the failure.

In principle, the distribution of stress and strain in the fuel and in the cladding can be predicted from the knowledge of the fuel element geometry, the material properties, the temperature distribution, and the operating conditions. The fuel clad gap closure and the fuel clad mechanical interaction can also be predicted from the parameters given above.

Ordinarily, in a code such as LIFE [1], the computations of the axial and radial variations in the fuel pin behavior involve a considerable amount of computer time. This dissertation develops a simplified code, named KRASS (Kwik Running Analysis for Stress and Strain), for the predictions of fast reactor fuel element behavior.

In large LMFBR, the creep rate in the fuel may be enhanced by the high neutron flux, and thus, it can be twice that at the same power rating for a fuel element in EBR II. A scheme is included in KRASS to provide a means for relatively precise creep calculations at higher creep rates in order to assure that this code can be applied to fuel element behavior prediction in a large LMFBR.

Assuming plane strain and axial symmetry for a long cylinder, elastic equivalent analysis [2] is applied to give a system of displacement-inelastic strain and stress-inelastic strain relations. The inelastic strains, which include the creep strain and the swelling strain accumulated in one time step in the cylinder, are first determined from existing empirical formulae and from the stress state in the previous time step. The displacement-inelastic strain and the stress-inelastic strain are then used, so that the stress variation and the boundary movements in this cylinder (that are induced by the corresponding type of inelastic strain) can be determined. Creep and the irradiation-induced swelling are considered both in the fuel and in the cladding. Hot pressing has also been considered in the fuel region.

After the fuel-clad gap closes, the mechanical interaction force between the fuel and the cladding can be determined by an iteration process, so that the displacement of the fuel outer boundary equals that of the clad inner boundary.

The fuel region is considered as two separate regions in the radial direction. The hot region has temperatures higher than 1500°C, the cool region has temperatures lower than 1500°C. In the hot region of the fuel the temperature is much higher than the brittle-to-ductile transition temperature ($T_c$=1350°C) [3]; plastic flow occurs



733 055

rapidly and the material is weak. Hence, for the sake of simplicity, we have assumed that this region is stress free, and the gas pressure in the central void is transmitted directly to its outer boundary through this region. The thermal stress that builds up as a result of the high temperature in the fuel region during the first start-up, will be quickly relaxed by creep and by fuel restructuring. It is assumed that the thermal stress originating from start-up effects in the fuel region can be neglected. Also, since fuel restructuring is usually completed in the first stage of operation, we assume that this effect has been completed prior to the beginning of our calculation. Fuel cracks are also neglected.

The temperature distribution in the fuel element may change due to the burn-up effects in the fuel region. This variation is usually small and slow; thus it is neglected in the current version of the code. In the preliminary calculations KRASS was used to compute results which could then be compared with those obtained from post-irradiation measurements and with results calculated using the LIFE III code. Then it was used for calculations involving actual applications. The fuel element behavior in CRBR, and in a conceptual CMFBR, has been studied using different correlations for the clad swelling. The major fuel properties have also been studied parametrically for CRBR fuel pins. It takes KRASS eleven hundred machine unit seconds on the UCLA IBM-360-91 to calculate fuel element behavior to 15% burn-up, with seven axial sections in the fuel column.

THERE IS NO TEXT ON THIS PAGE

733 057

## CHAPTER II. THEORY

### II.1 The Displacement-Inelastic Strain and the Stress-Inelastic Strain Relations.

The inelastic strain (consisting of the swelling strain and the creep strain) changes its value during fuel and clad irradiation in a nuclear reactor, thus changing the stress level within the material. Dimensional changes may also result.

In this section relations will be introduced between displacement and inelastic strain, and between stress and inelastic strains.

Let us consider a long cylinder with inner radius "a" and outer radius "b", subject to a uniform internal pressure $P_i$, and an outer pressure $P_o$. Let r, $\theta$, z be a set of cylindrical coordinates, and u,v,w the displacement along these three axes. The displacement w is initially assumed to be zero. Axial symmetry of the structure and of the loading is also assumed. The three principal stresses are $\sigma_r$, $\sigma_\theta$, and $\sigma_z$. The shear stresses and shear strains on these principal planes are zero.

Under the conditions described above, the strain-displacement relations are:

$$e_r = du/dr \qquad \text{II-1}$$

$$e_\theta = u/r \qquad \text{II-2}$$

where $e_r$, $e_\theta$ are the strain components.

According to the elastic equivalent relation the stress and the elastic component of the total strain should follow [2]:

$$\begin{cases} \sigma_r = \lambda(e - e'') + 2\mu(e_r - e_r'') \\ \sigma_\theta = \lambda(e - e'') + 2\mu(e_\theta - e_\theta'') \\ \sigma_z = \lambda(e - e'') + 2\mu(e_z - e_z'') \end{cases} \qquad \text{II-3}$$

Here $e_r''$, $e_\theta''$ and $e_z''$ are the inelastic strain components. $e_r$, $e_\theta$, and $e_z$ are the components of the total strain and

$$e'' = e_r'' + e_\theta'' + e_z''$$

$$e = e_r + e_\theta + e_z \quad .$$

Substituting Equations II-1 and II-2 into Equation II-3, we get:

$$\begin{cases} \sigma_r = (\lambda+2\mu)\ (\frac{du}{dr} - e_r'') + \lambda(\frac{u}{r} - e_\theta'') - \lambda e_z'' \\ \sigma_\theta = (\lambda+2\mu)\ (\frac{u}{r} - e_\theta'') + \lambda(\frac{du}{dr} - e_r'') - \lambda e_z'' \\ \sigma_z = -(\lambda+2\mu)e_z'' + \lambda(\frac{du}{dr} - e_r'') + \lambda(\frac{u}{r} - e_\theta'') \end{cases} \qquad \text{II-4}$$

The governing equation of equilibrium for a cylinder is:

$$\frac{d\sigma_r}{d_r} + \frac{\sigma_r - \sigma_\theta}{r} = 0 \qquad \text{II-5}$$

Substituting Equation II-4 into Equation II-5, and then integrating twice with respect to r, yields:

$$(\lambda+2\mu)u = \frac{\lambda}{r}\int_a^r (e_r'' + e_\theta'' + e_z'')\ rd_r + \frac{2\mu}{r}\int_a^r re_r''\ dr + \frac{2\mu}{r}\int_a^r r\int_a^r \frac{e_r'' - e_\theta''}{r}\ d_r d_r + \frac{c_1 r}{2} + \frac{c_2}{r} \qquad \text{II-6}$$

Substituting Equation II-6 into the first equation in II-4 we get:

733 059

$$\sigma_r = -\frac{2\mu\lambda}{(\lambda+2\mu)}\frac{1}{r^2}\int_a^r (e_r'' + e_\theta'' + e_z'')\,r\,dr - \frac{4\mu^2}{\lambda+2\mu}\frac{1}{r^2}\int_a^r r e_r''\,dr$$

$$-\frac{4\mu^2}{(\lambda+2\mu)}\frac{1}{r^2}\int_a^r r\int_a^r \frac{e_r''-e_\theta''}{-r}\,d_r d_r + 2\mu\int_a^r \frac{e_r''-e_\theta''}{r}\,dr$$

$$+\left(\frac{\lambda+\mu}{\lambda+2\mu}\right)c_1 - \frac{2\mu}{\lambda+2\mu}\frac{1}{r^2}c_2 \qquad \text{II-7}$$

The boundary conditions are:

$$\sigma_r = -P_i \quad \text{at} \quad r = a \qquad \text{II-8}$$

$$\sigma_r = -P_o \quad \text{at} \quad r = b \qquad \text{II-9}$$

The values of $c_1$ and $c_2$ and can be obtained from Equation II-7, using Equations II-8 and II-9. Resubstituting these values of $c_1$ and $c_2$ into Equation II-7 we get:

$$\sigma_r(r) = (\sigma_r(r))_e + (\sigma_r(r))_p \qquad \text{II-10}$$

$$u(r) = (u(r))_e + (u(r))_p\ . \qquad \text{II-11}$$

Similarly, we can write:

$$\sigma_\theta(r) = (\sigma_\theta(r))_e + (\sigma_\theta(r))_p \qquad \text{II-12}$$

$$\sigma_z(r) = (\sigma_z(r))_e + (\sigma_z(r))_p\ . \qquad \text{II-13}$$

Here:

$$(\sigma_r(r))_e = \frac{a^2}{b^2-a^2}(P_i-P_o)\left(1-\frac{b^2}{r^2}\right) - P_o \qquad \text{II-14}$$

$$(\sigma_\theta(r))_e = \frac{a^2}{b^2-a^2}\left(1+\frac{b^2}{r^2}\right)(P_i-P_o) - P_o \qquad \text{II-15}$$

$$(\sigma_z(r))_e = \frac{\lambda}{\lambda+\mu}\frac{1}{b^2-a^2}(a^2P_i-b^2P_o) \qquad \text{II-16}$$

$$(u(r))_e = \frac{a^2}{2(b^2-a^2)}\left[\frac{r}{\lambda+\mu}+\frac{b^2}{\mu r}\right](P_i-P_o) - \frac{r}{2(r+\mu)}P_o \qquad \text{II-17}$$

733 060

$$(\sigma_r(r))_p = -\left[I_1(r)+I_2(r)+I_3(r)-I_4(r)\right]$$

$$+ \frac{b^2}{b^2-a^2}\left(1-\frac{a^2}{r^2}\right)\left[I_1(b)+I_2(b)+I_3(b)-I_4(b)\right] \qquad \text{II-18}$$

$$(\sigma_\theta(r))_p = I_1(r)+I_2(r)+I_3(r)+\frac{\lambda}{\lambda+2\mu} I_4(r)-\frac{2\mu\lambda}{\lambda+2\mu}(e_\theta''+e_z'')-2\mu e_\theta''$$

$$+ \frac{b^2}{b^2-a^2}\left(1+\frac{a^2}{r^2}\right)\left[I_1(b)+I_2(b)+I_3(b)-I_4(b)\right] \qquad \text{II-19}$$

$$(\sigma_z(r))_p = \frac{\lambda}{\lambda+2\mu} I_4(r)-\frac{2\mu\lambda}{\lambda+2\mu}(e_\theta''+e_z'') - 2\mu e_z''$$

$$+ \frac{\lambda}{\lambda+\mu}\frac{b^2}{b^2-a^2}\left[I_1(b)+I_2(b)I_3(b)-I_4(b)\right] \qquad \text{II-20}$$

$$(u(r))_p = \frac{r}{2\mu}\left[I_1(r)+I_2(r)+I_3(r)\right]$$

$$+ \frac{b^2}{2(b^2-a^2)}\left[\frac{r}{\lambda+\mu}+\frac{a^2}{\mu r}\right]\left[I_1(b)+I_2(b)+I_3(b)-I_4(b)\right] \qquad \text{II-21}$$

Here the integrals are:

$$I_1(r) = \frac{2\mu\lambda}{\lambda+2\mu}\frac{1}{r^2}\int_a^r e'' r d_r \qquad \text{II-22}$$

$$I_2(r) = \frac{4\mu^2}{\lambda+2\mu}\frac{1}{r^2}\int_a^r e_r'' r dr \qquad \text{II-23}$$

$$I_3(r) = \frac{4\mu^2}{\lambda+2\mu}\frac{1}{r^2}\int_a^r r \int_a^r \frac{e_r''-e_\theta''}{r} d_r d_r \qquad \text{II-24}$$

$$I_4(r) = 2\mu \int_a^r \frac{e_r-e_\theta}{r} d_r \qquad \text{II-25}$$

$$e'' = e_r'' + e_\theta'' + e_z'' \qquad \text{II-26}$$

733 001

$\lambda$ and $\mu$ are Lame's Constants,

$$\lambda = \frac{2\mu\nu}{1-2\nu}, \qquad \mu = \frac{E}{2(1+\nu)} \qquad \text{II-27}$$

E and $\nu$ are the Young's modulus and the Poisson's ratio, respectively.

In the formulae listed above, an axial force must be applied to the ends of the cylinder to keep the axial displacement equal to zero. Saint-Venant's principle [4] can be applied for this effect. If the real restriction in the axial direction is $F_z$ and we superimpose a uniform axial stress $C_3$ so that the resultant axial force is equal to the restrictive force $F_z$, $C_3$ can be determined from:

$$\pi(b^2-a^2)C_3 + \int_a^b 2\pi r(\sigma_z)_{w=0}\,dr = F_z$$

i.e.

$$C_3 = \frac{F_z - \int_a^b 2\pi r(\sigma_z)_{w=0}\,dr}{\pi(b^2-a^2)} \qquad \text{II-28}$$

Here $(\sigma_z)_{w=0}$ is the axial stress for zero axial strain (w=0), described in Equation II-13.

The real axial stress should thus be:

$$\sigma_z = (\sigma_z)_{w=0} + C_3 = (\sigma_z)_{w=0} + \frac{F_z - \int_a^b 2\pi r(\sigma_z)_{w=0}\,dr}{\pi(b^2-a^2)} \qquad \text{II-29}$$

The displacement u is also affected by the superposed axial stress $C_3$. Therefore, the term, $\nu C_3 r/E$ [4] must be added to the right hand side of Equation II-11.

733 062

In Equations II-10 through II-13, the first term on the right hand side represents the effect induced by the pressure on the walls of the fuel and the cladding. The second term on the right hand side represents those effects that were induced by inelastic strains, e.g. the creep, the swelling, and the hot pressing strains. Thus:

$$e_i'' = e_i^{c''} + e_i^{sw} + e_i^{hp} = e_i^{c''} + e_i^{sw''} \qquad \text{II-30}$$

where $e_i^{c''}$ is the creep strain

$e_i^{sw}$ is the swelling strain

$e_i^{hp}$ is the hot pressing strain

$i$ represents the components in r, θ, and z directions.

Applying Equation II-30 to Equations II-22 through II-28, we can find the I values corresponding to the creep and swelling effects. If we substitute these I values into Equations II-10, II-11, II-12, II-13, and into Equations II-28 and II-29, the creep and swelling-induced stresses can be found.

## II.2 Inelastic Strains

The inelastic strain includes creep strain and irradiation induced strain.

### II.2.1 The Stress and Strain Relations in Creep Deformation

At low temperatures, the stress-strain curves are essentially time-independent. However, if the temperature of the material exceeds about half of its melting-point, a departure from this idealization becomes noticeable and the strain increases under constant load.

The creep strains should follow the Prandtl and Reuss assumption, i.e., the plastic-strain increment at any instant is proportional to the deviatoric stress. Using the principal stress axes, we get:

$$\frac{de_r^c}{s_r} = \frac{de_\theta^c}{s_\theta} = \frac{de_z^c}{s_z} = d_K \quad , \qquad \text{II-31}$$

where $de_r^c$, $de_\theta^c$, and $de_z^c$ are the increment of creep strains in the r, $\theta$ and z directions, respectively.

$S_r$, $S_\theta$ and $S_z$ are the deviatoric stress components.

$d_K$ is an instantaneous, positive constant of proportionality, which may vary during the loading process.

Equation II-31 satisfies the condition of zero dilation, i.e.,

$$de_r^c + de_\theta^c + de_z^c = 0 \qquad \text{II-32}$$

The effective stress $\sigma^*$ and strain $e^*$, are defined (in terms of the principal stresses and creep strains) as:

$$\sigma^* = \frac{1}{\sqrt{2}}\sqrt{(\sigma_r-\sigma_\theta)^2+(\sigma_\theta-\sigma_z)^2+(\sigma_r-\sigma_z)^2} \qquad \text{II-33}$$

$$e^* = \frac{\sqrt{2}}{3}\sqrt{(e_r^c-e_\theta^c)^2+(e_\theta^c-e_z^c)+(e_r^c-e_z^c)^2} \qquad \text{II-34}$$

It can be shown [5] that $\sigma^*$ is proportional to the total shear stress, which gives an accurate measurement for the gross amount of plastic creep deformation in a polycrystalline material.

In a uniaxial case $\sigma^*$ reduces to $\sigma_r$ and $e_c^*$ to $e_r^c$. Equation II-31 gives the relative proportion of the incremental plastic-strain components to the corresponding deviatoric-stress components. Also, in the uniaxial case $\sigma^* = \sigma_r = \frac{3}{2}S_r$. From these:

$$d_K = \frac{3}{2}\frac{de_c^*}{\sigma^*} \quad . \qquad \text{II-35}$$

733 064

Equation II-35 can be generalized to multiaxial cases by using $\sigma^*$ and $e_c^*$ defined in Equation II-33 and II-34.

II.2.2. The Creep Strain Rate

The creep strain rate can be represented by the following:

$$\frac{de_c^*}{dt} = Ae^{-\theta/RT}\sigma^{*m} + \left[\frac{A_1}{d^2} e^{-\theta_1/RT} + B\,\phi\right]\sigma^{*n} \qquad [1] \qquad \text{II-36}$$

For mixed oxide fuel, we are presently using

$$A = \frac{1.376\text{x}10^{-4}}{-90.5+D}$$

D = fuel density percentage.

If the calculated D value is less than 92, we shall substitute D = 92.

$\theta$ = 132000 cal/mole

$\theta_1$ = 90000 cal/mole

$A_1$ = 9.726x$10^6$/(-87.7+D)

d = grain diagram, $\mu$($\sim$10) II-37

B = 8.0x$10^{-24}$

m = 4.5

n = 1

$\phi$ = flux

For 316 cw S.S., used presently, the parameters are:

A = 2.7x$10^{-11}$

$\theta$ = 95000 cal/mole

$A_1$ = 0 II-38

B = 4.655x$10^{-34}$

m = 7

n = 3

733 065

Knowing $\sigma^*$, $de_c^*$ can be determined from Equation II-36. Then, from Equations II-31 and II-35 the increment of the creep components, i.e. $de_r^c$, $de_\theta^c$ and $de_z^c$, within a time step can be obtained.

II.2.3. The Swelling Strain

It is assumed that all swelling strain components are equal, i.e.:

$$e_r^{sw} = e_\theta^{sw} = e_z^{sw} = \frac{1}{3} e^{sw} \qquad \text{II-39}$$

where $e^{sw}$ is the total volumetric swelling strain.

II.2.3.1. The Swelling Strains in the Cladding

For 20% cw, 316 stainless steel, four options have been included in the code as possible correlations for irradiation-induced swelling. These are:

a) $$\frac{\Delta V}{V_o} = R\left[\phi t 10^{-22} + \frac{1}{\alpha}\,\ell n\left\{\frac{1+\text{Exp}\,[\alpha(\tau-\phi t)]}{1+\text{Exp}(\alpha\tau)}\right\}\right] \quad [6] \qquad \text{II-40}$$

where

$\Delta V/V_o$ = fractional volume change

$\phi t$ = fluence, unit = $n/cm^2$ (E > 0.1 Mev)

$$R = \beta\ \text{Exp}\Big[-88.5499+0.531072T-1.24156\text{x}10^{-3}T +1.37215\text{x}10^{-6}T^3-6.14\text{x}10^{-10}T^4\Big]$$

$$\alpha = -1.12+6.89\text{x}10^{-3}T$$

$$\tau = \text{Exp}\Big[-16.7382+0.130532T-3.81081\text{x}10^{-4}T^2 +5.51979\text{x}10^{-7}T^3-3.26491\text{x}10^{-10}T^4\Big]$$

T = neutron irradiation temperature in °C

$\beta$ = multiplicative factor to describe confidence limits, $\beta$ = 0.01 for nominal swelling

In this correlation there is a swelling threshold that is temperature dependent.

733 066

b) $\frac{\Delta V}{V} = \frac{1}{2} (9x10^{-35})(\phi t)^{1.5}(4.028-3.712x10^{-2}T+1.0145x10^{-4}T^2$

$-7.879x10^{-8}T^3)$ [7] II-41

The limits of applicability of this formula are $\phi t<10^{23} n/cm^2$, E>0.1 Mev, and 360°C<T<600°C. The confidence limits are ±50%.

c) $\frac{\Delta V}{V} = 9.71574x10^{-41}(\phi t)^{1.6877368} Exp[-(1.214x10^{-2}T$

$-6.0696)^2]$ [8] II-42

This gives a swelling which peaks at T = 500°C.

d) $\frac{\Delta V}{V} = 9.71574x10^{-41}(\phi t)^{1.6877368} Exp[-(1.214x10^{-2}T$

$-7.284)^2]$ [8] II-43

This gives a swelling which peaks at T = 600°C.

II.2.3.2. Swelling Strain in the Fuel Region

The isothermal tests described in Chubb's paper [9] give relation between the temperature and the strain rate induced by the fission gas swelling at a burnup rate of $2x10^{13}$ fissions/cc-sec.

The curves in Figure II-1 follow the formula:

$\dot{\Delta} = 10^{(0.001046T-5.08378)}$, II-44

where

$\dot{\Delta} = \frac{\Delta \dot{u}}{b}$ is the ratio of the displacement rate to the radius of the outer boundary.

T is the temperature in °F.

Assuming a linear relation between the fission gas swelling rate and the burnup rate in the fuel, the displacement of the fuel outer boundary during $\Delta t$ time will be:

733 067

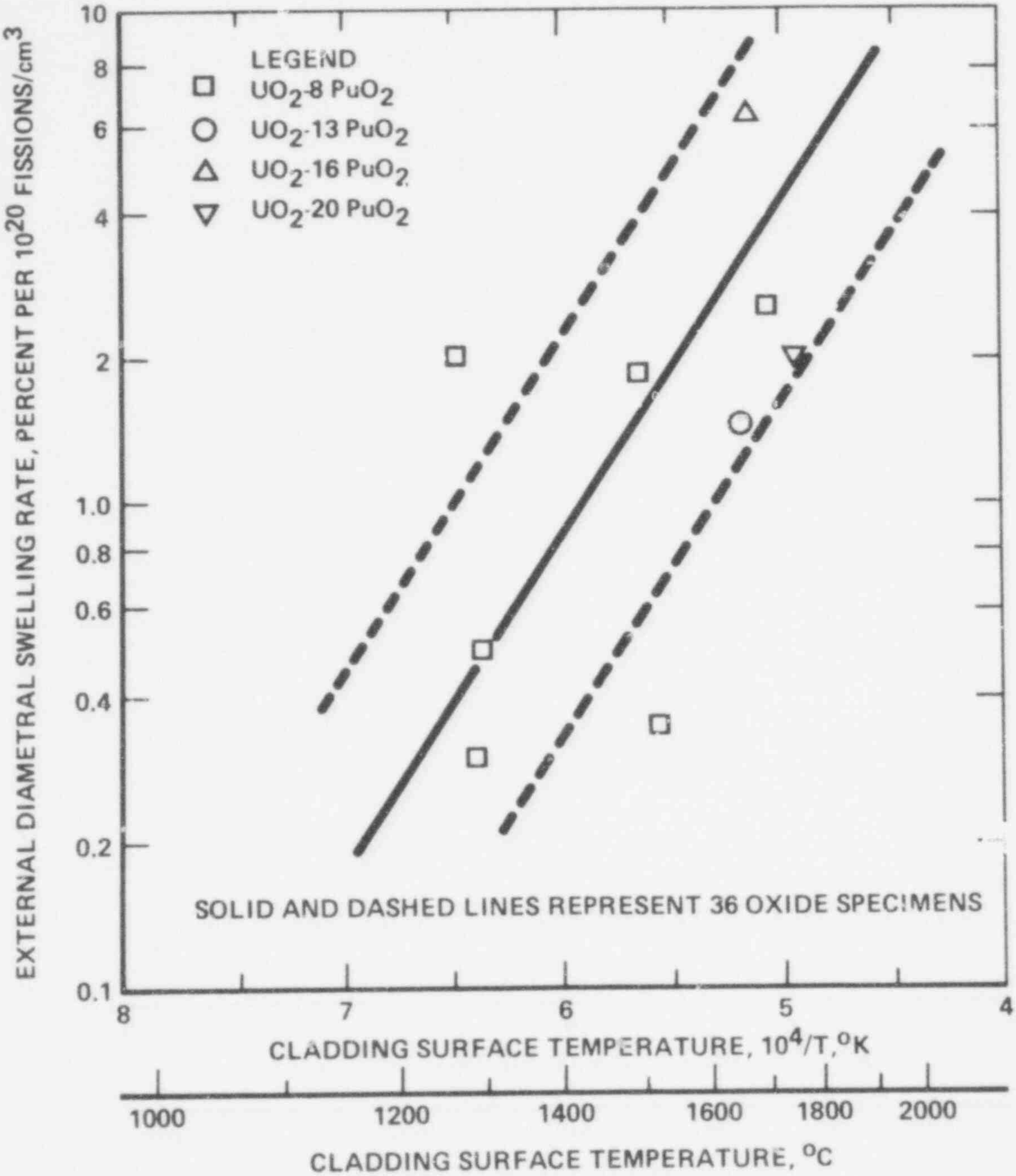


Figure II - 1. Effect of Alloying $UO_2$ with $PuO_2$.

733 008

$$\Delta u = b\dot{\Delta} \frac{(3600 x \Delta t) B}{10^{20}} = 3.6x10^{-17}\ b\dot{\Delta}B(\Delta t), \qquad \text{II-45}$$

where B is the burnup rate in fission/cc-sec.

On the other hand, from Equations II-21 and II-39, the relation between the swelling strains and the outer boundary displacement can be expressed by:

$$u(b) = (\lambda + \frac{2\mu}{3}) \frac{1}{\lambda+2\mu} \frac{1}{b} \left\{1 + \frac{\mu}{\lambda+\mu}\right\} e_{sw} \int_a^b rdr \ . \qquad \text{II-46}$$

Since the experiment in Reference [9] is almost isothermal, $e_{sw}$ is assumed to be constant across the fuel region.

By equating Equations II-45 and II-46, we get the fission gas swelling in the fuel as follows:

$$e_{sw}^{F} = 3.6x10^{-17} \frac{b}{G} \dot{\Delta}B(\Delta t) \ , \qquad \text{II-47}$$

where

$$G = (\lambda + \frac{2\mu}{3}) \frac{1}{\lambda+2\mu} \frac{1}{b} \left\{1 + \frac{\mu}{\lambda+\mu}\right\} \int_a^b rdr \qquad \text{II-48}$$

In order to achieve best fit to the results obtained from the LIFE-III code, an adjustable parameter AG = 3.4 is introduced in Equation II-47 for the low power calculations. This adjustment gives a fuel swelling rate that approximates the upper binding curve in Fig. II.1.

II.2.4 Hot Pressing

The temperature in the fuel region is usually high. Dislocation glide and stress-enhanced diffusional creep can reduce the volumetric strain under hydrostatic compression. The amount of change in the volumetric strain $\Delta e^{hp}$ caused by this hot pressing process can be expressed as: [8]

$$\Delta e^{hp} = \frac{C}{T} \exp\left(-\frac{\theta}{T}\right) \sigma\left(1 - \frac{\rho}{\rho_{th}} - e^{sw}\right) \Delta t \qquad \text{II-49}$$

where

$\sigma = \frac{1}{3}(\sigma_r + \sigma_\theta + \sigma_z)$ is the hydrostatic pressure (dyne/cm$^2$)

$c = 4.7 \times 10^6 \; \frac{cm^2 K°}{dyne\ sec}$

$Q = 4.43 \times 10^4$ °K

$\Delta t$ = time increment (sec)

$\rho$ = fuel density

$\rho_{th}$ = the theoretical fuel density

$e^{sw}$ = fission gas swelling in the fuel region

T = temperature in °K

It is assumed that all hot pressing strain components are equal, i.e.

$$\Delta e_r^{hp} = \Delta e_\theta^{hp} = e_z^{hp} = \frac{1}{3} \Delta e^{hp}$$

II.2.5 Fission Gas Release and the Gas Pressure

The fission gas bubbles migrate in the fuel region as a result of temperature and the stress gradient, and can be released through the grain boundaries and cracks that interconnect to the surface. The gas release percentage in the undisturbed fuel zone [10] can be expressed by:

$$F = 1 - \frac{\left\{\frac{1 - \exp(-6.84 \times 10^{-5} B)}{(6.84 \times 10^{-5}) B}\right\}}{\left\{0.421/\exp(10.05Q)\right\}} , \qquad \text{II-50}$$

where B is the burnup (MWD/MTM)

and Q is the linear heat rate (kw/ft).

733 070

100% gas release is assumed in the equiaxial grain zone and in the columnar grain zone. The relation between F and B is shown in Figure II-2.

At first, most of the gas atoms are released to the central void, and then to the plenum through the interconnected voids, cracks, and any separation between the fuel pellets. It is assumed that the gas pressure in the central void is equal to that in the plenum. The gas pressure can thus be determined by the ideal gas law as follows:

$$P_p = P_{cv} = \frac{(FN_F + N_I)R\bar{T}}{V_p + V_{cv}} \quad , \qquad \text{II-51}$$

$P_p$, $P_{cv}$, $V_p$, $V_{cv}$ are the pressures and the volumes of the plenum and of the central void, respectively.

$N_F$ is the number of total gas atoms generated

$N_I$ is the initial number of gas atoms

$F$ is the fraction of total gas atoms released

$\bar{T}$ is the average temperature in the plenum and in the central void.

733 071

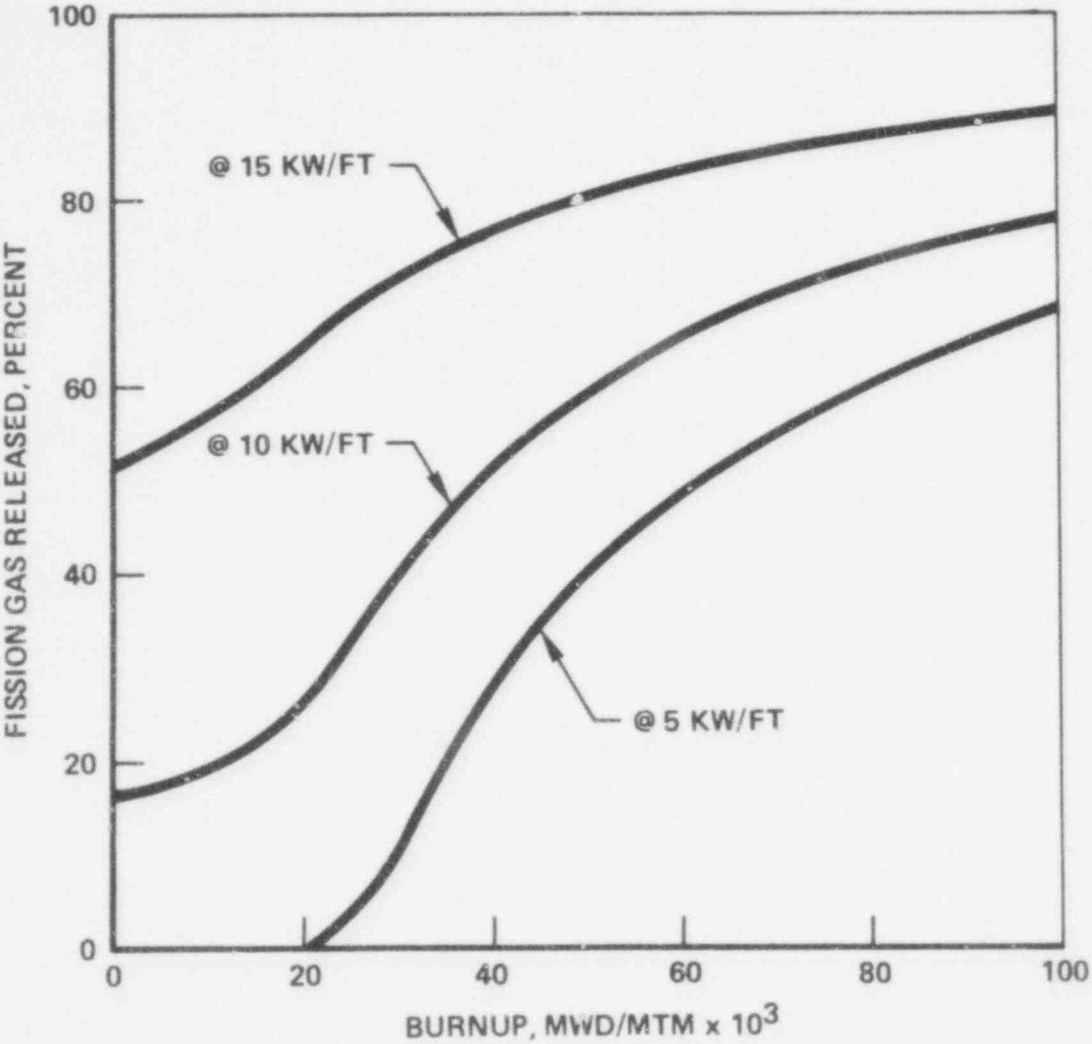


Figure II - 2. Predicted Gas Release for a Mixed-Oxide Fueled Pin.

733 072

THERE IS NO TEXT ON THIS PAGE

733 073

# CHAPTER III. THE PROCESS OF PROBLEM SOLVING

## III.1. The Basic Process

In the cooler fuel region the creep strain rate is about $10^{-4}$/hour, corresponding to a $10^{3}$ psi load. In the hot fuel region the creep strain rate is much higher. The thermal stress that has built up during the start-up period can thus be released quickly and should have negligible effect on fuel element behavior at later times. It is assumed in the code that this thermal stress is negligible.

The brittle-to-ductile transition temperature is approximately 1350°C for the fuel material. In the higher temperature region there is a heavy plastic flow and the material is very weak. This region can be considered stress free, with the gas pressure in the central void transmitted directly to the cooler boundary of the columnar region (Figure III.1).

This code treats steady state operations only. During such operation the variations of creep, swelling, and fission gas pressure are slow processes, therefore, the change in the stress state is also relatively slow. If the time intervals are small enough, it is a good assumption to calculate the creep strain using the stress state in the previous time step. An iteration process has been built into the code to assure that the ratio of the stress variation caused by the creep effect to the total stress state is less than a prescribed value. (See the simplified flow chart.) If this ratio is larger than the assigned value, the time interval of this step is linearly reduced to meet the prescribed value (Section III-3).

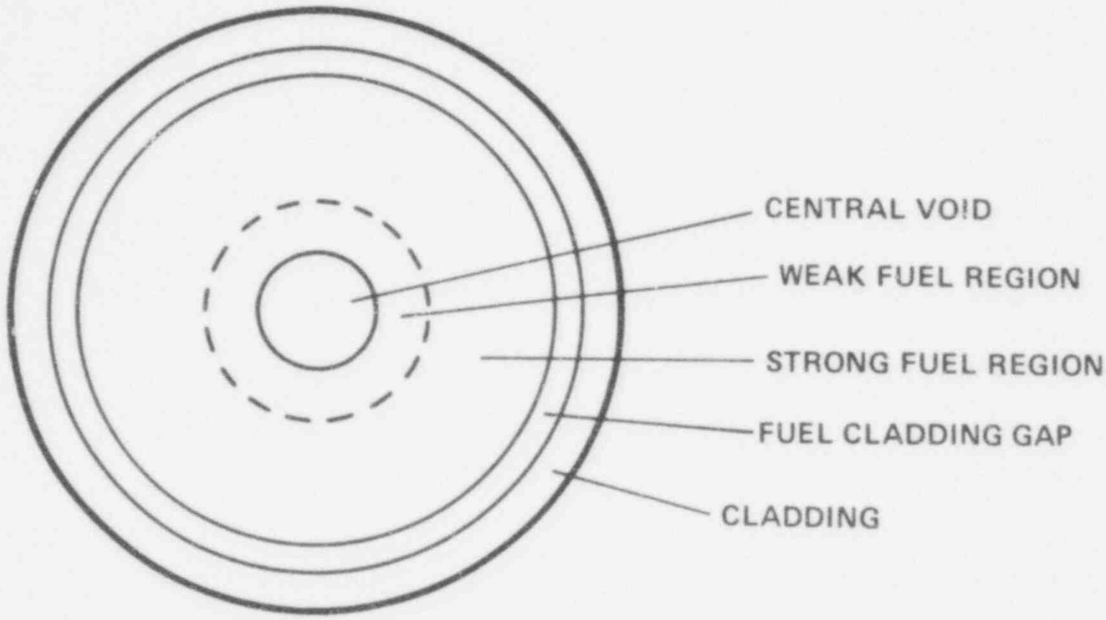


Figure III - 1. Radial Section of the Fuel Element.

733 075

The boundary displacements of the fuel and the cladding are calculated in each time step. Thus the closure of the fuel-cladding gap can be calculated by the differential displacement of the fuel and cladding boundaries. Before the gap closes, the plenum gas pressure acts on the fuel outer wall and on the cladding inner wall. After gap closure the mechanical interaction force can be determined by an iteration process so that the displacement of the fuel outer wall is equal to that of the cladding inner wall. A fast-converging iteration subroutine is included in the code to provide means for a fast determination of the interacting forces between the fuel and the clad after gap closure (Section III.2).

Once the pressure at the fuel and clad walls has been determined, the stress and strain distribution, caused by different physical effects, can be determined by the formulae in Chapter II.

The axial restriction $F_z$, used in Equation II-28, is different for the fuel column and for the cladding.

For the fuel column, as described in Figure III-2, the axial restriction is the plenum pressure $P_r$, acting at the end. After the fuel-clad gap is closed, the friction force $F_r$, acting between the fuel and the cladding, contributes to the axial restriction too. So, the total axial restriction, $F_z$ for the fuel column is:

$$F_z^F = \pi(b_f^2 - a_f^2)\, P_r + (2\pi b_f L)\, F_r q. \qquad \text{III-1}$$

Here $F_r = \mu P_{fc}$,

$\mu$ is the friction coefficient,

$P_{fc}$ is the mechanical interaction between the fuel and the cladding.

733 076

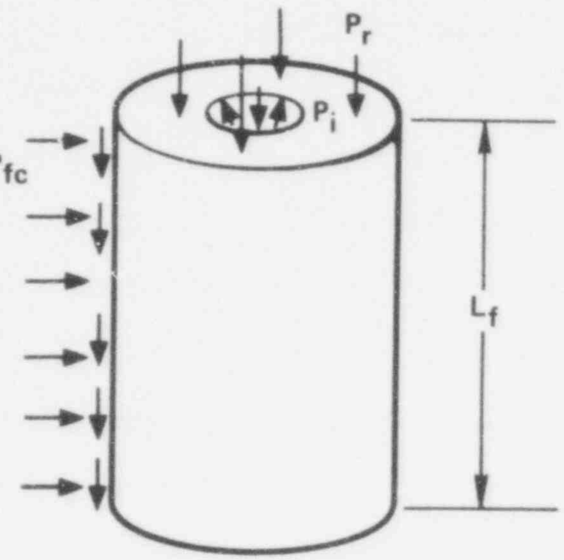


Figure III - 2. Free Body Diagram of the Fuel Region.

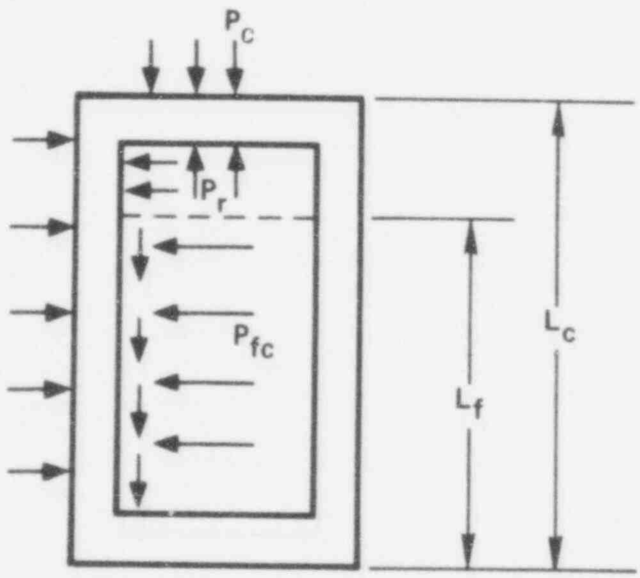


Figure III - 3. Free Body Diagram of the Cladding.

L is the distance to the upper end of the fuel column

q = 0, if the fuel-clad gap is open

q = 1, if the fuel-clad gap is closed.

As shown in Figure III-3, the axial restriction for the cladding can be written as:

$$F_z^c = \pi(b_c^2 P_c - a_c^2 P_r) + (2\pi a_c L)\ F_r q \quad . \qquad \text{III-2}$$

III.2. Determination of the Mechanical Force ($P_{fc}$) Between the Fuel and the Clad After the Gap Is Closed

After the fuel-clad gap is closed, there is a mechanical interaction force ($P_{fc}$) between the fuel and the clad. The increment of $P_{fc}$ in each time step should be such that the displacement of the outer boundary of the fuel and of the inner boundary of the clad is equal. An iteration process has been included in the code (see the simplified flow chart) to determine the change of $P_{fc}$(DP) in each time step.

Let us consider a coordinate system with $\Delta U_F$ displacement of the fuel outer wall along the X-axis, and with $\Delta U_c$ displacement of the clad inner wall along the Y-axis (see Figures III-4 and III-5) in a time interval $\Delta t_i$. $(DP)_1$, the first approximation of DP is equal to the change of $P_{fc}$ in the last time step. If the fuel-clad gap is still open in the last time step, then $(DP)_1$ is equal to the gas pressure change during the last time step. By applying $(DP)_1$ we get $(\Delta U_c)_1$ and $(\Delta U_F)_1$. If the absolute value of $\left[(\Delta U_c)_1 - (\Delta U_F)_1\right]/(\Delta U_c)_1$ is not smaller than a prescribed value (5% in this code), a second approximation, $(DP)_2$ should be tried.

733 078

As shown in Figure III-4, it is assumed that $(DP)_2$ is located at the crossing of lines $\bar{m}$ and $\bar{n}$. $\bar{m}$ contains all those points where $(\Delta U_c) = (\Delta U_F)$, $\bar{n}$ passes through point $(DP)_1$ and is perpendicular to line $\bar{m}$. Thus, $(DP)_2$ is expected to have a corresponding $(\Delta U_c)_2$ and $(\Delta U_F)_2$, so that $(\Delta U_c)_2 = (\Delta U_F)_2$. As shown in Figure III.4, $(\Delta U_c)_2$ and $(\Delta U_F)_2$ can be expressed by $(\Delta U_c)_1$ and $(\Delta U_F)_1$ as:

$$(\Delta U_F)_2 = (\Delta U_c)_2 = \frac{(\Delta U_c)_1 + (\Delta U_F)_1}{2} \quad .$$

In Figure III-4, $(DP)_1$ corresponds to a $(\Delta U_c)_1$ displacement of the cladding wall. As $\Delta P_{fc}$ varies from $(DP)_1$ to $(DP)_2$, the variation of $\Delta U_c$ is: $(\Delta U_c)_2 - (\Delta U_c)_1$. By assuming that

$$\frac{(DP)_1}{(DP)_2} = \frac{(\Delta U_c)_1}{(\Delta U_c)_2 - (\Delta U_c)_1}$$

$(DP)_2$ can be determined as:

$$(DP)_2 = (DP)_1 \frac{\left[(\Delta U_c)_1 + (\Delta U_F)_1\right]/2 - (\Delta U_c)_1}{(\Delta U_c)_1} \qquad \text{III-3}$$

If the absolute value of $\frac{(\Delta U_c)_2 - (\Delta U_F)_2}{(\Delta U_c)_2}$ is still not smaller than the allowed number, a more effective process is used to assure a fast convergence.

As shown in Figure III-5, $\bar{P}$ is the line connecting points $(DP)_1$ and $(DP)_2$. Point (DP) is assumed to be on P also and have $\Delta U_c = \Delta U_F$ displacement.

Figure III-5 shows that $\Delta U_c$ and $\Delta U_F$ can be expressed by the first and second trials as:

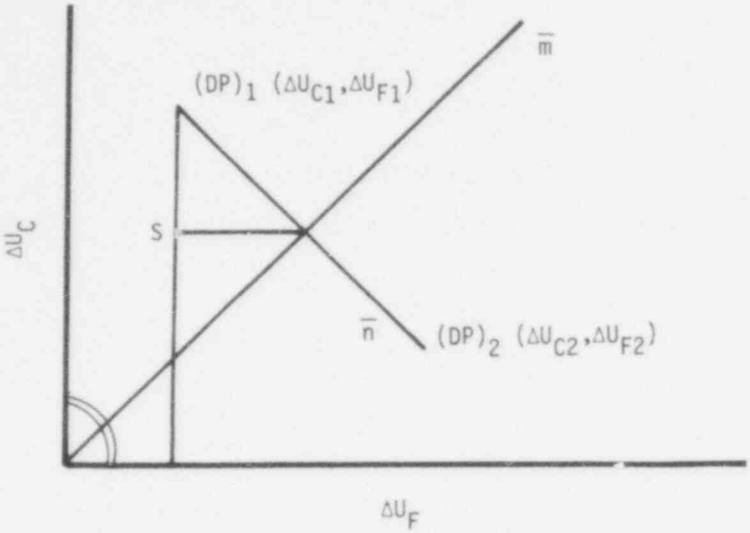


Figure III - 4. The Determination of $(DP)_2$

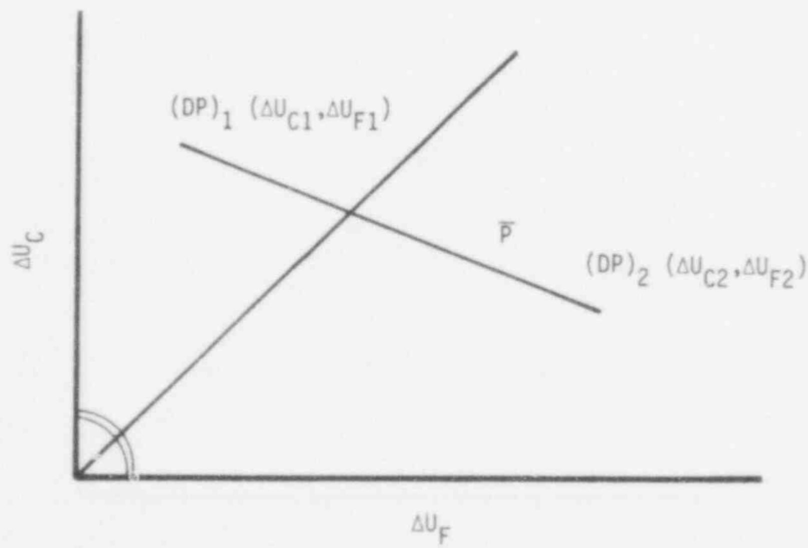


Figure III - The Determination of (DP)

733 000

$$\Delta U_c = \Delta U_F = b/(1-a) \qquad \text{III-4}$$

where $a = \dfrac{(\Delta U_c)_2 - (\Delta U_c)_1}{(\Delta U_F)_2 - (\Delta U_F)_1}$

and $b = (\Delta U_c)_2 - a(\Delta U_F)_2$ .

It can also be shown that the distance between points (DP) and $(DP)_2$ is:

$$LP2 = \sqrt{[(\Delta U_F) - (\Delta U_F)_2]^2 + [(\Delta U_c) - (\Delta U_c)_2]^2} \qquad \text{III-5}$$

and the distance between points $(DP)_1$ and $(DP)_2$ is:

$$L12 = \sqrt{[(\Delta U_F)_1 - (\Delta U_F)_2]^2 + [(\Delta U_c)_1 - (\Delta U_c)_2]^2} \ . \qquad \text{III-6}$$

Corresponding to the different $(\Delta U_c)$ and $(\Delta U_F)$ values in the first and second trial, the following relation is used to determine the third trial (DP):

(i) $(\Delta U_F)_1 > (\Delta U_c)_1$ and $(\Delta U_F)_2 > (\Delta U_c)_2$

$$DP = DP_2 - |DP_1 - DP_2| \frac{LP2}{L21} \qquad \text{III-7}$$

(ii) $(\Delta U_F)_1 < (\Delta U_c)_1$ and $(\Delta U_F)_2 < (\Delta U_c)_2$

$$DP = DP_2 - |DP_1 - DP_2| \frac{LP2}{L21} \qquad \text{III-8}$$

(iii) all other cases

$$DP = DP_2 + (DP_1 - DP_2) \frac{LP2}{L21} \qquad \text{III-9}$$

If $(DP)_{i-2} = (DP)_1$, $(DP)_2$, ... $(DP)_i$ are the steps of the iteration process, then the DP value will be reached when $(\Delta U_c - \Delta U_F)/\Delta U_c$ is smaller than the prescribed number.

## III-3. Iteration for Creep Precision in the Fuel

The increment of creep strain within a time step is determined by an empirical formula corresponding to the stress level in the previous

733 001

time step. In order to achieve precision in the creep increment calculation, a suitable time increment should be chosen for the time step, so that the creep increment and the stress variation (caused by this creep increment) is kept lower than a certain value (RV1).

If PH, PR and PZ are defined as:

$$\left.\begin{aligned} PH &= \Delta\sigma_\theta/\sigma_\theta \\ PR &= \Delta\sigma_r/\sigma_r \\ PZ &= \Delta\sigma_z/\sigma_z \end{aligned}\right\} \qquad \text{III-10}$$

where $\Delta\sigma_\theta$, $\Delta\sigma_r$, $\Delta\sigma_z$ are the stress increments caused by the creep affect within this time step, and $\sigma_\theta$, $\sigma_r$, $\sigma_z$ are the components of the total stress level in the previous time step. Also, let us designate:

$$AMX = \max\{PH, PR, PZ\} . \qquad \text{III-11}$$

To assure precision of the calculation, AMX should be kept smaller than RV1. But, in order to save computing time, AMX should be larger than another value RV2. We can thus adjust the time increment ($\Delta t$), so that RV1 < AMX < RV2 (See Fig. III-6).

Let $\Delta t_o$ be the initial time increment and let us determine $AMX_o$. If $AMX_o$ is not within the allowed interval for AMX, we adjust $\Delta t$ by a linear relation between $AMX_o$ and RV1, as described in Figure III-6. Thus, the first trial of time increment $\Delta t$ is:

$$\Delta t_1 = \Delta t_o \frac{RV1}{(AMX)_o} \qquad \text{III-12}$$

We can calculate $(AMX)_1$ by using $t_1$ in Equation III-7. If $(AMX)_1$ is still not in the allowed interval for AMX, we shall readjust $\Delta t$. As described in Figure III.11, the second trial of the time increment $\Delta t_2$ will be:

733 032

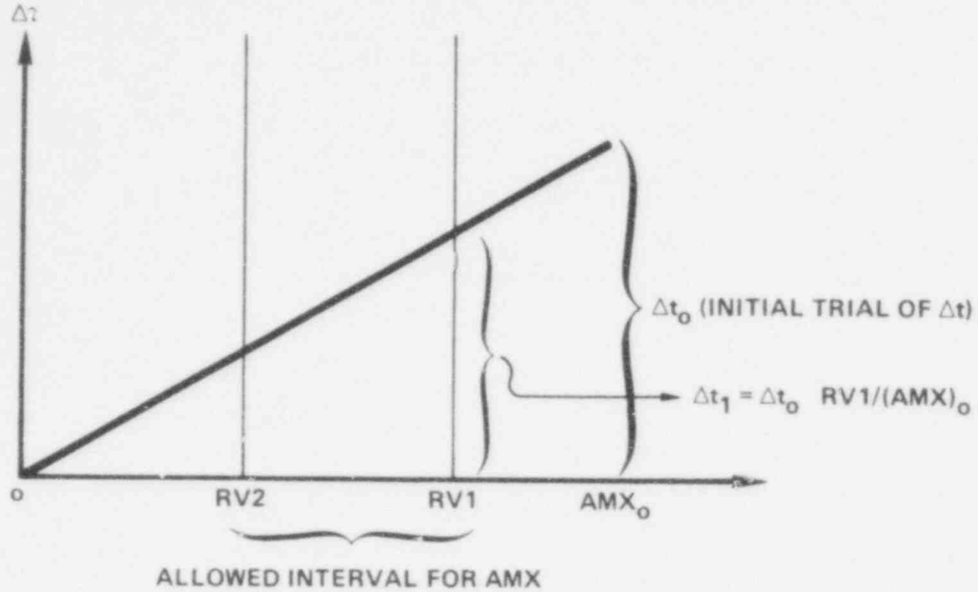


Figure III - 6. Adjusted Time Increment, Δt, Versus Maximum Fractional Stress Increment - First Trial.

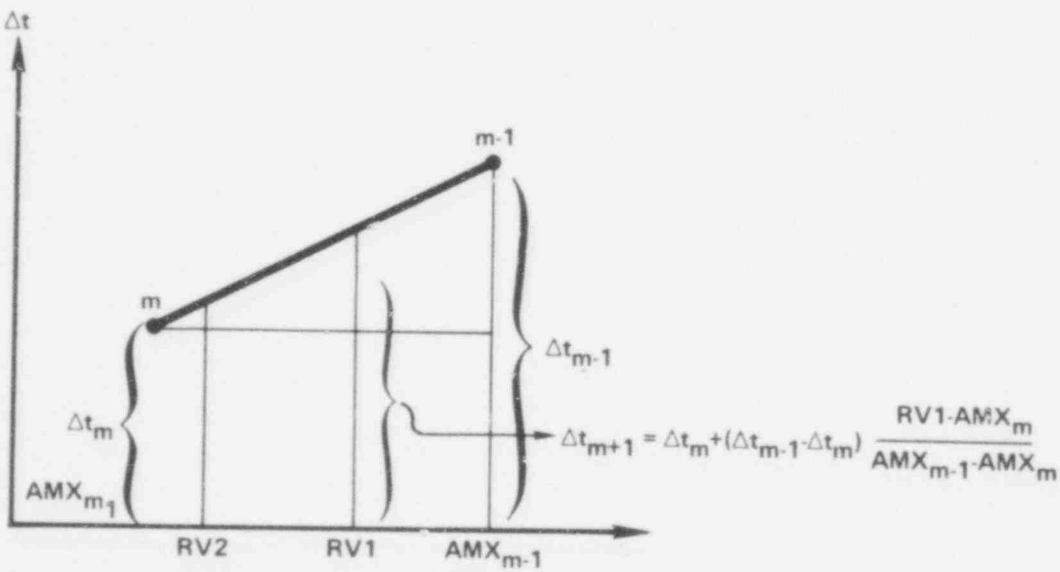


Figure III - 7. Adjusted Time Increment, Δt, Versus Maximum Fractional Stress Increment - $m^{th}$ Trial.

$$\Delta t_2 = \Delta t_1 + (\Delta t_o - \Delta t_1) \frac{RV1 - AMX_1}{AMX_o - AMX_1} \qquad \text{III-13}$$

This process can be repeated by using

$$\Delta t_{m+1} = \Delta t_m + (\Delta t_{m-1} - \Delta t_m) \frac{RV1 - AMX_m}{AMX_{m-1} - AMX_m} \qquad \text{III-14}$$

until AMX has a value inside the allowed interval.

A flow chart for the creep precision iteration is shown in Figure III-8.

III.4. A Simplified Flow Chart.

Figure III-9 illustrates the calculation of the strain change, boundary displacements, fuel-clad gap thickness and stress distribution. The process consists of the computation of:

1. The strain change ($\Delta e^c$) and the stress change ($\Delta\sigma^c$) caused by the creep effect. An iteration process is used to adjust $\Delta t$ so, that $\Delta\sigma^c/\sigma$ is small enough to result precise creep values.

2. The increment of the swelling strain and of the fission gas release. By knowing the available gas volume, the fission gas pressure can be determined.

3. The boundary displacements within this time step.

4. The fuel-clad gap thickness. If the gap is still open, the fission gas pressure acts at the outer boundary of the fuel and at the inner boundary of the clad. If the gap is closed, an iteration process is used to determine the fuel-clad mechanical interaction force ($P_{fc}$).

5. The stress distribution. This can be determined after the stress change (due to the swelling effect) and the pressures are calculated.

This process is repeated for all the axial sections and for all the time steps.

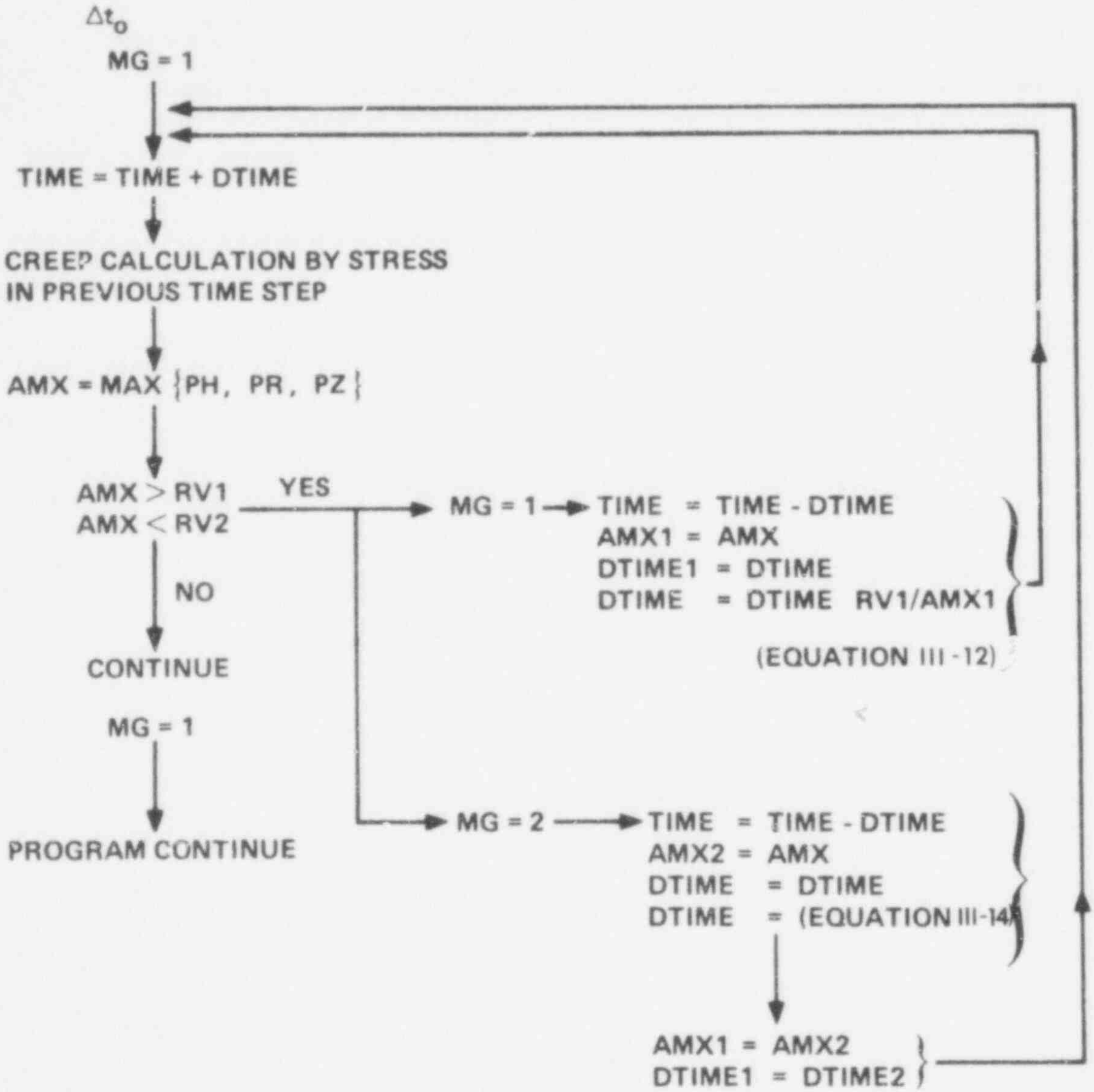


Figure III - 8. Flow Chart for Creep Precision Iteration.

733 086

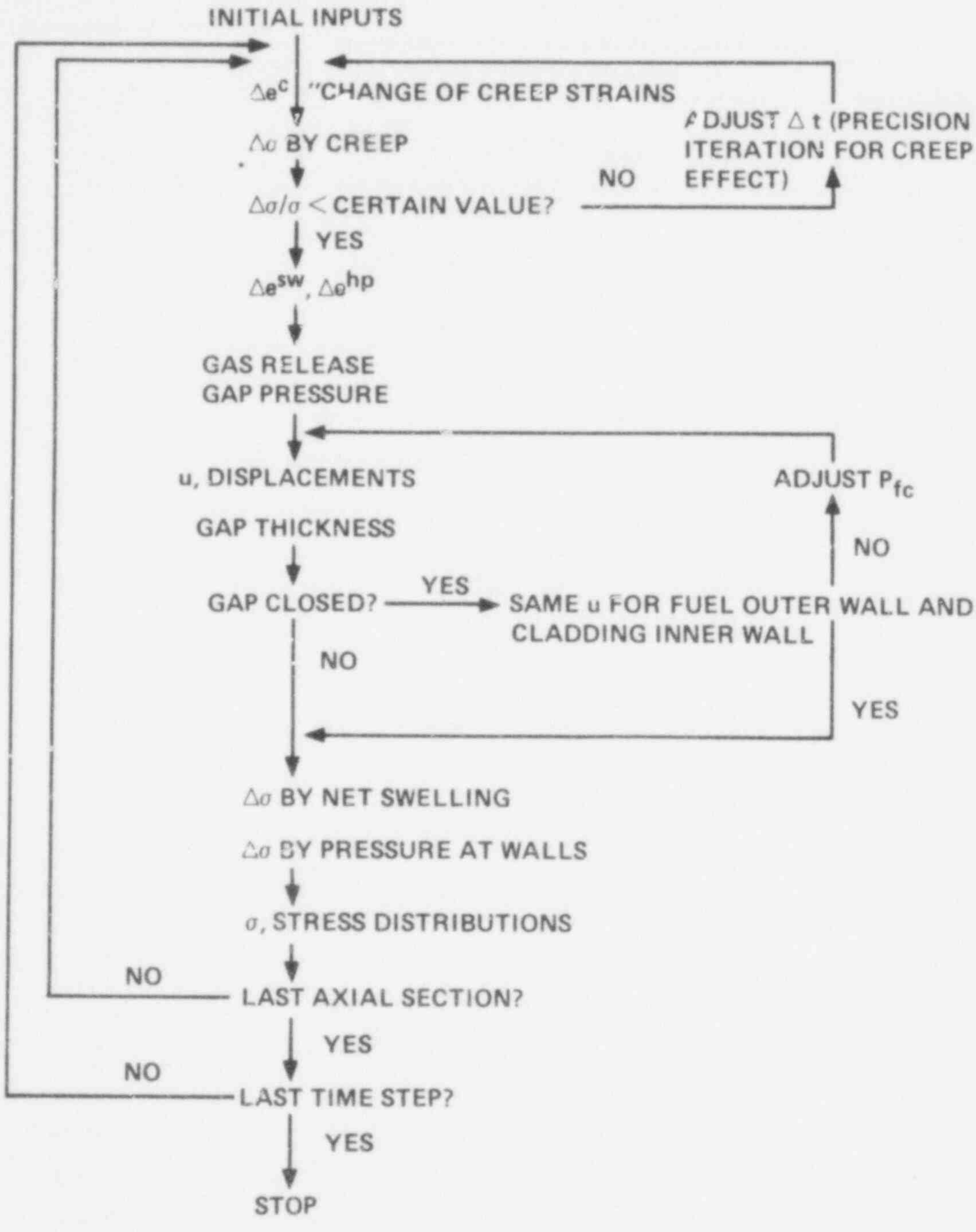


Figure III - 9. Simplified Flow Chart

733 007

# CHAPTER IV. PRELIMINARY CALCULATIONS

## IV.1. Calculations for Fuel Pin PNL-10-23

The fuel pin PNL-10-23, which had been irradiated in the EBR--II, has been chosen for comparison with the code. The specification of this fuel are the following: (11)

Fuel $UO_2$ - $PuO_2$ (65 wt % enriched U-235)

Fuel pellet diameter: 0.194 in., density: 90.9% TD

Fuel columnar length: 13.5 in.

Fuel smear density: 85.5% TD

Fuel-cladding gap width: 3 mils

Cladding material: 20% CW 316 S.S.

Cladding dimension: 0.23 in. OD x 0.015 in. thick

Gap plenum volume: 6.1 $cm^3$

Peak linear heat rating: 9.87 kW/ft

Peak burn-up: 5%

The post-irradiated fuel zone boundaries at the mid-plane are the following:

| Central Void Radius (mils) | Columnar Grain Radius (mils) | Equiaxed Grain Radius (mils) |
|---|---|---|
| 6.4 | 52.5 | 69.1 |

The mixed oxide fuel should be restructured completely above ~ 1650°C (columnar grain growth region), and the equiaxed grain growth is observed at about 1300°C. By normalizing the radius of the columnar zone and the equiaxial grain zone to 1650°C and 1300°C, respectively, the radial temperature distribution in the fuel region can be determined. The reported cladding surface temperature can also be used to determine the radial temperature distribution in the cladding.

By using the above values as inputs, the stresses, strains, boundary deformations, and the gap closures for the fuel PIN PNL-10-23 have been calculated.

A second sample case, with a smaller (2.4 mils) initial gap, has also been calculated. The gap closed at a 3.5% burn-up.

The results of these two primary calculations are shown in Figure E-1 through Figure E-3.

Figure E-1 shows the boundary movements of the fuel outer wall and the clad inner wall. In the first case, the initial gap thickness is larger, and the gap does not close before a 5% burn-up. In the second case, a small initial gap has been used that closed at 3.2% burn-up after 10,800 hours of irradiation. After 2 years of irradiation (5% burn-up), the post irradiation measurement of the clad boundary displacement was 1.26 mils. The calculated value is 1.5 mils; it is close to the measured value.

Figure E-2 shows the displacement of the clad wall ($U_c$) in the first and in the second case, after the clad has been irradiated for 10,800 hours. The fuel-clad mechanical interaction ($P_{fc}$) in the second case is also shown in this figure. Because the gap is closed and $P_{fc}$ acts on the cladding boundary, $U_c$ is larger than it was in the first case.

The maximum radial hoop stress $(\sigma_\theta^c)_{max}$ acts in the outer wall of the clad. Figure E-3 shows the time behavior of this stress. $(\sigma_\theta^c)_{max}$, that was induced by the start-up heating, is first relaxed by the creep effect, then, it is increased by the irradiation-induced



733 009

swelling of the clad. After the gap closure in the second case, $(\sigma_\theta^c)_{max}$ is increased by the $P_{fc}$ acting on the clad inner wall.

IV.2. Calculations for 6 kW/ft and 15 kW/ft Fuel Pins Irradiated in EBR-II.

In order to compare the results of our code to that of LIFE III, two sample calculation inputs of the LIFE III code (6 kW/ft and 15 kW/ft) have been used as inputs for the KRASS code.

IV.2.1. The Low Power Case (6kW/ft).

This is a calculation for a test fuel element that was irradiated in EBR. The specifications of the fuel element are the following:

Fuel: $UO_2$ - $PuO_2$ (65% wt enriched)

Fuel pellet radius: 0.11148 inch

Fuel density: 92.9% TD

Fuel columnar length: 13.5 inch

Cladding length: 36 inch

Fuel-cladding gap width: 1 mils

Cladding materials: 20% CW 316 S.S.

Cladding dimension: 0.25 inch OD x 12.5 mils thickness

Peak linear heat rating: 9.87 kW/ft

Coolant inlet temperature: 700°F

Coolant outlet temperature: 980°F

Neutron Flux: $0.65 \times 10^{15}$ neut/cm$^2$sec

The temperature after the start-up period (printed by LIFE III) was used as the input for the KRASS code. The stresses, strains, boundary movements and the gap closures were calculated for this 6 kW/ft fuel element.

733 0̣0

The fuel is divided into three axial components in the computation. The results of the KRASS code were compared to those of the LIFE III code in Figures E-4 and E-5. As Figure E-4 shows, the fuel-clad closure is calculated 980 hours by LIFE III, and at 1150 hours by KRASS. After the gap closure the $P_{fc}$ values given by both codes are very similar. The maximum radial hoop stress in the clad is measured at the outer wall by both codes. Because of fuel-clad interaction $P_{fc}$ at the inner wall, the stress and strain magnitudes start to increase in the clad in about 260 hours after the gap closure. At this time the value of $P_{fc}$ is large enough to compensate the outward swelling of the fuel; the increase rate of $P_{fc}$ is thus reduced, and the hoop stress in the clad starts to be relaxed by the creep effect.

Comparing the results of the two codes after 2750 hours of irradiation (Figure E-4) we find:

| | KRASS | LIFE III |
|---|---|---|
| $(\sigma_\theta^c)_{max}$ | 28 ksi | 25.4 ksi |
| $e_t^c$ | 0.87% | 0.67 % |

After 7500 hours of irradiation:

| | KRASS | LIFE III |
|---|---|---|
| $(\sigma_\theta^c)_{max}$ | 27.5 ksi | 29.7 ksi |
| $(e_\theta^c)_t$ | 2.46% | 2.70 % |

Figure E-5 shows the displacement of the fuel outer wall ($U_F$) and of the clad inner wall ($U_c$). As this figure indicates, after 2750 hours and 7500 hours, the $U_F$ and $_c$ values calculated by the KRASS code are similar to those given by the LIFE-III code.

733 021

IV.2.2. The High Power Case (15.2 kW/ft).

This is a calculation for a test fuel element irradiated in the EBR-II. The specifications are the following:

Fuel: $UO_2$ - $PuO_2$ (65% wt enriched)

Fuel pellet radius: 0.1085 inch

Fuel density: 90.8% TD

Fuel columnar length: 13.5 inch

Cladding length: 36 inch

Fuel-clad gap width: 1.8 mils

Cladding material: 20% CW 316 S.S.

Cladding dimension: 0.22 mils x 28 mils thickness

Peak linear power rating: 15.2 kW/ft

Coolant inlet temperature: 700°F

Coolant outlet temperature: 860° F

Neutron flux: $1.16 \times 10^{15}$ neut/cm$^2$ sec

Figure E6 shows the fuel-clad gap closure, the fuel-clad interaction force, the total hoop strain $(e^c_\theta)_t$, and the $(\sigma^c_\theta)_{max}$, calculated by the FRASS code. The fuel-clad gap closes at 1600 hours. Before gap closure the irradiation-induced swelling strain is the main contributor to the $(e^c_\theta)_t$. After gap closure the creep strain induced by $P_{fc}$ in the clad gives a larger $(e^c_\theta)_t$. 150 hours after gap closure $P_{fc}$ reaches a large enough value to compensate the outward swelling of the fuel. The increase rate of $P_{fc}$ is thus reduced. 150 hours after gap closure $P_{fc}$ increases by 750 psi, which results in a 5.9 ksi increase of $(\sigma^c_\theta)_{max}$. After 1750 hours, the creep rate in the clad is $1.9 \times 10^{-7}$/hr.

733 092

This is three times that of the 6 kW/ft case. This large creep rate is due to the higher neutron flux used in this calculation. Because of this creep in the clad, and the small reduction of $P_{fc}$ due to the fuel creep, $(\sigma_\theta^c)_{max}$ starts to reduce its magnitude 150 hours after the gap closure. At 4% burn-up, $P_{fc}$, $(\sigma_\theta^c)_{max}$, and $(e_\theta^c)_t$ is 550 psi, 4.8 ksi, and 0.06%, respectively.

In this high power case, the available version of LIFE III gave results which oscillate in their values, because the code did not have a subroutine to control creep stability in the fuel region. In the KRASS code, a control scheme was included to assure that in each time step, the change of state caused by the creep effect is small enough to allow accurate calculations.

The results of the KRASS code are within the envelope of the oscillatory results given by LIFE III.

## CHAPTER V. APPLICATIONS

### V.1. List of Applications.

The KRASS code is used for the calculations of the fuel element behavior in CRBR and in a large conceptual LMFBR. The fuel element specifications in these reactors are the following:

| | CRBR | Conceptual LMFBR |
|---|---|---|
| Fuel material: | $(U - Pu)O_2$ | $(U - Pu)O_2$ |
| Fuel pellet radius: | 0.097 inch | 0.135 inch |
| Fuel density: | 91.3% TD | 85% TD |
| Fuel smear density: | 85.5% TD | 80% TD |
| Core column length: | 36 inch | 42.8 inch |
| Fuel-clad gap: | 3.25 mils | 2.5 mils |
| Cladding material: | 20% CW, 316 S.S. | 20% CW, 316 S.S. |
| Cladding radius: | 0.115 inch | 0.14 inch |
| Cladding thickness: | 15 mils | 17 mils |
| Fission gas plenum length: | 48 inches | 37.6 inches |
| Peaking linear power: | 12 kW/ft | 16.03 kW/ft |
| Coolant inlet temperature: | 730°F | 760°F |
| Coolant outlet temperature: | 1050°F | 1170°F |

12 kW/ft, 9 kW/ft and 6 kW/ft fuel elements have been analyzed in CRRB applications and calculations were made for the 15 kW/ft and 9 kW/ft elements used in a conceptual large LMFBR. Different correlations are used to calculate the irradiation swelling in the clad. The creep rate in the fuel, the smear density, and the fuel density are also varied. The cases of calculations are listed in the following.



733 094

Symbols: LP: linear power (kW/ft)

NCSW: options for the correlation of swelling in the clad (Equations in Section 2.3.1 of Chapter II).

NZ: total number of axial sections for the fuel column. 1st axial section is the bottom section of the fuel pin.

$\phi$: neutron flux (x $10^{15}$ neut/$cm^2$ sec)

(1) Basic Cases

| Case | Reactor | LP | NCSW | NZ | $\phi$ |
|---|---|---|---|---|---|
| A0 | CRBR | 12 | II-40 | 3 | 4.7 |
| A1 | CRBR | 12 | II-41 | 3 | 4.7 |
| A3 | CRBR | 12 | II-42 | 3 | 4.7 |
| A4 | CRBR | 12 | II-43 | 3 | 4.7 |
| R1 | CRBR | 12 | II-40 | 7 | 4.7 |
| B0 | CRBR | 9 | II-40 | 3 | 3.5 |
| B1 | CRBR | 9 | II-41 | 3 | 3.5 |
| B3 | CRBR | 9 | II-42 | 3 | 3.5 |
| B4 | CRBR | 9 | II-43 | 3 | 3.5 |
| R2 | CRBR | 9 | II-40 | 7 | 3.5 |
| N0 | CRBR | 6 | II-40 | 3 | 2.4 |
| N1 | CRBR | 6 | II-41 | 3 | 2.4 |
| N3 | CRBR | 6 | II-42 | 3 | 2.4 |
| N4 | CRBR | 6 | II-43 | 3 | 2.4 |
| H0 | Conceptual LMFBR | 15 | II-40 | 3 | 8.5 |
| H1 | Conceptual LMFBR | 15 | II-41 | 3 | 8.5 |
| H5 | Conceptual LMFBR | 15 | II-40 | 5 | 8.5 |
| M0 | Conceptual LMFBR | 9 | II-40 | 3 | 5.2 |
| M1 | Conceptual LMFBR | 9 | II-41 | 3 | 5.2 |

The ratio of the axial section lengths is:

1:1:1 for NZ = 3 cases in CRBR

1:2:1 for NZ = 3 cases in the conceptual reactor.

The axial section lengths were equal for NZ = 5 and NZ = 7 cases.

(2) Sensitivity of the fuel properties

NCSW = II-40 for all cases

NZ = 3 for all cases

$\rho_D$ = fuel density

$\rho_S$ = smear density

$\dot{\Delta} = 10^{8.368 \times 10^{-4} T(°F) - 4.6628668}$ (Equation II-44.1)

$\dot{\Delta} = 10^{5.23 \times 10^{-4} T(°F) - 4.031495}$ (Equation II-44.2)

Equation II-44.1 and Equation II-44.2 represent two different fuel swelling models from that of Equation II-44. In these two equations the temperature dependence of the fuel swelling has a slope 0.8 and 0.5 times that of Equation II-44. The amount of fuel swelling is the same for all three cases at an average cold fuel region temperature. The cases for this sensitivity study are listed on the following page.

V.2. Calculation of the Fuel Element Behavior in CRBR

(1) Case A0 (CRBR, 12 kW/ft)

Figure A0-1 shows the time history of the fuel-clad gap closure and the fuel-clad mechanical interaction force. As the figure shows, the gap closes after 1831 hours, 1498 hours, and 1971 hours in the 1st, 2nd, and 3rd axial sections, respectively. After the gap closes, the highest $P_{fc}$ is in the 1st axial section. After 13000 hours (12% burn-up), $P_{fc}$ has the value of 5.1 ksi, 1.4 ksi, and 3.3 ksi in the 1st, 2nd and 3rd axial sections, respectively. The plenum pressure is 1.0 ksi at this burn-up.

| Case | Reactor | L.P. | $\phi$ | Changes of Parameters from the Basic Case | Basic Case |
|---|---|---|---|---|---|
| AA | CRBR | 12 | 4.7 | creep rate in the fuel x 1.5 | AO |
| AB | CRBR | 12 | 4.7 | creep rate in the fuel x 0.5 | AO |
| AG | CRBR | 12 | 4.7 | $\rho_S$ = 88% TD | AO |
| AH | CRBR | 12 | 4.7 | $\rho_S$ = 83% TD | AO |
| AI | CRBR | 12 | 4.7 | $\rho_D$ = 85% TD, $\rho_S$ = 80% TD | AO |
| AN | CRBR | 12 | 4.7 | $\dot{\Delta}$ = eqn. II-44.1 | AO |
| AS | CRBR | 12 | 4.7 | $\dot{\Delta}$ = eqn. II-44.2 | AO |
| BA | CRBR | 9 | 3.5 | creep rate in the fuel x 1.5 | BO |
| BB | CRBR | 9 | 3.5 | creep rate in the fuel x 0.5 | BO |
| BG | CRBR | 9 | 3.5 | $\rho_S$ = 88% TD | BO |
| BH | CRBR | 9 | 3.5 | $\rho_S$ = 83% TD | BO |
| BI | CRBR | 9 | 3.5 | $\rho_D$ = 85% TD, $\rho_S$ = 80% TD | BO |
| BN | CRBR | 9 | 3.5 | $\dot{\Delta}$ = eqn. II-44.1 | BO |
| BS | CRBR | 9 | 3.5 | $\dot{\Delta}$ = eqn. II-44.2 | BO |
| NA | CRBR | 6 | 2.4 | creep rate in the fuel x 1.5 | NO |
| NB | CRBR | 6 | 2.4 | creep rate in the fuel x 0.5 | NO |
| NG | CRBR | 6 | 2.4 | $\rho_S$ = 88% TD | NO |
| NH | CRBR | 6 | 2.4 | $\rho_S$ = 83% TD | NO |
| NI | CRBR | 6 | 2.4 | $\rho_D$ = 85% TD, $\rho_S$ = 80% TD | NO |
| NN | CRBR | 6 | 2.4 | $\dot{\Delta}$ = eqn. II-44.1 | NO |
| NS | CRBR | 6 | 2.4 | $\dot{\Delta}$ = eqn. II-44.2 | NO |

733 097

Figure A0-2 shows the clad swelling rate at each radial node in each axial section. The difference between the swelling rate curves in each axial section represents the differential swelling rate, which can generate hoop tension across the clad wall. The swelling rate starts to have significant value after 8000 hours, 4800 hours, and 3200 hours irradiation in the first, the second, and the third axial section, respectively. As in Figure A0-2, the differential swelling rate is $10^{-6}$/hr at 10500 hours in the first axial section. In the second axial section, the differential swelling rate is $1.4 \times 10^{-6}$/hr, $3.0 \times 10^{-6}$/hr, and $1.2 \times 10^{-6}$/hr at t = 5200 hours, 6200 hours and 10000 hours, respectively. In the third axial section the differential swelling rate changes its direction at 6600 hours and has values of $1.2 \times 10^{-6}$/hr, $3.8 \times 10^{-6}$/hr and $0.8 \times 10^{-6}$/hr at t = 4000 hours, 5200 hours, and 10000 hours, respectively.

Figure A0-3 shows the stress rate at the clad outer wall, the creep ($\dot{\sigma}_{cp}$), the swelling ($\dot{\sigma}_{sw}$), and the pressure ($\dot{\sigma}_{p}$) effects.

From the differential swelling rate across the clad wall described above, the behavior of $\dot{\sigma}_{sw}$ in each axial section can be understood. In the first axial section $\dot{\sigma}_{sw}$ becomes significant after 10500 hours radiation. After 13000 hours it has a value of 5 psi/hr. In the second axial section $\dot{\sigma}_{sw}$ becomes significant at 4800 hours with a peak value of 12.5 psi/hr at 6050 hours, and is almost a constant 6 psi/hr after 8000 hours. In the third axial section $\dot{\sigma}_{sw}$ becomes significant at 3400 hours. It has a peak of 21 psi/hr at 5200 hours. Because the differential swelling changes direction, at 6600 hours $\dot{\sigma}_{sw}$ changes to negative and has a constant -4 psi/hr value after 7500 hours.

Several days after gap closure the $P_{fc}$ induced $\dot{\sigma}_p$ reaches a peak value of 8 psi/hr, 5.5 psi/hr, and 7.1 psi/hr in the first, second, and third axial sections, respectively.

Because of the thin wall geometry of the clad, any change of $\dot{\sigma}_{sw}$ and $\dot{\sigma}_p$ can generate a shear force, which can produce $\dot{\sigma}_{cp}$ in the clad. As Figure A0-3 shows, $\dot{\sigma}_{cp}$ always tries to relax the stress produced by the swelling or the pressure. Before the gap closure there is also a large creep rate in each axial section due to the relaxation of the thermal stress that was induced during the start-up period.

The sum of $\dot{\sigma}_p$, $\dot{\sigma}_{cp}$ and $\dot{\sigma}_{sw}$, in Figure A0.3, represents the net stress rate at the clad outer wall. The stress variation can also be obtained from this net stress rate.

Figure A0-4 shows the time behavior of the maximum clad stress $(\sigma_\theta^c)_{max}$ at the clad outer wall. The thermal stress, induced by the start-up heating, at first is relaxed by the creep effect. After the gap closes, the stress suddenly increases due to the effect of $P_{fc}$. This stress increment induces shear, which in turn relaxes the stress a few hundred hours after the sudden increase. The stress is then increased by the action of $P_{fc}$. In the time period during which the differential swelling in the clad becomes active, the stress increases its value. This stress increase is followed by a decrease. At 13000 hours (12% burn-up), the maximum clad stress is 19.4 ksi, 9.4 ksi, 13.5 ksi in the first, the second, and the third axial section, respectively.

Figure A0-5 shows the radial distribution of the clad hoop stress as a function of time. The start-up thermal stress has a large radial slope in each axial section. At 1315 hours (1.3% burn-up), this stress is relaxed by the creep effect. At 4050 hours (3.9% burn-up peak) it increases to a positive value due to the action of $P_{fc}$ after gap closure. At 8053 hours (7.7% burn-up), the radial slopes of the stress distribution increase in the second and the third axial sections. This is the result of the differential swelling in the clad in these two sections. At 12818 hours (11.8% burn-up peak). The clad swelling increases the slope in the first axial section, and the creep decreases the slope in the other two sections.

Figure A0-6 shows the total hoop strain in the clad for each axial section. After 13000 hours of irradiation, the total hoop strain $(e_\theta^c)_{tot}$ is 5.1%, 1.9%, and 4.2% in the first, second and third axial section, respectively.

Figure A0-7 shows the radial distribution of the total hoop strain and the swelling strain in the clad. In the first axial section the swelling strain is small; the creep strain induced by $P_{fc}$ is the major contributor to the total strain. In the second and the third axial section the contribution of the swelling strain to the total strain is 67.1% and 25%. The remaining part of the total strain is mainly creep strain.

(2) Case A1 (CRBR, 12 kW/ft)

Figure A1-1 shows the temperature dependence of the swelling in the clad. It also shows the temperature range across the clad wall in each axial section. The differential swelling across the clad wall is small.

Figure A1-2 shows the fuel-clad gap closures and the fuel-clad interaction force ($P_{fc}$). The gap closes at 1800 hours, 1650 hours, and 2000 hours in the first, second, and third axial sections, respectively. At 13000 hours (12% peak burn-up), the $P_{fc}$ is 4.9 ksi. 1.6 ksi, and 3.4 ksi in each axial section, respectively. The plenum pressure is 1.0 ksi at that time.

Figure A1-3 shows the clad hoop stress rate due to the irradiated swelling ($\dot{\sigma}_{sw}$), the creep ($\dot{\sigma}_{cp}$), and the pressure ($\dot{\sigma}_p$). Because of the small differential swelling, $\dot{\sigma}_{sw}$ is small in all three axial sections. In the second axial section, the fuel temperature is higher, the fuel is softer and so $P_{fc}$ is smaller. The combination of $\dot{\sigma}_{sw}$, $\dot{\sigma}_{cp}$ and $\dot{\sigma}_p$ gives the net hoop stress rate, which determines the stress variation in the clad.

Figure A1-4 shows the history of $(\sigma_\theta^c)_{max}$ in each axial section. In the second and third axial sections, the maximum hoop at the clad outer wall is caused by the $P_{fc}$. After 13000 hours irradiation, $(\sigma_\theta^c)_{max}$ is 20 ksi, 10.2 ksi, and 15.7 ksi in each axial section, respectively.

Figure A1-5 shows the radial distribution of the hoop stress across the clad wall. The thermal stress induced by start-up heating is first relaxed by the creep effect. After the fuel-clad gap closes, $P_{fc}$ causes tension across the clad wall.

Figure A1-6 shows the total hoop strain in each clad axial section. At 13000 hours, the total strain is 5.4%, 1.8% and 4.2% in the first, second, and third axial section.

Figure A1-7 shows the radial distribution of the total hoop strain and the creep strain across the clad wall. At 1000 hours the creep strain is 86.1%, 34.0%, and 76.9% of the total strain in the first, second and third axial sections, respectively. The rest of the total strain is mainly swelling strain.

(3) Case A3 (CRBR, 12 kW/ft)

Figure A3-1 shows the temperature dependence of the clad swelling and the temperature range across the clad wall in each axial section. The swelling is larger at the hot region (inner wall) in the first axial section while in the second and the third axial sections, it is larger at the cooler region (outer wall). The differential swelling across the clad wall is larger in the first and the second axial sections than in the third one.

Figure A3-2 shows the fuel-clad gap closure and the fuel-clad interaction force. The gaps close at 1900 hours, 1600 hours and 1970 hours in the first, second and third axial sections, respectively. At 13000 hours (12.0% peak burn-up), $P_{fc}$ is 4.7 ksi, 1.2 ksi, and 3.5 ksi in each axial section, respectively.

Figure A3-3 shows the hoop stress rate at the outer wall of the clad due to the pressure ($\dot{\sigma}_p$), the swelling ($\dot{\sigma}_{cw}$), and the creep ($\dot{\sigma}_{cp}$). Because of the differential irradiated swelling across the clad wall, $\dot{\sigma}_{sw}$ is positive in the first axial section and negative in the second and the third axial sections at the outer wall of the clad. The combination of $\dot{\sigma}_p$, $\dot{\sigma}_{sw}$, and $\dot{\sigma}_{cp}$ gives the net hoop stress rate ($\dot{\sigma}_\theta$) which governs the behavior of the hoop stress at the outer wall of the clad.

733 102

Figure A3-4 shows the history of the maximum hoop stresses. In the first axial section, the maximum hoop is 20.5 ksi at 13000 hours at the clad outer wall because of the smaller swelling in this region. In the second axial section, the clad inner wall has smaller swelling and so the maximum hoop stress is found in this region at 13000 hours with a value of 11.5 ksi. In the third axial section, the maximum hoop occurs in the clad inner wall. After 9800 hours, the $P_{fc}$ is large enough to induce larger tensions and causes maximum hoop stress in the clad outer wall. At 13000 hours, the maximum hoop stress is 15.5 ksi in this axial section.

Figure A3-5 shows the hoop stress distribution across the clad wall at 0 hours, 1310 hours, 3920 hours, 7920 hours, and 11730 hours.

Figure A3-6 shows the total hoop strain in the clad. At 13000 hours (12% peak burn-up), it is 6.6%, 4.6%, and 4.3% in the first, second and third axial section, respectively.

Figure A3-7 shows the radial distribution of the total hoop strain and the creep strain across the clad wall. At 10000 hours, the creep strain is 66.7%, 6.8%, and 75.8% of the total hoop strain in the first, second, and third axial sections, respectively. The rest of the total strain is mainly swelling strain.

(4) Case A4 (CRBR, 12 kW/ft)

Figure A4-1 shows the clad swelling pattern as a function of the temperature. The temperature range across the clad wall in each axial section is also shown. The third axial section has the largest clad swelling, while the second axial section has the largest differential swelling across the clad wall.

Figure A4-2 shows the gap thickness and the fuel-clad interaction force in each axial section. The gap closes at 1830 hours, 1550 hours, and 2100 hours in the first, the second and the third axial section, respectively. After the gap closure $P_{fc}$ is highest in the first axial section because of the lower fuel temperature and less clad swelling. $P_{fc}$ is 5 ksi, 1.4 ksi and 3.5 ksi in the first, the second, and the third axial section, respectively at 13000 hours (12.0% peak burn-up). The plenum pressure is 1 ksi at this time.

Figure A4-3 shows the clad-hoop stress rate due to creep, swelling, and pressure. In the second axial section $\dot{\sigma}_{sw}$ is large because of the large differential swelling across the clad wall. This $\dot{\sigma}_{sw}$ can generate $\dot{\sigma}_{cp}$ and relax the stress induced by the differential swelling effect. Because of the higher fuel temperature in this axial section, the fuel is softer and $\dot{\sigma}_{p}$ is smaller. In the first and the second axial sections, the stresses induced by swelling and pressure can also be relaxed by the creep effect. In all three axial sections the summation of $\dot{\sigma}_{sw}$, $\dot{\sigma}_{cp}$, and $\dot{\sigma}_{p}$ represents the net rate for the hoop stress in the clad. The behavior of the hoop stress variation (Figure A4-4) can thus be understood clearly by knowing this net hoop stress.

Figure A4-4 shows the maximum hoop stress in the clad. First the start-up thermal stress is relaxed by the creep effect. After the gap is closed, the stress is first relaxed by the high shear generated by a sudden jump of $P_{fc}$. Then the stress is increased by the clad differential swelling and the acting of $P_{fc}$. At 13000 hours (12.0% burn-up peak), the maximum hoop stress is 20.5 ksi, 12.2 ksi, and



733 104

16.0 ksi in the first, the second, and the third axial sections, respectively.

Figure A4-5 shows the radial distribution of the hoop stress across the clad wall at different times. Because of the differential thermal expansion during the start-up period, the thermal stress at t = 0 hour has a large slope across the clad wall. This stress can be relaxed by the creep effect to a flatter slope. In the second axial section, the differential swelling causes a larger slope even at large burn-ups. In the first and the second axial sections, $P_{fc}$ causes tension across the clad wall.

The total hoop strain is shown in Figure A4-6. The radial distribution of the total strain and the creep strain across the clad wall is shown in Figure A4-7. Because of the large $P_{fc}$ in the first axial section, the creep strain is the main contributor to the total strain. As a result of the large clad swelling in the third axial section, the swelling strain makes the largest contribution to the total strain in that section. At 10000 hours (9.2% peak burn-up), the creep strain is 88.2%, 29.4%, and 45.0% of the total strain in the first, second and the third axial section, respectively. The rest of the total strain is mainly swelling strain. At 13000 hours (12% peak burn-up), the total hoop strain is 4.8%, 3.0%, and 5.9% in each axial section, respectively.

The percentage of the axial displacement for the fuel and the clad is shown in Figure A4-8. Before 1700 hours, the fuel axial displacement is small because the fuel-clad gap is still open and there is no clad confinement in the radial direction. At 12000 hours (11% peak burn-up), 21.3% and 0.36% of the axial displacement is in the fuel and the clad, respectively.

(5) Case R1 (CRBR, 12 kW/ft)

Figure R1.1 shows $P_{fc}$ in each axial section. After 13000 hours of irradiation, $P_{fc}$ is 6.6 ksi, 3.0 ksi, 1.8 ksi, 1.4 ksi, 1.7 ksi, 2.2 ksi, and 4.5 ksi in each axial section, respectively.

Figure R1.2 shows $(\sigma_\theta^c)_{max}$ in each axial section. $(\sigma_\theta^c)_{max}$ exhibits peaks at 6400 hours, 5400 hours, and 6500 hours in fourth, fifth and sixth axial sections, respectively. After 13000 hours of irradiation $(\sigma_\theta^c)_{max}$ is 23.5 ksi, 14.8 ksi, 10.9 ksi, 8.5 ksi, 9.5 ksi, 12.6 ksi, and 18.4 ksi in each axial section, respectively.

Figure R1.3 shows $(e_\theta^c)$. After 13000 hours of irradiation, it is 6.3%, 3.0%, 1.9%, 1.6%, 2.3%, 3.3%, and 5% in each axial section, respectively.

(6) Case BO (CRBR, 9 kW/ft)

Figure BO-1 shows the fuel-clad gap closure and the fuel-clad interaction force after the closure. The gap closed at 2160 hours, 1780 hours, and 2140 hours in the first, second, and third axial sections, respectively. $P_{fc}$ increases to 3.5 ksi, 0.8 ksi, and 1.7 ksi at 8000 hours (Bu = 6% peak) and is 6 ksi, 1.1 ksi, and 2.4 ksi at 13000 hours (Bu = 9.2% peak) in each axial section, respectively. The plenum pressure is 0.66 ksi at 13000 hours.

Figure BO-2 shows the swelling rate at each radial node across the clad wall. The swelling rate becomes significant at 10000 hours, 7000 hours and 6000 hours in the first, the second and the third axial sections. The differential swelling rate across the clad wall can result in stress change. In the first axial section, the differential swelling rate across the clad is $0.7 \times 10^{-6}$/hr at 13000 hours. In the second axial section, it is $1.0 \times 10^{-6}$/hr, $1.2 \times 10^{-6}$/hr and $1.1 \times 10^{-6}$/hr at 8000 hours, 10000 hours and 13000 hours, respectively. In the 3rd axial section, it is $0.9 \times 10^{-6}$/hr, $2.6 \times 10^{-6}$/hr, and $-0.2 \times 10^{-6}$/hr at 6500 hours, 8000 hours, and 13000 hours, respectively. The differential swelling rate changes its direction at 10000 hours in the third section.

Figure B0-3 shows the rate of the hoop stress, due to creep, swelling and pressure at the outer wall of the clad. In the second axial section, the clad stress rate (due to $P_{fc}$) is lower than that in the other two sections, because the fuel temperature is higher, and so the fuel is softer. The stress due to swelling becomes significant at 10000 hours, 7000 hours, and 6000 hours in each section, respectively. In the second axial section, the differential swelling rate stays almost constant, and so does the stress rate due to swelling after 9400 hours. In the third axial section, the stress rate due to the swelling reaches a maximum at 8400 hours and then decreases due to a decrease in the differential swelling across the clad wall. After 11200 hours, this swelling stress becomes negative with a value of -0.5 psi/hr at 13000 hours.

As we can see in Figure B0-3, any change in the stress rate, due to pressure and swelling, can induce a creep stress rate which relaxes the stress. The combination of the stress rate due to the pressure, swelling, and creep effects, gives the net stress rate which determines the stress variations.

Figure BO-4 shows the history of $(\sigma_\theta^c)_{max}$ in each axial section. The thermal stresses, induced by the start-up heating, are first relaxed by the creep effect. The gap closure is followed by a stress jump under the influence of $P_{fc}$. This induces shear to the clad and the creep effect can relax the stress several hundred hours after the stress jump. The clad differential swelling results in stress variations at about 8000 hours in the second and the third axial sections. In the first axial section, the increase of $P_{fc}$ results in stress increment. At 13000 hours (9.2% peak burn-up), the hoop stress at the clad outer wall is 21.5 ksi, 9 ksi, and 13 ksi in the first, second, and third axial sections.

Figure BO-5 shows the radial distribution of the hoop stress across the clad wall at different times. The start-up thermal stress is first relaxed to a flatter shape. After gap closure $P_{fc}$ adds tension to the hoop stress all across the clad wall. The slope increment of the hoop curves in the second and third axial section at 13000 hours and 8075 hours is due to the differential swelling across the clad wall.

Figure BO-6 shows the total hoop strain at the clad outer wall. It is 5.2%, 1.4 % and 2.2% at 13000 hours (9.2% peak burn-up) in each axial section, respectively.

Figure BO-7 shows the radial distribution of the total hoop strain and the creep strain across the clad wall. At 10000 hours, the creep strain is 90%, 40%, and 60% of the total strain in the first, the second, and the third axial sections, respectively. The remaining part of the total strain is mainly swelling strain.

(7) Case B1 (CRBR, 9 kW/ft)

Figure B1-1 shows the temperature dependence of the swelling in the clad. It also shows the temperature range across the clad wall in each axial section. The swelling is the largest in the third axial section, and is the smallest in the first axial section.

Figure B1-2 shows the gap closure (GAP) and the interaction force between the fuel and the clad. The gap closes at 2100 hours, 1800 hours, and 2200 hours in each axial section, respectively. After gap closure, $P_{fc}$ is largest in the 1st axial section and is smallest in the second axial section. After 13000 hours of irradiation (Bu = 9.5%), $P_{fc}$ is 5.6 ksi, 0.9 ksi, and 2.3 ksi in each axial section, respectively. At this time, the plenum pressure is 0.5 ksi.

Figure B1-3 shows the maximum hoop stress in the clad. The radial maximum of the hoop stress is located at the outer wall of the clad in all three axial sections. Because of the larger $P_{fc}$ in the first axial section, $(\sigma_\theta^c)_{max}$ is larger there than in the other two sections. After 13000 hours of irradiations, $P_{fc}$ is 20.6 ksi, 9.8 ksi, and 13.9 ksi, in each axial section, respectively.

Figure B1-4 shows the total hoop strain in the clad. Because of the large $P_{fc}$ in the first axial section, the total hoop strain is also larger there than in the other two sections. After 13000 hours of irradiation, the total hoop strain is 5.3%, 2.5%, and 3.5%, in each axial section, respectively.

Figure B1-5 shows the radial distribution of the hoop strain across the clad wall. It also shows the creep strain. The creep strain is 94%, 26.7%, and 28.6% of the total hoop strain in each axial section, respectively.

(8) Case B3 (CRBR, 9 kW/ft)

Figure B3-1 shows the temperature dependence of the swelling pattern in the clad. It also shows the temperature range across the clad wall in each axial section. The clad has larger swelling at the cooler region (outer wall) in the second and the third axial section. In the first axial section, the swelling is larger in the hotter region (inner wall). The differential swelling across the clad wall is large in the first and third axial section and small in the second axial section.

Figure B3-2 shows the fuel-clad gap closure, and the fuel-clad interaction force after the closure. The gap closes at 2212 hours, 2008 hours, and 2187 hours in the first, second, and third axial section, respectively. $P_{fc}$ has its highest value in the first axial section. At 13000 hours (9.2% peak burn-up), it is 5.6 ksi, 1.0 ksi, and 2.9 ksi in each axial section, respectively. At 12000 hours, the plenum pressure is 0.6 ksi.

Figure B3-3 shows the hoop stress rate at the clad outer wall due to differential swelling ($\dot{\sigma}_{sw}$), creep ($\dot{\sigma}_{cp}$), and pressure ($\dot{\sigma}_{p}$). In the first axial section the $\dot{\sigma}_{sw}$ is positive and $\dot{\sigma}_{p}$ is larger than in the other two axial sections. In the second and the third axial section $\dot{\sigma}_{sw}$ is negative. The combination of the $\dot{\sigma}_{sw}$, $\dot{\sigma}_{cp}$, and $\dot{\sigma}_{p}$ gives the net stress rate which determines the stress variation in the clad.

Figure B3-4 shows the maximum hoop stress in the clad in each axial section. The stress behavior at the clad outer wall can be understood by examining Figure B3-3. In the second and the third axial sections the maximal hoop stress occurs at the inner wall of the clad. This is due to the larger swelling at the outer wall, results in hoop tension to the inner wall, and hoop compression to the outer wall of the clad. At 13000 hours (9.2% peak burn-up), the maximum hoop stress is 22.5 ksi, 7.7 ksi, and 15.5 ksi in the first, second, and third axial section, respectively.

Figure B3-5 shows the radial distribution of the hoop stress across the clad wall. The thermal stresses, induced by the start-up heating, are first relaxed to a flatter shape by the creep effect (1380 hours). At 4130 hours, 8000 hours, and 12000 hours, $P_{fc}$ induces tension to all three axial sections, and the differential swellings increase the slope of the curves. Because of the different direction of the differential swelling, the sign of the slope of the hoop curve in the first axial section is opposite to those in the other two axial sections.

Figure B3-6 shows the total hoop strain in the clad. At 13000 hours, the total strain is 5.9%, 4.2% and 2.4% in the first, second, and third axial section, respectively.

Figure B3-7 shows the radial distribution of the total hoop strain and the creep strain across the clad wall. At 10000 hours (7% peak burn-up), the contribution of the creep strain to the total strain is 70.4%, 3.3%, and 44.4% in each axial section, respectively. The remainder is mostly swelling strain.

733 111

(9) Case B4 (CRBR, 9 kW/ft)

Figure B4-1 shows the temperature dependence of the swelling in the clad and the temperature range across the clad wall in each axial section. The swelling is highest in the third axial section and lowest in the first axial section. The differential swelling across the clad wall is highest in the second axial section.

Figure B4-2 shows the fuel-clad gap closure and the fuel-clad interaction force in each axial section. The gaps close at 2150 hours, 1800 hours, and 2250 hours in the first, second and third axial section, respectively. At 13000 hours, $P_{fc}$ is 5.4 ksi, 1.0 ksi, and 2.9 ksi in each axial section. The plenum pressure is 0.55 ksi at that time.

Figure B4-3 shows the hoop stress rate, at the outer wall of the clad, due to the differential swelling ($\dot{\sigma}_{sw}$), the creep effect ($\dot{\sigma}_{cp}$), and the pressure ($\dot{\sigma}_p$). As this figure shows, $\dot{\sigma}_{sw}$ is high and $\dot{\sigma}_p$ is low in the second axial section. The summation of $\dot{\sigma}_{sw}$, $\dot{\sigma}_{cp}$, and $\dot{\sigma}_p$ gives the net stress rate at the outer wall of the clad. The net stress rate is low in the second axial section.

Figure B4-4 shows the time history of the maximum hoop stress in the clad. The hoop stress is maximal at the outer wall of the clad in all three axial sections. At 13000 hours the maximum hoop stress is 21 ksi, 10.5 ksi, and 16.2 ksi in the axial sections.

Figure B4-5 shows the radial distribution of the hoop stress across the clad wall. The thermal stress induced by the start-up heating is first relaxed by the creep effect. After an irradiation of 4020 hours, 8060 hours, and 11700 hours, $P_{fc}$ is the main contributor



733 112

to the hoop tensile in the first axial section. The differential clad swelling causes the larger slope in the second axial section. In the third axial section, both the $P_{fc}$ and the differential clad swelling contribute to the stress change across the clad wall.

Figure B4-6 shows the time history of the total hoop strain in the clad. At 13000 hours it is 5.0%, 1.75%, and 3.9% in each axial section, respectively.

Figure B4-7 shows the radial distribution of the total hoop strain and the creep strain across the clad wall. At 10000 hours, the creep strain is 97%, 25%, and 22.5% of the total strain in each axial section, respectively. The rest of the total strain is mainly the swelling strain.

Figure B4-8 shows the percentage of the axial displacement for the fuel and the clad. At 13000 hours, it is 24.5% for the fuel and 0.24% for the clad.

(10) Case R2 (CRBR, 9 kW/ft)

Figure R2-1 shows the gap closure and the interaction force between the fuel and the clad, in each axial section. This figure shows that the gap closes at 2400 hours, 1900 hours, 1750 hours, 1750 hours, 2100 hours, 2200 hours, and 2450 hours in each axial section, respectively. After 13000 hours of irradiation (Bu = 9.5%), $P_{fc}$ is 6.4 ksi, 4.0 ksi, 1.8 ksi, 0.7 ksi, 1.0 ksi, 2.8 ksi, and 5.9 ksi in each axial section.

Figure R2-2 and Figure R2-3 show $(\sigma_\theta^c)_{max}$ and the total hoop strain in each axial section. After 13000 hours of irradiation, $(\sigma_\theta^c)_{max}$ is 22.8 ksi, 18.3 ksi, 11.6 ksi, 7.7 ksi, 6.1 ksi, 15 ksi, and 16.6 ksi; the total hoop strain is 6.2%, 3.6%, 1.7%, 1.5%, 1.6%, 2.6%, and 4.3% in each axial section, respectively.

(11) Case NO (CRBR, 6 kW/ft)

Figure NO-1 shows the fuel-clad gap closure and the fuel-clad interaction forces. The gap closes at 7200 hours, 3700 hours, and 5800 hours in the first, second, and the third axial sections, respectively. At 17000 hours (Bu = 8%) the fuel-clad interaction force is 1.4 ksi, 2.6 ksi, and 1.7 ksi in each axial section, respectively. The plenum pressure is 500 psi.

Figure NO-2 shows the hoop stress rate, at the outer wall of the clad, due to swelling ($\dot{\sigma}_{sw}$), the creep effect ($\dot{\sigma}_{cp}$), and the pressure ($\dot{\sigma}_p$). $\dot{\sigma}_p$ becomes significant after the gap closes. $\dot{\sigma}_{sw}$ becomes significant at 12800 hours, 11200 hours, and 13200 hours in the first, second, and third axial sections. The combination of $\dot{\sigma}_{cp}$, $\dot{\sigma}_{sw}$, and $\dot{\sigma}_p$ is the net stress rate $\dot{\sigma}$ which governs the behavior of the hoop stress at the outer wall of the clad.

Figure NO-3 shows the maximum hoop stress in the clad. It appears at the outer wall in all three axial sections. At 17000 hours, it is 9.4 ksi, 14.0 ksi, and 10.6 ksi in the axial sections, respectively.

Figure NO-4 shows the radial distribution of the hoop stress across the clad wall.

Figure NO-5 shows the total hoop strain in the clad. At 17000 hours, the total hoop strain is 0.60%, 2.7%, and 1.7% in the first, second, and third axial sections, respectively.

733 114

Figure NO-6 shows the radial distribution of the total hoop strain and the creep strain across the clad wall. At 15100 hours, the creep strain is 46.7%, 57.3%, and 33.3% of the total strain in each axial section, respectively. The rest of the total strain is mainly swelling strain.

(12) Case N1 (CRBR, 6 kW/ft)

Figure N1-1 shows the temperature dependence of irradiation induced swelling in the clad, and the temperature range across the clad wall.

Figure N1-2 shows the fuel-clad gap closure and the fuel-clad interaction force in each axial section. The gap closes at 7100 hours, 3800 hours, and 5800 hours in the first, second, and third axial sections, respectively. At 17000 hours, the $P_{fc}$ is 1.2 ksi, 2.4 ksi, and 1.6 ksi in each axial section, respectively. The plenum pressure is 0.5 ksi.

Figure N1-3 shows the maximum hoop stress in the clad. It occurs at the outer wall of the clad in all three axial sections. At 17000 hours, it is 11.0 ksi, 14 ksi, and 12.5 ksi in the axial sections, respectively.

Figure N1-4 shows the radial distribution of the hoop stress across the clad walls at 0 hour, 1310 hours, 3870 hours, 8040 hours, and 10140 hours.

Figure N1-5 shows the total hoop strain in the clad. At 17000 hours, it is 1.5%, 2.6%, and 2.0% in the first, the second, and the third axial section, respectively.

Figure N1-6 shows the radial distribution of the total hoop strain and the creep strain across the clad wall at 5000 hours, 7500 hours, and 10000 hours. The rest of the total strain is mainly the swelling strain.

(13) Case N3 (CRBR, 6 kW/ft)

Figure N3-1 shows the temperature dependence of swelling in the clad, and the temperature range across the clad wall in each axial section. The swelling in the clad is high in the second and the third axial sections and is lower in the first axial section.

Figure N3-2 shows the fuel-clad gap closures and the fuel-clad interaction forces. The gap closes at 8100 hours, 4500 hours, and 7700 hours in the first, second, and third axial section, respectively. At 17000 hours, the $P_{fc}$ is 0.94 ksi, 1.62 ksi, and 1.04 ksi in each axial section, respectively. The plenum pressure is 0.5 ksi.

Figure N3-3 shows the maximum hoop stress in the clad. It occurs at the outer wall in the first and the second axial section, and at the clad inner wall in the third axial section. At 17000 hours, it is 10.8 ksi, 12.6 ksi and 8.4 ksi in each axial section, respectively.

Figure N3-4 shows the radial distribution of the hoop stress across the clad wall at 0 hr, 4600 hrs, 8100 hrs, and 100000 hrs. The slope of the hoop curves in the third axial section have an opposite sign from those in the other two axial sections. This is due to the different direction of the differential swelling across the clad wall and in the axial sections.

Figure N3-5 shows the total hoop strain in the clad. At 17000 hours, it is 2.7%, 5.9%, and 4.4% in each axial section, respectively.

Figure N3-6 shows the radial distribution of the total hoop strain and the creep strain across the clad wall at 5000 hrs, 7500 hrs, and 10000 hrs. At 10000 hrs, the creep strain is 6.7%, 8.3%, and 2.8% of the total strain in each axial section, respectively. The rest of the total strain is mainly the swelling strain.

(14) Case N4 (CRBR, 6 kW/ft)

Figure N4-1 shows the temperature dependence of the swelling in the clad, and the temperature range across the clad wall in each axial section. The clad swelling is small in the first axial section and larger in the third axial section. The swelling is larger at the clad inner wall (hotter region) than that at the clad outer wall (cooler region) in all three axial sections.

Figure N4-2 shows the fuel-clad gap closures and the fuel-clad interaction forces. The gap closes at 7170 hours, 3700 hours, and 6000 hours in the first, second, and third axial sections, respectively. The plenum pressure is 0.5 ksi.

Figure N4-3 shows the maximum hoop stress in the clad. It occurs at the outer wall of the clad in all three axial sections. At 17000 hours, it is 7.0 ksi, 13.8 ksi, and 11.4 ksi in each axial section, respectively.

Figure N4-4 shows the radial distribution of the hoop stress across the clad wall at 0 hr, 1314 hrs, 3870 hrs, 7930 hrs, and 10030 hrs.

Figure N4-5 shows the total hoop strain in each axial section. At 17000 hours, it is 0.2%, 1.8%, and 2.1% in the first, second, and third axial sections, respectively.

Figure N4-6 shows the distribution of the total hoop strain and the creep strain across the clad wall at 5000 hours, 7500 hours, and 10000 hours. At 10000 hours, the creep strain is 50%, 60%, and 15.3% of the total strain in each axial section, respectively. The rest of the total strain is mainly the swelling strain.

## V.3. Calculations for Fuel Element Behavior in a Conceptual 1000 MW LMFBR

### (1) Case HO (LMFBR, 15 kW/ft)

Figure HO-1 shows the time history of the fuel-clad gap closures and the fuel-clad interaction forces. The gap closes at 1915 hours, 830 hours, and 2270 hours in the first, second and third axial sections, respectively. The gap of the second axial section reopens at 3230 hours and has a value of 4.4 mils at 13000 hours. The $P_{fc}$ increases with time and has a value of 860 psi and 840 psi at 13000 hours in the first and third section, respectively. The plenum pressure is 810 psi at that time.

Figure HO-2 shows the displacement of the fuel outer boundary (FUB) and the clad inner boundary in the second axial section. Before the fuel-clad gap closure, the movement of the fuel outer boundary reduces the gap and closes it at 830 hours. After 830 hours, the clad confinement reduces the rate of FUB. After 2800 hours, the swelling in the clad beocmes higher, the clad starts to swell faster than the fuel boundary, and the gap reopens at 3230 hours.

Figure HO-3 shows the effect of clad confinement on the fuel boundary movement. During the 400 hours of gap closure in the second axial section, the clad limits the fuel movement in the radial direction within two mils.

Figure HO-4 shows the rate of swelling strain at the radial nodes across the clad wall. The swelling rate becomes significant at 4000 hours, 2000 hours, and 600 hours in the first, second and third axial sections, respectively. The differential swelling strain across the clad wall can induce stresses in the clad. In the first axial section, the differential swelling is $2 \times 10^{-6}$/hr and $3.8 \times 10^{-6}$/hr at 4800 hours and 6800 hours, respectively. After 4800 hours, it is constant. The hotter region always has larger swelling and the cooler region has smaller swelling in the second axial section. The differential swelling is $3 \times 10^{-6}$/hr, $1.1 \times 10^{-6}$/hr, and $4.5 \times 10^{-6}$/hr at 2200 hrs, 3000 hrs, and 3400 hrs, respectively in this region. After 3440 hrs, the peak of the swelling rate shifts to the center node (b). The differential swelling rate is about $2 \times 10^{-6}$/hr after 4200 hours. In the third axial section, the differential swelling is $1.8 \times 10^{-6}$/hr and $3.5 \times 10^{-6}$/hr at 800 hours and 1400 hours. Before 1440 hours, the hotter node (a) has a higher swelling rate and the cooler node (c) has a smaller swelling rate. After 2400 hours, the direction of the differential swelling changes, i.e., the cooler node (c) has the higher swelling rate and the hotter node (a) has the smaller one. The differential swelling is $4.1 \times 10^{-6}$/hr and stays almost constant after 2450 hours.

Figure HO-5 shows the hoop stress rate at the outer wall of the clad due to swelling ($\dot{\sigma}_{sw}$) and the creep ($\dot{\sigma}_{cp}$). $\dot{\sigma}_{sw}$ is caused by the differential swelling rate across the clad wall, described in

Figure HO-4. In the first axial section, $\dot{\sigma}_{sw}$ becomes significant at 3900 hours and stays almost constant (20 psi/hr) after 5800 hours. In the second axial section, $\dot{\sigma}_{sw}$ becomes significant at 1900 hours and reaches a peak value of 65 psi/hr, at 3050 hours. After 4400 hours, $\dot{\sigma}_{sw}$ is small because the differential swelling across the clad wall is small. In the third axial section $\dot{\sigma}_{sw}$ becomes significant at 750 hours and reaches a peak of 23 psi/hr at 1600 hours. After 1900 hours $\dot{\sigma}_{sw}$ becomes negative because the direction of the differential swelling across the clad wall is changed. The change of $\dot{\sigma}_{sw}$ is always followed by the change of $\dot{\sigma}_{cp}$ in the same direction to relax the swelling stress in the clad. Because of the high temperature and neutron flux in this case, the fuel-clad mechanical interaction force is small. The combination of $\dot{\sigma}_{sw}$ and $\dot{\sigma}_{cp}$ represents the net stress rate ($\dot{\sigma}$) which governs the stress variations at the outer wall of the clad. The net stress is negative in the first several hundred hours because the creep relaxes the thermal stress, induced by the start-up heating. $\dot{\sigma}$ becomes positive at 3900 hours, 2000 hours, and 600 hours in the first, second, and third axial section, respectively. In the first axial section, $\dot{\sigma}$ is positive and small after 6000 hours. In the second axial section $\dot{\sigma}$ is positive between 2000 hours and 3000 hours, and is negative between 3000 hours and 4600 hours. After 4600 hours $\dot{\sigma}$ is positive, but small. In the third axial section, $\dot{\sigma}$ is positive between 600 hours and 1570 hours and becomes negative at 1570 hours.

Figure HO-6 shows the maximum hoop stress in the clad. It occurs at the outer wall in the first axial section and at the inner wall in the second and the third axial sections after 800 hours and 2500 hours, respectively. The hoop stress has a peak at 3200 hours and 1500 hours, 10.5 ksi and 8.2 ksi in the second and the third axial section. The time variation of the hoop stress at the outer wall of the clad can be seen in Figure HO-5. At 14000 hours, the maximum hoop stress is 9.2 ksi, 6.4 ksi, and 7.6 ksi in the first, second and third axial sections, respectively. The maximal hoop stress is 10.5 ksi at 3200 hours at the outer wall of the clad in the second axial section.

Figure HO-7 shows the radial distribution of the hoop stress across the clad wall. The thermal stress is relaxed at t = 0 by the creep effect and then it is influenced by the differential swelling rate and the creep relaxation across the clad wall.

Figure HO-8 shows the total hoop strain at the outer wall of the clad at 13000 hours. It is 2.5%, 6.2% and 3.7% in the first, second and third axial sections, respectively.

Figure HO-9 shows the radial distribution of the total hoop strain and the swelling strain across the clad wall. At 12000 hours the swelling strain is 80%, 93.8%, and 82.2% in each axial section, respectively.

Case H1 (LMFBR, 15 kW/ft)

Figure H1-1 shows the temperature dependence of the irradiation-induced swelling in the cladding and the temperature range across the clad wall.

The first axial section has higher differential swelling across the clad wall than the other two axial sections.

Figure H1-2 shows the fuel-clad gap closure and the fuel-clad interaction forces in each axial section. The gap closes at

2230 hours, 1000 hours, and 2100 hours in each axial section, respectively. At 13500 hours, the clad swells away from the fuel and the fuel-clad gap reopens in the second axial section. At 12000 hours, the $P_{fc}$ is 830 psi, 775 psi, and 800 psi in each axial section, respectively. The fission gas pressure is 760 psi at that time.

Figure H1-3 shows the maximum hoop stress in the clad. It occurs at the clad outer wall in the first and second axial sections and at the clad inner wall in the third axial section. At 13000 hours, the maximum hoop stress is 7.5 ksi, 6.8 ksi, and 6.3 ksi in the first, second, and third axial sections, respectively.

Figure H1-4 shows the radial distribution of the hoop stress across the clad wall. The thermal stress, induced by the start-up heat, at first is relaxed by the creep effect. The slope of the curves in the third axial section is opposite to those in the first and second axial sections after 8300 hours and 16000 hours. This is due to the differential irradiated swelling of the clad in the third axial section. Its direction is opposite to those in the other two axial sections.

Figure H1-5 shows the total hoop strain in the clad. At 13000 hours, the total strain is 2.5%, 4.5%, and 3.4% in each axial section, respectively.

Figure H1-6 shows the radial distribution of the total hoop strain and the swelling strain across the clad wall. At 15000 hours, the swelling strain is 88.9%, 94%, and 84.6% of the total strain in each axial section, respectively.

Figure H1-7 shows the percentage of the axial displacement for the fuel and the clad. At 13000 hours it is 16% for the fuel and 1.1% for the clad.

(3) Case H5 (LMFBR, 15 kW/ft)

Figure H5-1 shows the gap closure and $P_{fc}$. The gap closes at 2100 hours, 1400 hours, 800 hours, 1200 hours, 2500 hours in each axial section, respectively. The gaps in the second, the third, and the fourth axial sections reopen at 4400 hours, 3200 hours, and 2700 hours, respectively. The gaps in the first and the fifth section do not reopen. After 13000 hours irradiation, $P_{fc}$ is 960 psi and 900 psi, respectively in these two gaps.

Figure H5-2 shows $(\sigma_\theta^c)_{max}$ in the clad. It reaches a peak value at 3200 hours, 2300 hours, and 1400 hours in the third, fourth, and fifth axial section, respectively. In the first and second axial section $(\sigma_\theta^c)_{max}$ starts to increase rapidly at 4100 hours and 3200 hours, respectively, and appears at the outer wall of the clad. In the other axial sections $(\sigma_\theta^c)_{max}$ occurs at the inner wall of the clad after 5000 hours of irradiation.

Figure H5-3 shows the hoop strain in the clad. After 13000 hours of irradiation, $(e_\theta^c)$ is 2.6%, 5.1%, 6.7%, 6.0%, and 4.2% in each axial section, respectively.

(4) Case MO (LMFBR, 9 kW/ft)

Figure MO-1 shows the fuel-clad gap closures and the fuel-clad interaction forces. The gap closes at 2100 hours, 1300 hours, and 2600 hours in the first, second, and third axial sections, respectively. After 14000 hours of irradiation, $P_{fc}$ is 1280 psi, 500 psi, and 660 psi in each axial section, respectively. Because of the faster clad swelling, $P_{fc}$ reduces its magnitude at 4400 hours and at 5000 hours in the second and the third axial sections, respectively. The plenum pressure is 450 psi at 14000 hours.

Figure MO-2 shows the swelling rate of the radial nodes in each axial section of the clad. The differential swelling across the clad wall becomes significant at 5400 hours, 5000 hours, and 4400 hours in the first, second, and third axial sections, respectively. The smallest swelling rate occurs at the outer wall of the clad in all three axial sections. The differential swelling across the clad wall is constant after 6600 hours, 6200 hours, and 7200 hours. The differential swelling induces tension to the hoop stress at the outer wall of the clad.

Figure MO-3 shows the hoop stress rate at the outer wall of the clad due to swelling ($\dot{\sigma}_{sw}$), creep ($\dot{\sigma}_{cp}$), and pressure ($\dot{\sigma}_{p}$). As an effect of the differential swelling across the clad wall, $\dot{\sigma}_{sw}$ is positive in each axial section. The combination of $\dot{\sigma}_{sw}$, $\dot{\sigma}_{cp}$, and $\dot{\sigma}_{p}$ gives the net hoop stress rate ($\dot{\sigma}_{\theta}$), which governs the variation of the hoop stress at the outer wall of the clad. $\dot{\sigma}_{\theta}$ has a significant positive value between 5200 hours and 6600 hours, 4600 hours and 6000 hours, and 4200 hours and 6200 hours in the first, second, and third axial sections, respectively. In the third axial section $\dot{\sigma}_{\theta}$ is negative between 6300 hours and 7200 hours.

Figure MO-4 shows the maximum hoop stress in the clad. It occurs at the outer wall of the clad in all three axial sections. In the third axial section there is a peak at 6300 hours with a

733 124

7.5 ksi magnitude. The time behavior of the maximum hoop stress can be understood by knowing the net hoop stress rate (Figure MO-3). At 14000 hours, the maximum hoop stress is 9.3 ksi, 7.6 ksi, and 6.8 ksi in the first, second, and third axial section, respectively.

Figure MO-5 shows the distribution of the hoop stress across the clad wall at 0 hr, 1260 hrs, 4020 hrs, 8150 hrs, and 12030 hrs.

Figure MO-6 shows the total hoop strain in the clad. At 14000 hrs, it is 1.4%, 2.9%, and 3.3% in the first, second, and third axial section, respectively.

Figure MO-7 shows the distribution of the total hoop strain and the creep strain across the clad wall. At 10000 hours, the swelling strain is 43%, 78.7%, and 85.8% of the total strain in each axial section, respectively. The rest of the total strain is mostly creep strain.

(5) Case M1 (LMFBR, 9 kW/ft)

Figure M1-1 shows the fuel-clad gap closure (GAP) and the fuel-clad interaction forces ($P_{fc}$). The gap closes at 2100 hours, 1800 hours, and 3400 hours in the first, second, and third axial sections, respectively. At 14000 hrs, the $P_{fc}$ is 128 ksi, 0.5 ksi, and 0.76 ksi in each axial section, respectively. The plenum pressure is 0.45 ksi.

Figure M1-2 shows the maximum hoop stress in the clad. It appears at the outer wall of the clad in all three axial sections. At 14000 hrs, it is 8.7 ksi, 5.6 ksi, and 5.4 ksi in each axial section, respectively.

Figure M1-3 shows the radial distribution of the hoop stress across the clad wall at 0 hr, 1580 hrs, 4080 hrs, 8200 hrs, and 11810 hrs.

Figure M1-4 shows the total hoop strain in the clad. At 14000 hours, it is 1.4%, 2.1%, and 2.0% in the first, second, and third axial sections, respectively.

Figure M1-5 shows the radial distribution of the total hoop strain and the creep strain across the clad wall at 5000 hours, 7500 hours, and 10000 hours. At 10000 hours the swelling strain is 77.8%, 92%, and 90% of the total strain in each axial section, respectively.

V.4. The Rate of the Fuel Swelling

The calculated rates of the fuel swelling for cases HO, MO, and NO are shown in Figure FSW. Some other data for the fuel swelling are also shown in this figure.

V.5. Discussion of Applications

In sections V.5.1, V.5.2, and V.5.3 the fuel-clad mechanical interaction, the stress in the clad, and the strain in the clad are discussed for cases AO, BO, NO, R1 and R2 in CRBR, and cases HO, MO, and H5 are for the conceptual reactor. In section V.5.4, the sensitivity of the clad-swelling correlation is discussed.

V.5.1 The Fuel-Clad Mechanical Interaction

In the 12 kW/ft linear power case for CRBR, a large portion of the fuel is in the columnar and equiaxed zone. The undisturbed zone is relatively small. This undisturbed fuel is mechanically strong and can prevent the outward swelling of the weak fuel region. After the fuel-clad gap closure, the interaction force is dependent on the amount of mechanically strong fuel which can push the clad effectively as it swells. In 12 kW/ft and 9 kW/ft fuel elements the amount of the strong fuel is relatively small in the second axial section, the fuel temp rature and the creep rate are higher; $P_{fc}$ is thus smaller than in the other sections. Because of the lower temperature distribution in the first axial section, there is more cold fuel zone and less fuel creep rate. The fuel can push the clad stronger after gap closure. $P_{fc}$ is thus higher in this section than in the other two sections.

As Figure AO-1 and Figure BO-1 show, $P_{fc}$ is larger in the first, and smaller in the second axial section throughout the whole irradiation history. After 10800 hours of irradiation (Bu = 10.%) in the 12 kW/ft case, the calculated $P_{fc}$ is 4.2 ksi, 1.2 ksi, and 2.8 ksi in the first, second, and third axial section, respectively. After 13700 hours of irradiation (Bu = 9.8%) in the 9 kW/ft case, the calculated $P_{fc}$ is 6.2 ksi, 1.1 ksi, and 2.6 ksi, in the axial sections, respectively. Figures R1-1 and R2-1 also show larger $P_{fc}$ in the bottom half of the fuel pin.

In the 9 kW/ft case, the temperature distribution and the neutron flux are lower, hence the creep rate in the fuel is lower than 12 kW/ft case. Consequently the strong fuel can push the clad more effectively and at the same burn-up it results in a higher $P_{fc}$ for the 9 kW/ft than for the 12 kW/ft fuel element.

In 6 kW/ft fuel elements, the linear power is low and the fuel is strong. In this case, the higher linear power and the relatively higher temperature in the second axial section causes the fuel to swell faster and push the clad stronger. As Figure NO-1 shows, $P_{fc}$ is larger in the second axial section than in the other sections.

After 17000 hours of irradiation (Bu=8%), the calculated $P_{fc}$ is 1.4 ksi, 2.6 ksi, and 1.7 ksi in each axial section, respectively.

As the neutron flux increases from the assumed $4.6 \times 10^{15}$ neut/cm$^2$-sec in CRBR to $8.5 \times 10^{15}$ neut/cm$^2$-sec in the conceptual LMFBR, there is a faster generation rate of interstatials and vacancies in the fuel, which enhances the creep rate. This effect reduces the fuel-clad interaction forces after gap closure. Also, the high flux leads to faster swelling in the clad which further reduces the mechanical interaction. For fuel elements irradiated 19000 hours in the conceptual reactor, and 10900 hours in CRBR, both with 8% burn-up, the calculated $P_{fc}$ in the first axial section is 1.6 ksi in the conceptual LMFBR and 4.9 ksi in CRBR (Figures MO-1 and BO-1). In the case of 15 kW/ft fuel element in the conceptual LMFBR, the fuel-clad gap closes after 1300 hours of irradiation in the second axial section. This gap reopens after 3200 hours of irradiation (Figure HO-1). If the fuel column has five axial sections instead of three, the gap reopens at 4400 hours, 3200 hours, and 2800 hours in the second, third, and fourth axial sections, respectively (Figure HO-0). This gap reopening is caused by the larger rate of clad swelling. No gap reopening has been calculated for CRBR's with $4.6 \times 10^{15}$ neut/cm$^2$-sec flux.

V.5.2 The Stress in the Clad

The stresses in the clad are induced mainly by the action of $P_{fc}$ and by the differential irradiation-induced swelling across the clad wall. For the 12 kW/ft and the 9 kW/ft fuel element in CRBR, $P_{fc}$, and thus $(\sigma_\theta^c)_{max}$, is higher in the first section than those in the

733 128

other two sections. Because of the low $P_{fc}$ in the second section, $(\sigma_\theta^c)_{max}$ has its lowest value there. As Figures AO-4 and BO-4 show, at a 10% of burn-up (10800 hours irradiation in 12 kW/ft case and 13700 hours in 9 kW/ft case), $(\sigma_\theta^c)_{max}$ is 17.6 ksi, 8.5 ksi, and 12.6 ksi for the 12 kW/ft case, and is 22.0 ksi, 9.2 ksi, and 13.5 ksi in 9 kW/ft case, in each axial section, respectively. The calculations, performed for seven axial sections in 12 kW/ft and 9 kW/ft fuel elements, show that the bottom half of the fuel pin has larger $(\sigma_\theta^c)_{max}$ than the upper half (Figures R1-2 and R2-2).

In 6 kW/ft fuel elements in CRBR, $P_{fc}$, $(\sigma_\theta^c)_{max}$ have the highest value in the second section, while their lowest value is in the first section. At an 8% burn-up (after 17000 hours of irradiation), $(\sigma_\theta^c)_{max}$ is 9.4 ksi, 14 ksi and 10.6 ksi in each axial section, respectively (Figure NO-3).

In the conceptual LMFBR, $(\sigma_\theta^c)_{max}$ is much lower than in CRBR. This is due to a much lower $P_{fc}$ in the conceptual reactor, where the fuel creep rate is much larger. In the first and third axial sections of a 9 kW/ft fuel element, $(\sigma_\theta^c)_{max}$ is about half of that in CRBR.

As Figures MO-4 and BO-4 show, a 9 kW/ft fuel element irradiated for 19000 hours in conceptual reactor or 10900 hours in CRBR (8% burn-up), $(\sigma_\theta^c)_{max}$ is 10.4 ksi, 8 ksi and 7.4 ksi in the conceptual reactor, and is 20 ksi, 9 ksi and 11.5 ksi in CRBR, for each axial section, respectively.

At certain burn-ups, depending on the clad temperature distribution, the vacancies, induced by the neutron irradiation in the clad, reach supersaturation. The rate of the void growth, which causes the irradiation-induced swelling in the clad, can thus increase rapidly (Figure AO-2). Because of the differential temperature, there is also a differential swelling, which generates stress peaks in the clad. This stress peak appears in the third section of the fuel elements in CRBR after 5200 hours and 8700 hours of irradiation, in the 12 kW/ft and the 9 kW/ft cases, respectively. These peaks are smaller than the axial maximum of the hoop stress in the first section. There is no stress peak in the first section because of the relatively low temperature. In the 6 kW/ft fuel elements, the neutron flux and the differential swelling across the clad wall are low, therefore no stress peak is observed (Figure NO-3).

Because of the higher neutron flux in the conceptual LMFBR, the stress peaks occur earlier, at 3200 hours and at 1500 hours of irradiation, in the second and third sections, respectively, for the 15 kW/ft case. Because of the higher temperature and the larger differential swelling in the clad, these peaks are high. The one in the second section is the highest stress in the life-time of the fuel element (Figure HO-6). The peak magnitudes are 10.5 ksi and 8.2 ksi, in the second and the third sections, respectively. There is also a rapid increase of $(\sigma_\theta^c)_{max}$ in the first section at 4300 hours, with an increase of 5.6 ksi in a 1300 hour time interval.

The 9 kW/ft fuel elements in the conceptual LMFBR have lower temperatures than the 15 kW/ft element, so the stress peaks are reduced in the clad. The maximum stress peak is 7.5 ksi in the third axial section which is lower than most of the $(\sigma_\theta^c)_{max}$ in the first axial section during the irradiation history. $(\sigma_\theta^c)_{max}$ rapidly increases in the first and the second axial sections too, at 5200 hours and 4600 hours, respectively. The magnitude of increase is 2.8 ksi and 4.0 ksi in these two sections, respectively (Figure MO-4).

V.5.3. The Strain in the Clad

The total strain in the clad results from the clad swelling and from the creep strain induced by the acting $P_{fc}$ at the inner boundary of the clad. Because of the relatively large $P_{fc}$ for fuel elements in CRBR, a significant part of the total strain in the clad is the creep strain. Because of the larger $P_{fc}$ in the first section of 12 kW/ft and 9 kW/ft fuel elements in CRBR, the contribution of the creep strain to the total strain is large, more than 90%. In the second axial section about 33% and 40% of the total hoop strain is the creep strain. In 6 kW/ft fuel elements in CRBR, the creep strain in the clad is 46.7%, 53.7%, and 33.3% in the first, second, and third axial sections, respectively. The larger creep strain in the second section is caused by the larger $P_{fc}$. For fuel elements of 8% burn-up (irradiated 8640 hours in the 12 kW/ft, 10900 hours in 9 kW/ft, and 17000 hours in 6 kW/ft case) in CRBR, the total hoop strain in the clad is 2.4%, 0.6%, and 1.6% for the 12 kW/ft, 3.7%, 0.8%, and 1.4% for the 9 kW/ft, and 0.6%, 2.7%, and 1.7% in 6 kW/ft case, in the first, second, and third axial sections, respectively. At the same burn-up of irradiation, the larger hoop strain in the first axial section in 9 kW/ft and 12 kW/ft case is caused by a larger creep strain. There is a larger hoop strain in the second

733 151

axial section in the 6 kW/ft than in the 12 kW/ft and the 9 kW/ft case, because of the larger creep strain.

In the conceptual LMFBR the $P_{fc}$ is small; therefore, the creep strain is a smaller fraction of the total strain in the clad. In the first axial section, where the largest $P_{fc}$ occurs at 15 kW/ft and 9 kW/ft, about 20% of the total hoop strain in the clad is the creep strain. For fuel element of 8% burn-up after 13000 hours (15 kW/ft), and 19000 hours (9 kW/ft) irradiation in the conceptual reactor, the total hoop strain in the clad is 2.8%, 7.1%, and 4.0% in 15 kW/ft case, and 2.5%, 4.6%, and 5.1% in the 9 kW/ft case in the axial sections, respectively. The total strain in the first axial section is less than in the other sections because there is less clad swelling resulting from the cooler temperature in this section. In the 15 kW/ft case, the maximum clad swelling occurs in the second section, the total strain is thus higher there than in the other sections. In the 9 kW/ft case the maximal clad swelling occurs in the third axial section; the total strain is thus higher there. Because of the cooler temperature in the 9 kW/ft case, the average clad swelling, and therefore the average total strain, is smaller than in the 12 kW/ft case.

V.5.4. Sensitivity of the Clad Swelling Correlation

As different correlations are used for the clad swelling, different fuel pin behavior may follow.

V.5.4.1. High Power Case

For 12 kW/ft fuel elements in CRBR, different correlations are used for the irradiated swelling in the clad for cases A0, A1, A3, and

and A4. In these cases, the fuel boundary movements, induced by the fuel creep and by the fuel swelling, are the major contributors to the $t_G$ and $P_{fc}$ values. Since the same fuel creep and fuel swelling model are used, $t_G$ and $P_{fc}$ values are similar in these cases. The average $t_G$ is 1850 hours, 1590 hours, and 1960 hours, the average $P_{fc}$ at 13000 hours is 4.9 ksi, 1.5 ksi, and 3.4 ksi in the first, second, and third axial sections, respectively. The variation of $t_G$ and $P_{fc}$ relative to their average value is within 9%. Right after the gap closure, a rapid increase of $P_{fc}$ and of $(\sigma_\theta^c)_{max}$ follows. The average time for these fast increases is 96 hours. In that period the average $P_{fc}$ increase is 1.1 ksi, 0.5 ksi, and 0.9 ksi and the average $(\sigma_\theta^c)_{max}$ increase is 6.2 ksi, 2.7 ksi, and 5.3 ksi in the first, second, and third axial sections, respectively. The smaller $P_{fc}$ increase in the second section is due to the higher fuel temperature, which induces softer mechanical properties. In cases A1, A3 and A4, the swelling in the clad is a linear function of time. There is thus no peak of $(\sigma_\theta^c)_{max}$ in these cases. If the peak of the clad swelling is at 600°C, the swelling strain is larger at the hotter region (inner wall) than at the cooler region (outer wall), so, as in cases A0, A1, and A4, $(\sigma_\theta^c)_{max}$ occurs at the outer wall of the clad. When the clad swelling peak shifts to 500°C (case A3), the differential swelling across the clad wall reverses its direction in the second and the third sections, and so, $(\sigma_\theta^c)_{max}$ shifts to the inner wall of the clad. But, in case A3, because of the increased $P_{fc}$ (2.6 ksi after 8300 hours irradiation), $(\sigma_\theta^c)_{max}$ in the third axial section shifts to the outer wall of the clad. As in case A0, A1, A3, and A4 cases have their highest $(\sigma_\theta^c)_{max}$ in the first section and the lowest $(\sigma_\theta^c)_{max}$ in the second section. Because of the large $P_{fc}$ in the first section, the change of the clad swelling has small effect on $(\sigma_\theta^c)_{max}$ in this section. After 13000 hours of irradiation (Bu = 12%), the average $(\sigma_\theta^c)_{max}$ in the first axial section is 20.1 $\pm$ 0.3 ksi. In the second axial section, $P_{fc}$ is smaller, the variation of $(\sigma_\theta^c)_{max}$ is larger due to the changing of the clad swelling. In cases A0, A1, and A4, the average $(\sigma_\theta^c)_{max}$ is 10.8 $\pm$ 1.1 ksi.

The hoop strain magnitude in the clad is affected significantly by the change of the clad swelling model. In cases A0 and A1, their values are similar. The average of the total hoop strain after 13000 hours of irradiation is 5.3%, 1.8%, and 4.2% in each axial section, respectively.

In case A3, the peak of the clad swelling moves to 500°C, the swelling strain in the first and the second section increases significantly; $(e_\theta^c)_{tot}$ is larger than in cases A0 and A1. The largest $(e_\theta^c)$ is in the first axial section. After 13000 hours of irradiation, it is 6.6%, and is larger in the second section than in the third one. In case A4, because of the larger swelling in the second and the third axial sections of the clad, $(e_\theta^c)$ is larger than in cases A0 and A1. The swelling in the third axial section is also significantly increased. The largest $e_\theta^c$ is 5.9% in this axial section after 13000 hours of irradiation.

For 15 kW/ft fuel element in the conceptual reactor with $8 \times 10^{15}$ neut/cm$^2$-sec neutron flux, the variation of $t_G$ and $P_{fc}$ in the first and the third sections are small as the swelling model in the

733 134

clad is varied. The average $t_G$ is 2100 hours, 950 hours, and 2150 hours in each axial section, respectively. The average variation is 5.6%. Because of the high neutron flux level in the second axial section, the time variation of the gap reopening is large. It reopens after 3200 hours of irradiation in case H0, and after 13500 hours of irradiation in case A1. The gap is 5.7 mils in case H0 and 0.2 mils in case H1 after 15000 hours of irradiation (Bu = 9%). In case H1, the rate of clad swelling is a linear function of time, thus there is no peak for $(\sigma_\theta^c)_{max}$. In the conceptual reactor fuel element $P_{fc}$ is relatively small; a change of the swelling in the clad can thus have a more significant effect on $(\sigma_\theta^c)_{max}$ than in CRBR. As Figures H0-6 and H1-3 show, $(\sigma_\theta^c)_{max}$ behaves differently in cases H0 and H1. After 8000 hours of irradiation, this difference is 2.3 ksi, 0.2 ksi, and 1.7 ksi; after 13000 hours of irradiation, it is 1.6 ksi, 0.7 ksi, and 1.3 ksi in the first, second and third axial sections, respectively. As Figures H0-7 and H1-4 show, the hoop stress radial distribution across the clad wall is very different in the two cases. All these relatively large differences are caused by the effect of the clad swelling model if $P_{fc}$ is low. In the conceptual reactor $(e_\theta^c)$ is less in case H1 than in case H0. Especially in the second axial section, where it is 64% of that in case H0. These decreases are due to the small clad swelling in case H1.

V.5.4.2. Mid-Power Case

For 9 kW/ft fuel elements in CRBR, different irradiated swelling correlations are used for cases B0, B1, B3 and B4. The effect of the changed model for the clad swelling is similar to those in the 12 kW/ft cases. $t_G$ and $P_{fc}$ variations are small, within 11%. The average $t_G$ is 2190 hours, 1860 hours, and 2210 hours; the average $P_{fc}$ is 5.1 ksi, 0.9 ksi, and 2.6 ksi, in the first, second and third axial sections, respectively. After gap closure the average duration of $P_{fc}$ and of the hoop stress increase in the clad is 89 hours. In this time the average $P_{fc}$ increase is 1.2 ksi, 0.4 ksi, and 0.8 ksi, and the average $(\sigma_\theta^c)_{max}$ increase is 6.6 ksi, 1.9 ksi, and 3.6 ksi in each axial section, respectively. Both $P_{fc}$ and $(\sigma_\theta^c)_{max}$ show the largest magnitude in the first section and the smallest one in in the second section in all, B0, B1, B3 and B4 cases. In B1, B3, and B4 cases, the swelling is a linear function of time, so there is no peak of $(\sigma_\theta^c)_{max}$. In cases B0, B1, and B4, the swelling is larger in the hotter region (inner wall) than in the cooler region (outer wall) of the clad, so $(\sigma_\theta^c)_{max}$ occurs at the outer wall. In case B3, the direction of the differential swelling across the clad wall changes its direction in the second and the third sections, so $(\sigma_\theta^c)_{max}$ is at the inner wall in these two sections. After 12000 hours of irradiation (Bu = 8.9%) the average $(\sigma_\theta^c)_{max}$ is 20.8 ksi, 8.6 ksi and 15.0 ksi in each axial section, respectively. The average variation is 8.5%.

$(e_\theta^c)$ is greatly dependent on the swelling model in the clad. In case B4, the swelling strain in the third section is increased; therefore, $(e_\theta^c)$ increases significantly and exceeds that in the second section, it is 1.8 times larger in case B4 than in case B0. As the peak of the clad swelling model shifts to 500°C (case B3), the swelling strain in the second and third sections is increased. In the second axial section it is 2.8 times larger than that in case B0.

733 136

Because of a large $P_{fc}$, and a large creep strain in the first section, the maximum value of $e_\theta^c$ is in this section for all B0, B1, B3, and B4 cases. The average $(e_\theta^c)$ in the first axial section is 5.37%. The average variation of this value is 9%.

For 9 kW/ft fuel elements in the conceptual reactor with $8.5 \times 10^{15}$ neut/cm$^2$-sec neutron flux, as the model of the clad swelling is changed in cases M0 and M1, the average $t_G$ is 2075 hours, 1425 hours, and 2950 hours in the first, second, and third axial sections, respectively. After 13000 hours of irradiation, the average $P_{fc}$ is 1.14 ksi and 0.6 ksi in the first and in the third axial sections, respectively. The average variation of $t_G$ is 10%, the average variation of $P_{fc}$ in the first and in the third axial section is 5.8%. No gap reopening has been calculated for either the M0 or the M1 case.

The swelling rate in the clad is linear in time in case M1, thus there is no peak for $(\sigma_\theta^c)_{max}$. As Figure M0-4 and Figure M1-3 show, the difference of $(\sigma_\theta^c)_{max}$ in these two cases at 6000 hours is relatively large, 1.3 ksi, 1.9 ksi, and 1.35 ksi in each axial section, respectively. The differences are small at 16000 hours, 0.3 ksi, 1.2 ksi, and 0.9 ksi in each axial section, respectively. $(\sigma_\theta^c)_{max}$ is smaller in case M1 than in case M0 throughout the calculated history. As Figures M0-5 and M1-4 show, the slope of $(\sigma_\theta^c)$ across the clad wall is larger in case M0 than in case M1.

In case M1 $(e_\theta^c)$ is less in the second and the third section than in case M0. It is 0.73 and 0.61 of the value in case M0 for the second and the third axial sections, respectively. In the first axial



733 137

section ($e_\theta^c$) is similar in the two cases. The differences in the ($e_\theta^c$) values are due to the different swelling of the clad.

V.5.4.3. Low Power Case

Different swelling correlations are used in cases N0, N1, N3, and N4 for 6 kW/ft fuel element calculations in CRBR. In cases N0, N1, and N4 the $t_G$ and $P_{fc}$ differences are small. The average $t_G$ is 7150 hours, 3717 hours, and 5817 hours in the first, second, and third axial section, respectively. After 17000 hours of irradiation, the average $P_{fc}$ is 1.20 ksi, 2.41 ksi, and 1.53 ksi in each section, respectively. In case N3, the peak swelling shifts from 600°C to 500°C, thus there will be more clad swelling within the same temperature range. Because of the small rate of the fuel swelling in the low linear power cases, the clad swelling effects are relatively large. Hence, the changes of $t_G$ and $P_{fc}$ in case N3 are significant. Because of the larger clad swelling, $t_G$ is larger and $P_{fc}$ is smaller in case N3 than in case N0. $t_G$ is 8100 hours, 4500 hours and 7700 hours in the first, second and third axial sections, respectively. After 17000 hours of irradiation (Bu = 8%), $P_{fc}$ is 1.62 ksi in the second axial section, (1.0 ksi lower than in case N0). Right after the gap closure, the average time for the rapid increases of $P_{fc}$ and of $(\sigma_\theta^c)_{max}$ is 67 hours. In this time, the average increase of $P_{fc}$ is 0.49 ksi, 0.59 ksi, and 0.57 ksi, and the average $(\sigma_\theta^c)_{max}$ increase is 2.7 ksi, 3.3 ksi, and 2.9 ksi in each axial section, respectively. Because of the linear time function of the swelling rate in cases N1, N3, and N4, the $(\sigma_\theta^c)_{max}$ behavior is almost linear in time after gap closure.

In cases N0, N1, and N4 $(\sigma_\theta^c)_{max}$ occurs at the outer wall of the clad. In case N3, in the first and the second axial sections it is at the outer wall, and in the third axial section at the inner wall of the clad. This is due to the larger swelling at the outer wall of the clad for the third axial section in case N3. In all cases with 6 kW/ft fuel elements, $(\sigma_\theta^c)_{max}$ has a higher magnitude in the second axial section than in the other ones. After 17000 hours of irradiation the average $(\sigma_\theta^c)_{max}$ is 9.5 ksi, 13.6 ksi and 10.7 ksi in each axial section, respectively. The variation of this average value is within 2.6% in the second, and within 5.6% in the first and third sections.

$(e_\theta^c)$ is greatly dependent on the swelling model in the clad. In case N1, because of a larger swelling strain in the first axial section, $(e_\theta^c)$ is twice that of case N0. In the first and the second axial sections of case N4, the smaller swelling strain and creep strain result in smaller $(e_\theta^c)$ than in case N0. It is 0.3 and 0.7 that of case N0. In the third axial section, $(e_\theta^c)$ is 1.3 times larger in case N4 than in case N0. In case N3, the peak of the clad swelling shifts from 600°C to 500°C, the swelling strain is significantly increased in all the three axial sections, and $(e_\theta^c)$ thus is 4.5, 2.2, and 2.6 times that of case N0 for the first, second, and third axial sections, respectively.

After 17000 hours of irradiation (Bu = 8%) in cases N0, N1, and N4 the average $(e_\theta^c)$ is 1.0%, 2.3%, and 1.9% in each axial section, respectively. The variation from this average value is 37%. In case N3, $(e_\theta^c)$ is 2.7%, 5.9%, and 4.4% in each axial section, respectively. For cases N0, N1, N3, and N4, the average creep strain is 26% of the total strain.

V.5.4.4. The Average Values of $t_G$, $P_{fc}$, $(\sigma_\theta^c)_{max}$, and $(e_\theta^c)$.

As discussed previously, different correlations for the clad swelling give different results. For fuel pins with 8% burn-up, the average $t_G$, $P_{fc}$, $(\sigma_\theta^c)_{max}$, and $(e_\theta^c)$ is listed as follows:

$$\overline{t_G} \pm \overline{t_G}$$

| Reactor | Linear Power (kW/ft) | Axial Section | $\overline{t_G} \pm \overline{\Delta t_G}$ hr | $\overline{P_{fc}} \pm \overline{\Delta P_{fc}}$ ksi | $\overline{\sigma_\theta} \pm \overline{\Delta\sigma_\theta}$ ksi | $\overline{e_\theta} \pm \overline{\Delta e_\theta}$ % |
|---|---|---|---|---|---|---|
| CRBR | 12 | 1 | 1850± 25 | 3.3 ± 0.10 | 16.4± 0.4 | 2.4± 0.3 |
| | | 2 | 1550± 75 | 1.0 ± 0.25 | 9.1± 1.4 | 1.3± 0.7 |
| | | 3 | 2075± 74 | 2.3 ± 0.03 | 12.4± 0.5 | 2.1± 0.6 |
| | 9 | 1 | 2217± 22.3 | 4.7 ± 0.25 | 19.9± 0.6 | 3.9± 0.3 |
| | | 2 | 1767± 44.3 | 0.87 ± 0.1 | 8.8± 0.7 | 1.8± 0.8 |
| | | 3 | 2117± 55.7 | 1.90 ± 0.30 | 12.8± 0.9 | 2.2± 0.5 |
| | 6 | 1 | 7387± 356 | 1.1 ± 0.17 | 9.6± 1.30 | 1.2± 0.80 |
| | | 2 | 3912± 294 | 2.2 ± 0.30 | 13.6± 0.50 | 3.3± 1.40 |
| | | 3 | 6325± 172 | 1.4 ± 0.25 | 10.6± 0.80 | 2.6± 0.90 |
| Conceptual LMFBR | 15 | 1 | 2100± 200 | 0.9 ± 0.02 | 8.4± 0.8 | 2.6± 0.2 |
| | | 2 | 900± 50 | (open) | 6.5± 0.3 | 5.7± 1.3 |
| | | 3 | 2100± 10 | 0.85 ± 0.02 | 6.8± 0.7 | 3.7± 0.3 |
| | 9 | 1 | 2075± 75 | 1.6 ± 0.01 | 10.5± 0.1 | 2.4± 0.2 |
| | | 2 | 1425±162.5 | 0.68 ± 0.01 | 7.3± 0.7 | 4.0± 0.7 |
| | | 3 | 2950± 450 | 0.96 ± 0.02 | 7.6± 0.2 | 2.6± 0.5 |

This table shows that for the 12 kW/ft and 9 kW/ft fuel pin in CRBR with 8% burn-up, the axial maximum of $\overline{P_{fc}}$, $(\overline{\sigma_\theta^c})$, and $(\overline{e_\theta})$ is in the first axial section, thus the axial weak point of the clad is in that section. In a 6 kW/ft fuel pin, the weak point of the clad shifts to the second axial section.

733 140

In the conceptual LMFBR, $\overline{P_{fc}}$ and $(\overline{\sigma_\theta^c})$ is smaller than in CRBR. In the 15 kW/ft fuel pin, the fuel-clad gap reopens at 8200 hours average irradiated time. In both the 15 kW/ft and 9 kW/ft fuel pins, the axial maximum of $P_{fc}$ and $(\sigma_\theta^c)_{max}$ occurs in the first axial section, while that of $(\overline{e_\theta})$ is in the second axial section.

### V.5.5. The Rate of Fuel Swelling

As Figure FSW shows, the calculated rates of the fuel swelling are close to the results reported in CONF-731004.

## V.6. Results and Discussion of Sensitivity Calculation for the Fuel Properties

Because of the higher neutron flux and temperature, the fuel is soft in the conceptual LMFBR. The fuel properties thus are less sensitive to the clad behavior than in CRBR. Fuel creep rate, fuel density, smear density and fuel swelling have been studied parametrically for CRBR fuel pins. Cases A0, B0, and N0 have been used as bases for these studies for the 12 kW/ft, 9 kW/ft, and 6 kW/ft cases, respectively.

### V.6.1. The 12 kW/ft Fuel Element

For the 12 kW/ft cases, Figures SA-1 through SA-3 show the variations of $P_{fc}$, the clad stress, and the clad hoop strain, by varying the fuel creep to 1.2 (Case AA) and 0.5 (Case AB) times that in case A0. As we can see in these figures, the gap closure times $(t_G)$ are not changed significantly. The $P_{fc}$ reduces by 250 psi, and increases by 205 psi as the fuel creep rate is varied to 1.5 and 0.5 times its value in A0, respectively.

Because of the changing $P_{fc}$, the stress differences in the clad (cases A0, AA, and AB) are significant, especially prior to 6000 hours irradiation. At 3000 hours, the clad stress for case AB increases by 1.8 ksi, 2.0 ksi, and 1.4 ksi, with respect to that in case A0, for the first, second and third axial sections, respectively. After 6000 hours, the differences of clad stress for these three cases decrease by several hundred psi.

The strains in the clad decrease by increasing the fuel creep and increase by decreasing the fuel creep. This changing clad strain is mainly due to the change of the creep strains induced by the fuel-clad interaction forces. After 13000 hours of irradiation, the average variation of the hoop strain is 0.3%.

In case A0, the fuel density is 91.3% and the smear density is 85.5% of the theoretical density (with 3 mils initial fuel-clad gap). In case AG, the smear density is changed to 88%, which is equivalent to a initial gap that closes at 400 hours, 100 hours, and 550 hours in each axial section, respectively. After the gap is closed, the $P_{fc}$ magnitudes, and consequently the stress and the strain in the clad, do not change significantly with respect to those in case A0. In case AH, the smear density is changed to 83% which is equivalent to a 5 mils initial gap. $t_G$ is thus 2900 hours, 2800 hours and 3200 hours in each axial section, respectively (Figure SA-4). $P_{fc}$, the stress, and the strain in the clad are smaller than in case A0. At 13000 hours, the difference in the clad stress is 800 psi, 500 psi, and 750 psi, and in the hoop strain is 0.6%, 0.28%, and 0.4% in each axial section, respectively (Figures SA-5, SA-6).

In case AI, the initial gap is 3 mils and the fuel density is 85% of the theoretical density (with 80% smear density). Because of the same initial gap as in case AO, $t_G$ will also be similar (Figure SA-7). The reduction of the fuel density enhances the creep rate in the fuel, thus, $P_{fc}$, the stress, and the strain in the clad are reduced in case AI. At 13000 hours, the reduction of $P_{fc}$ with respect to that in case AO, is 1 ksi, 0.3 ksi, and 0.65 ksi (Figure SA-7). The reduction of the maximum hoop stress in the clad is 2.2 ksi, 0.6 ksi, and 1.3 ksi. The reduction of the hoop strain in the clad is 1.2%, 0.32%, and 0.91% in each axial section, respectively (Figures SA-8 and SA-9).

In cases AN and AS, the model of the fuel swelling is varied. As shown in Figure SA-10, $t_G$ and $P_{fc}$ are reduced significantly in all axial sections. In the first axial section, where the highest $P_{fc}$ occurs, it is reduced by 25.7% and by 50.5%, compared to case AO. This reduction of $P_{fc}$ is caused by less bulk swelling in the fuel.

Figure SA-11 shows the maximum hoop stress in the clad for AN, AS, and AO. Because of the great reduction of $P_{fc}$ in cases AN and AS, the maximum clad stresses are also reduced significantly. At 13000 hours, the maximum hoop stress in the first axial section is reduced by 14% and by 31% for cases AN and AS, respectively.

Figure SA-12 shows the total hoop strain in the clad. This is reduced in all three axial sections because $P_{fc}$ is reduced, and as a consequence, the creep strain in the clad will also be reduced. At 13000 hours, the total hoop strain in the first axial section is reduced by 1.8% and 3.5% for cases AN and AS, respectively.

V.6.2. The 9 kW/ft Fuel Element

For the 9 kW/ft fuel element, Figures SB-1 through SB-12 show the values of $t_G$, $P_{fc}$, the stress, and the strain in the clad for cases BO, BA, and BB. In case BA, $t_G$, $P_{fc}$ and $(\sigma_\theta^c)_{max}$ are not changed significantly. At 13000 hours, $P_{fc}$ is smaller than in case BO by 200 psi. The average decrease of $e_\theta^c$ is 0.2%.

In case BB, $t_G$ is larger than in case BO, it is 2550 hours, 1800 hours, and 2250 hours in each axial section, respectively. $P_{fc}$, $(\sigma_\theta^c)$ and $(e_\theta^c)$ are larger than in case BO. After 13000 hours of irradiation, the average changes of $P_{fc}$, $(\sigma_\theta^c)$, and $(e_\theta^c)$ are 250 psi, 750 psi and 0.4%, respectively (Figures SB-1 through SB-3).

In cases BG and BH, the smear density is changed to 88% and 83%, respectively. This is equivalent to an initial gap of 1.87 mils for case BG and 5 mils for case BH. As shown in Figure SB-4 for case BG, the gap closes at 860 hours, 280 hours, and 630 hours, in each axial section, respectively. After the gap closure $P_{fc}$ is similar in cases BO and BG. In case BH the gap closes at 3400 hours, 3200 hours, and 3480 hours in the first, second and third axial section, respectively. The $P_{fc}$ is slightly smaller in each axial section. At 14000 hours in case BH, $P_{fc}$ is 420 psi, 108 psi, and 230 psi lower in each axial section than in case BO.

Figure SA-5 shows $(\sigma_\theta^c)_{max}$ in cases BO, BG, and BH. After the fuel-clad gap closes, the difference of $(\sigma_\theta^c)_{max}$ is induced by the $P_{fc}$ variation. After 5000 hours, $(\sigma_\theta^c)_{max}$ is similar for cases BO and BG, and is lower in case BH than in case BO. At 14000 hours, it is lower by 850 psi, 500 psi, and 690 psi than that in case BO. Figure SB-6 shows the total hoop strain in these cases. It is similar to that in case BO. In case BH at 14000 hours it is lower by 0.38%, 0.2%, and 0.22% than that in case BO, for each axial section, respectively.

In case BI, the initial gap is kept the same (i.e. 3 mils) as that in case BO, but the fuel density is reduced to 85% of the theoretical density. This effect hastens the fuel creep, and thus reduces $P_{fc}$ in each axial section. As shown in Figure SB-7, the gap closure time is not changed significantly. After the gap closes, $P_{fc}$ is lower in case BI than in case BO. At 14000 hours, this difference is 910 psi, 130 psi, and 330 psi for each axial section, respectively.

Figure SB-8 shows the $(\sigma^c)_{max}$ for cases BO and BI. The differences of $(\sigma^c)_{max}$ are mainly due to the differences of $P_{fc}$. In case BI at 14000 hours it is lower by 1600 psi, 510 psi, and 900 psi than that in case BO in each axial section, respectively. Figure SB-9 shows the total hoop strain in the clad for these two cases. Because of the lower $P_{fc}$ in case BI, the total hoop strain in the clad is lower. At 14000 hours, the difference of the total hoop strain in the clad for cases BO and BI is 0.9%, 0.14% and 0.3%, in each axial section, respectively.

In cases BN and BS, the model of the fuel swelling is varied. Because of slower fuel swelling in these two cases, $P_{fc}$, the clad stress, and the strain are lower than in case BO. As shown in Figure SB-10, the reduction of $P_{fc}$ is 6.4 ksi, 4.3 ksi, and 2.6 ksi in the first axial section; 1.2 ksi, 0.9 ksi, and 0.7 ksi in the second axial section; and 2.7 ksi, 1.7 ksi, and 1.0 ksi in the third axial section, for cases BO, BN, and BS, respectively.

Figure SB-11 shows the $(\sigma_\theta^c)_{max}$ in the clad. Because the same clad swelling model has been used, the shape of $(\sigma_\theta^c)_{max}$ is similar in each axial section for cases BO, BN, and BS. The difference in the $(\sigma_\theta^c)_{max}$ magnitude is due to the difference in $P_{fc}$. At 14000 hours, $(\sigma_\theta^c)_{max}$ is 22.5 ksi, 19 ksi, and 15 ksi in the first axial section; 9.3 ksi, 8.8 ksi, and 8.2 ksi in the second axial section; and 13.7 ksi, 10.2 ksi, and 7.0 ksi in the third axial section for cases BO, BN, and BS, respectively.

Figure SB-12 shows the hoop strain in the clad for these three cases. Because of the lower $P_{fc}$ and creep strain, the total hoop strain in the clad is lower for cases BN and BS than that in case BO. At 14000 hours, the total hoop strain is 5.9%, 3.7%, and 1.5% in the first axial section; 1.9%, 1.7%, and 1.3% in the second axial section; 2.6%, 2.1%, and 1.4% in the third axial section, for cases BO, BN, and BS, respectively.

V.6.3. The 6 kW/ft Fuel Element

For 6 kW/ft cases, Figures SN-1 through SN-10 show the variation caused in $P_{fc}$, $t_G$, the stress, and the strain in the clad by varying the fuel creep to 1.5 (case NA) and 0.5 (case NB) times that in case NO.

As Figure SN-1 shows, the gaps close earlier in case NA than in case NB. This happens because in case NA the fuel boundary movement is retarded by the slower creep rate in the fuel. The magnitude of $P_{fc}$ is not changed significantly. At 14000 hours, $P_{fc}$ is similar for cases NO and NA. In case NB it is 130 psi and 204 psi lower for the second and the third axial section than that of case NO.

733 146

Figure SN-2 shows the maximum clad hoop stress $(\sigma_\theta^c)_{max}$ for cases NO, NA, and NB. Because of the same swelling model for each case, the shape of $(\sigma_\theta^c)_{max}$ is similar and its magnitude is influenced by the gap closure time and by the magnitude of $P_{fc}$. After 12400 hours, the magnitudes of $(\sigma_\theta^c)_{max}$ are similar in cases NO and NA. In case NB it is 340 psi and 580 psi lower for the second and the third axial sections, respectively.

Figure SN-3 shows the hoop strain in the clad in cases NO, NA, and NB. Because of the similar clad swelling and $P_{fc}$, the amount of the total strain is similar in each case. At 14000 hours, it is 0.1% and 0.07% lower, in case NB, for the second and the third axial sections, respectively. These differences are caused by the lower $P_{fc}$.

Figures SN-4 and SN-5 show $P_{fc}$, the gap closure times, and the clad stress for cases NO, NG, and NH. In cases NG and NH, the smear density is changed to 88% and 83%, respectively, i.e., the initial gap is changed to 3 mils in case NO, to 1.87 mils and 5 mils in cases NG and NH. Figure SN-4 shows that the gaps close earlier in case NG and later in case NH. Because of the same swelling rate in the fuel, the $P_{fc}$ is almost the same in these low power cases after gap closure.

Figure SN-5 shows $(\sigma_\theta^c)_{max}$ in cases NO, NG, and NH. Because $P_{fc}$ is almost the same after the gap closure, and the swelling model is the same for the fuel and the clad, the $(\sigma_\theta^c)_{max}$ values are the same for all three cases. The total hoop strain change in the clad is not significant.

Figures SN-6 and SN-7 show case NI, where the initial gap is kept at 3 mils and the fuel density is changed from 91.3% in case NO, to 85% of the theoretical density in case NI. As the density is lowered, there is a faster creep effect in the fuel and so the fuel-clad gap can close earlier. In case NI, the gap closes at 6700 hours, 3750 hours, and 5700 hours in each axial section, respectively. The $P_{fc}$ is also smaller in case NI than that in case NO. At 12000 hours, this difference is about 150 psi in each axial section. Figure SN-7 shows $(\sigma_\theta^c)_{max}$ for cases NO and NI. The differences of $(\sigma_\theta^c)_{max}$ in these two cases are mainly due to the differences in $t_G$. Because the difference of $P_{fc}$ is not significant, the $(\sigma_\theta^c)_{max}$ differences are negligible after gap closure. The difference of the total hoop strain in the clad is insignificant.

The model for the fuel swelling is varied in cases NN and NS. Because of the lower fuel temperature and lower fuel swelling, the changes of $P_{fc}$ and of $(\sigma_\theta^c)_{max}$ are not as significant as in higher linear power fuel elements. As shown in Figure SN-8, at 14000 hours, in case NN $P_{fc}$ is lower by 160 psi, and by 70 psi than in case NO for the second and third axial sections, respectively. In case NS $P_{fc}$ is lower by 510 psi and 208 psi than in case NO for the second and third axial section, respectively. These $P_{fc}$ differences induce $(\sigma_\theta^c)_{max}$ differences in each axial section. As Figure SN-9 shows, in case NS at 14000 hours, $(\sigma_\theta^c)_{max}$ is lower by 1240 psi and 720 psi than that in case NO for the second and third axial section, respectively. The total hoop strains in cases NO, NN and NS are shown in Figure SN-10. In case NS at 14000 hours, the hoop strain is 0.4% and 0.1% lower than in case NO for the second and the third axial sections, respectively.



733 148

THERE IS NO TEXT ON THIS PAGE

## CHAPTER VI. CONCLUSIONS

1. The KRASS code is a simplified computer code which can be used for the prediction of axial and radial variations of fuel element behavior in an LMFBR under steady state irradiation. It takes eleven hundred machine unit seconds on the UCLA IBM-360-91 to calculate fuel element behavior to 15% burn-up with seven axial sections in the fuel column.

2. At 12 kW/ft and 9 kW/ft, the axial maximum of $P_{fc}$ and $(\sigma_\theta^c)_{max}$ occurs in the bottom section, while at 6 kW/ft, it occurs in the mid-section of the fuel element.

3. The higher neutron flux in the large LMFBR may enhance the creep rate in the fuel and lower the fuel-clad mechanical interactions. The hoop stress in the clad is thus lower in the large LMFBR than in the CRBR in most cases.

4. Because of the high neutron flux in the large LMFBR, the fuel-clad gap in the mid-section of the fuel pin with higher linear power may reopen. The time for this reopening is greatly dependent on the clad swelling model. No gap reopening has been calculated for fuel pins in the CRBR.

5. As the temperature changes from 600°C to 500°C for peak clad swelling, the radial maximum of the hoop stress can move from the clad outer wall to the clad inner wall in some of the axial sections. The radial stress distribution across the clad wall is also significantly changed.

6. Because of the larger $P_{fc}$ in CRBR, a large fraction of the total strain in the clad is due to creep strain. In the bottom section

733 150

of the 12 kW/ft element, where $P_{fc}$ is high and the clad swelling is low, the fraction of the creep strain could be 80%. In large LMFBR, $P_{fc}$ is low, thus irradiation induced swelling is the main contributor to the total strain.

7. The amount of the total clad strain is greatly dependent on the irradiation induced swelling model. In CRBR, the total strain in the clad is also significantly influenced by the $P_{fc}$-induced creep strain.

8. As the correlation of the clad swelling with the swelling threshold (Equation II-40) used in the calculation shows, a stress peak is induced in the clad by the larger differential swelling across the clad wall near the threshold burn-up. In the large LMFBR, these stress peaks are high and occur at low burn-up.

9. As the creep rate of the fuel, the fuel pin smear density, or the fuel density is varied, modest variations of the fuel pin behavior are calculated. As the fuel swelling model is varied, the variations in fuel pin behavior become significant.

733 151

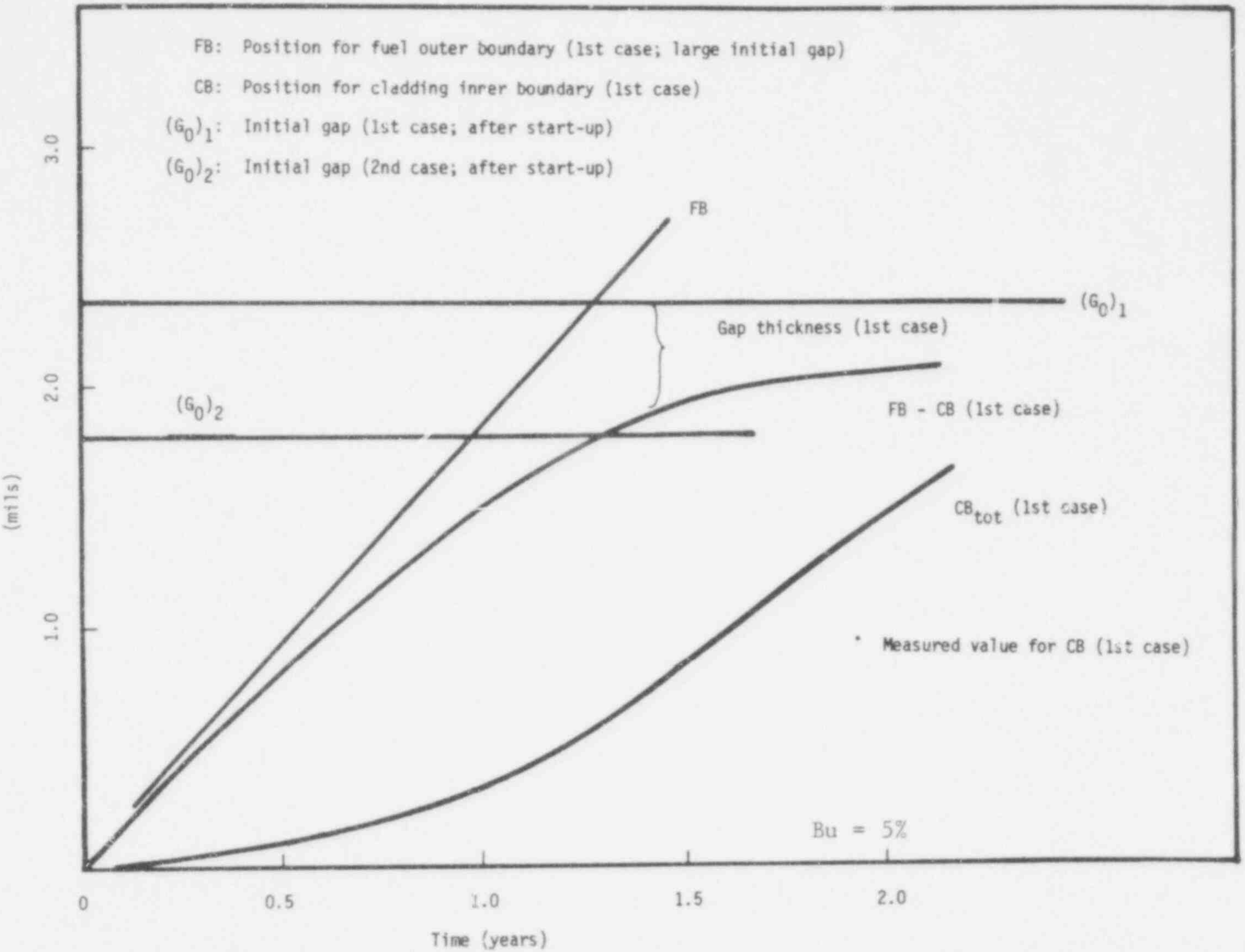


Figure E - 1. Fuel Element Boundary Positions.

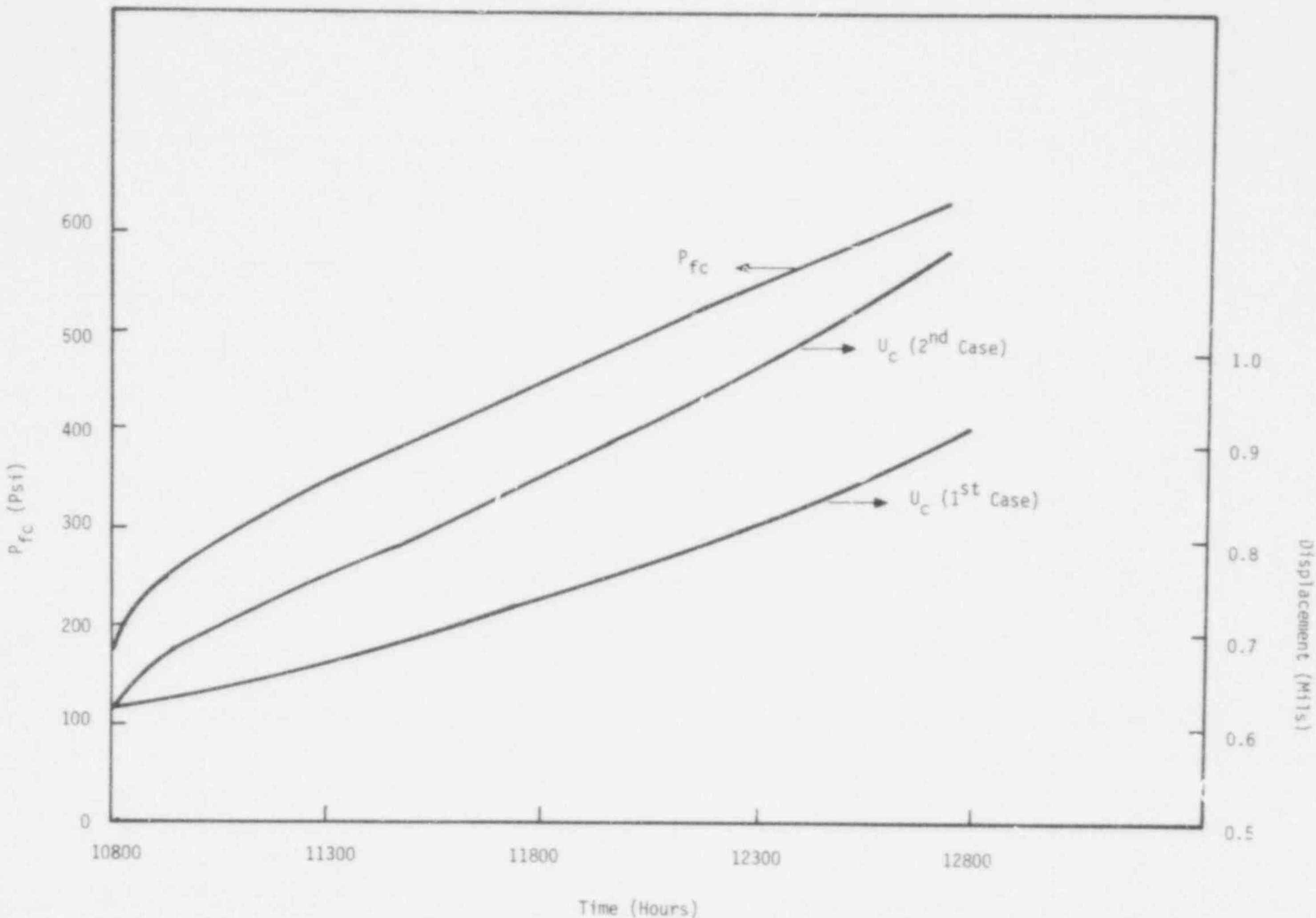


Fig.E-2 The Fuel-Clad Mechanical Interaction($P_{fc}$), and the Displacement of the Cladding Inner Surface ($U_c$)

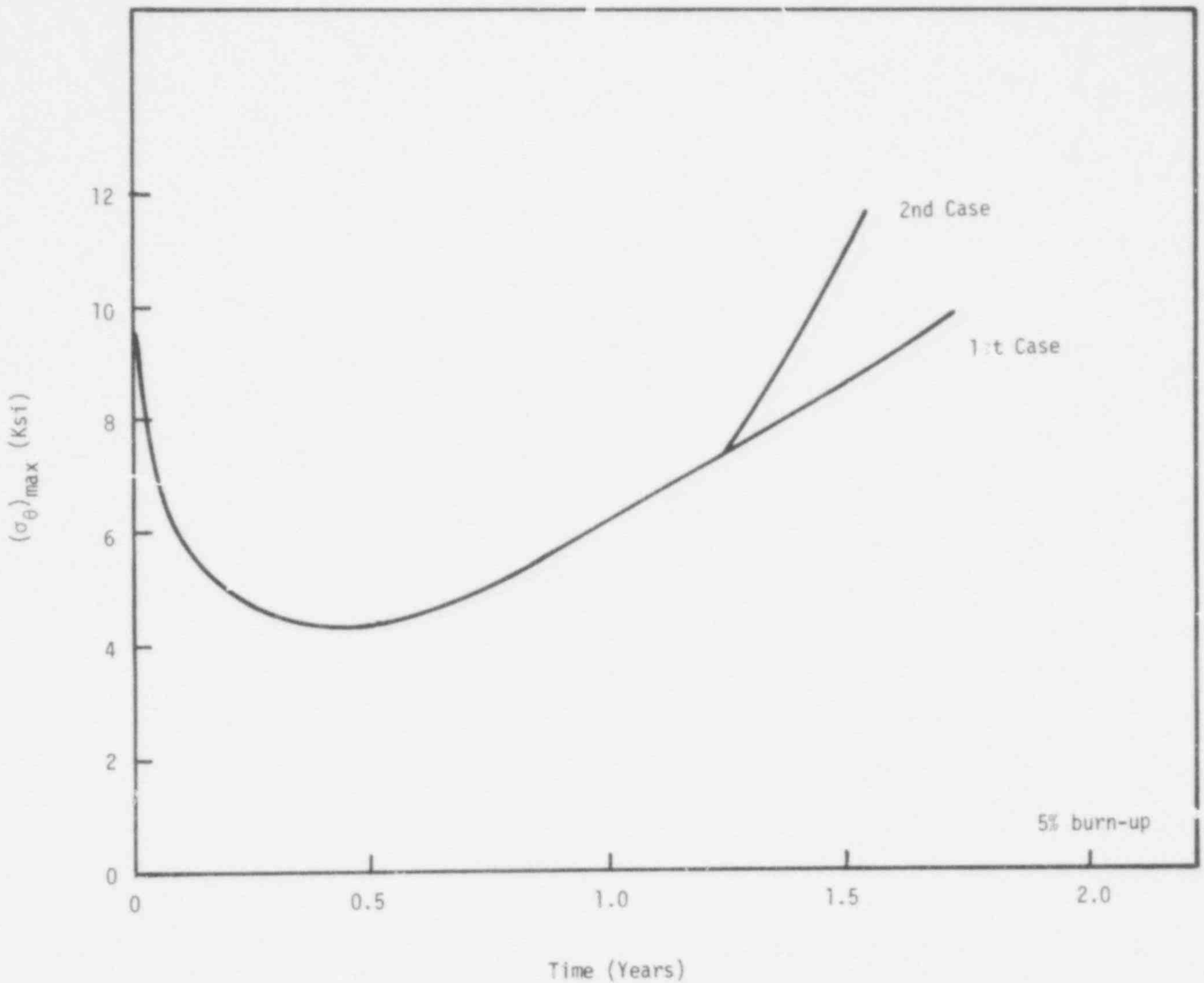


Figure E-3. The Maximum Hoop Stress in the Clad.

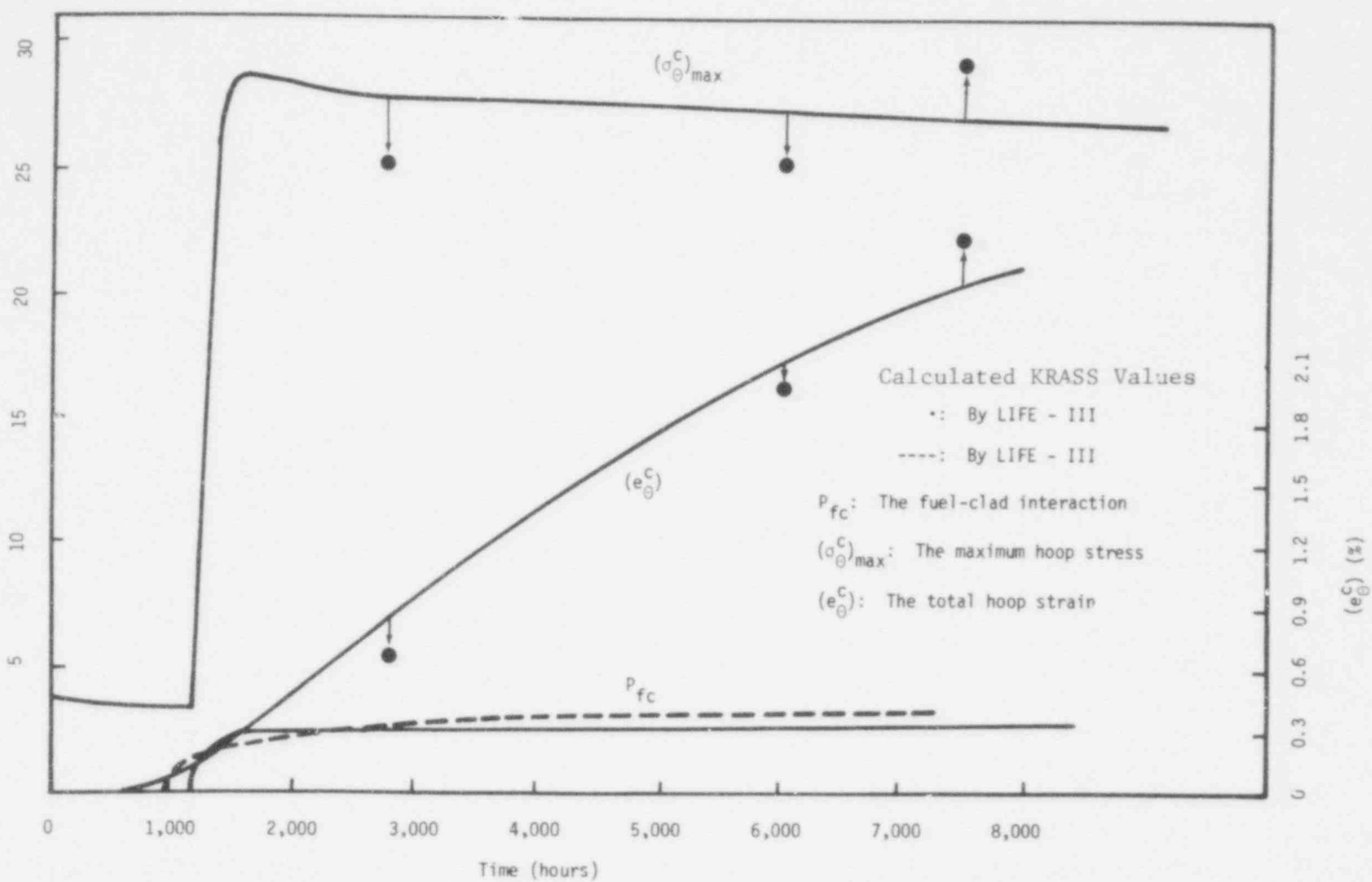


Figure E - 4. The Fuel-Clad Interaction, the Maximum Hoop Stress, and the Total Hoop Strain in the Clad.



733 155

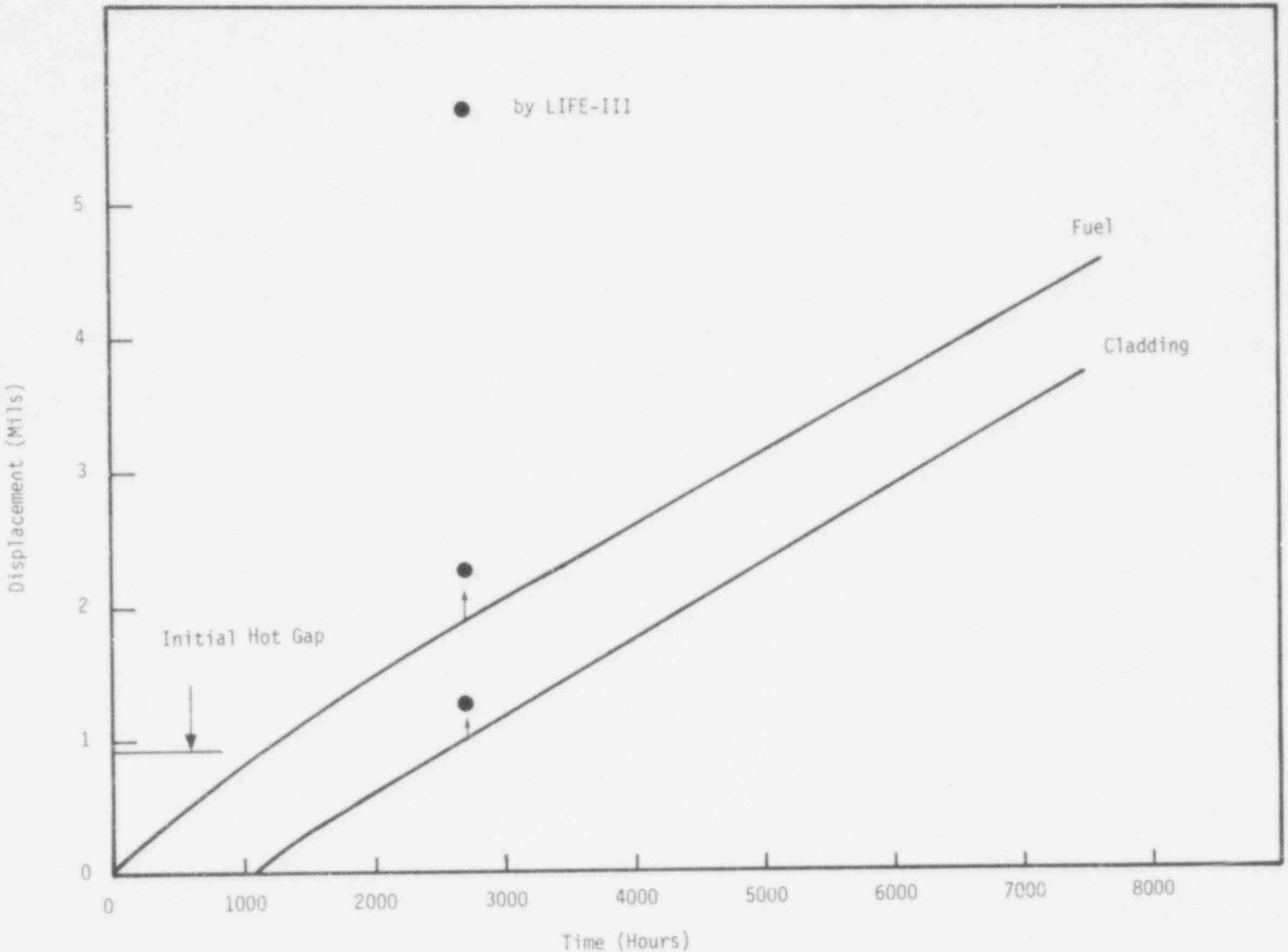


Fig. E-5 The Fuel and the Cladding Boundary Movements

733 156

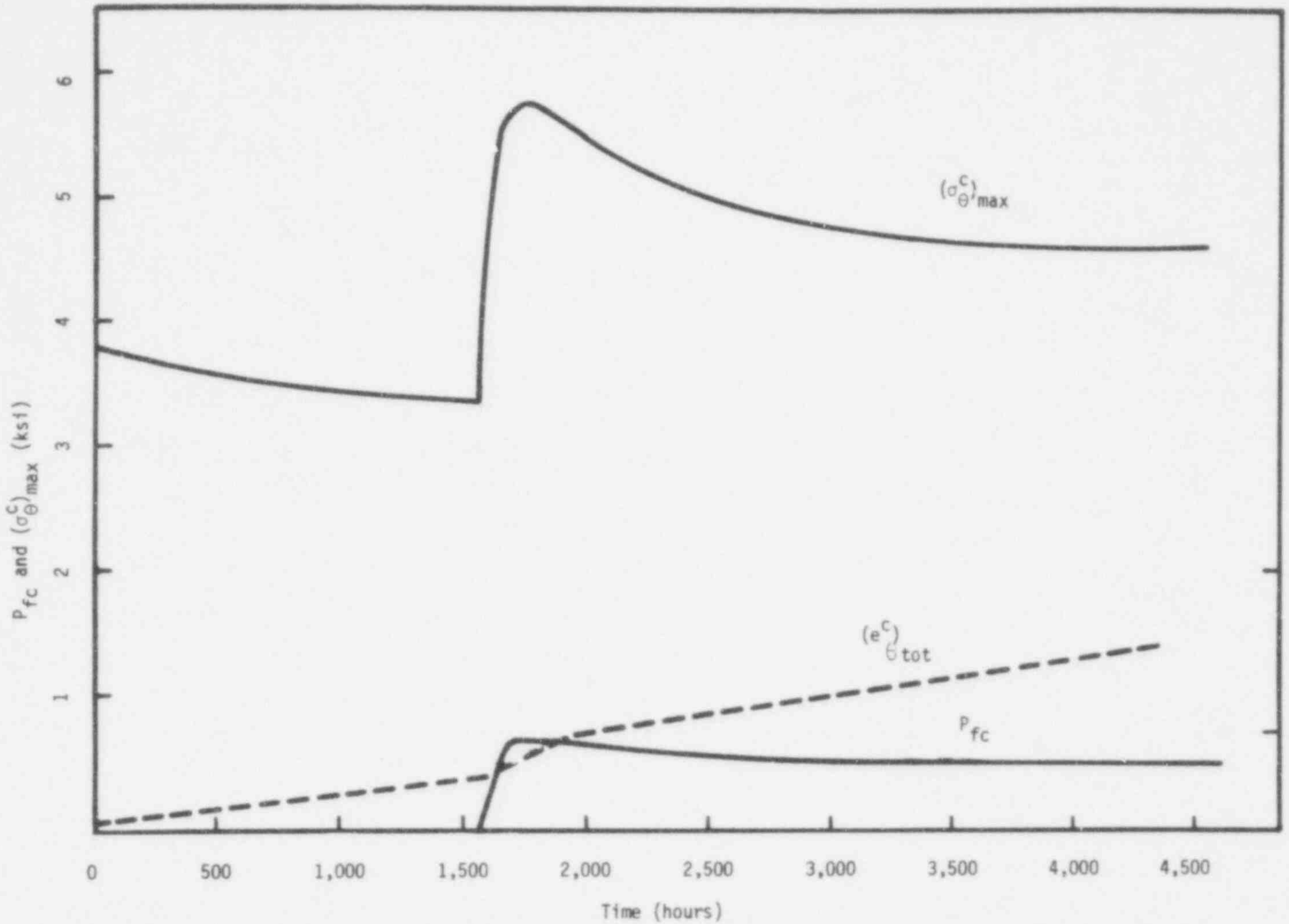


Figure E - 6. The Fuel-Clad Interaction ($P_{fc}$), the Maximum Hoop Stress ($(\sigma_\theta^c)_{max}$), and the Hoop Strain ($e_\theta^c$) in the Clad (Case EBR - 15 KW/Ft).

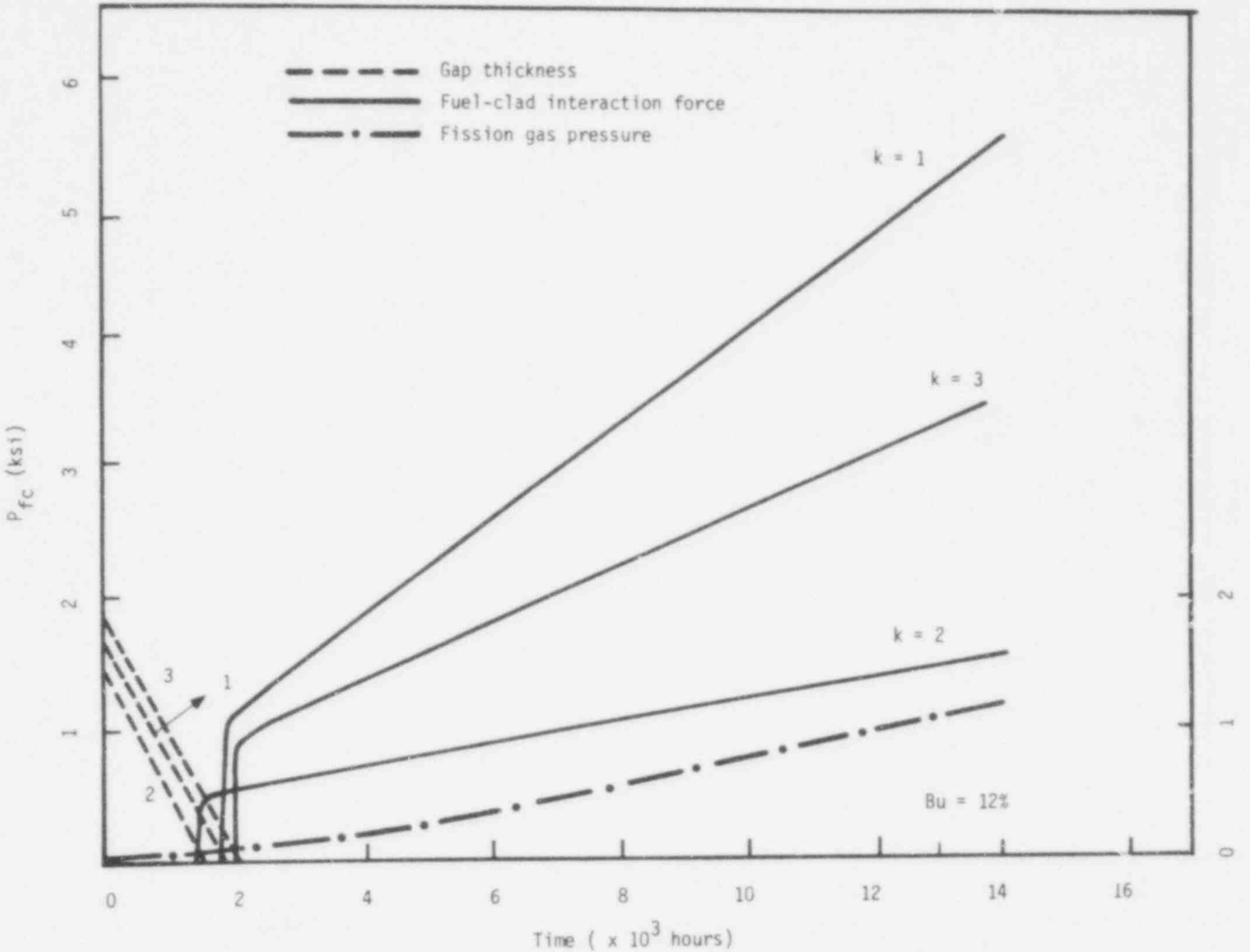


Figure AO - 1. The Gap Thickness, the Fuel-Clad Interaction Force, and the Fission Gas Pressure. (Case AO)

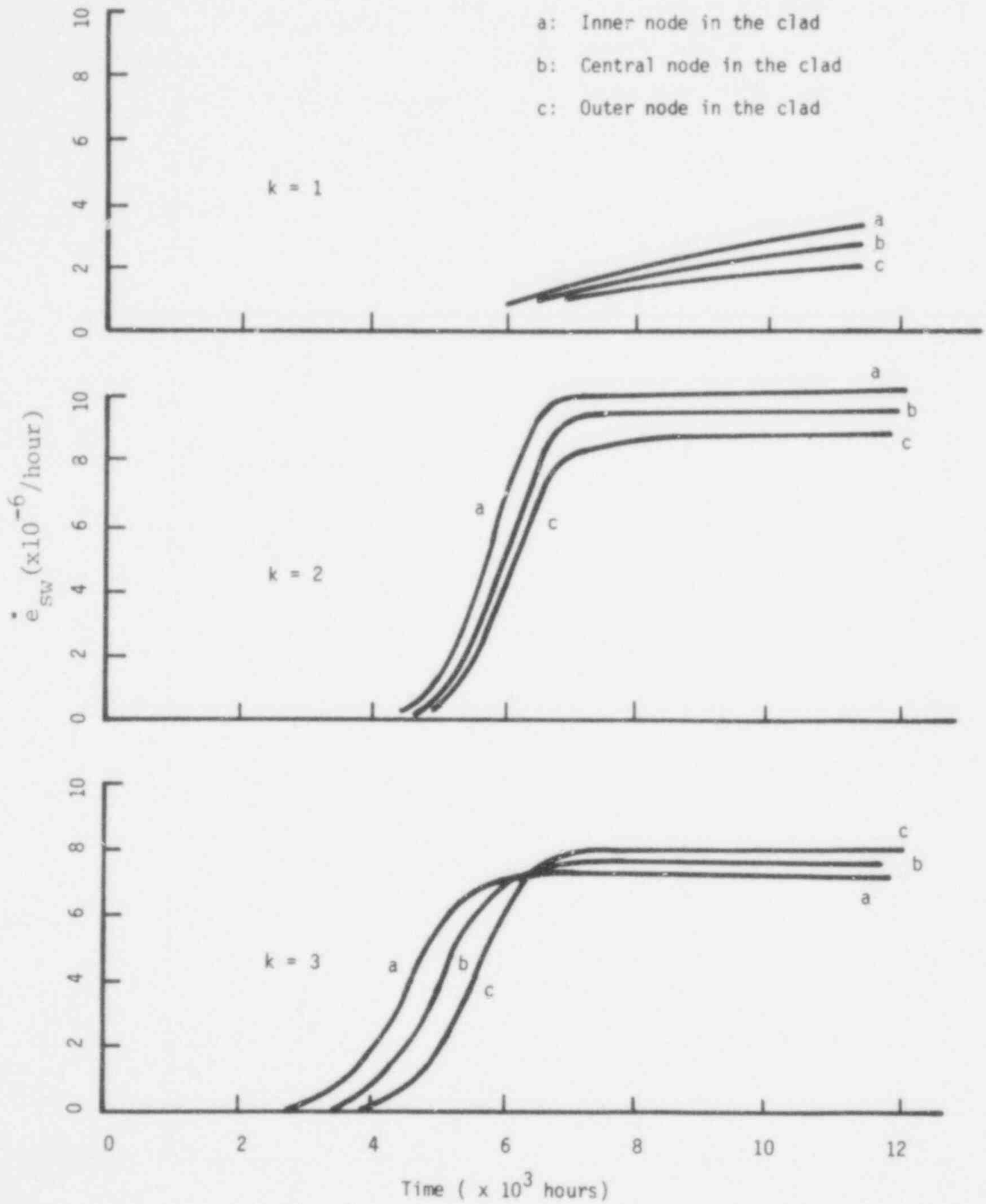


Figure A0 - 2. The Swelling Strain Rate (per hour) in Each Axial Section. (Case A0)

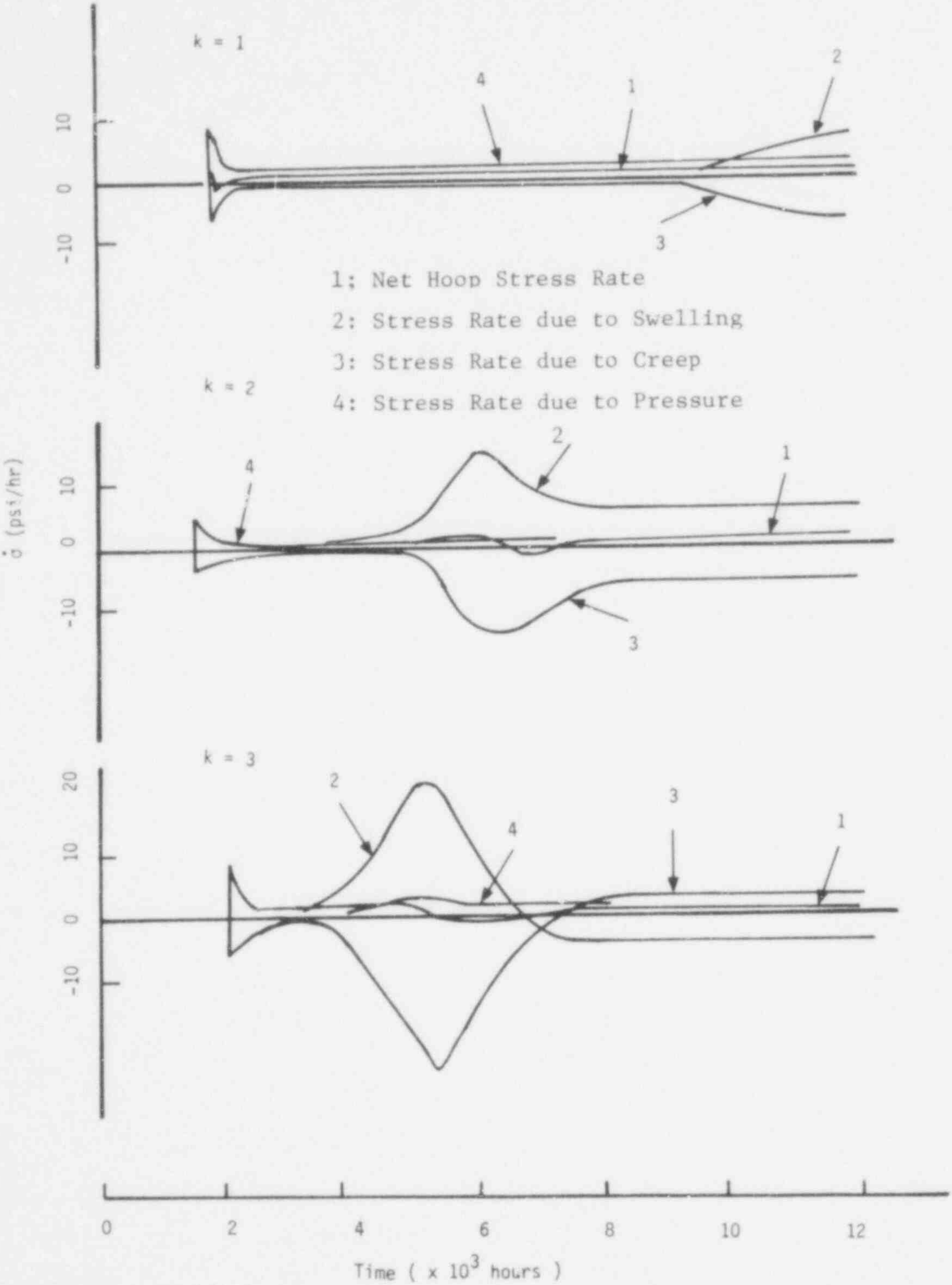


Figure A0-3. The Net Hoop Stress and the Stress Rate, Due to Swelling, Creep, and Pressure at the Outer Wall of the Clad.

733 180

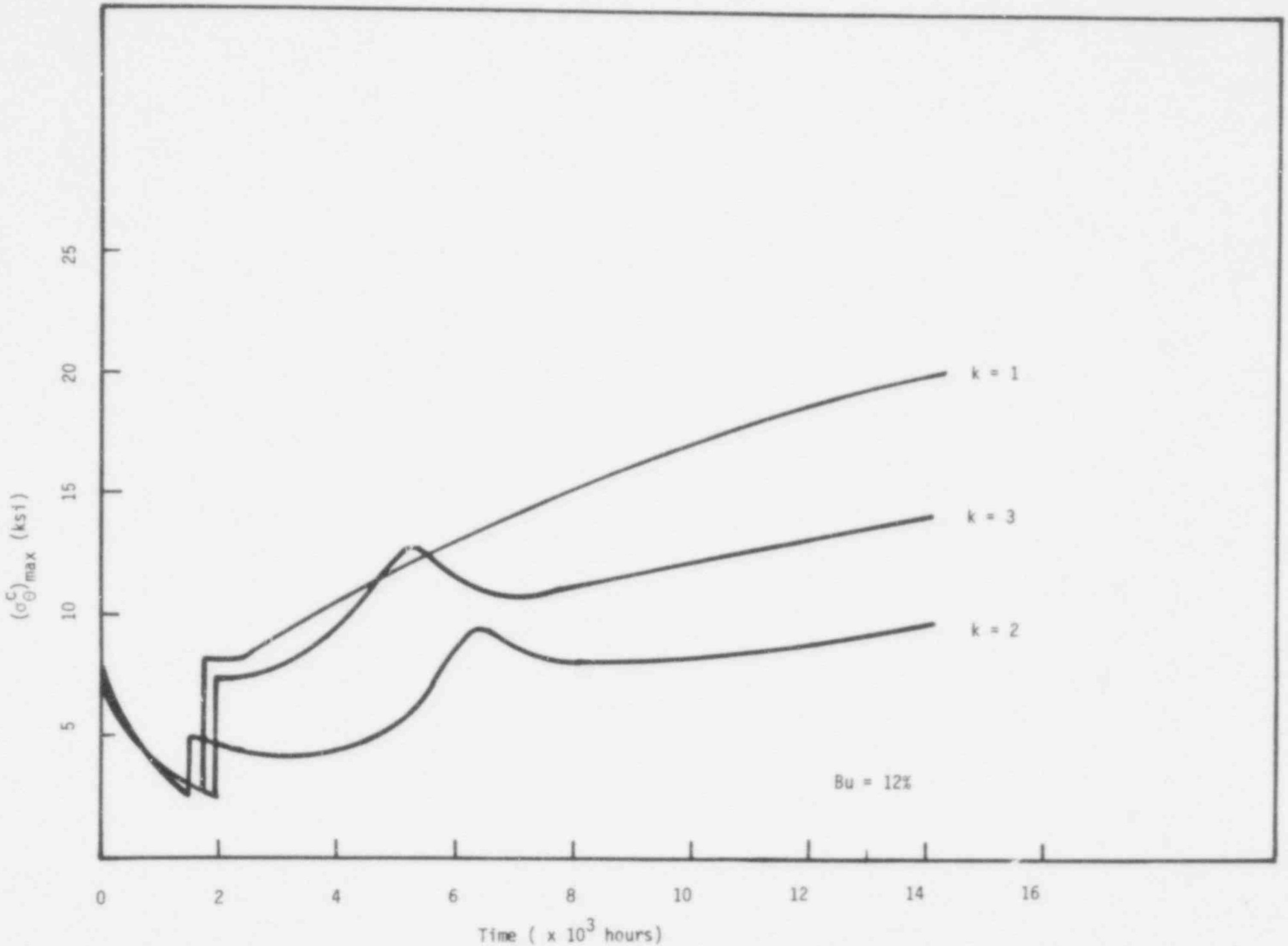


Figure AO - 4. The Maximum Clad Stress in Each Axial Section. (Case AO)

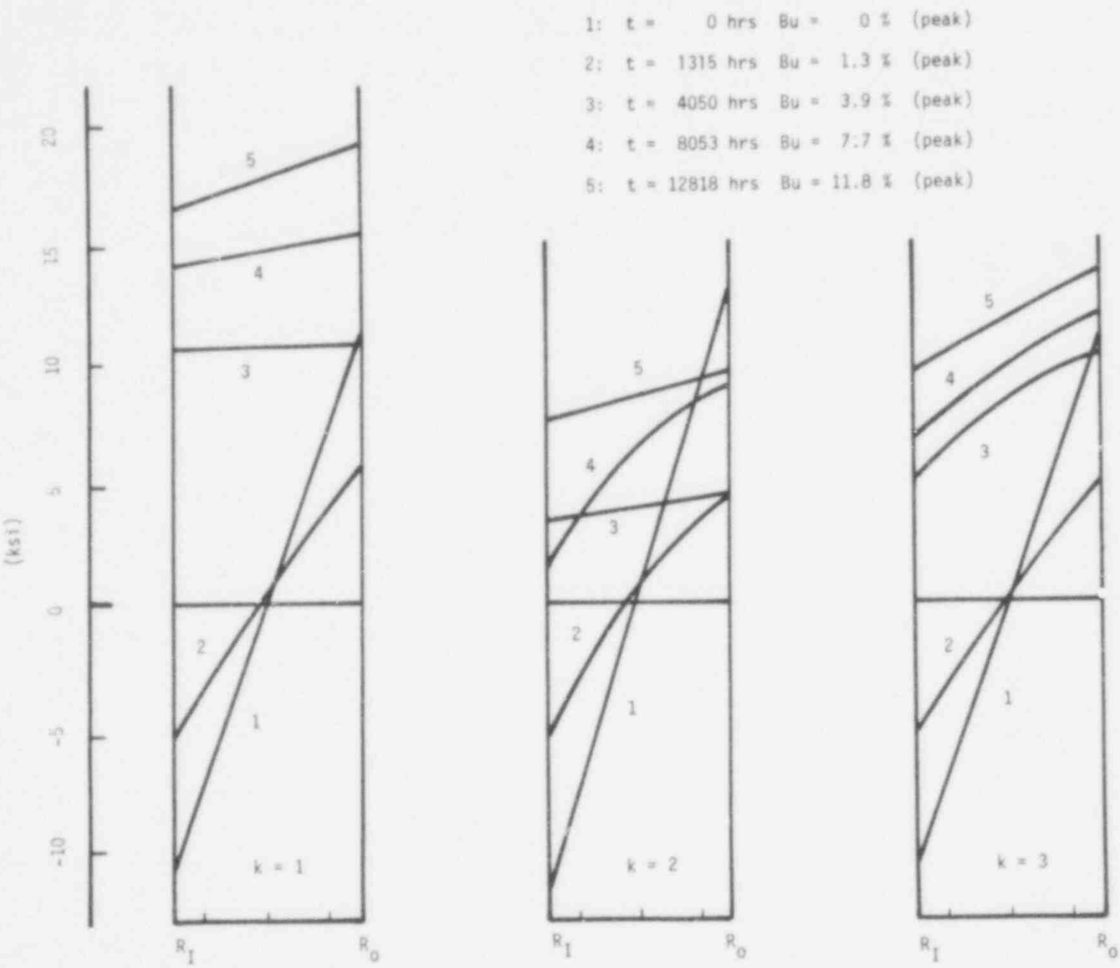


Figure AO-5. The Hoop Stress Distribution Across the Clad Wall.

733 162

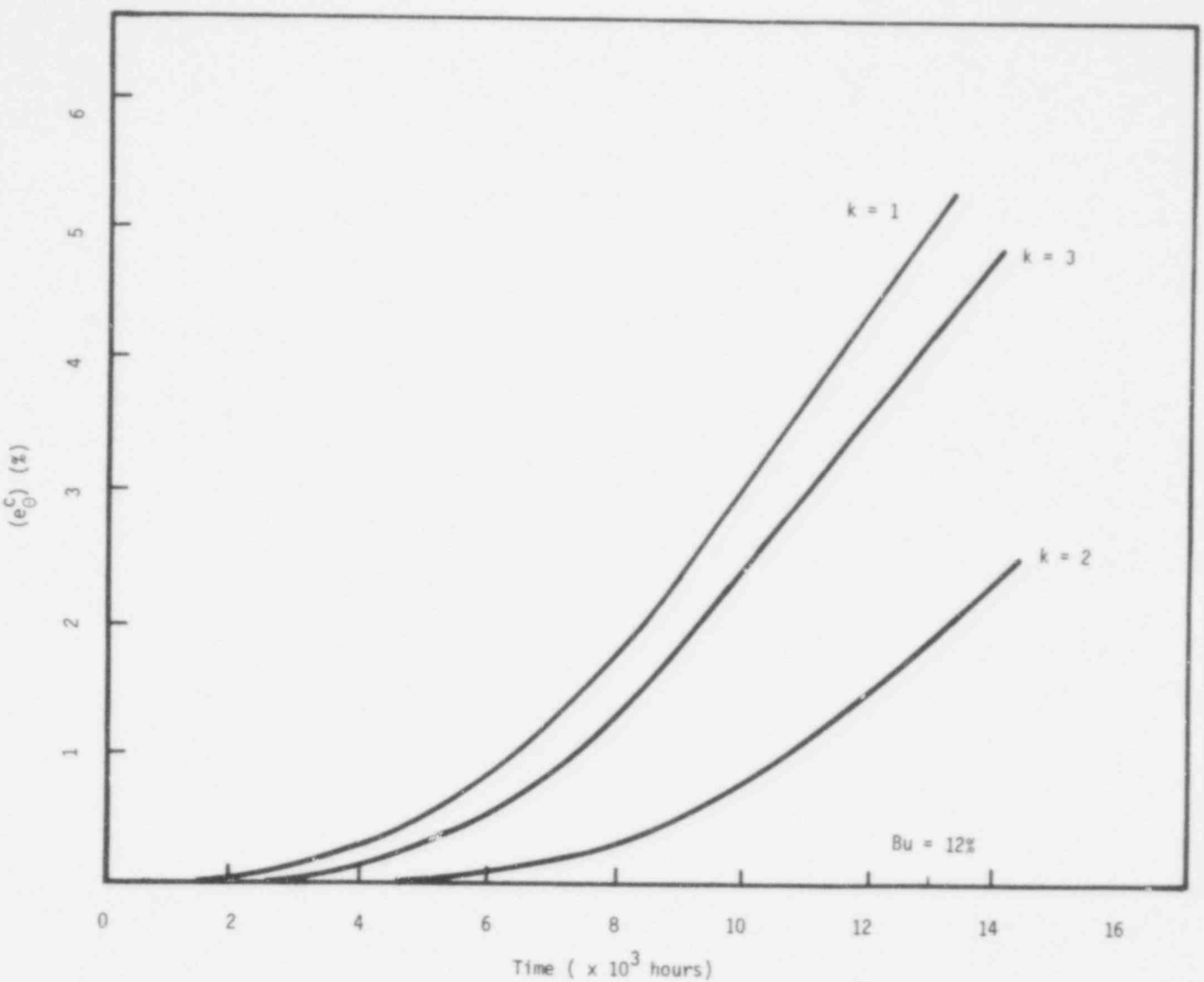


Figure AO - 6. The Hoop Strain in the Clad. (Case AO)



733 16

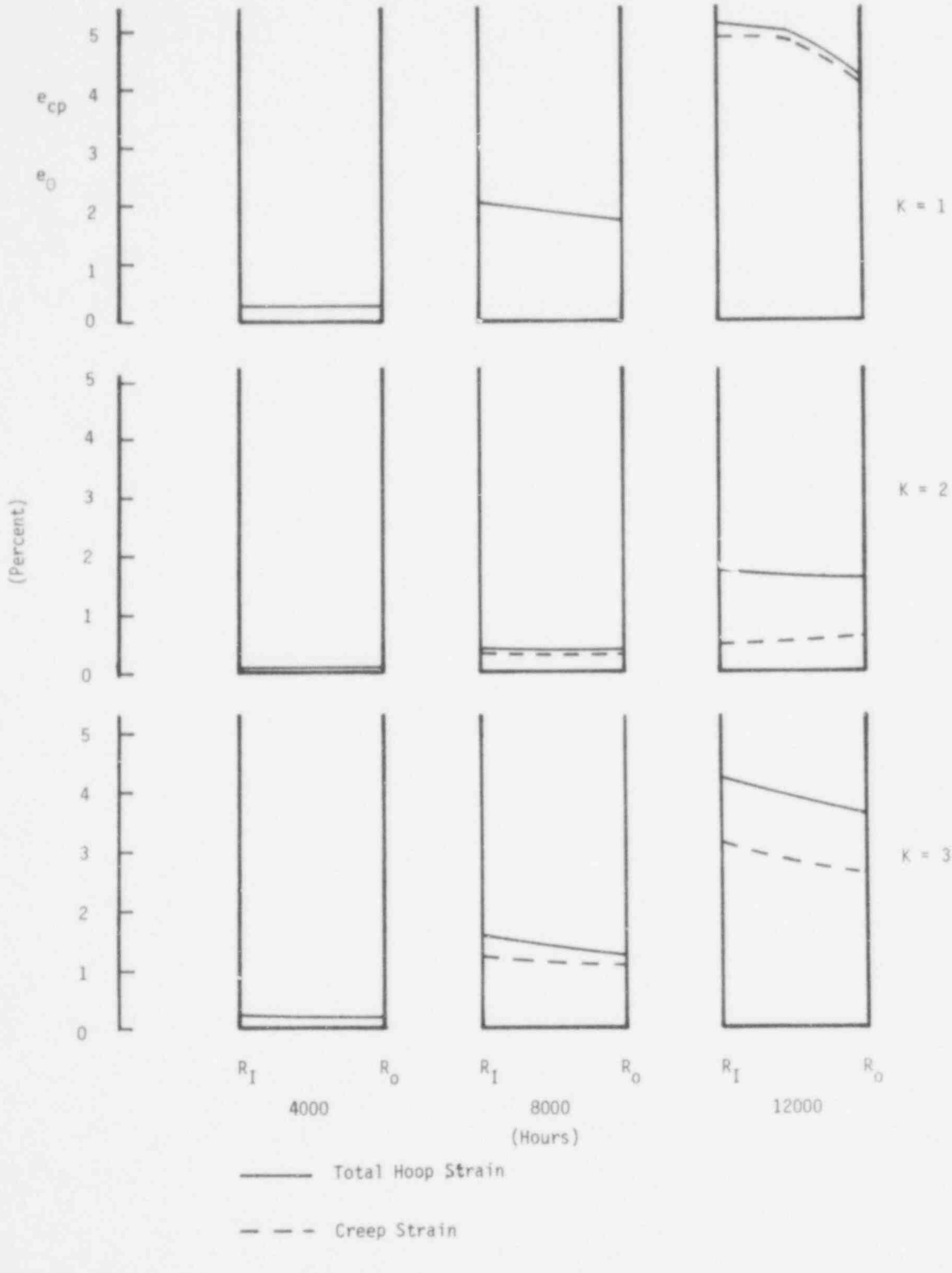


Fig. A0.7 The Total Hoop Strain and the Creep Strain Across the Clad Wall ( Case A0 )

733 164

12 kW/ft Cases

Case A1

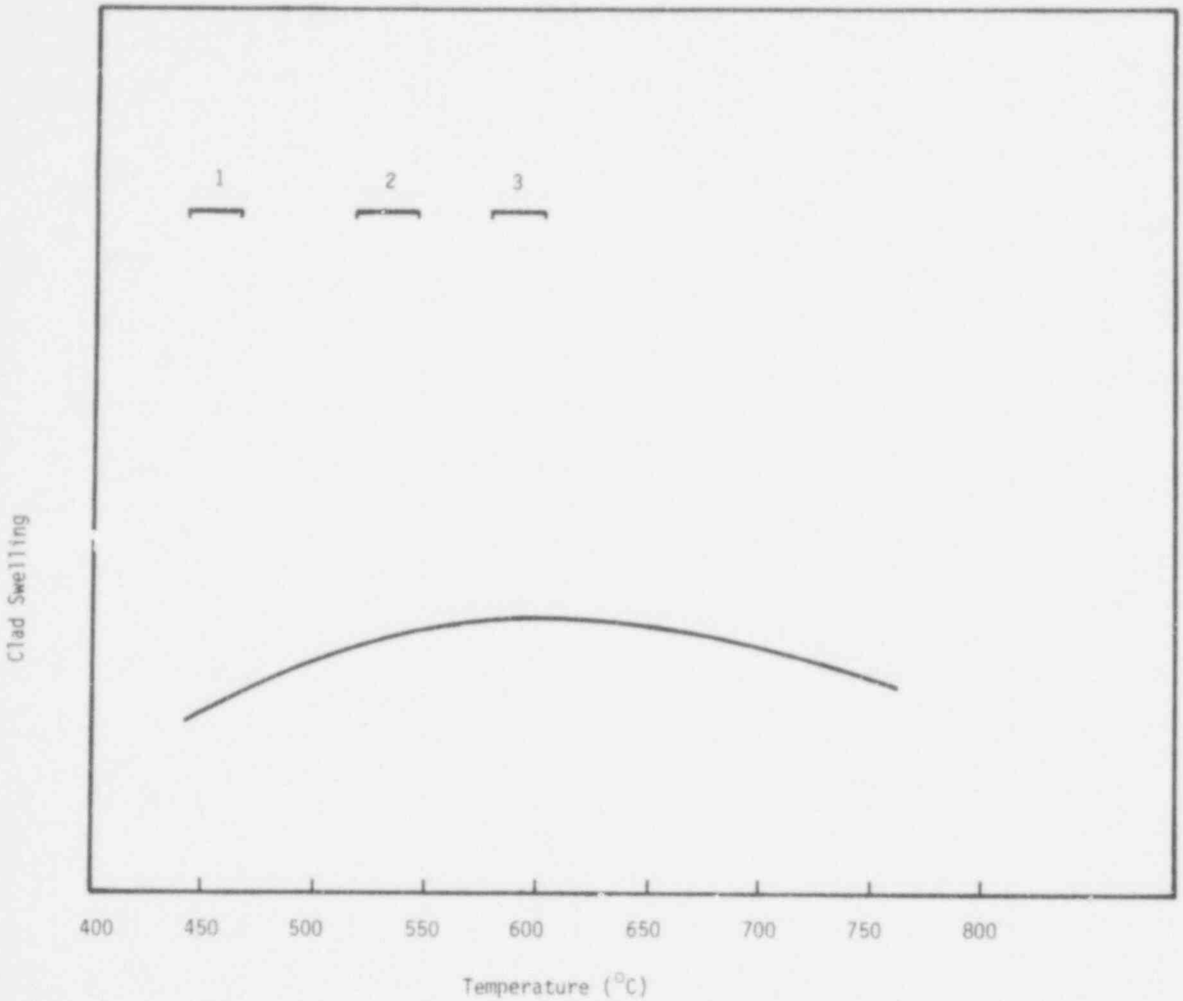


Figure A1.1 The Temperature Dependance of the Irradiation Swelling and the Temperature Range Across the Clad Wall ( Case A1-1 )

733 165

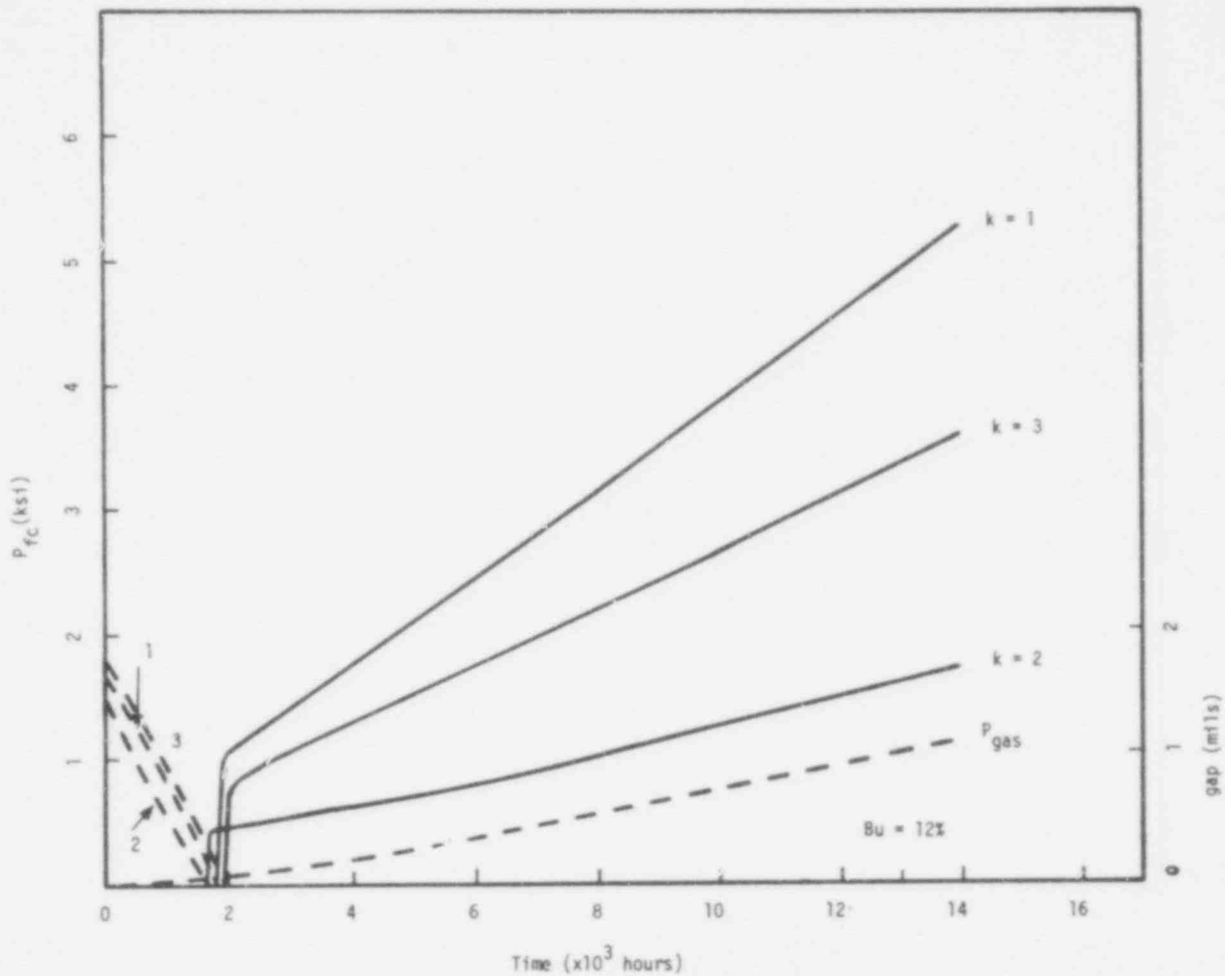


Figure A1 - 2 The Plenum Pressure ($P_{gas}$), The Gap Thickness and The Fuel-Clad Interaction Force in Each Axial Section. (Case A1)

733 166

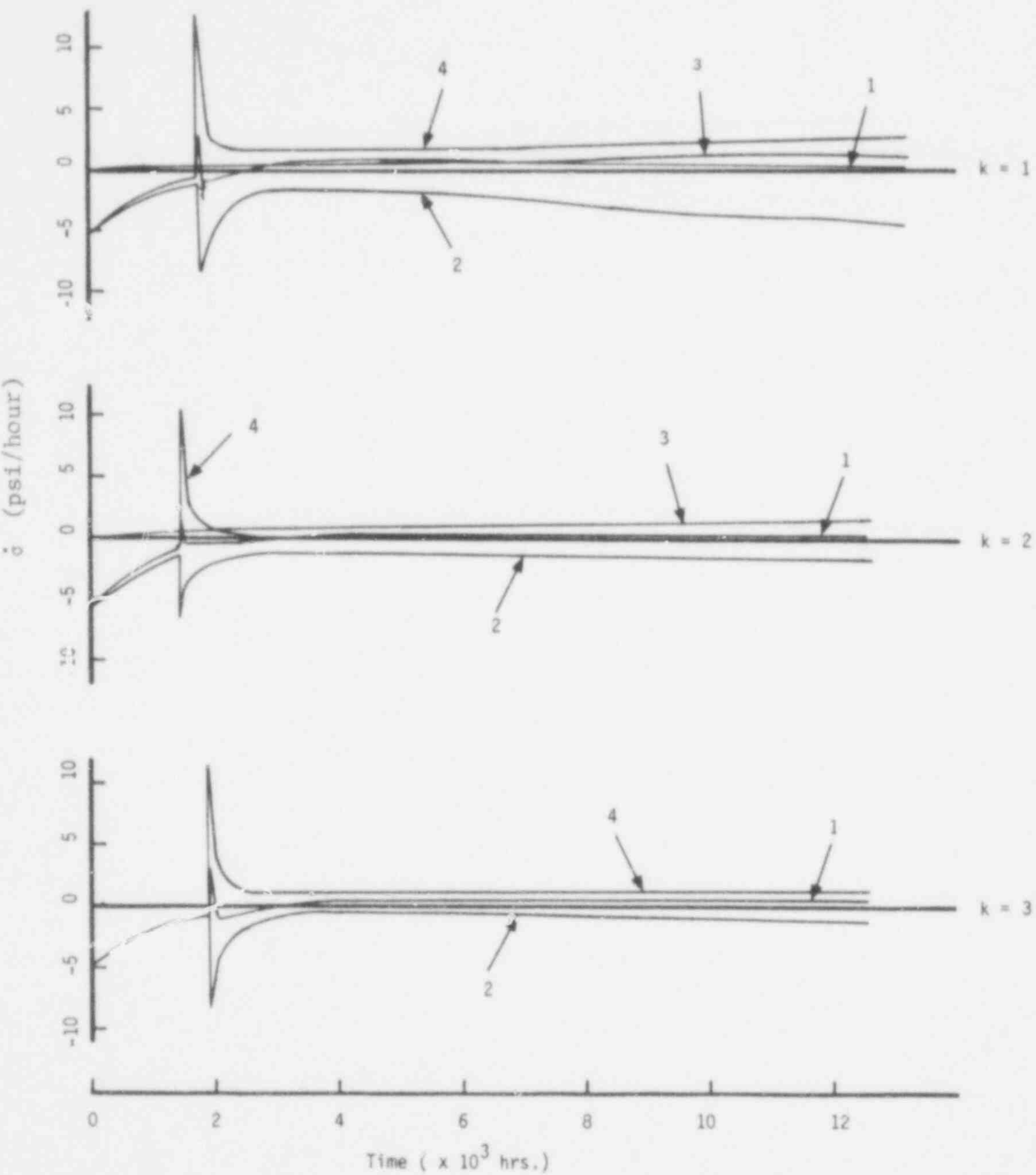


Fig. A1-3. The Net Hoop Stress Rate (1) and the Stress Rate at the Clad Outer Wall Due to the Creep (2), the Swelling (3), and the Pressure (4). (Case A-1)



733 167

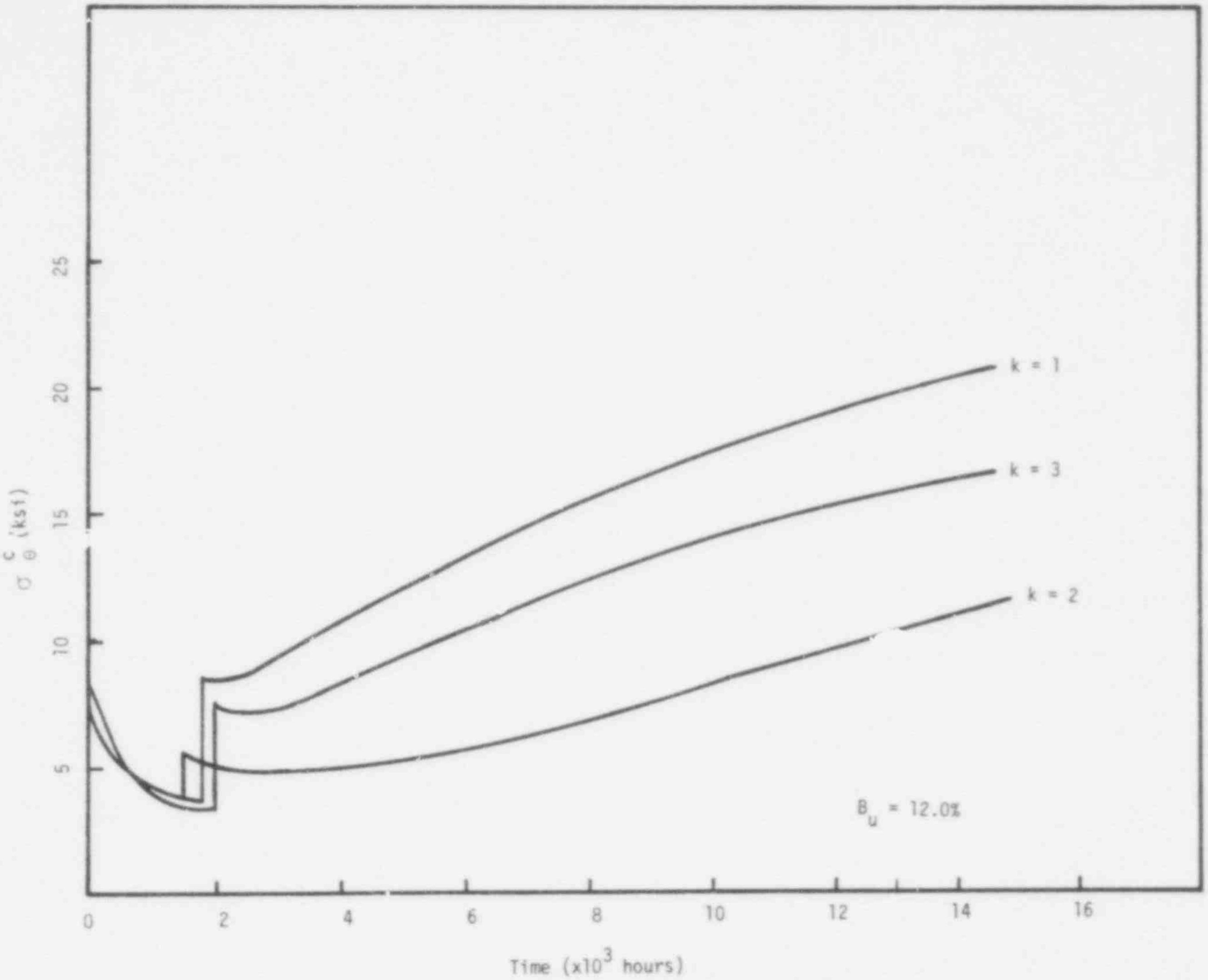


Figure A1-4 The Maximum Clad Hoop Stress in Each Axial Section.
(Case A1)

733 168

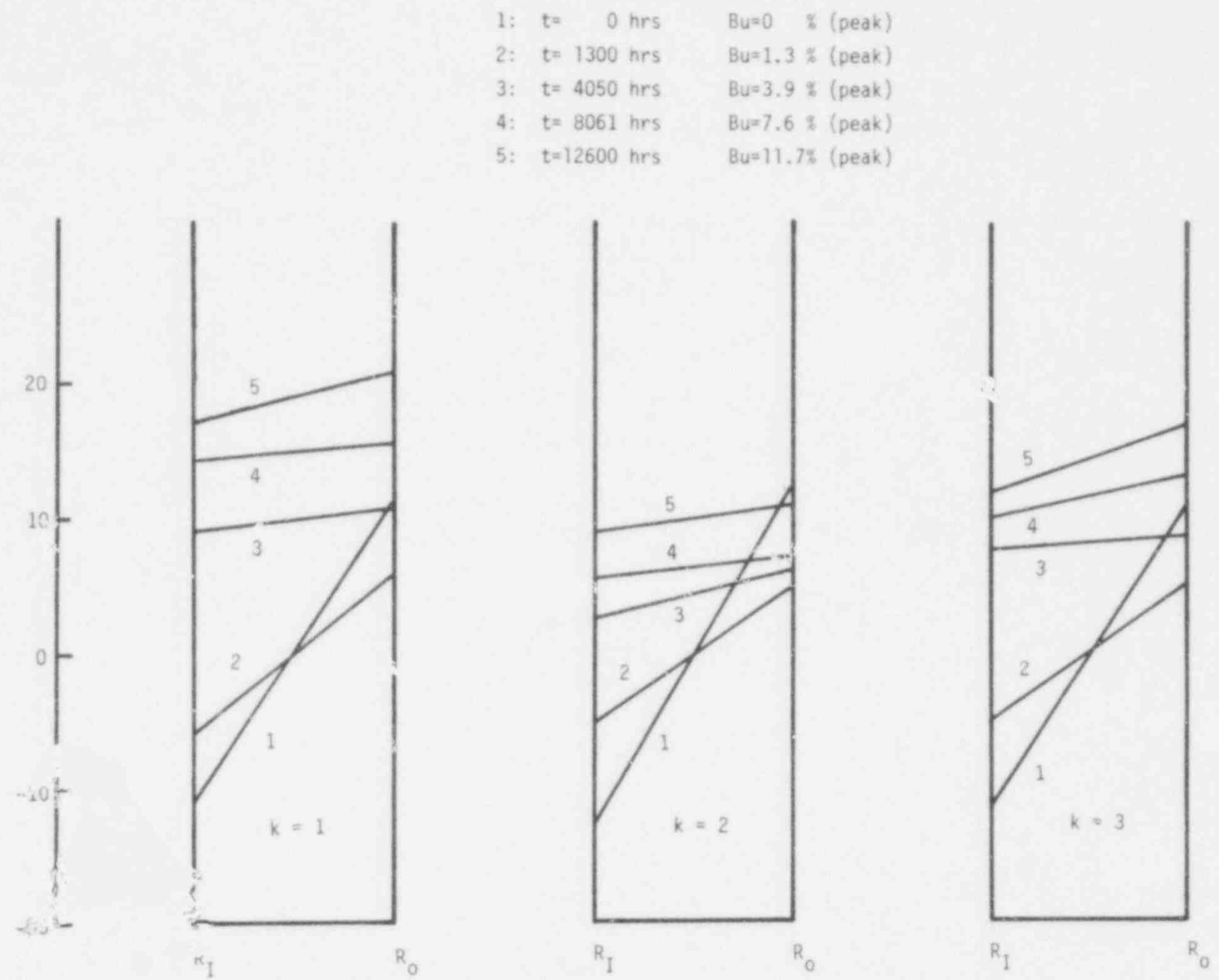


Figure A1-5. The Distribution of the Hoop Stress Across the Clad Wall.

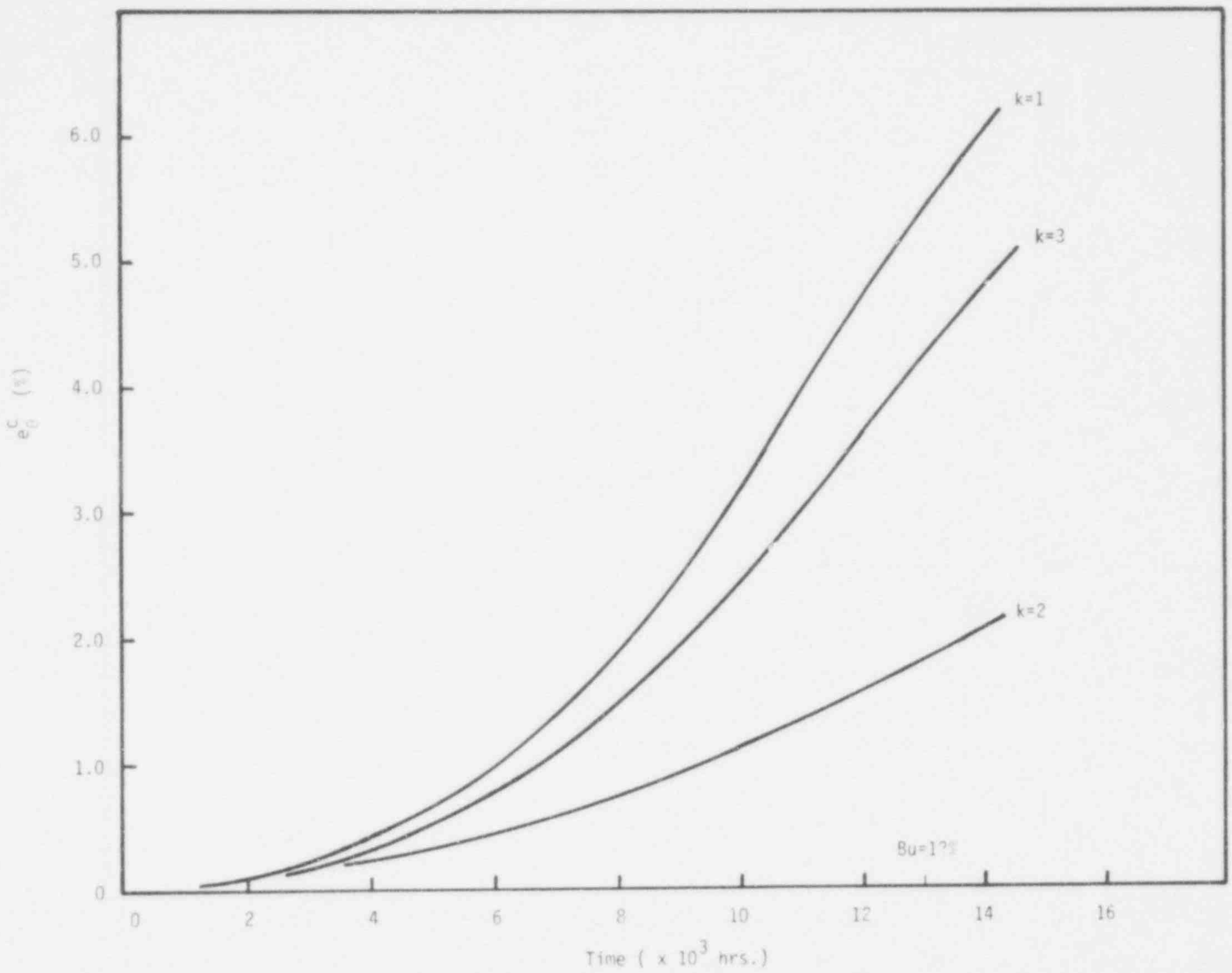


Fig. A1.6 The Hoop Strain in the Clad. (Case A1)

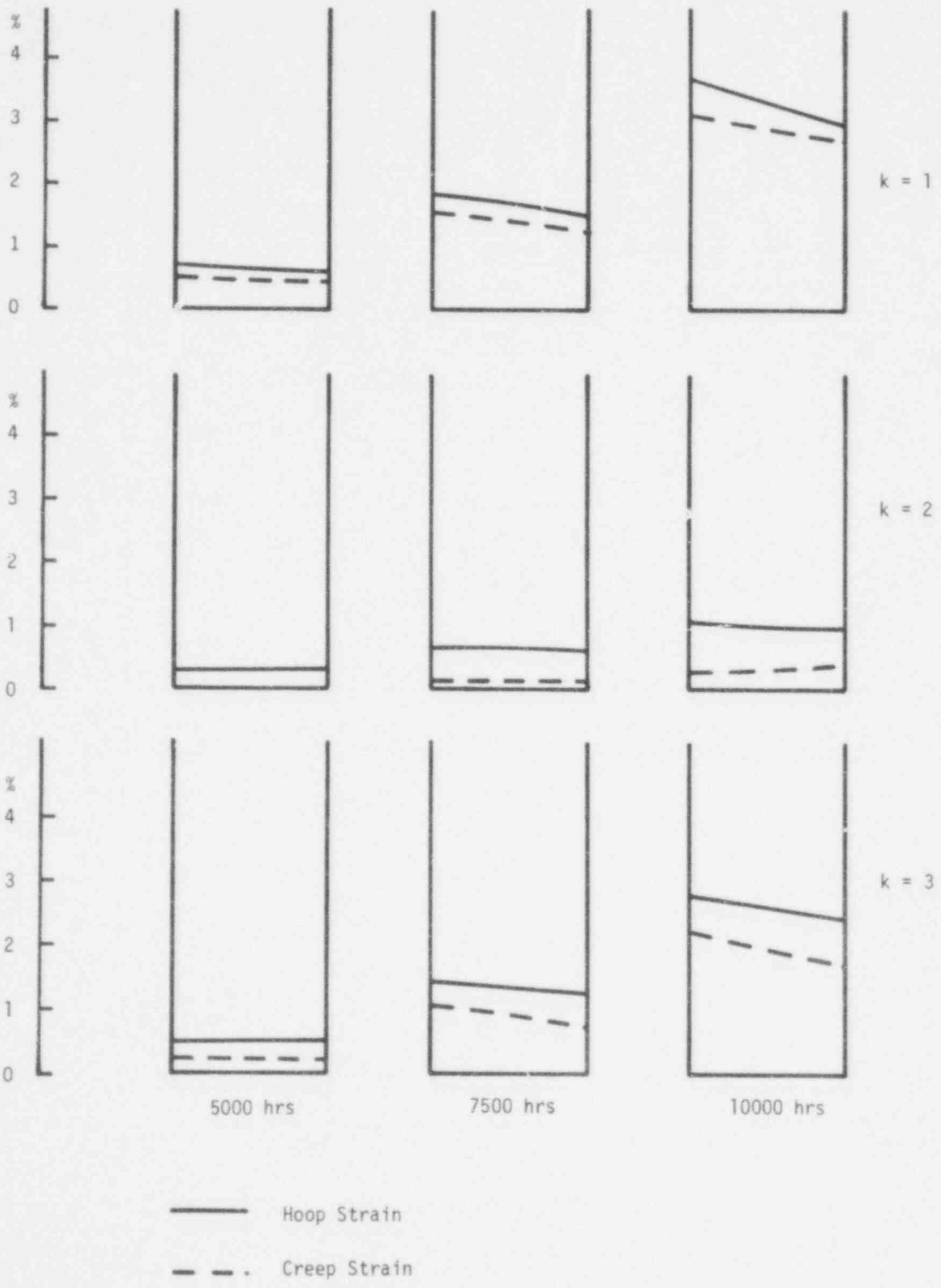


A1-7 The Distribution of the Total Hoop Strain and the Creep Strain Across the Clad Wall (Case A1)

733 171

12 kW/ft Cases

Case A3

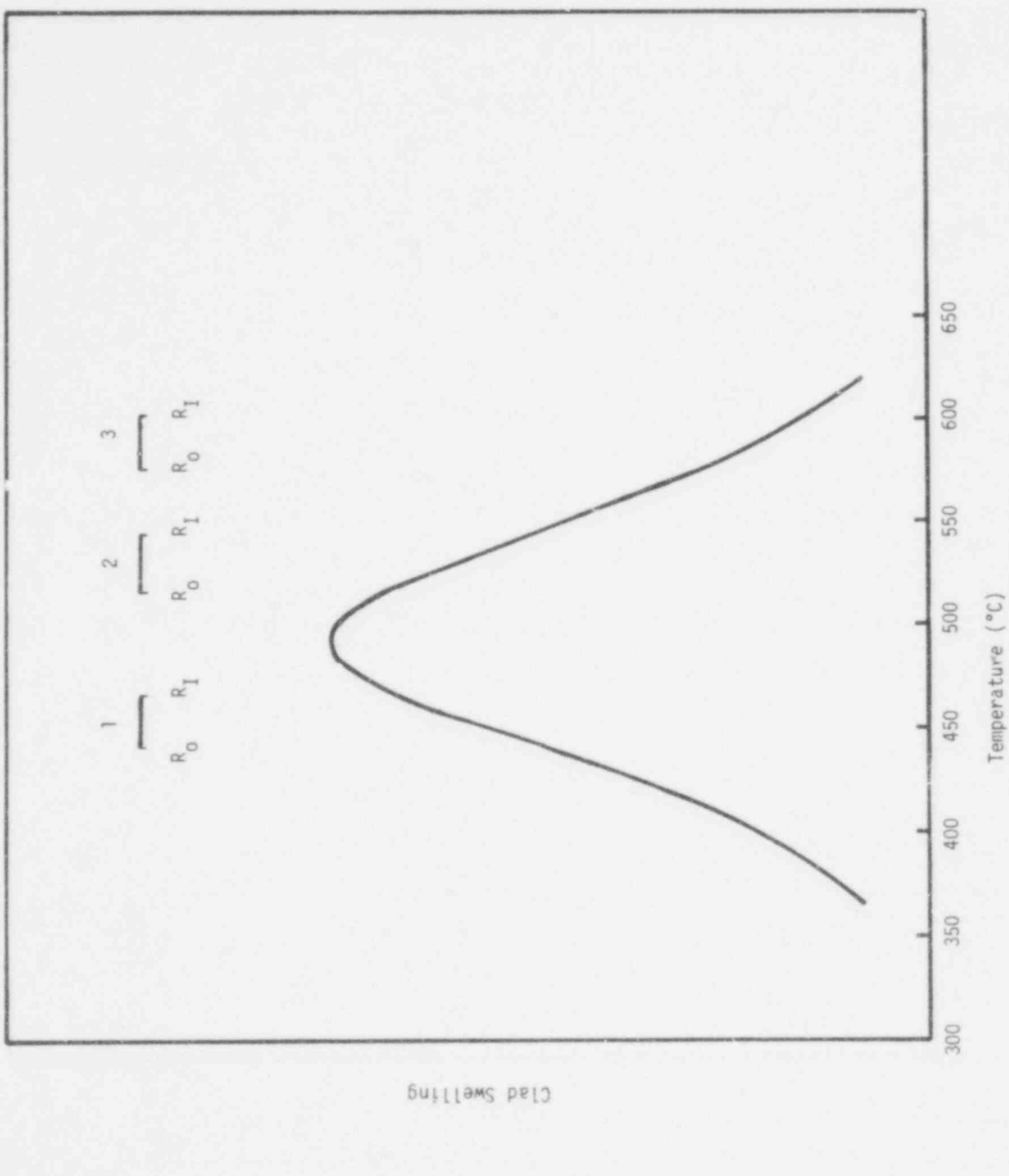


Figure A3-1 The Temperature of the Irradiated Swelling, and the Temperature Range Across the Clad Wall.

733 172

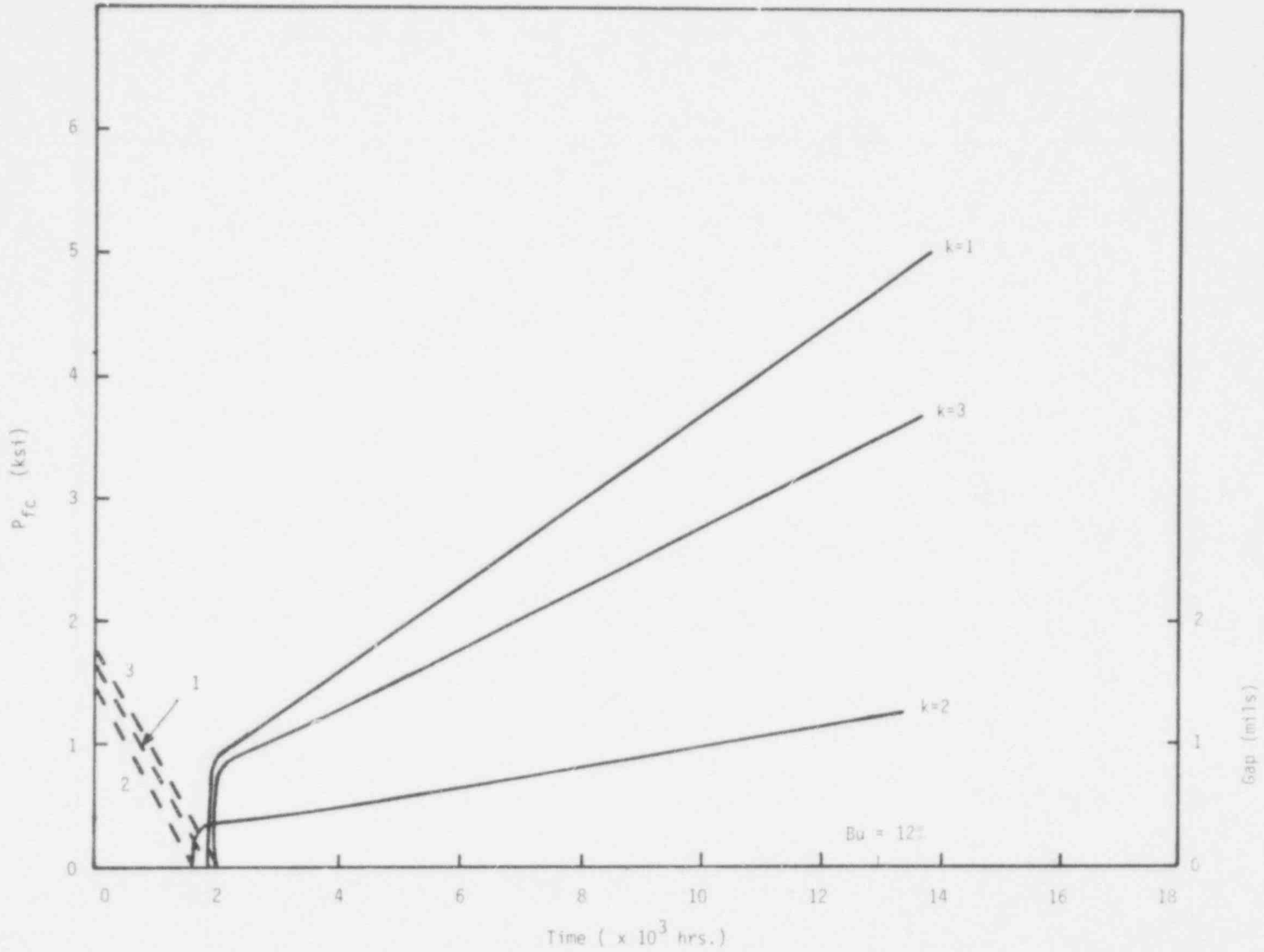


Fig. A3.2 The Fuel-Clad Gap Thickness and the Fuel-Clad Interaction Force. (Case A3)

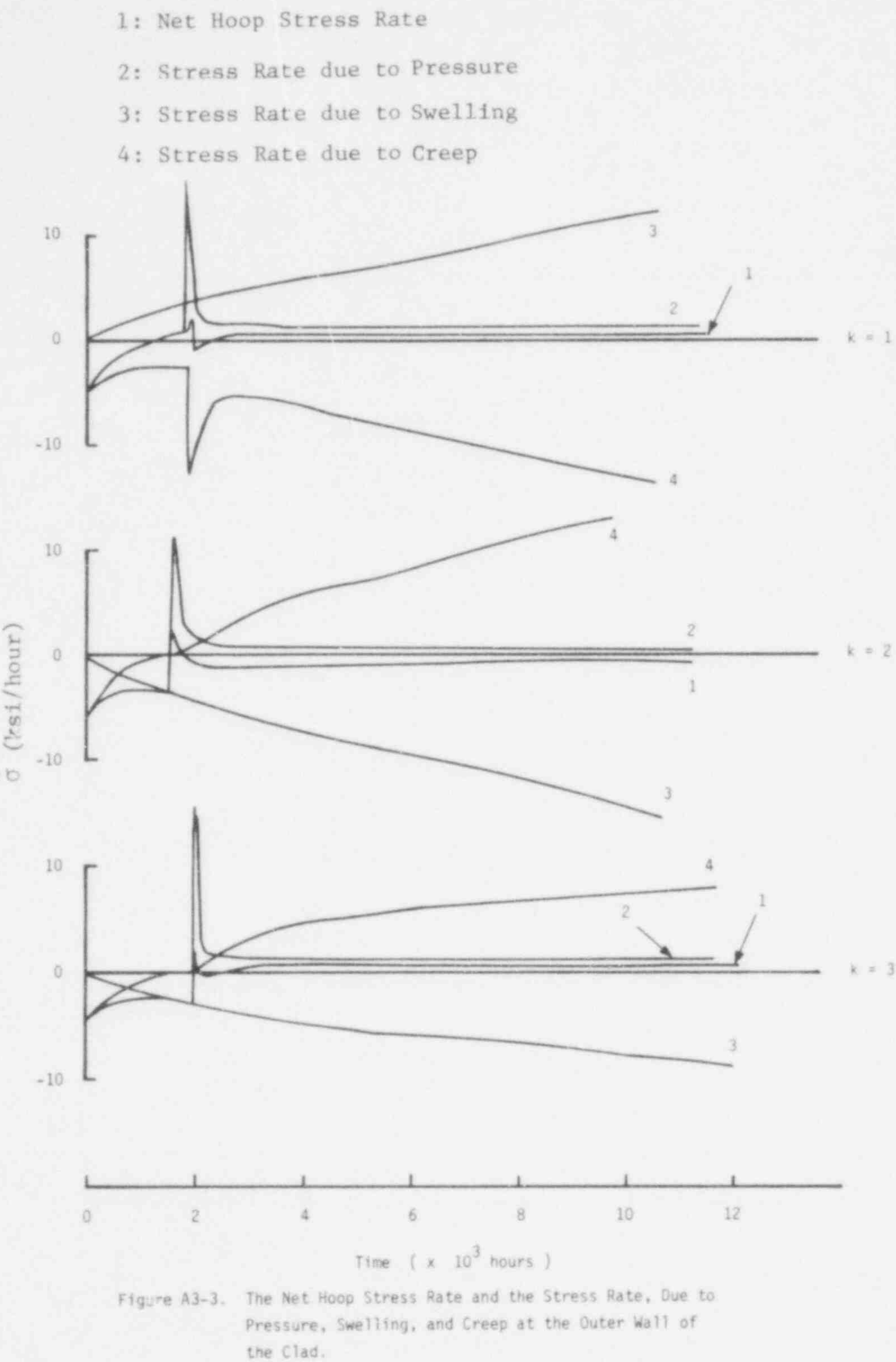


Figure A3-3. The Net Hoop Stress Rate and the Stress Rate, Due to Pressure, Swelling, and Creep at the Outer Wall of the Clad.

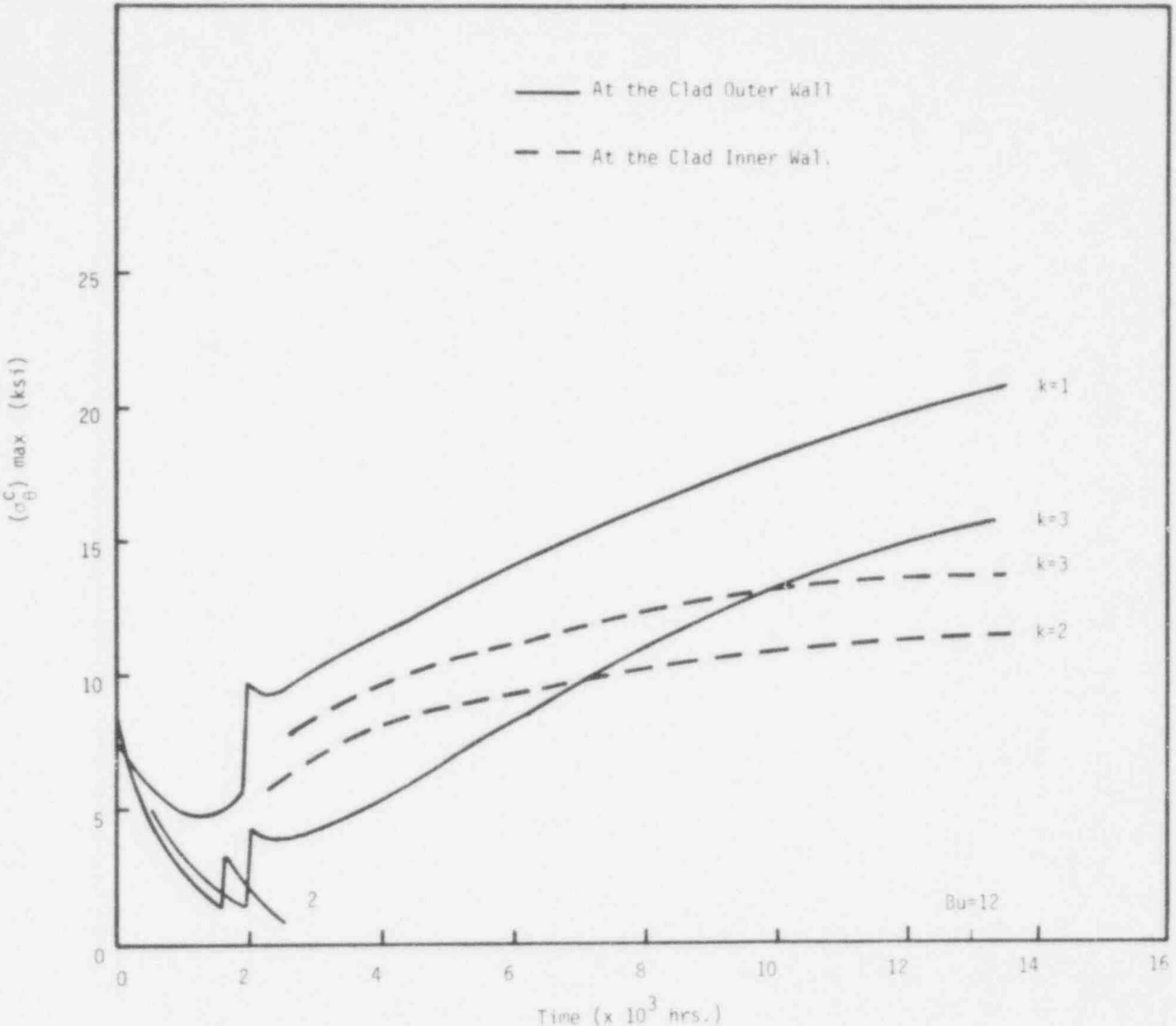


Fig. A3.4 The Maximium Hoop Stress in the Clad. (Case A3)

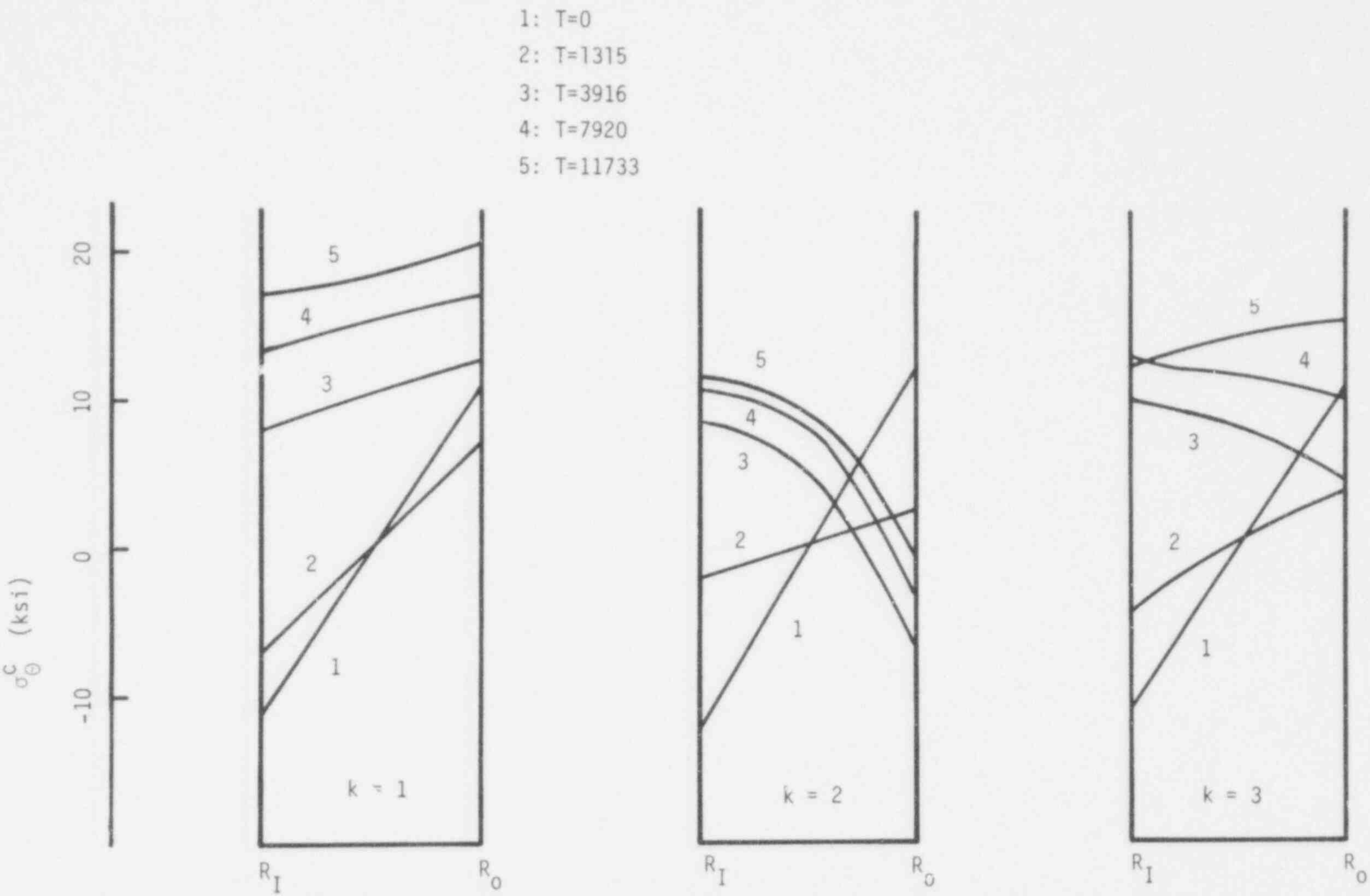


Figure A3-5. The Distribution of the Hoop Stress Across the Clad Wall

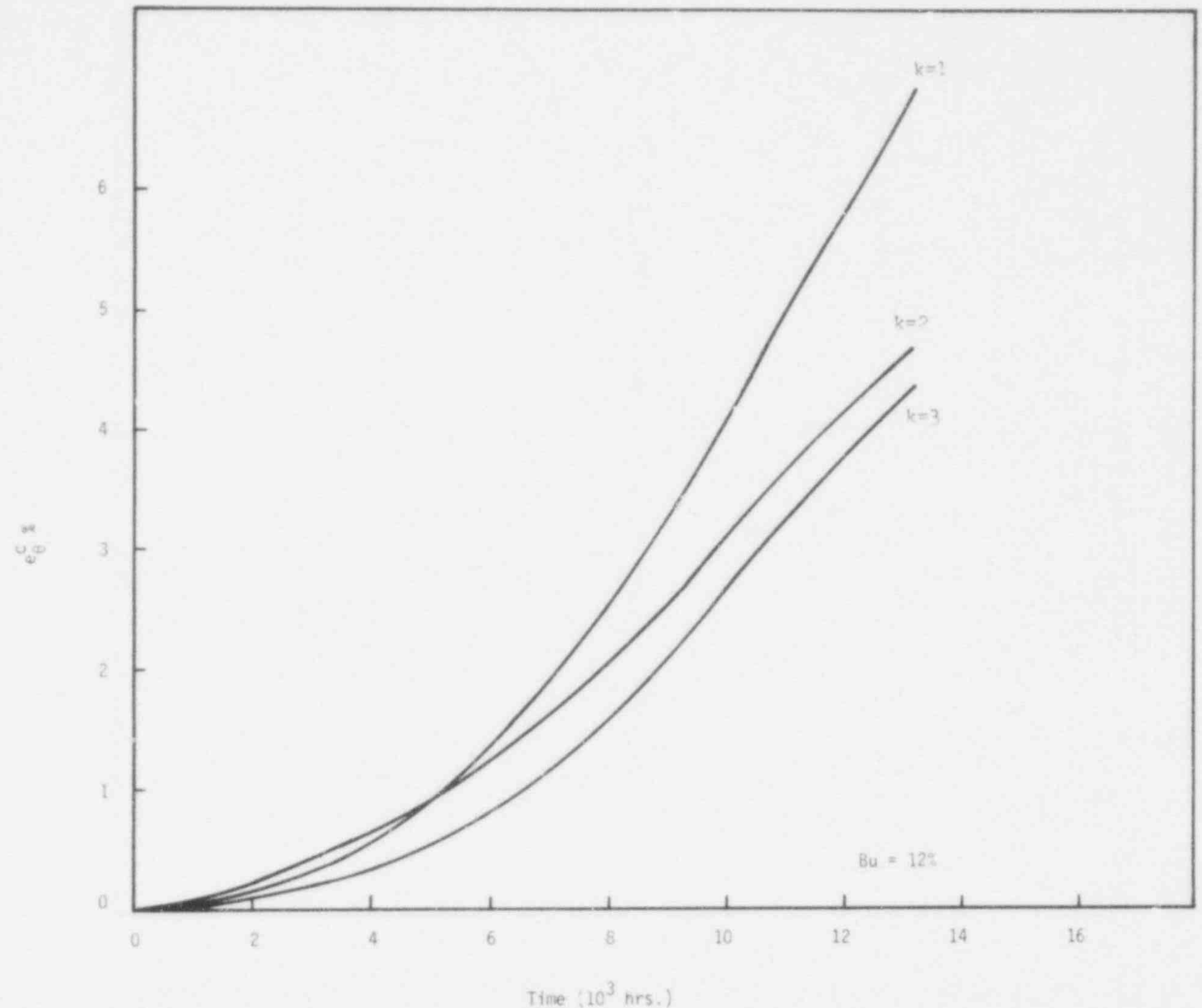


Fig. A3-6 The Hoop Strain in the Clad (Case A3)



733 17

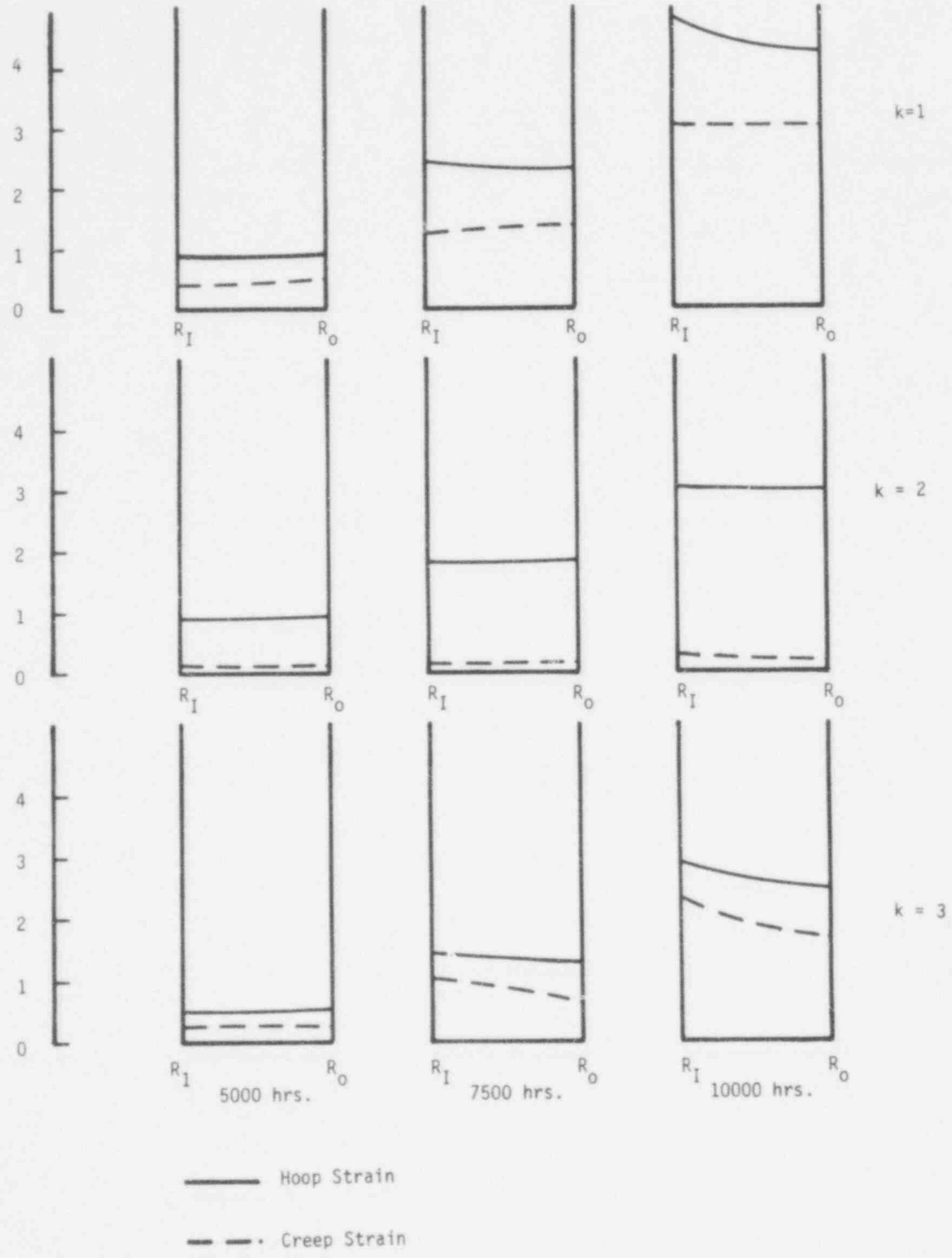


Figure A3 - 7. The Distribution of the Hoop Strain and the Creep Strain Across the Clad Wall.

12 kW/ft Cases

Case A4

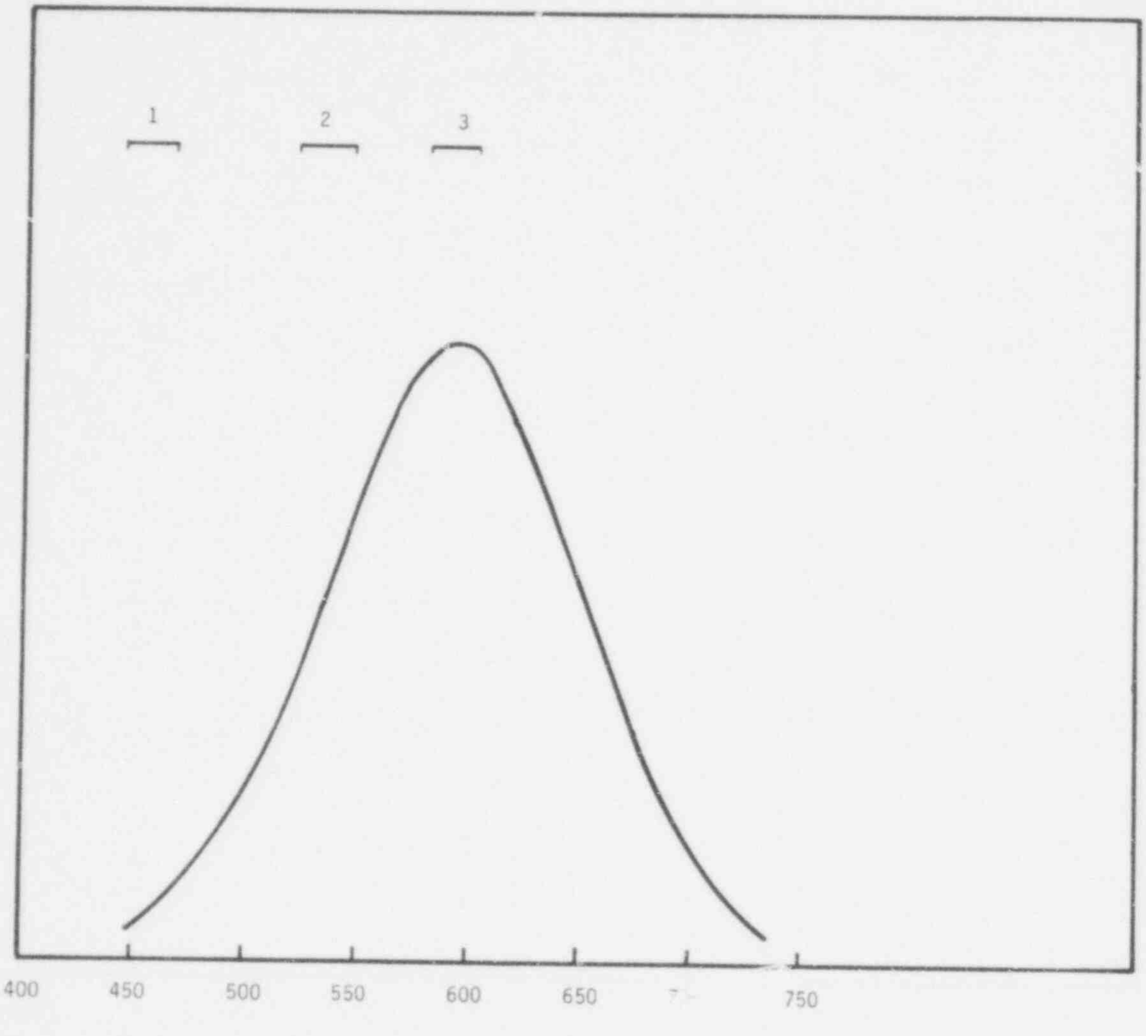


Fig. A4-1 The Temperature Dependence of the Irradiated Swelling and the Temperature Range Across the Clad Wall.

733 179

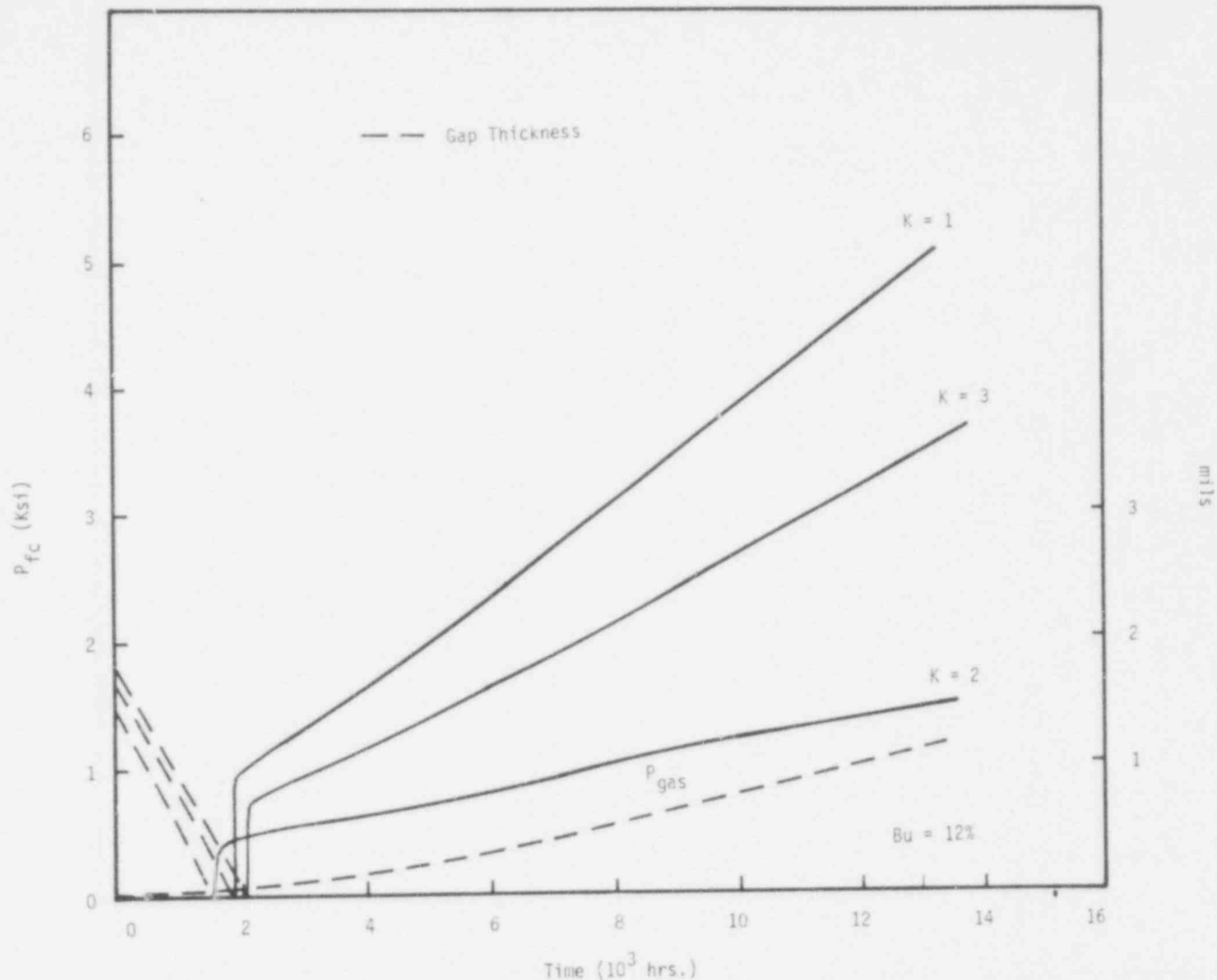


Fig. A4-2 The Fuel-Clad Interaction Force ($P_{fc}$), the Gap Thickness, and the Plenum Pressure in Each Axial Section (Case A4).

733 100

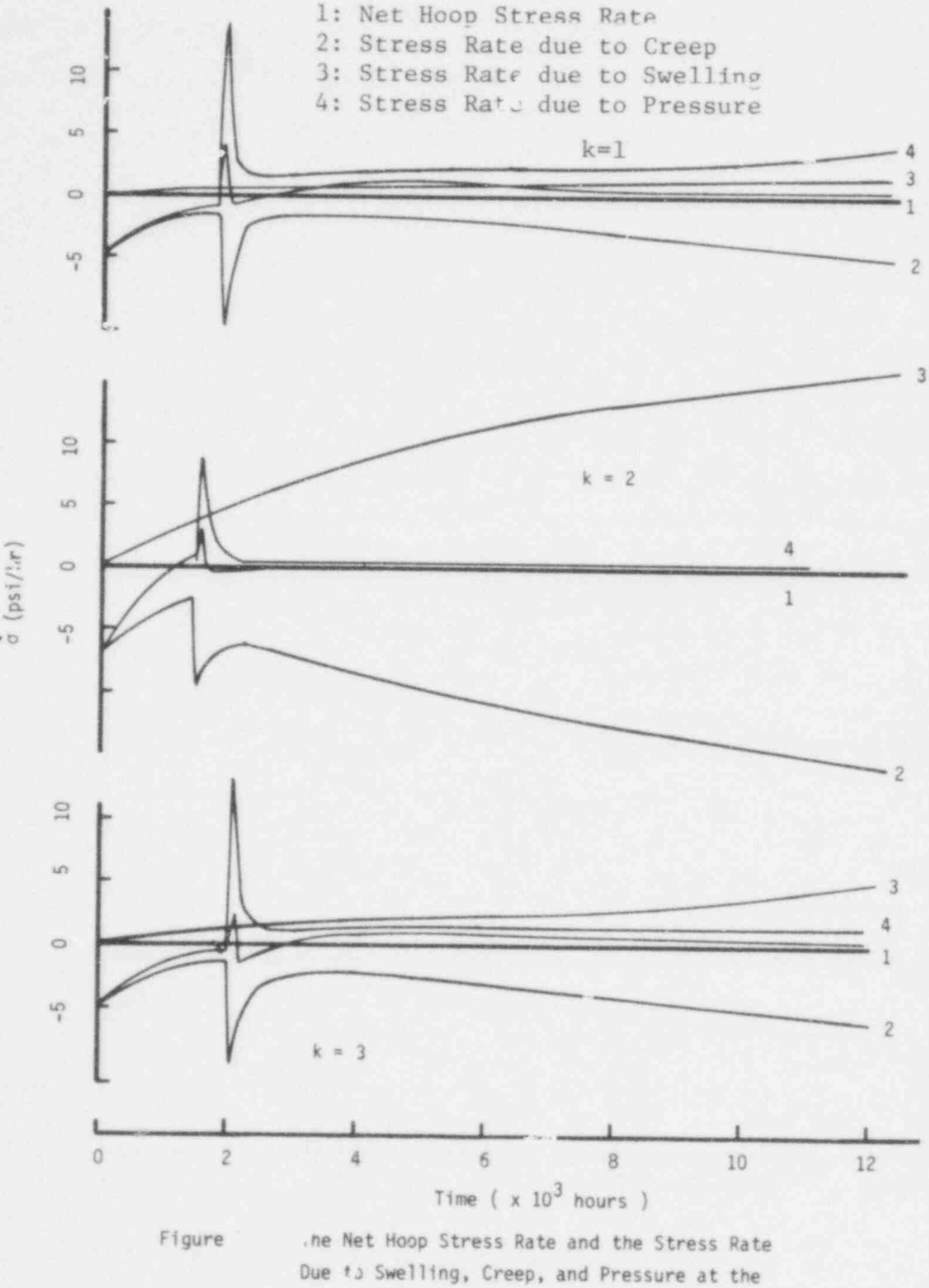


Figure .he Net Hoop Stress Rate and the Stress Rate Due to Swelling, Creep, and Pressure at the Clad Outer Wall.

733 181

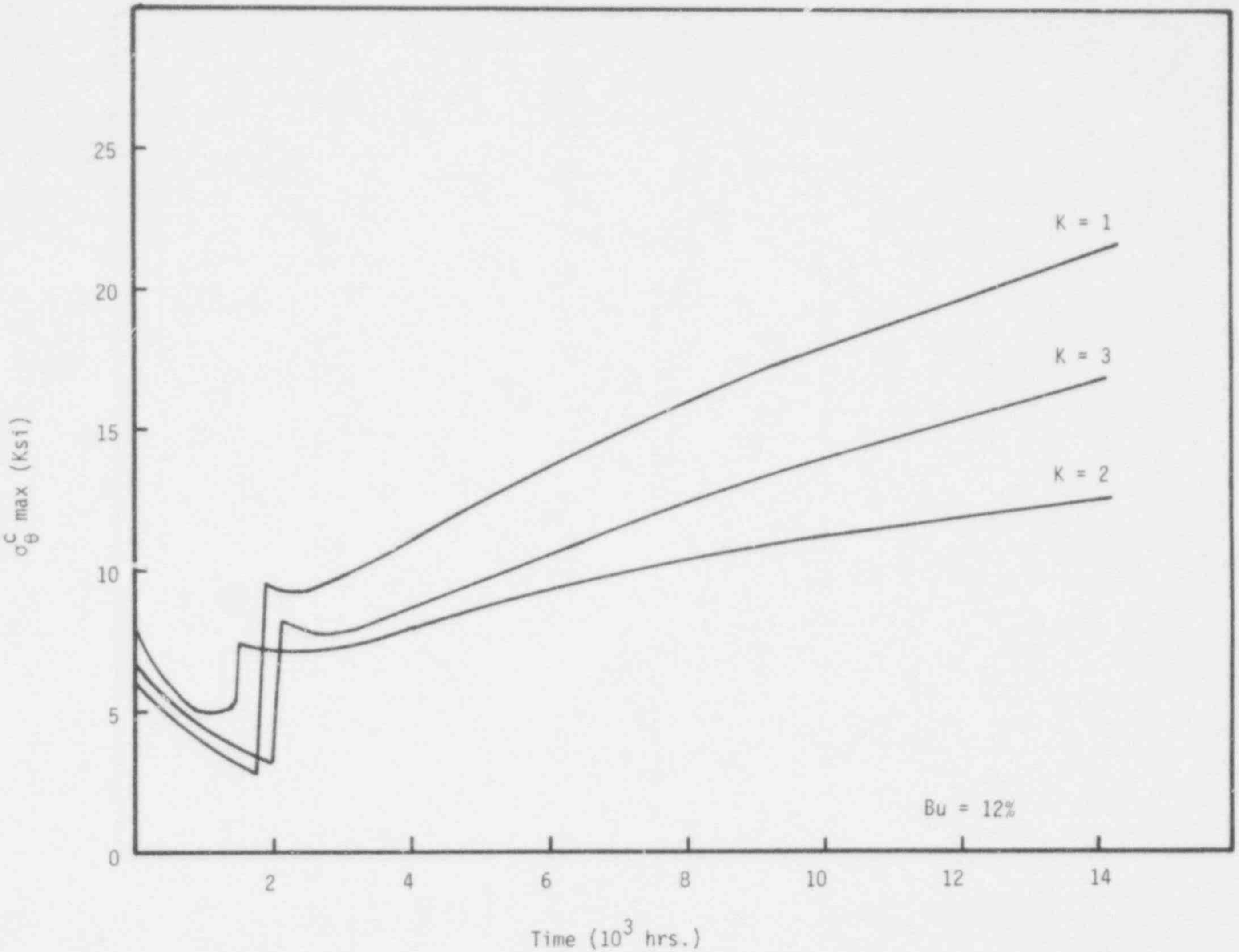


Fig. A4-4 The Maximum Hoop Stress in the Clad (Case A4).

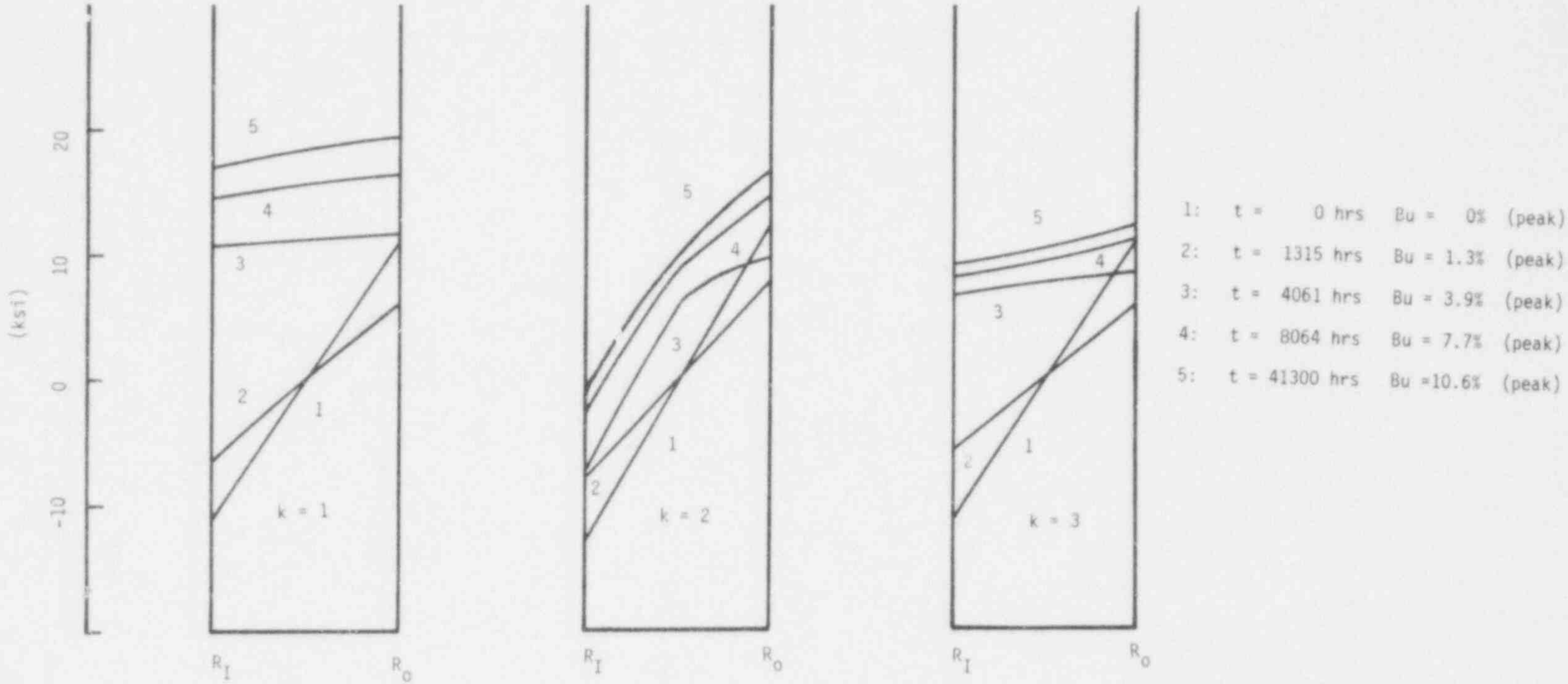


Figure A4-5. The Hoop Stress Distribution Across the Clad Wall.

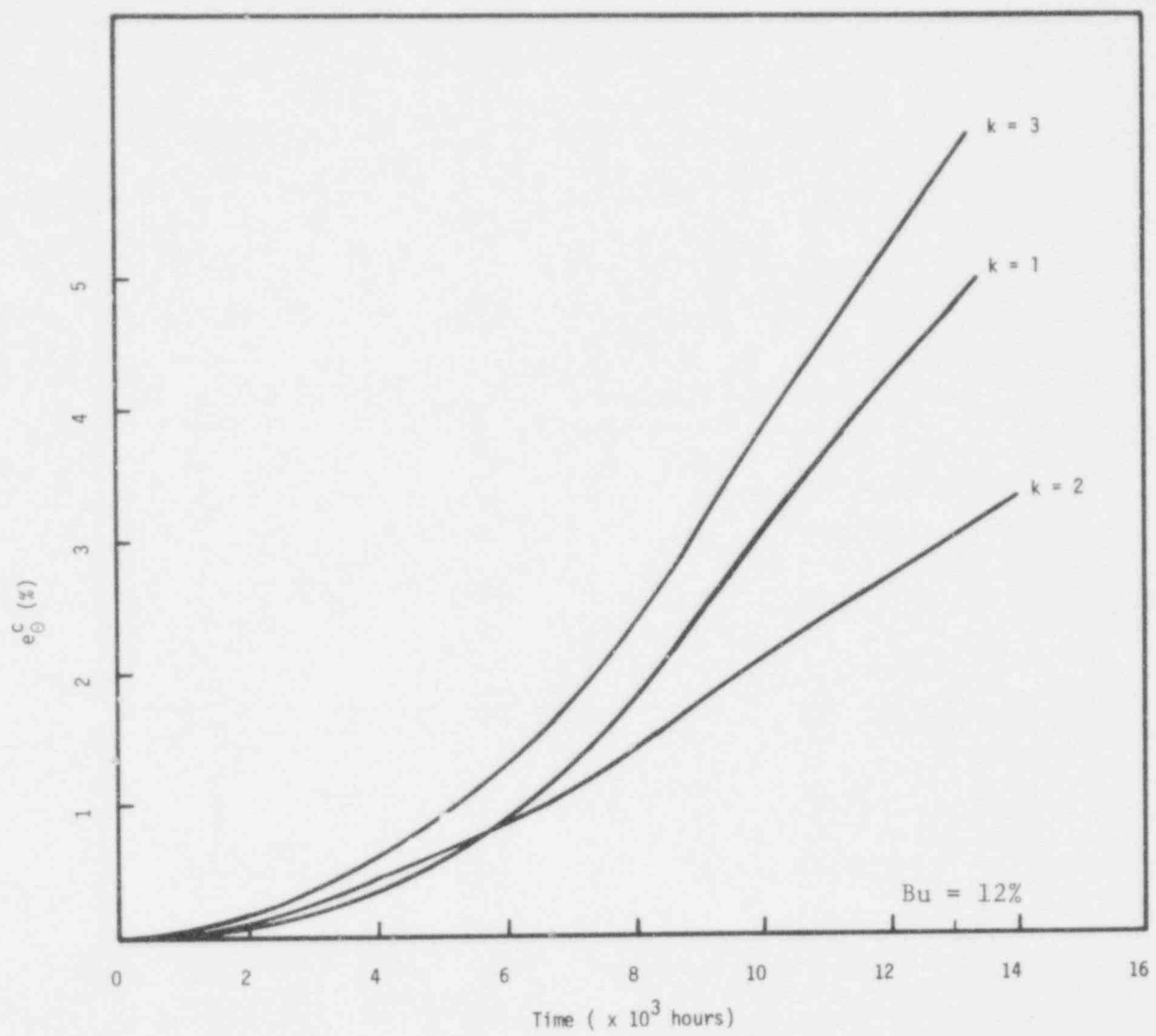


Figure A4 - 6. The Hoop Strain in the Clad. (Case A4)

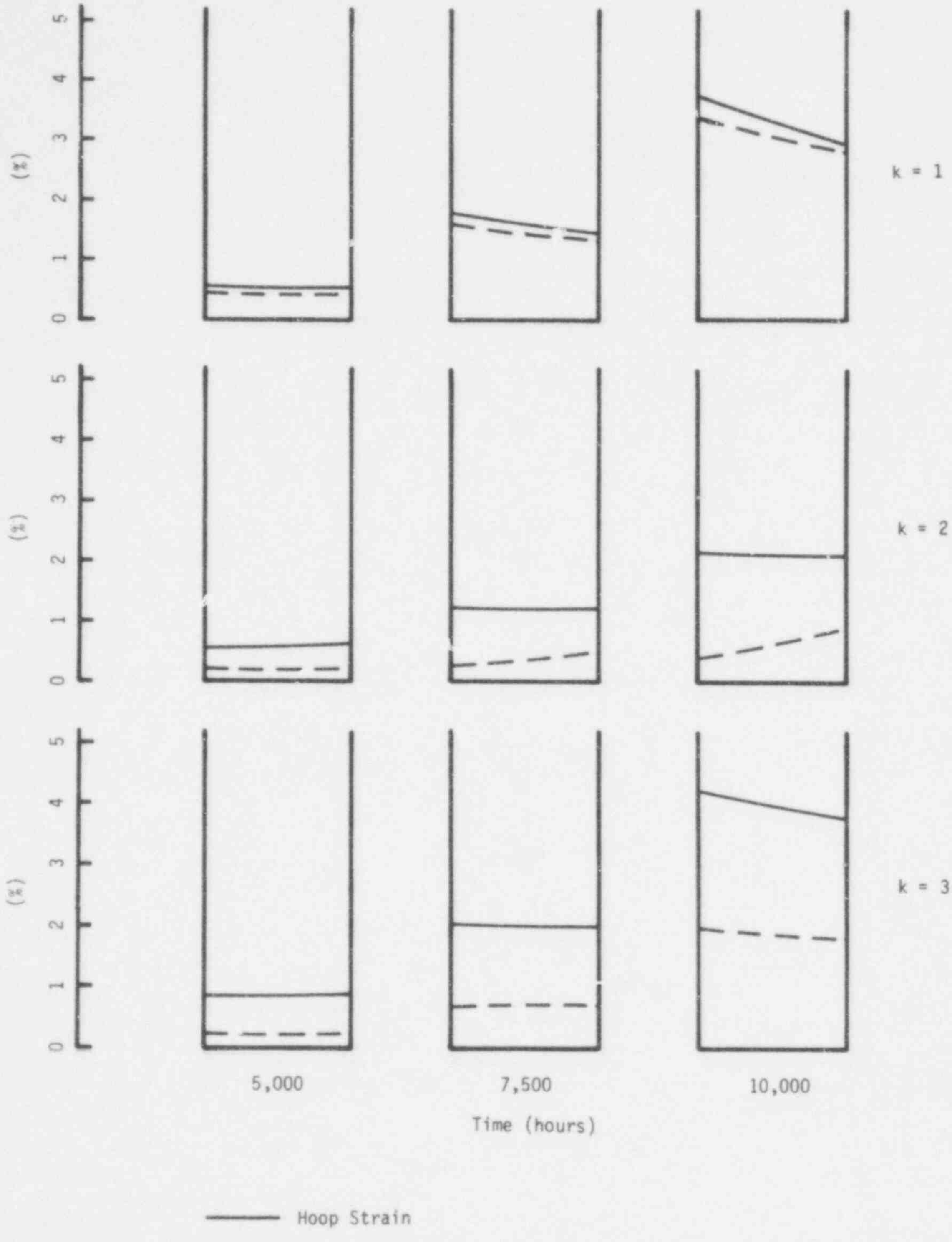


Figure A4 - 7. The Hoop Strain and the Creep Strain Across the Clad Wall. (Case A4)

733 195

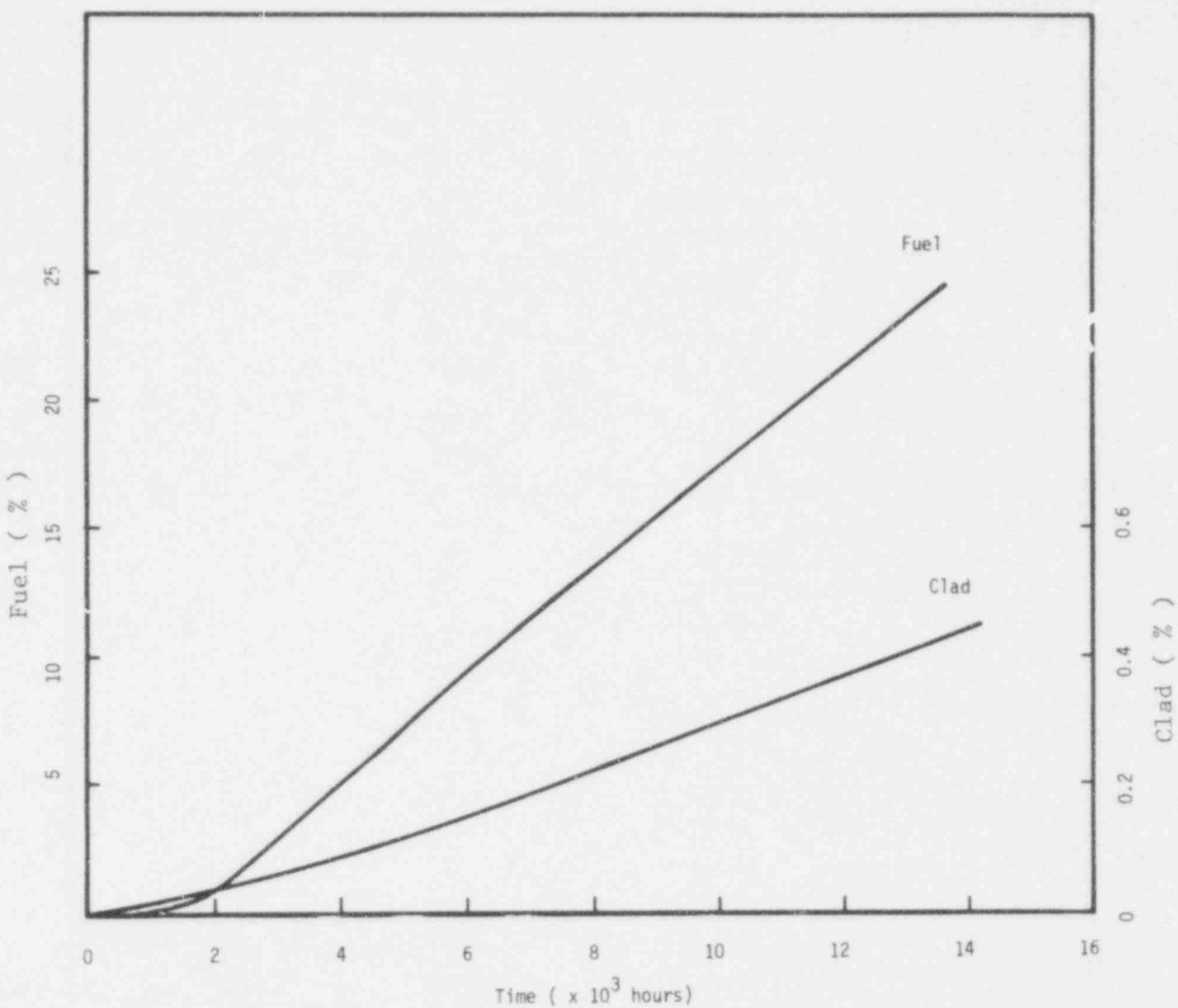


Figure A4 - 8. The Percentage of the Axial Displacement for the Fuel and the Clad (Case A4)

733 186

12 kW/ft Cases

Case R1

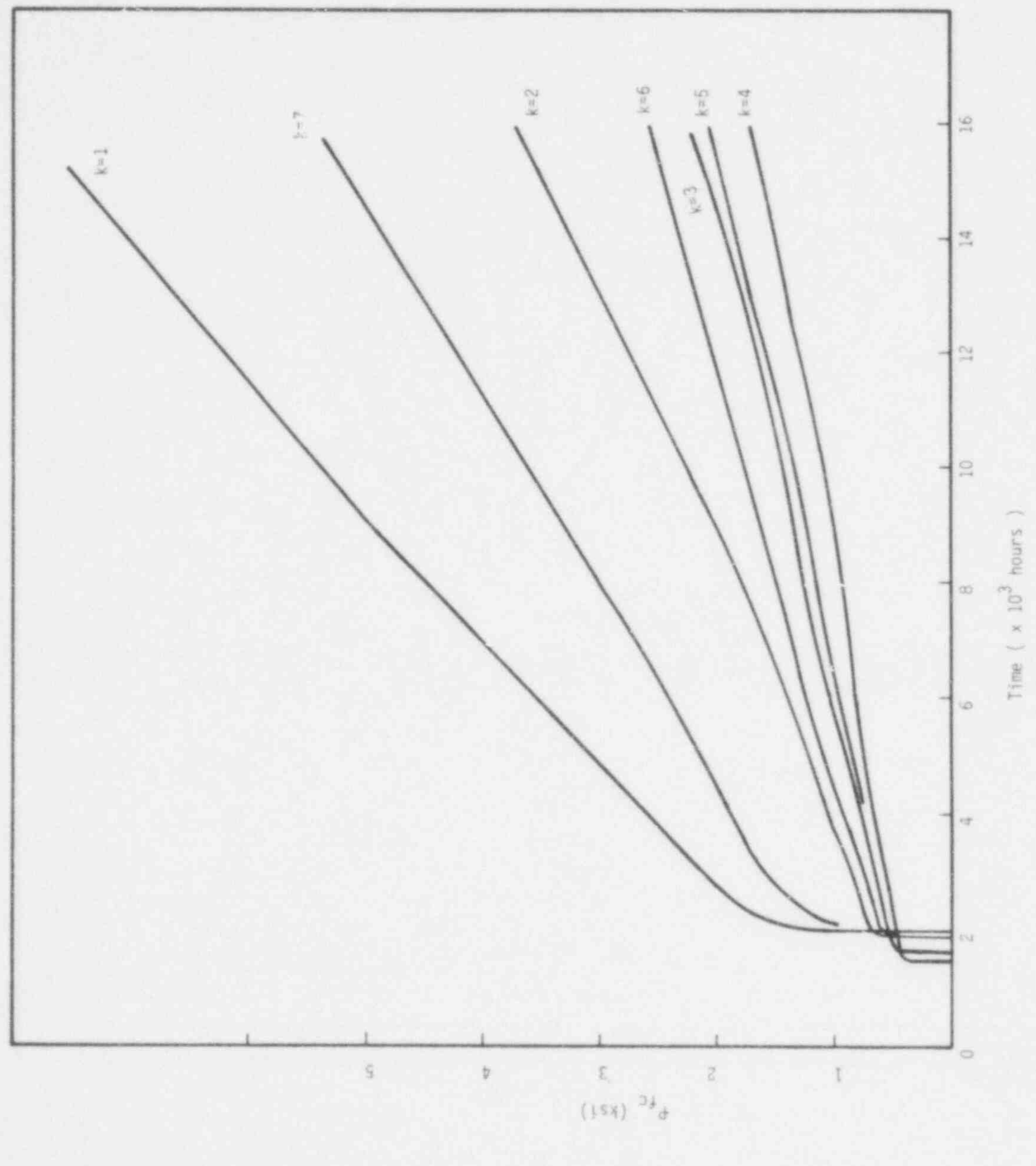


Figure R1 - 1. The Fuel-Clad Interaction Force.

133

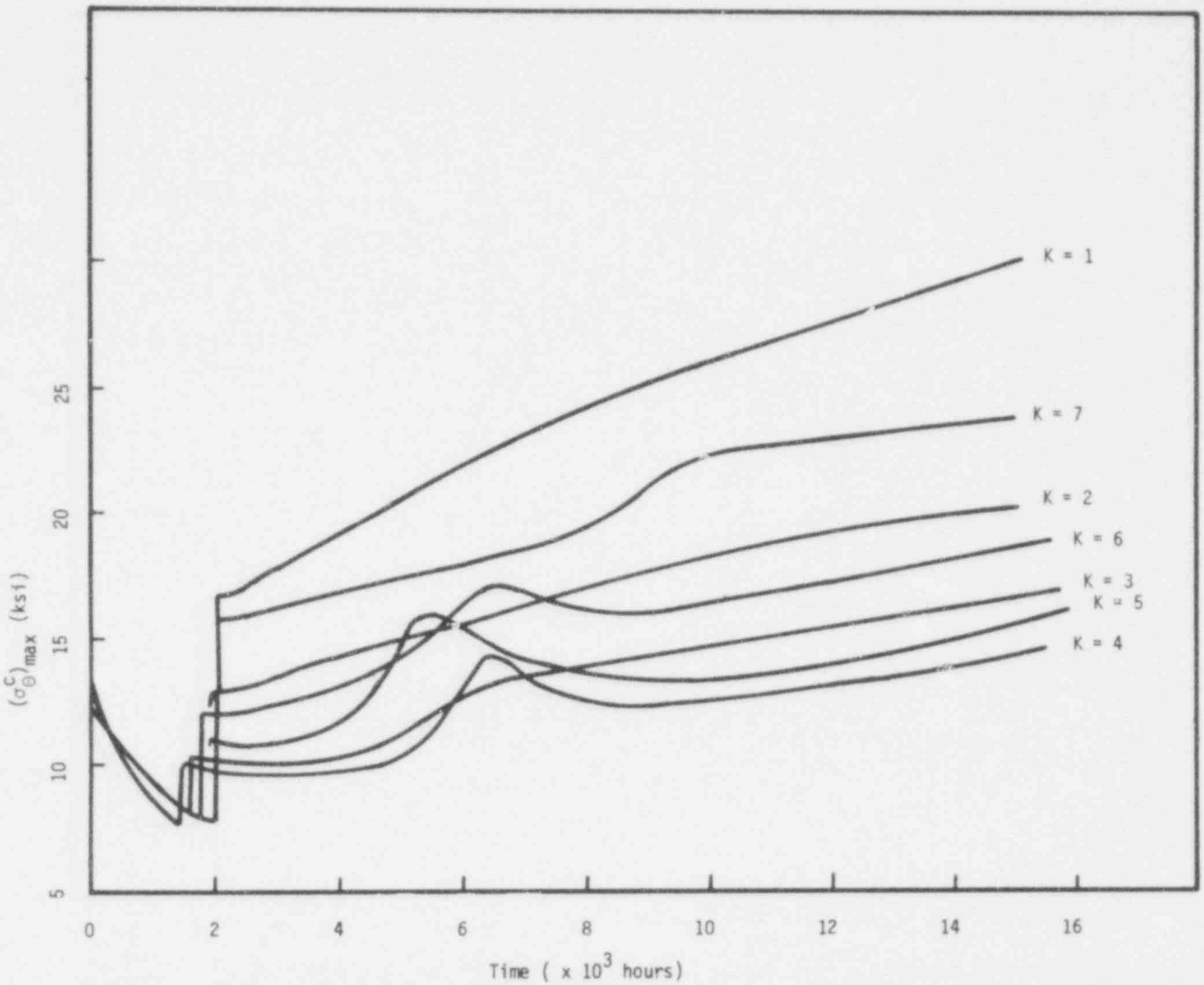


Figure R1 - 2. The Maximum Hoop Stress in the Clad. (Case R1)

733 188

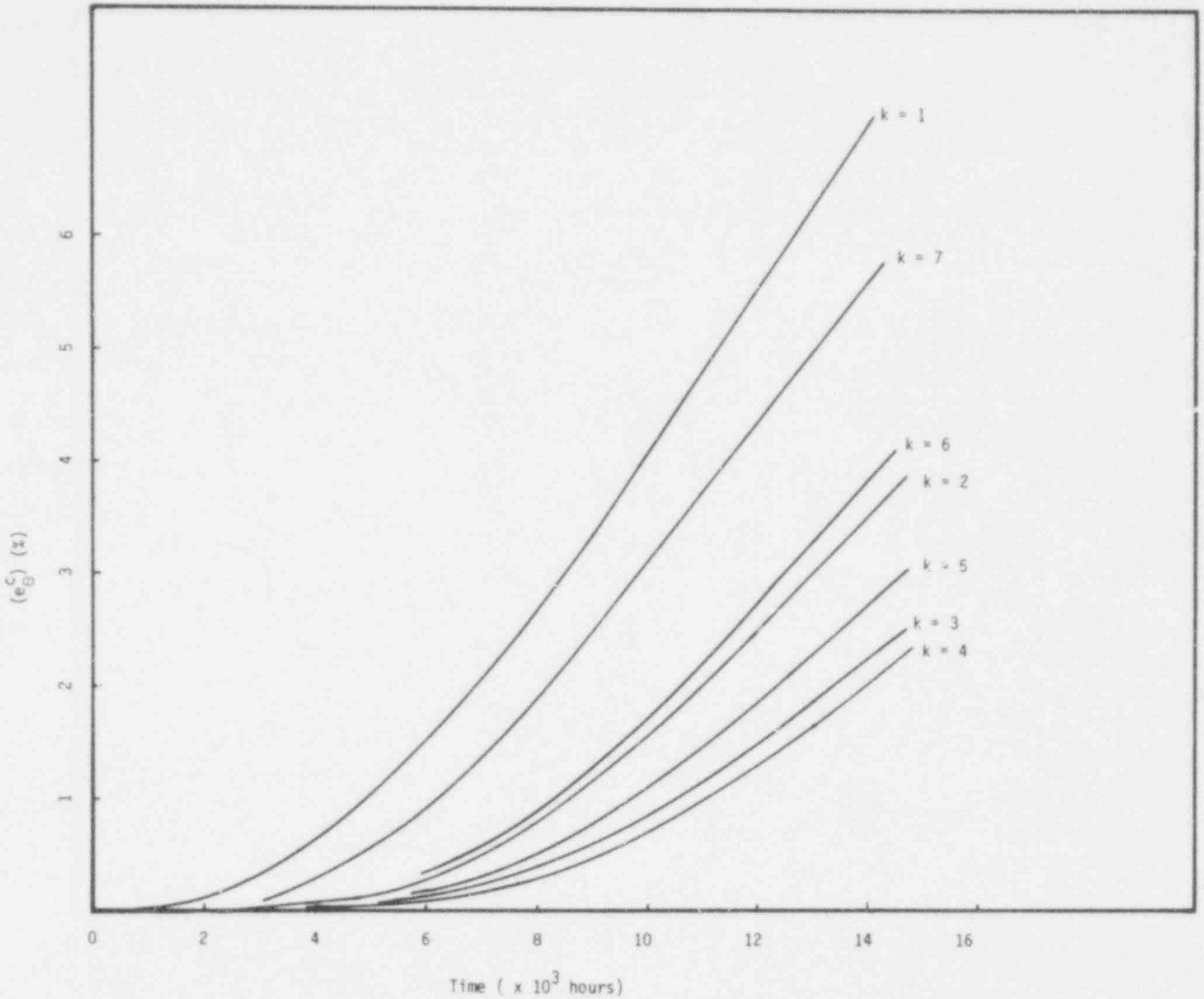


Figure R1 - 3. The Hoop Strain in the Clad. (Case R1)



733 189

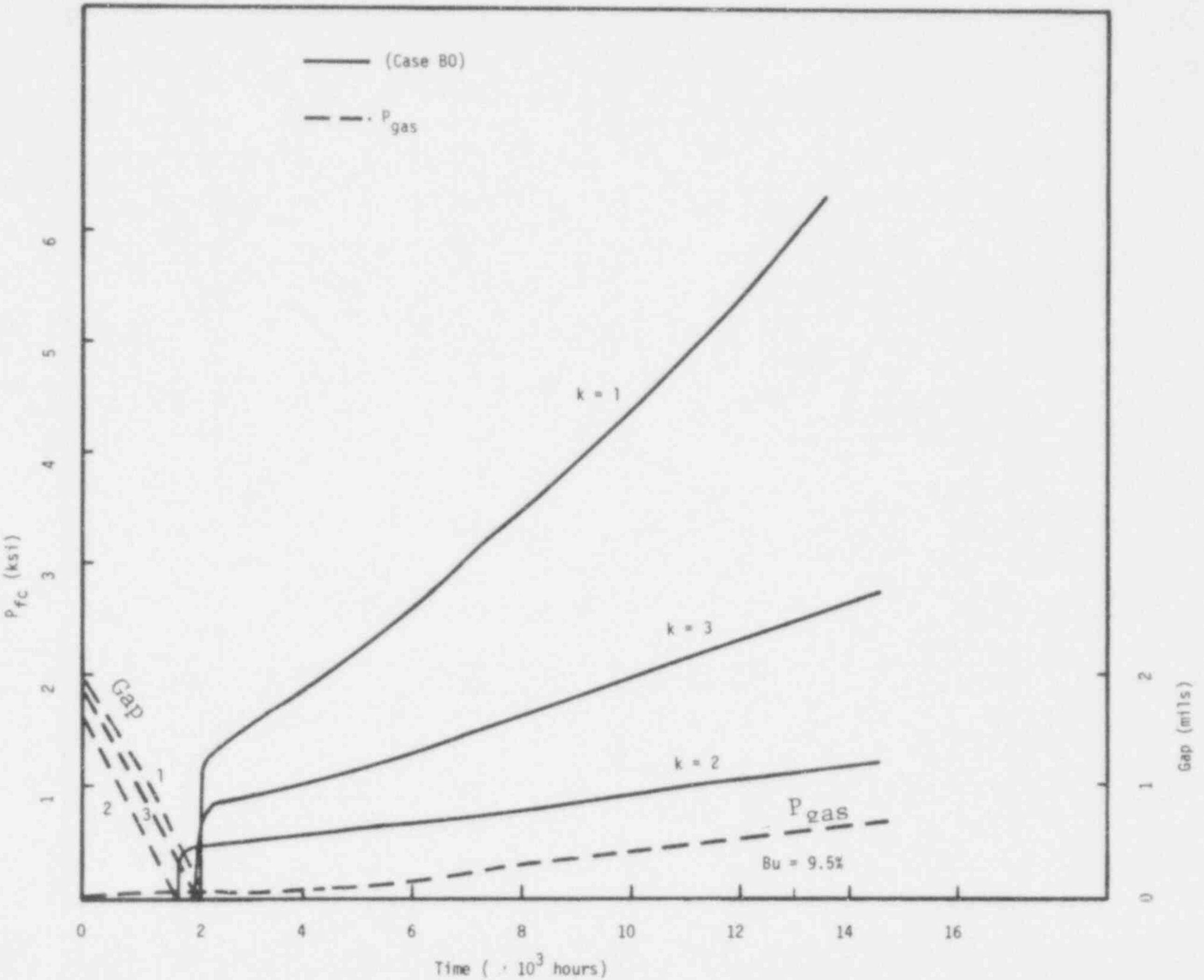


Figure B0 - 1. The Fuel-Clad Interaction Forcc, the Gap Thickness, and the Plenum Pressure in Each Axial Section (Case B0)



733 100

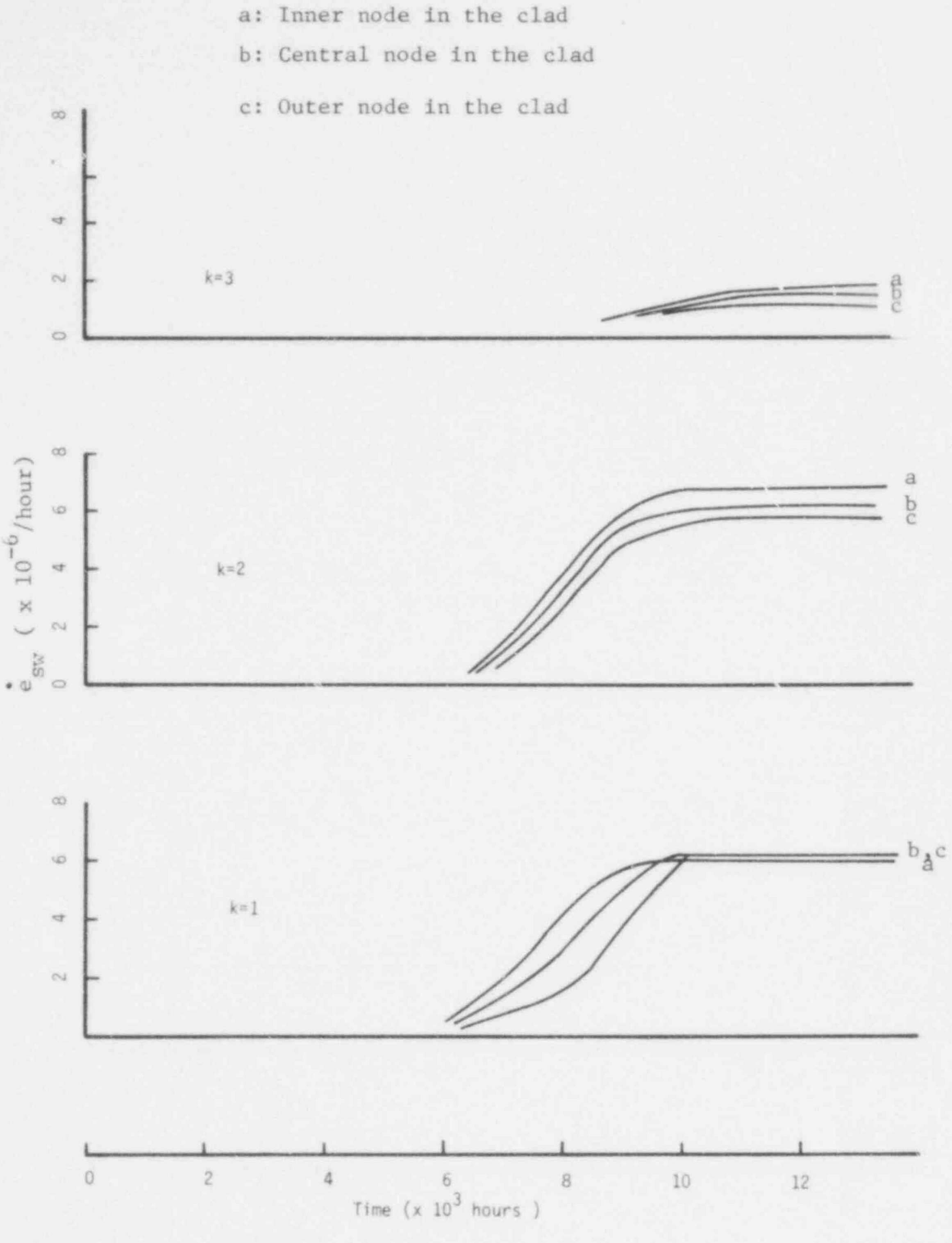


Figure BO - 2. The Swelling Rate Across the Clad Wall.

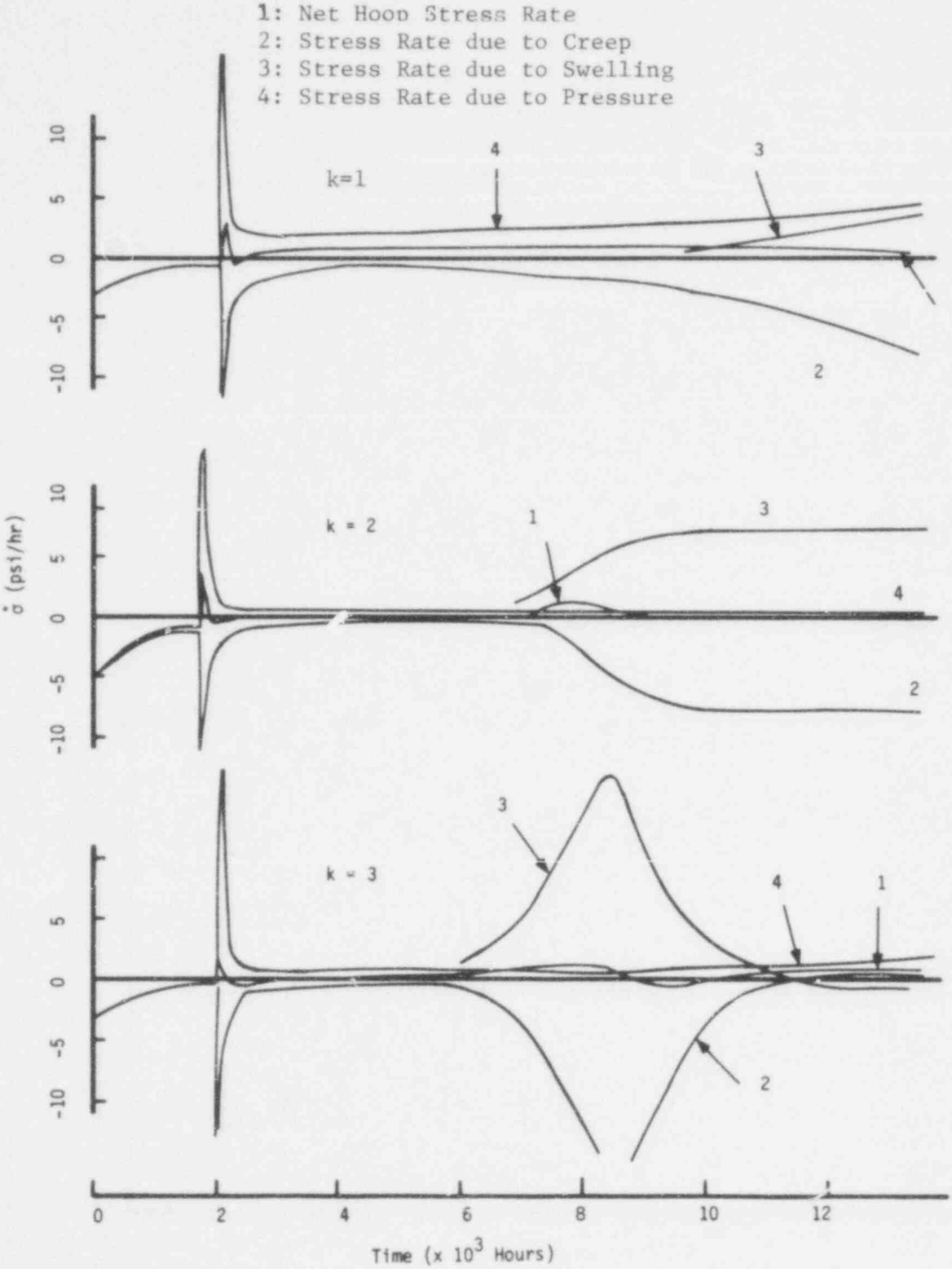


Figure BO-3. The Net Hoop Stress Rate and the Stress Due to Pressure, Creep, and Swelling at the Clad Outer Wall.

733 192

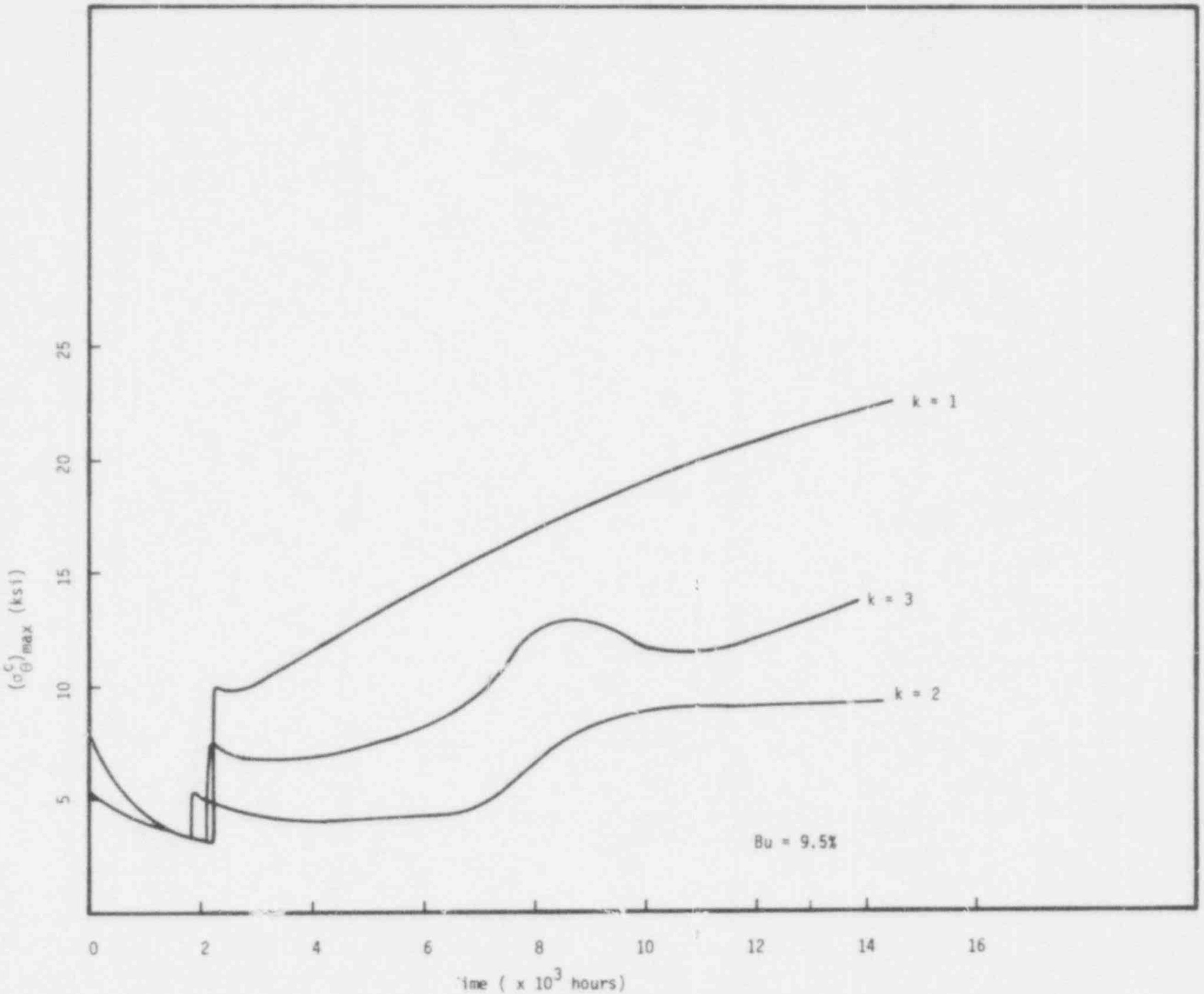


Figure B0 - '. The Maximum Hoop Stress in the Clad. (Case B')

733 193

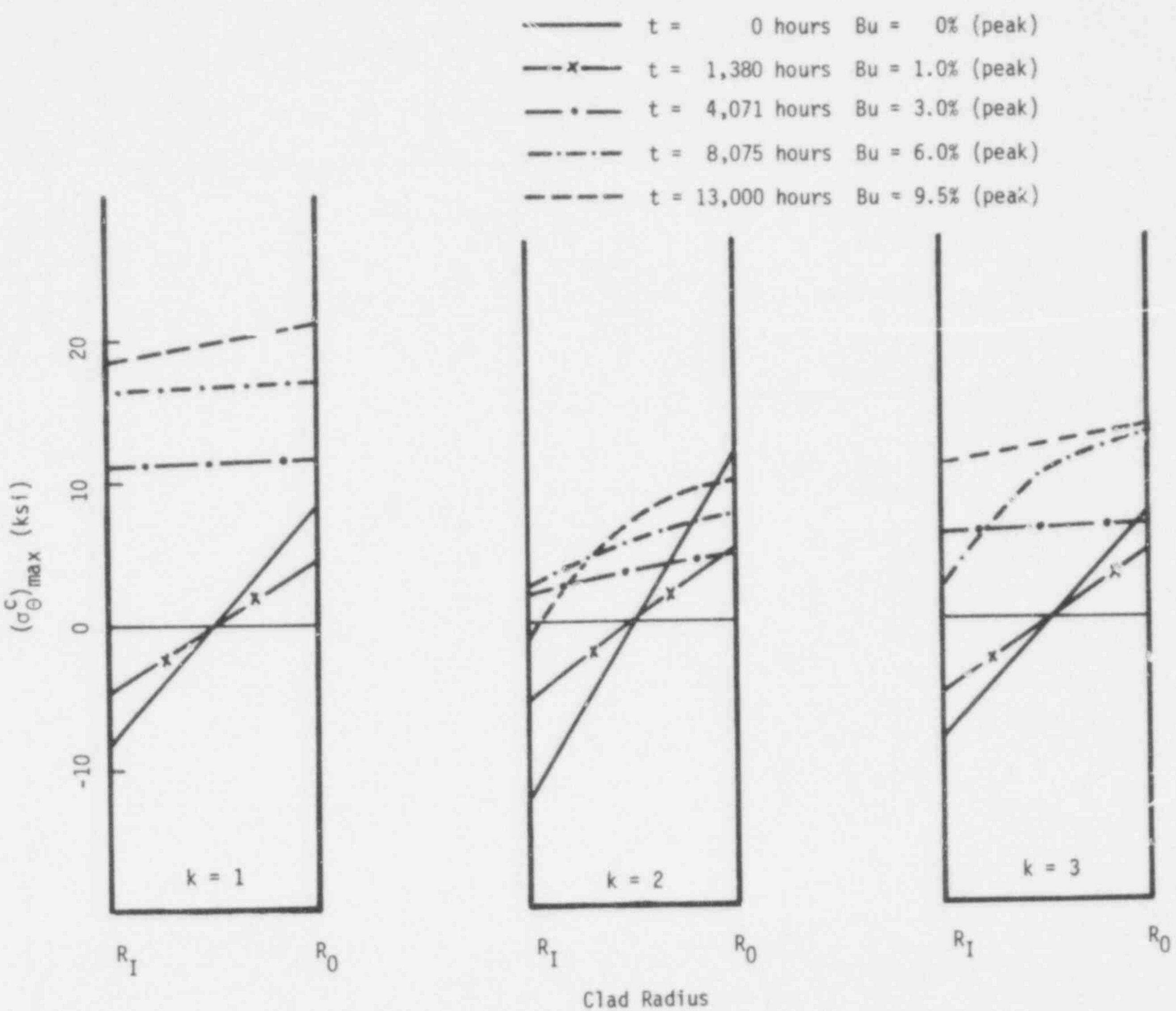


Figure BO - 5. The Hoop Stress Distribution Across the Clad Wall. (Case BO)

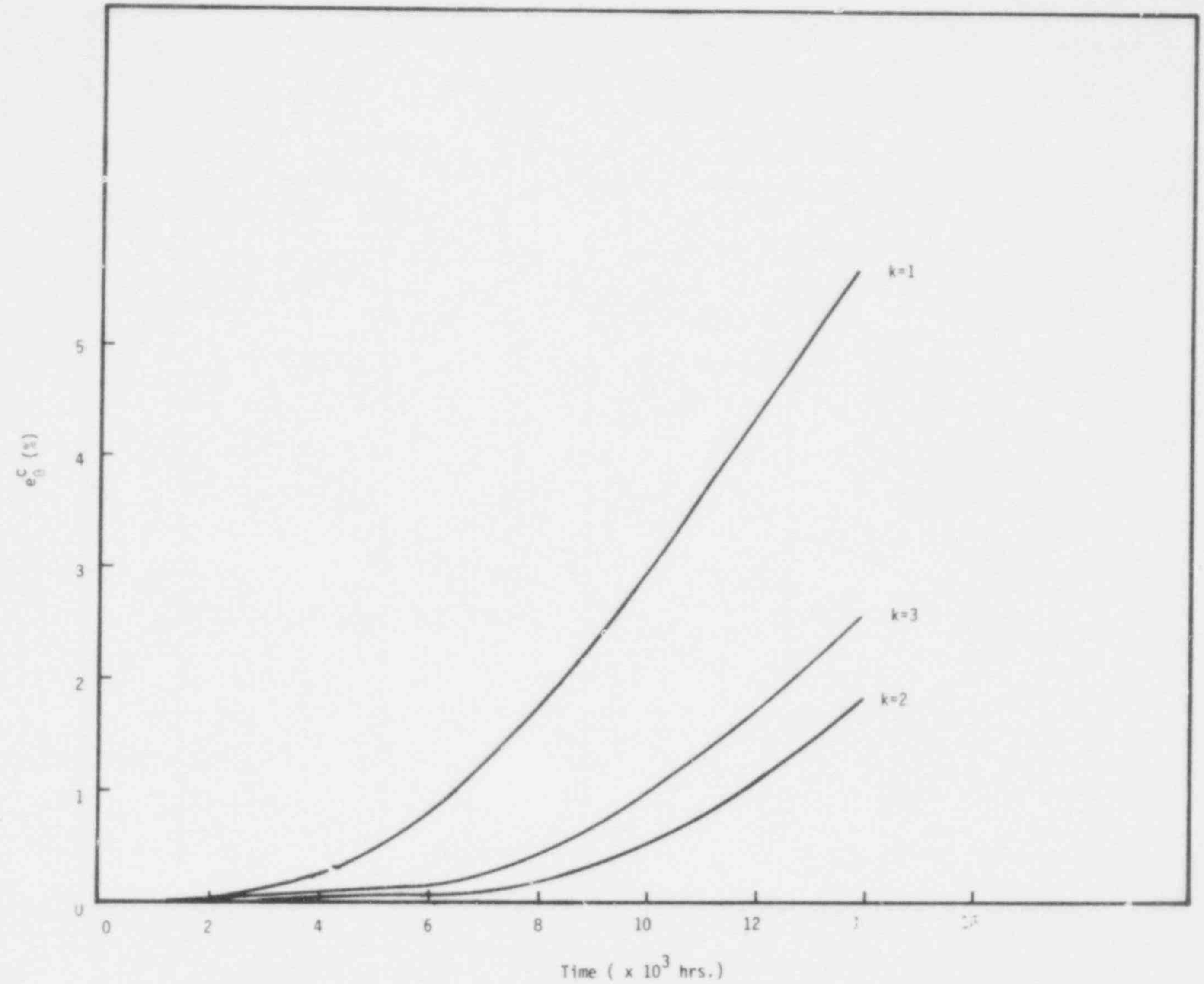


Figure B0-6. The Hoop Strain in the Clad. (Case B0)



733 195

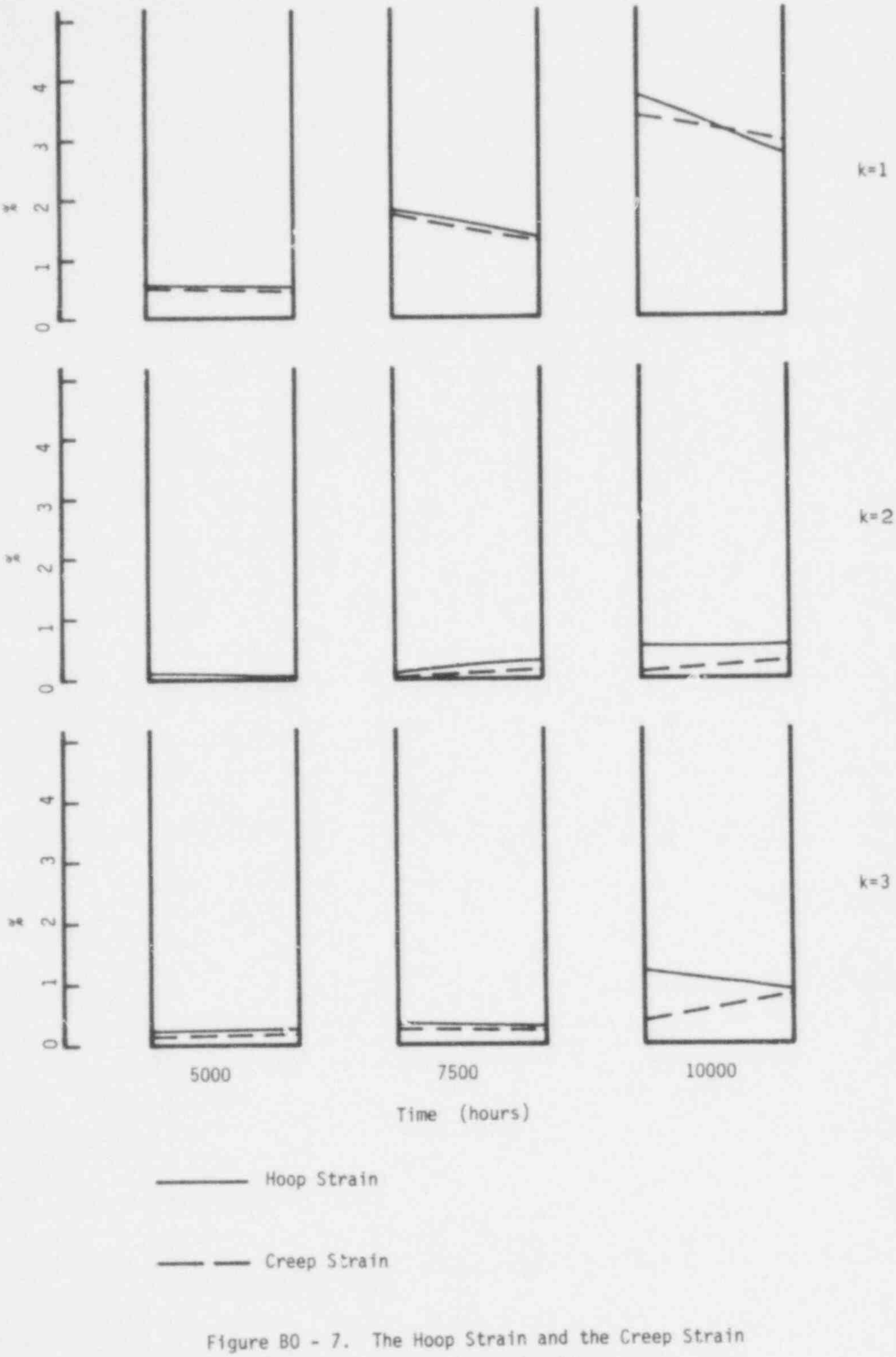


Figure BO - 7. The Hoop Strain and the Creep Strain Across the Clad Wall

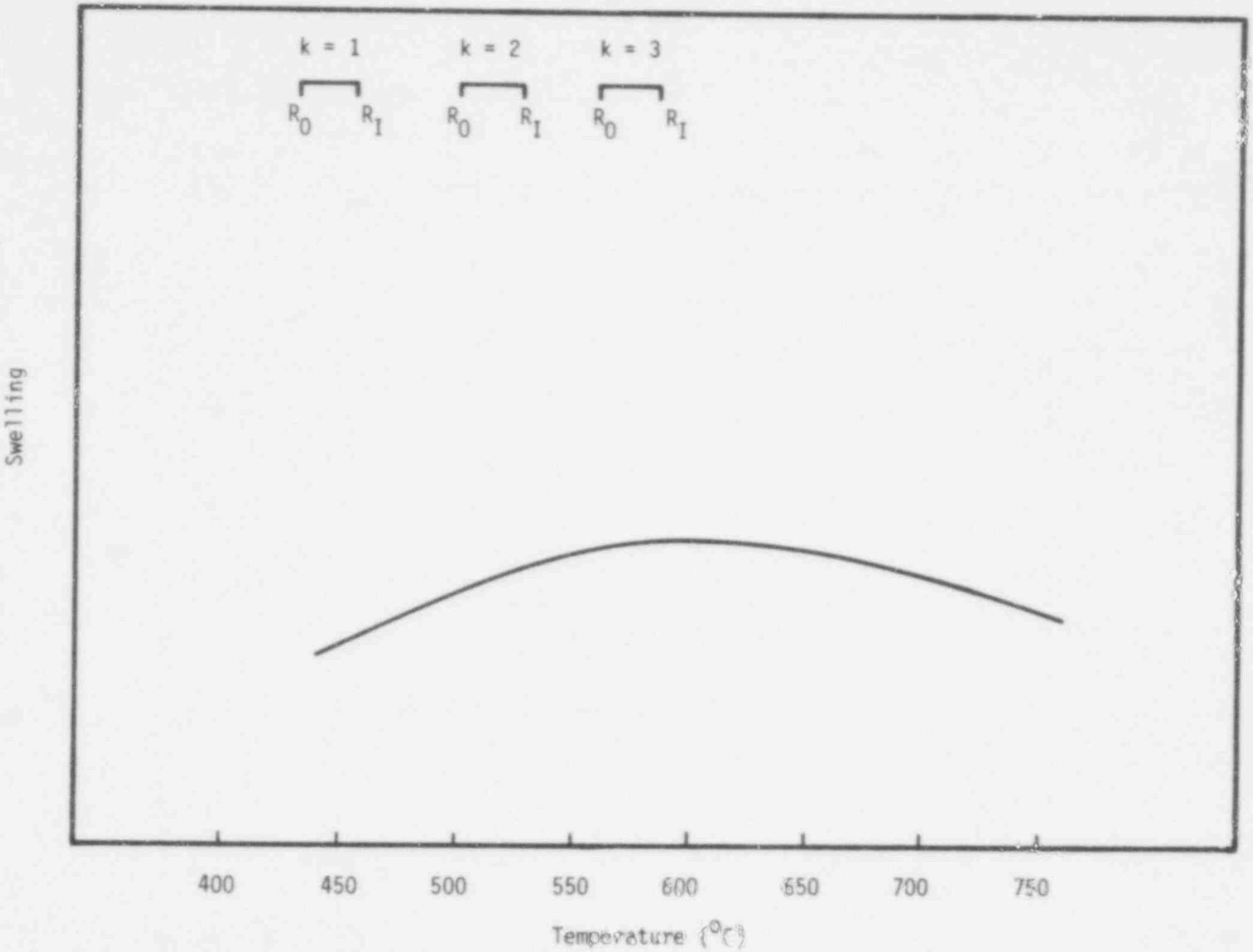


Figure B1 - 1. The Temperature Dependence of the Irradiated Swelling and the Temperature Range Across the Clad Wall. (Case B1)

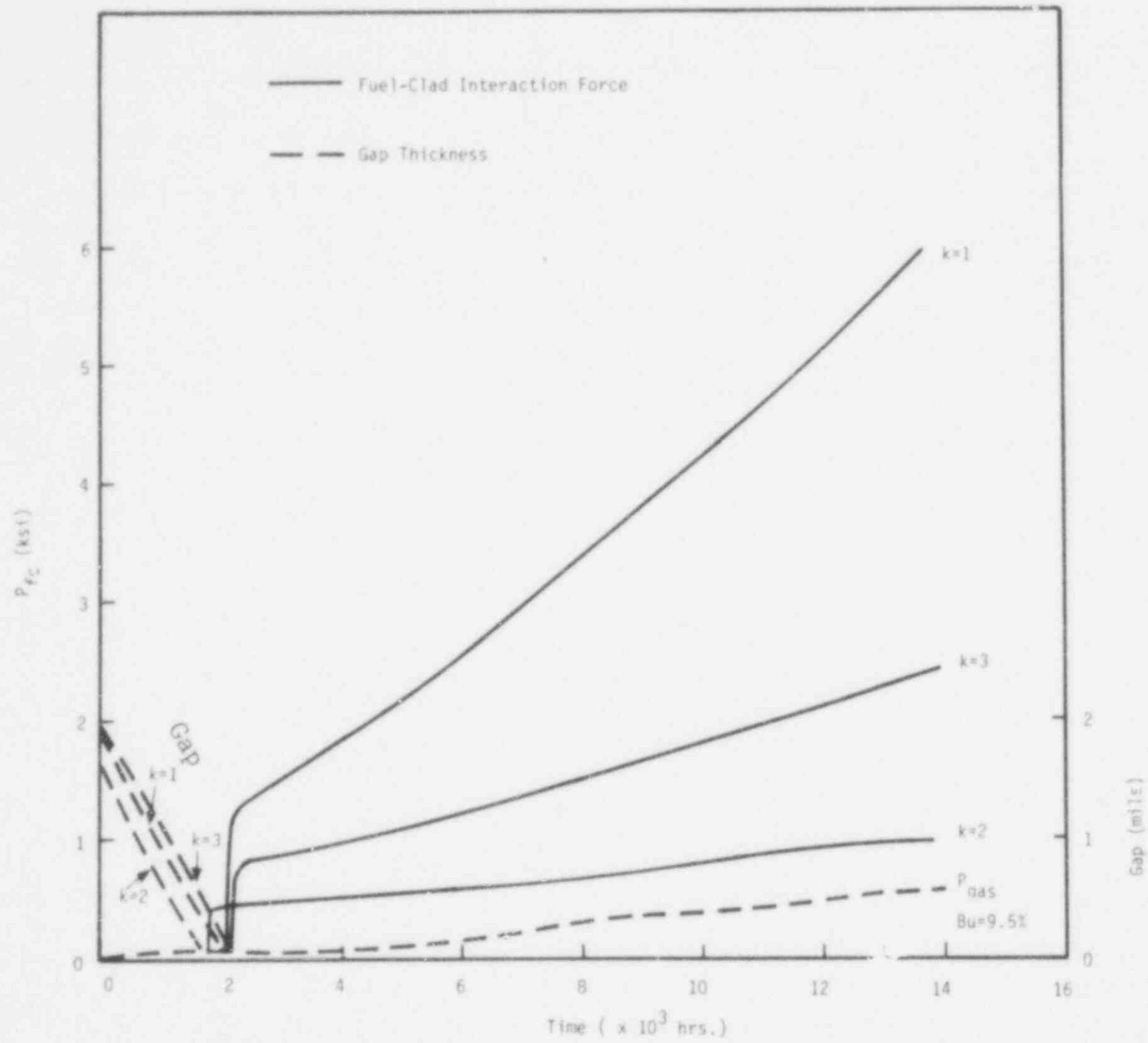


Fig. B1.2 The Fuel-Clad Interaction Force ($P_{fc}$), the Gap Thickness, and the Plenum Pressure ($P_{gas}$) in each Axial Section. (Case B1)

733 198

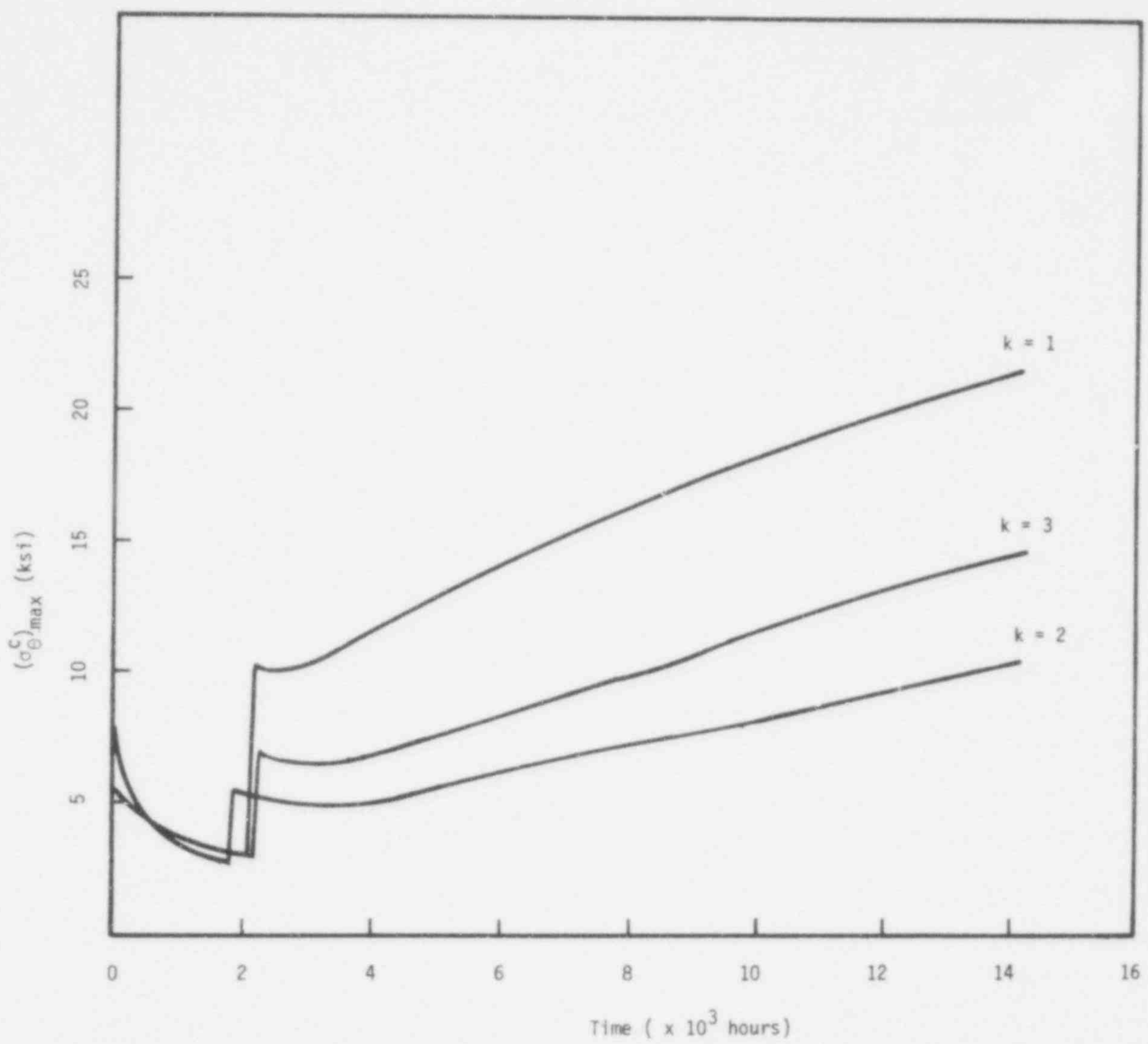


Figure B1 - 3. The Maximum Hoop Stress in the Clad. (Case B1)

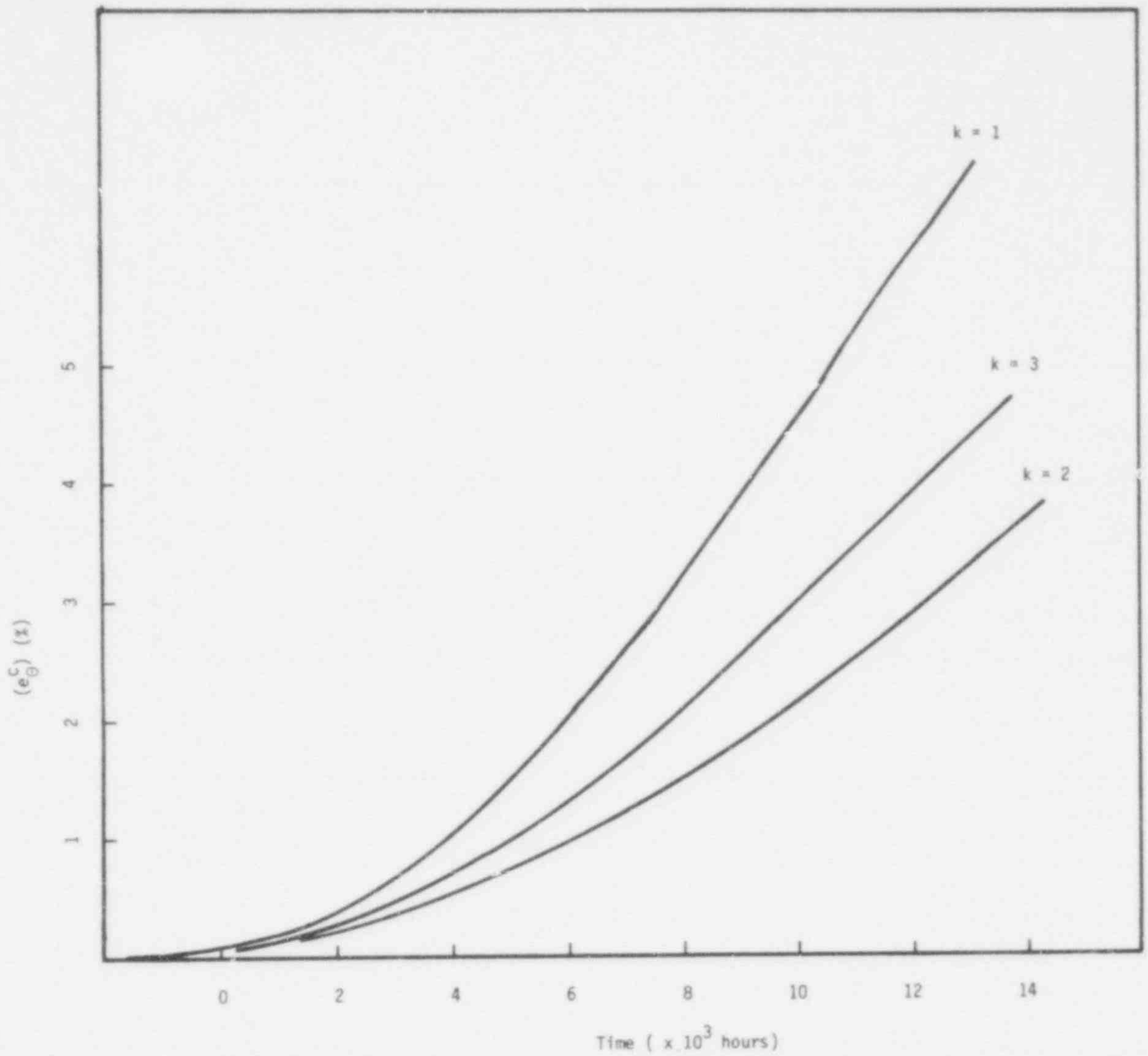


Figure B1 - 4. The Hoop Strain in the Clad. (Case B1)



733 200

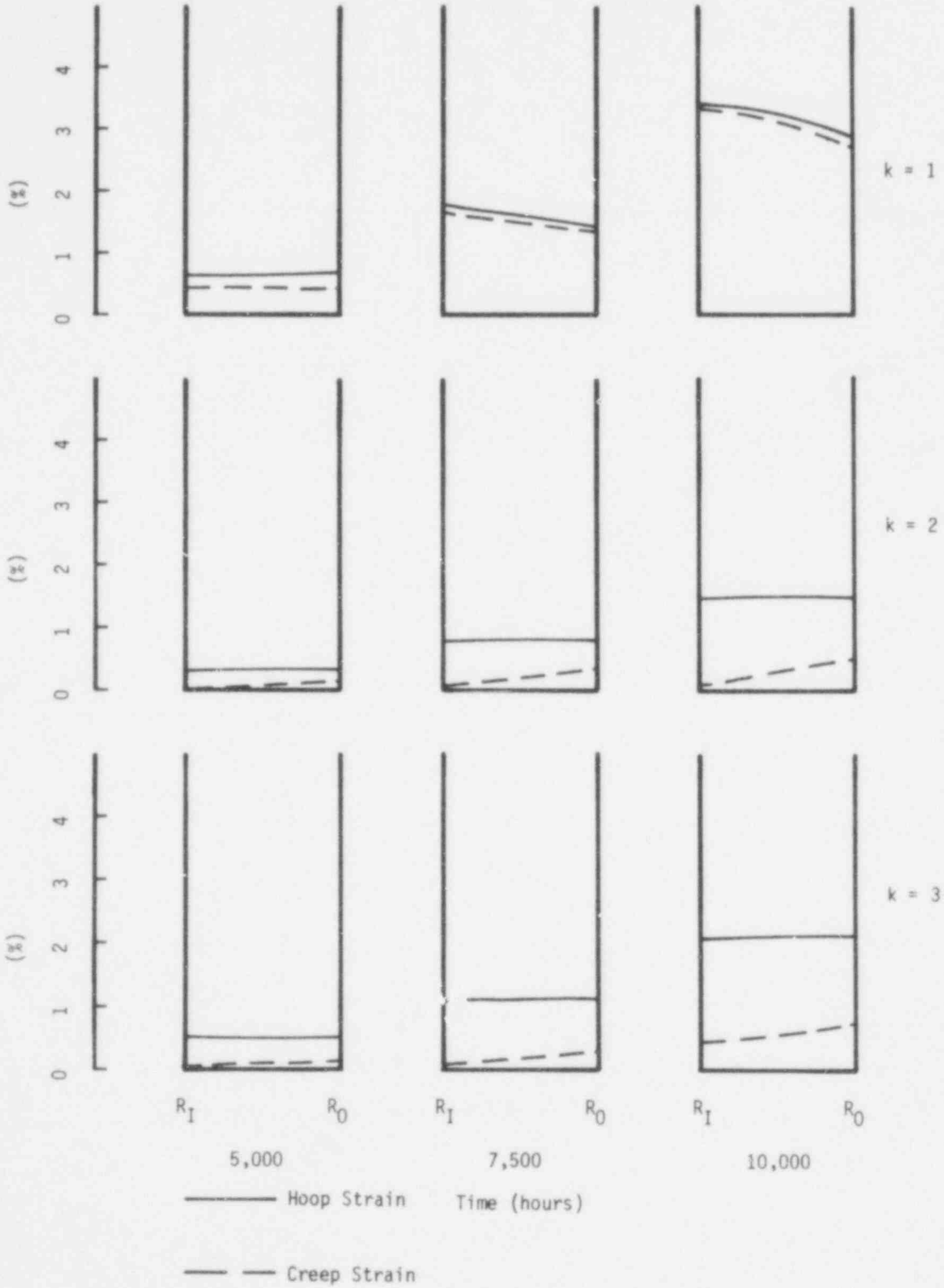


Fig. B1-?. The Distribution of the Total Hoop Strain and the Creep Strain Across the Clad Wall.

733 201

9 kW/ft Cases

Case B3

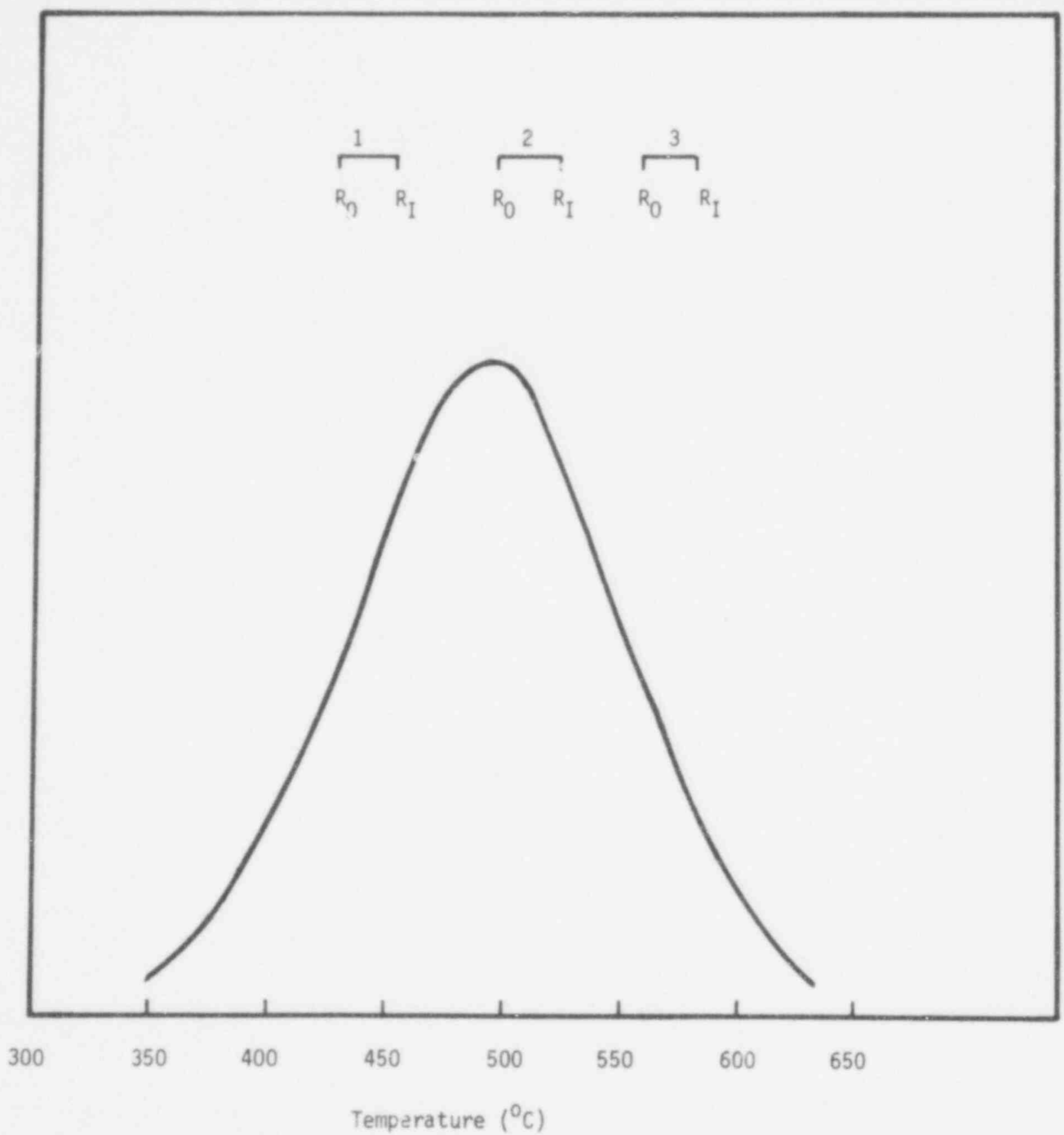


Figure B3 - 1. The Temperature Dependence of the Irradiated Strain, and the Temperature Range across the Clad Wall.

733 202

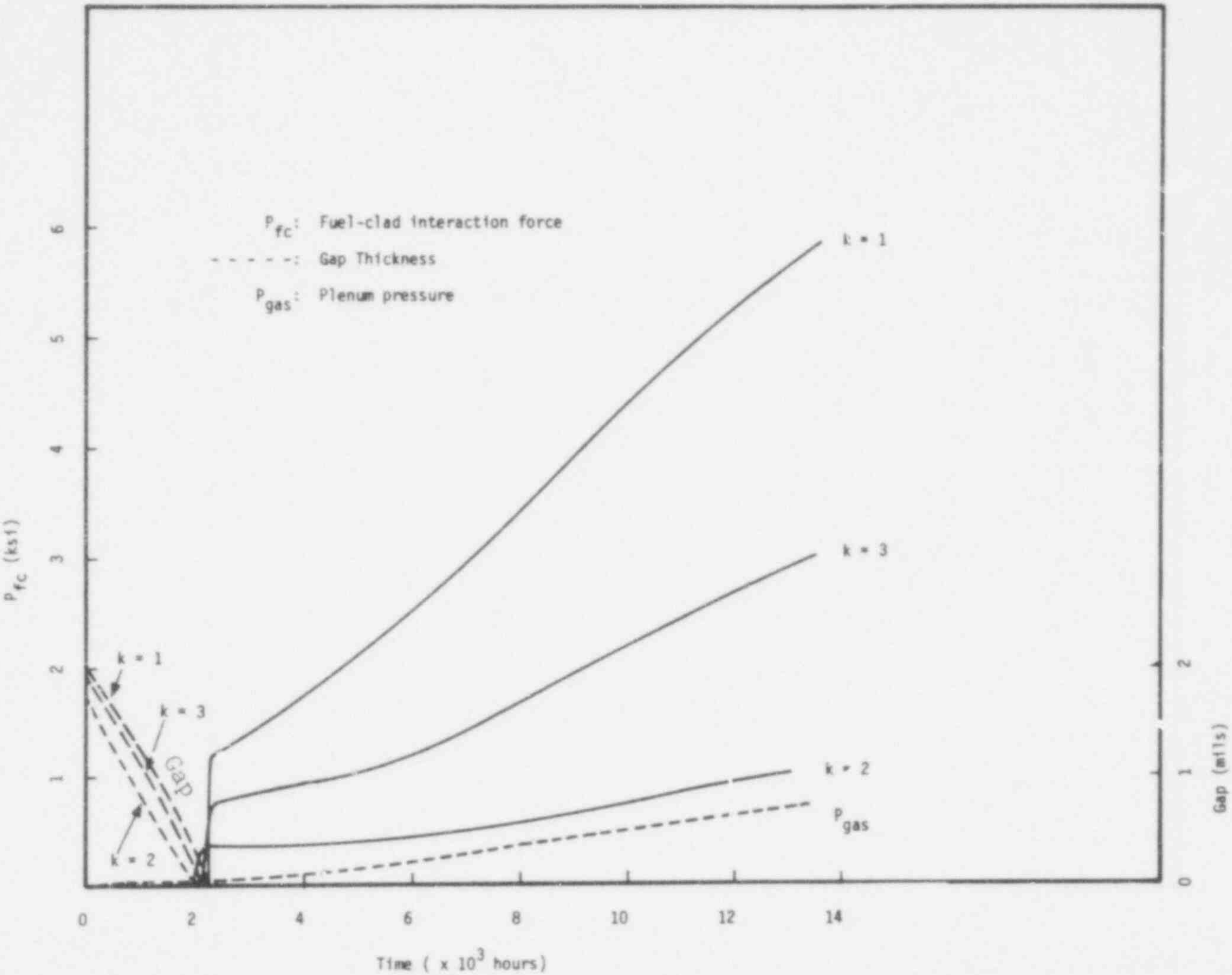


Figure B3 - 2. The Fuel-Clad Interaction Force, the Gap Thickness, and the Plenum Pressure in Each Axial Section.

(Case B3)

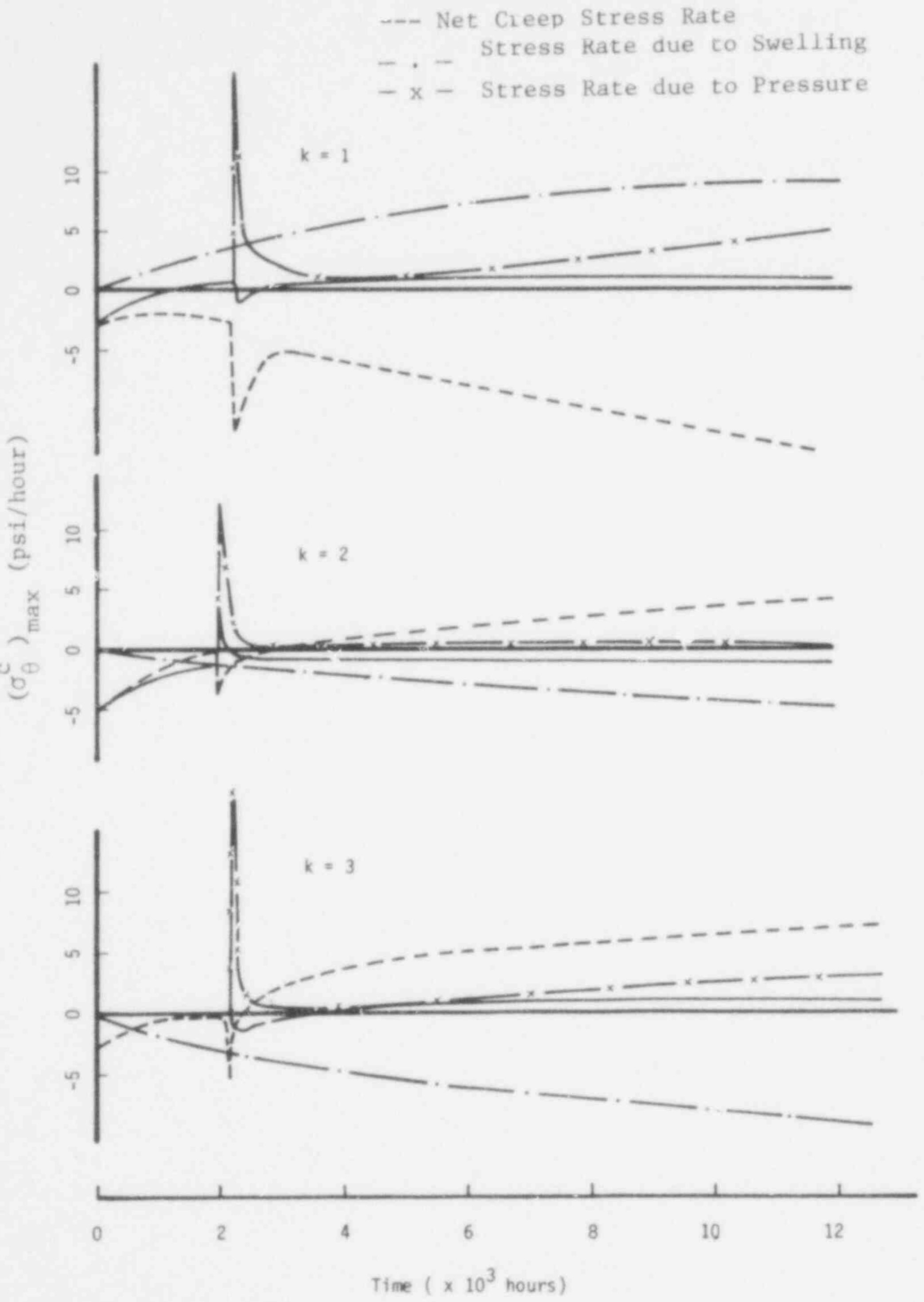


Figure B3 - 3. The Net Rate of the Hoop Stress, the Stress Rate Due to the Creep, the Clad Swelling, and the Pressure at the Clad Outer Wall. (Case B3)

POOR ORIGINAL

733 204

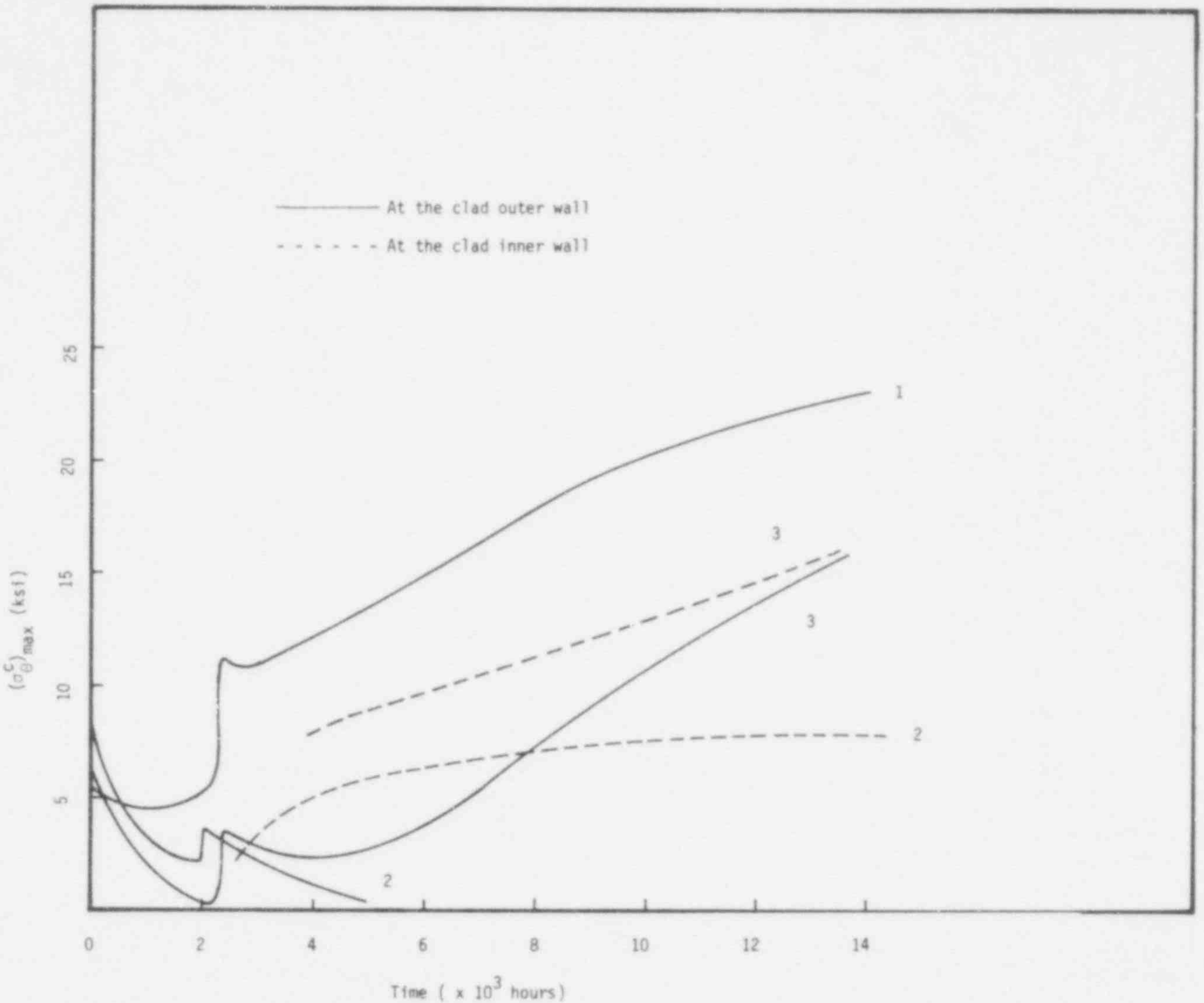


Figure B3 - 4. The Maximum Hoop Stress in the Clad. (Case B3)

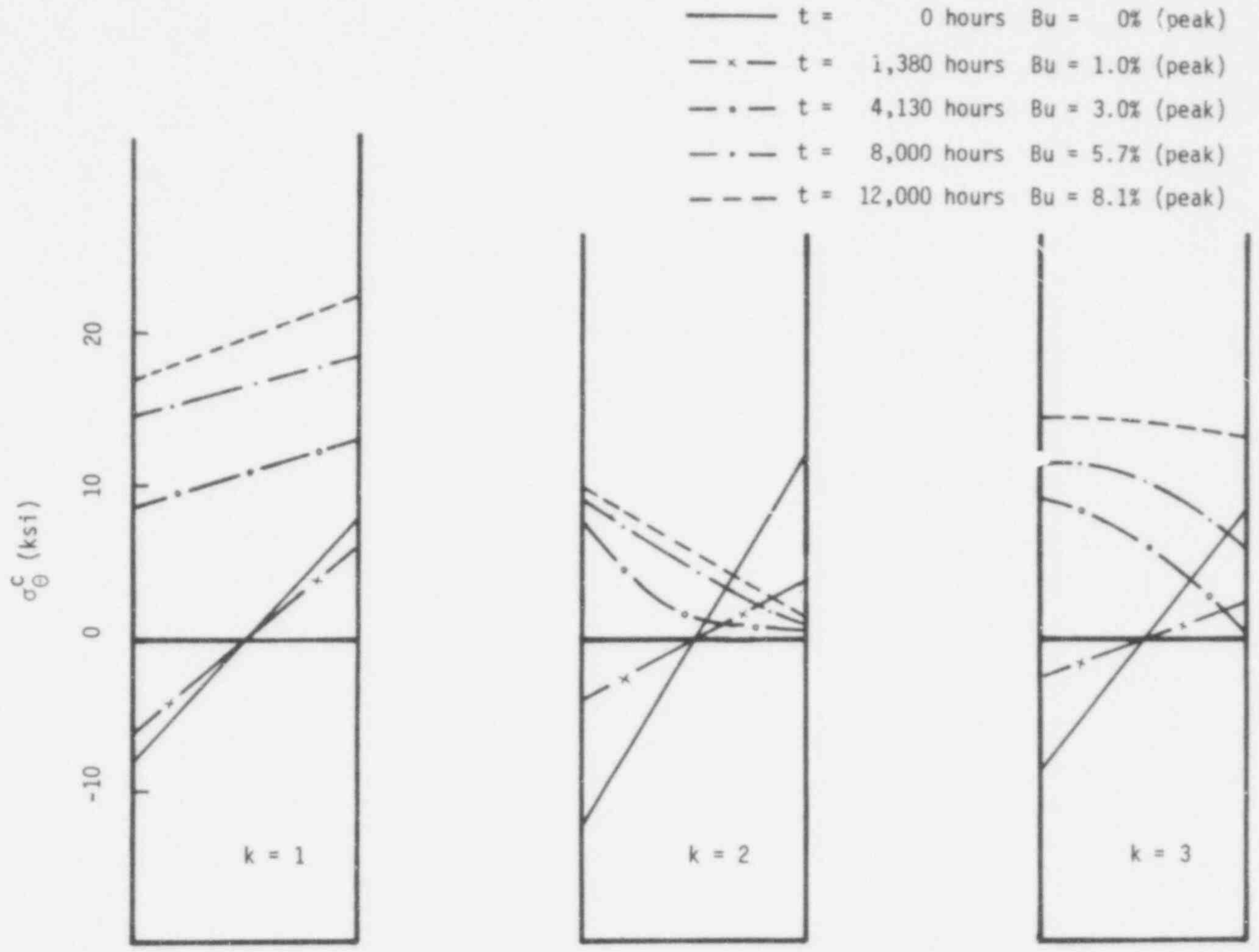


Figure B3 - 5. The Distribution of the Hoop Stress across the Clad Wall. (Case B3)

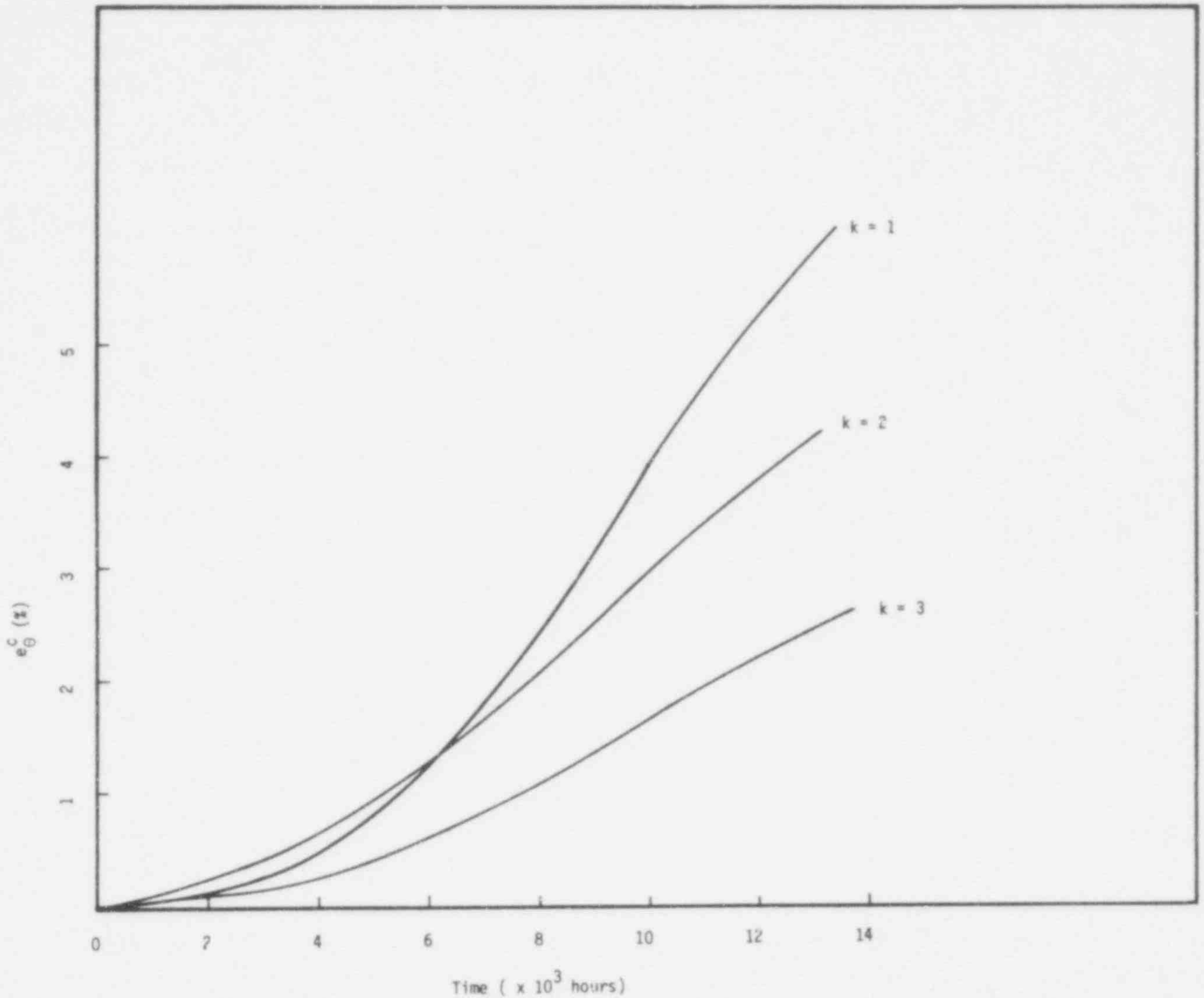


Figure B3 - 6. The Hoop Strain in the Clad. (Case B3)

733 207

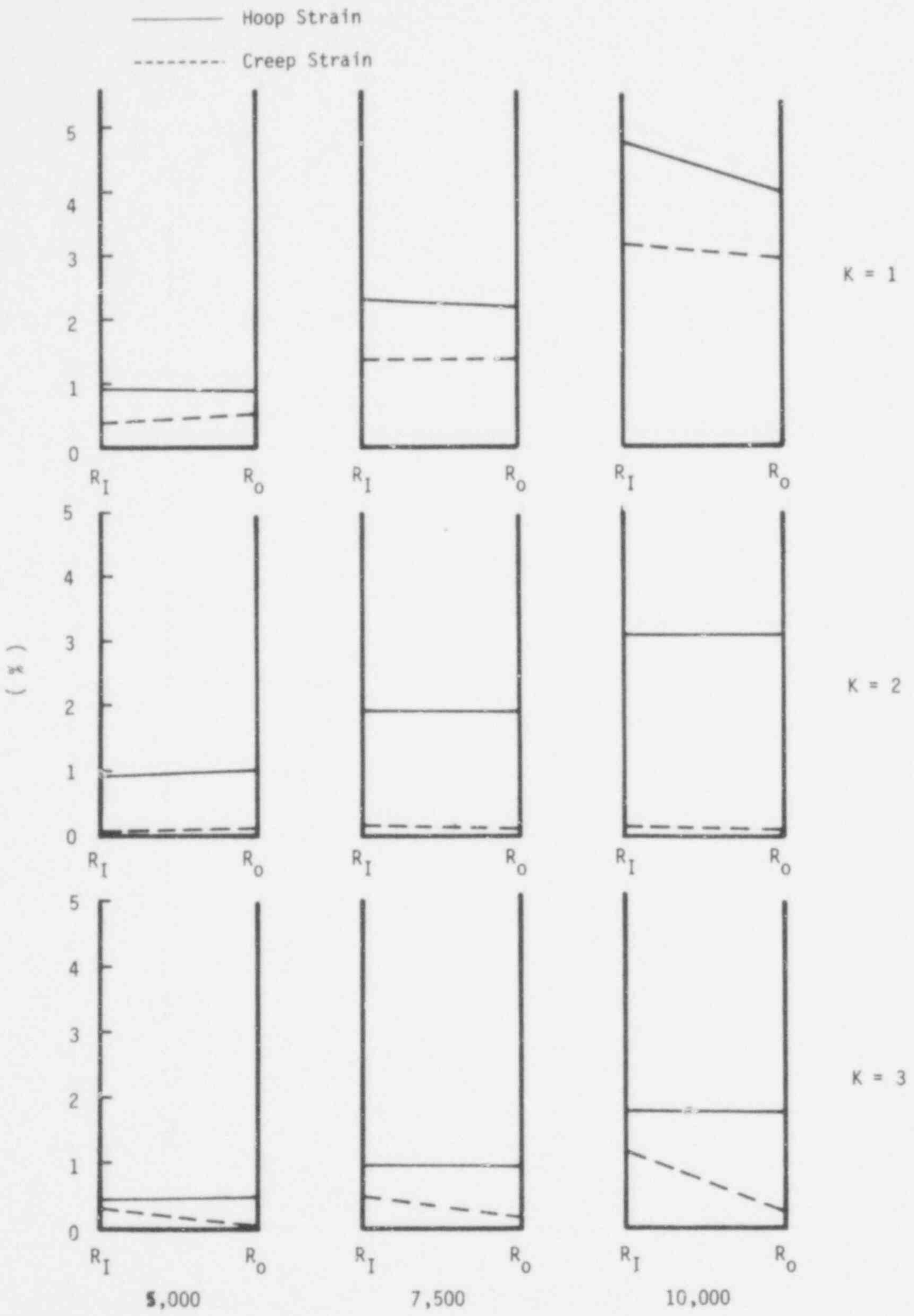


Figure B3 - 7. The Hoop Strain and the Creep Strain Across the Clad Wall (Case B-3)

208

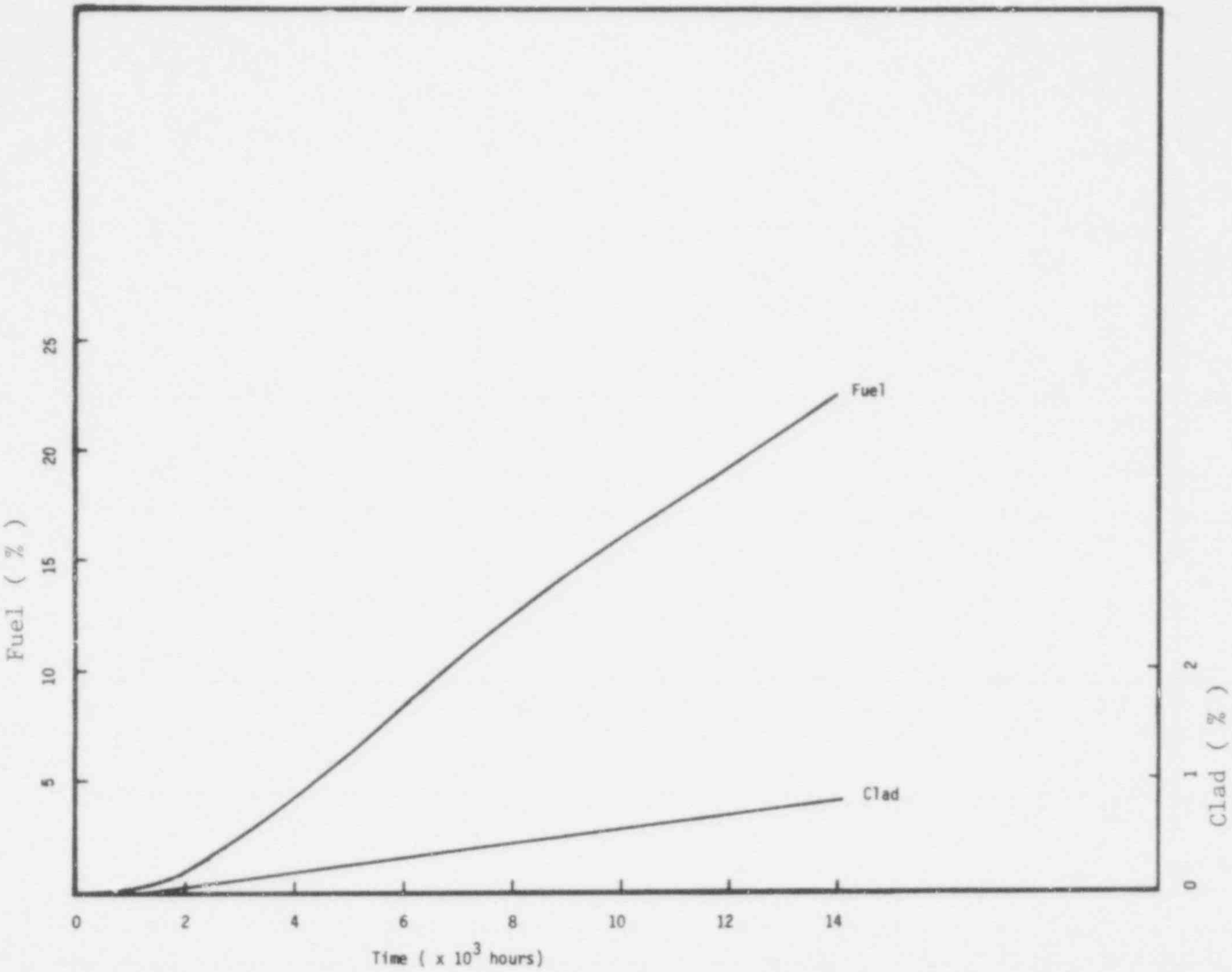


Figure B3 - 8. The Percentage of the Axial Displacement for the Fuel and the Clad. (Case B3)



733 209

9 kW/ft Cases

Case B4

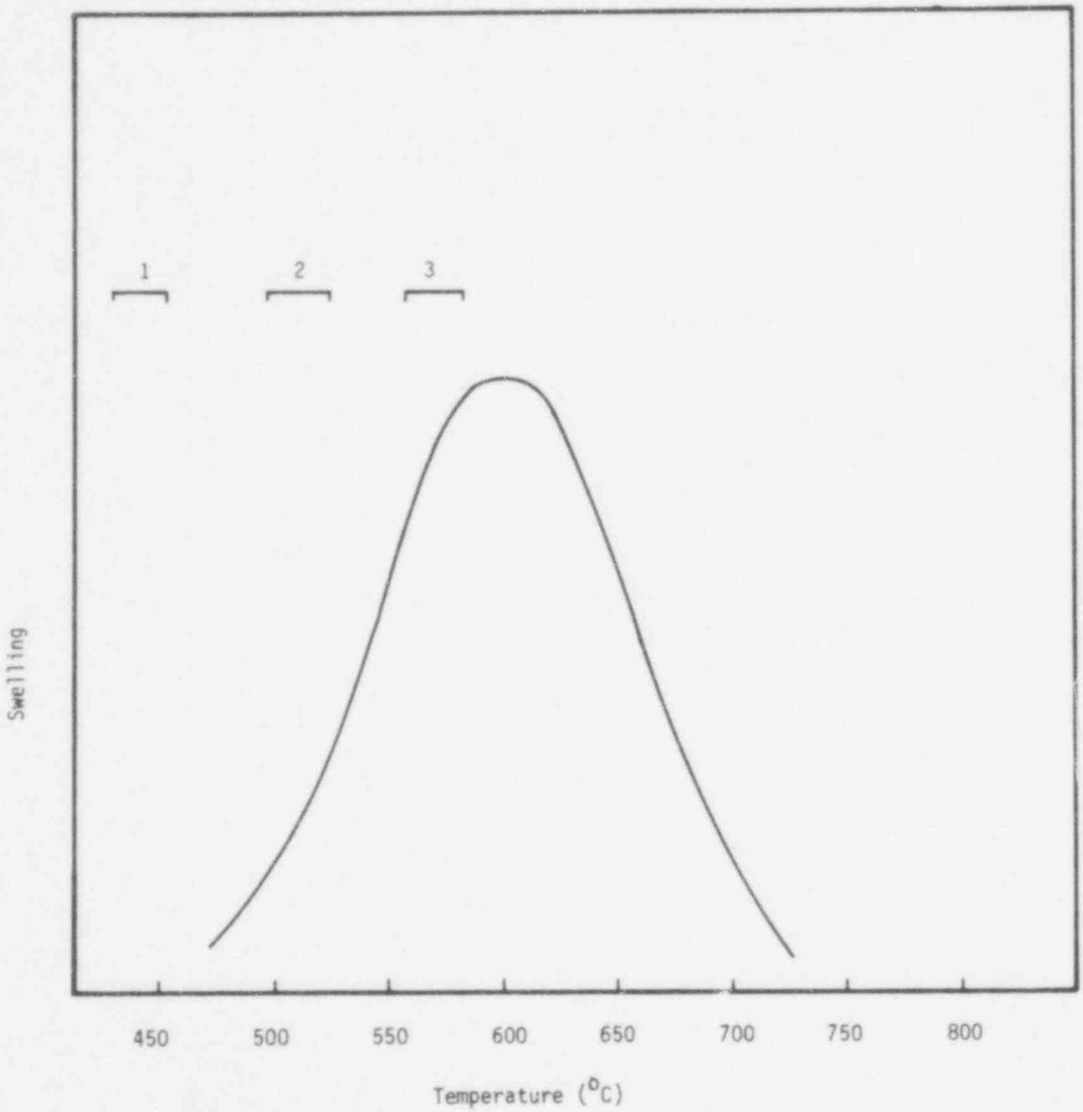


Figure B4 - 1. The Temperature Dependence of the Irradiated Swelling, and the Temperature Range Across the Clad Wall



733 210

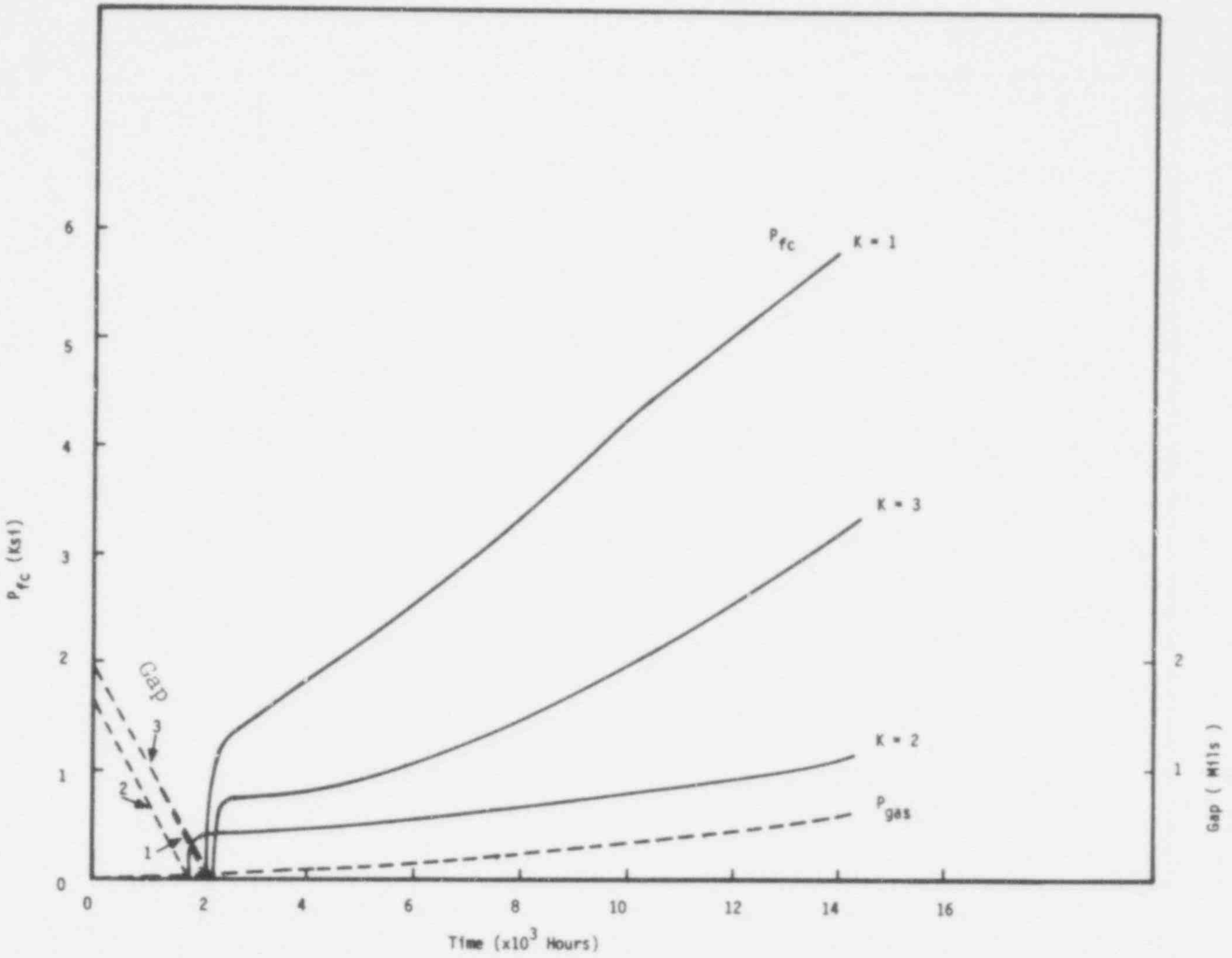


Figure B4 - 2. The Fuel Clad Gap Closure, the Fuel-Clad Interaction Force ($P_{fc}$), and the Plenum Pressure (Case B4)

1: Net Hoop Stress Rate

2: Stress Rate due to Creep

3: Stress Rate due to Swelling

4: Stress Rate due to Pressure

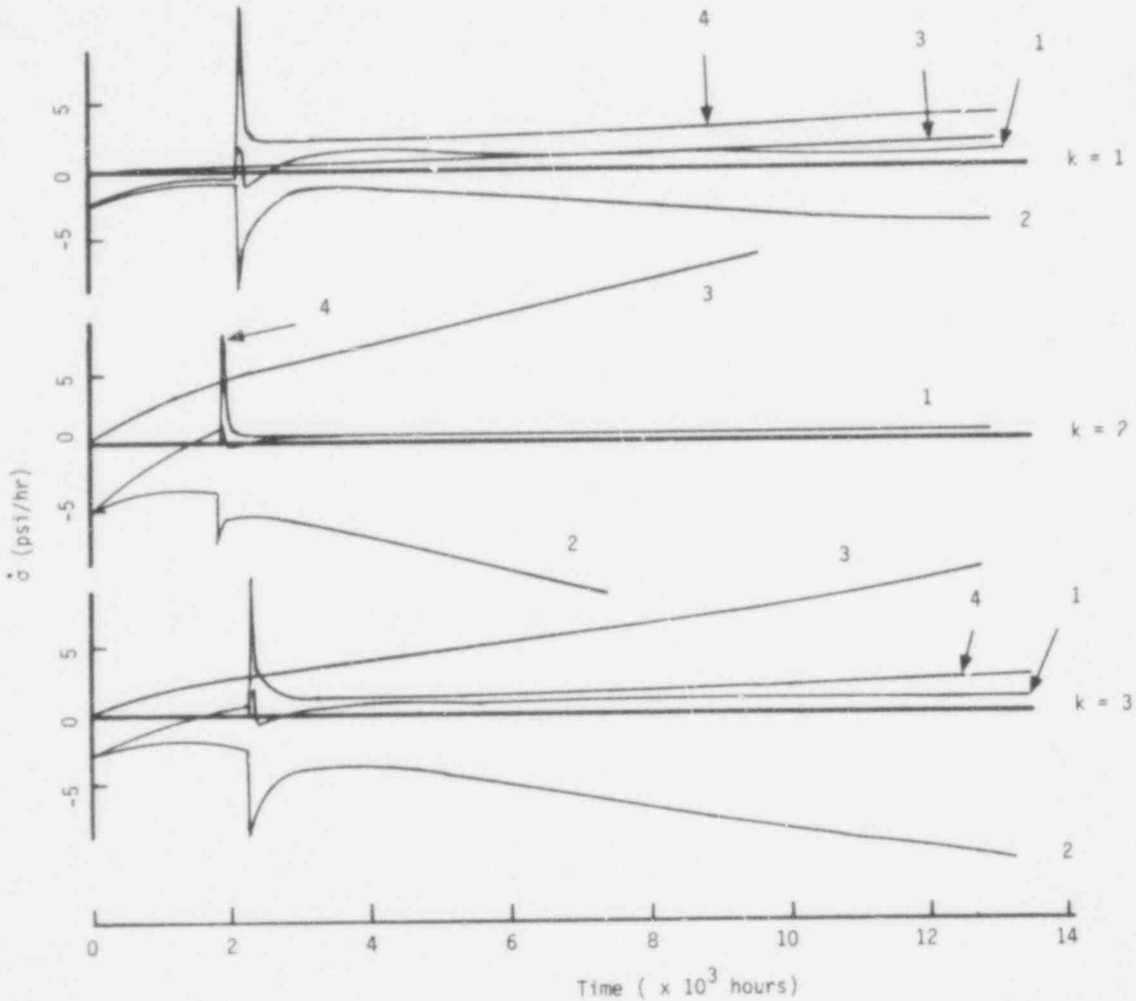


Figure B4-3.
The Net Hoop Stress Rate and the Stress Rate, Due to Creep, Swelling, and Pressure at the Outer Wall of the Clad.

733 212

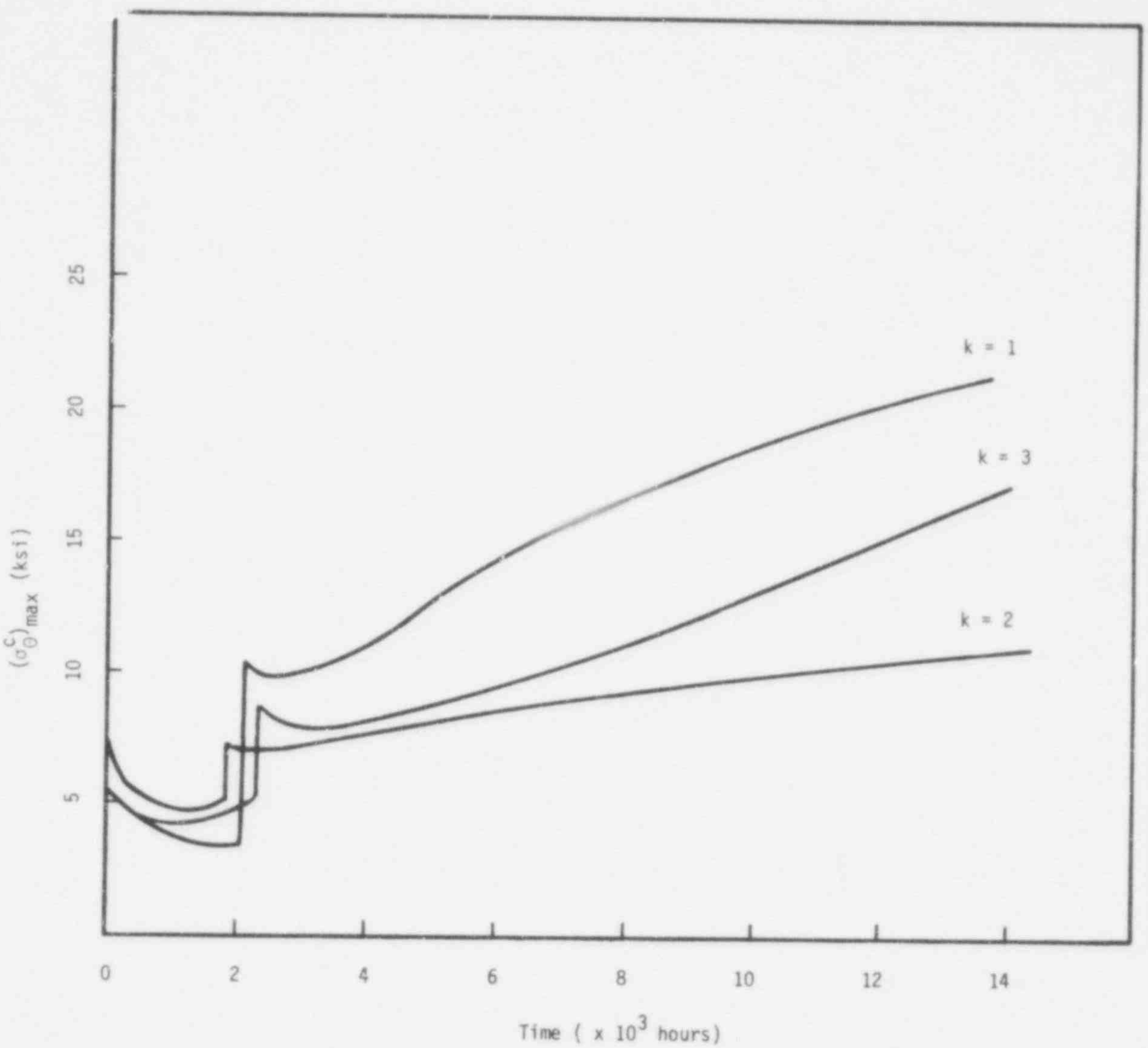


Figure B4 - 4. The Maximum Hoop Stress in the Clad. (Case B4)

733 213

1: t = 0 hrs Bu = 0 % (peak)

2: t = 1250 hrs Bu = 0.9 % (peak)

3: t = 4020 hrs Bu = 3.0 % (peak)

4: t = 8050 hrs Bu = 6.0 % (peak)

5: t = 11700 hrs Bu = 8.6 % (peak)

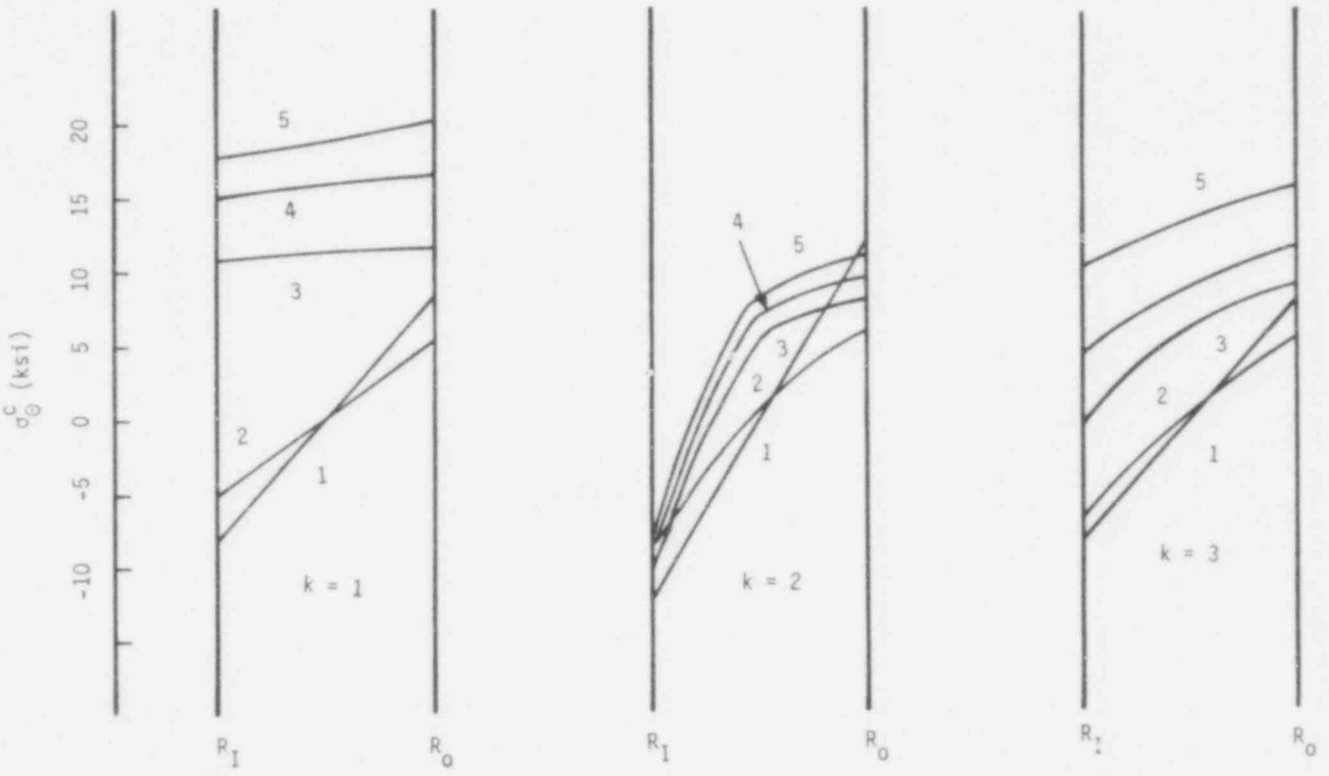


Figure B4-5. The Hoop Stress Distribution Across the Clad.

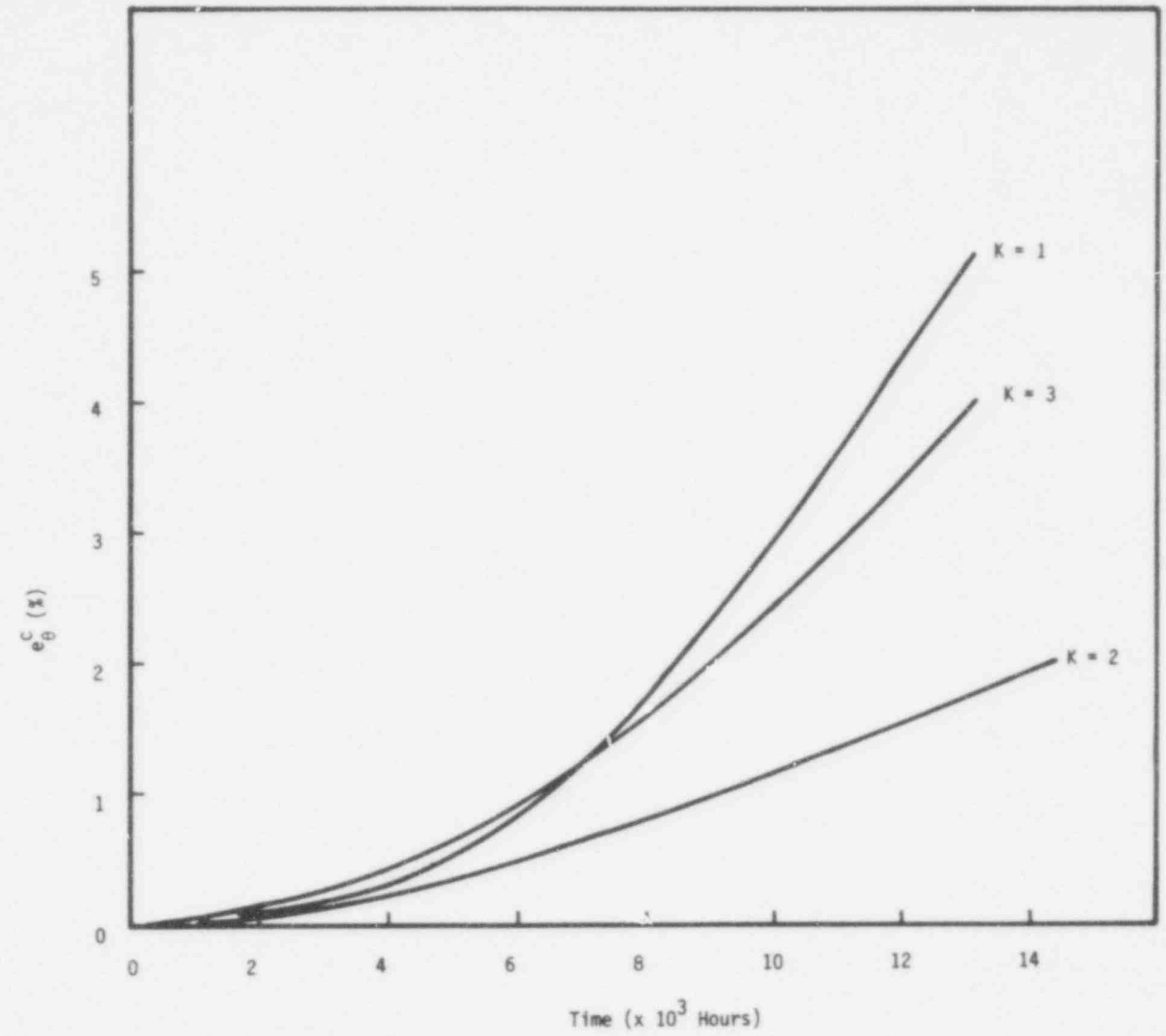


Figure B4 - 6. The Hoop Strain in the Clad (Case B4)

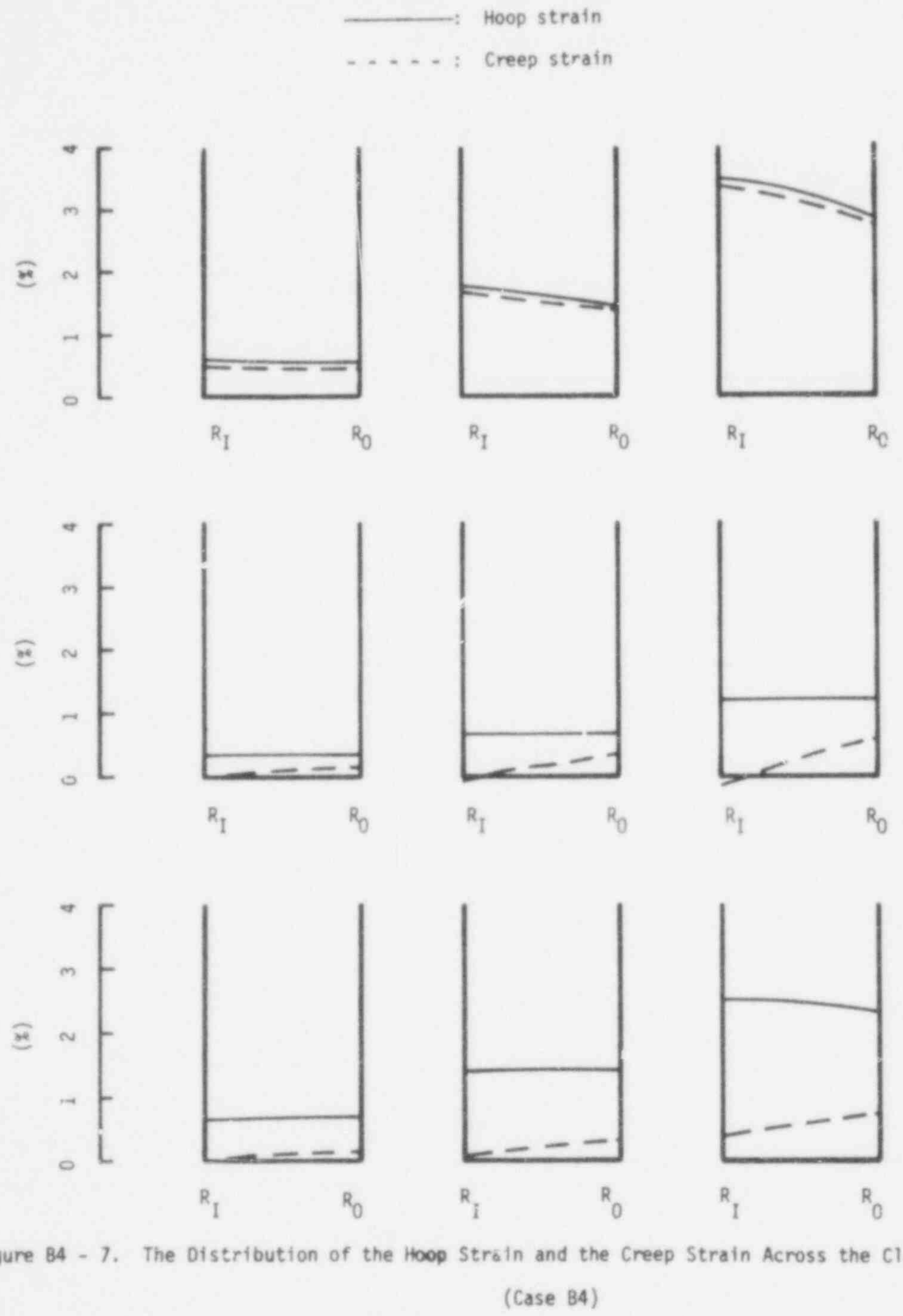


Figure B4 - 7. The Distribution of the Hoop Strain and the Creep Strain Across the Clad Wall.

(Case B4)

733 216

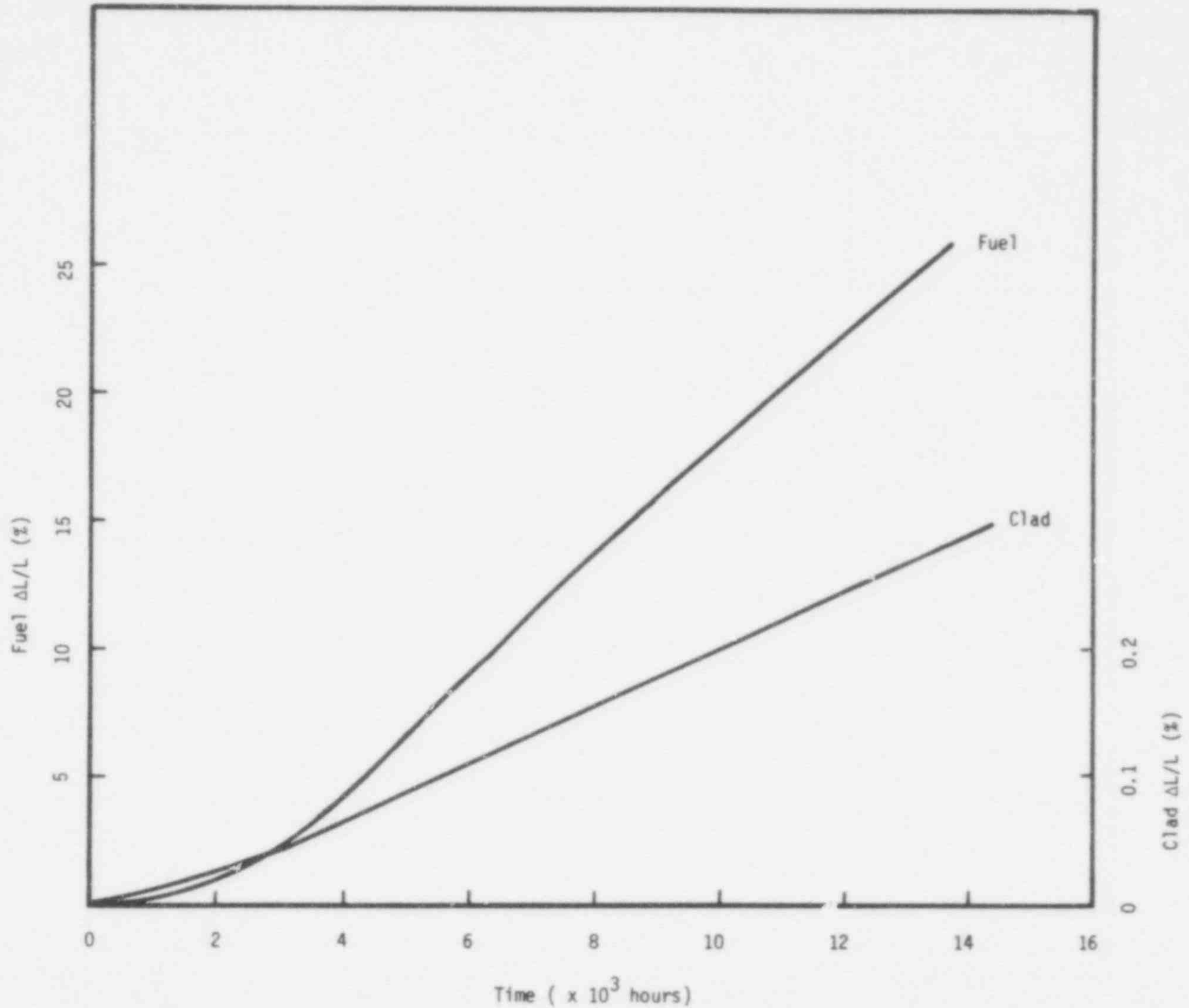


Figure B4 - 8. The Percentage of Axial Displacement for the Fuel and the Clad. (Case B4)



733 217

9 kW/ft Cases

Case R2

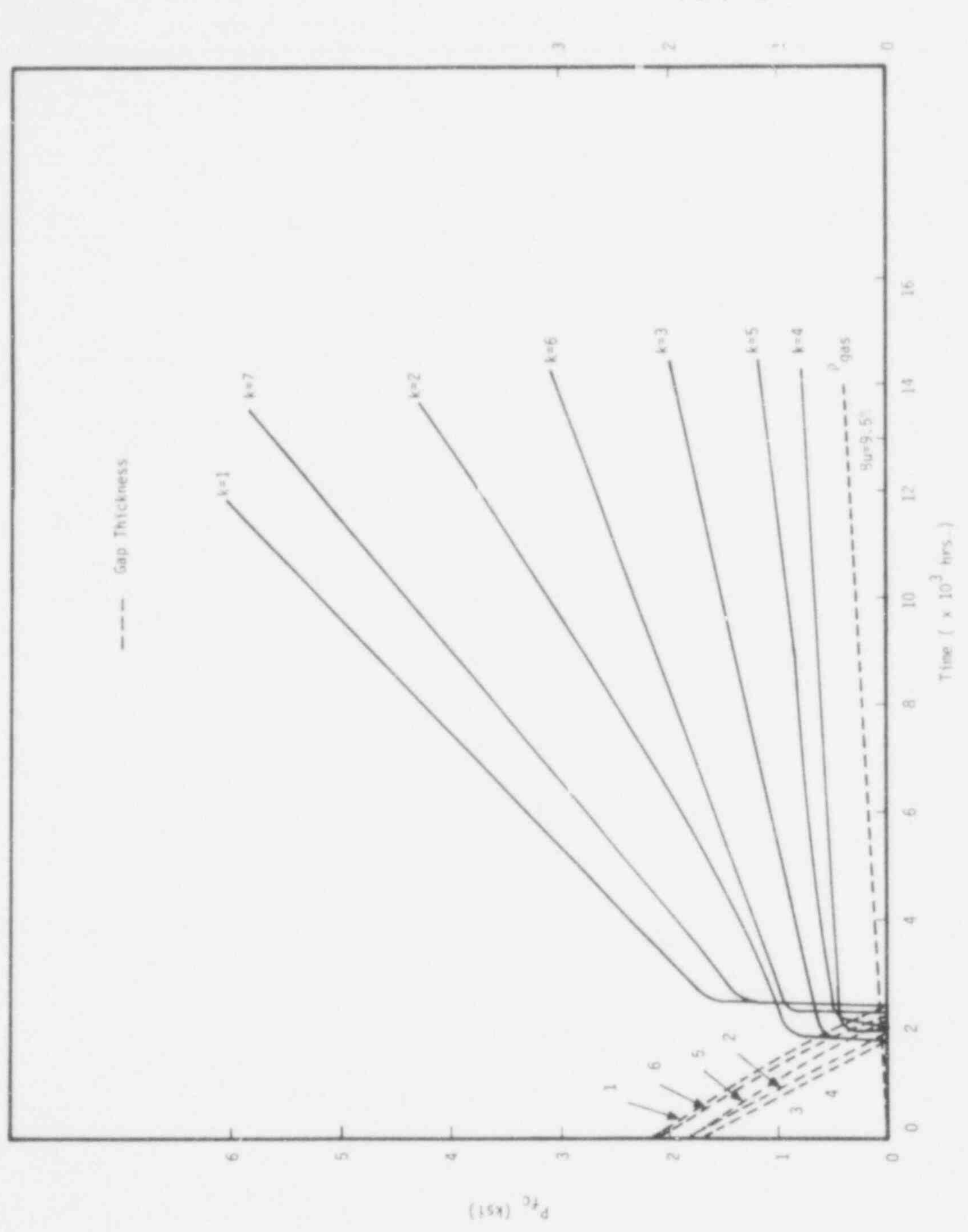


Fig. R2.1 The Fuel-Clad Interaction Force ($P_{fc}$), the Gap Thickness, and the Plenum Pressure ($P_{gas}$) in Each Axial Section. (Case R2)

733 218

POOR ORIGINAL

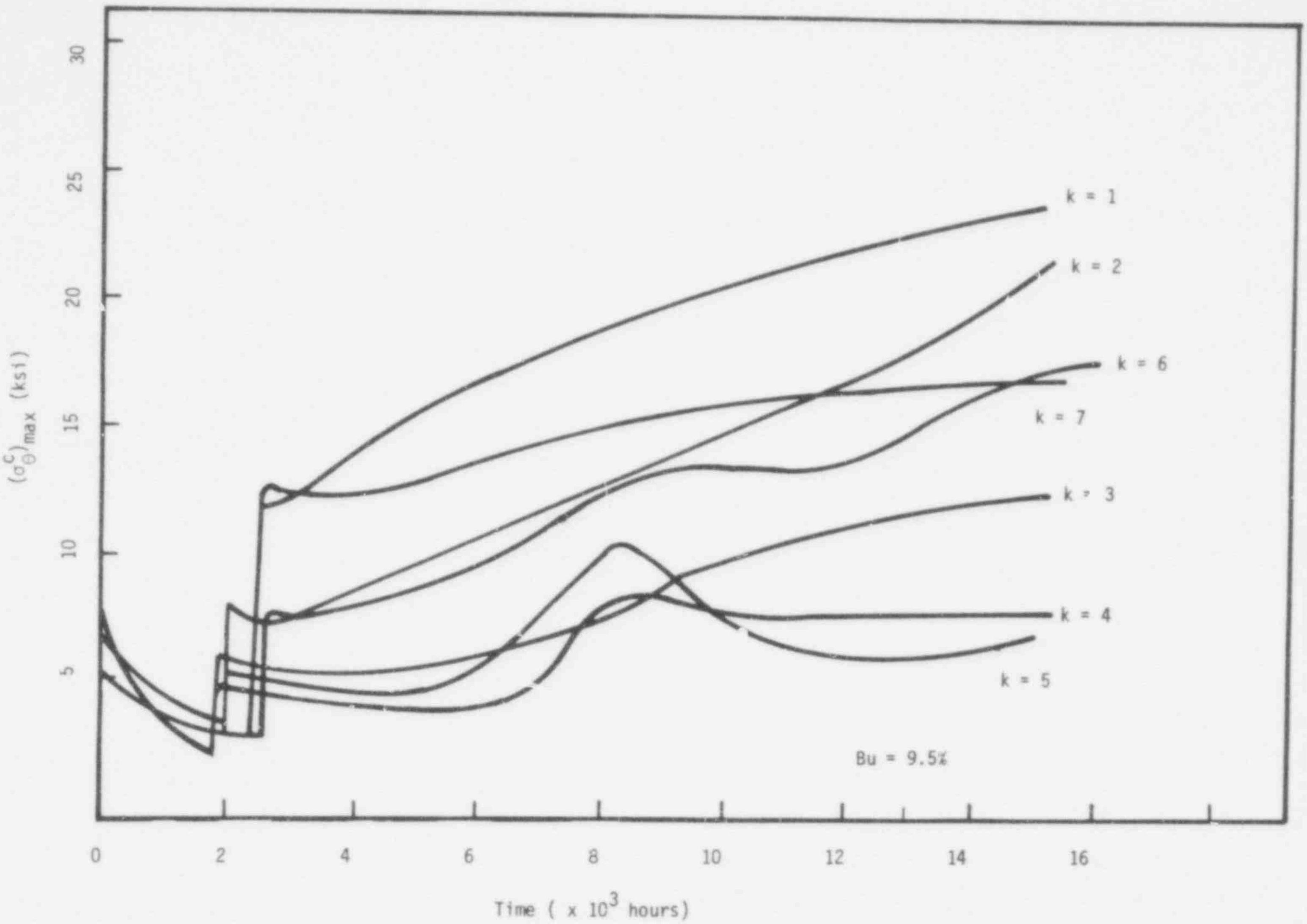


Figure R2 - 2. The Maximum Hoop Strain in the Clad. (Case R2)

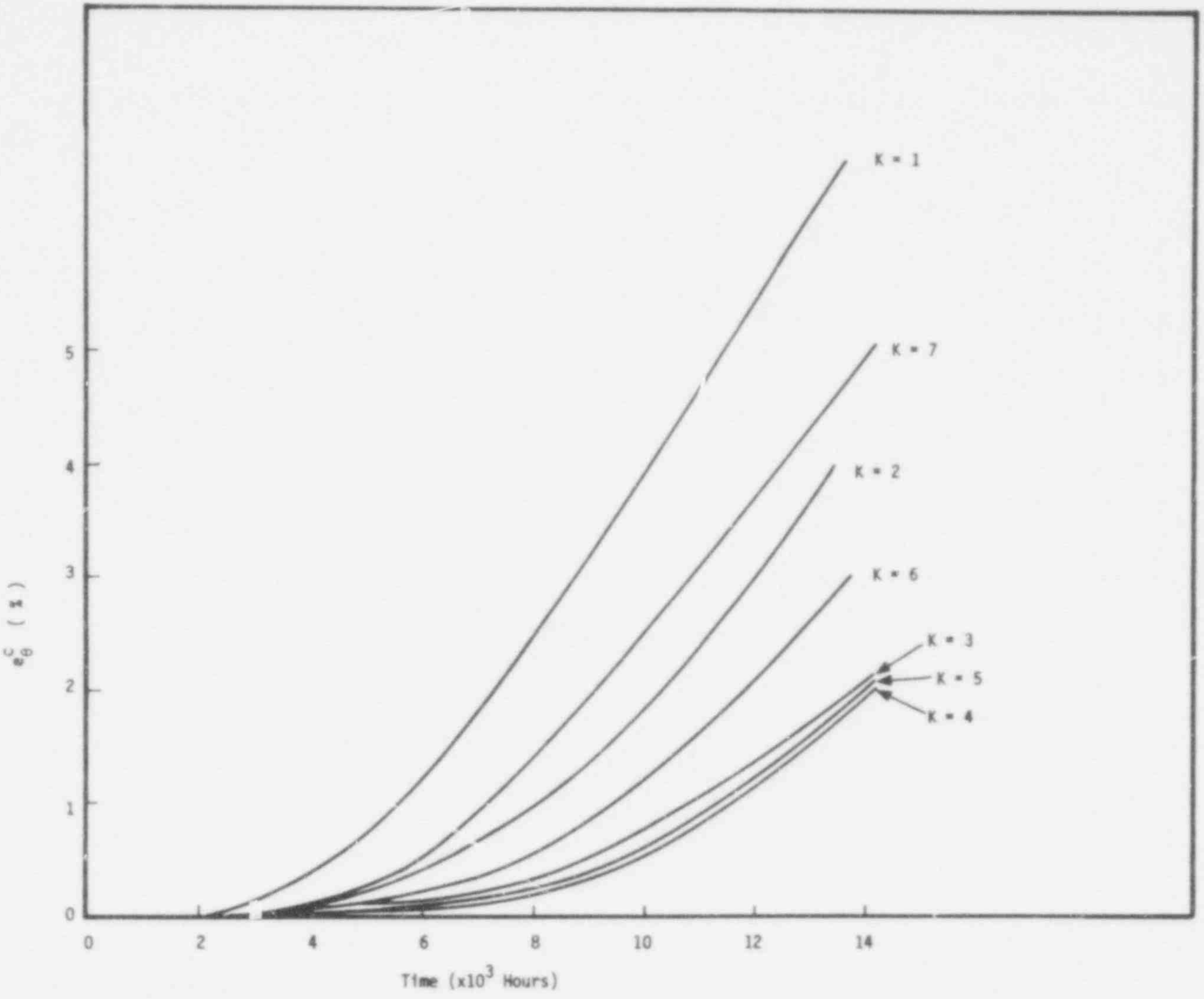


Figure R2 - 3. The Hoop Strain in the Clad (Case R2)

733 220

6 kW/ft Cases

Case NO

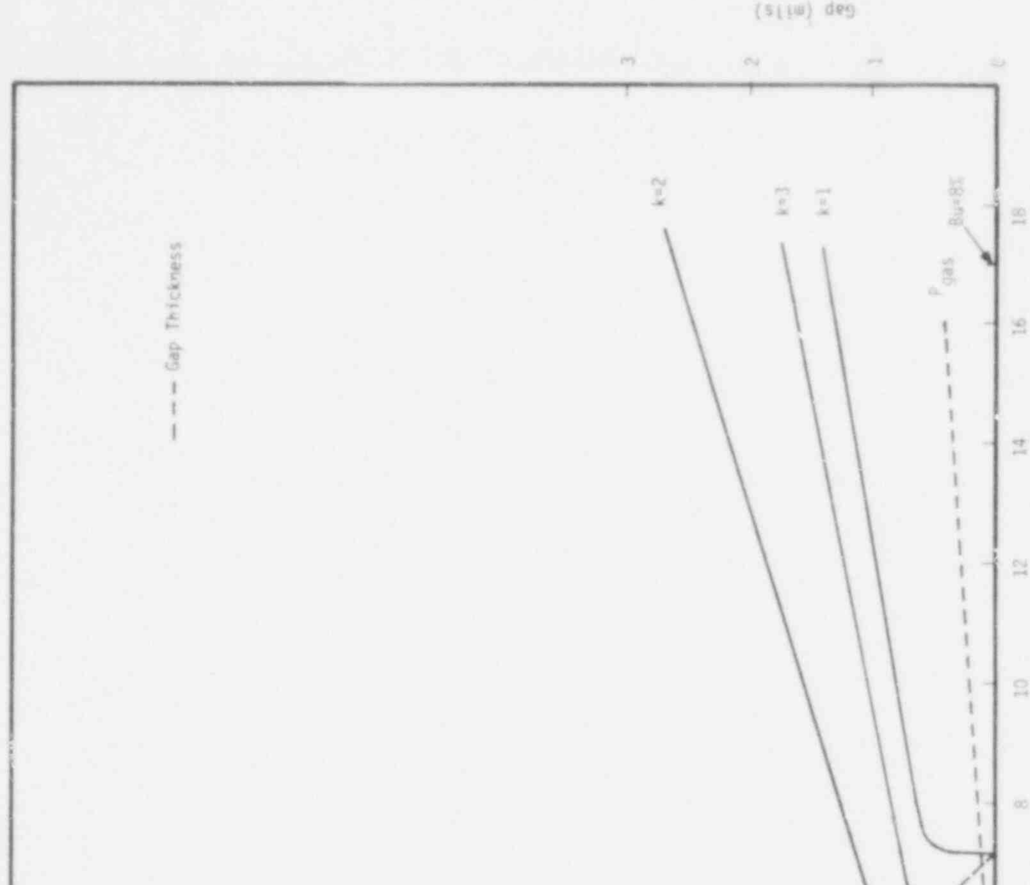


Fig. NO.1 The Fuel-Clad Interaction Force ($P_{fc}$), the Gap Thickness, and the Plenum Pressure ($P_{gas}$) In Each Axial Section (Case NO)

POOR ORIGINAL

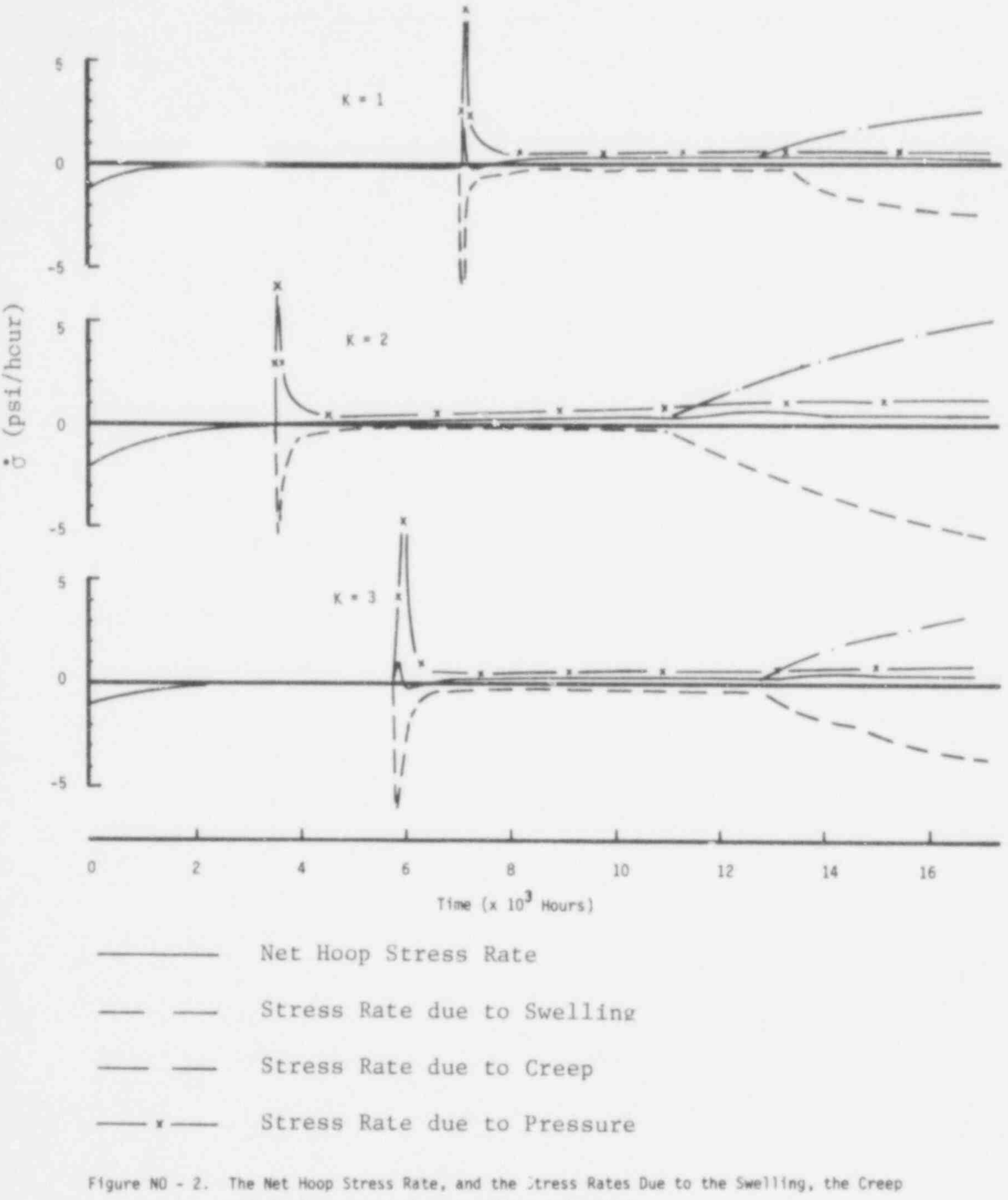


Figure NO - 2. The Net Hoop Stress Rate, and the Stress Rates Due to the Swelling, the Creep and the Pressure at the Outer Wall of the Clad

733 222

POOR ORIGINAL

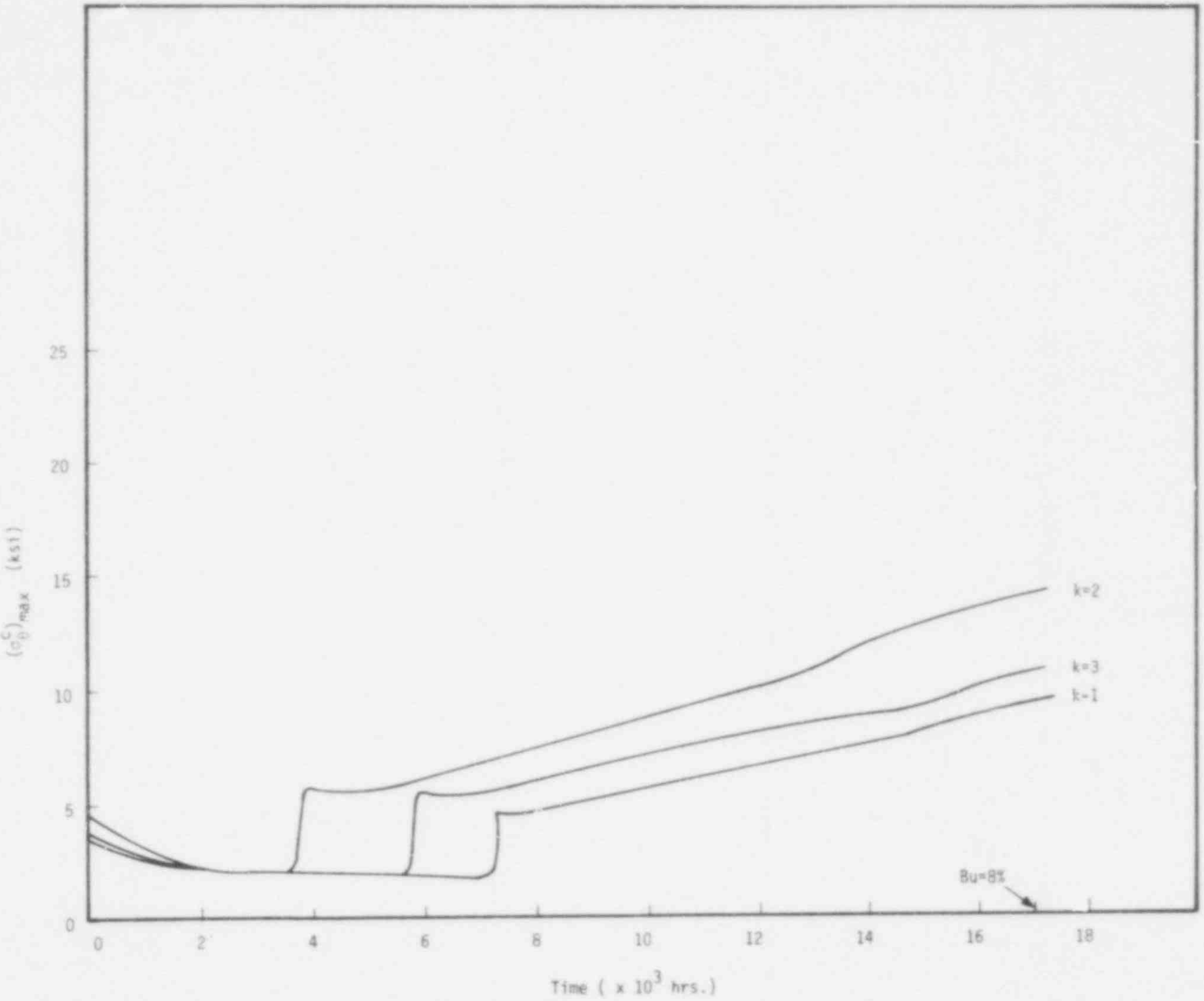


Fig. NO.3 The Maximum Hoop Stress in the Clad (Case NO).



733 223

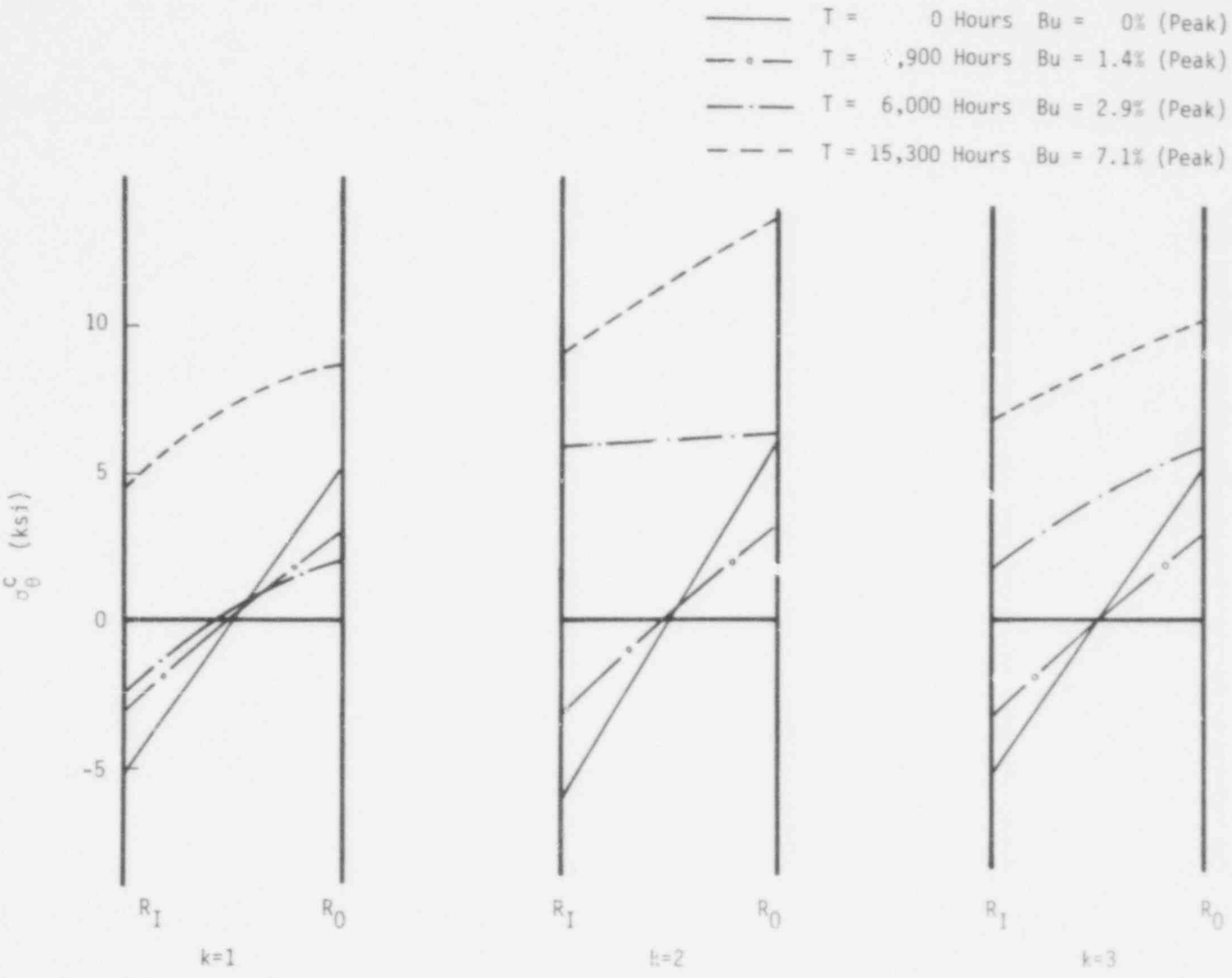


Fig. NO.4 The Distribution of the Hoop Stress Across the Clad Wall (Case NO)

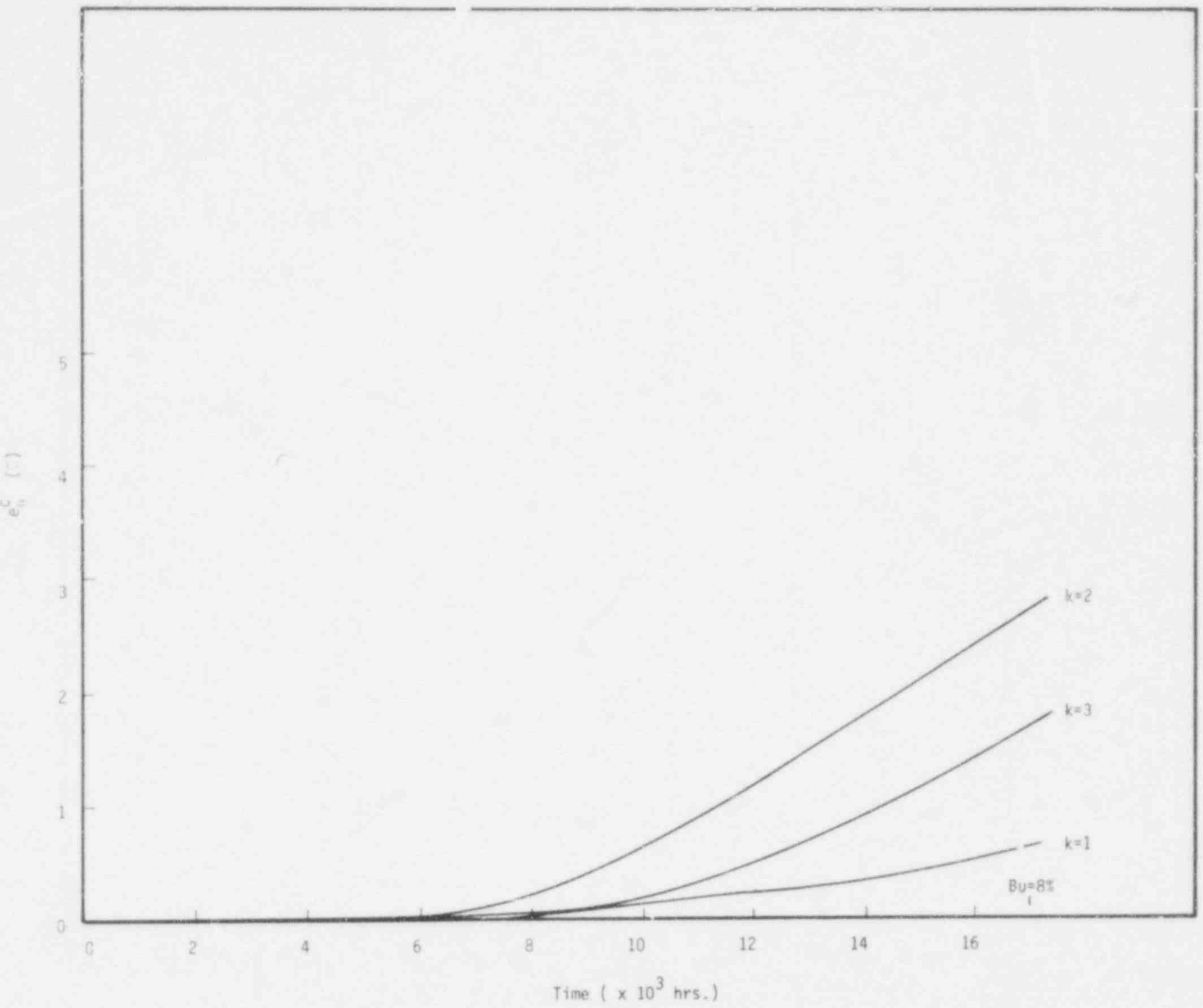


Fig. NO.5 The Hoop Strain in the Clad. (Case NO)

733 225

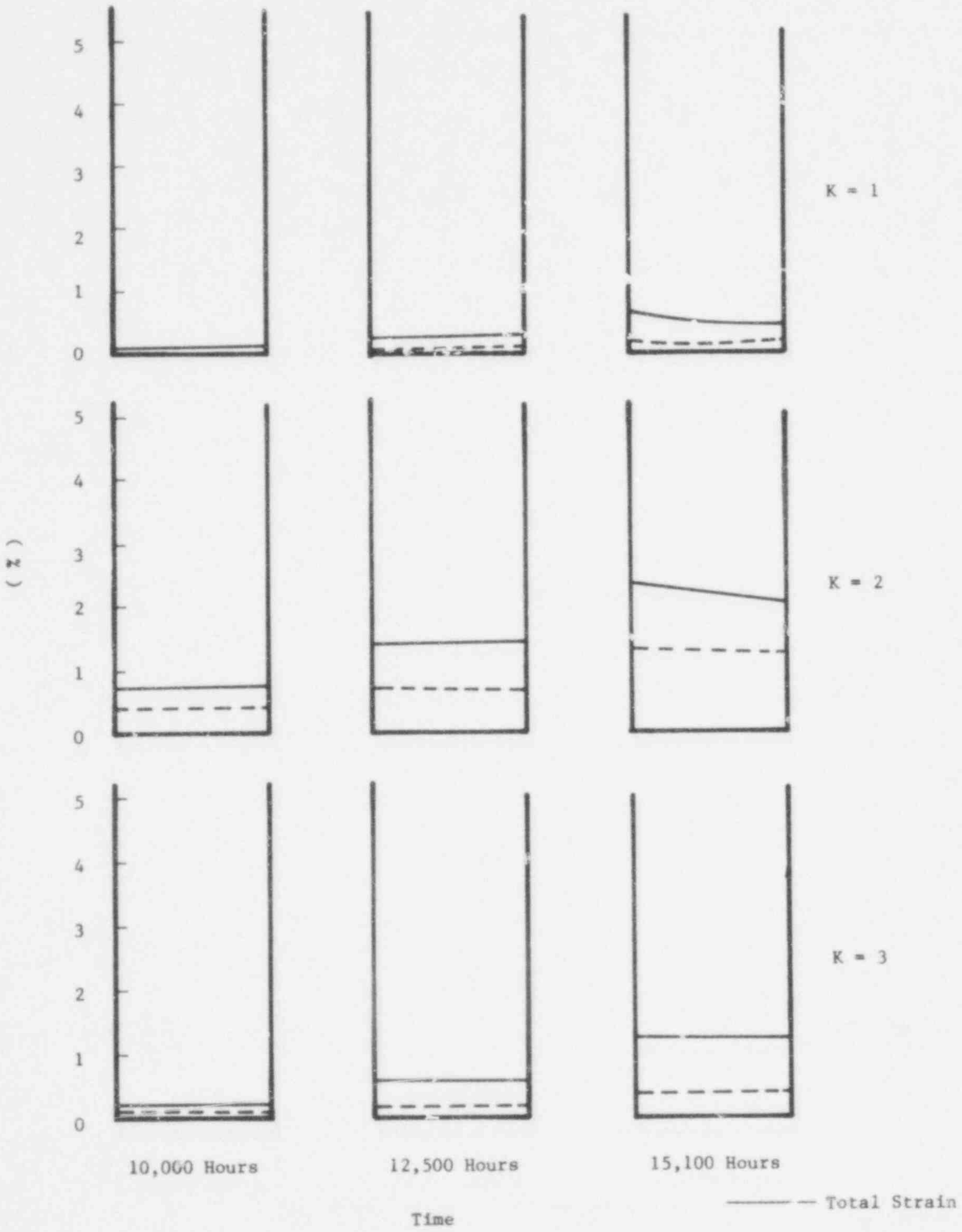


Figure NO - 6. The Total Strain and the Creep Strain Across the Clad Wall (Case NO)

733 226

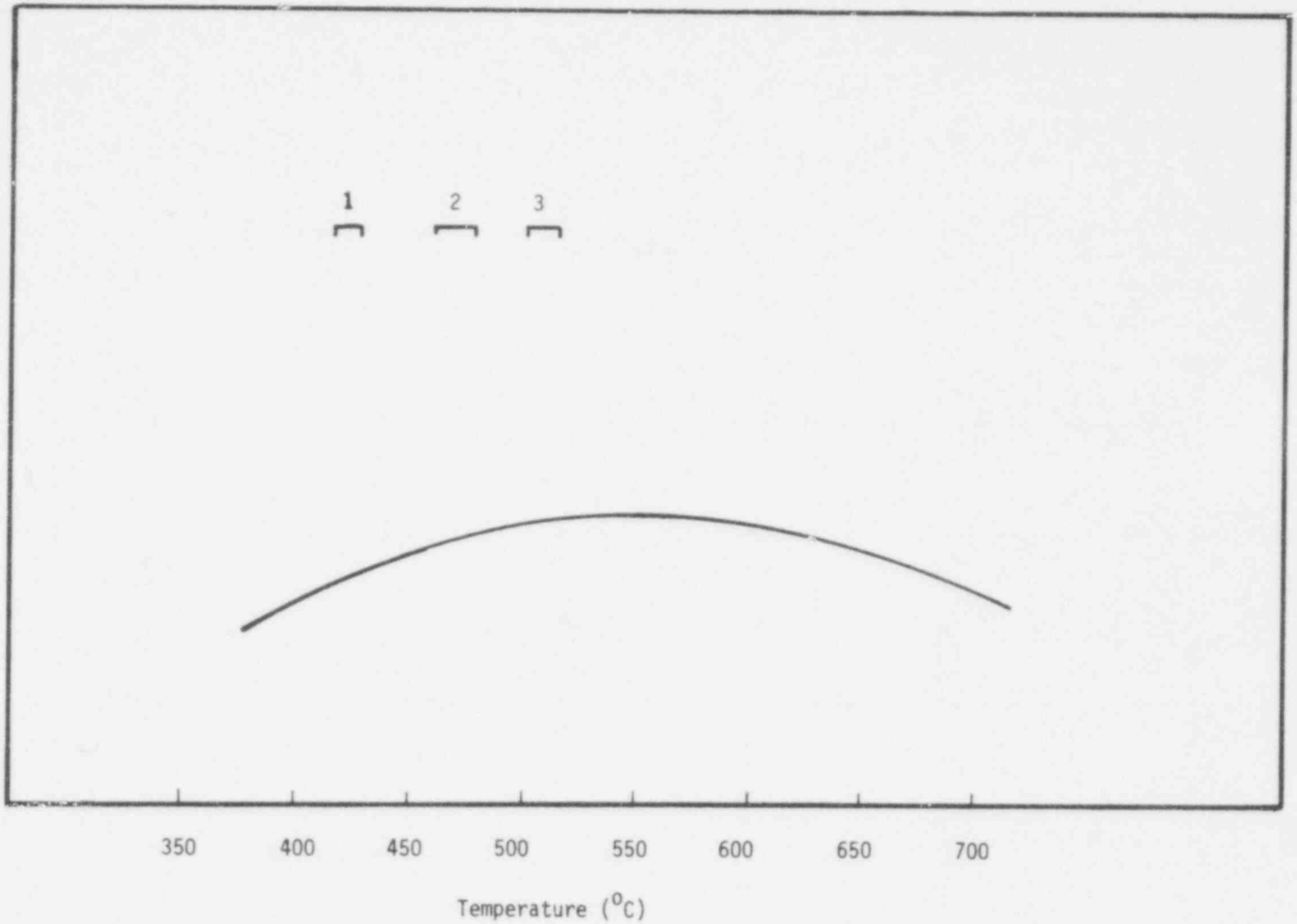


Figure N1 - 1. The Temperature of the Irradiated Swelling, and the Temperature Range Across the Clad Wall

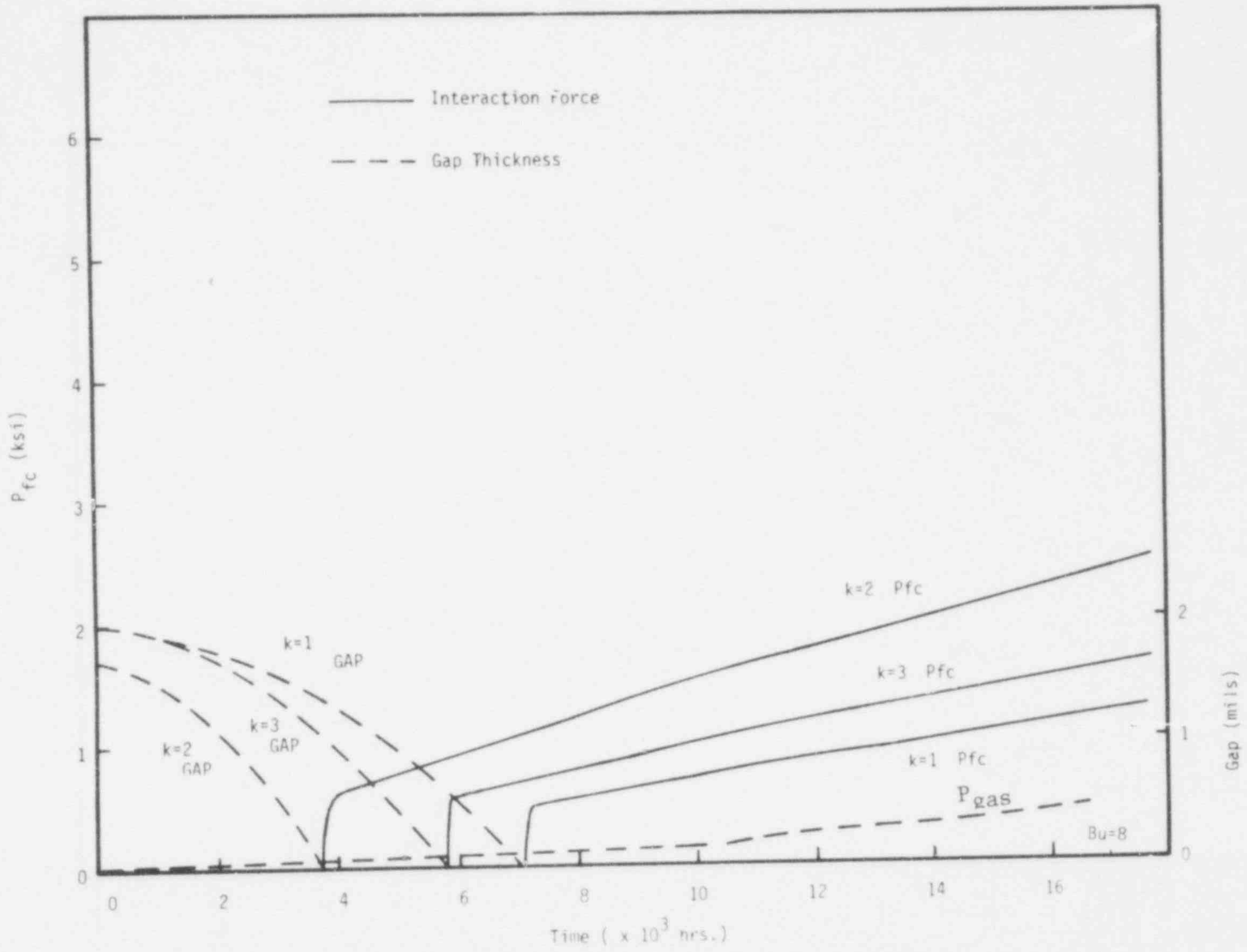


Fig. N1.2 The Fuel-Clad Gap Thickness and the Fuel-Clad Interaction Force. (Case N1)

733 228

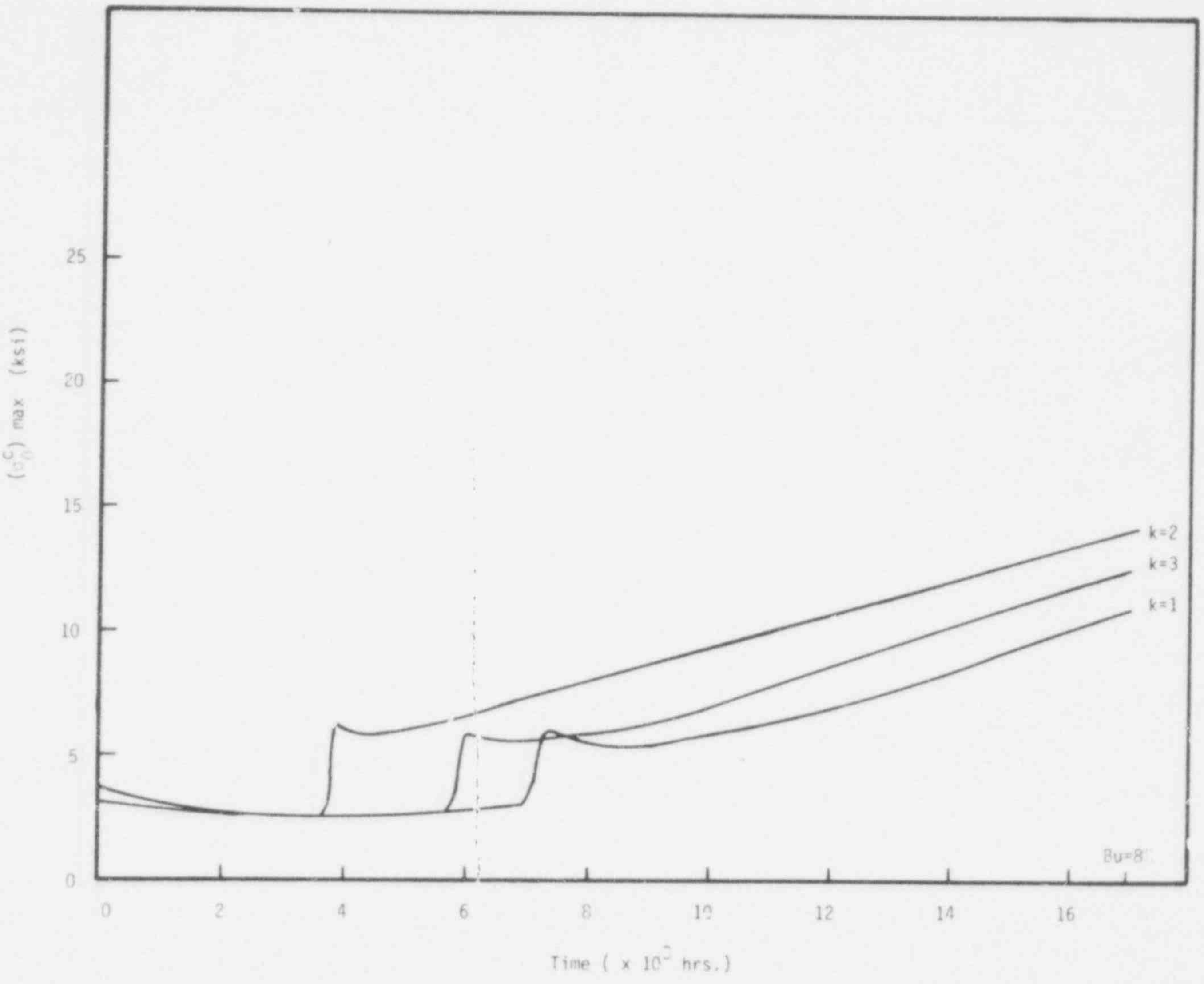


Fig. N1.3 The Maximum Hoop Stress in the Clad.

733 229

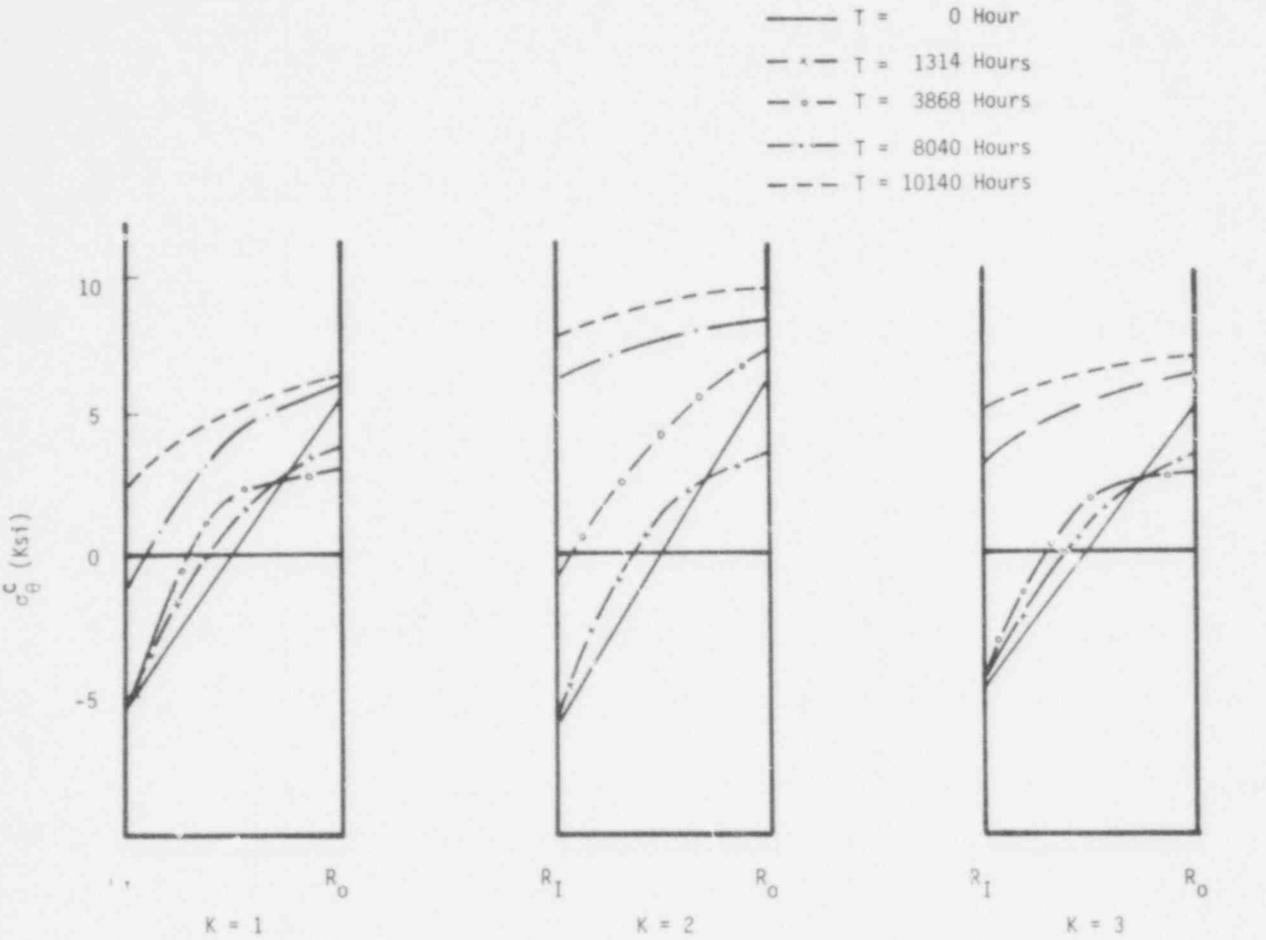


Figure N1 - 4. The Distribution of the Hoop Stress Across the Clad Wall ( Case N1 )

733 230

POOR ORIGINAL

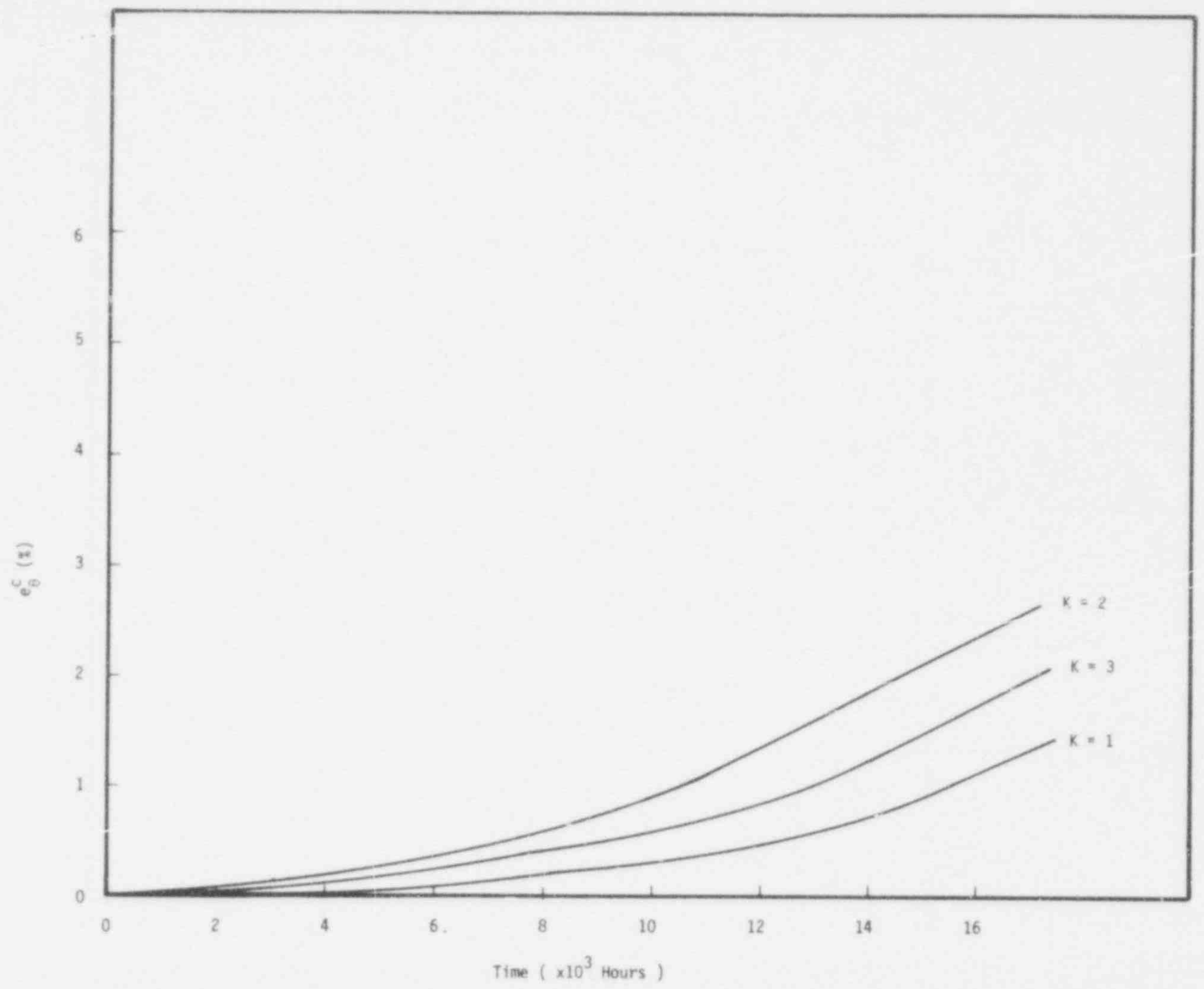


Figure N1 - 5. The Hoop Strain in the Clad (Case N1)

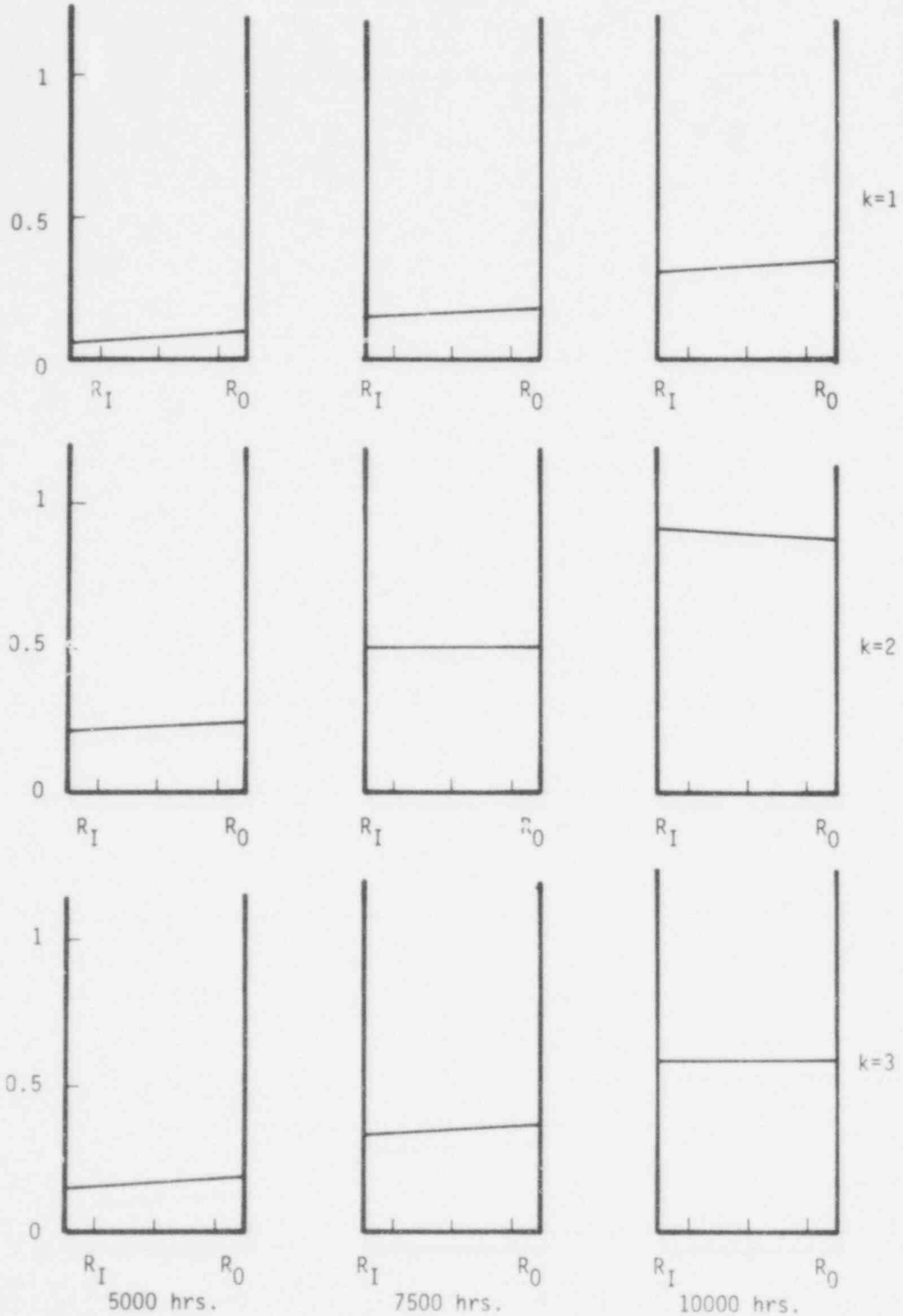


Fig. N1.6 The Distribution of the Hoop Strain (——) and the Creep Strain (– –) Across the Clad Wall. (Case N1)

733 232

6 kW/ft Cases

Case N3

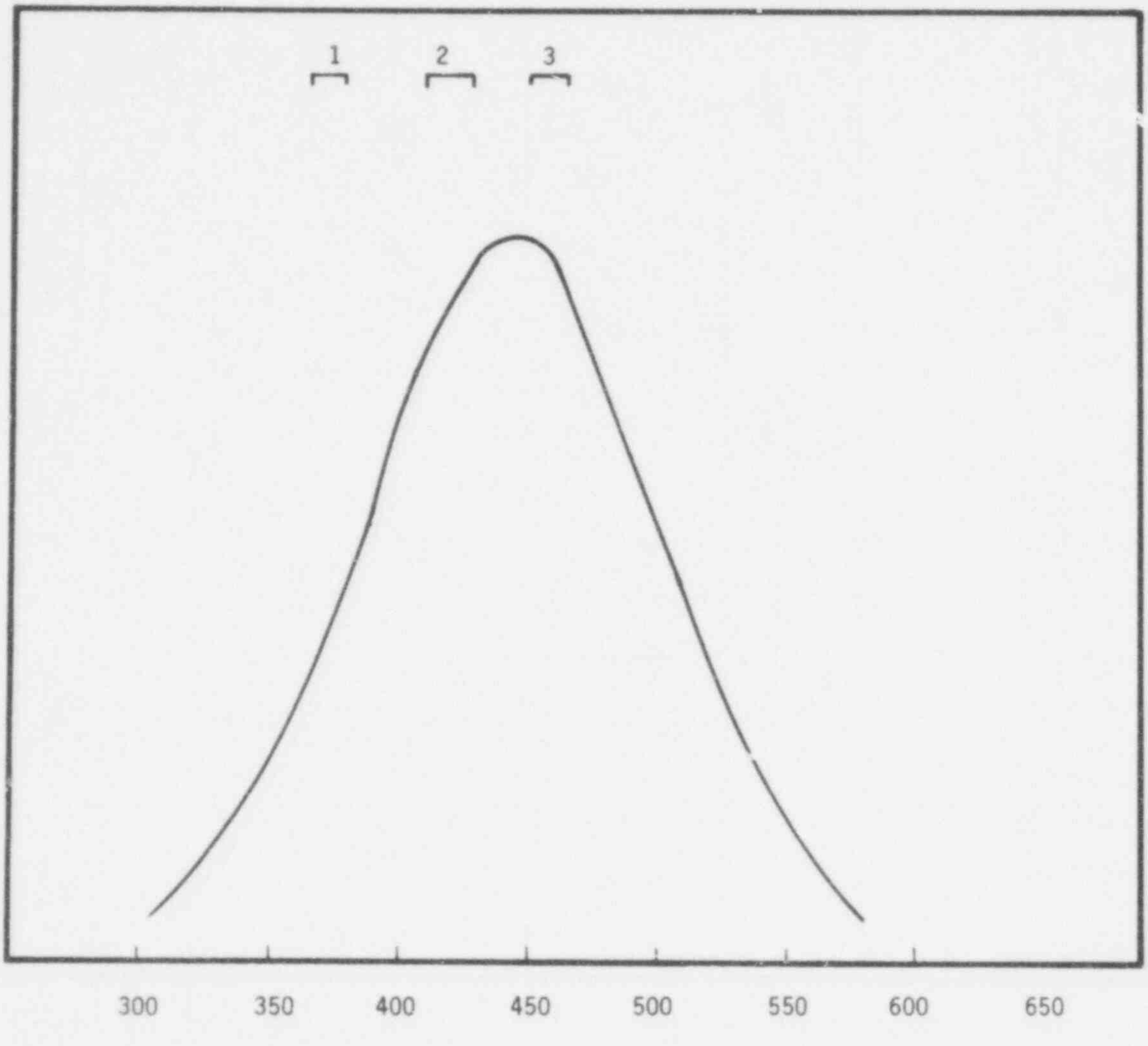


Figure N3 - 1. The Temperature of the Irradiated Swelling, and the Temperature Range Across the Clad Wall

733 233

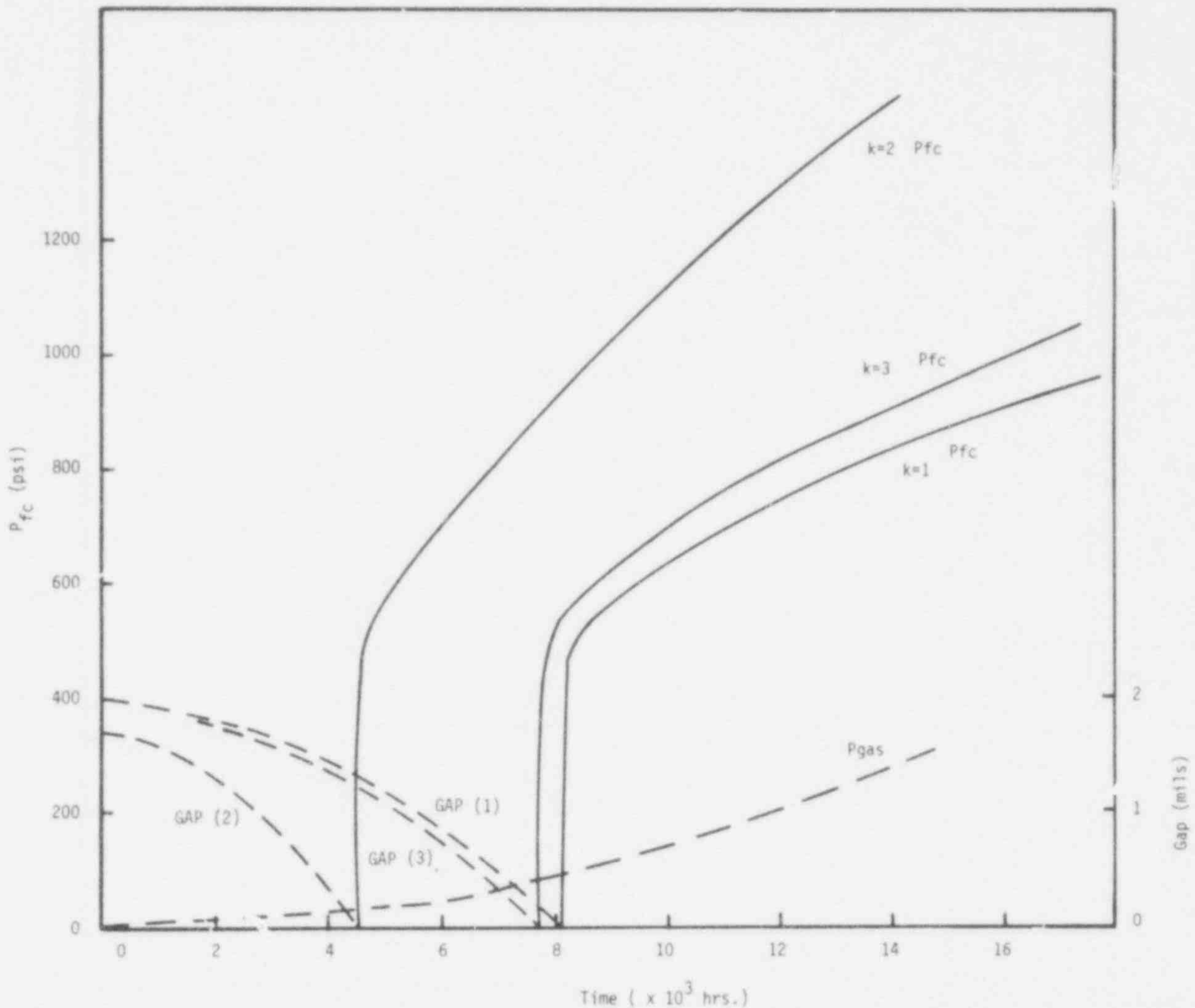


Fig. N3.2 The Fuel-Clad Gap Closure (GAP), the Fuel-Clad Interaction Force (Pfc), and the Plenum Pressure (Pgas). ( Case N3)

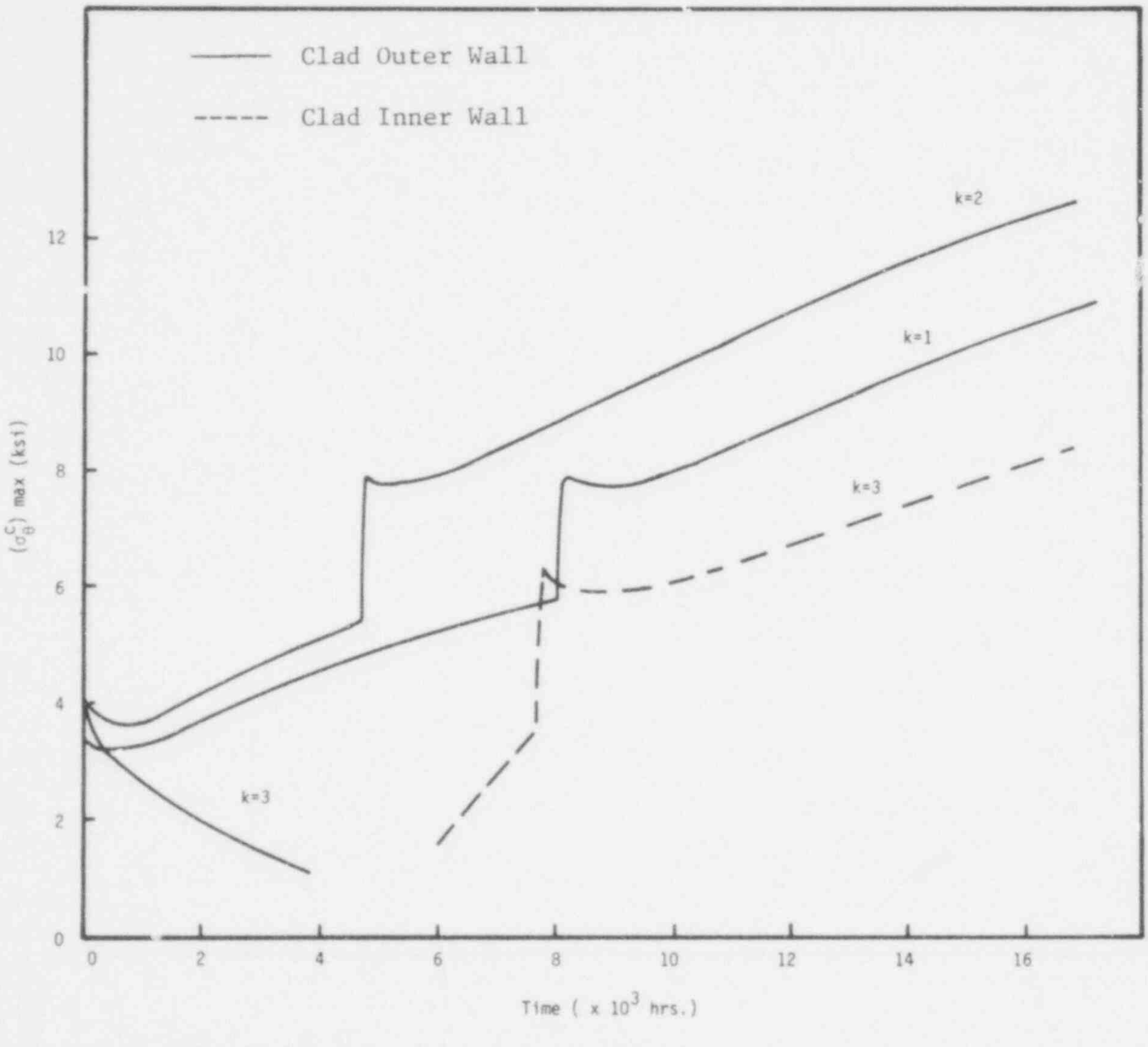


Fig. N3.3 The Maximum Hoop Stress in the Clad (Case N3).

733 235

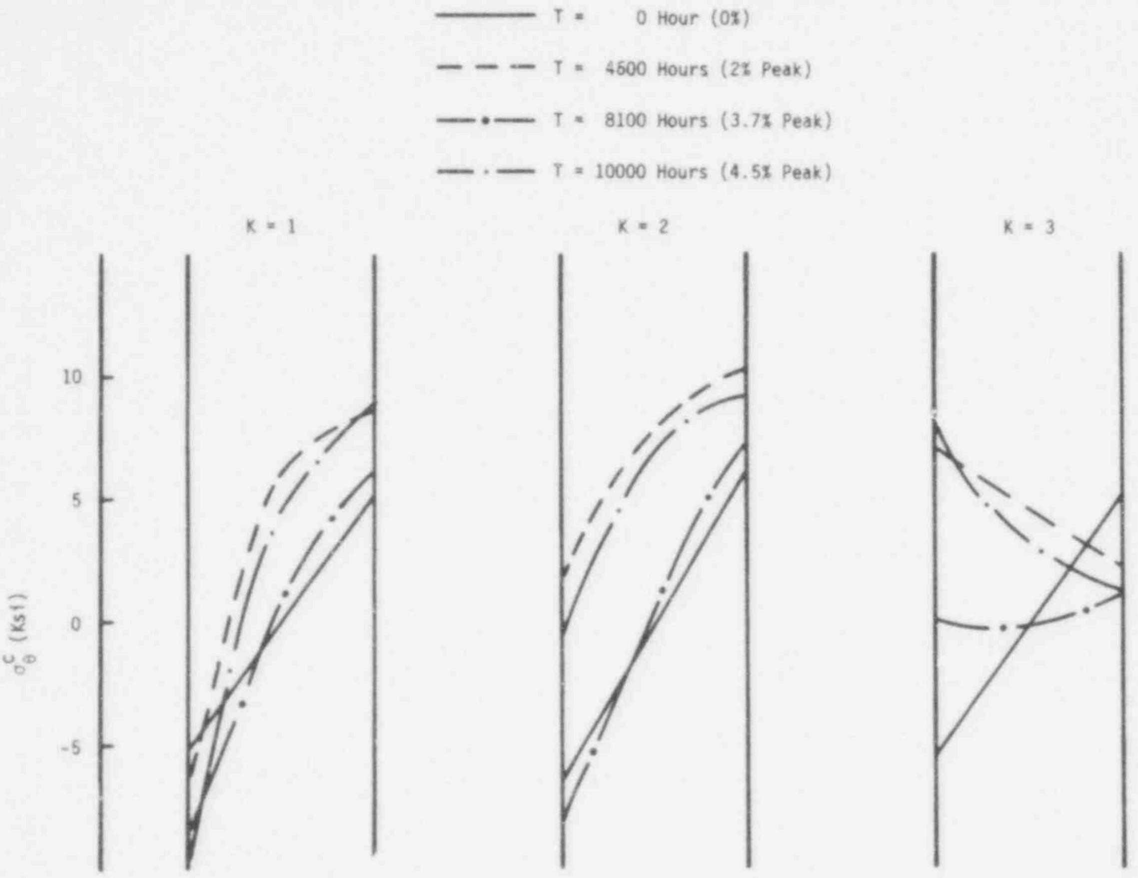


Figure N3 - 4. The Distribu'ion of the Hoop Stress Across the Clad Wall
( Case N3 )

733 236

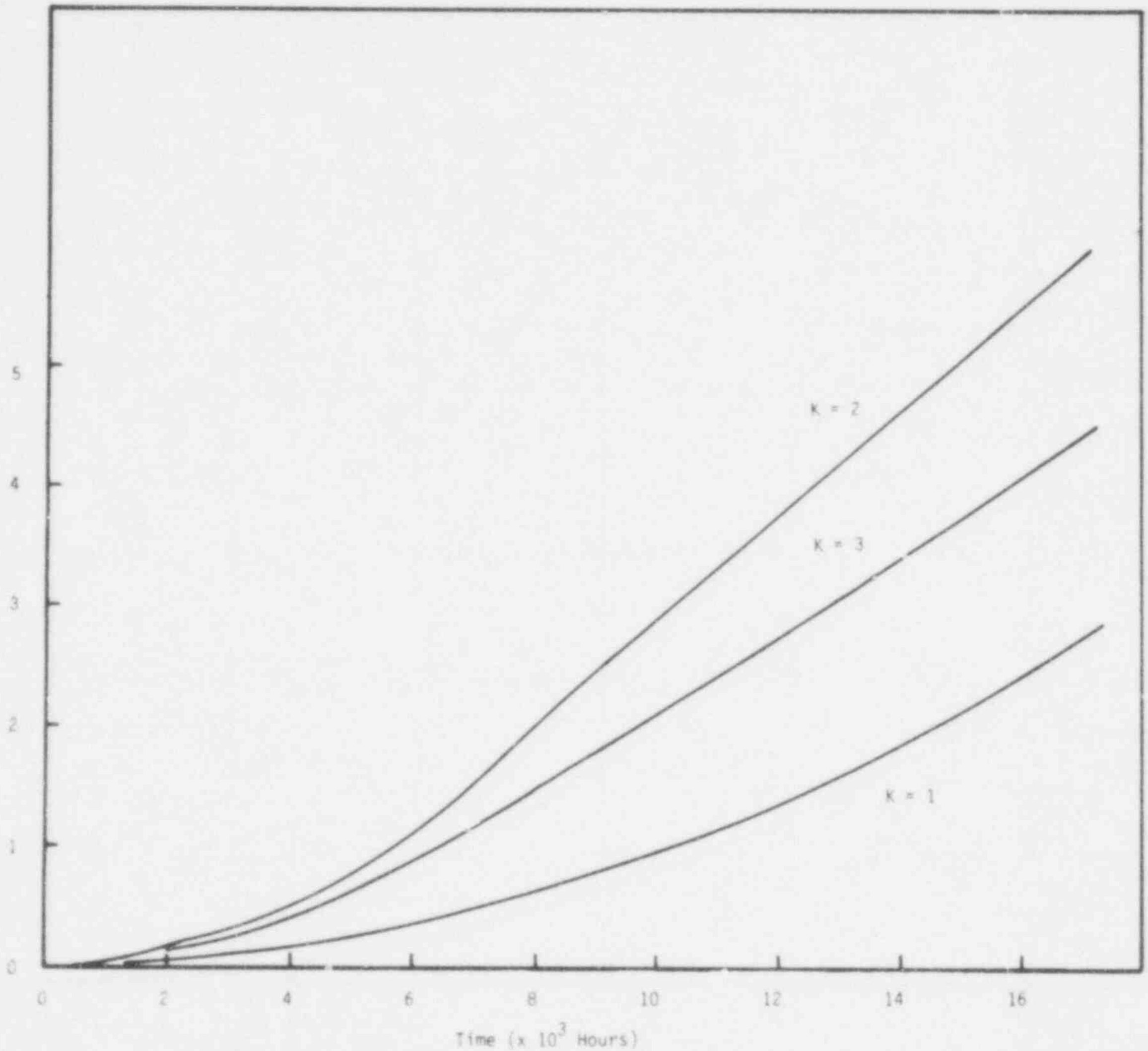


Figure N3 - 5. The Hoop Strain in the Clad ( Case N3 )

733 237

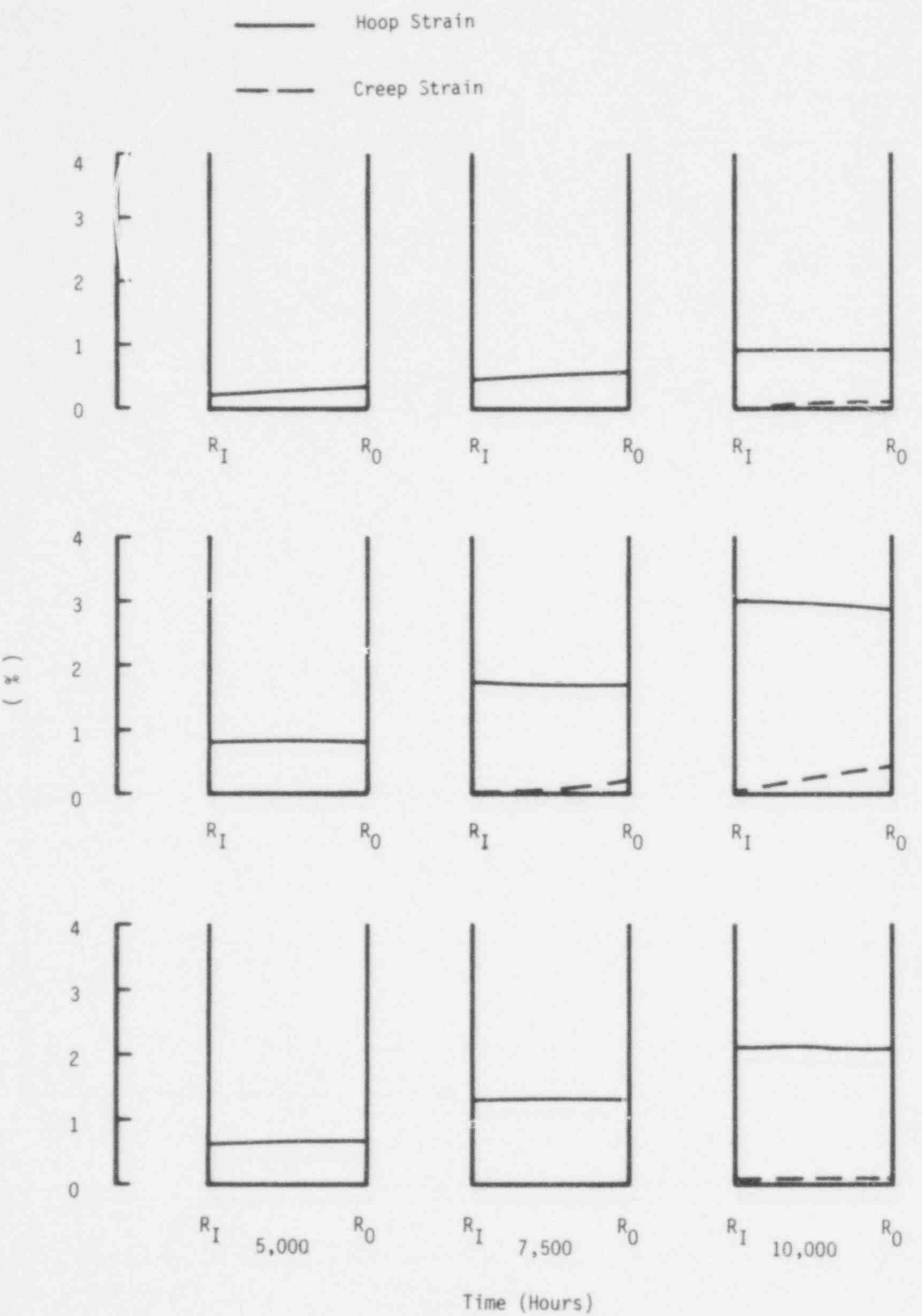


Figure N3 - 6. The Distribution of the Hoop Strain and the Creep Strain Across the Clad Wall (Case N3)

733 238

6 kW/ft Cases

Case N4

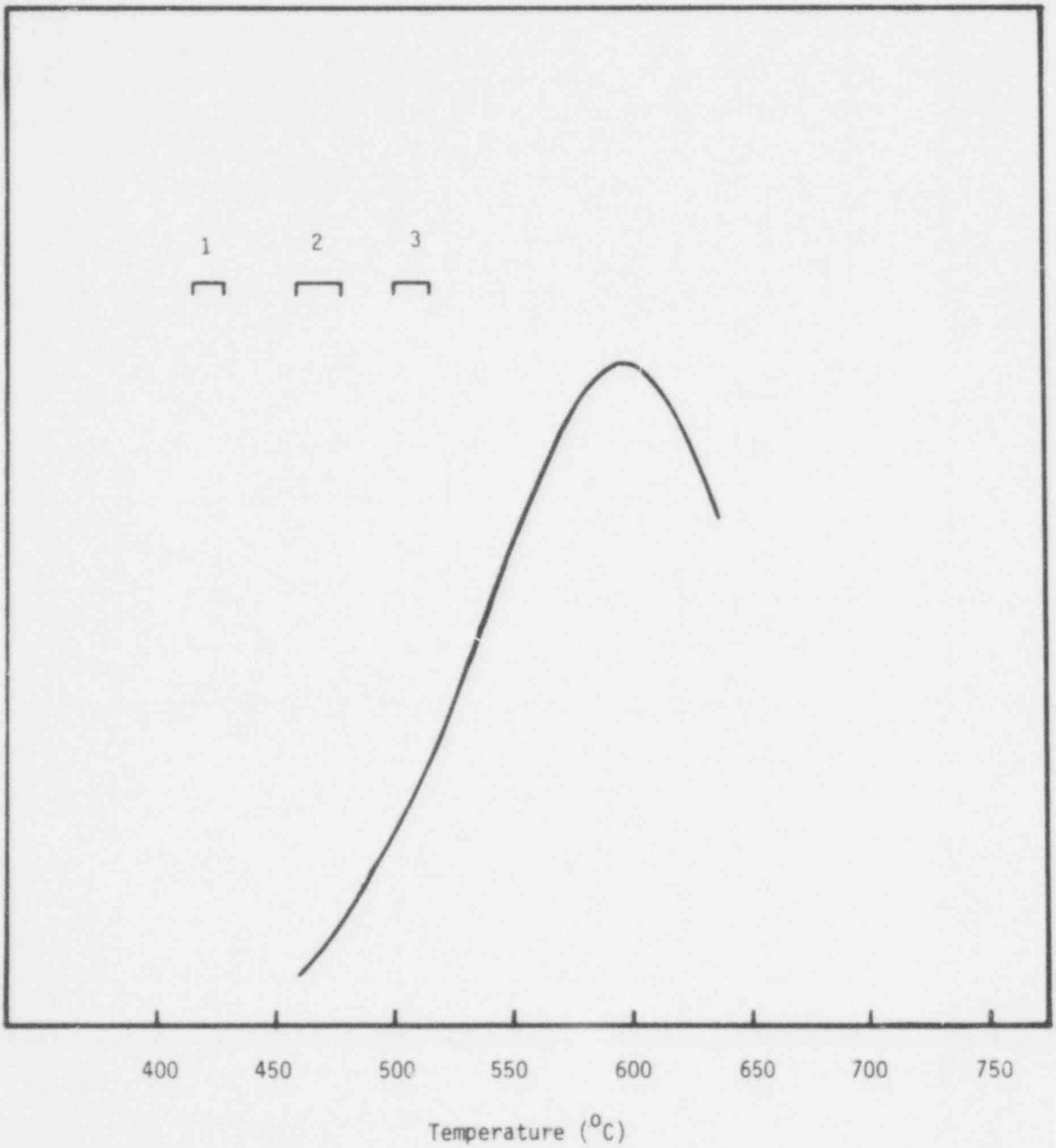


Figure N4 - 1. The Temperature Dependence of the Irradiated Swelling, and the Temperature Range Across the Clad

733 239

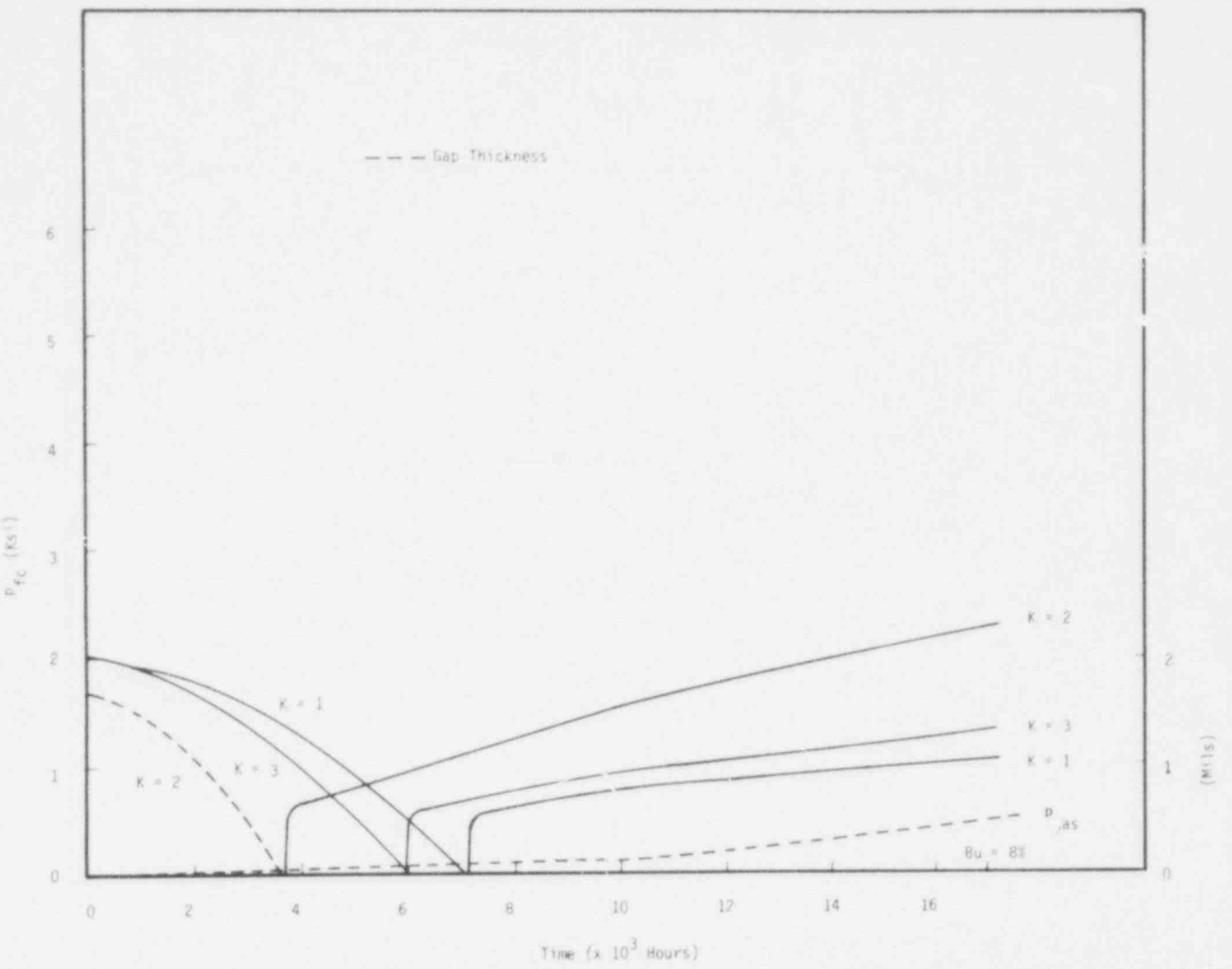


Figure N4 - 2. The Fuel-Clad Interaction Force ($P_{fc}$), the Gap Thickness and the Plenum Pressure ($P_{gas}$) in Each Axial Section (Case N4)



733 240

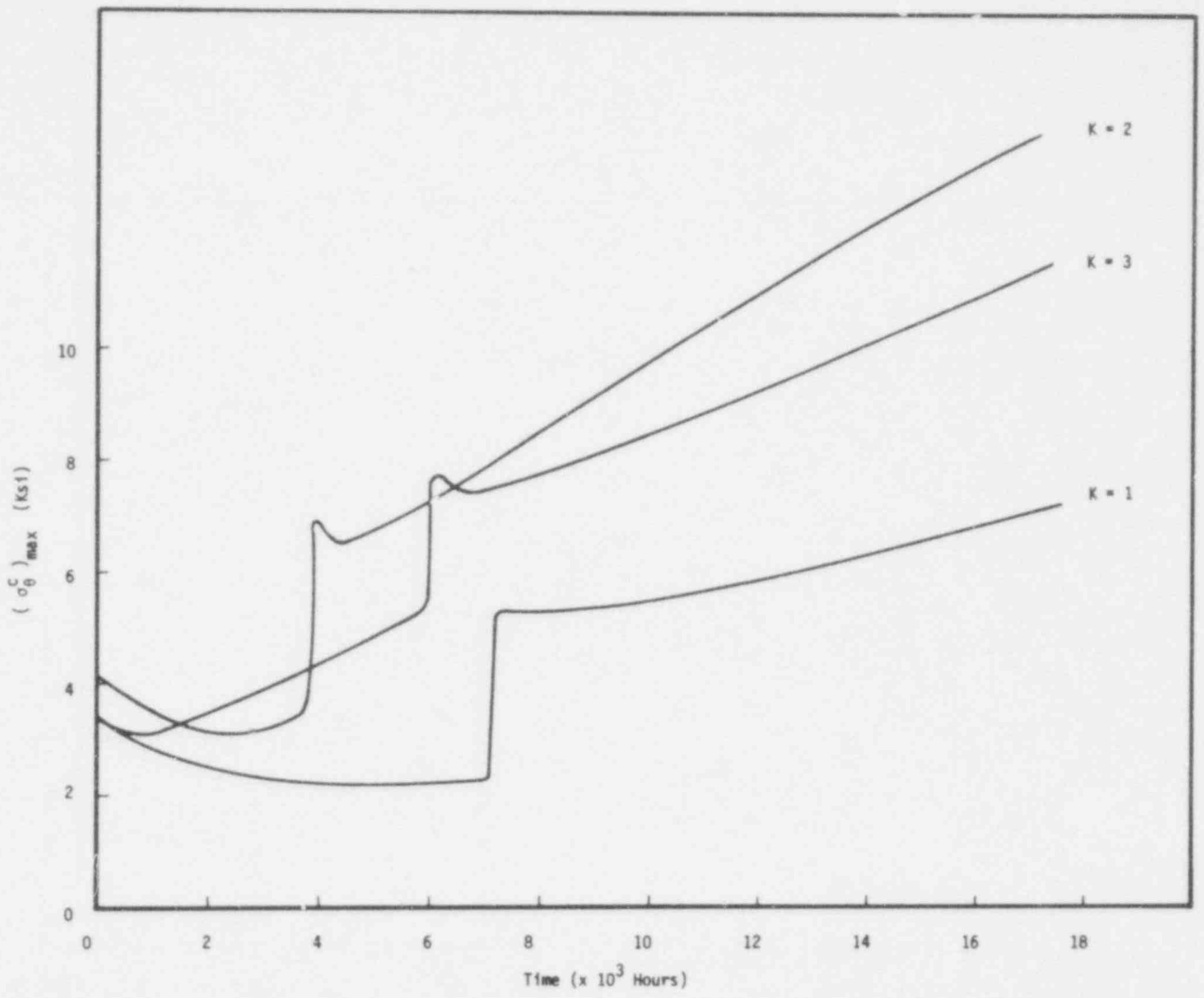


Figure N4 - 3. The Maximum Hoop Stress in the Clad (Case N4)

733 241

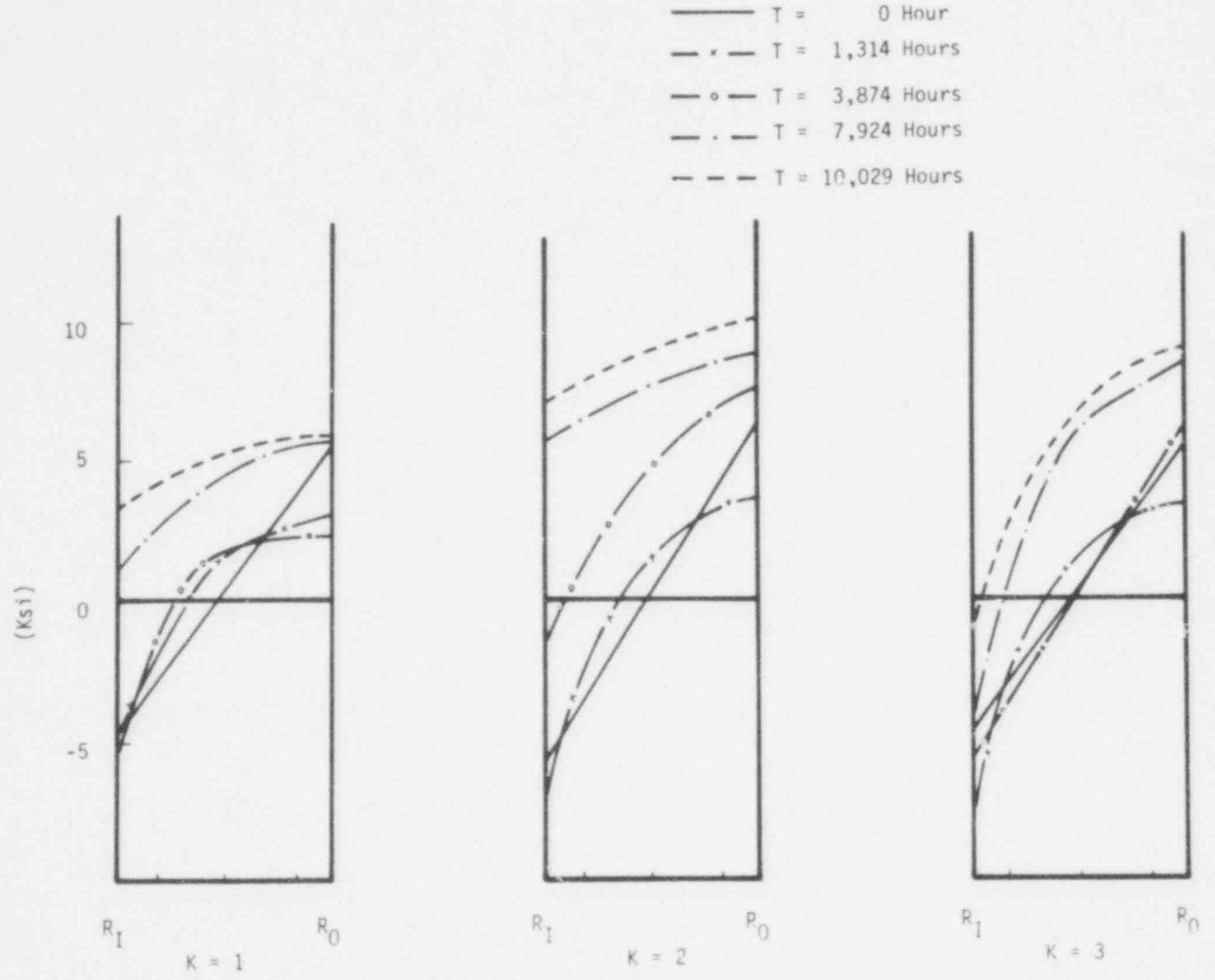


Figure N4 - 4. The Distribution of Hoop Stress Across the Clad Wall ( Case N4 )

733 242

POOR ORIGINAL

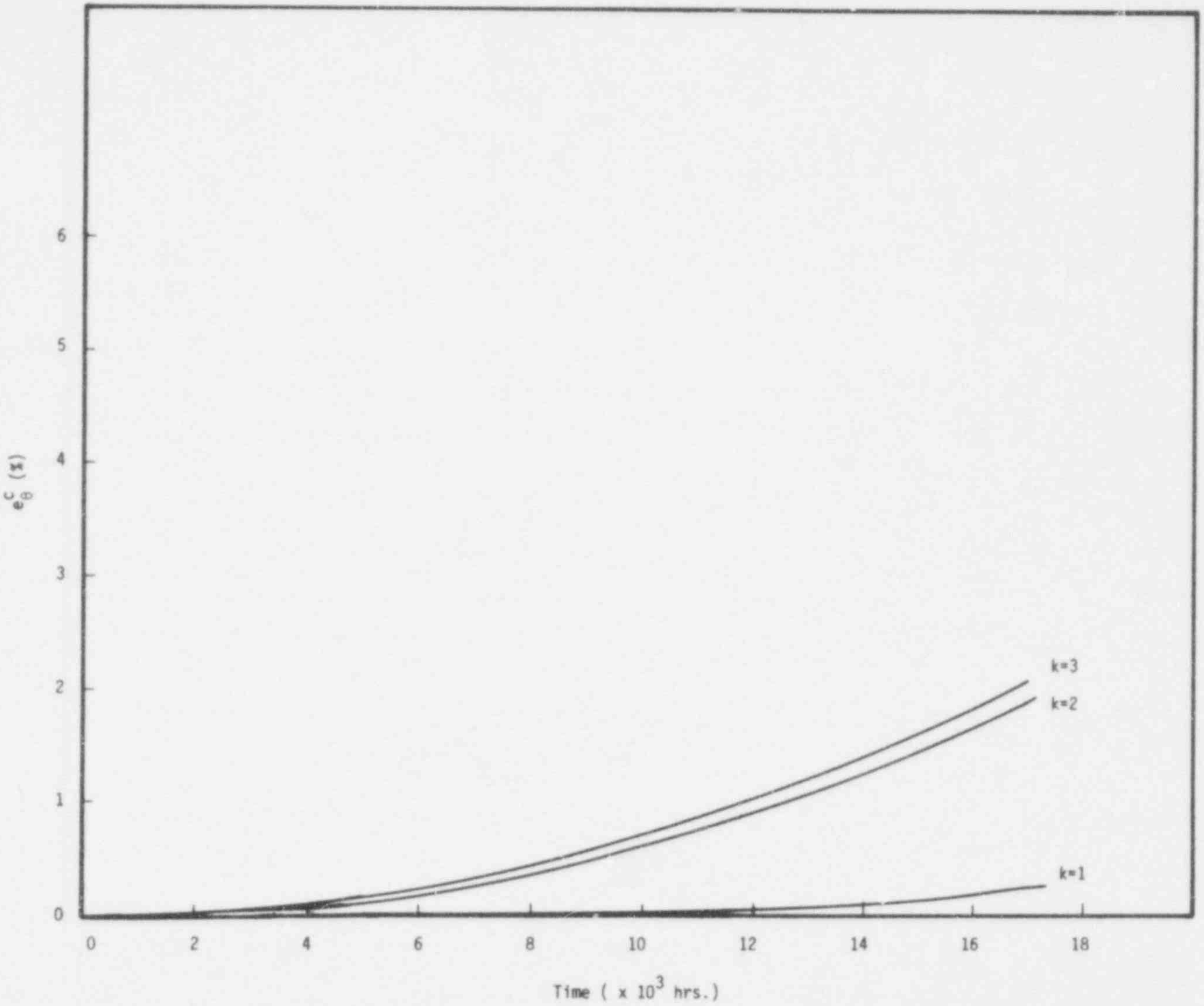


Fig. N4.5 The Hoop Strain in the Clad.



733 243

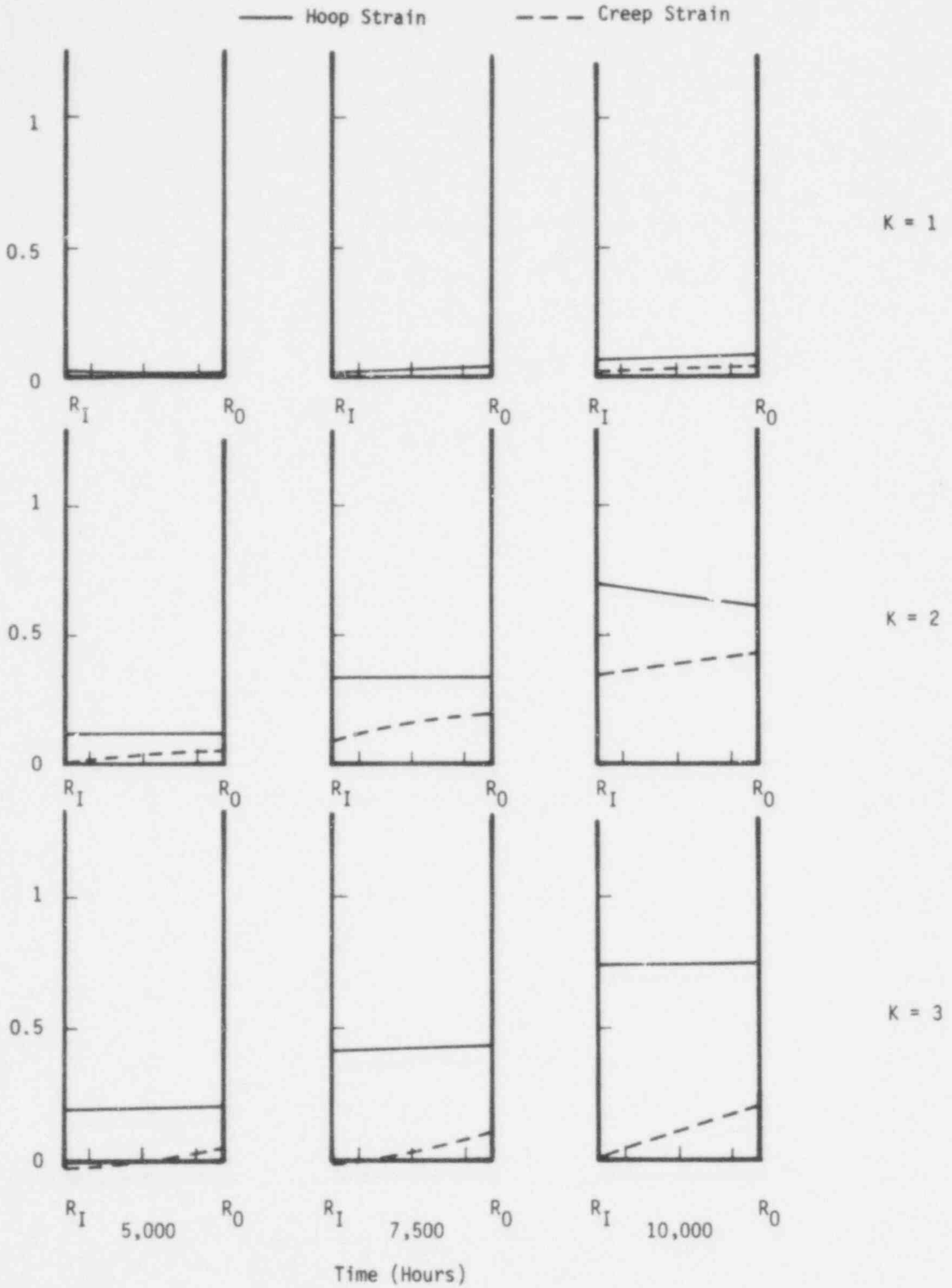


Figure N4 - 6. The Distribution of the Hoop Strain and the Creep Strain Across the Clad Wall ( Case N4 )

733 214

CONCEPTUAL LMFBR CALCULATIONS

15 kW/ft Cases

Case H0

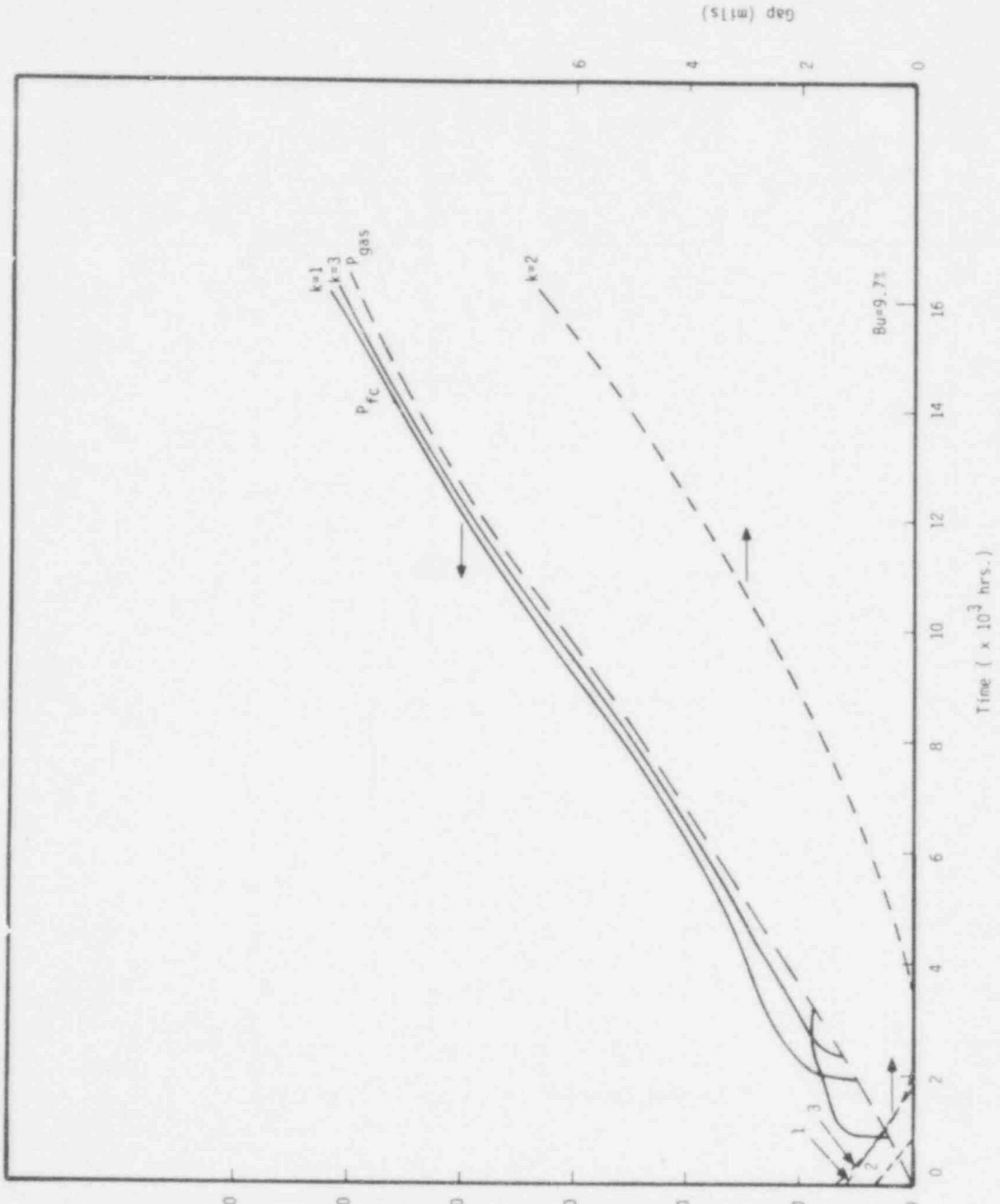


Fig. H0.1 The Fuel-Clad Gap Closure, the Fuel-Clad Interaction Force ($P_{fc}$), and the Plenum Pressure (Case H0)

POOR ORIGINAL

733 245

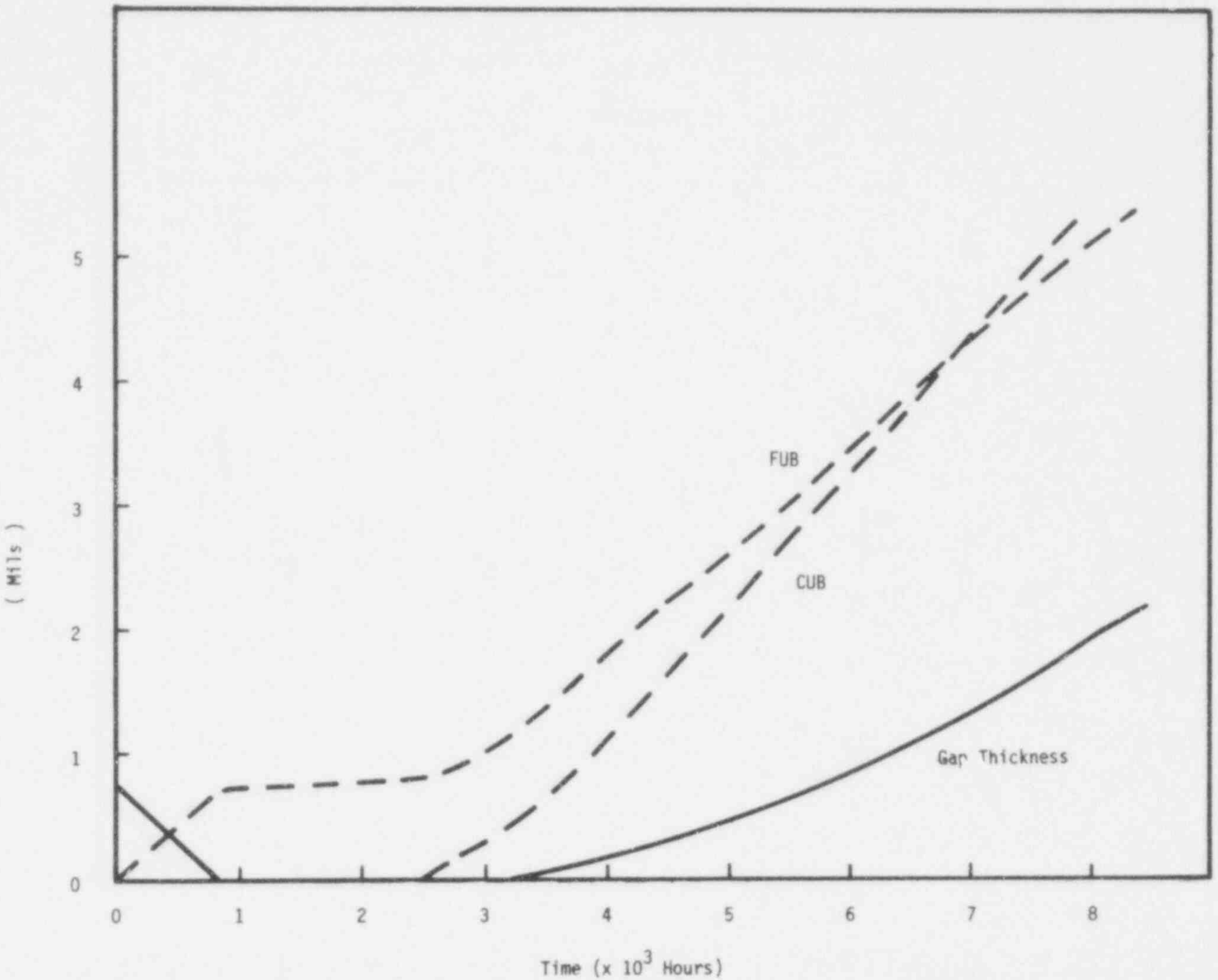


Figure HO - 2. Fuel Outer Boundary Displacement (FUB), Clad Inner Wall Displacement (CUB) and Gap Thickness of 2nd Axial Section in Case HO

733 246

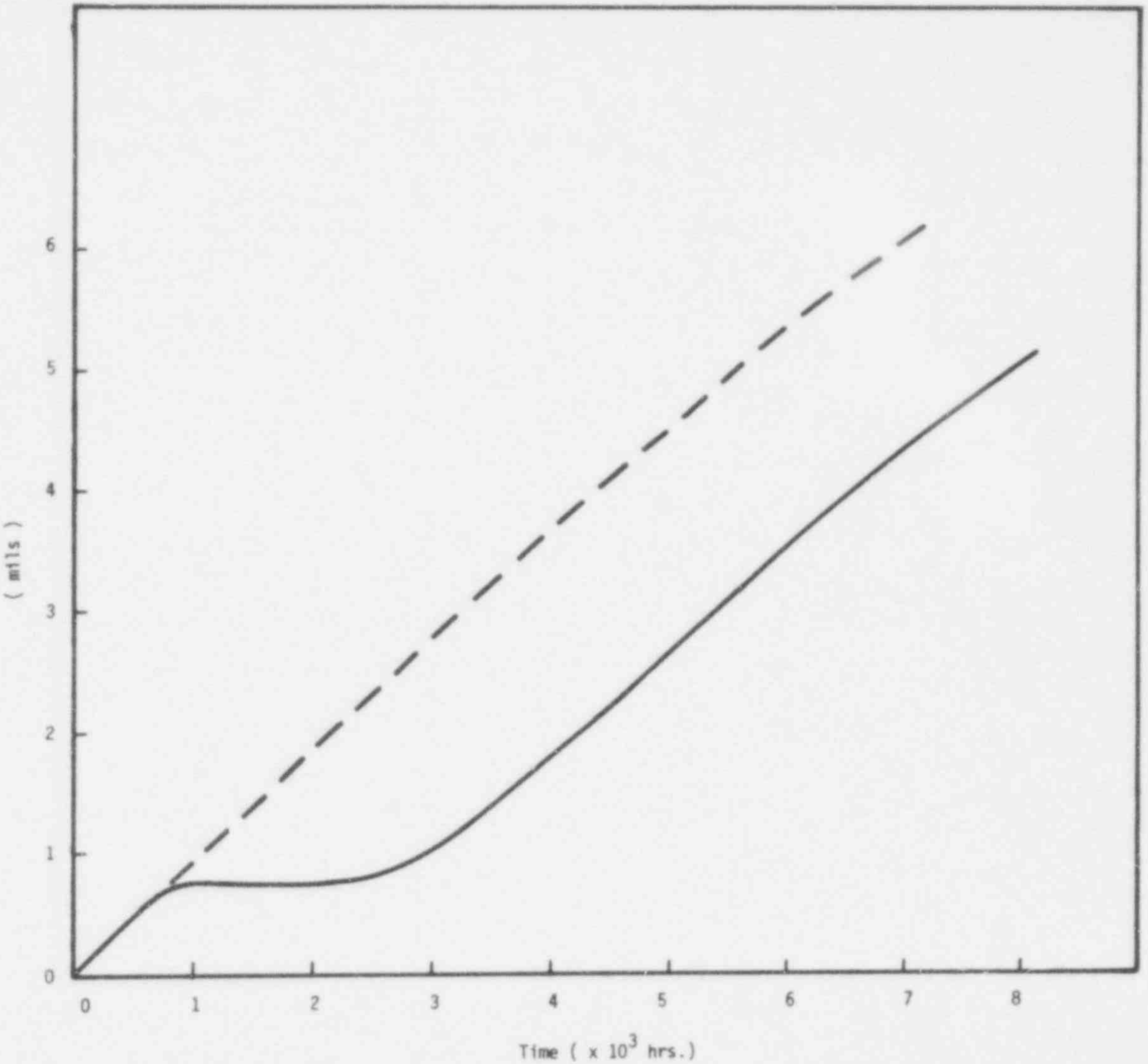


Fig. H0.3 Fuel Boundary Movement and the Effect of Clad Confinement in the Second Axial Section. (Case H0)

733 247

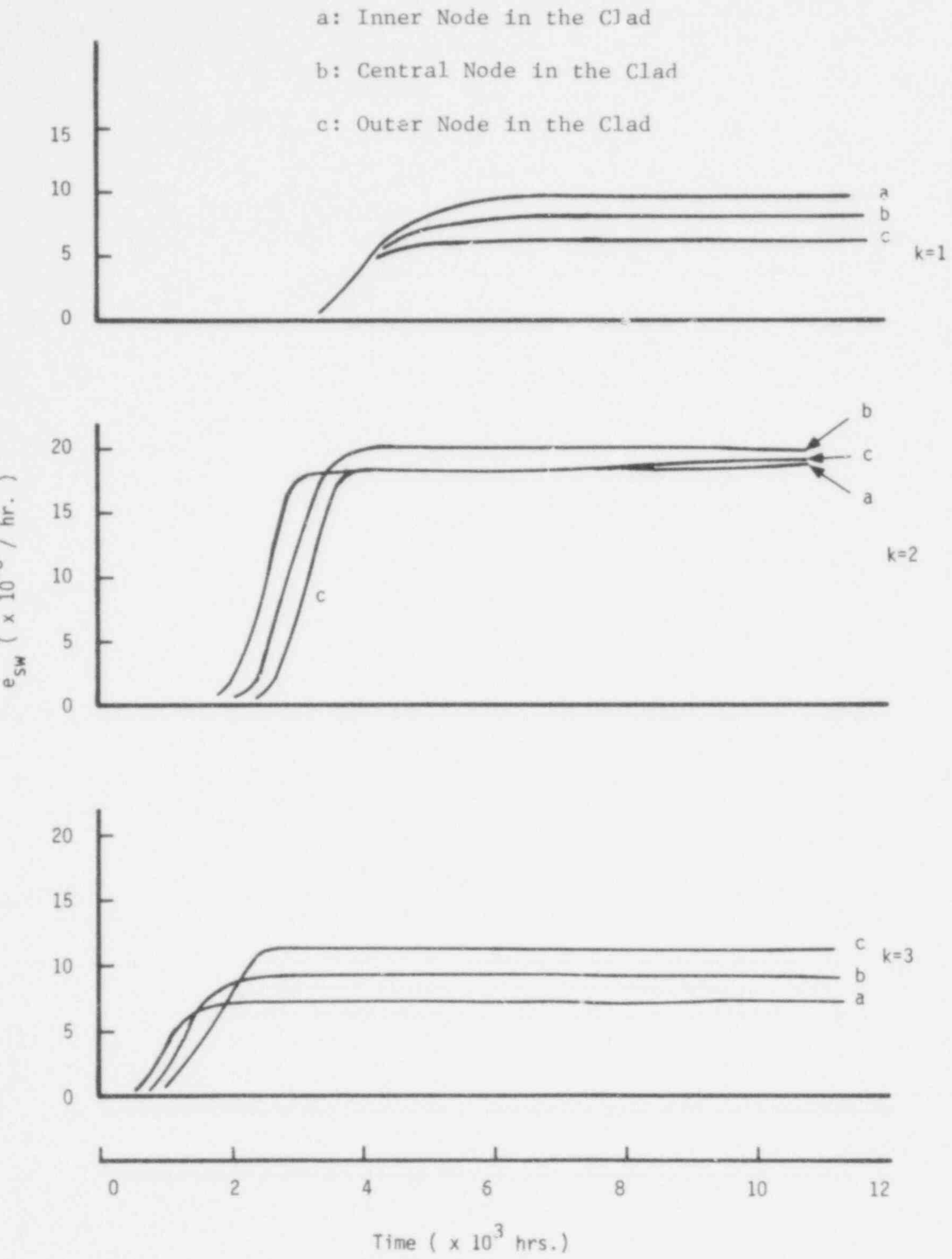


Fig. HO.4 The Rate of the Irradiated Swelling Strain Across the Clad Wall. (Case HO)

733 248

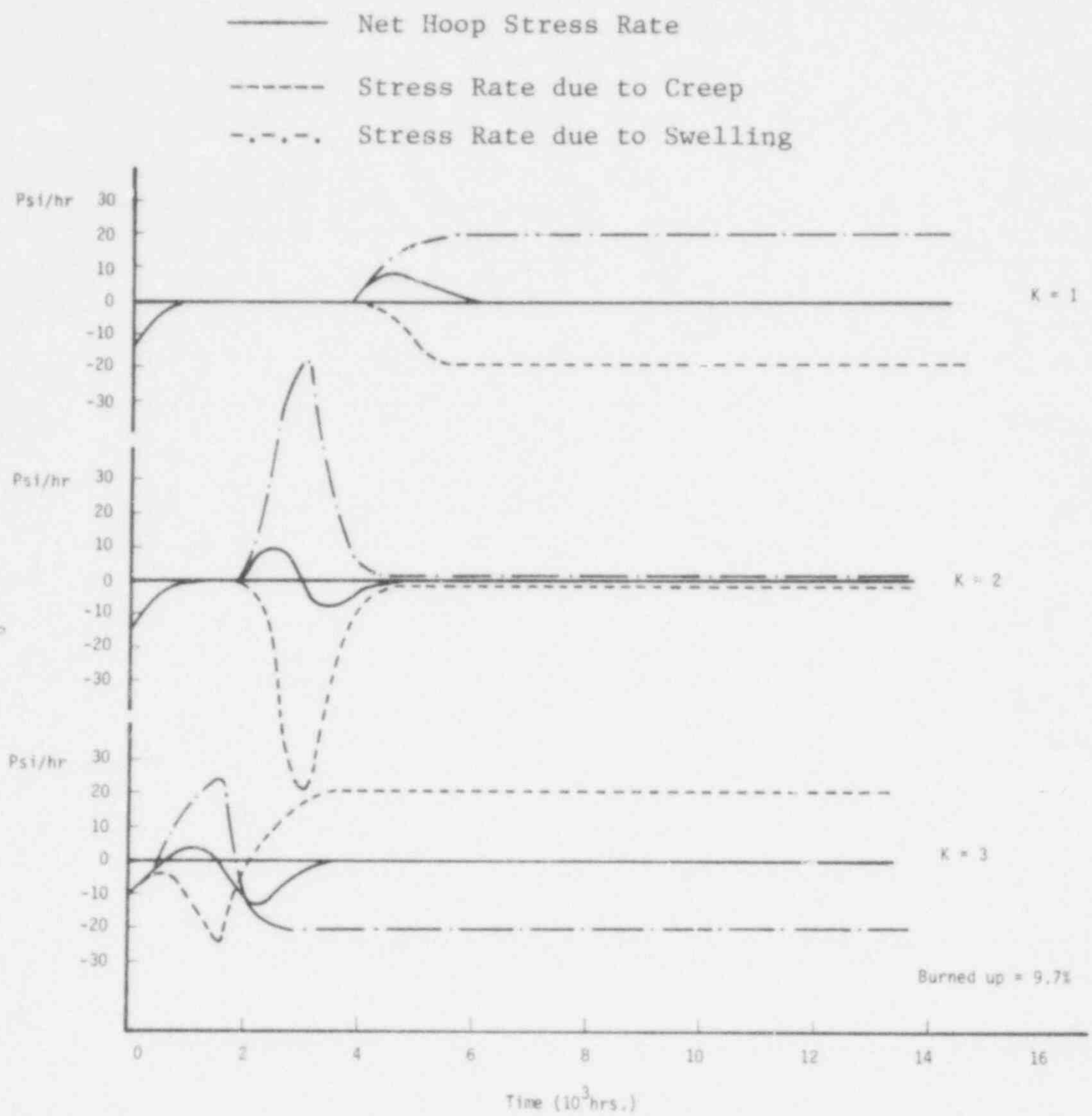


Fig. HO-5 The Net Hoop Rate, and the Hoop Stress Rate Due to the Creep and the Swelling at the Outer Wall of the Clad (Case HO).

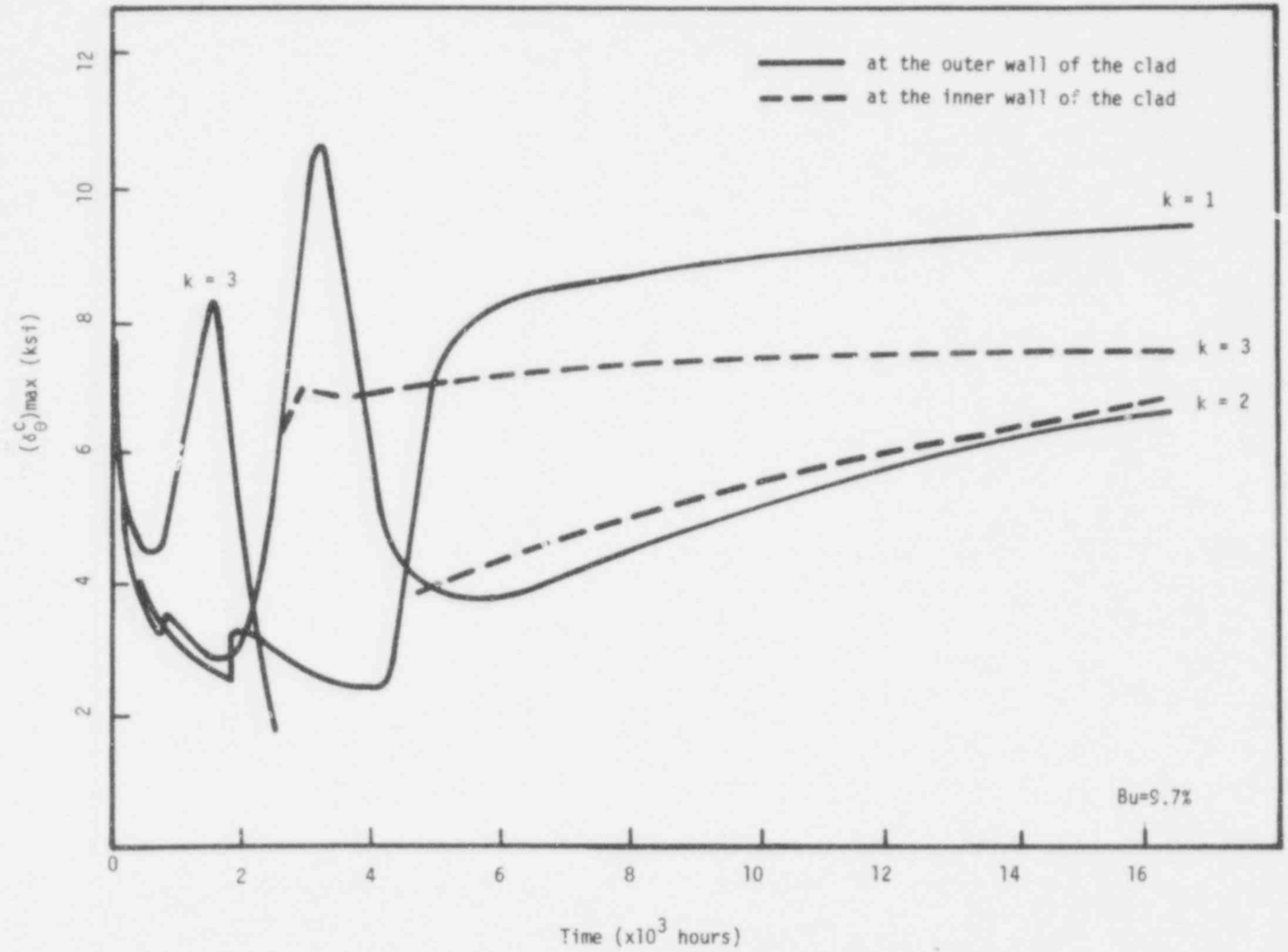


Figure HO - 6. The Maximum Hoop Stress in the Clad for Each Axial Section (Case HO)



733 250

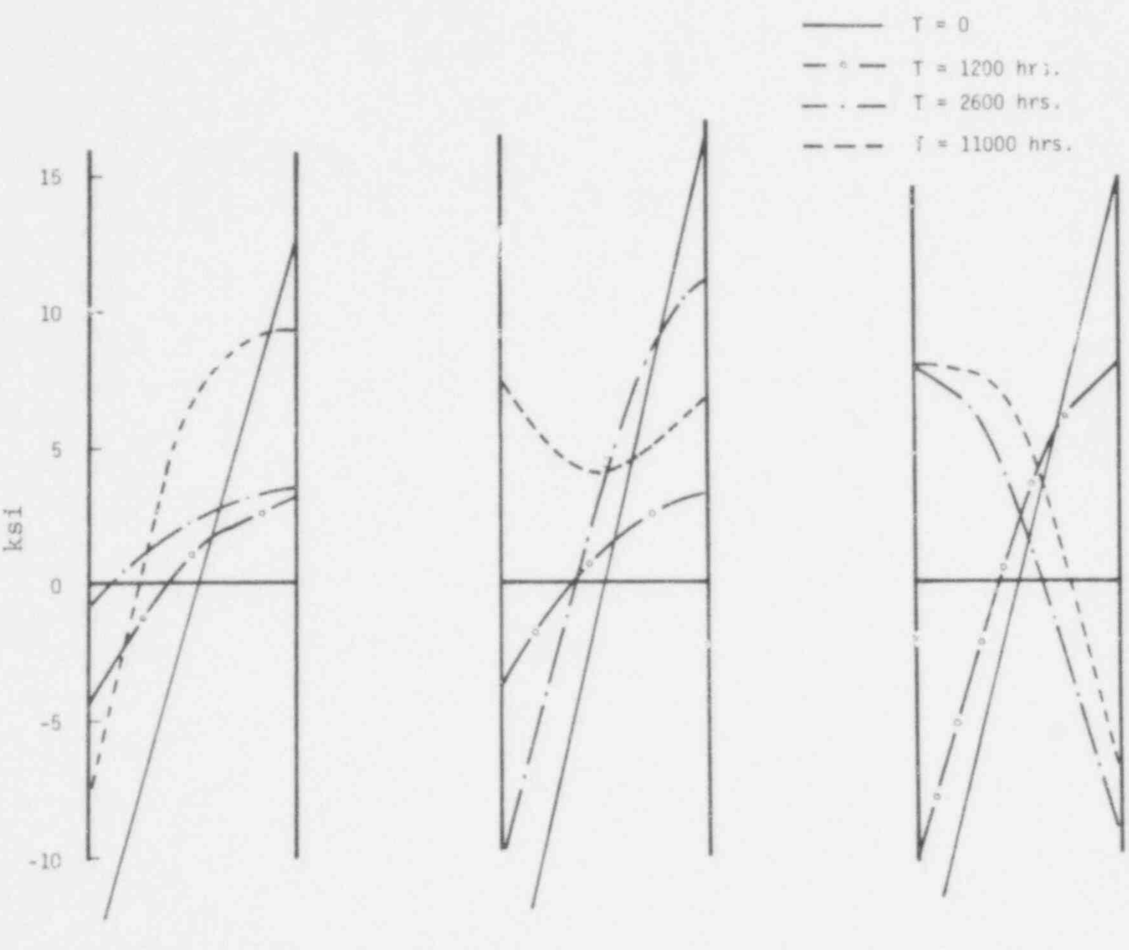


Fig. HO-7 The Distribution of Hoop Stress Across the Clad Wall (Case HO).

POOR ORIGINAL 733 251

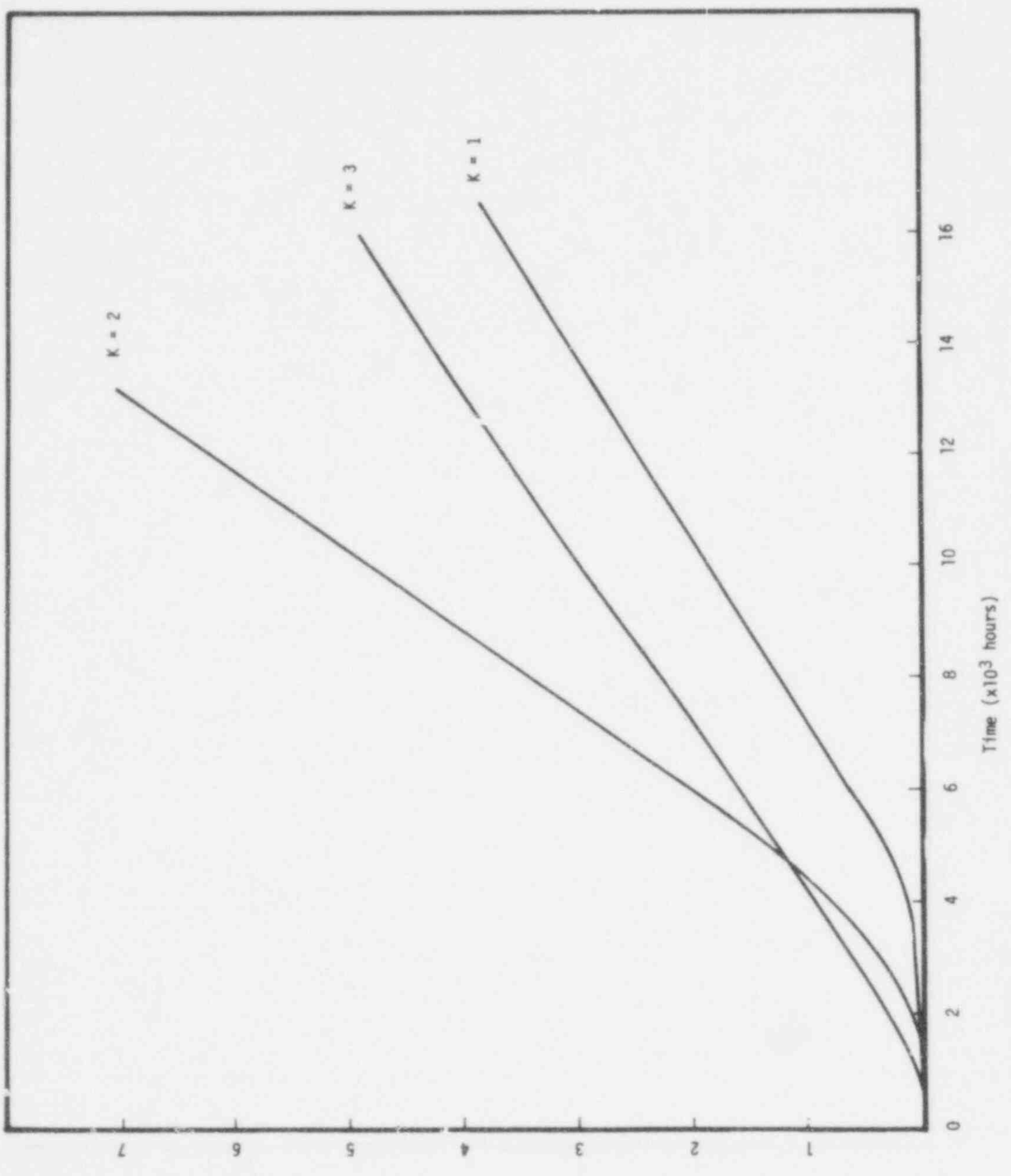


Figure Ho-8 The Hoop Strain at the Outer Wall of the Clad (Case Ho)

733 252

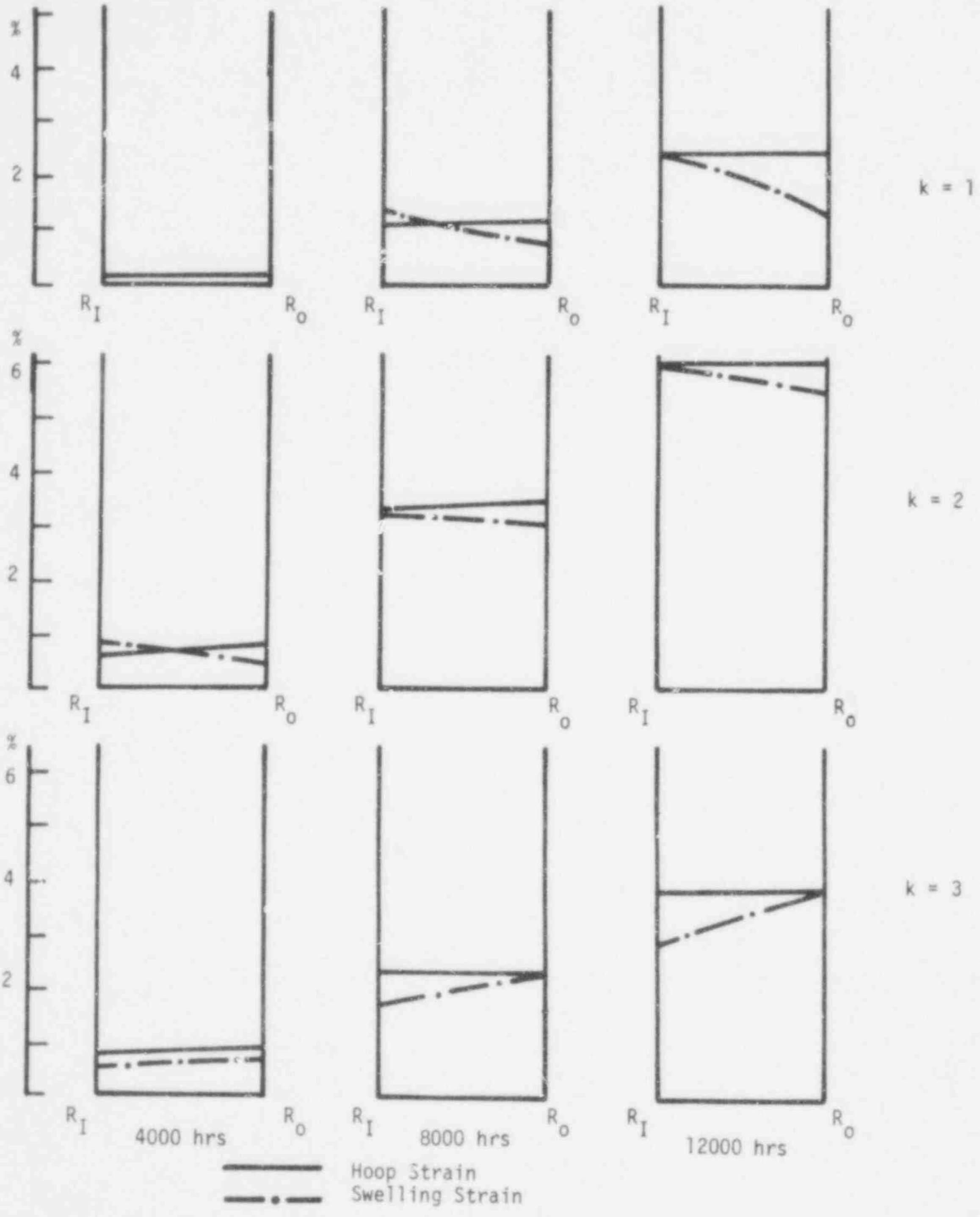


Figure HO - 9. The Distribution of the Hoop Strain and the Swelling Strain Across the Clad Wall (Case Ho)



733 253

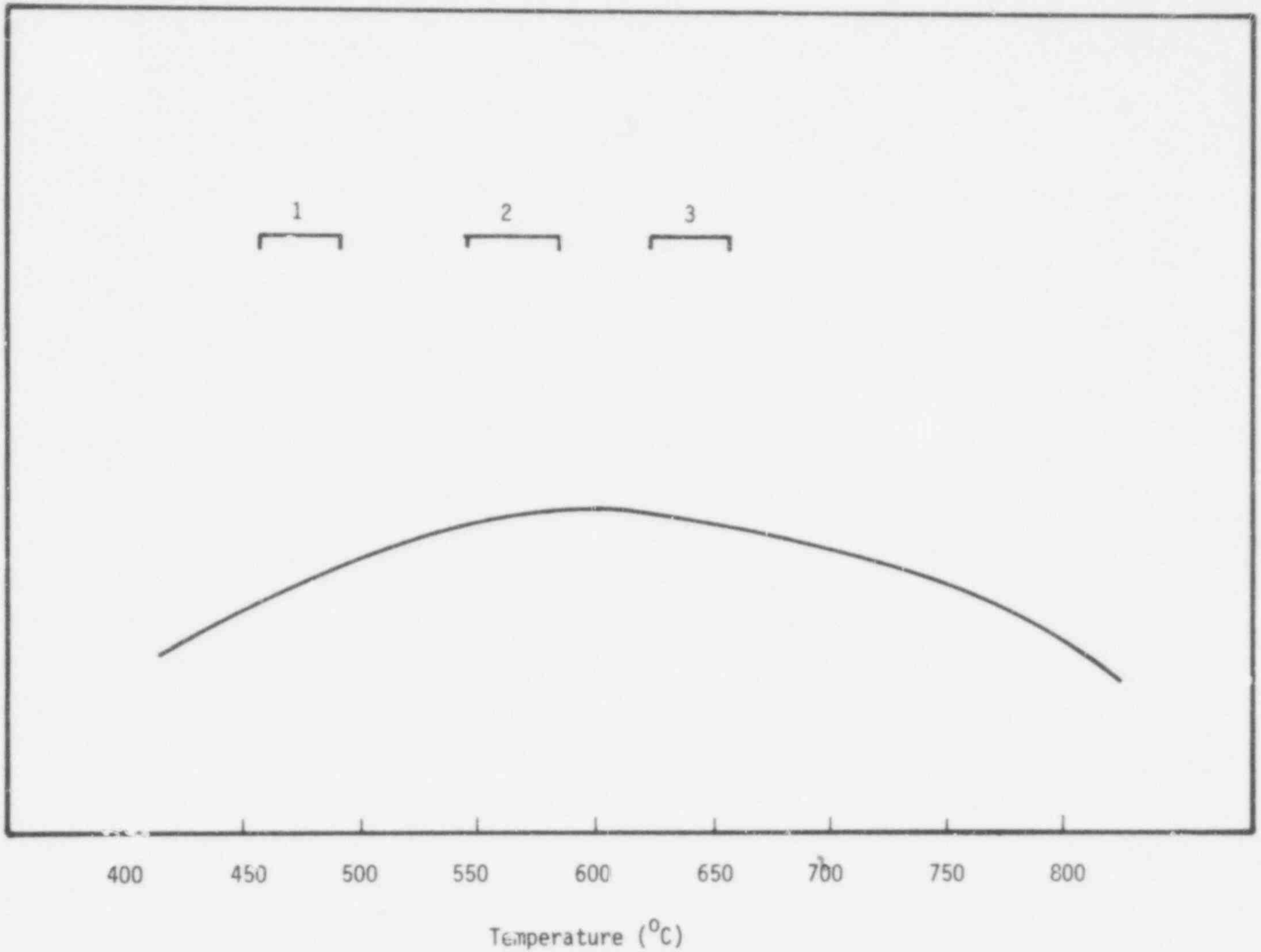


Fig. H1.1 The Temperature Dependance of the Irradiated Swelling, and the Temperature Range Across the Clad Wall.

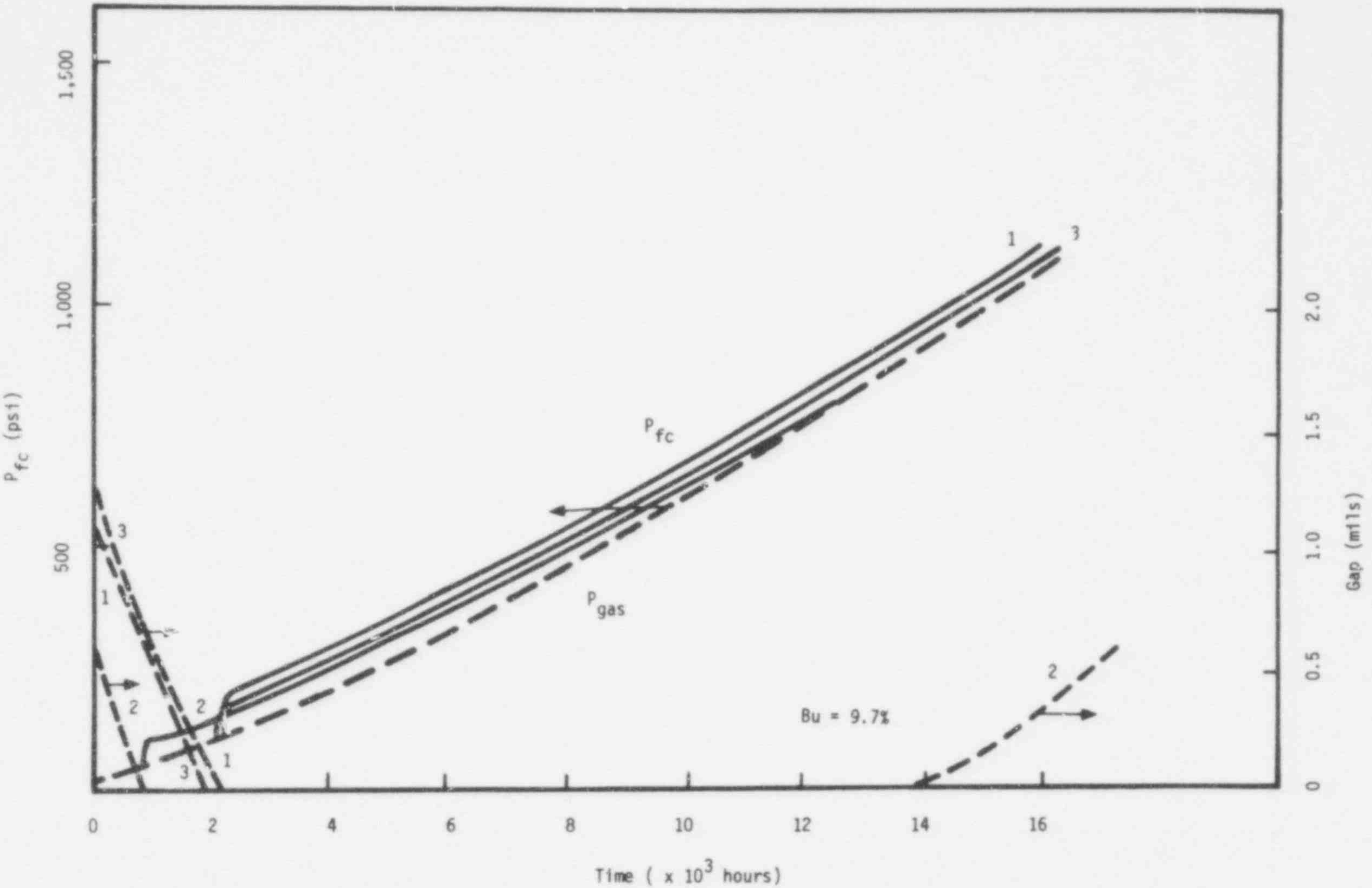


Figure H1 - 2. The Plenum Pressure ($P_{gas}$), the Fuel-Clad Interaction Force ($P_{fc}$), and the Fuel-Clad Gap Closure.

(Case H1)



733 255

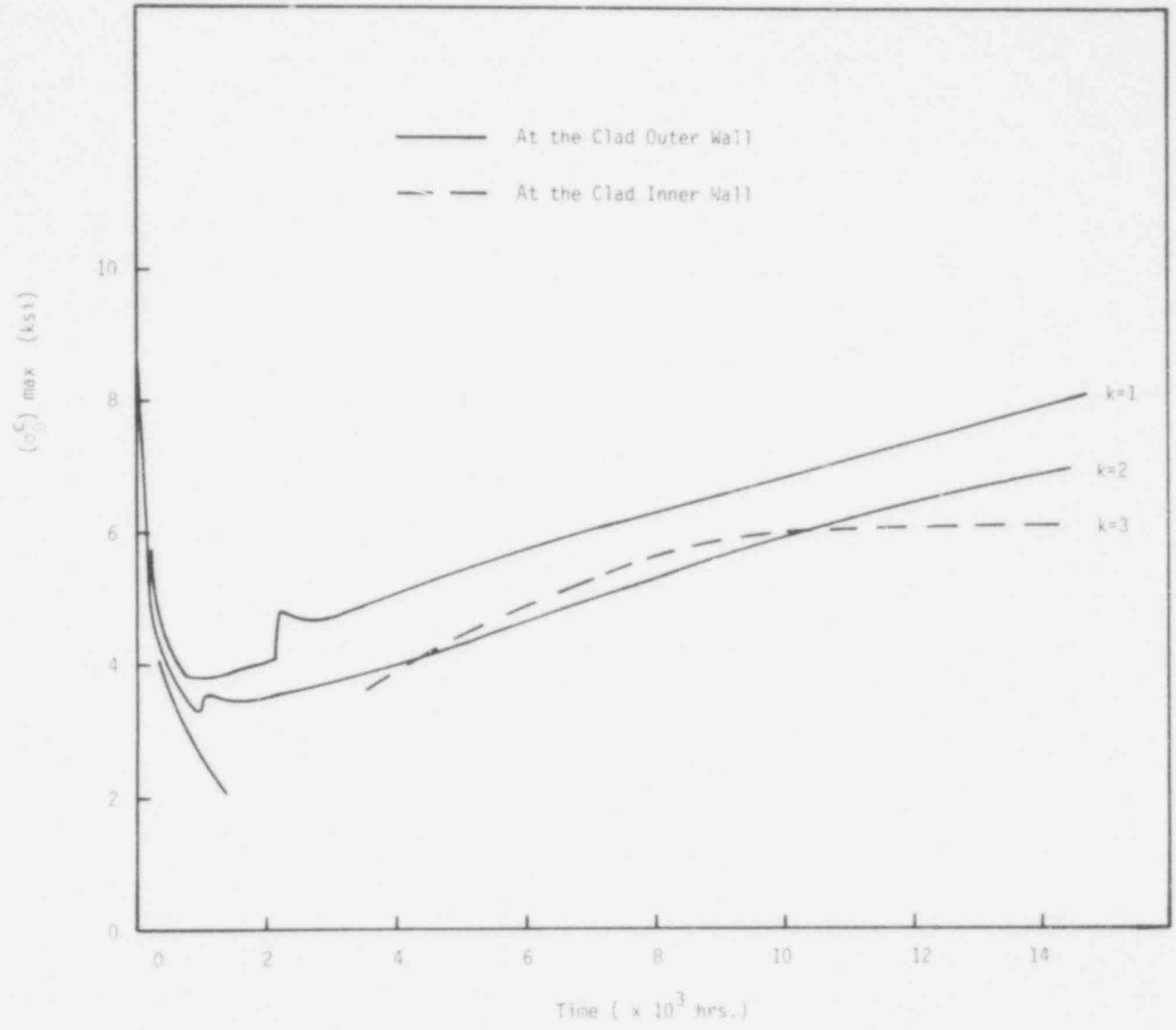


Fig. H1.3 The Maximum Hoop Stress in the Clad. (Case H1)

733 256

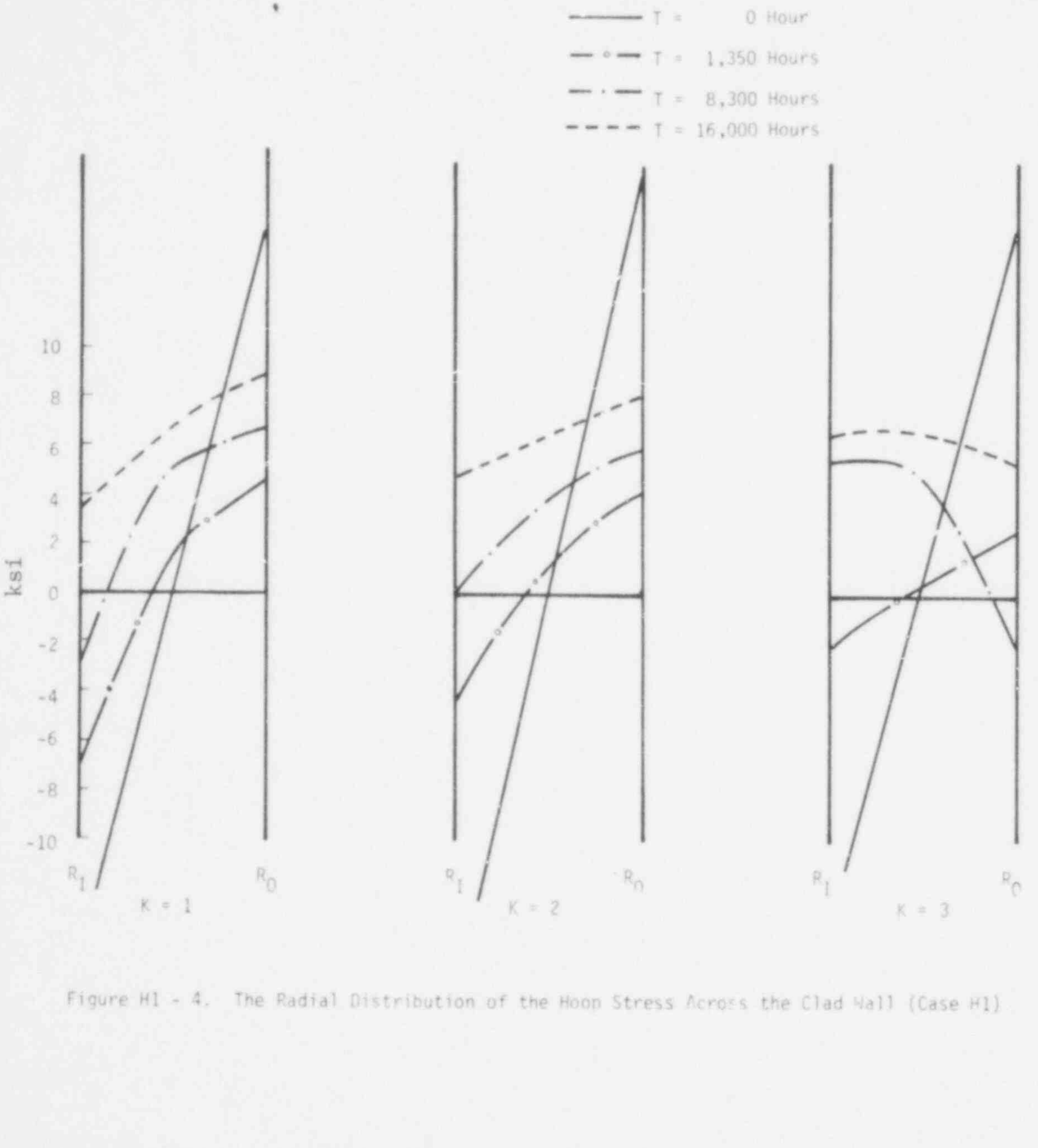


Figure H1 - 4. The Radial Distribution of the Hoop Stress Across the Clad Wall (Case H1)

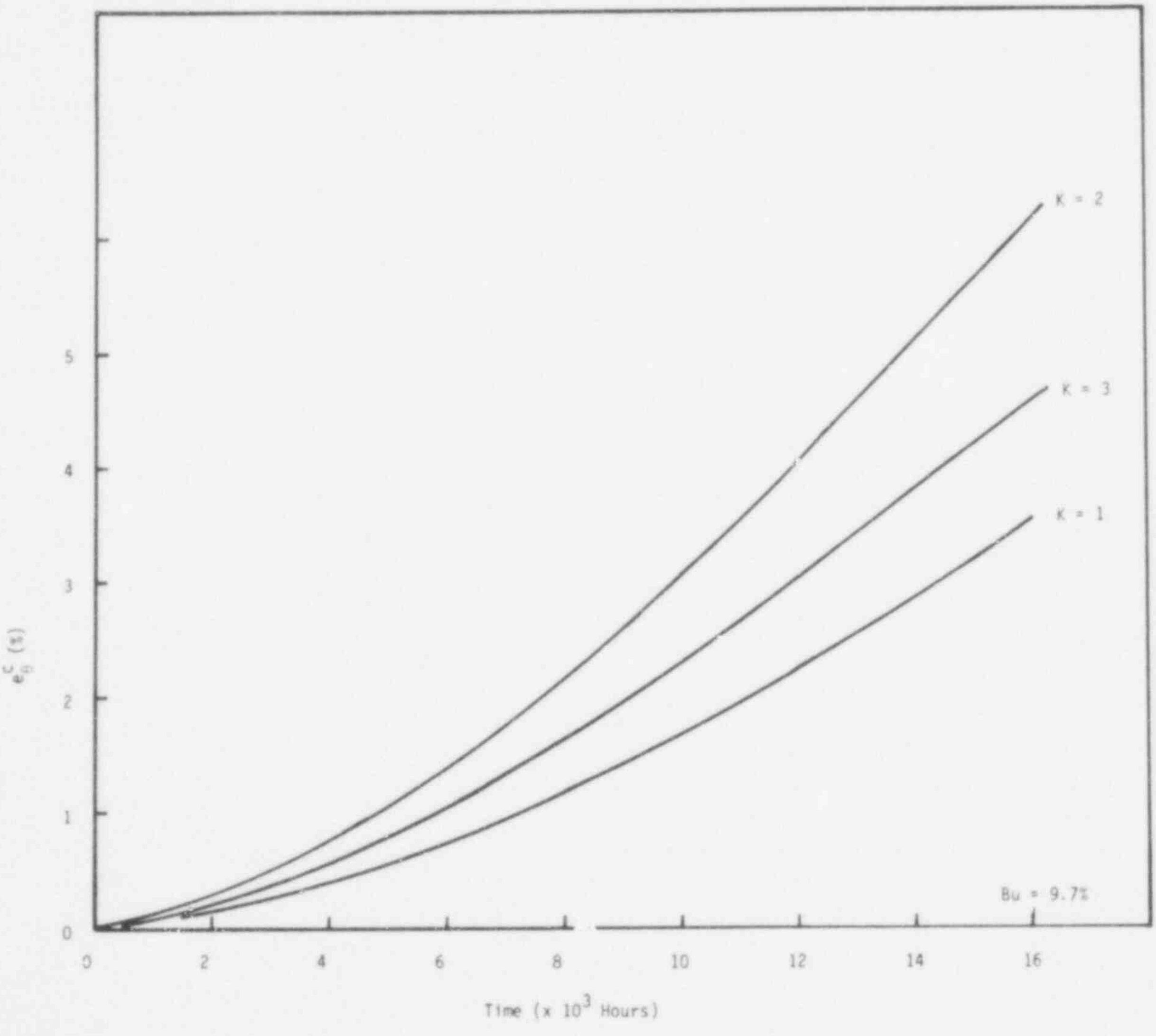


Figure H1 5. The Hoop Strain in the Clad ( Case H1 )

733 258

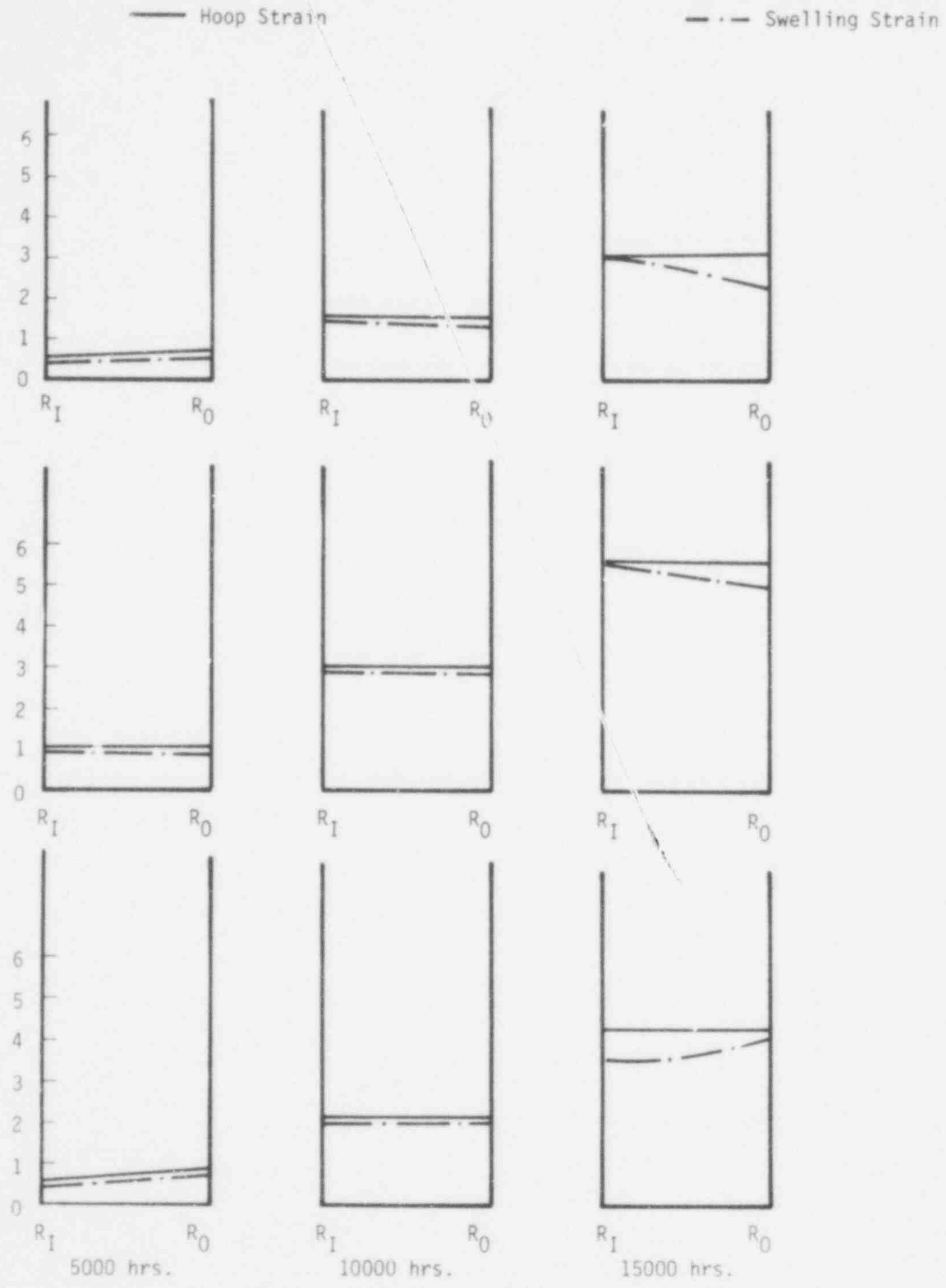


Fig. H1.6 The Distribution of the Hoop Strain and the Irradiated Swelling Strain Across the Clad Wall. (Case H1)

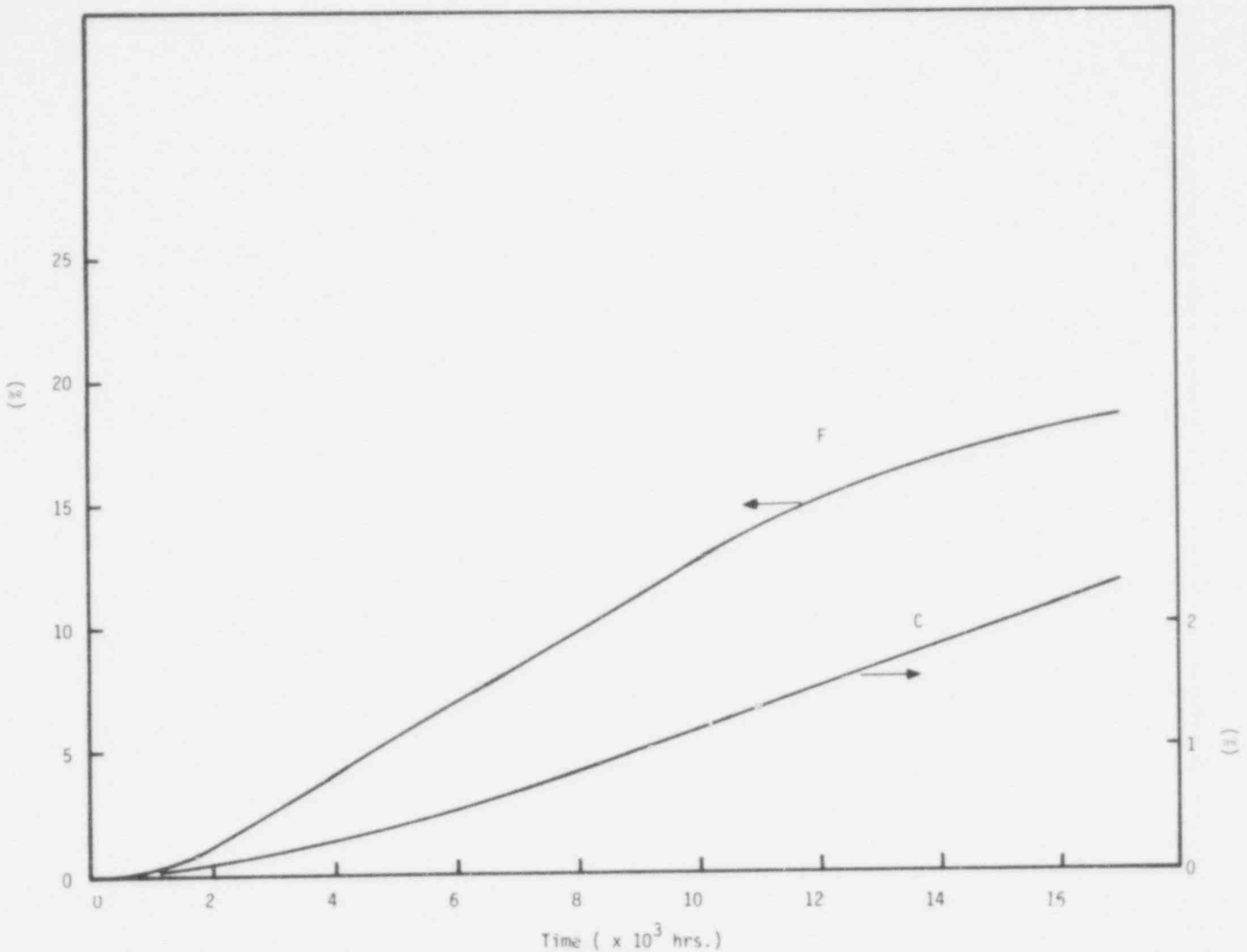


Fig. H1.7 The Percentage of Axial Displacement for the Fuel and the Clad. (Case H1)

733 260

15 kW/ft Cases
Case H5

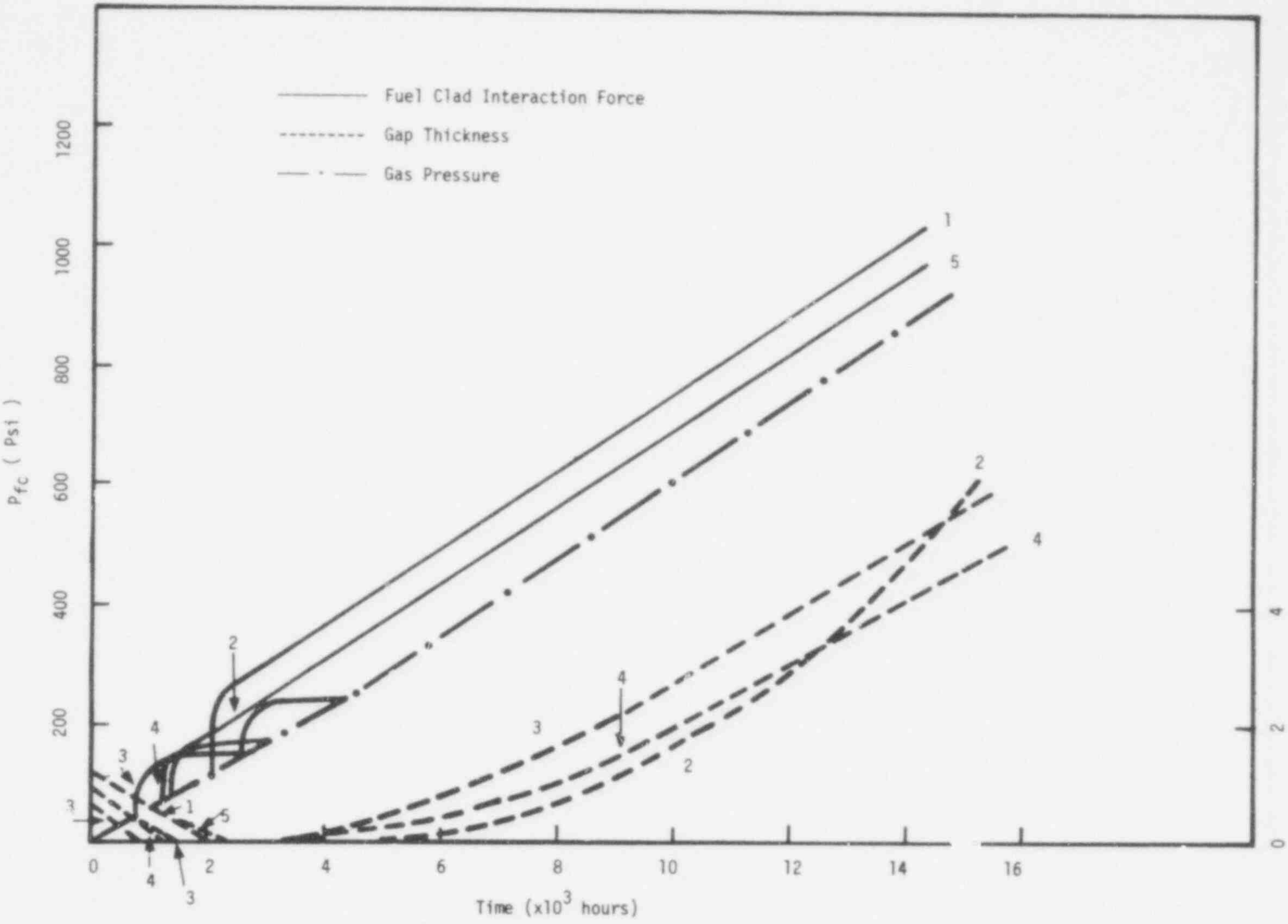


Figure H5 - 1. The Gap Thickness, the Fuel Clad Interaction Force and the Gas Pressure (Case H5).

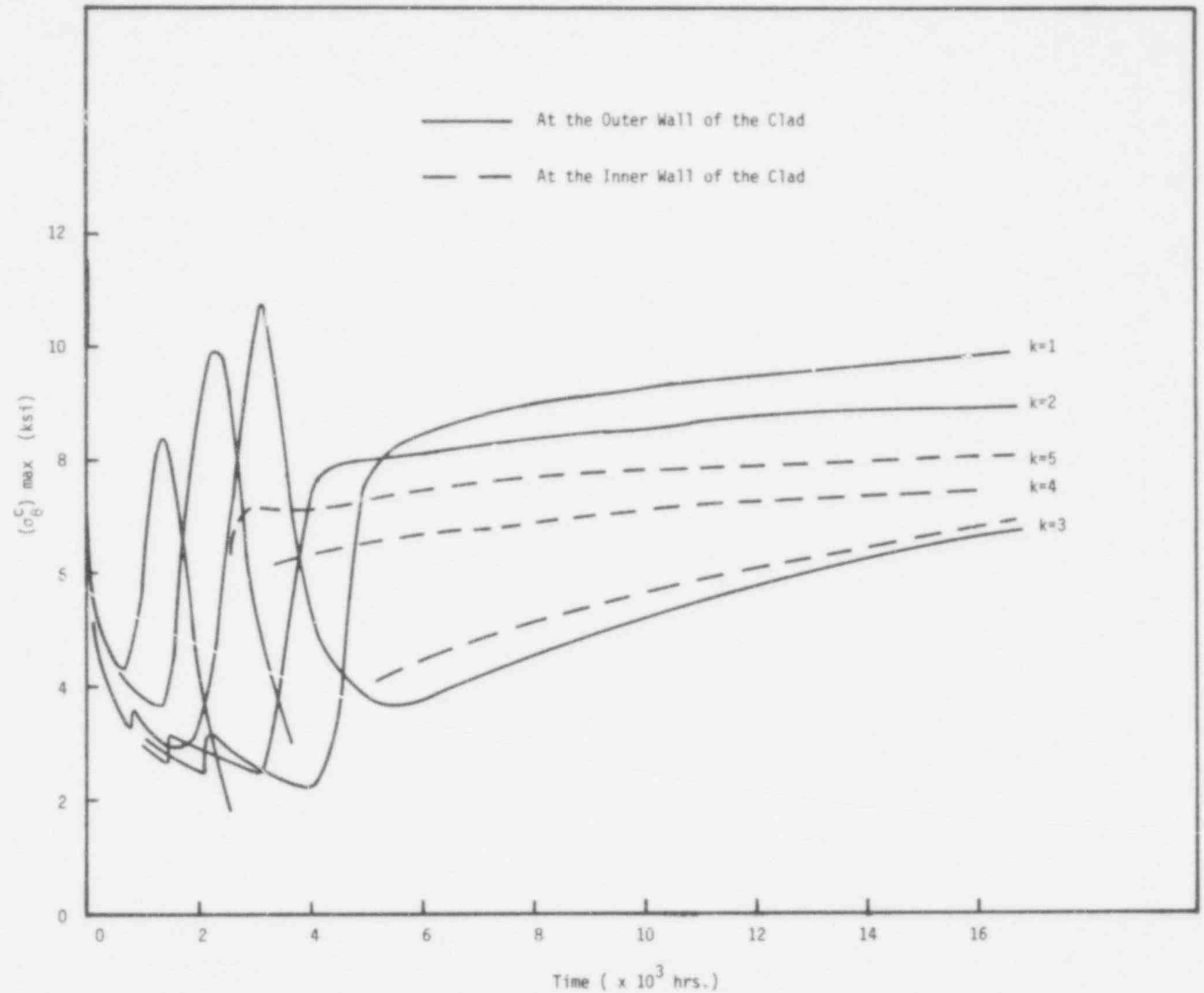


Fig. H5.2 The Maximum Hoop Stress in the Clad. (Case H5)

733 262

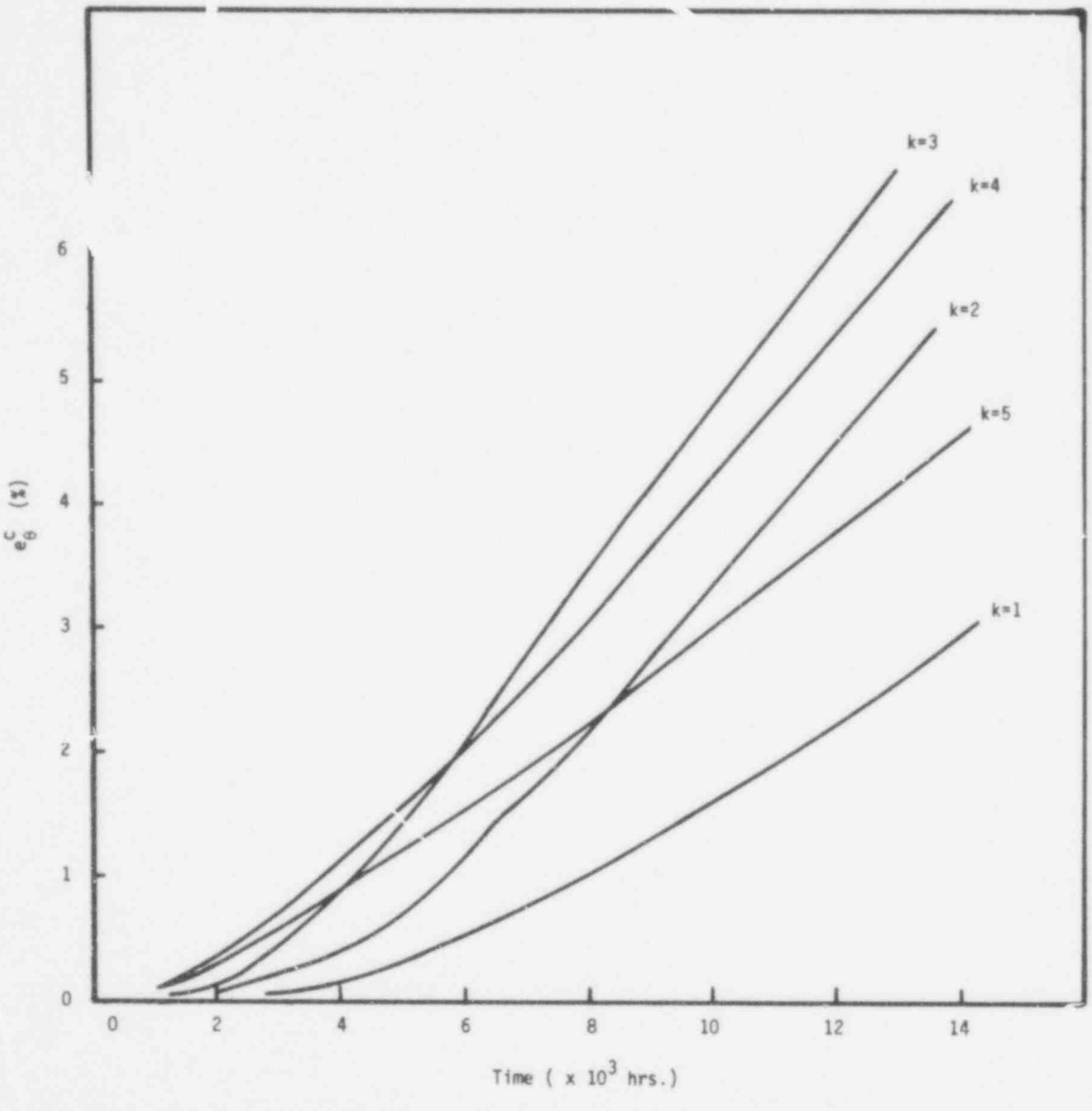


Fig. H5.3 The Hoop Strain in the Clad. (Case H5)

9 kW/ft Cases

Case MO

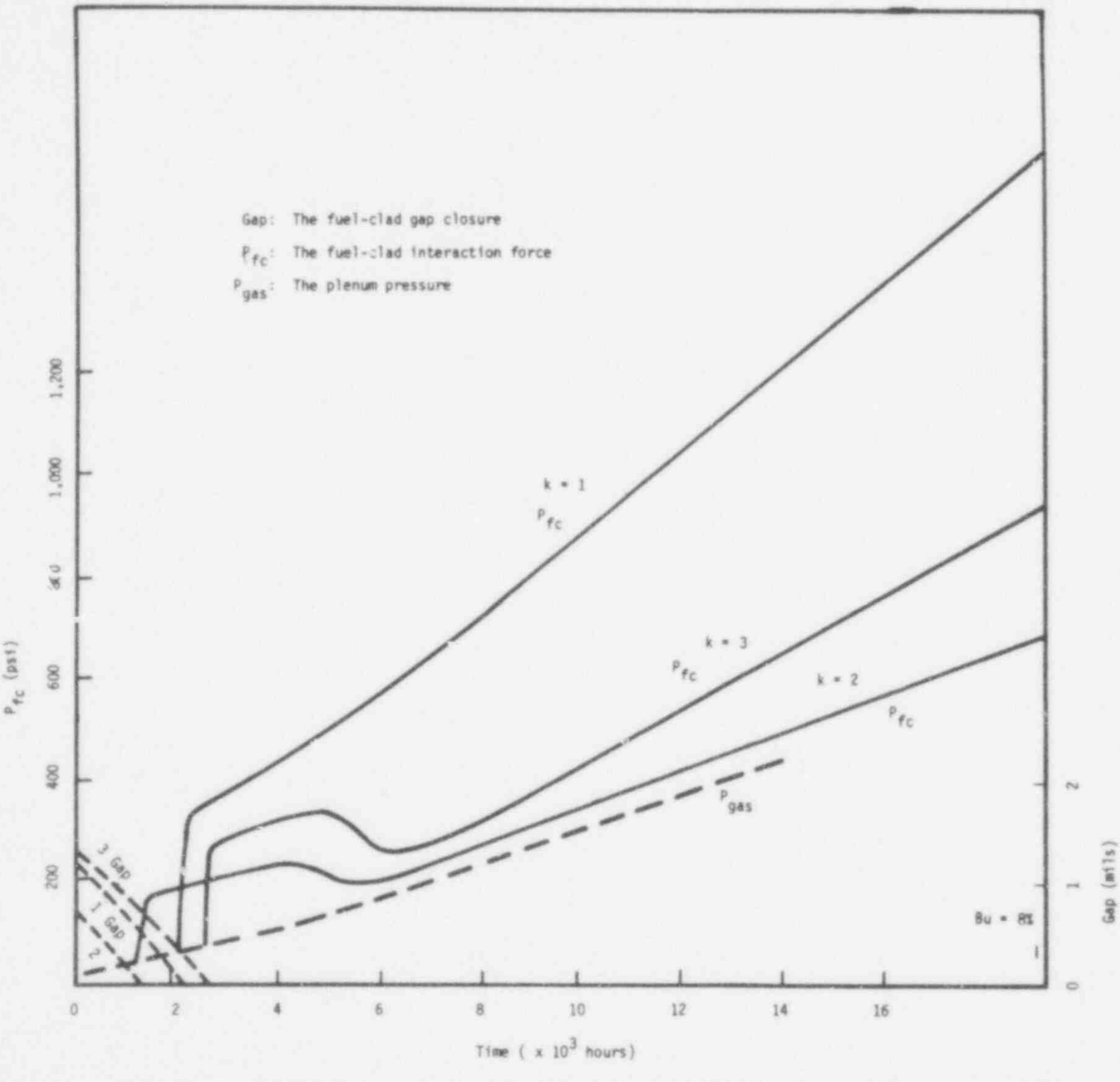


Figure MO - 1. The Fuel-Clad Gap Closure, the Fuel-Clad Interaction Force, and the Plenum Pressure. (Case MO)

733 264

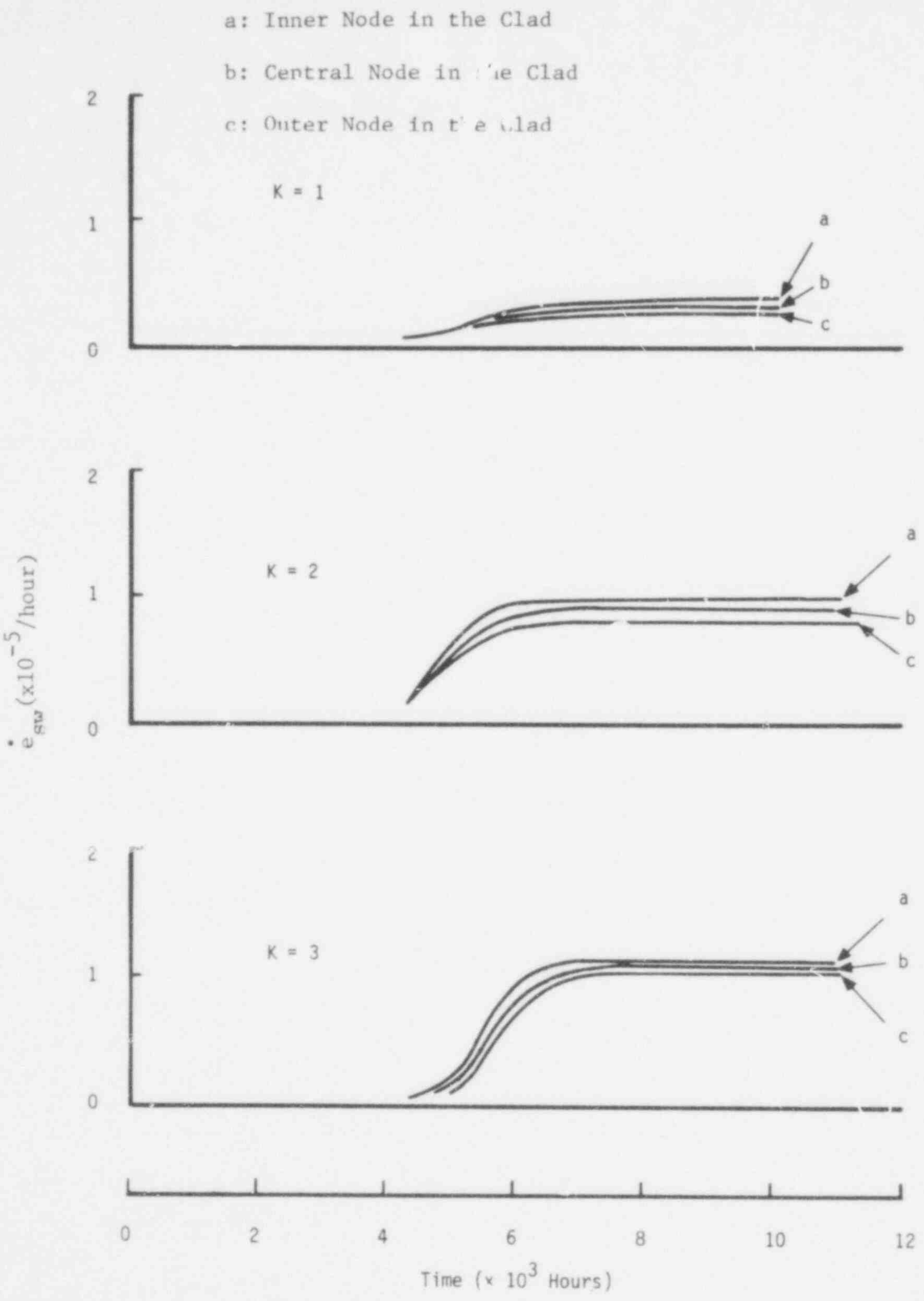


Figure MO - 2. The Rate of Irradiated Swelling on Radial Nodes of the Clad

733 265

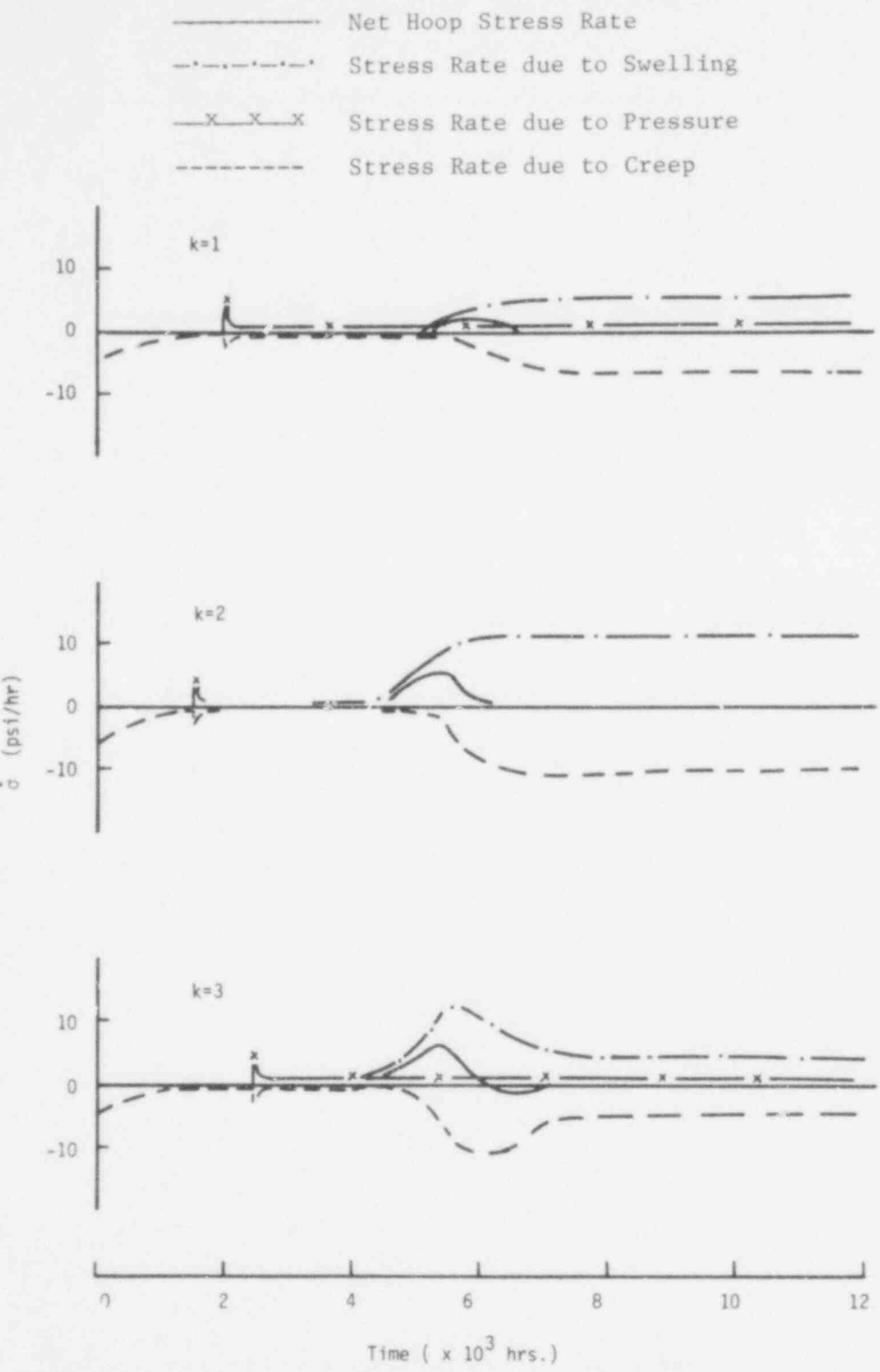


Fig. MO.3 The Net Hoop Rate and the Stress Rate Due to the Creep, the Swelling, and the Pressure at the Outer Wall of the Clad.

733 266

POOR ORIGINAL

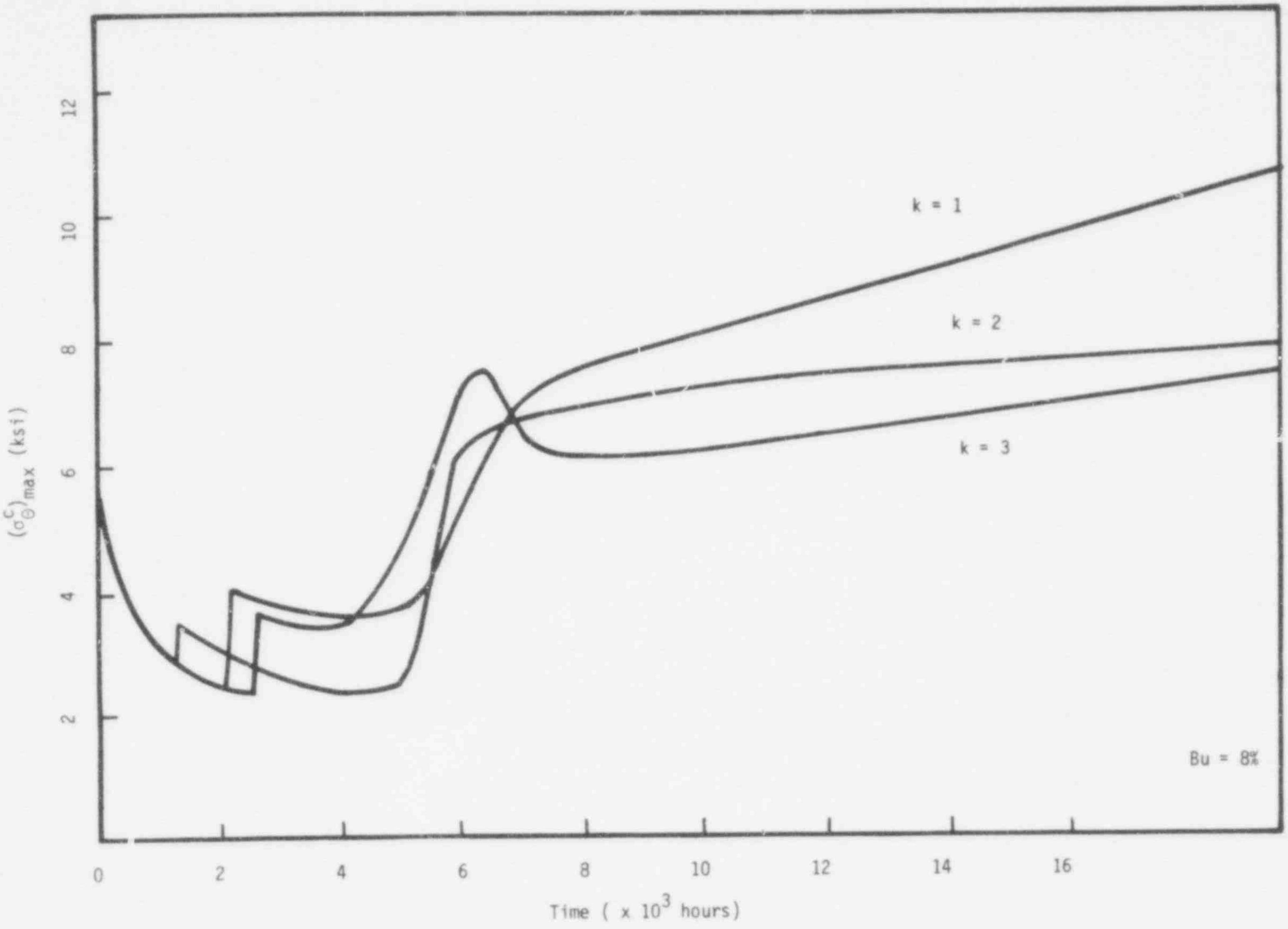


Figure MO - 4. The Maximum Hoop Stress in the Clad. (Case MO)



733 267

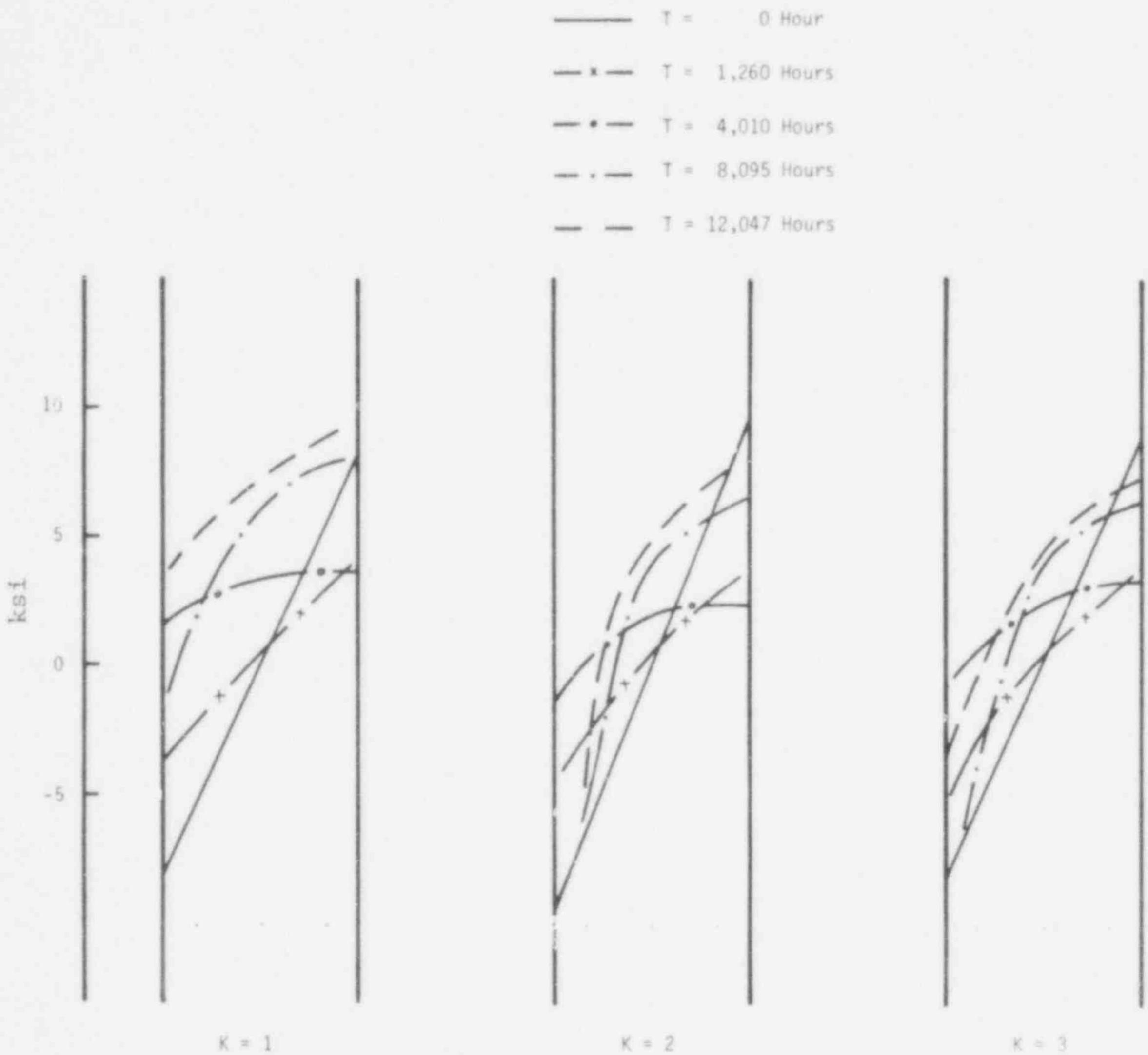


Figure MO - 5. The Distribution of the Hoop Stress Across the Clad Wall

733 268

POOR ORIGINAL

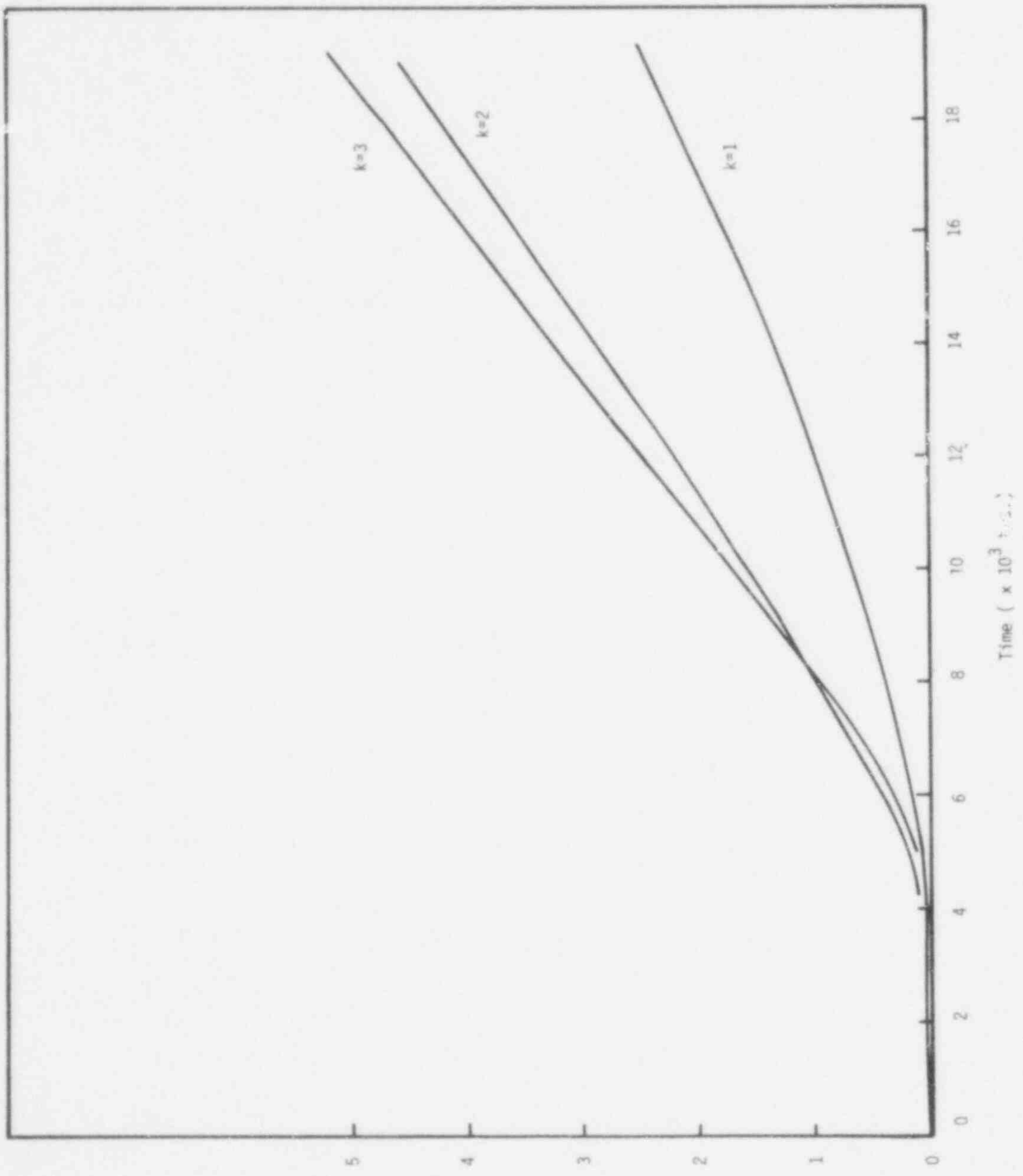


Fig. MO.6 The Total Hoop Strain in the Clad. (Case MO)

733 269

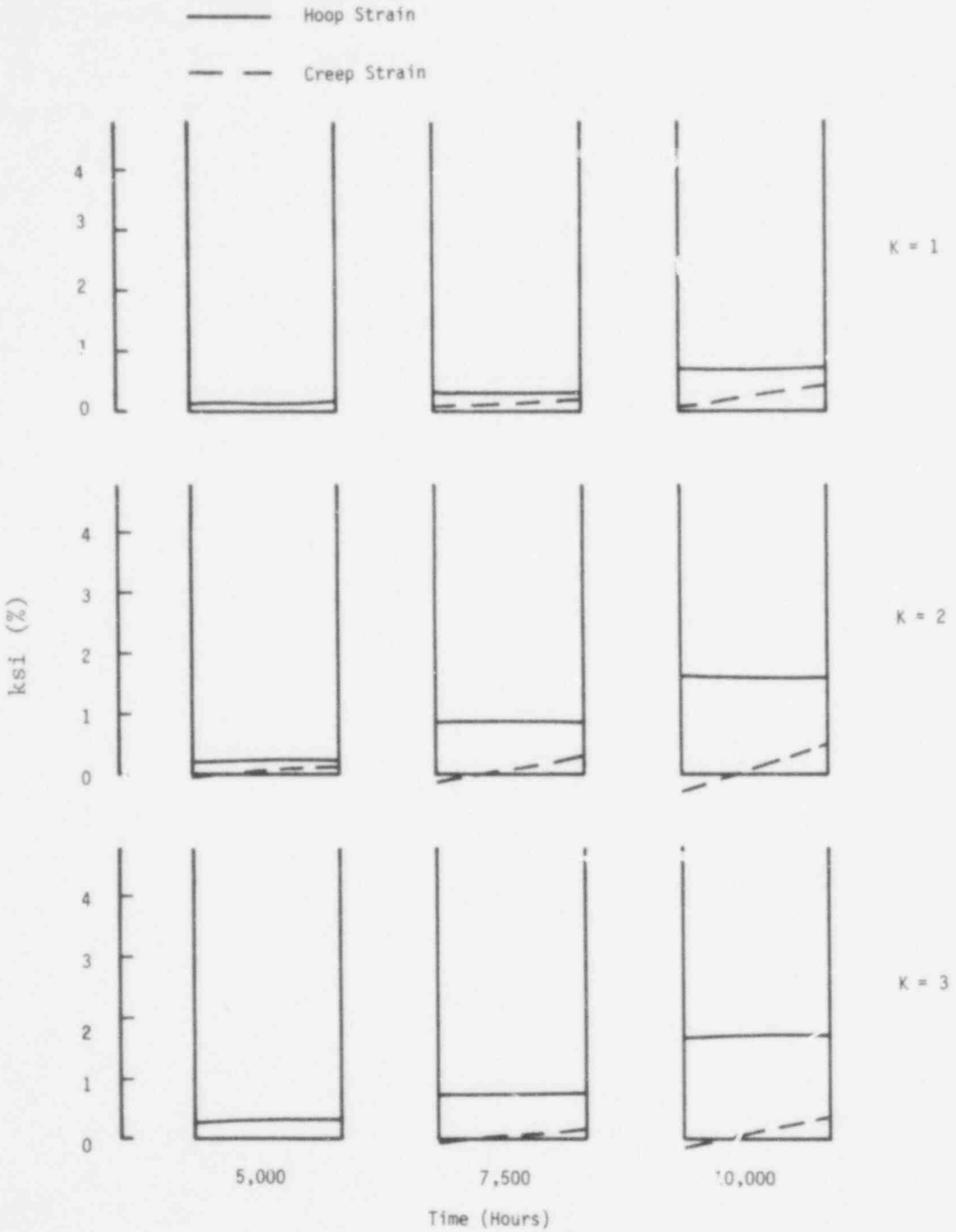


Figure MO - 7. The Distribution of the Hoop Strain and the Creep Strain Across the Clad Wall

733 270

9 kW/ft Cases

Case M1

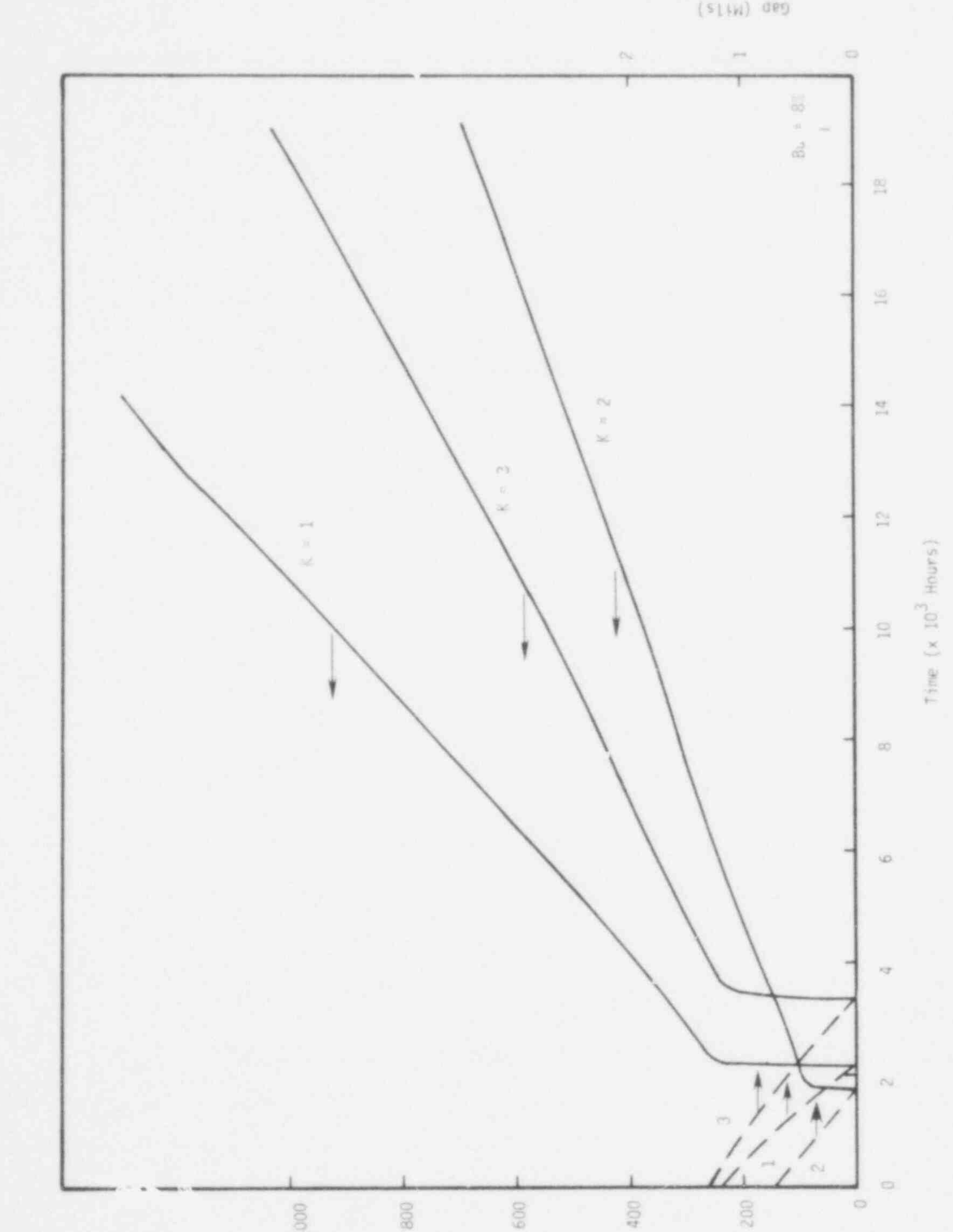


Figure M1 - 1. The Fuel-Clad Gap Thickness and the Fuel-Clad Interaction Force (Case M1)

733 271

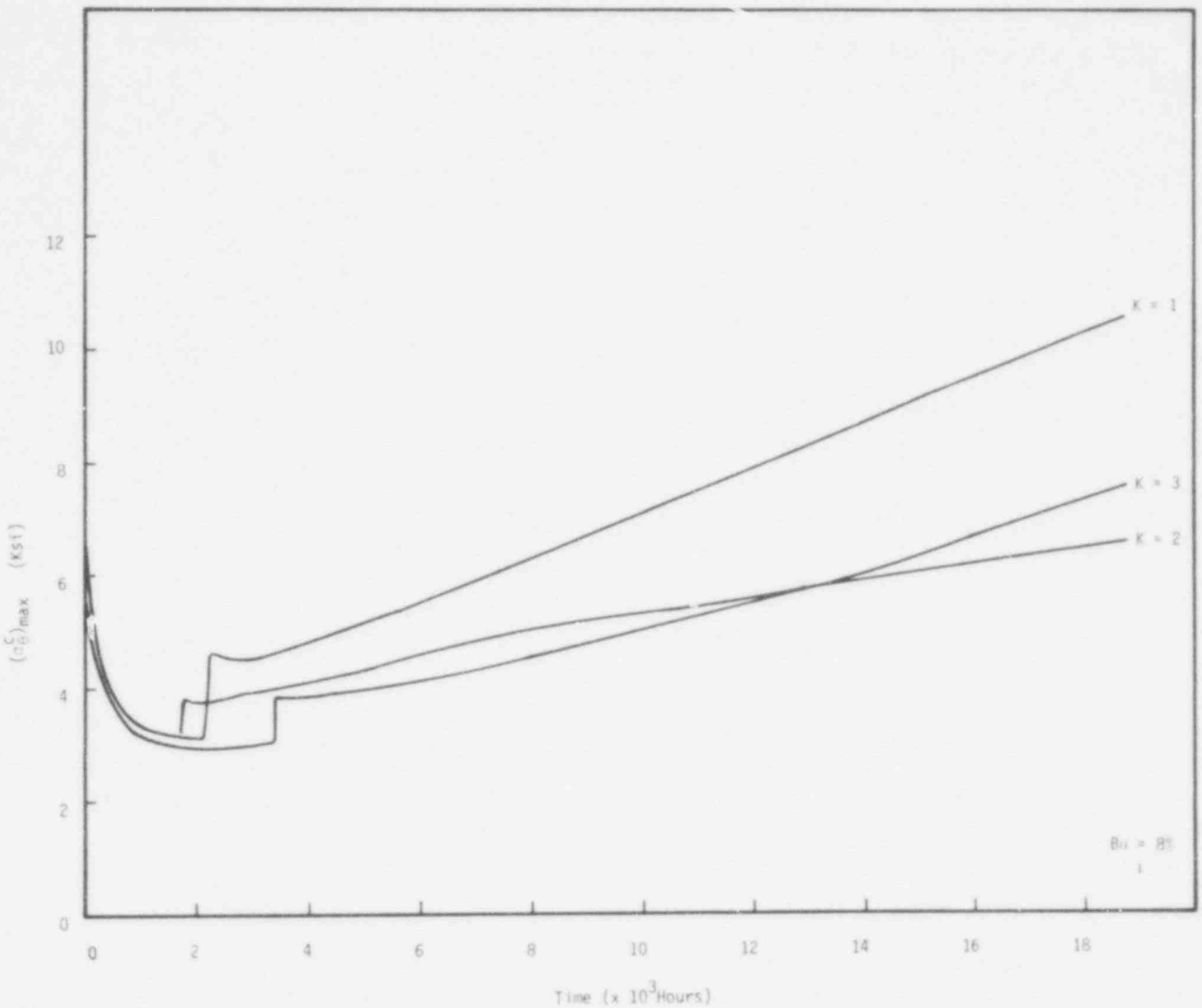


Figure M1 - 2. The Maximum Hoop Stress in the Clad ( Case M1 )

733 272

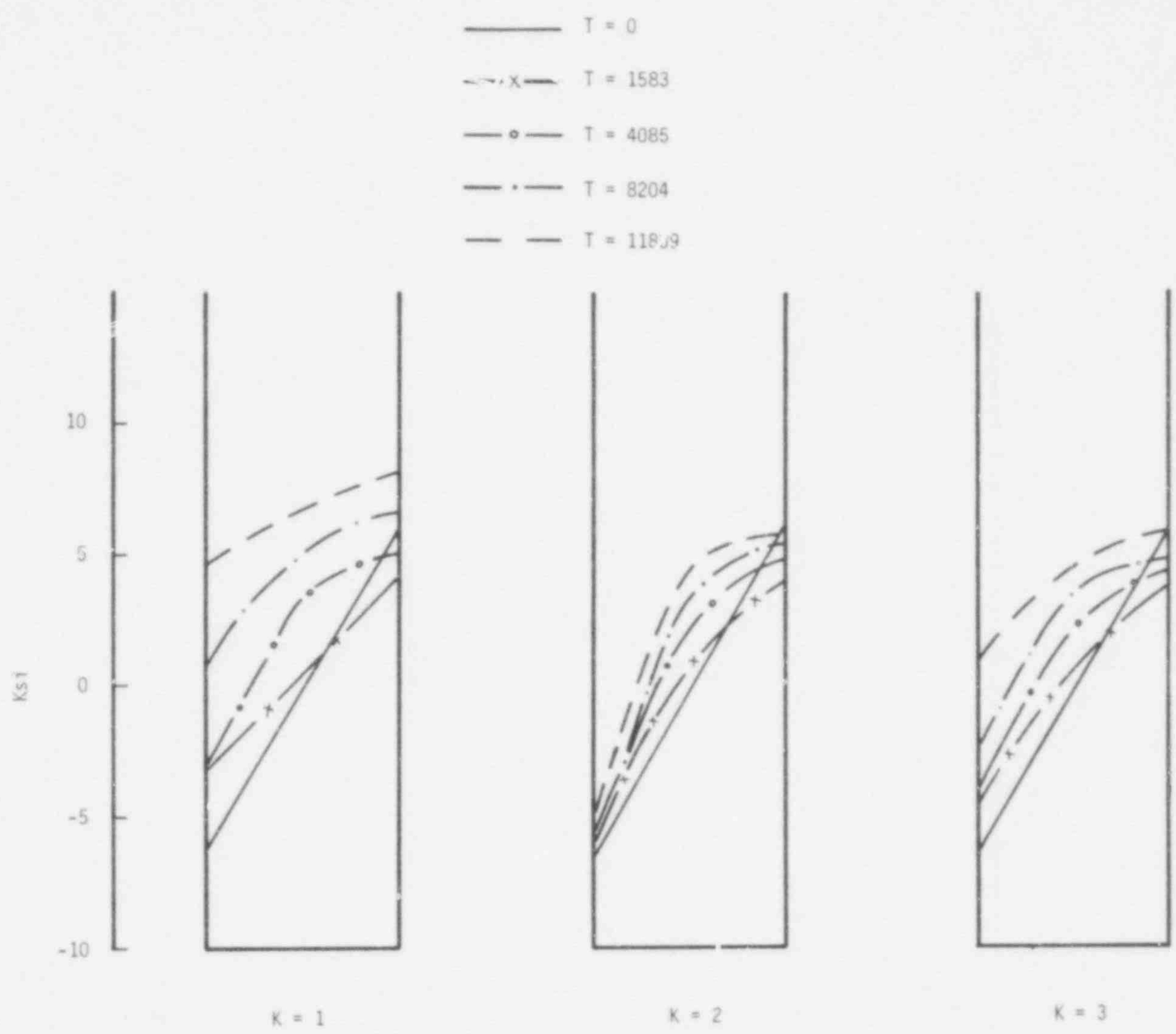


Fig. M1-3 The Radial Distribution of the Hoop Stress Across the Clad Wall.



733 273

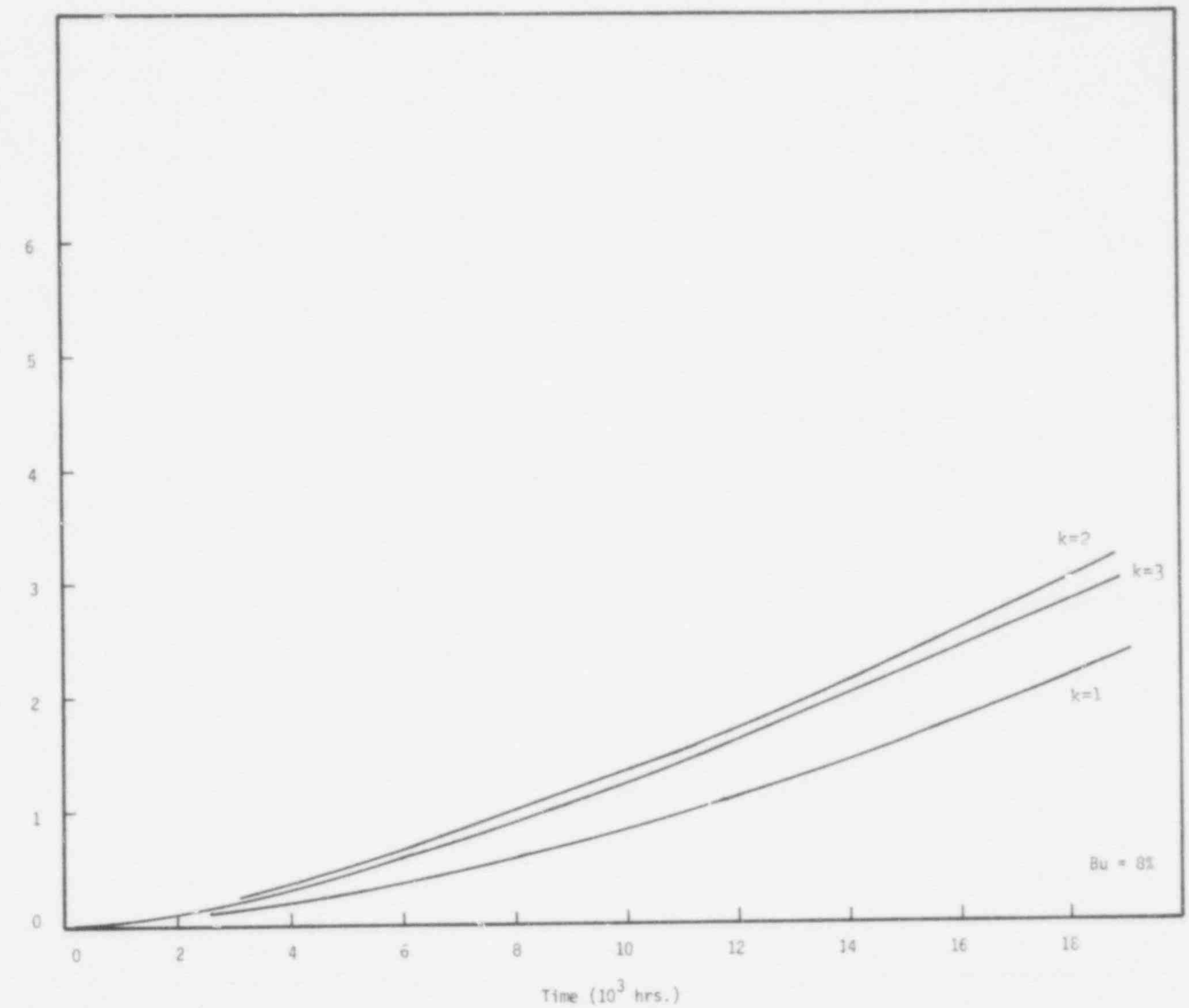


Fig. M1-4 The Total Hoop Strain in the Clad (Case M1).

733 274

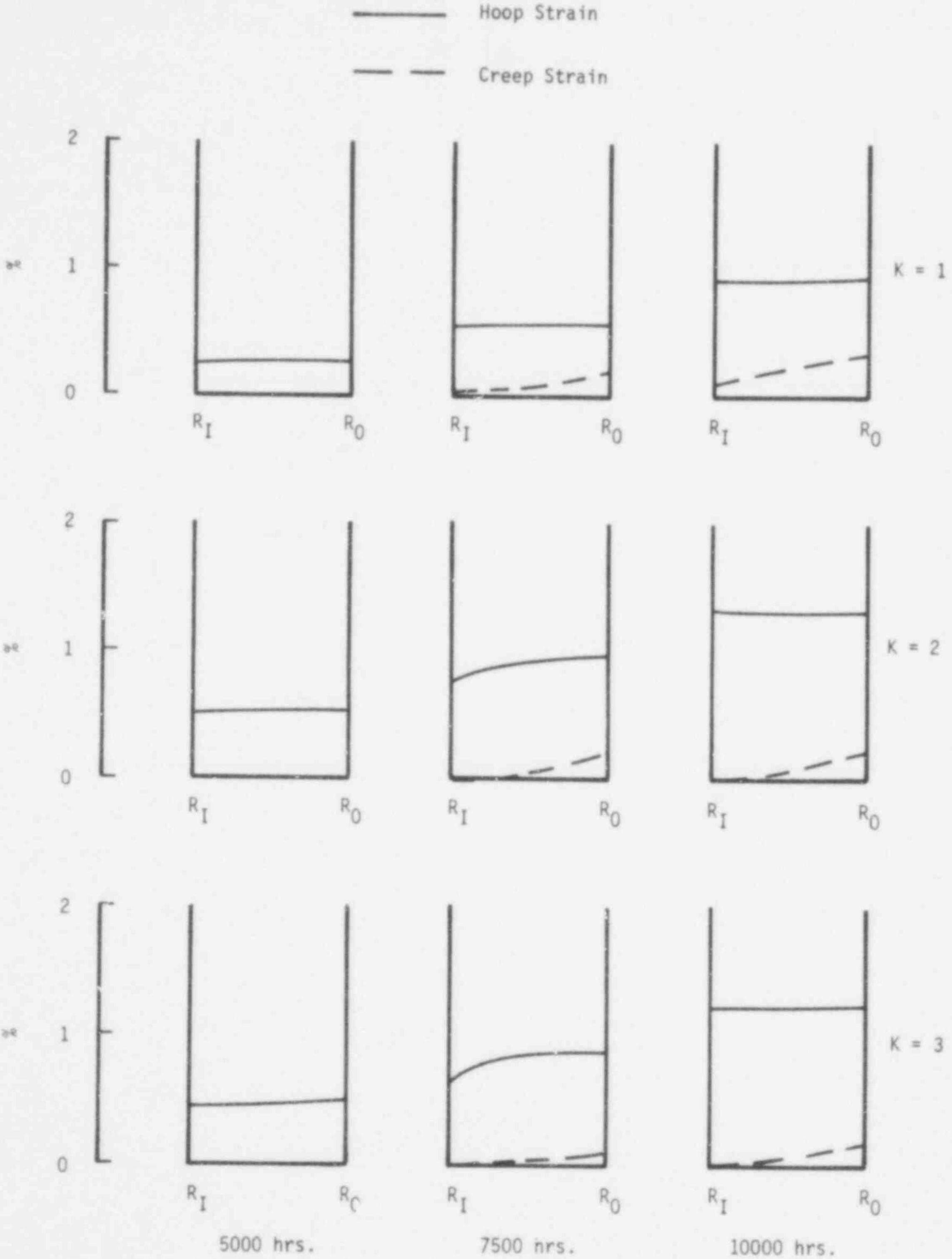


Fig. M1-5 The Distribution of the Hoop Strain and the Creep Strain Across the Clad Wall (Case M-1).

733 275

RATE OF FUEL SWELLING

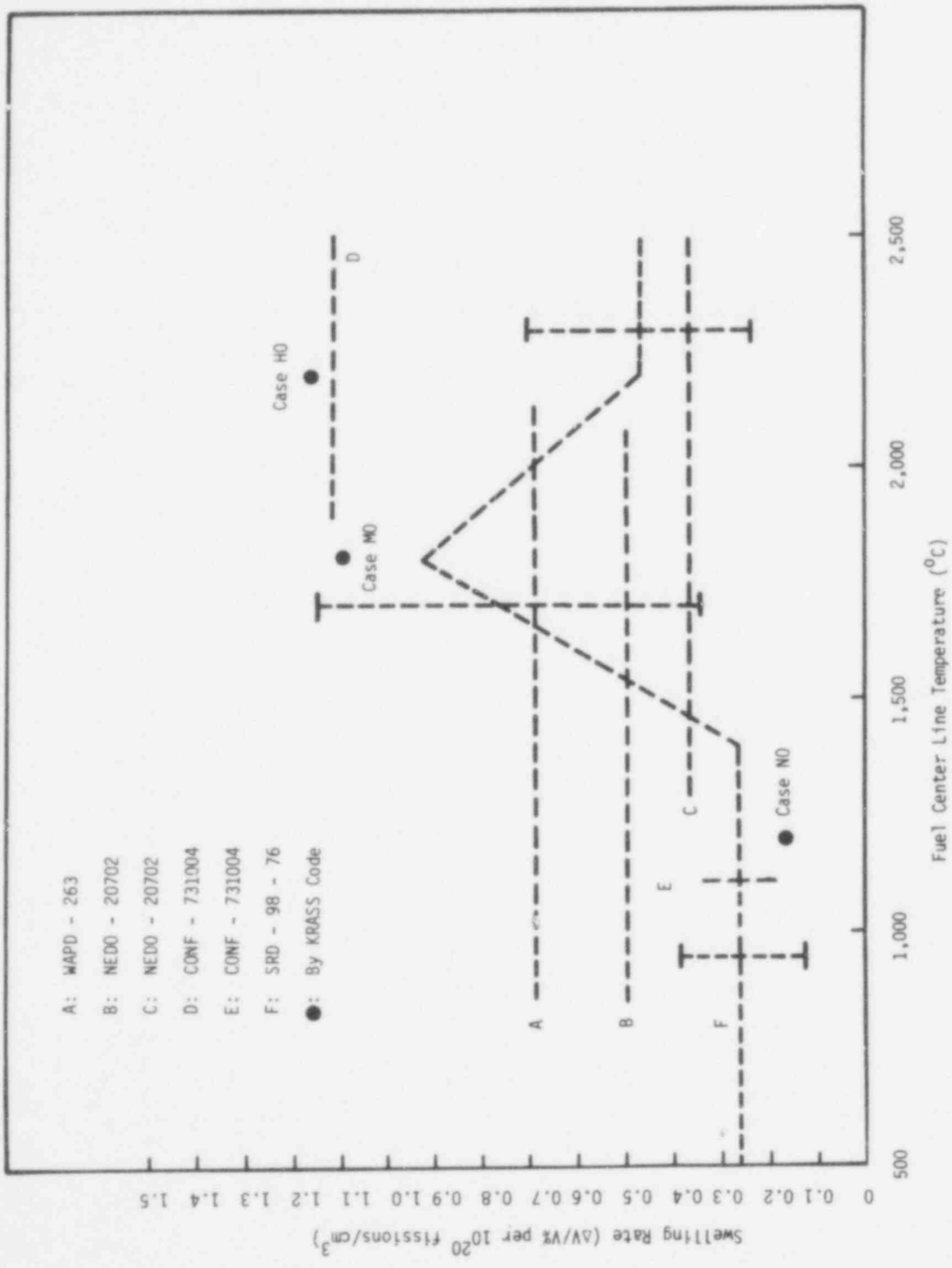


Figure FSW. The Rate of Fuel Swelling.

733 276

SENSITIVITY CALCULATIONS FOR FUEL PROPERTIES

12 kW/ft Cases

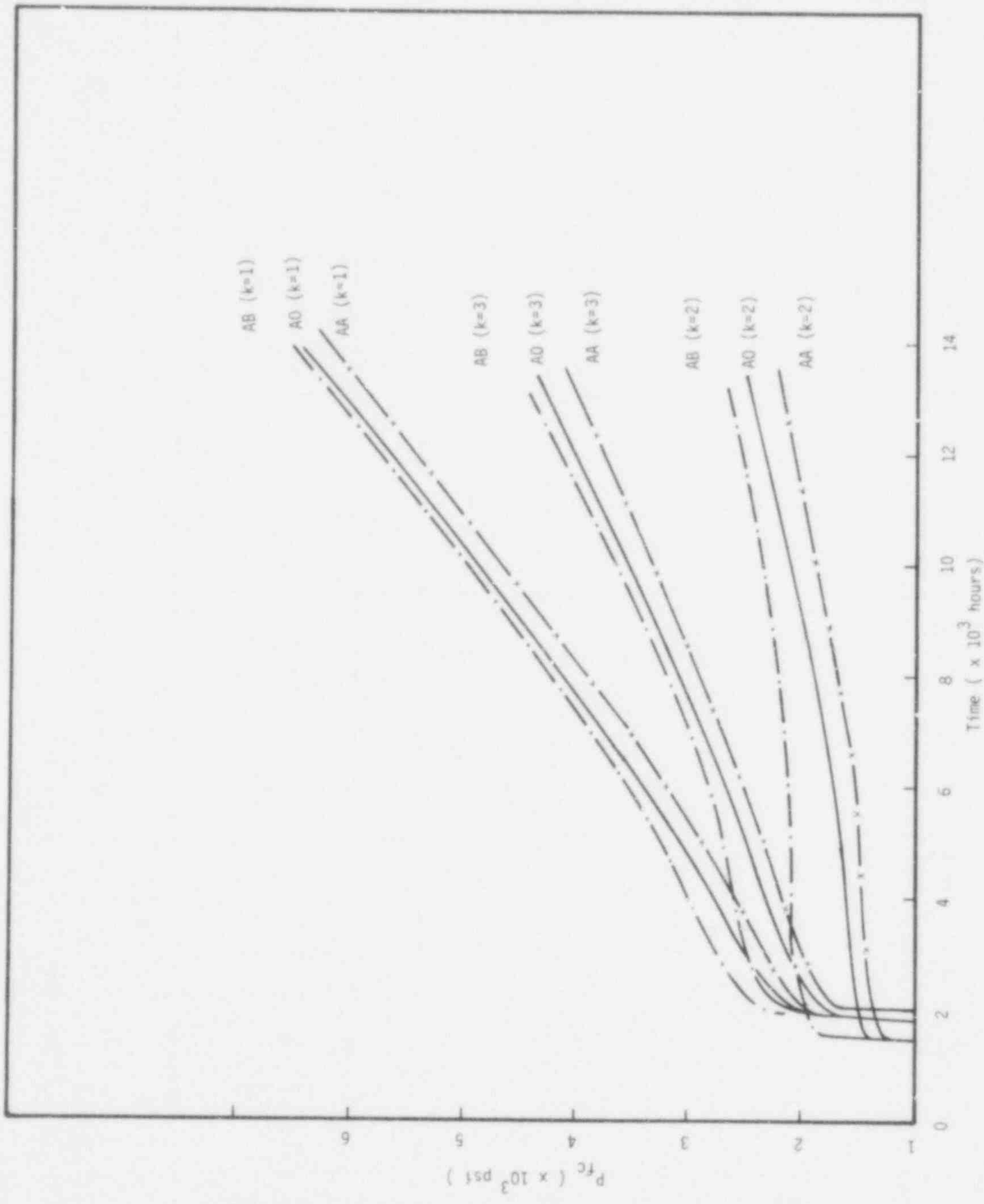


Figure 5A - 1. The Fuel - Clad Interaction Forces.

POOR ORIGINAL

733 277

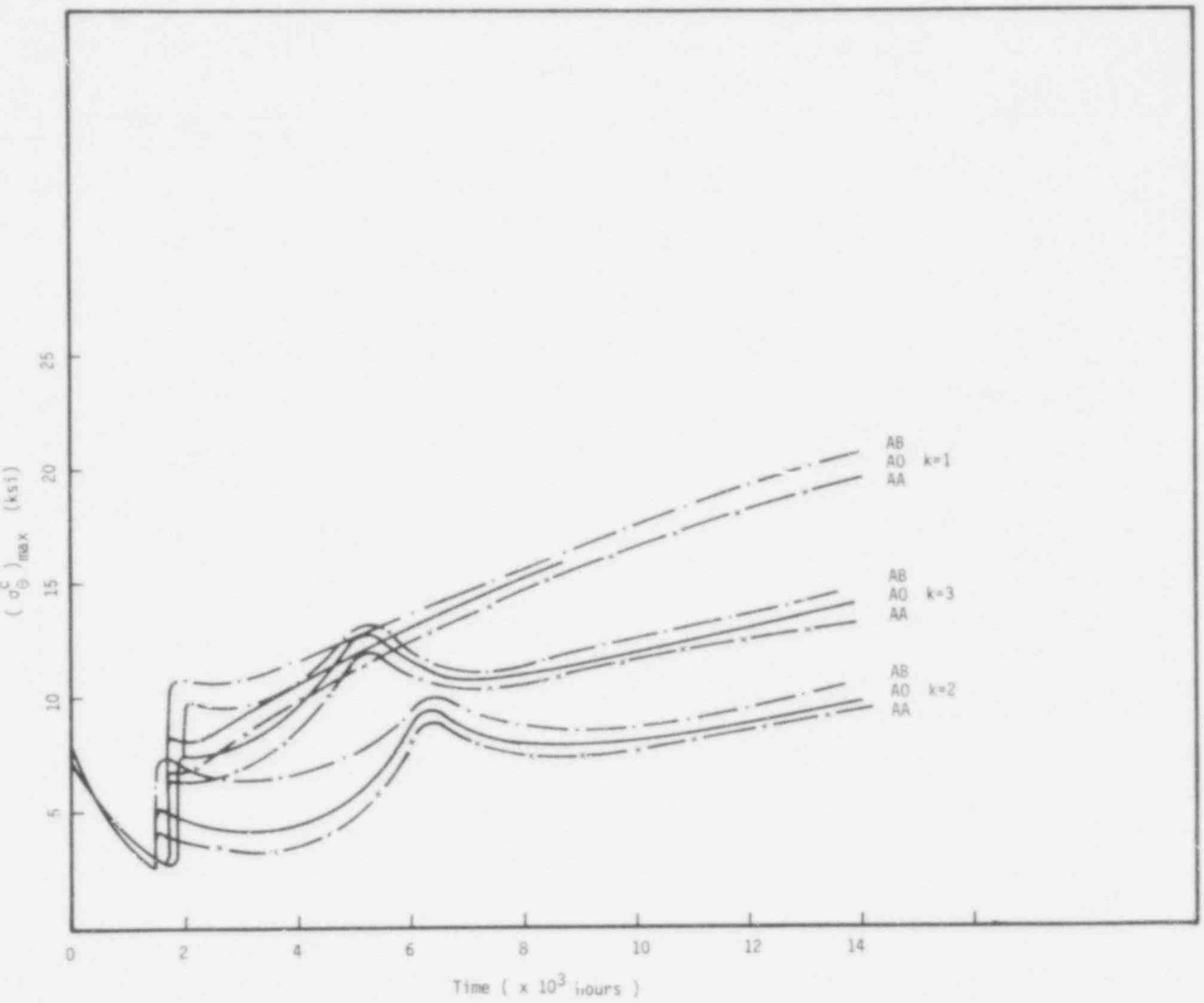


Figure SA - 2. The Maximum Hoop Stress in the Clad.

733 278

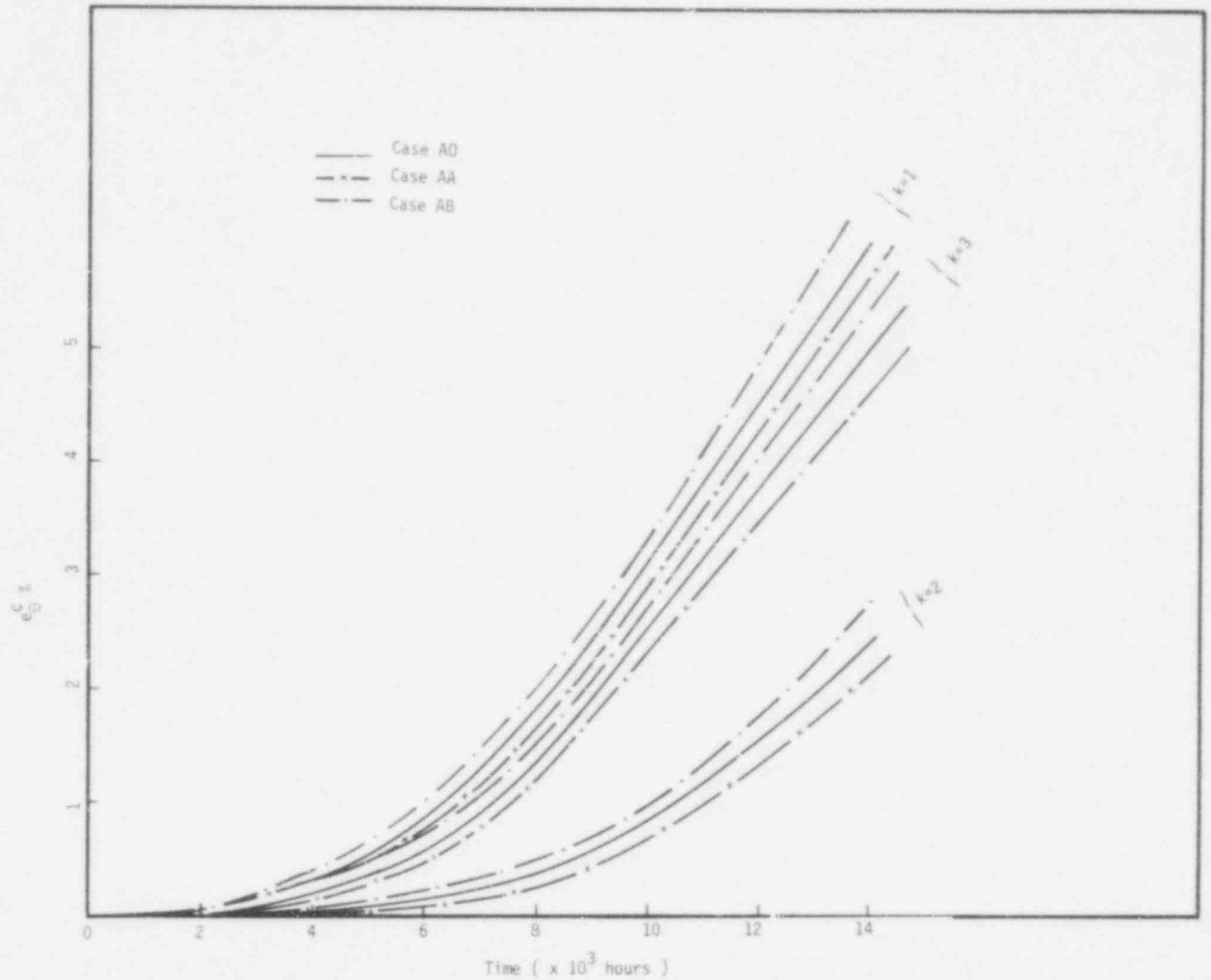


Figure SA - 3. The Total Strain in the Clad.

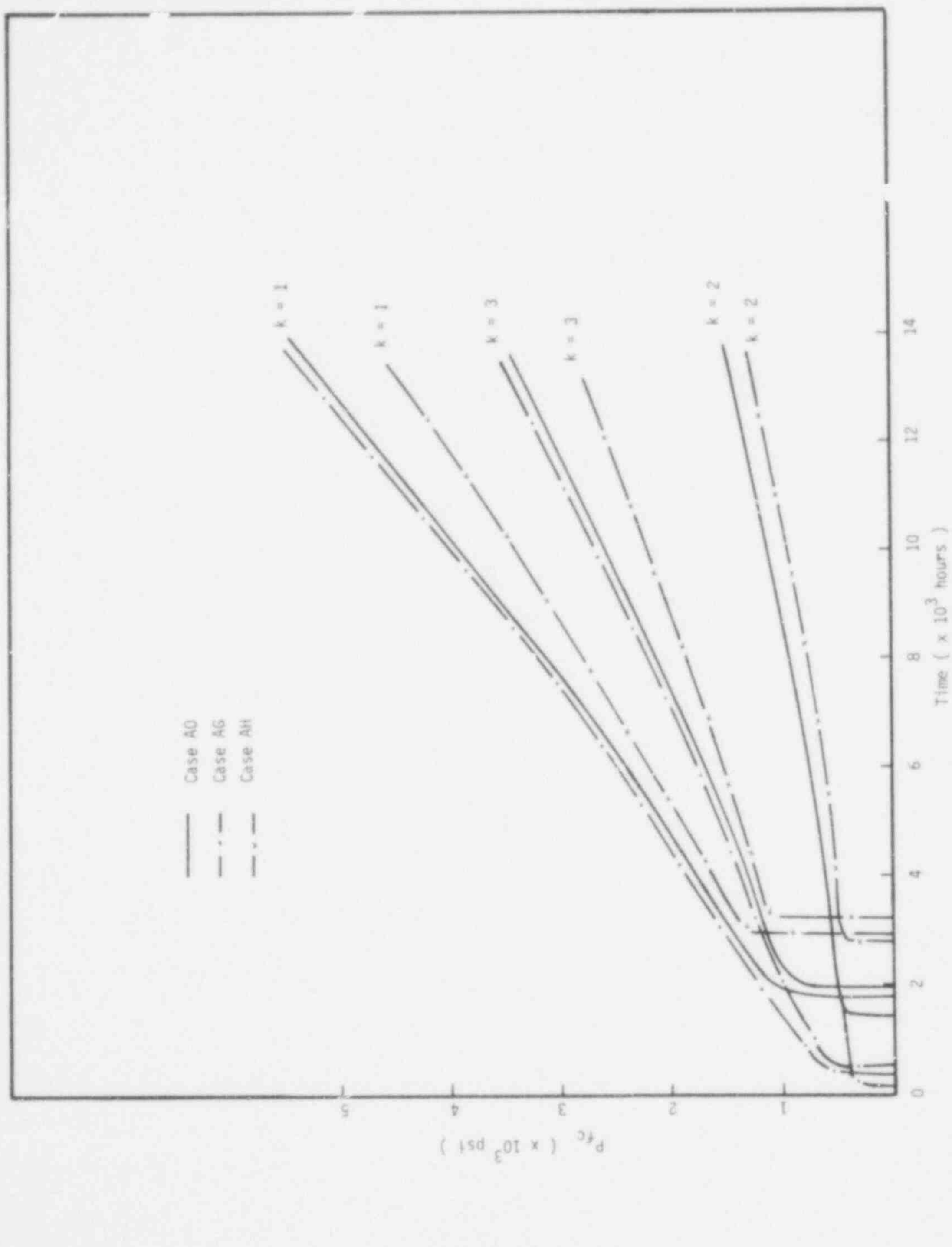


Figure SA - 4. The Fuel-Clad Interaction Force.

733 280

POOR ORIGINAL

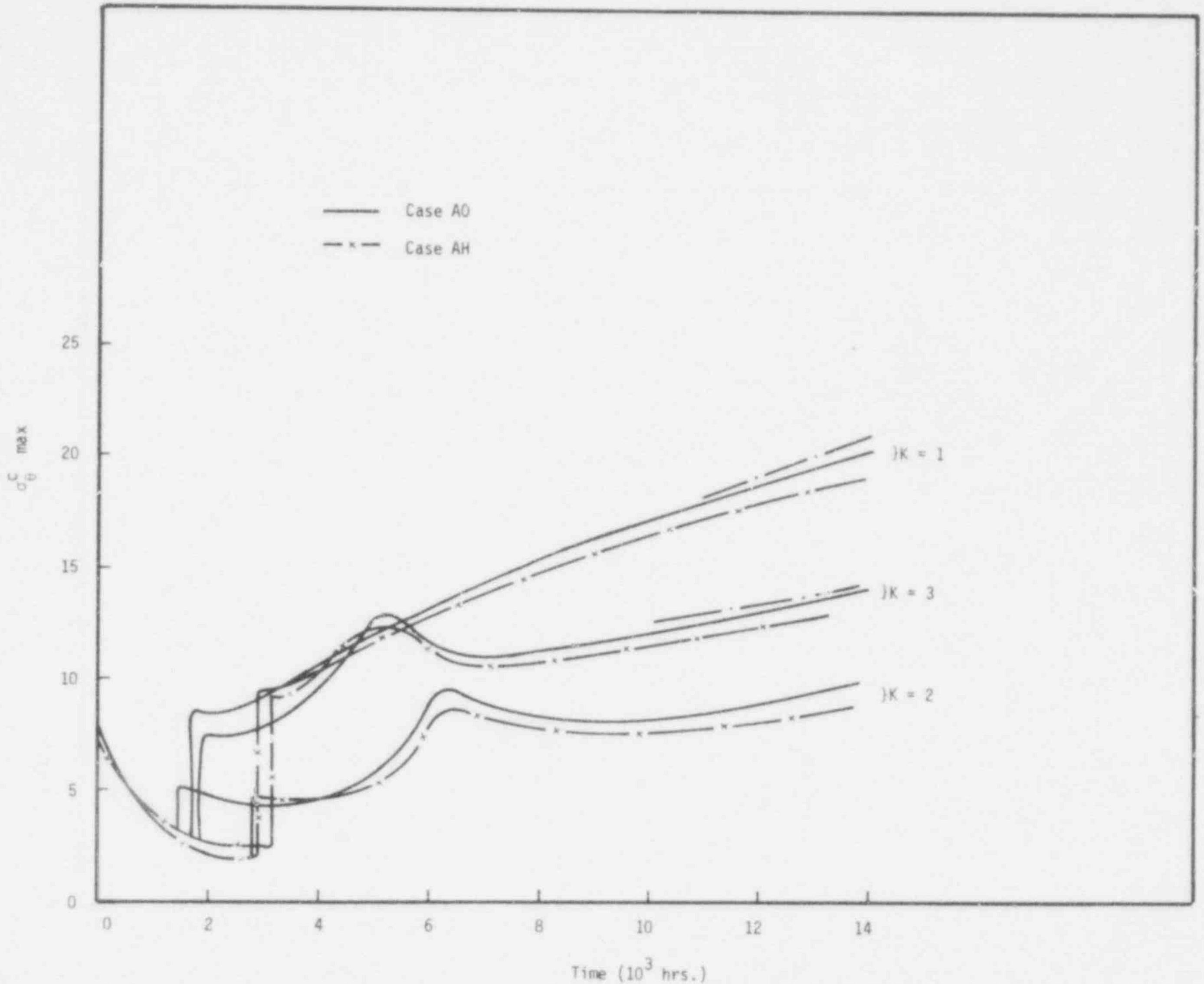


Fig. SA-5 The Maximum Hoop Stress in the Clad.

POOR ORIGINAL

733 281

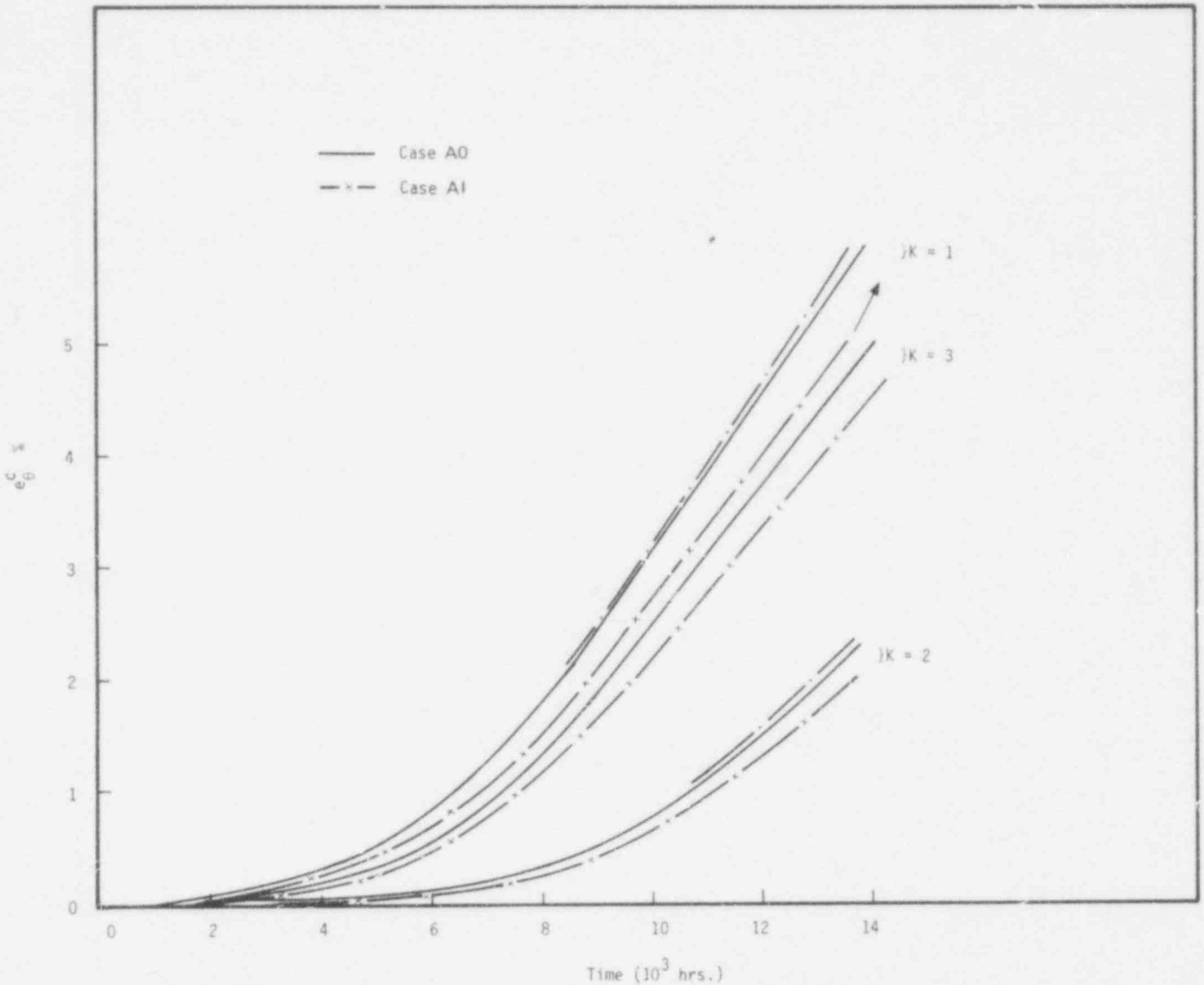


Fig. SA-6 The Total Strain in the Clad.

POOR ORIGINAL

733 202

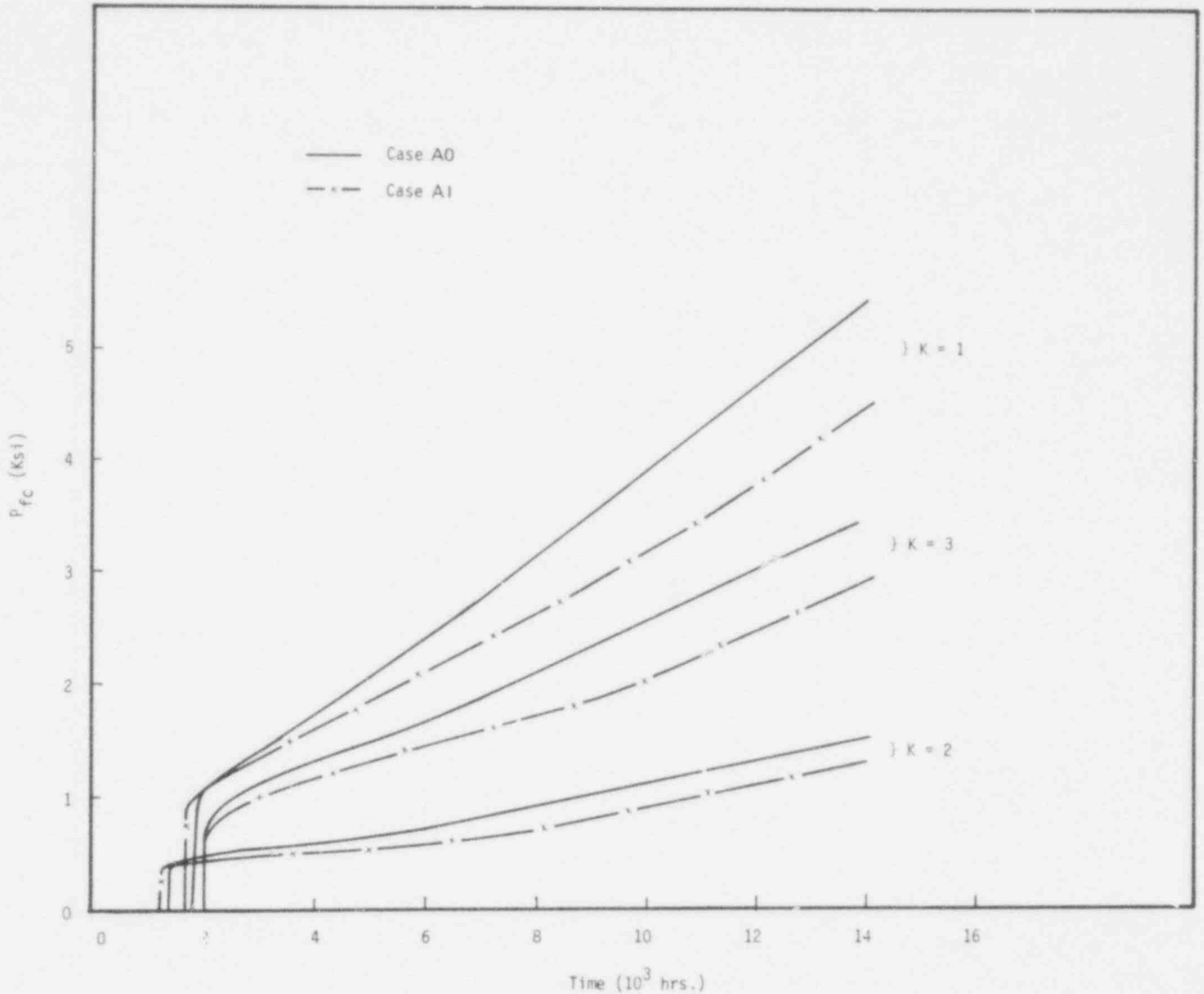


Fig. SA-7 The Fuel-Clad Interaction Force.

733 283

POOR ORIGINAL

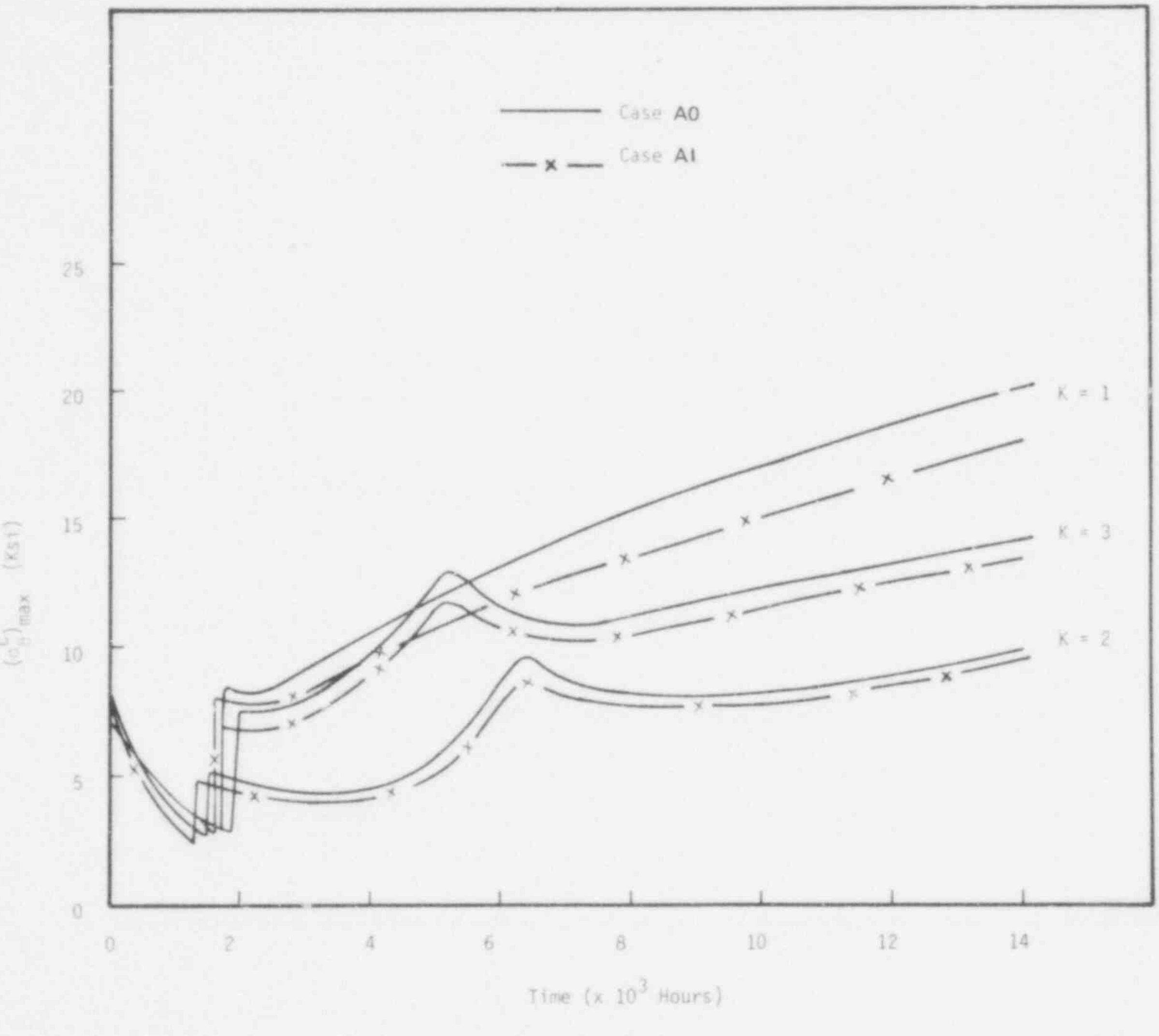


Figure SA - 8. The Maximum Hoop Stress in the Clad

733 294

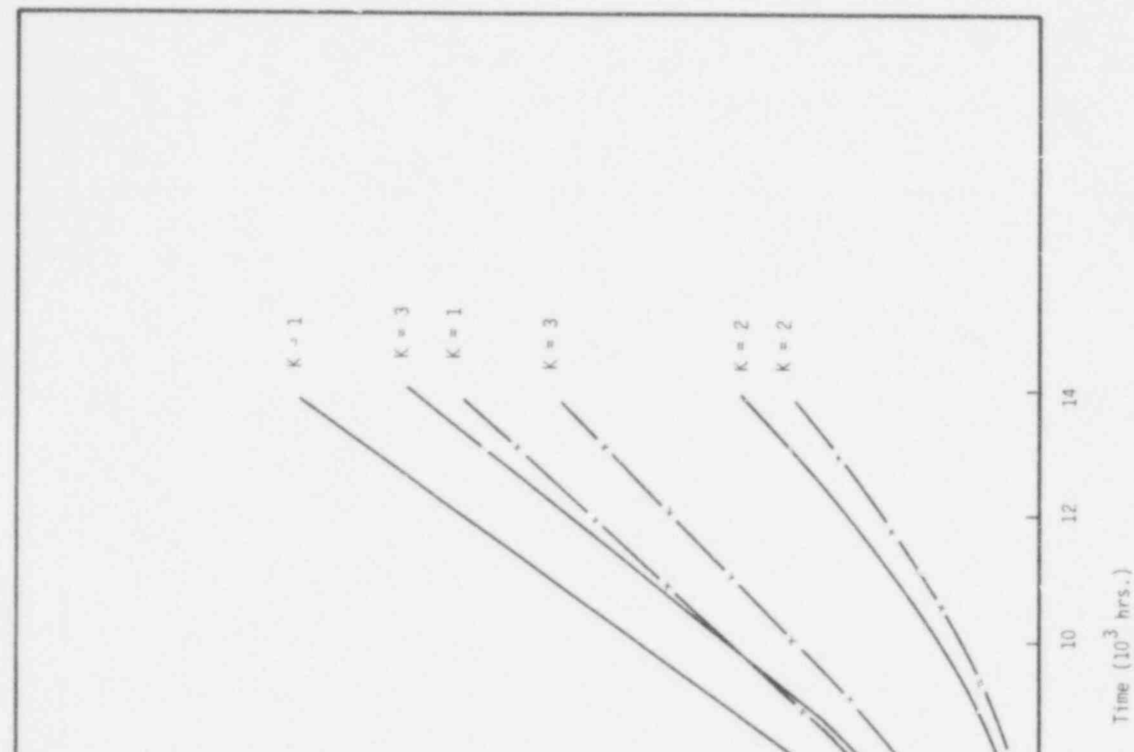


Fig. SA-9 The Total Strain in the Clad.

POOR ORIGINAL

733 285

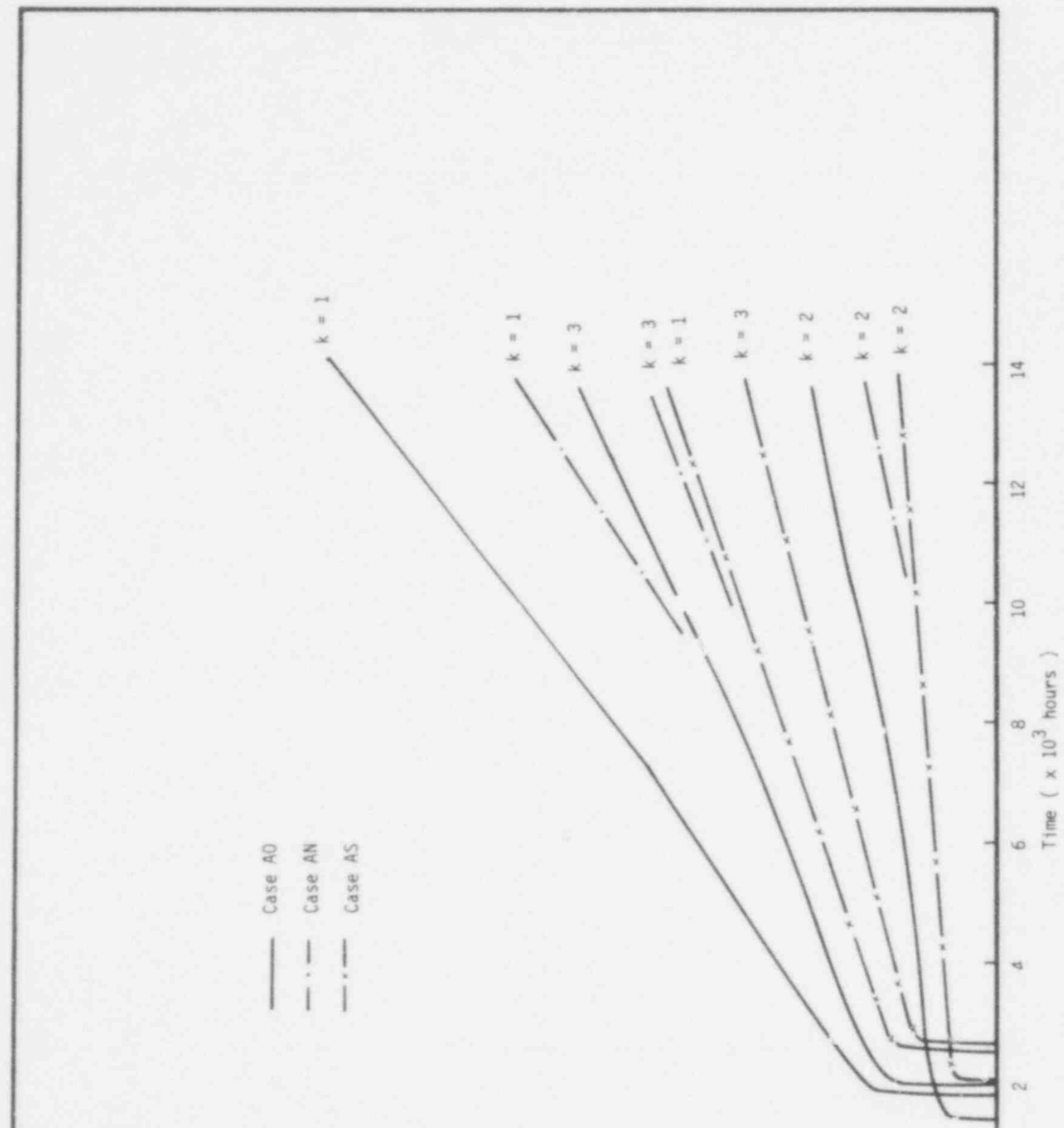


Figure SA - 10. The Fuel-Clad Interaction Force.

POOR ORIGINAL

733 286

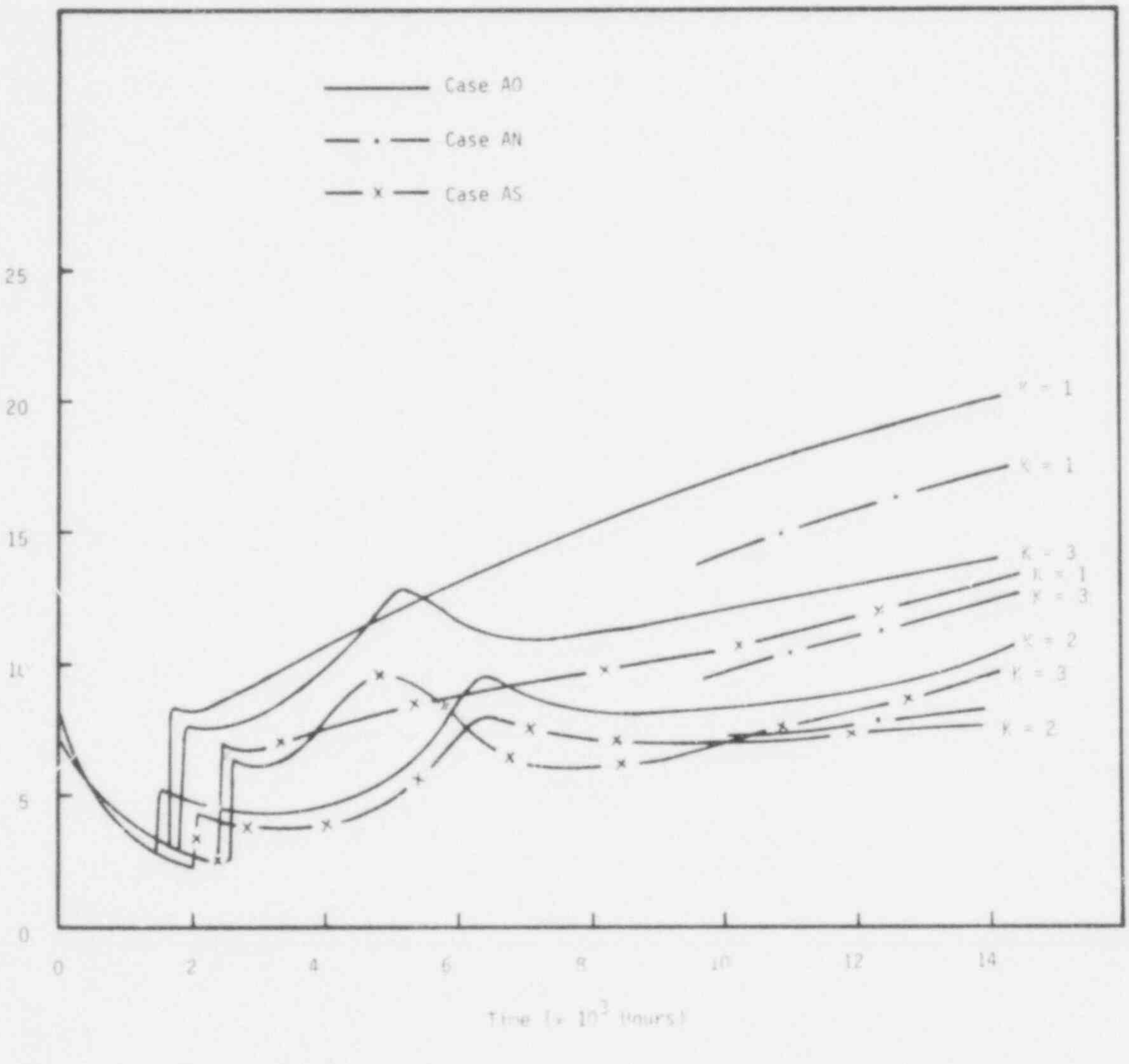


Figure 5A - 11. The Maximum Hoop Stress in the Clad

POOR ORIGINAL

733 287

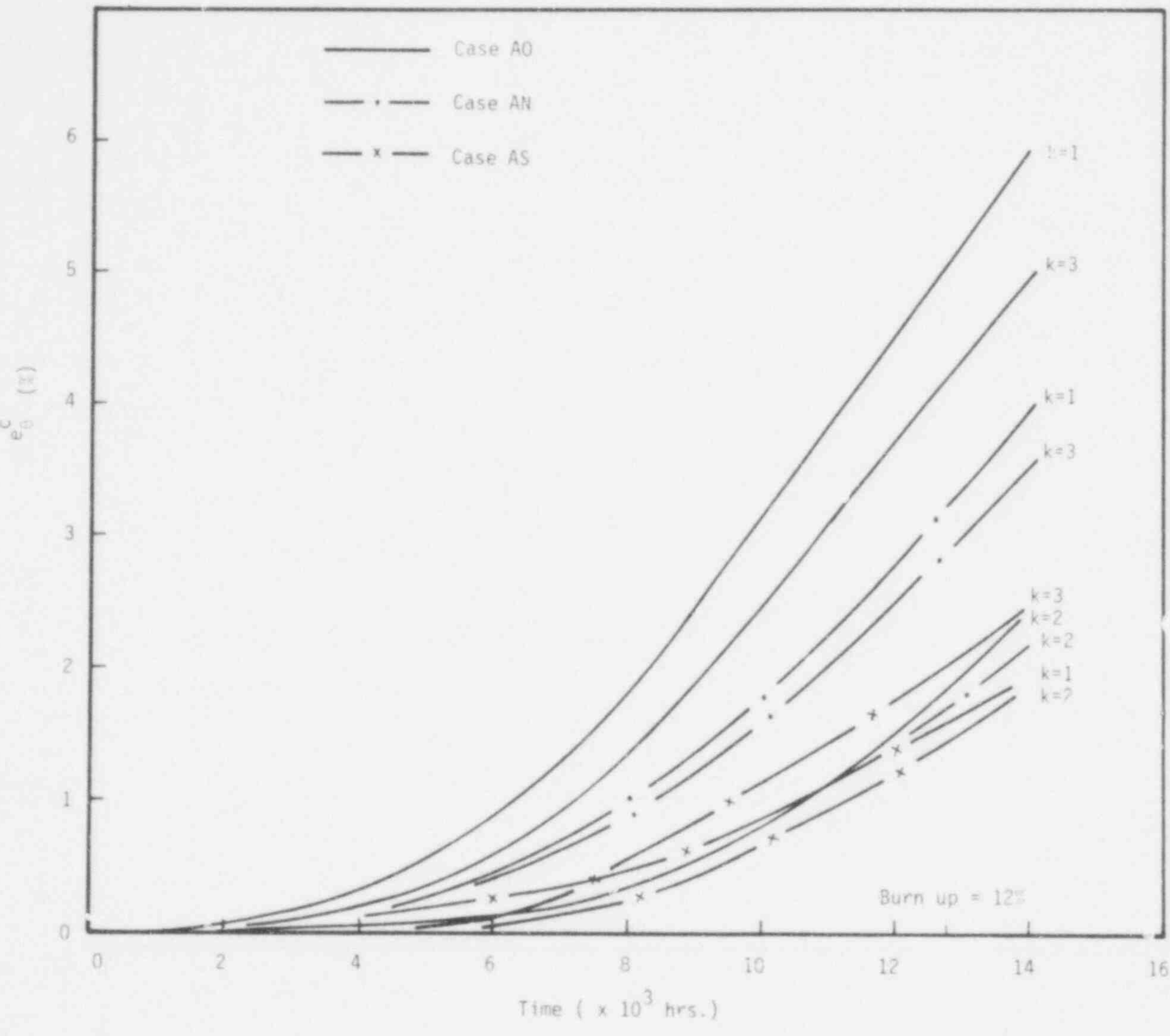


Fig. SA-12 The Total Hoop Strain in the Clad.

POOR ORIGINAL

733 288

9 kW/ft Cases

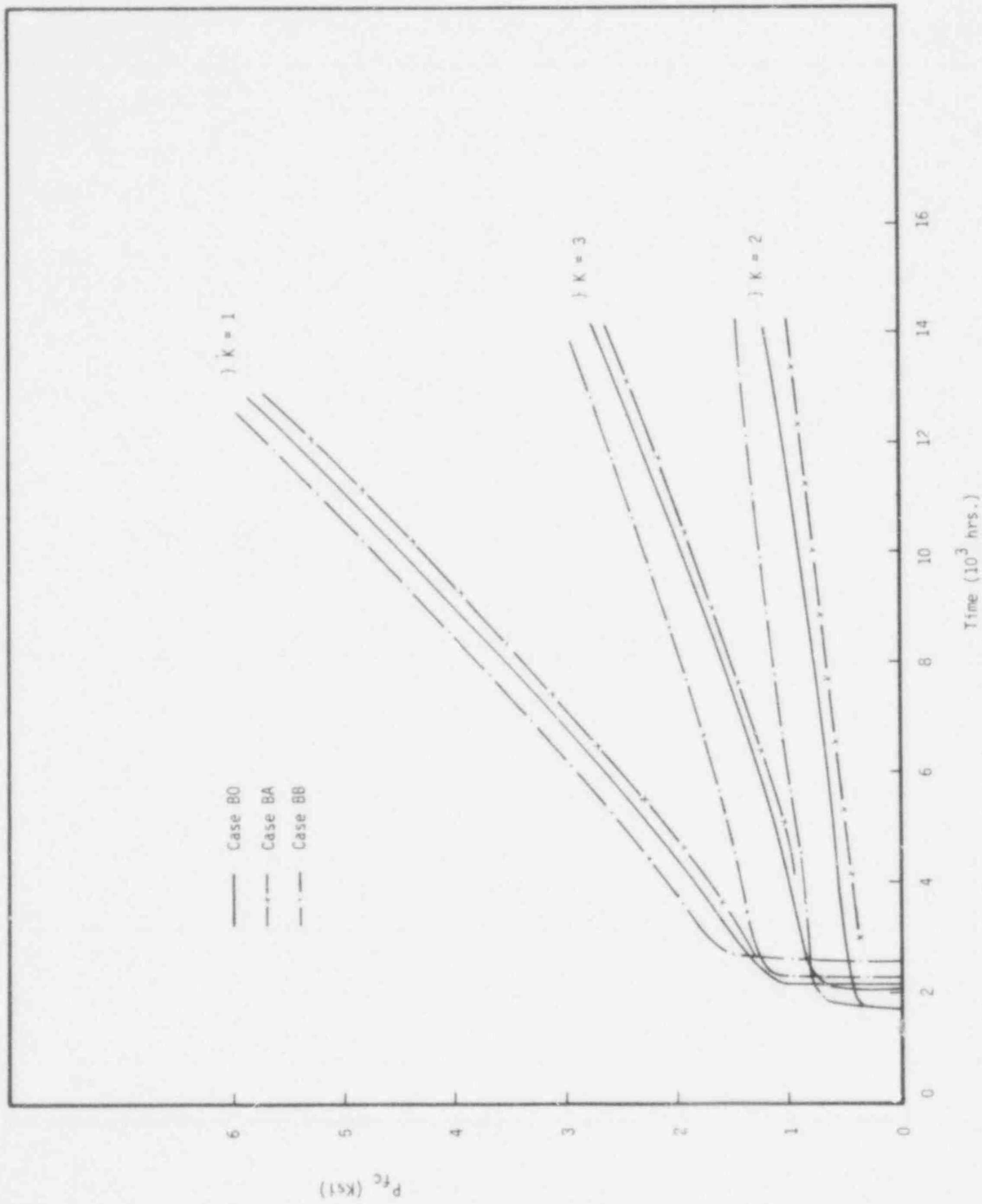


Fig. SB-1 The Fuel-Clad Interaction Force.

733 209

POOR ORIGINAL

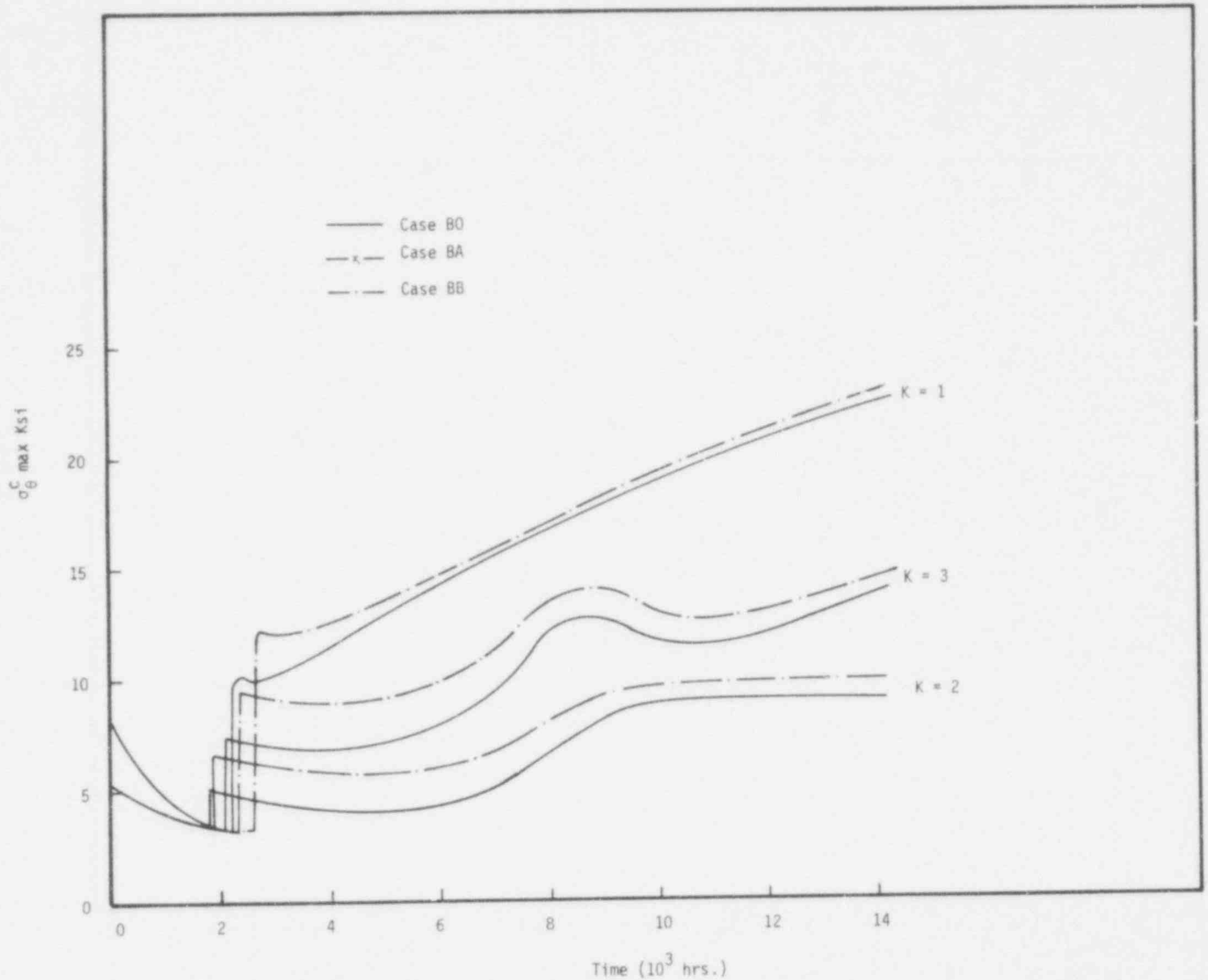


Fig. SB-2 The Maximum Hoop Stress in the Clad.



733 290

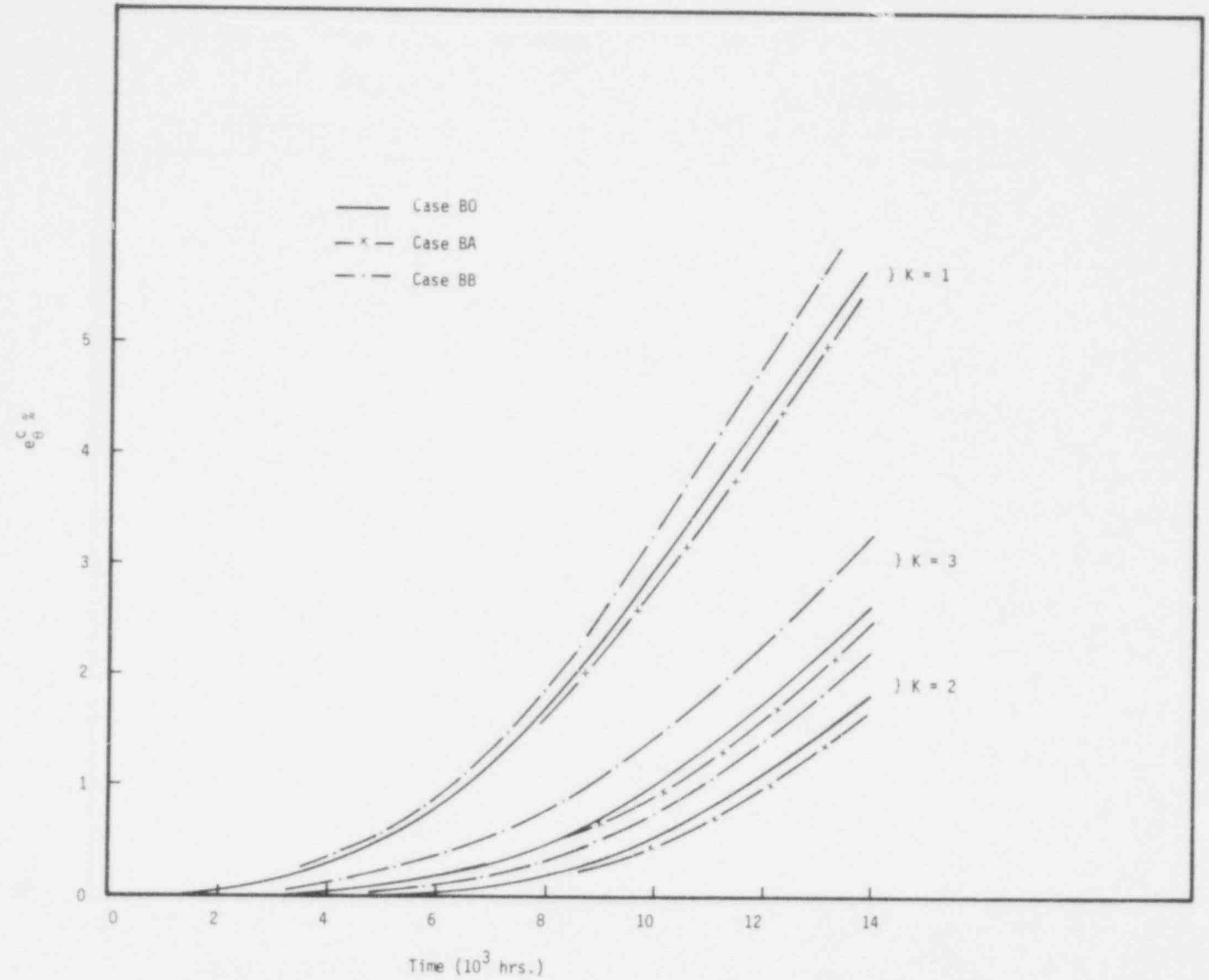


Fig. 5B-3 The Total Strain in the Clad.

POOR ORIGINAL

733 291


Figure 5B - 4. The Fuel-Clad Interaction Force

733 292

POOR ORIGINAL

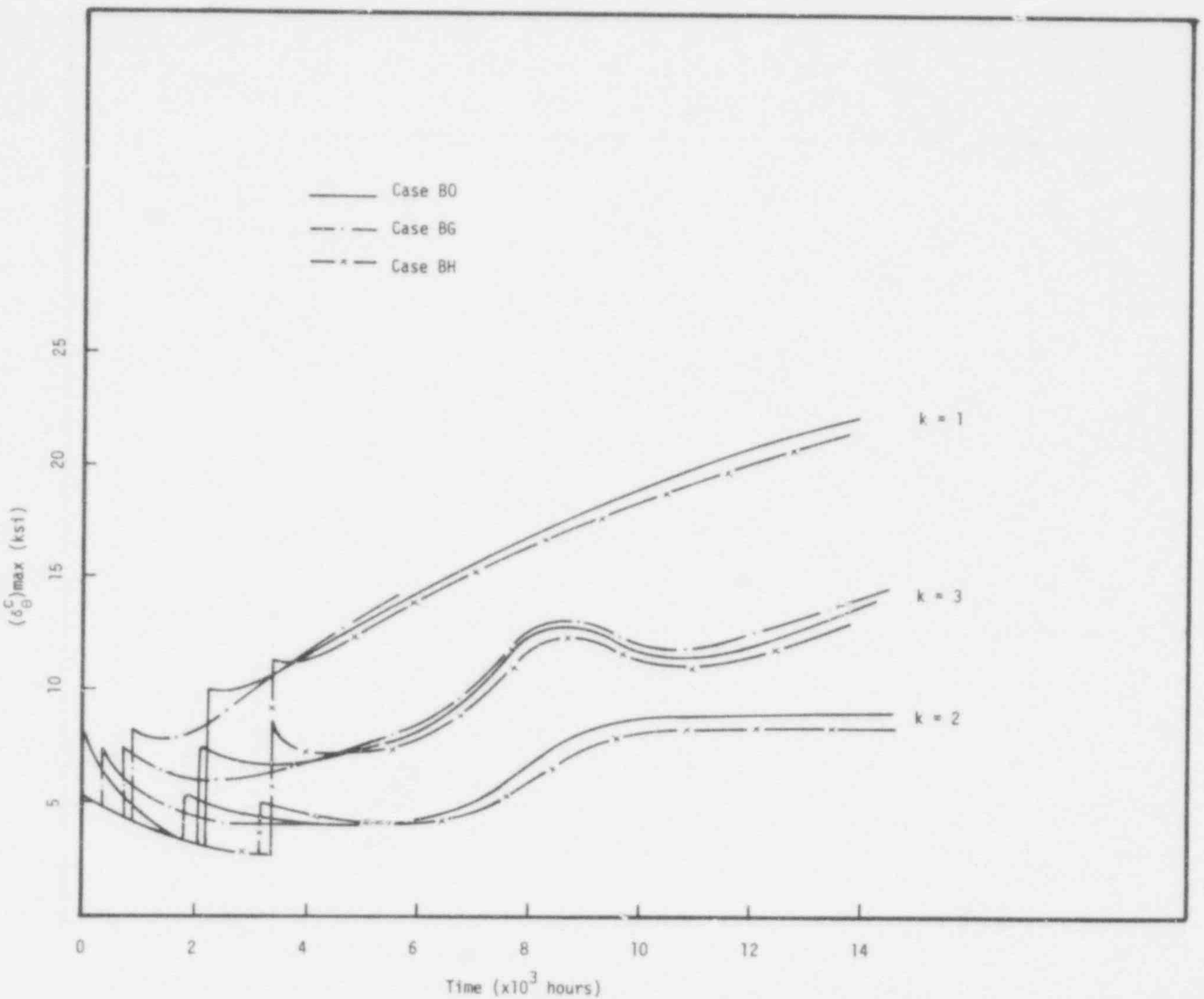


Figure 5B-5 The Maximum Hoop Stress in the Clad





733 293

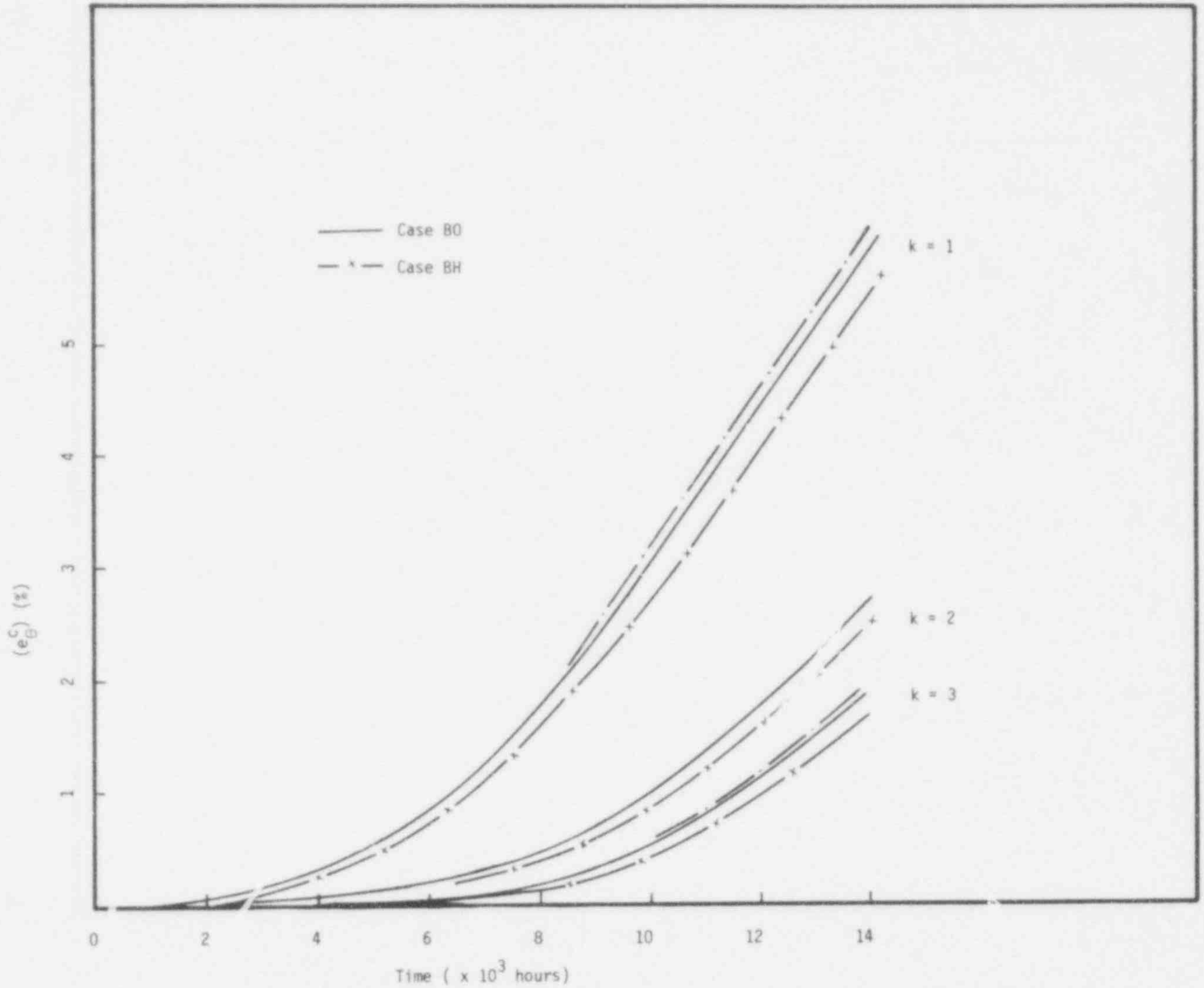


Figu e SB - 6. The Tot*l Strain in the Clad.

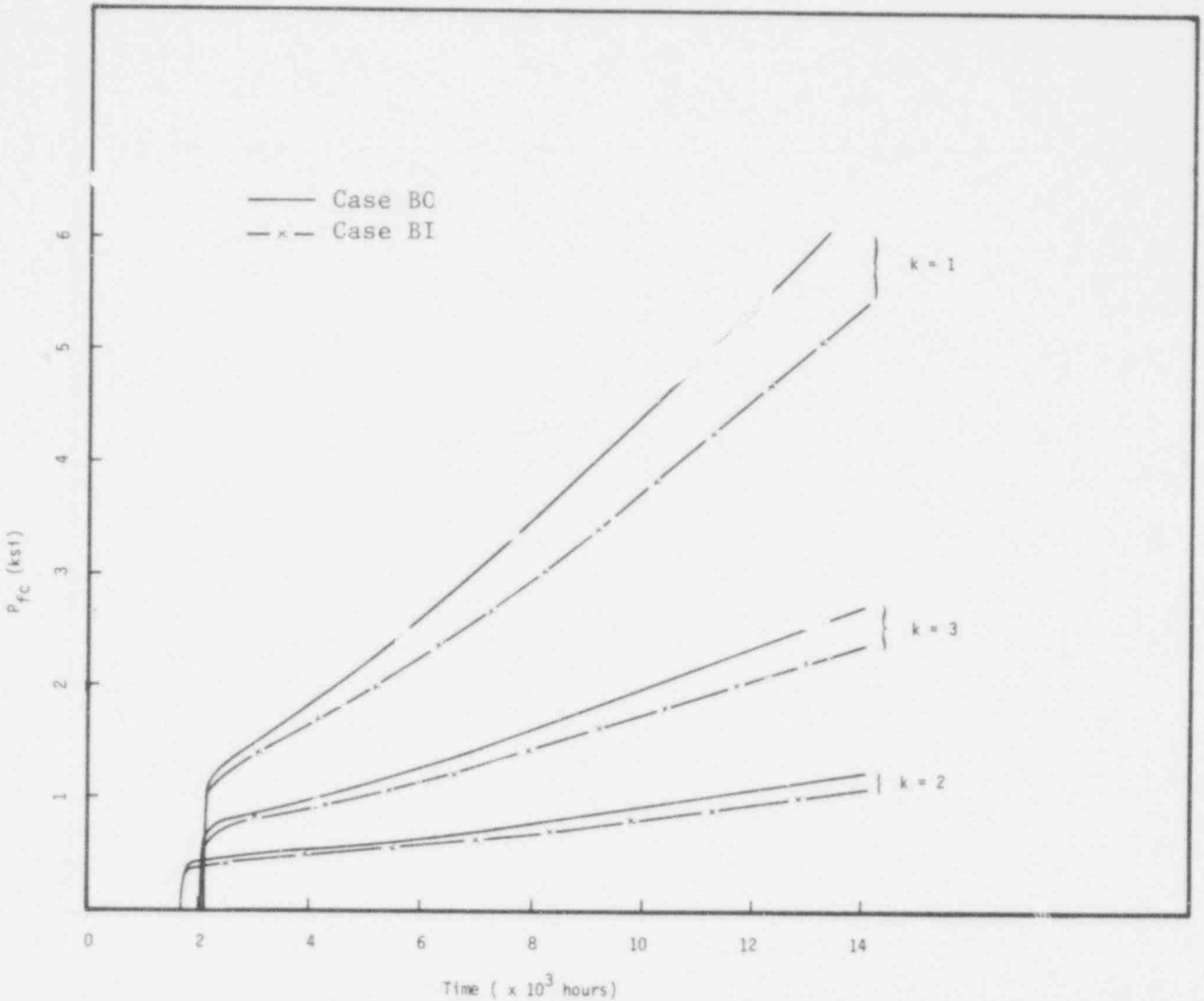


gure 5B - 7. The Fuel-Clad Interaction Force.

POOR ORIGINAL



733 295

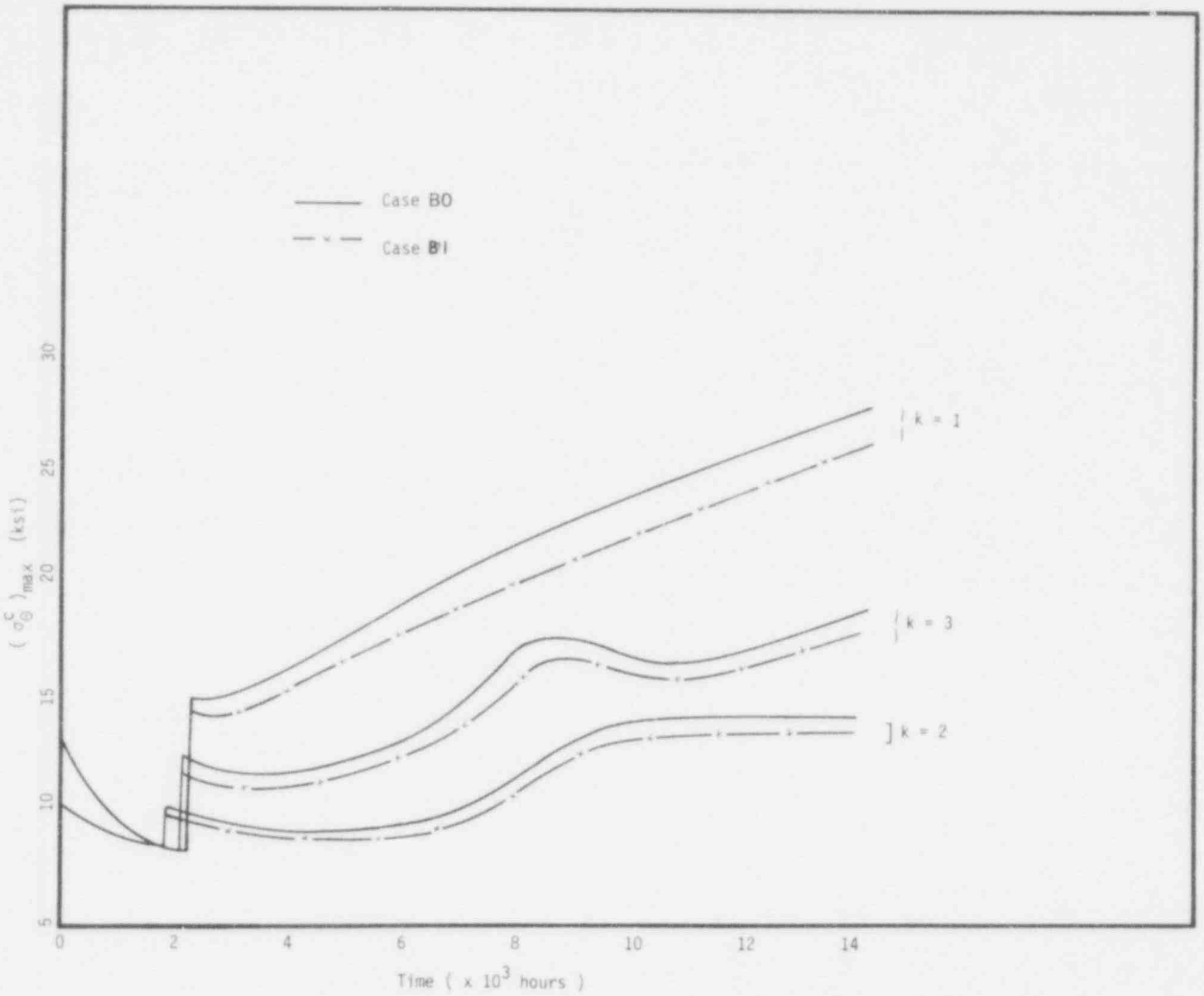


Figure 5B - 8. The Maximum Hoop Stress in the Clad.

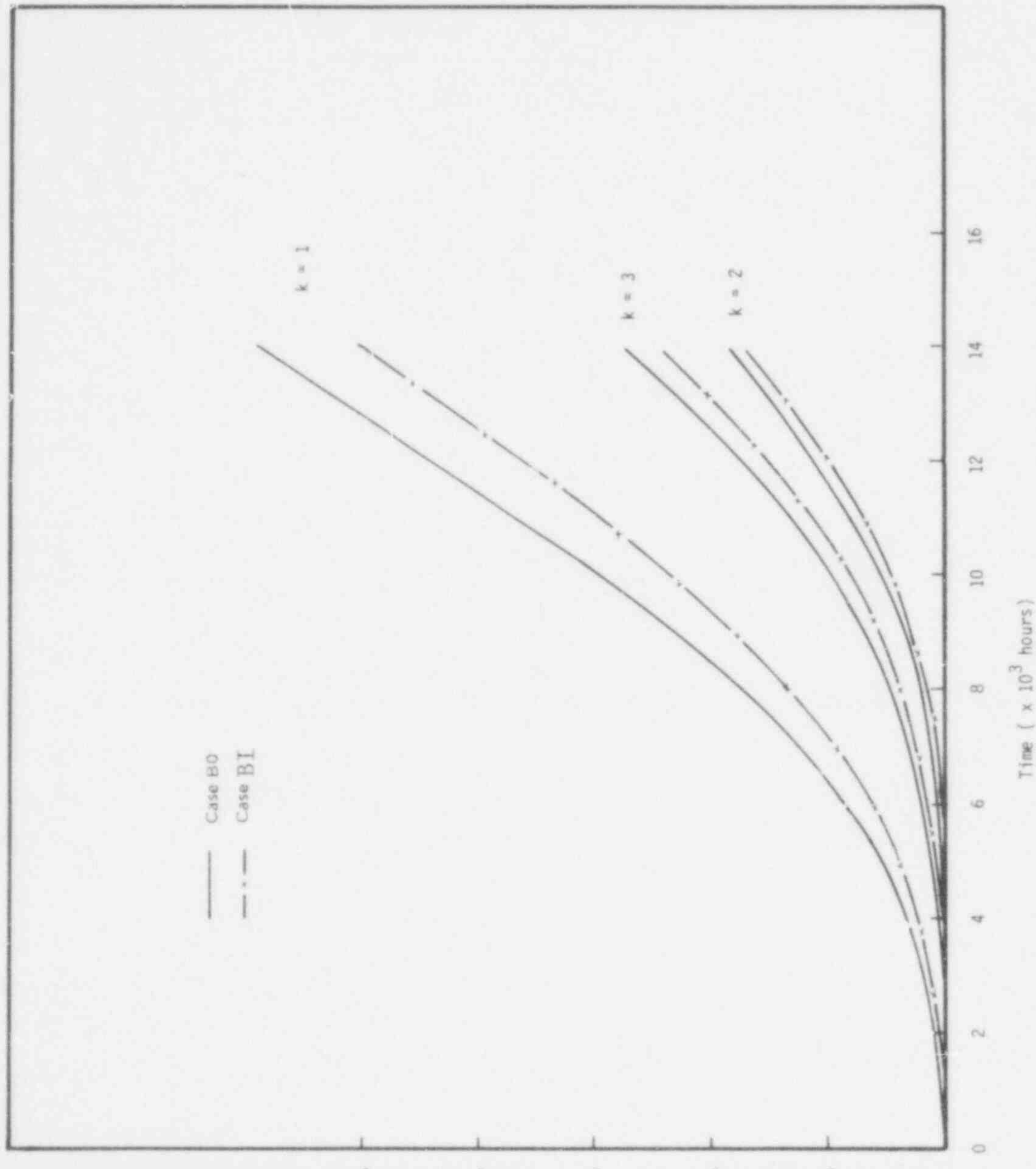


Figure 5B - 9. The Total Strain in the Clad.

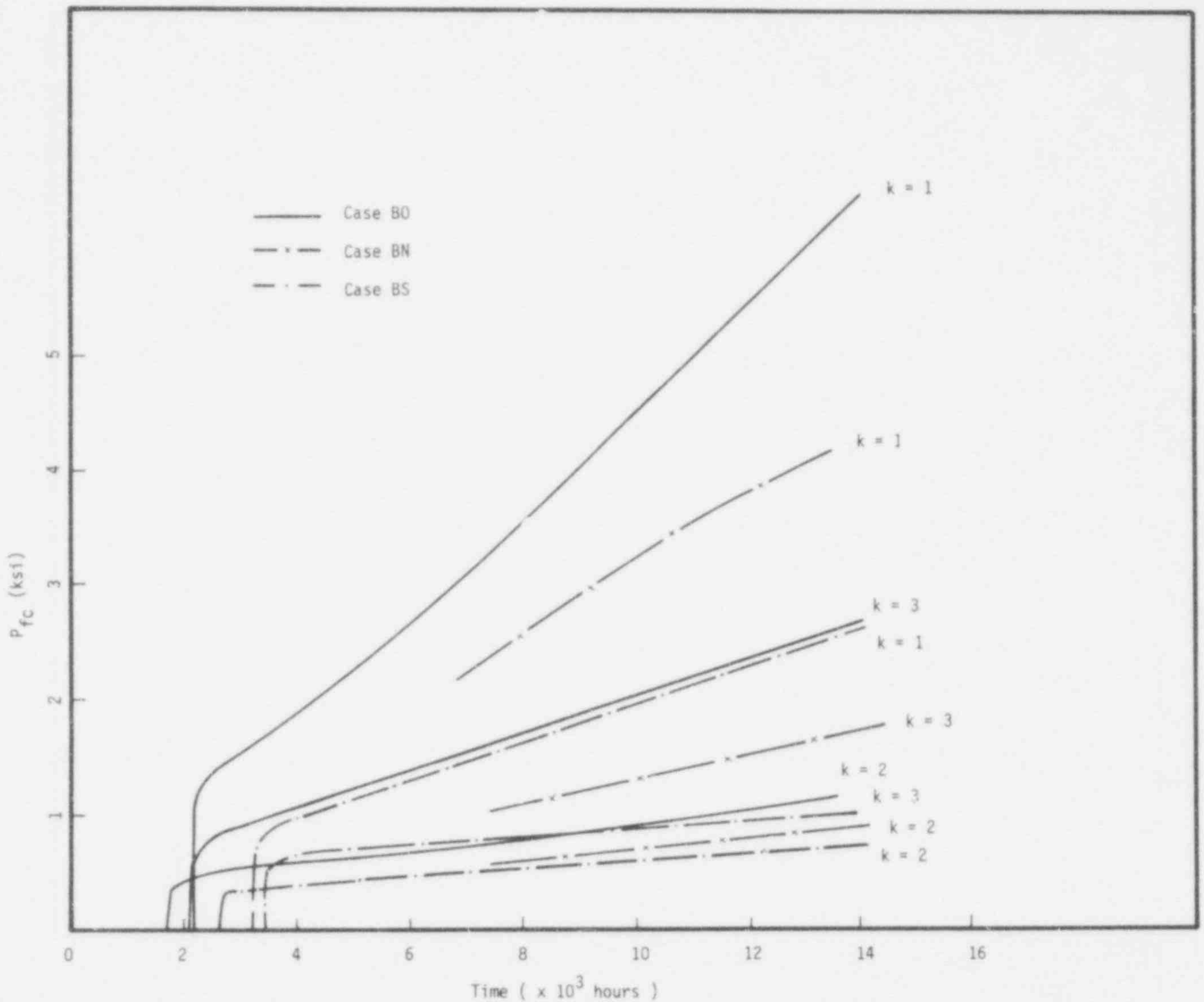


Figure 5B - 10. The Fuel-Clad Interaction Force.



733 298

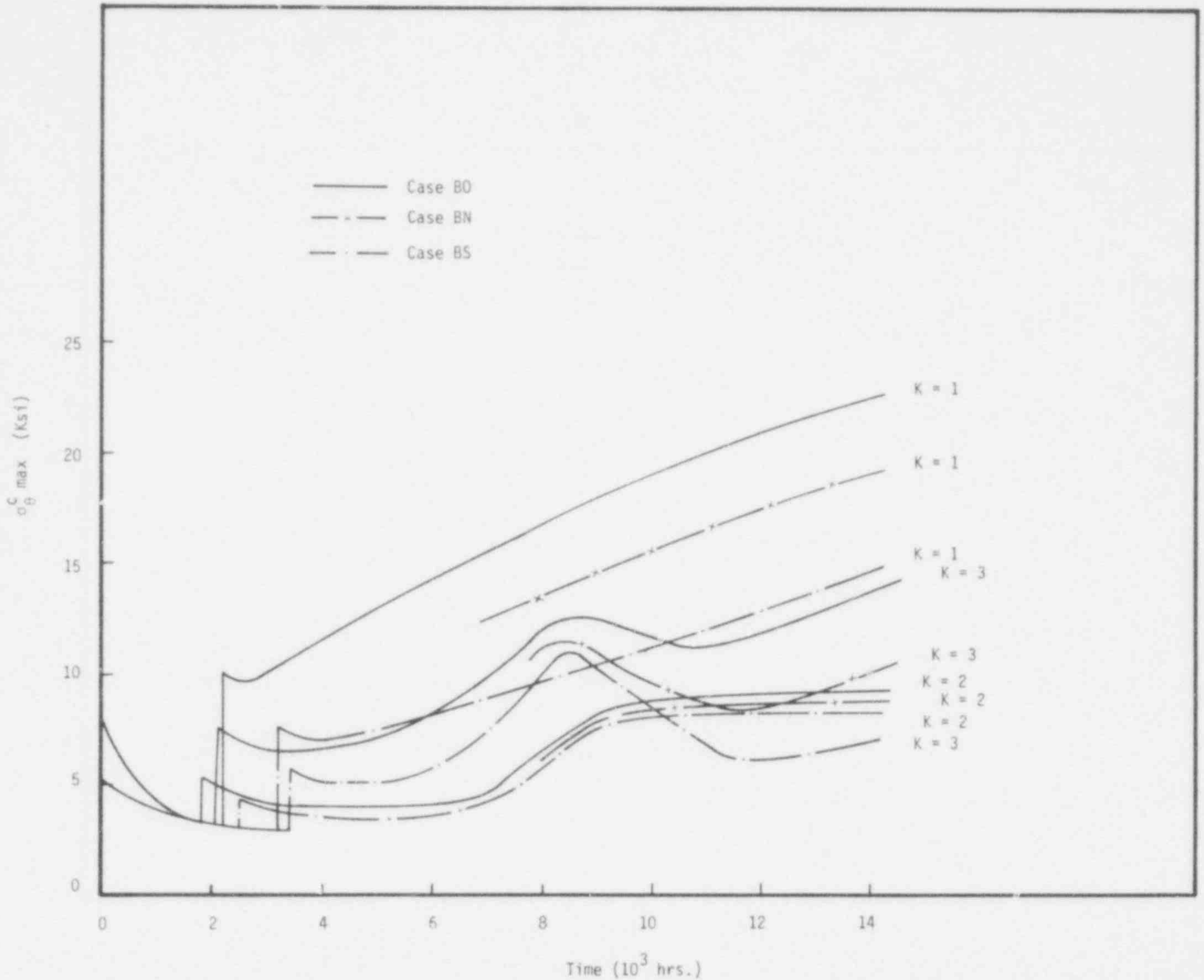


Fig. SB-11 The Maximum Hoop Stress in the Clad.

POOR ORIGINAL

733 299

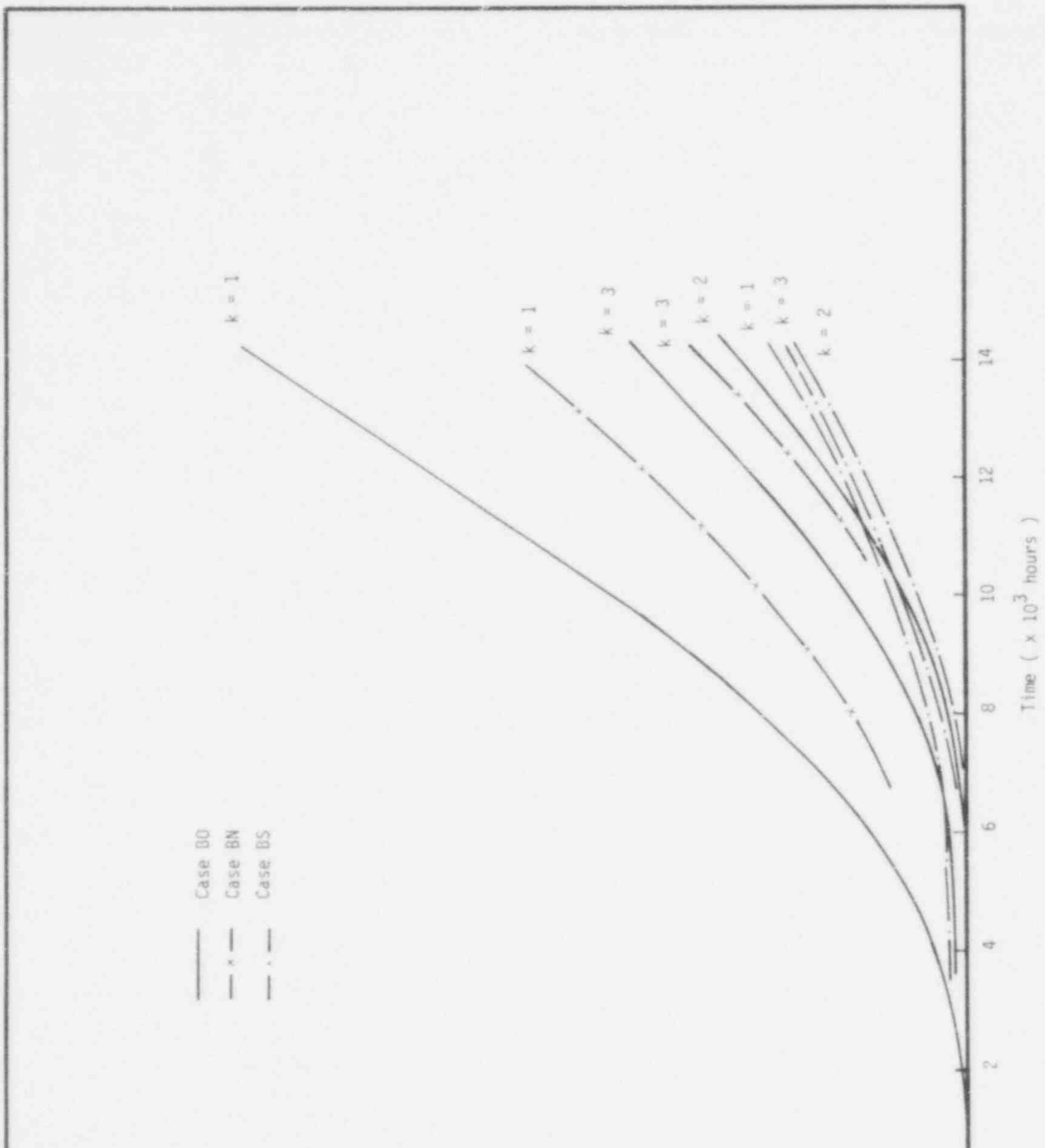


Figure SB - 12. The Total Strain in the Clad.

6 kW/ft Cases

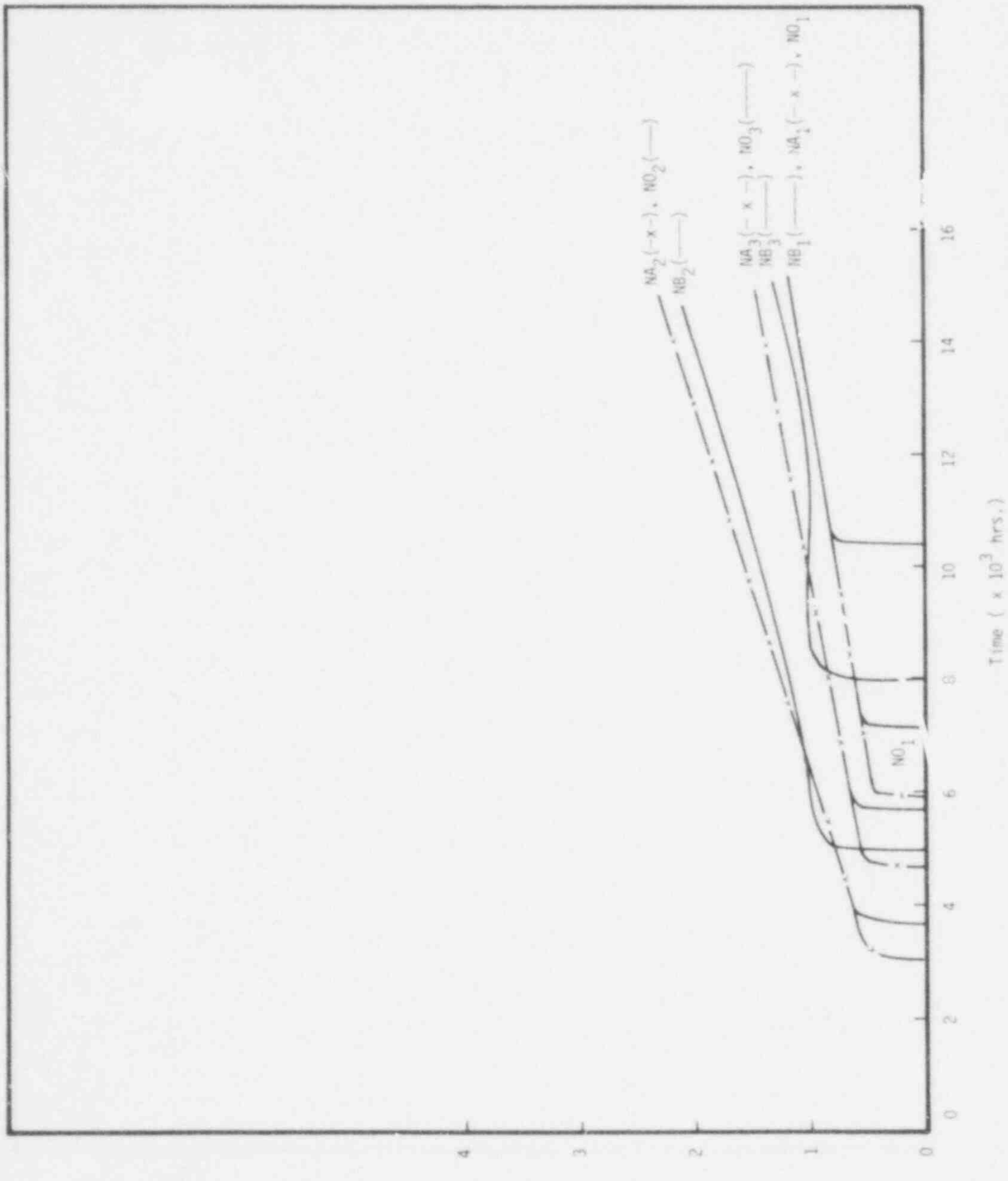


Fig. SN-1 The Fuel-Clad Interaction Force.

POOR ORIGINAL



133 301

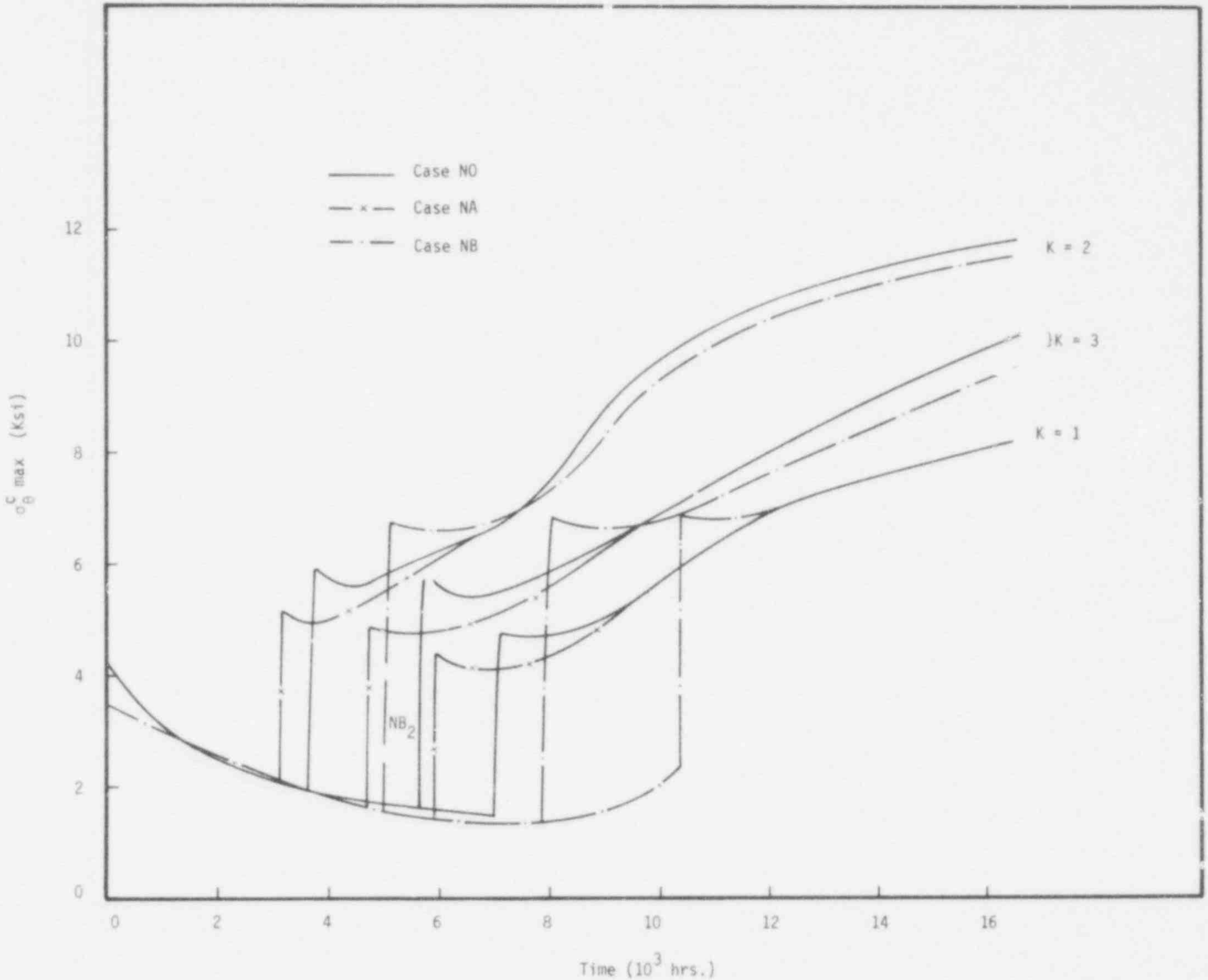


Fig. SN-2 The Maximum Stress in the Clad.

POOR ORIGINAL

733 302

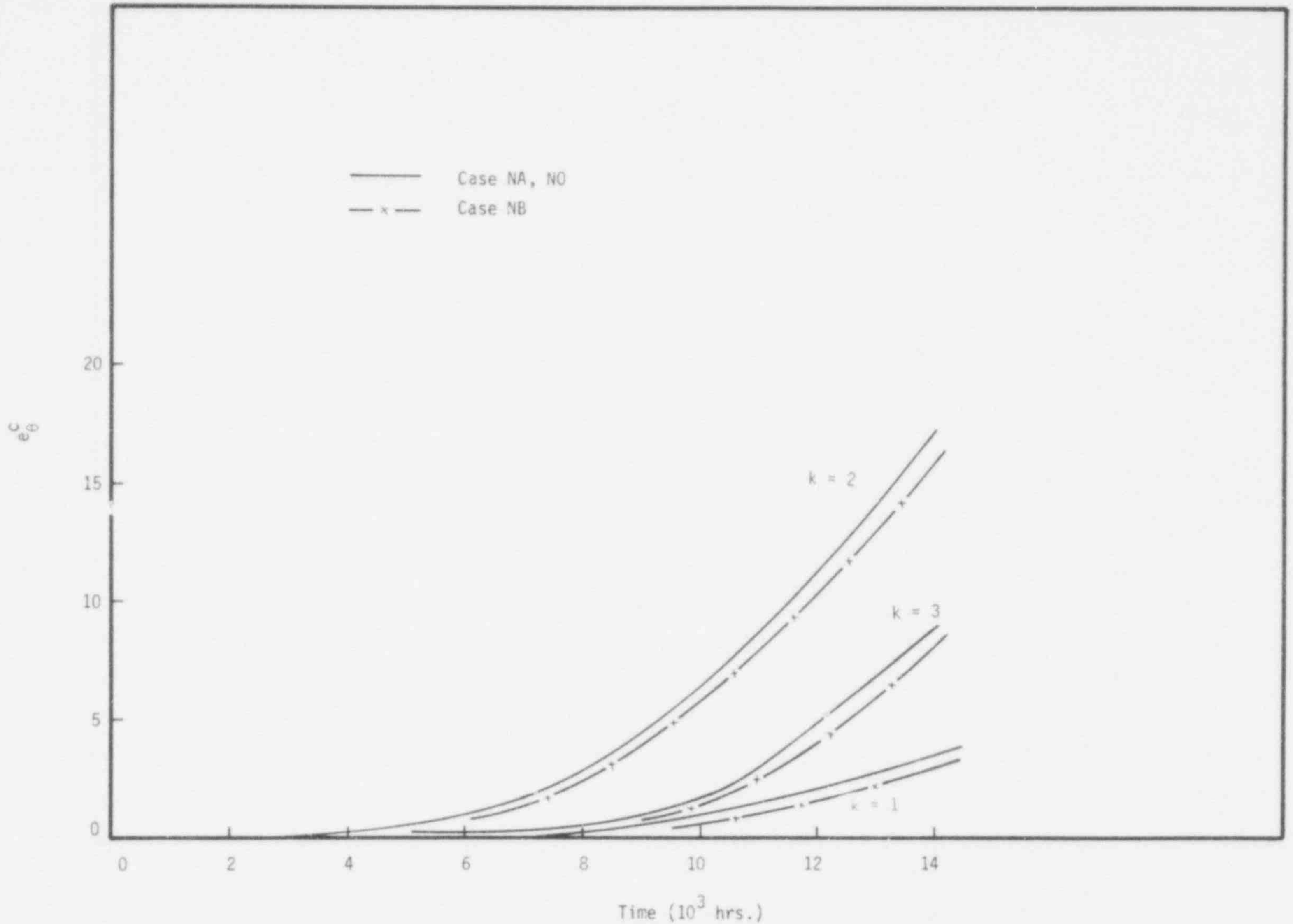


Fig. SN-3 The Total Strain in the Clad.





733 303

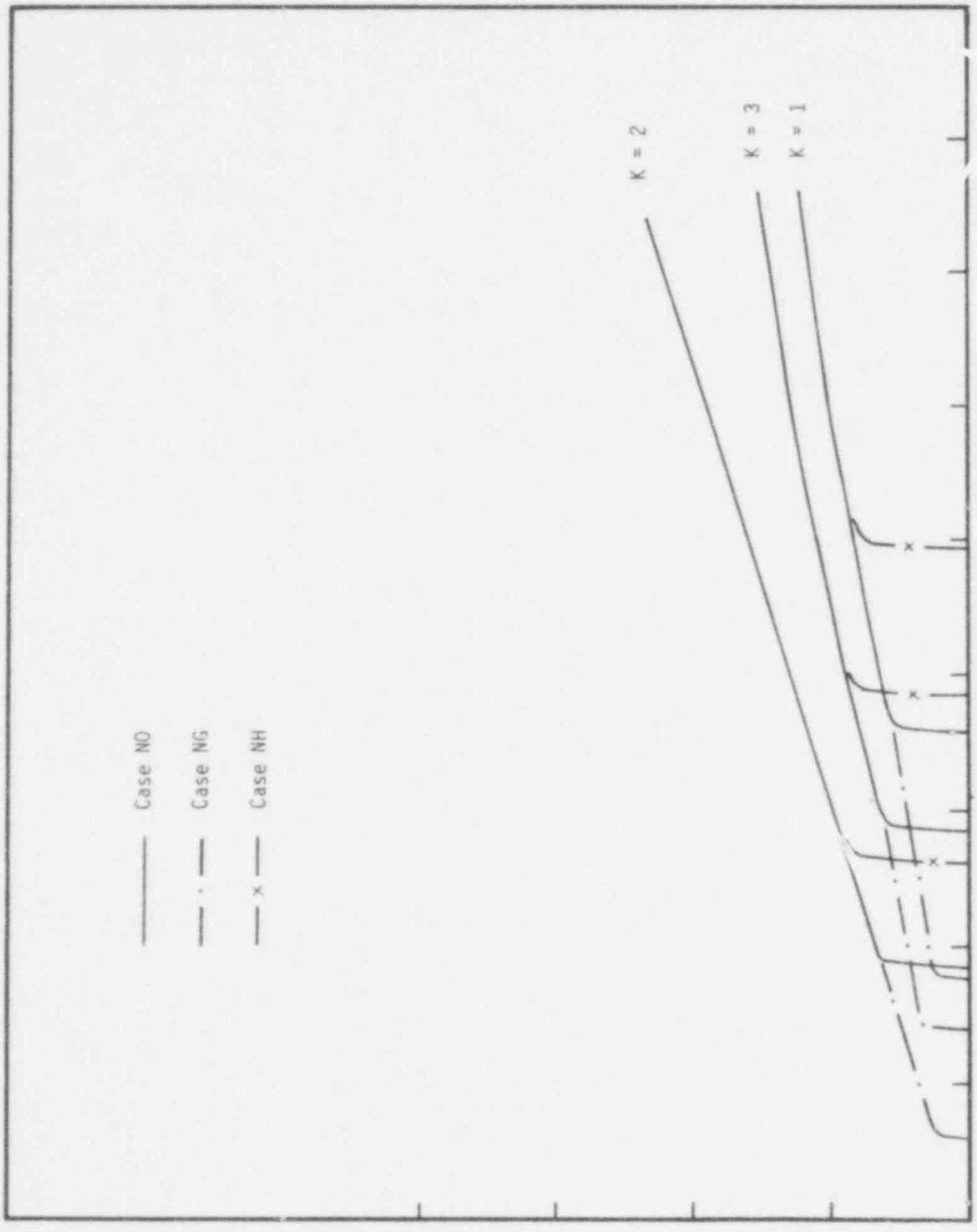


Fig. SN-4 The Fuel-Clad Interaction Force.

POOR ORIGINAL

733 204

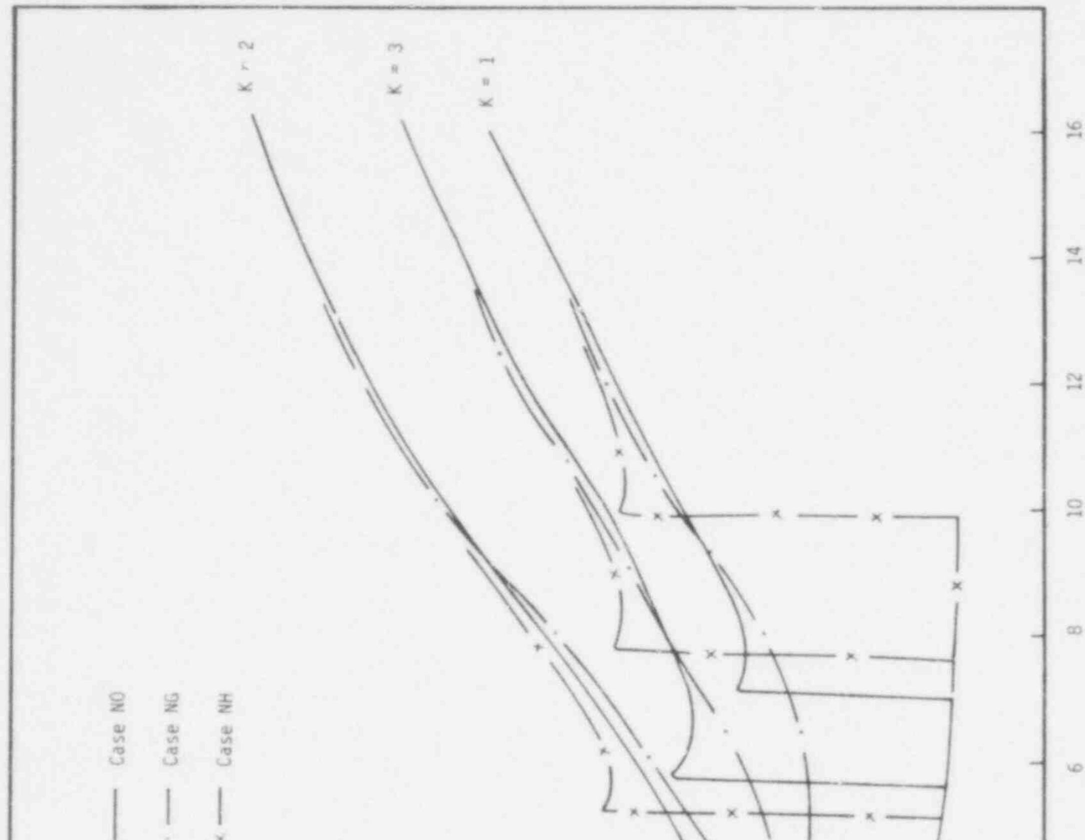


Fig. 2N-5 The Maximum Hoop Stress in the Clad.

POOR ORIGINAL

733 305

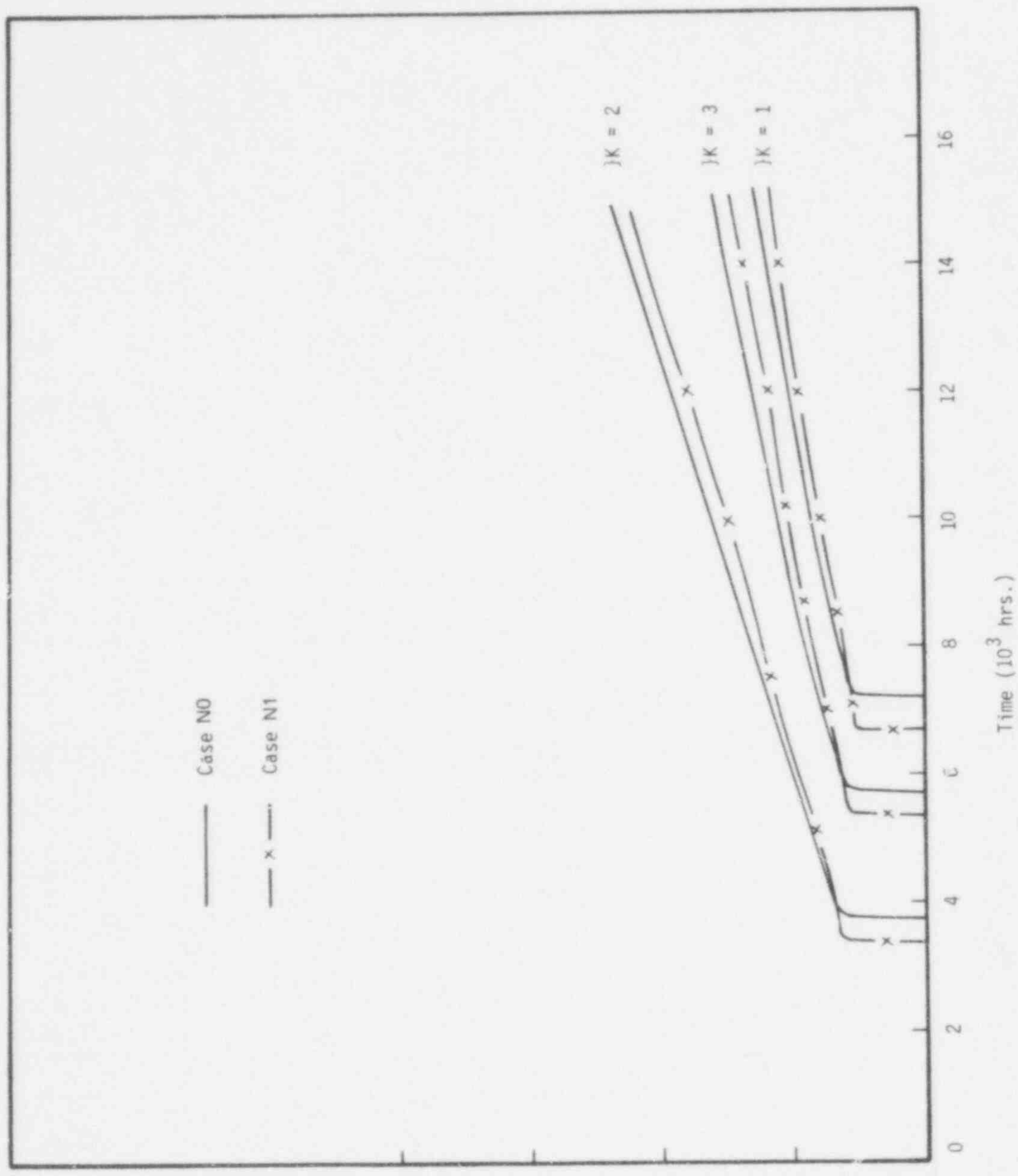


Fig. SN-6 The Fuel-Clad Interaction Force.

733 306

POOR ORIGINAL

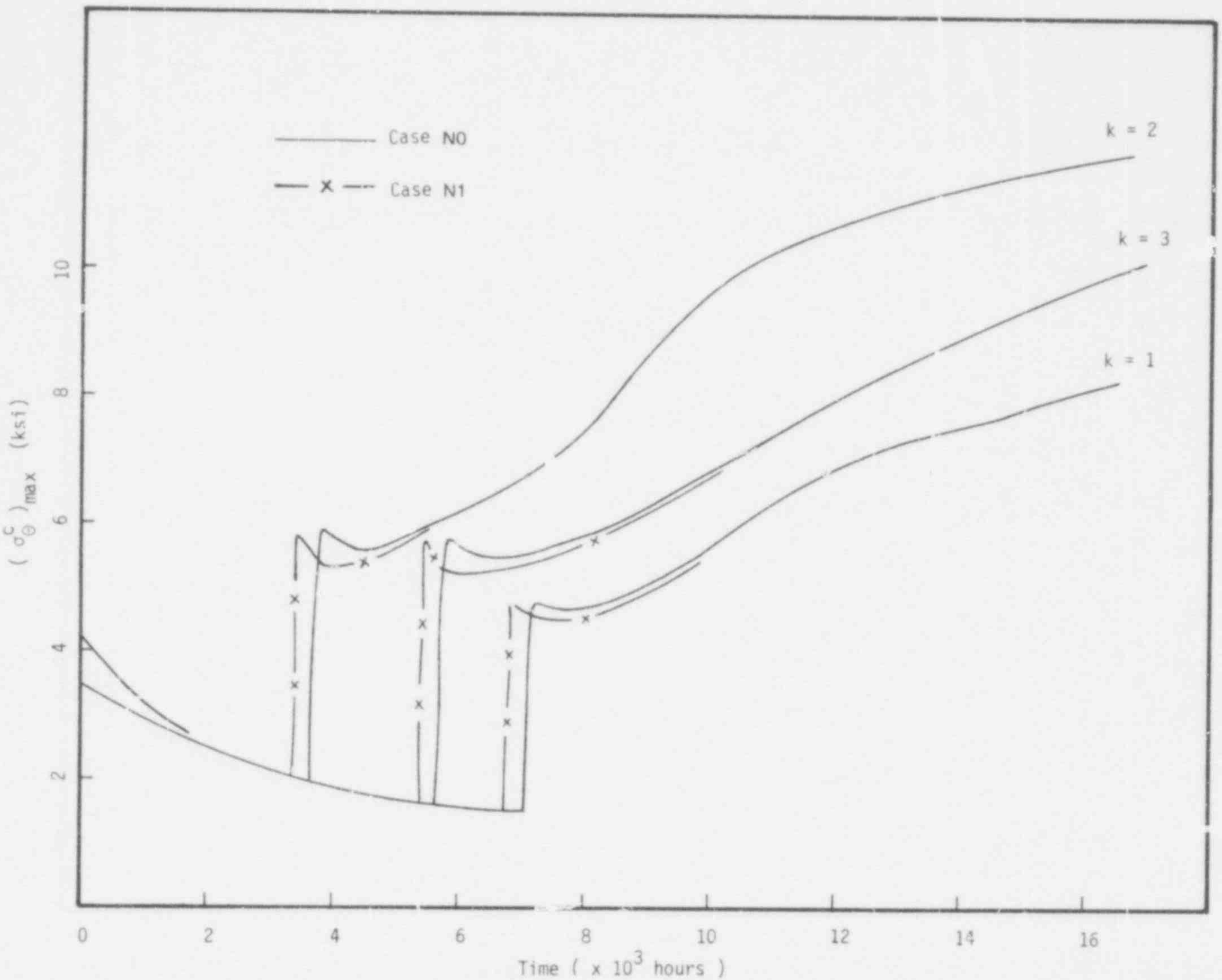


Figure SN - 7. The Maximum Hoop Stress in the Clad.

POOR ORIGINAL



733 307

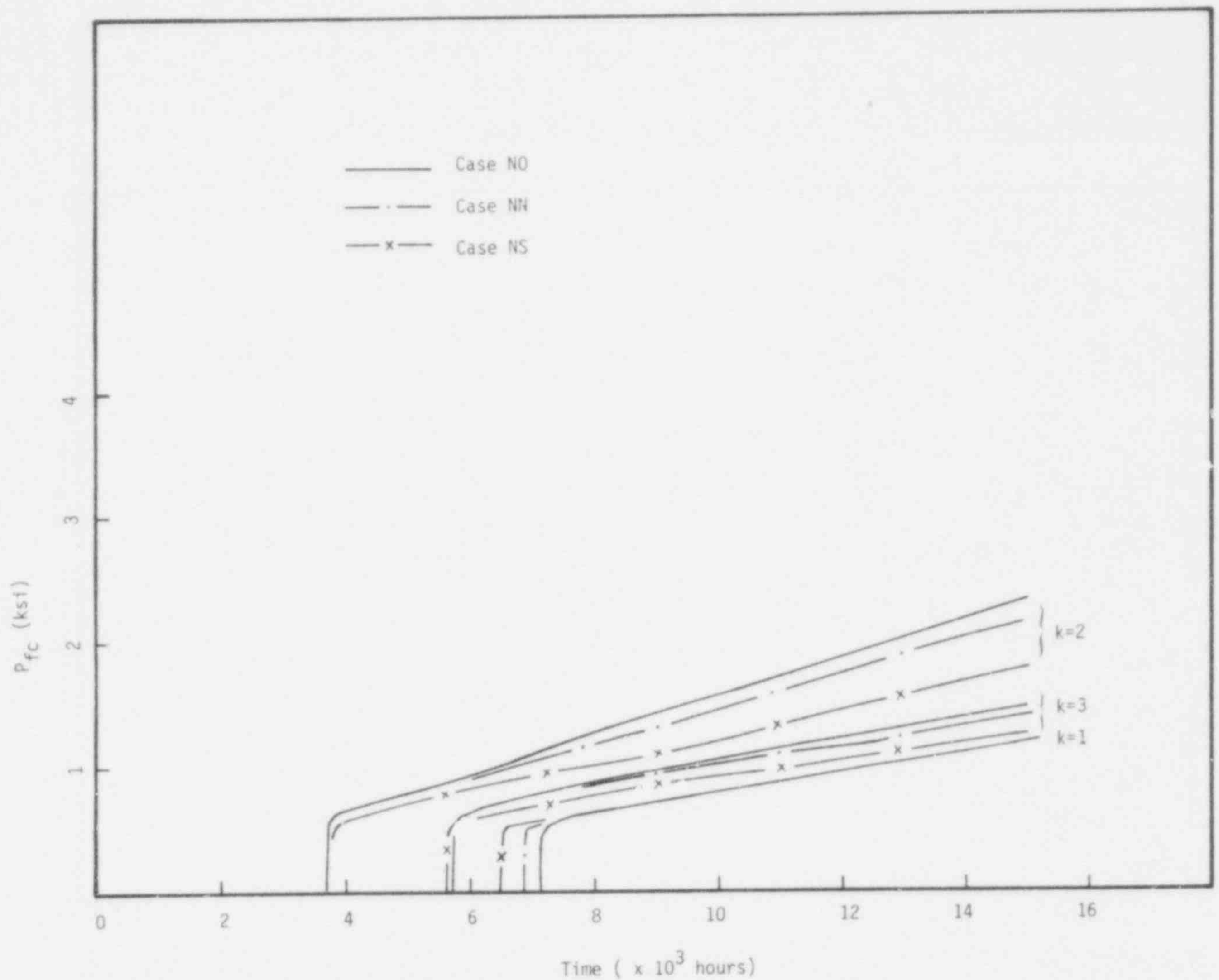


Figure SN-8. The Fuel - Clad Interaction Force.

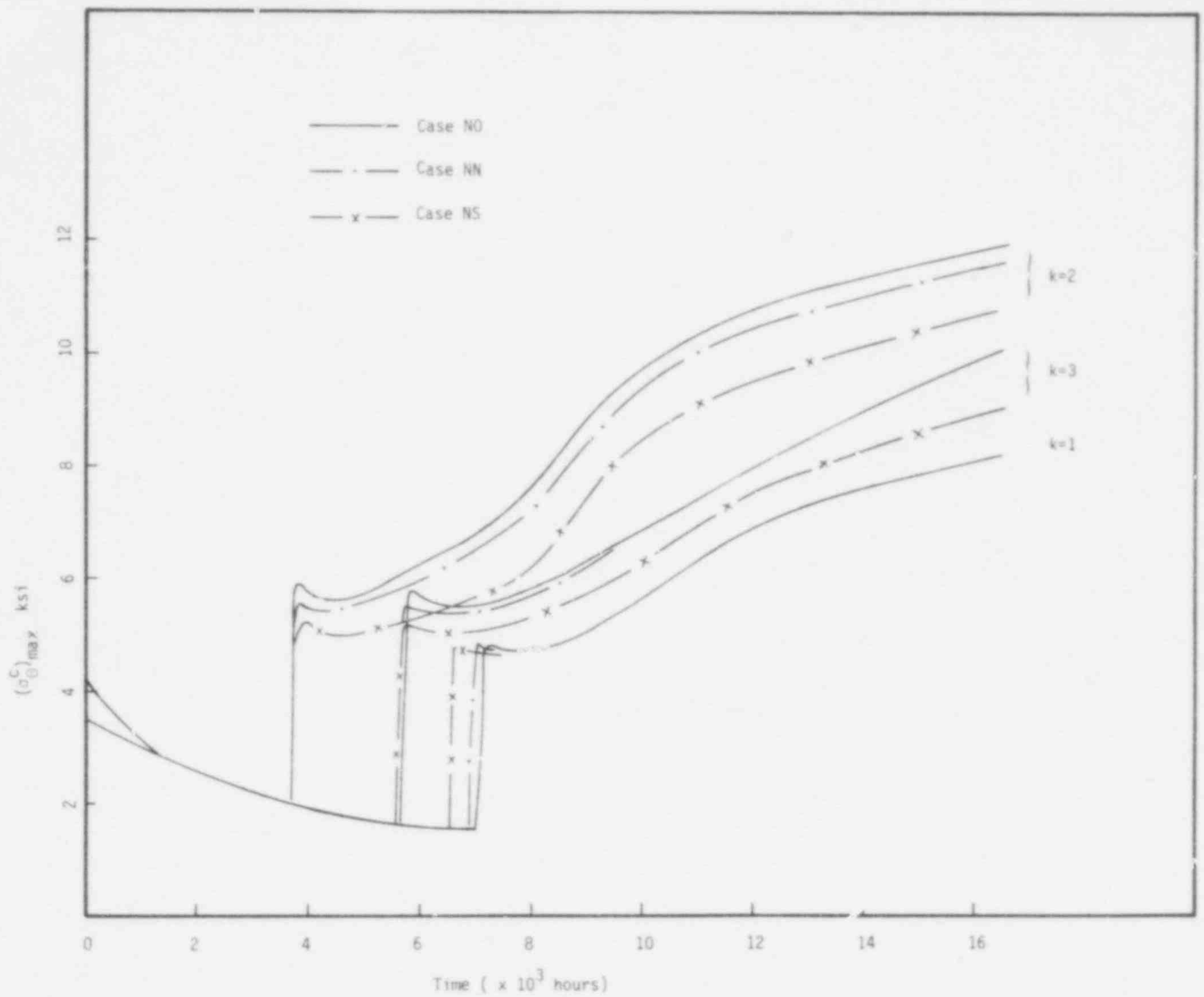


Figure SN-9. The Maximum Hoop Stress in the Clad



733 309

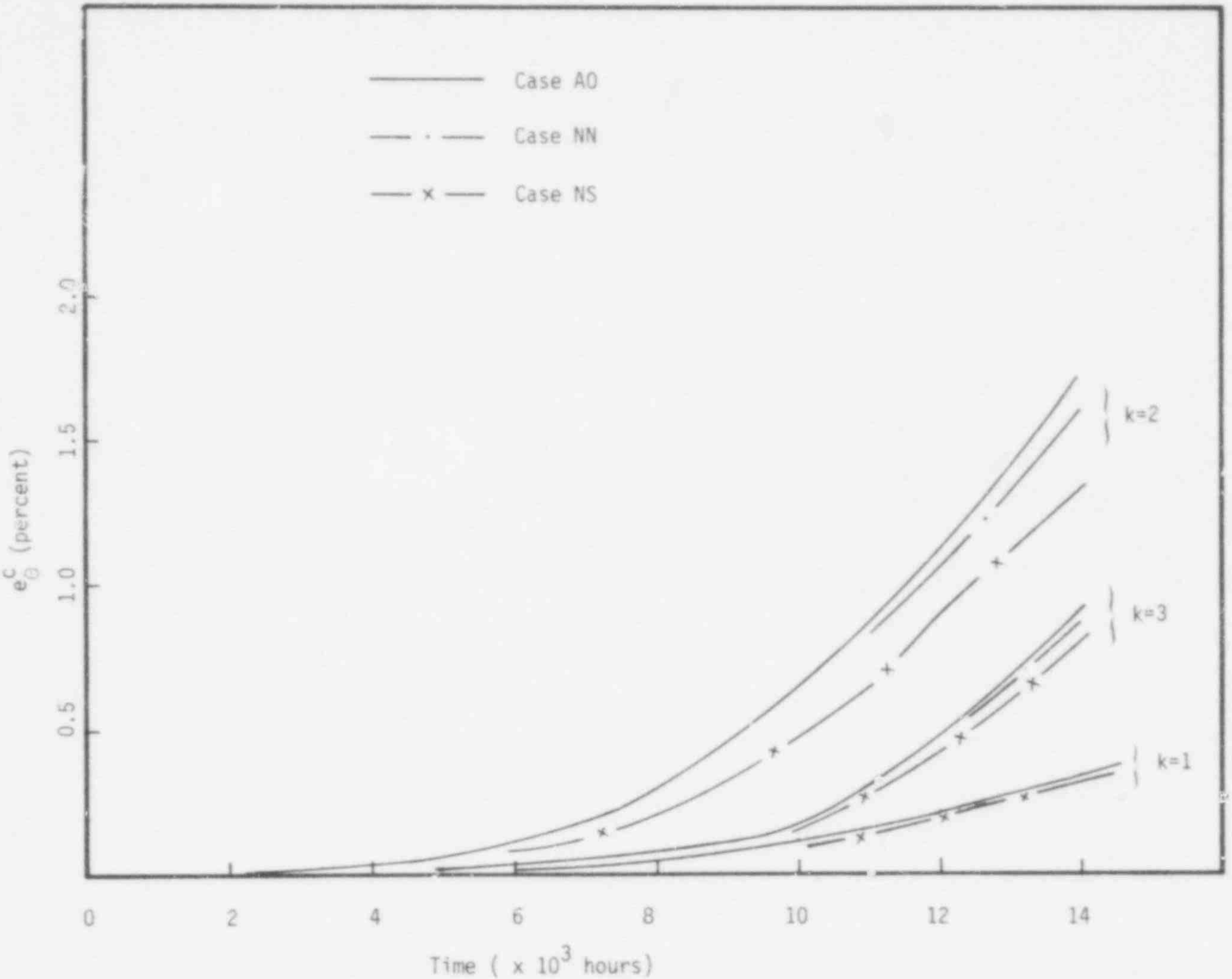


Figure SN-10. The Total Hoop Strain In the Clad

733 310

POOR ORIGINAL

THERE IS NO TEXT ON THIS PAGE

733 711

## REFERENCES


1. V. Z. Jankus and R. W. Weeks, "LIFE-I, a Fortran-IV Computer Code for the Prediction of Fast Reactor Fuel Element Behavior," ANL-7736, 1970.

2. T. H. Lin, "Theory of Inelastic Structures," John Wiley and Sons, Inc., 1968.

3. J. T. A. Roberts and B. J. Wrona, "Deformation and Fracture of $UO_2$ - 20% $PuO_2$," ANL-7945, June 1972.

4. Timoshenko and Goodier, "Theory of Elasticity," McGraw-Hill Book Co.

5. George Sines, "Elasticity and Strength," a UCLA Engineering Syllabus.

6. Nuclear System Handbook, Vol. 1, Design Data, June 19, 1974 Revision.

7. P. Soo, et al., "Type 304 and Type 316 Stainless Steel Data for High Temperature Design," WARD-3045T2C-3, Nov. 1972.

8. Private communication with ANL.

9. W. Chubb, V. W. Storhok, and D. L. Keller, "Factors Affecting the Swelling of Nuclear Fuels at High Temperatures," Nucl. Tech., Vol. 18, p. 231, June 1973.

10. D. S. Dutt, et al., "A Correlated Fission Gas Release Model for Fast Reactor Fuels," ANS Trans. 15, No. 1, p. 198, 1972.

11. J. H. Scott, et al., "Post Irradiation Examination of Fuel Pins PNL-10-23 and PNL-10-63," HEDO-TME-74-23, May 1974.


735 312

THERE IS NO TEXT ON THIS PAGE

733 313

```
*********************************************************************************************$
QCK2501 QCL CARD ENCOUNTERED->$NLB211LL.LIST.LEE
C*********FUEL STRESSES AND BOUNDARY DISPLACEMENT BY CREEP.SWELLING.      DRU00280
C*********HOT PRESS..AND GAS PRESS.. AT STEADY STATE /5CV                 DRU00300
C********* STRESSES ALL RELAXED WITHIN REGION T .GT. 1650 DEGREE C        DRU00320
C******* CLADDING STRESSES AND DISPLACEMENT AT STEADY STATE                DRU00340
C******* CREEP AND SWELLING                                                DRU00360
C****** BAOLEE=1 : GAP OPEN                                                DRU00960
C****** BAOLEE=2 : GAP CLOSED                                              DRU00980
      COMMON/FCBV/ACB(15),BCB(15),AFB(15),BFB(15),FTIME,ET,EIT,RF1,        YHS00100
     1 RF2,DPO,MF,MG,JF,MPRINT,RV1,RV2,MPUNCH,MBULF,TCLB,TFLB,RPFS(15)     YHS00120
     2,VOLM,VOLU,VOL,AVETK,GAS,AC(15),BC(15),AF(15),BF(15),FL(15)
      COMMON/COMFC/J,K,TIME,DTIME,FR(5,15),FDR(5,15),FSTSH(5),             YHS00160
     1 FSTSR(5),FSTSZ(5),CR(5,15),CDR(5,15),CSTSH(5),CSTSR(5),             YHS00180
     2 CSTSZ(5),NZ,NR,MFR,MP,BAOLEE,MTEST,FLUX(15)                         YHS00200
      COMMON/CONSTC/CA,CB,A2,B2,BA2,UA1,CAA,CUU,CE,CP,CTF(5,15),           YHS00220
     1 CUA(15),CUB(15),TDCA,TDCB,A1U,A2U,UA2,UA3,U2,UA5,UA6,B2BA2,         YHS00240
     2 CUA3UU,CADBA2,CBDBA2                                                YHS00260
      COMMON/CONSTF/FA,FB,FA2,FB2,FBA2,FC,FP,FU2,FUA1,FUA2,FUA3,           YHS00280
     1 FUA5,FUA6,FTF(5,15),TDFA,TDFB,FDEB,FUU(15),FAA,FUU,FBBA2,           YHS00300
     2 FBA22,FBB26,FUA3UU,U1,U3,FADBA2,FBDBA2,FA1U                         YHS00320
      COMMON/FCREPM/FC3,FDTSH(5),FDTSR(5),FDTSZ(5),FS1(5),FS2(5),          YHS00340
     1 FS3(5),FDSTRH(5),FDSTRR(5),FDSTRZ(5),FSTSHB(5,15),FSTSRB(5,15),     YHS00360
     2 FSTSZB(5,15),SHB(5,15),SRB(5,15),SZB(5,15),PN(5),SE(5),SH(5),       YHS00380
     3 SR(5),SZ(5),FMX                                                     YHS00400
      COMMON/CCREPM/CDTSH(5),CDTSR(5),CDTSZ(5),CDSTRH(5),CDSTRR(5),        YHS00420
     1 CDSTRZ(5),S1(5),S2(5),S3(5),CP3,CSTSHB(5,15),CSTSRB(5,15),          YHS00440
     2 CSTSZB(5,15),SHCB(5,15),SRCB(5,15),SZCB(5,15),CN(5),CSE(5),         YHS00460
     3 CSH(5),CSR(5),CSZ(5)                                                YHS00480
      COMMON/CSWLM/CSWW(5),CSW1(5),CSW(5),CSWH(5),CSWR(5),CSWZ(5),         YHS00500
     1 CUSWA(15),CUSWB(15),CTSW(5),CSWB(5,15)                              YHS00520
      COMMON/MIX1/FDHE(5),FDRE(5),FDZE(5),FDCPB,UCPA(15),UCPB(15),         YHS00540
     1 PL(15),CUEA(15),CUEB(15),FUBB(15),BULE(15),CUAB(15),CUBB(15),       YHS00560
     2 UCPAB(15),UCPBB(15),CUEAB(15),CUEBB(15),CUSWAB(15),CUSWBB(15),      YHS00580
     3 CTSWB(15),CSWB2(5,15),BU,GF,PNB(5,15),FNTSW(5,15),CE3,CW3,          YHS00600
     4 TCE3,TCW3,TCP3,C3,FW3,TFE,TFP,TFW,FCPZB(5,15),FCPRB(5,15),          YHS00620
     5 FCPHB(5,15),CCPHB(5,15),CCPRB(5,15),CCPZB(5,15),FSWUBB(15),         YHS00640
     6 FCPBB(15),FUEB(15),FUEBB(15),FERH(5),FERR(5),FERZ(5),FCPZ(5,15)     YHS00660
     7 ,FCPR(5,15),FCPH(5,15),CCPH(5,15),CCPR(5,15),CCPZ(5,15),            YHS00680
     8 FSWUB(15),FCPB(15),FTRH(5),FTRR(5),FTRZ(5),CTRH(5),CTRR(5),         YHS00700
     9 CTRZ(5),CERH(5),CERR(5),CERZ(5)                                     YHS00720
      COMMON/MIX2/DPGAS,PGAS,FPJ,FDPU,FPI,FDPI,PFC(15),DPFC,CPO,CP1,       YHS00740
     1 FDSWUB,FDSWH(5),FDSWR(5),FDSWZ(5),FDSW(5,15),CDP1,CDP2,CDCHE(5)     YHS00760
     2 ,CDCRE(5),CDCZE(5),DUEA,DUEB,TDCA1,TDCA2,TDFB1,TDFB2,DP1,DP2,       YHS00780
```

POOR ORIGINAL



733 214

```
      3 FTSW(5,15)
        DIMENSION FGR(5,15),VV(5,15),FGVP1(5,15),FGVP2(5,15),V1(5),
      1 V2(5),          MPFC(15),REOPEN(15),TDHP(5),DDHP(5),V(5),
      2 SI1(5),SI2(5),SEK(5,15),CPR(5),DCP(5),F(5),CTZ(5),DSTU(5),
      3 CPRK(5,15),H(5),RR(5),Z(5),PCB(5,15),GAP(15),SSW(5),UW(15),
      4 V3(5),FDTS(5),CDTS(5),PEF( 5),NBOLE(15),FTSWH(5,15),DPFCK(15),
      5 FFLUX(15)
       CALL READ(CTR,DTIMEL ,DPFCK,MPFC,CIPFC,FJMX,NBOLE,RCC,
      1 FSQ1,FSQ2,TFSQ1,TFSQ2,NFSW,NCSW,FTSWB,SPFC,FPFC,SPC,TCLOSE,
      2  DCL,DFL,REOPEN,MSHP,TGRM,TGSM,AVCV,FPDEN,FFLUX)
       PORO=1.-FPDEN
        FE=(3.292E7)*(1.-2.35*PORO)
       FP=0.317*(1.-0.46*PORO)
       FP=0.91986*FP+0.0401
        CP=0.3
        CE=2.9E7
       CALL WINP
        J=J+1
       MFM1=MFR-1
       MFM2=MFR-2
       NZ1=NZ-1
       DO 60 K=1,NZ1
       DO 60 I=1,MFR
       PNB(I,K)=(FSTSHB(I,K)+FSTSRB(I,K)+FSTSZB(I,K))/3.
       SHB(I,K)=FSTSHB(I,K)-PNB(I,K)
       SRB(I,K)=FSTSRB(I,K)-PN3(I,K)
 60    SZB(I,K)=FSTSZB(I,K)-PN3(I,K)
       DO 61 K=1,NZ
       DO 61 I=1,NR
       PCB(I,K)=(CSTSHB(I,K)+CSTSRB(I,K)+CSTSZB(I,K))/3.
       SHCB(I,K)=CSTSHB(I,K)-PC3(I,K)
       SRCB(I,K)=CSTSRB(I,K)-PC3(I,K)
 61    SZCB(I,K)=CSTSZB(I,K)-PC3(I,K)
       CAA=1.32E7
       CUU=0.88E7
        FDPA=(1.+FP)*(1.-2.*FP)
        FAA=FP*FE/FDPA
        FUU=FE/(2.*(1.+FP))
        FA1U=FAA+FUU
        FA2U=FAA+2.*FUU
        FUA1=4.*(FUU**2)/FA2U
        FUA2=FAA/FA2U
        FUA3=2.*FUU*FAA/FA2U
        FU2=2.*FUU
        FUA5=FAA/(FAA+FUU)
        FUA6=FUA5*FUA1
        FUAA2=FU2*FAA
       FUA3UU=(FUA3+FUU)*2./3.
        A1U=CAA+CUU
        A2U=CAA+2.*CUU
        UA1=4.*(CUU**2)/A2U
        UA2=CAA/A2U
        UA3=2.*CUU*CAA/A2U
        U2=2.*CUU
        UA5=CAA/(CAA+CUU)
        UA6=UA5*UA1
        UAA6=U2*CAA
       CUA3UU=(UA3+CUU)*2./3.
       GF=(FAA+2.*FUU/3.)*(1.+FUU/FA1U)*0.1/(2.*FA2U)
       AVPL=0.
```

```
205   IF(BOLE(K) .EQ. 2.) GAP(K)=0.
      DO 206 K=1,NZ1
      IF(BOLE(K) .EQ. 2. .AND. NBOLE(K) .EQ. 1 ) GO TO 207
      GO TO 206
 207   NBOLE(K)=2
      TCLOSE=TIME
      GO TO 208
 206  CONTINUE
 208  CONTINUE
      TTS=(1.-1./FSQ1)*TIME/TFSQ1
      CRLM=CTR*(TTS+1./FSQ1)
      IF(TIME.GT. TFSQ1) CRLM=CTR
      DO 209 K=1,NZ1
      IF(BOLE(K) .EQ.2.)  GO TO 202
 209   CONTINUE
      GO TO 203
 202  T1=(TIME-TCLOSE)/TFSQ2
      T2=CTR/FSQ2
      CRLM=T1*(CTR-T2)+T2
 203   CONTINUE
      NZD2=NZ/2
       IF (CPRK(1,NZD2) .LT. 1.E-10) CPRK(1,NZD2)=1.E-10
      DTIME=(CRLM   )/CPRK(1,NZD2)
      IF(DTIME.GT.DTIMEL) DTIME=DTIMEL
      IF(TIME  .LT.  5.) DTIME=0.5
      NZ2=NZ-2
      GP=PFC(1)
      DO 75 K=1,NZ2
      K1=K+!
 75   GP=AMAX1(GP,PFC(K1))
       APFC=(1./SPO-1.)*DTIMEL/(FPFC-SPFC)
       BPFC=DTIMEL-APFC*SPFC
       IF(GP.GT.SPFC)DTIME=APFC*GP+BPFC
       IF(GP.GT.FPFC)DTIME=DTIMEL/SPO
       TIME=TIME+CTIME
      VCV=0.
      VGAP=0.
       DO 70 K=1,NZ1
 70   FL(K)=TFLB/NZ1
      DO 71 K=1,NZ1
      VCV=VCV+3.1416*(   AVCV**2)*FL(K)
 71   VGAP=VGAP+3.1416*FL(K)*(ACB(K)**2-BFB(K)**2)
      VPL=3.1416*(TCLB-TFLB)*(ACB(NZ)**2)
      VOL=VCV+VGAP+VPL
      VOLM=0.
      VOLU=0.
      DO 72 K=1,NZ1
      VOLM=3.1416*FL(K)*(RRES(K)**2             )+VOLM
 72   VOLU=3.1416*FL(K)*(BFB(K)**2-RRES(K)**2)+VOLU
      DTCK=0.
      DTFK=0.
      BUAV=(2.56567E-6)*AVPL*TIME/3.1416/AVBF2
      F1=0.66427*BUAV
      RUF=1.-((1.-EXP(-F1))/F1)/(0.421*EXP(0.05*AVPL))
      IF(RUF .LT. 0.) RUF=0.
      GFFM=GAS*3600./(6.02E23)
      TGRMN=GFFM* TIME*(RUF*VOLU+VOLM)
      TGGM=GFFM* TIME*(VOLU+VOLM)
      DGRM=TGRMN-TGRM
      TGRM=TGRMN
```





733 317

```
      AVBF=0.
      DO 73 K=1,NZ1
      AVPL=AVPL+PL(K)/NZ1
   73 AVBF=AVBF+BFB(K)/NZ1
      AVBF2=AVBF**2
      GAS=(6.1474E11)*AVPL/(3.1416*AVBF2)
      TGRM=0.
       FVO=RF2+(RF1-RF2)/4.
       CVO=RV2+(RV1-RV2)/4.
       GO TO 23                                                          DR001980
C****** ITERATION FOR CREEP PRECISION                                    DR002320
  350  IF(MF .EQ. 1) GO TO 351                                           DR002000
       IF(MF .EQ. 2) GO TO 352                                           DR002020
  351  TIME=TIME-DTIME                                                   DR002040
       FMX1=FMX                                                          DR002060
       DTIME1=DTIME                                                      DR002080
       DTIME=DTIME*FVO/FMX                                               DR002100
       MF=2                                                              DR002120
       GO TO 23                                                          DR002140
  352  TIME=TIME-DTIME                                                   DR002160
       FMX2=FMX                                                          DR002180
       DTIME2=DTIME                                                      DR002200
       IF(FMX1 .EQ. FMX2) GO TO 353                                      DR002220
       DTIME=DTIME2+(DTIME1-DTIME2)*(RF1-FMX2)/(FMX1-FMX2)               DR002240
       FMX1=FMX2                                                         DR002260
       DTIME1=DTIME2                                                     DR002280
       GO TO 23                                                          DR002300
   23  CONTINUE                                                          DR002340
      CSCPD=0.
      FSCPD=0.
       DO 58 K=1,NZ1
       DO 59 I=1,NFR                                                     DR010440
      SS=(FSTSHB(I,K)-FSTSRB(I,K))**2+(FSTSHB(I,K)-FSTSZB(I,K))**2
     1 +(FSTSRB(I,K)-FSTSZB(I,K))**2
       SEK(I,K)=(SS/2.)**0.5
      FTR=FTF(I,K)+459.69
      TS=SEK(I,K)**4.5
      EXP1=EXP((-1.1963E5)/FTR)
      EXP2=EXP((-8.1566E4)/FTR)
C75    FORMAT(2X,'T1,T2,SE,EXP1,EXP2,TS',6E14.3)                          DR010720
      FPDEN1=FPDEN
      IF(FPDEN .LT. 0.92) FPDEN1=0.92
      FCPA=(1.376E-4)/(-90.5+100*FPDEN1)
      FCPA1=(9.726E 6)/(-87.7+100*FPDEN1)/100.
       CPRK(I,K)=(FCPA      )*EXP1*TS+((FCPA1    )*(EXP2)+(8.E-24)
     1 *FLUX(K))*SEK(I,K)
   59  CONTINUE                                                          DR011080
   58  CONTINUE
      PPP=0.
      DO 205 K=1,NZ1
      BOLE(K)=2.
      GAP(K)=ACB(K)-BFB(K)
      IF(GAP(K) .GT. 0.) BOLE(K)=1.
       IF(BOLE(K).EQ.2. .AND. PFC(K).LT.PGAS) REOPEN(K)=2.
       IF(REOPEN(K).EQ.2.) GO TO 355
       GO TO 356
  355 BOLE(K)=1.
      IF(GAP(K).LT.0.) GAP(K)=0.
  356 CONTINUE
      IF(BOLE(K) .EQ. 2.) PPP=PPP+1.
```

POOR ORIGINAL

733 316

```
      PERGR=(TGRMN/TGGM)*100.
      AVETK=(CTF(1,NZ)-32.)*0.556+273.
      DPGAS=73.578*AVETK*DGRM/VOL
      PGAS=PGAS+DPGAS
       K=1
       FKMX=0.
      SFTRZK=0.
      SCTRZK=0.
 26    CONTINUE                                                        DRU02680
      IF(K.EQ.NZ) GO TO 67
       CA=ACB(K)
       CB=BCB(K)
 67   CONTINUE
       IF(K .EQ. NZ) GO TO 65                                          DRU03920
       FA=AFB(K)
       FB=BFB(K)
       DO 66 I=1,MFR
       CPR(I)=CPRK(I,K)
       SE(I)=SEK(I,K)
 66   CONTINUE
       DO 5 I=1,MFM2
       AI=I-1                                                          DRU02780
       FDR(I,K)=(FB-FA)/MFM1
 5     FR(I,K)=FA+FDR(I,K)*(AI+0.5)                                    DRU02820
      FDR(MFM1,K)=FDR(MFM2,K)/2.
      FDR(MFR,K)=FDR(MFM1,K)
      FR(MFM1,K)=FR(MFM2,K)+FDR(MFM2,K)/2.+FDR(MFM1,K)/2.
      FR(MFR,K)=FR(MFM1,K)+FDR(MFM1,K)/2.+FDR(MFR,K)/2.
      FGR(1,K)=FA
      MPR1=MFR+1
       DO 69 I=2,MPR1
      I1=I-1
 69    FGR(I,K)=FGR(I1,K)+FDR(I1,K)
      FGVP2(1,K)=0.
      DO 400 I=1,MFR
       I1=I+1
      FGVP1(I,K)=(FR(I,K)**2-FGR(I,K)**2)/2.
      FGVP2(I1,K)=(FGR(I1,K)**2-FGR(I,K)**2)/2.
 400  CONTINUE
 999   CONTINUE                                                        DRU03060
       FA2=FA**2                                                       DRU03140
       FB2=FB**2                                                       DRU03160
       FBA2=FB2-FA2                                                    DRU03180
        A2=CA**2                                                       DRU15960
        B2=CB**2                                                       DRU15980
        BA2=B2-A2                                                      DRU16000
      FBBA2=FB2/FBA2                                                   DRU14680
      FBA22=FBBA2/2.
      FBB26=FUAS*FBBA2
      FADBA2=FA2/FBA2
      FBDBA2=FB2/FBA2
      CADBA2=A2/BA2
      CBDBA2=B2/BA2
       U1=FA2*FB/(2.*FBA2)/FA1U
       U3=FA2*FB2 /FU2/FB/FBA2                                         DRU13500
C******** FUEL CREEP                                                   DRU03200
      CALL FCREP(DSTB,KGG,JF,CPR,FGVP1,FGVP2,FGR,FS1B,FS25,FS38      )
      BU=(2.56567E-6)*PL(K)      /3.1416/(FB*FB)
      DBU=BU*DTIME
      BU=BU*TIME
```

```
         MF=1                                                            ORU03920
C******* ELASTIC PRESSURE EFFECTS
      CALL FPE(FGVP2 ,DPFCK,MPFC                              )
      CALL        FSWHP(FGR,FGVP1,FGVP2,SIB,DBU,NFSW,FTSWB
C********* BOUNDARY CONDITIONS IN AXIAL DIRECTION
      FC3=0.
      DO 74 I=1,MFR
      I1=I+1
      FDTS(I)=FDTSZ(I)+FDSWZ(I)+FDZE(I)
   74  FC3=FC3+FDTS(I)*FGVP2(I1,K)*2.
      IF(BOLE(K) .EQ. 1.) GO TO 76
      QP=1.
      IF(DFL .GT. DCL) QP=-1.
      IF(DFL .EQ. DCL ) QP=0.
      DFRZ=2.*FB*RCC*DPFCK(K)*QP*TFLB*PPP/NZ1-DPGAS*(FBA2)
      GO TO 77
   76 DFRZ=0.-DPGAS*(FBA2)
   77 FC3=( DFRZ-FC3)/FBA2
      DO 78 I=1,MFR
      FDTS(I)=FDTS(I)+FC3
   78 FSTSZ(I)=FSTSZB(I,K)+FDTS(I)
      DTFK=DTFK+FC3
      FMX=0.
      PPGS=1.E-10
      DO 83 I=1,MFR
      SS=(FSTSH(I)-FSTSR(I))**2+(FSTSH(I)-FSTSZ(I))**2
     1 +(FSTSR(I)-FSTSZ(I))**2
      SEFC=(SS/2.)**0.5
      IF(SE(I) .LT. PPGS) GO TO 84
      PEF(I)=ABS(1.-SEFC/SE(I))
      GO TO 85
   84 PEF(I)=0.
   85 CONTINUE
      FMX=FMX+PEF(I)
   83  CONTINUE
      FMX =FMX/MFR
      IF(J.GT.JF) GO TO 354
      GO TO 353
  354 CONTINUE
        IF(K .GT.1) GO TO 353                                            ORU03840
      IF(FMX.EQ.0.) GO TO 353
        IF(FMX .GT. RF1) GO TO 350                                       ORU03860
        IF(FMX .LT. RF2) GO TO 350                                       ORU03880
 353    CONTINUE                                                         ORU03900
C*****FUEL BOUNDARY DISPLACEMNT
      CALL FUBCWP(FS1B,FS2B,FS3B,SIB                          )
   65   CONTINUE                                                         ORU04100
        DO 6 I=1,NR                                                      ORU02840
        AI=I-1                                                           ORU02860
      ANR=NR
       CDR(I,K)=(CB-CA)/ANR
 6      CR(I,K)=CA+CDR(I,K)*(AI+0.5)                                     ORU02900
C***** CLADDING CREEP EFFECT                                             ORU04120
      CALL CCREP(S1B,S2B,S3B                          )                  ORU04140
       NG=1                                                              ORU04740
C****** WALL PRESSURE EFFECT                                             ORU04780
      CALL CGP(DPFCK                                                     ORU04800
C****** CLADDING SWELLING                                                ORU04940
      CALL CSWL(DUSWA,DUSWB,SIBC,NCSW,FFLUX                    )
      CP3=0.
```

POOR ORIGINAL



733 315

```
      DO 79 I=1,NR
      I1=I+1
      CDTS(I)=CSWZ(I)+CDTSZ(I)+CDCZE(I)
 79   CP3=CP3+CDTS(I)*CR(I,K)*CDR(I,K)*2.
      DCRZ=-DFRZ
      CP3=(DCRZ-CP3)/BA2
      DO 82 I=1,NR
      CDTS(I)=CDTS(I)+CP3
 82   CSTSZ(I)=CSTSZB(I,K)+CDTS(I)
      DTCK=DTCK+CP3
      CALL CBCWP (DUFA,DUFB,S1B,S2B,S3B,S1BC
      IF(K .EQ. NZ) GO TO 101                                   DR004980
       IF(BOLE(K).EQ. 1.) GO TO 101                             DR_05000
       BDD=TDCA-TDFB                                            DR005020
       BDC=BDD/TDCA                                             DR005040
       ABDD=ABS(BCD)                                            DR005060
       IF(ABDD .LT. CIPFC ) GO TO 101
      CALL PPRCI(DPFCK,MPFC
       IF(MP .GT. 20) GO TO 1000                                DR005200
       GO TO 999                                                DR005220
101    CONTINUE                                                 DR005240
       MP=1                                                     DR005260
       IF(K .EQ. NZ) GO TO 30                                   DR005280
       BF(K)=BF3(K)+TDFB
       DO 8 I=1,MFM2
       AI=I-1                                                   DR005360
       FDR(I,K)=(BF(K)-FA)/MFM1
8      FR(I,K)=FA    +FDR(I,K)*(AI+0;5)                         DR005380
      FDR(MFM1,K)=FDR(MFM2,K)/2.
      FDR(MFR,K)=FDR(MFM1,K)
      FR(MFM1,K)=FR(MFM2,K)+FDR(MFM2,K)/2.+FDR(MFM1,K)/2.
      FR(MFR,K)=FR(MFM1,K)+FDR(MFM1,K)/2.+FDR(MFR,K)/2.
      FGR(1,K)=FA
      DO 12 I=2,MFR
      I1=I-1
 12    FGR(I,K)=FGR(I1,K)+FDR(I1,K)
30     AC(K)=ACB(K)+TDCA
       BC(K)=BCB(K)+TDCB
       DO 9 I=1,NR                                              DR005440
       AI=I-1                                                   DR005460
      ANR=NR
       CDR(I,K)=(BC(K)-AC(K))/ANR
9      CR(I,K)=AC(K)+CDR(I,K)*(AI+0.5)                          DR005500
       IF(K.EQ.NZ) GO TO 103                                    DR005520
       IF(BOLE(K).EQ.2.) AC(K)=BF(K)                            DR005540
103    CONTINUE                                                 DR005660
      EXT=ET
      IF(TIME.LT. EIT) EXT=0.
       IF(K .EQ. NZ) GO TO 105                                  DR006200
      DO 150 I=1,MFR
      SS=(FSTSH(I)-FSTSR(I))**2+(FSTSH(I)-FSTSZ(I))**2+(FSTSR(I)-
     1 FSTSZ(I))**2
      SE(I)=(SS/2.)**0.5
      PN(I)=(FSTSH(I   )+FSTSR(I   )+FSTSZ(I   ))/3.
      SH(I)=FSTSH(I   )-PN(I)
      SR(I)=FSTSR(I   )-PN(I)
      SZ(I)=FSTSZ(I   )-PN(I)
150   PNB(I,K)=PN(I)
      DO 151 I=1,MFR
      SHB(I,K)=SH(I)
```

```
      SRB(I,K)=SR(I)
151   SZB(I,K)=SZ(I)
      DO 152 I=1,WFR
      FSTSHB(I,K)=SHB(I,K)+PNB(I,K)
      FSTSRB(I,K)=SRB(I,K)+PNB(I,K)
152    FSTSZB(I,K)=SZB(I,K)+PNB(I,K)
      FUBB(K)=FUB (K)
      BFB(K)=BF (K)
      DO 153 I=1,WFR
      FCPHB(I,K)=FCPH (I,K)
      FCPRB(I,K)=FCPR (I,K)
153   FCPZB(I,K)=FCPZ (I,K)
      DO 154 I=1,WFR
      FSWUBB(K)=FSWUB (K)
      FCPBB(K)=FCPB (K)
154   FUEBB(K)=FUEB (K)
      DO 155 I=1,WFR
      FERH(I)= (FSTSH(I)-FP*(FSTSR(I)+FSTSZ(I)))/FF
      FERR(I)= (FSTSR(I)-FP*(FSTSH(I)+FSTSZ(I)))/FF
155   FERZ(I)= (FSTSZ(I)-FP*(FSTSH(I)+FSTSR(I)))/FE
      DO 156 I=1,WFR
       FNTSW3=FNTSW(I,K)/3.
      FTRH(I)=FERH(I)+FNTSW3+FCPH(I,K)
      FTRR(I)=FERR(I)+FNTSW3+FCPR(I,K)
156   FTRZ(I)=FERZ(I)+FNTSW3+FCPZ(I,K)
105   DO 100 I=1,NR
      SS=(CSTSH(I)-CSTSR(I))**2+(CSTSH(I)-CSTSZ(I))**2+(CSTSR(I)-
     1 CSTSZ(I))**2
      CSE(I)=(SS/2.)**0.5
      CN(I)=(CSTSH(I   )+CSTSR(I   )+CSTSZ(I   ))/3.
      CSH(I)=CSTSH(I   )-CN(I)
      CSR(I)=CSTSR(I   )-CN(I)
      CSZ(I)=CSTSZ(I   )-CN(I)
100   PCB(I,K)=CN(I)
      DO 110 I=1,NR
      SHCB(I,K)=CSH(I)
      SRCB(I,K)=CSR(I)
110   SZCB(I,K)=CSZ(I)
      DO 111 I=1,NR
      CSWB(I,K)=CSWB2(I,K)
      CSTSHB(I,K)=SHCB(I,K)+PCB(I,K)
      CSTSRB(I,K)=SRCB(I,K)+PCB(I,K)
111   CSTSZB(I,K)=SZCB(I,K)+PCB(I,K)
      DO 112 I=1,NR
      CCPHB(I,K)=CCPH (I,K)
      CCPRB(I,K)=CCPR (I,K)
112   CCPZB(I,K)=CCPZ (I,K)
      DO 113 I=1,NR
      CERH(I)= (CSTSH(I)-CP* (CSTSR(I)+CSTSZ(I)))/CF
      CERR(I)= (CSTSR(I)-CP* (CSTSH(I)+CSTSZ(I)))/CE
113   CERZ(I)= (CSTSZ(I)-CP* (CSTSH(I)+CSTSR(I)))/CF
      DO 114 I=1,NR
      CSW3=CSWW(I)/3.
      CTRH(I)=CERH(I)+CSW3+CCPH(I,K)
      CTRR(I)=CERR(I)+CSW3+CCPR(I,K)
114   CTRZ(I)=CERZ(I)+CSW3+CCPZ(I,K)
      CUAB(K)=CUA (K)
      CUBB(K)=CUB (K)
      UCPAB(K)=UCPA (K)
      UCPBB(K)=UCPB (K)
```





733 321

```
      CUEAB(K)=CUEA (K)
      CUEBB(K)=CUEB (K)
      CUSWAB(K)=CUSWA (K)
      CUSWBB(K)=CUSWB (K)
      ACB(K)=AC (K)
      BCB(K)=BC (K)
       MTEST=MOD(J,MPRINT)
       IF(MTEST .NE. 0) GO TO 24
      IF (K.EQ.NZ) GO TO 200
      CALL FWRITE(FDTS                   )
200   CALL CWRITE (CDTS                  )
       IF(K.EQ.NZ) GO TO 35
       IF(BOLE(K).EQ. 1.) GO TO 361
       WRITE(6,370)
370    FORMAT(' GAP IS CLOSED')
       WRITE(6,373) PFC(K),DPFCK(K)
       GO TO 31
361    WRITE(6,371) GAP(K)
371    FORMAT(' GAP IS OPEN,GAP(K)=',E12.4)
31    CONTINUE
373    FORMAT(' PFC = ,E12.4,'  DPFC =',E12.4)
       WRITE(6,378) AC(K),BC(K),BF(K)
       WRITE(6,379) (CR(I,K),I=1,NR)
       WRITE(6,380) (FR(I,K),I=1,MFR)
378   FORMAT(' AC(K)=',1PE14.6,'    BC(K)=',1PE14.6,'   BF(K)=',
     1  1PE14.6)
379    FORMAT(' CR(K)=',5E12.4)
380    FORMAT(' FR(K)=',4E12.4,/)
       GO TO 24
35     CONTINUE
       WRITE(6,381) AC(K),BC(K)
       WRITE(6,379) (CR(I,K),I=1,NR)
381    FORMAT(' AC(K)=',E12.4,' BC(K)=',E12.4)
24     CONTINUE
      IF(K .EQ. NZ) GO TO 1210
      SFTRZ=0.
      SCTRZ=0.
      DO 1219 I=1,MFR
1219  SFTRZ=SFTRZ+FTRZ(I)/MFR
      DO 1218 I=1,NR
1218   SCTRZ=SCTRZ+CTRZ(I)/NR
1210   CONTINUE
      IF(K.EQ.NZ)   GAP(K)=111.
       IF(K.EQ.NZ) GO TO 36
      IF(BOLE(K) .EQ. 1.) PFC(K)=PGAS
36     K=K+1
       IF(K .GT. NZ) GO TO 25
       FKMX=FKMX+FMX/NZ1
      SFTRZK=SFTRZK+SFTRZ/NZ1
      SCTRZK=SCTRZK+SCTRZ/NZ1
       GO TO 26
25     CONTINUE
      DFL=SFTRZK*TFLB
      DCL=SCTRZK*TFLB
      TCL=TCLB+DCL
      TFL=TFLB+DFL
       FJMX=FJMX+FKMX
       FJAV=FJMX/J
       MSHO=MOD(J,MSHP)
       IF(MSHO .NE. 0) GO TO 1891
```

```
      CALL QPRINT (NZ1.CPRK.GAP
 1891  CONTINUE
       IF(MTEST .NE. 0) GO TO 1215
       WRI(E(6.374) PGAS.DPGAS
 374   FORMAT(' PGAS=',E12.4,'  DPGAS=',E12.4)
      PRINT 1217.TGRM.PERGR
 1217 FORMAT(2X,'TOTAL GAS RELEASE(MOLES)=',E12.?,'  %RELEASE OF THE FISS
     1ION GAS =',F10.3)
       WRITE(6.1214) DCL.TCL.DFL.TFL.FJAV
 1214  FORMAT(2X,'DCL.TCL',2E13.4.5X,'DFL.TFL', E13.4.8X.'FJAV',
     1  E13.4,/)
 1215  CONTINUE
      MPUN=MOD(J.MPUNCH)
      IF(MPUN .NE. 0) GO TO 1002
      CALL PUNCH(CTR.DTIMEL .DPFCK.MPFC.CIPF .FJMX.NBOLE.RCC.
     1 FSQ1.FSQ2.IFSQ1.TFSQ2.NFSW.NC  .FTS  .SPFC.FPFC.SPC.TCLOSE.
     2  DCL.DFL.REOPEN.MSHP.TGRM.TGGM.   .FPDEN.FFLUX)
 1002 CONTINUE
       J=J+1                                                             DRU06740
       IF(J .GT. JF) GO TO 1000                                          DRU06300
       IF(TIME .LT. FTIME) GO TO 23                                      DRU06320
 1000  CONTINUE
 1001 STOP
      END
      SUBROUTINE  QPRINT (NZ1.CPRK.GAP
       COMMON/COMFC/J.K.TIME.DTIME.FR(5.15).FDR(5.15).FSTSH(5),          YHS00160
     1 FSTSR(5).FSTSZ(5).CR(5.15).CDR(5.15).CSTSH(5).CSTSR(5),           YHS00180
     2 CSTSZ(5).NZ.NR.MFR.MP.BADLEE.MTEST.FLUX(15)                       YHS00200
       COMMON/MIX2/DPGAS.PGAS.FPO.FDPO.FPI.FDPI.PFC(15).DPFC.CPO.CPI.    YHS00740
     1 FDSWUB.FDSWH(5).FDSWR(5).FDSWZ(5).FDSW(5.15).CDPI.CDPO.CDCHE(5)   YHS00760
     2 .CDCRE(5).CDCZE(5).DUEA.DUEB.TDCA1.TDCA2.TDFB1.TDFB2.DP1.DP2.     YHS00780
     3 FTSW(5.15)                                                        YHS00800
      DIMENSION          GAP(15) .CPRK(5.15)
       PRINT 1980. J.TIME.DTIME.CPRK(1.3).PFC(1).PFC(2).PFC(3).PFC(4).
     1 PFC(5).PFC(6).GAP(1).GAP(2).GAP(3).GAP(4).GAP(5).GAP(6)
 1980  FORMAT(I7.F7.1.F5.2.E9.2.6F6.1. 1X.6E9.2)
       RETURN
       END
       SUBROUTINE FSWHP(FGR.FGVP1.FGVP2.SIB.DBU.NFSW.FTSWB    )
       COMMON/COMFC/J.K.TIME.DTIME.FR(5.15).FDR(5.15).FSTSH(5).          YHS00160
     1 FSTSR(5).FSTSZ(5).CR(5.15).CDR(5.15).CSTSH(5).CSTSR(5).           YHS00180
     2 CSTSZ(5).NZ.NR.MFR.MP.BADLEE.MTEST.FLUX(15)                       YHS00200
       COMMON/CONSTF/FA.FB.FA2.FB2.FBA2.FE.FP.FU2.FUA1.FUA2.FUA3.        YHS00280
     1 FUA5.FUA6.FTF(5.15).TDFA.TDFB.FDEB.FUB(15).FAA.FUU.FBBA2.         YHS00300
     2 FBA22.FBB26.FUA3UU.U1.U3.FADBA2.FBDBA2.FA1U                       YHS00320
       COMMON/MIX1/FDHE(5).FDRE(5).FDZE(5).FDCPB.UCPA(15).UCPB(15).      YHS00540
     1 PL(15).CUEA(15).CUEB(15).FUBB(15).BOLE(15).CUAB(15).CUBB(15).     YHS00560
     2 UCPAB(15).UCPBB(15).CUEAB(15).CUEBB(15).CUSWAB(15).CUSWBB(15).    YHS00580
     3 CTSWB(15).CSWB2(5.15).BU.GF.PNB(5.15).FNTSW(5.15).CE3.CW3.        YHS00600
     4 TCE3.TCW3.TCP3.C3.FW3.TFE.TFP.TFW.FCPZB(5.15).FCPRB(5.15).        YHS00620
     5 FCPHB(5.15).CCPHB(5.15).CCPRB(5.15).CCPZB(5.15).FSWUBB(15).       YHS00640
     6 FCPBB(15).FUEB(15).FUEBB(15).FERH(5).FERR(5).FERZ(5).FCPZ(5.15)   YHS00660
     7 .FCPR(5.15).FCPH(5.15).CCPH(5.15).CCPR(5.15).CCPZ(5.15).          YHS00680
     8 FSWUB( 5).FCPB(15).FTRH(5).FTRR(5).FTRZ(5).CTRH(5).CTRR(5).       YHS00700
     9 CTRZ(  ).CERH(5).CERR(5).CERZ(5)                                  YHS00720
       COMMO /MIX2/DPGAS.PGAS.FPO.FDPO.FPI.FDPI.PFC(15).DPFC.CPO.CPI.    YHS00740
     1 FDSWUB.FDSWH(5).FDSWR(5).FDSWZ(5).FDSW(5.15).CDPI.CDPO.CDCHE(5)   YHS00760
     2 .CDCRE(5).CDCZE(5).DUEA.DUEB.TDCA1.TDCA2.TDFB1.TDFB2.DP1.DP2.     YHS00780
     3 FTSW(5.15)                                                        YHS00800
      DIMENSION FGVP1(5.15).FGVP2(5.15).FTSWB(5.15)
```



733 323

```
      DIMENSION       TDHP(5),VV(5)  ,V(5),SI1(5),SI2(5),FGR(5,15)        DR014020
        SUM=0.                                                            DR014040
       DO 111 I=1,MFR
C***** FUEL SWELLING FROM ISOTHERMAL EXPERIMENT                           DR014060
      DD1=0.001046*FTF(I,K)-5.08378                                       DR014080
       DD=10.**DD1
      FS=(2.0712E-6)*0.1*DD*PL(K)/(GF*FB*FB)
      FDSW(I,K)=FS*DTIME
      FTSW(I,K)=FS* TIME                                                  DR014140
C**** HOT PRESSING TO COMPACT THE SWELLING BY CREEP
       TFK=(FTF(I,K)-32.)*0.556+273.
      HPHP=PNB(I,K)*(1.45E-5)                                             DR014200
       IF(HPHP .GT. 0.)GO TO 237
      EQHP=EXP((-4.43E4)/TFK)
       HPDW=1.-0.900-FNTSW(I,K)
       TDHP(I)= (1.692E10/TFK)*EQHP*HPHP*HPDW*DTIME
C      WRITE(6,456)HPDW,HPHP,EQHP
C456   FORMAT(2X,'HPDW,HPHP,EQHP,    ',3E11.3)                            DR014400
       GO TO 238                                                          DR014420
 237   TDHP(I)=0.                                                         DR014460
 238   CONTINUE                                                           DR014480
       FDSW(I,K)=     TDHP(I)+FDSW(I,K)
      FNTSW(I,K)=FNTSW(I,K)+FDSW(I,K)
C     WRITE(5,1) FDSW(I,K),TDHP(I),FNTSW(I,K),FNTSW(I,K)                  DR014500
       IF(FDSW(I,K).LT.0.)FDSW(I,K)=0.                                    DR014520
 111   CONTINUE
      DO 101 I=1,MFR
 101  VV(I)=FDSW(I,K)*FGVP1(I,K)
      VP=0.
      DO 100 I=1,MFR
       I1=I+1
      V(I)=VP+VV(I)
 100  VP=VP+FDSW(I,K)*FGVP2(I1,K)
 99   CONTINUE
       DO 102 I=1,MFR
       SI1(I)=(FUA3     )*V(I)/(FR(I,K)**2)
 102   SI2(I)=(FUA1/3.)*V(I)/(FR(I,K)**2)
      SIB=(FUA3+FUA1/3.)*VP/FB2                                           DR014640
       DO 113 I=1,MFR                                                     DR014660
       R2=FR(I,K)**2
       FDSWH(I)=SI1(I)+SI2(I)-FUA3UU*FDSW(I,K)
      FDSWH(I)=FDSWH(I)+FBBA2 *(1.+FA2/R2)*SIB
      FDSWR(I)=-SI1(I)-SI2(I)+FBBA2*(1.0-FA2/R2)*SIB
 113  FDSWZ(I)=FBB26 *SIB-FUA3UU  *FDSW(I,K)                              DR014900
       DO 104 I=1,MFR                                                     DR014980
       FSTSH(I )=FSTSH(I)+FDSWH(I)                                        DR015000
       FSTSR(I )=FSTSR(I)+FDSWR(I)                                        DR015040
 104   CONTINUE                                                           DR015120
       RETURN                                                             DR015140
        END
      SUBROUTINE FCREP(DSTB,KGG,JF,CPR,FGVP1,FGVP2,FGR,FS13,FS2B,FS3B)
       COMMON/COMFC/J,K,TIME,DTIME,FR(5,15),FDR(5,15),FSTSH(5),           YHS00160
     1 FSTSR(5),FSTSZ(5),CR(5,15),CDR(5,15),CSTSH(5),CSTSR(5),            YHS00180
     2 CSTSZ(5),NZ,NR,MFR,MP,BAOLEE,MTEST,FLUX(15)                        YHS00200
       COMMON/CONSTF/FA,FB,FA2,FB2,FBA2,FE,FP,FU2,FUA1,FUA2,FUA3,         YHS00280
     1 FUA5,FUA6,FTF(5,15),TDFA,TDFB,FDEB,FUB(15),FAA,FUU,FBBA2,          YHS00300
     2 FBA22,FBB26,FUA3UU,U1,U3,FADBA2,FBDBA2,FA1U                        YHS00320
       COMMON/FCREPM/FC3,FDTSH(5),FDTSR(5),FDTSZ(5),FS1(5),FS2(5),        YHS00340
     1 FS3(5),FDSTRH(5),FDSTRR(5),FDSTRZ(5),FSTSHB(5,15),FSTSRB(5,15),    YHS00360
     2 FSTSZB(5,15),SHB(5,15),SRB(5,15),SZB(5,15),PN(5),SE(5),SH(5),      YHS00380
```

```
      3 SR(5).SZ(5).FMX
       COMMON/MIX1/FDHE(5).FDRE(5).FDZE(5).FDCPB.UCPA(15).UCPB(15).         YHS00400
      1 PL(15).CUEA(15).CUEB(15).FUBB(15).BOLE(15).CUAB(15).CUBB(15).       YHS00540
      2 UCPAB(15).UCPBB(15).CUEAB(15).CUEBB(15).CUSWAB(15).CUSWBB(15).      YHS00560
      3 CTSWB(15).CSWB2(5.15).BU.GF.PNB(5.15).FNTSW(5.15).CE3.CW3.          YHS00580
      4 TCE3.TCW3.TCP3.C3.FW3.TFE.TFP.TFW.FCPZB(5.15).FCPRB(5.15).          YHS00600
      5 FCPHB(5.15).CCPHB(5.15).CCPRB(5.15).CCPZB(5.15).FSWUBB(15).         YHS00620
      6 FCPBB(15).FUEB(15).FUEBB(15).FERH(5).FERR(5).FERZ(5).FCPZ(5.15)     YHS00640
      7 .FCPR(5.15).FCPH(5.15).CCPH(5.15).CCPR(5.15).CCPZ(5.15).            YHS00660
      8 FSWUB(15).FCPB(15).FTRH(5).FTRR(5).FTRZ(5).CTRH(5).CTRR(5).         YHS00680
      9 CTRZ(5).CERH(5).CERR(5).CERZ(5)                                     YHS00700
       DIMENSION       CPR(5).DCP(5).F(5).CTZ(5).PEF(5).DSTB(5)             YHS00720
       DIMENSION FGVP1(5.15).FGVP2(5.15).V1(5).V2(5).V3(5) .FGR(5.15)
   78  DO 81 I=1.MFR
        DCP(I)=CPR(I)*DTIME
        IF(SE(I) .EQ. 0.) GO TO 12                                          DRJ10860
        DK    =(DCP(I)/SE(I))*1.5
        GO TO 14                                                            DRJ10900
   12   DK    =0.
   14  FDSTRH(I)=DK*SHB(I.K)
       FDSTRR(I)=DK*SRB(I.K)
       FDSTRZ(I)=DK*SZB(I.K)
C      WRITE(6.100) CPR(I).DCP(I).SE(I).DK.I
C 100   FORMAT(2X.'CPR.DCP.SE.DK.I-Z'.4E12.3.I4)
C       WRITE(6.101)FDSTRH(I).FDSTRR(I).FDSTRZ(I)
C 101   FORMAT('*DSTRH.DSTRR.DSTRZ'.3E12.4)
   81  CONTINUE
C      WRITE(6.93) DTIME
C 93    FORMAT(2X.'DTIMEB'.F10.5)
       DO 70 I=1.MFR
       FCPH(I.K)=FCPHB(I.K)+FDSTRH(I)
       FCPR(I.K)=FCPRB(I.K)+FDSTRR(I)
   70  FCPZ(I.K)=FCPZB(I.K)+FDSTRZ(I)
       DO 63 I=1.MFR
       V1(I)=FDSTRR(I)*FGVP1(I.K)
       V3(I)=(ALOG(FR(I.K))-ALOG(FGR(I.K)))*(FDSTRR(I)-FDSTRH(I))
   63  CONTINUE
       VP=0.
        DO 64 I=1.MFR
       I1=I+1
       FS1(I)=VP+V1(I)
       VP=VP+FDSTRR(I)*FGVP2(I1.K)
   64   CONTINUE
       FS1B=VP
       VP=0.
       DO 65 I=1.MFR
       I1=I+1
        FS3(I)=VP +V3(I)
       VP=VP+(ALOG(FGR(I1.K))-ALOG(FGR(I.K))) *(FDSTRR(I)-FDSTRH(I))
   65   CONTINUE
       FS3B=VP
       VP=0.
        DO 66 I=1.MFR
       I1=I+1
       V2(I)=FS3(I)*FGVP1(I.K)
       FS2(I)=VP+V2(I)
       VP=VP+FS3(I)*FGVP2(I1.K)
   66   CONTINUE
       FS2B=VP
       R1=FR(1.K)
```

```
      T1=(R1**2)*(0.5*ALOG(R1)-0.25)
       T2=FA2*(0.5*ALOG(FA)-0.25)
       T3=0.5*(R1**2-FA2)*ALOG(FA)
       FS2(I)=(FDSTRR(I)-FDSTRH(I))*(T1-T2-T3)
       DO 61 I=1,MFR                                                    DRO11420
       R2=FR(I,K)**2                                                    DRO11440
       RA2 =(R2+FA2)                                                    DRO11460
       T1=FS1(I)/R2+FS1B     *RA2/(R2*FBA2)
       T2=FS2(I)/R2+FS2B     *RA2/(R2*FBA2)
       T3=FS3(I)*FUA2 -FS3B     *RA2*FBDBA2 /(R2)
       FDTSH(I )=(FUA1)*(T1+T2)+(FU2)*T3-(FUA3)*(FDSTRH(I)+FDSTRZ(I))
     1 -(FU2)*FDSTRH(I)
       RR2=R2-FA2                                                       DRO11600
       D1=-FS1(I)/R2+FS1B     *RR2/(R2*FBA2)
       D2=-FS2(I) /R2+FS2B     *RR2/(R2*FBA2)
       D3=FS3(I)-FS3B     *RR2*FB2/(R2*FBA2)
       FDTSR(I )=(FUA1   )*(D1+D2)+(FU2   )*D3                          DRO11680
      Z1=((FUA6)/FBA2)*(FS1B+FS2B,
       Z2=(FU2   )*(FUA2 *FS3(I)-FUA5*(FBBA2    )*FS3B)
       Z3=(FUA3     )*(FDSTRH(I)+FDSTRZ(I))+(FU2   )*(FDSTRZ(I))          DRO11740
      FDTSZ (I)=Z1+Z2-Z3
  61   CONTINUE                                                         DRO11840
       DO 77 I=1,MFR                                                    DRO11960
       FSTSH(I   )=FSTSHB(I,K)+FDTSH(I)                                 DRO11980
       FSTSR(I   )=FSTSRB(I,K)+FDTSR(I)                                 DRO12000
  77   CONTINUE                                                         DRO12040
       RETURN
       END                                                              DRO12080
      SUBROUTINE CCREP(S1B,S2B,S3B                    )
       COMMON/COMFC/J,K,TIME,DTIME,FR(5,15),FDR(5,15),FSTSH(5),         YHS00160
     1 FSTSR(5),FSTSZ(5),CR(5,15),CDR(5,15),CSTSH(5),CSTSR(5),          YHS00180
     2 CSTSZ(5),NZ,NR,MFR,MP,BADLEE,MTEST,FLUX(15)                      YHS00200
       COMMON/CONSTC/CA,CB,A2,B2,BA2,UA1,CAA,CUU,CC,CP,CTF(5,15),       YHS00220
     1 CUA(15),CUB(15),TDCA,TDCB,A1U,A2U,UA2,UA3,U2,UA5,UA6,B2BA2,      YHS00240
     2 CUA3UU,CADEA2,CBDBA2                                             YHS00260
       COMMON/CCREPM/CDTSH(5),CDTSR(5),CDTSZ(5),CDSTRH(5),CDSTRR(5),    YHS00420
     1 CDSTRZ(5),S1(5),S2(5),S3(5),CP3,CSTSHB(5,15),CSTSRB(5,15),       YHS00440
     2 CSTSZB(5,15),SHCB(5,15),SRCB(5,15),SZCB(5,15),CN(5),CSE(5),      YHS00460
     3 CSH(5),CSR(5),CSZ(5)                                             YHS00480
       COMMON/MIX1/FDHE(5),FDRE(5),FDZE(5),FDCPB,UCPA(15),UCPB(15),     YHS00540
     1 PL(15),CUEA(15),CUEB(15),FUBB(15),BOLE(15),CUAB(15),CUEB(15),    YHS00560
     2 UCPAB(15),UCPBB(15),CUEAB(15),CUEBB(15),CUSWAB(15),CUSWBB(15),   YHS00580
     3 CTSWB(15),CSWB2(5,15),BU,CF,PNB(5,15),FNTSW(5,15),CE3,CW3,       YHS00600
     4 TCE3,TCW3,TCP3,C3,FW3,TFE,TFP,TFW,FCPZB(5,15),FCPRB(5,15),       YHS00620
     5 FCPHB(5,15),CCPHB(5,15),CCPRB(5,15),CCPZB(5,15),FSWUBB(15),      YHS00640
     6 FCPBB(15),FUEB(15),FUEBB(15),FERH(5),FERR(5),FERZ(5),FCPZ(5,15)  YHS00660
     7 ,FCPR(5,15),FCPH(5,15),CCPH(5,15),CCPR(5,15),CCPZ(5,15),         YHS00680
     8 FSWUB(15),FCPB(15),FTRH(5),FTRR(5),FTRZ(5),CTRH(5),CTRR(5),      YHS00700
     9 CTRZ(5),CERH(5),CERR(5),CERZ(5)                                  YHS00720
      DIMENSION SE(5),CPR(5),DCP(5),F(5),FF(5)
       DO 59 I=1,NR                                                     DRO16040
       R2=CR(I,K)**2                                                    DRO16060
      R4=R2**2
      SS=(CSTSHB(I,K)-CSTSRB(I,K))**2+(CSTSHB(I,K)-CSTSZB(I,K))**2
     1 +(CSTSRB(I,K)-CSTSZB(I,K))**2
       SE(I)=(SS/2.)**0.5                                               DRO16180
       TC=CTF(I,K)+460.                                                 DRO16240
C      WRITE(6,1840)S,U                                                 DRO16340
C1840  FORMAT('  S,U',2E8.2)                                             DRO16360
      IF(SE(I).EQ.0.)GO TO 160
```



733 326

POOR ORIGINAL

```
      G1=(- 8.61E4/TC)+ 7*ALOG(SE(I))-11.*ALOG(10.)+ALOG(2.7)
      G2=ALOG(FLUX(K))+ 3*ALOG(SE(I))-34.*ALOG(10.)+ALOG(4.655)
       IF( G1 .LT.-170.  ) GO TO 140
        E1=EXP(G1)                                                      DRO16540
       GO TO 141                                                        DRO16560
 140   E1=0.                                                            DRO16580
 141   CONTINUE                                                         DRO16600
      IF( G2 .LT.-170.  ) GO TO 150
       E2=EXP(G2)                                                       DRO16640
       GO TO 151                                                        DRO16660
 150   E2=0.                                                            DRO16680
 151   CONTINUE                                                         DRO16700
       CPR(I)=E1+E2                                                     DRO16760
      GO TO 161
 160  CPR(I)=0.
 161   DCP(I)=CPR(I)*DTIME
       IF(SE(I) .EQ. 0.) GO TO 12                                       DRO16940
      DK     =(DCP(I)/SE(I))*1.5
       GO TO 14                                                         DRO16980
 12   DK     =0.
 14   CDSTRH(I)=DK*SHCB(I,K)
      CDSTRR(I)=DK*SRCB(I,K)
      CDSTRZ(I)=DK*SZCB(I,K)
C      WRITE(6,100) SDH(I),SDR(I),SDZ(I),SE(I),CPR(I),DCP(I),DK(I)     DRO17080
C 100  FORMAT('$$$$$$',7E15.4)                                          DRO17100
C      WRITE(6,101)DSTRH(I),DSTRR(I),DSTRZ(I)                          DRO17120
C 101  FORMAT('*****',3E15.4)                                           DRO17140
 59    CONTINUE                                                         DRO17160
      DO 70 I=1,NR
      CCPH(I,K)=CCPHB(I,K)+CDSTRH(I)
      CCPR(I,K)=CCPRB(I,K)+CDSTRR(I)
 70   CCPZ(I,K)=CCPZB(I,K)+CDSTRZ(I)
       SF=0.
       DO 58 I=1,NR
       GG=(CDSTRR(I)-CDSTRH(I))*CDR(I,K)*0.5/CR(I,K)
      AI= SF+GG
       SF=SF+(CDSTRR(I)-CDSTRH(I))*CDR(I,K)/CR(I,K)
       FF(I)=SF
 58   F(I)=AI
      S3B=SF
       S1S=0.                                                           DRO17280
       S2S=0.
       S3S=0.
       DO 60 I=1,NR
       G1=CDSTRR(I)*CR(I,K)*CDR(I,K)*0.5
      G2=F(I)*CR(I,K)*CDR(I,K)*0.5
      AI1=S1S+G1
       AI2=S2S+G2
       S1S=S1S+CDSTRR(I)*CR(I,K)*CDR(I,K)
       S2S=S2S+FF(I)*CR(I,K)*CDR(I,K)
       S1(I)=AI1
       S2(I)=AI2
 60   S3(I)=F(I)
      S1B=S1S
       S2B=S2S
C      WRITE(6,115) (S1(I),I=1,5)                                      DRO17500
C      WRITE(6,116) (S2(I),I=1,5)                                      DRO17520
C      WRITE(6,117) (S3(I),I=1,5)                                      DRO17540
C 115  FORMAT(2X,'S1(I)',5E12.4)                                       DRO17560
C 116  FORMAT(2X,'S2(I)',5E12.4)                                       DRO17580
```

POOR ORIGINAL



733 327

```
C117     FORMAT(2X,'S3(I)',5E12.4)                                              DRO17600
         DO 61 I=1,NR                                                           DRO17620
         R2=CR(I,K)**2                                                          DRO17640
         RA2=(R2+CA**2)                                                         DRO17660
         T1=S1(I)/R2+ S1B*RA2/(R2*BA2)
C        WRITE(6,119) TG1,TG2,T1                                                DRO17740
C 119    FORMAT(2X,'TG1,TG2,T1',3E12.4)                                         DRO17760
         T2=S2(I)/R2+S2B    *RA2/(R2*BA2)
         T3=S3(I)*UA2   -S3B    *RA2*CBDBA2/R2
         T4=(UA3)*(CDSTRH(I)+CDSTRZ(I))+(U2)*(CDSTRH(I))
         CDTSH(I)=(UA1)*(T1+T2)+(U2)*T3-T4
         RR2=R2-A2
         D1=-S1(I)/R2+S1B    *RR2/(R2*BA2)
         D2=-S2(I)/R2+S2B    *RR2/(R2*BA2)
         D3=S3(I)-S3B*RR2*CBDBA2/R2
         CDTSR(I)=(UA1     )*(D1+D2)+(U2    )*D3                                DRO17960
        Z1=((UA6)/BA2)*(S1B+S2B)
         Z2=(U2)*(UA2*S3(I)-UA5 *CBDBA2*S3B    )
         Z3=(UA3     )*(CDSTRH(I)+CDSTRZ(I))+(U2    )*(CDSTRZ(I))               DRO18020
         CDTSZ(I)=Z1+Z2-Z3                                                      DRO18040
C        WRITE(6,110)       DTSH(I  ),T1,T2,T3,T4,TT                            DRO18060
C        WRITE(6,111)           D1,D2,D3,Z1,Z2,DTSZ(I,J)                        DRO18080
C110     FORMAT(2X,'DTSH ,T1,T2,T3,T4,TT',6E12.4)                               DRO18100
C111     FORMAT(2X,'DTSZ ,D1,D2,D3,Z1,Z2',6E12.4)                               DRO18120
  61     CONTINUE                                                               DRO18140
         JTT=J                                                                  DRO18280
         DO 133 I=1,NR                                                          DRO18300
         CSTSH(I )=CSTSHB(I,K)+CDTSH(I)                                         DRO18320
         CSTSR(I )=CSTSRB(I,K)+CDTSR(I)                                         DRO18340
 133     CONTINUE                                                               DRO18360
        RETURN                                                                  DRO18400
        END                                                                     DRO18420
        SUBROUTINE WINP
         COMMON/FCBV/ACB(15),BCB(15),AFB(15),BFB(15),FTIME,ET,EIT,RF1,         YHS00100
       1 RF2,DPO,MF,MG,JF,MPRINT,RV1,RV2,MPUNCH,MBOLE,TCLB,TFLB,RRES(15)       YHS00120
       2,VOLM,VOLU,VOL,AVETK,GAS,AC(15),BC(15),AF(15),BF(15),FL(15)            YHS00   0
         COMMON/COMFC/J,K,TIME,DTIME,FR(5,15),FDR(5,15),FSTSH(5),
       1 FSTSR(5),FSTSZ(5),CR(5,15),CDR(5,15),CSTSH(5),CSTSR(5),
       2 CSTSZ(5),NZ,NR,MFR,MP,BAOLEE,MTEST,FLUX(15)
         COMMON/CONSTC/CA,CB,A2,B2,BA2,UA1,CAA,CUU,CE,CP,CTF(5,15),            Y
       1 CUA(15),CUB(15),TDCA,TDCB,A1U,A2U,UA2,UA3,U2,UA5,UA6,B2BA2,           YHS0024
       2 CUA3UU,CADBA2,CBDBA2
         COMMON/CONSTF/FA,FB,FA2,FB2,FBA2,FE,FP,FU2,FUA1,FUA2,FUA3,
       1 FUA5,FUA6,FTF(5,15),TDFA,TDFB,FDEB,FUB(15),FAA,FUU,FBBA2,             YHS
       2 FBA22,FBB26,FUA3UU,U1,U3,FADBA2,FBDBA2,FA1U
         COMMON/FCREPM/FC3,FDTSH(5),FDTSR(5),FDTSZ(5),FS1(5),FS2(5),           YHS003
       1 FS3(5),FDSTRH(5),FDSTRR(5),FDSTRZ(5),FSTSHB(5,15),FSTSRB(5,15),       YHS00360
       2 FSTSZB(5,15),SHB(5,15),SRB(5,15),SZB(5,15),PN(5),SE(5),SH(5),         YH
       3 SR(5),SZ(5),FMX
         COMMON/CCREPM/CDTSH(5),CDTSR(5),CDTSZ(5),CDSTRH(5),CDSTRR(5),         Y
       1 CDSTRZ(5),S1(5),S2(5),S3(5),CP3,CSTSHB(5,15),CSTSRB(5,15),            YH
       2 CSTSZB(5,15),SHCB(5,15),SRCB(5,15),SZCB(5,15),CN(5),CSE(5),           Y
       3 CSH(5),CSR(5),CSZ(5)
         COMMON/CSWLM/CSWW(5),CSWI(5),CSW(5),CSWH(5),CSWR(5),CSWZ(5),          Y
       1 CUSWA(15),CUSWB(15),CTSW(5),CSWB(5,15)
         COMMON/MIX1/FDHE(5),FDRE(5),FDZE(5),FDCPB,UCPA(15),UCPB(15),
       1 PL(15),CUEA(15),CUEB(15),FUBB(15),BOLE(15),CUAB(15),CUBB(15),         YH
       2 UCPAB(15),UCPBB(15),CUEAB(15),CUEBB(15),CUSWAB(15),CUSWBB(15),        YHS00
       3 CTSWB(15),CSWB2(5,15),BU,GF,PNB(5,15),FNTSW(5,15),CE3,CW3,            YHS0060
       4 TCE3,TCW3,TCP3,C3,FW3,TFE,TFP,TFW,FCPZB(5,15),FCPRB(5,15),            YHS
```

```
 5 FCPHB(5.15).CCPHB(5.15).CCPRB(5.15).CCPZB(5.15).FSWUBB(15 .           YHS006
 6 FCPBB(15).FUEB(15).FUEBB(15).FERH(5).FERR(5).FERZ(5).FCPZ(5.15)       YHS
 7 .FCPR(5.15).FCPH(5.15).CCPH(5.15).CCPR(5.15).CCPZ(5.15).              YHS0
 8 FSWUB(15).FCPB(15).FTRH(5).FTRR(5).FTRZ(5).CTRH(5).CTRR(5).           YH
 9 CTRZ(5).CERH(5).CERR(5).CERZ(5)
   NZ1=NZ-1
   PRINT 2.(BFB(K).K=1.NZ1)
  PRINT 3.(ACB(K).K=1.NZ)
   PRINT 4.(BCB(K).K=1.NZ)
   PRINT 5.(PL(K).K=1.NZ)
   PRINT 6.(FLUX(K).K=1.NZ)
   PRINT 7.((FTF(I.K).I=1.MFR).K=1.NZ1)
   PRINT 8.((CTF(I.K).I=1.NR).K=1.NZ)
   PRINT 9.((FSTSHB(I.K).I=1.MFR).K=1.NZ1)
   PRINT 9.((FSTSRB(I.K).I=1.MFR).K=1.NZ1)
   PRINT 9.((FSTSZB(I.K).I=1.MFR).K=1.NZ1)
   PRINT 10.((CSTSHB(I.K).I=1.NR).K=1.NZ)
   PRINT 10.((CSTSRB(I.K).I=1.NR).K=1.NZ)
   PRINT 10.((CSTSZB(I.K).I=1.NR).K=1.NZ)
 2  FORMAT('   BF   '.15F8.5)
 3  FORMAT('   AC   '.15F8.5)
 4  FORMAT('   BC   '.15F8.5)
 5  FORMAT('   PL   '.15F8.2)
 6  FORMAT('   FLUX'.15E8.1)
 7  FORMAT  ('   FTF '.12F9.1)
 8  FORMAT  ('   CTF '.12F9.1)
 9  FORMAT('   FSTRESS'.12F9.1)
10  FORMAT('   CSTRESS'.12F9.1)
    RETURN
    END
    SUBROUTINE CSWL(DUSWA.DUSWB.SIBC.NCSW.FFLUX        )
    COMMON/COMFC/J.K.TIME.DTIME.FR(5.15).FDR(5.15).FSTSH(5).              YHS00160
 1 FSTSR(5).FSTSZ(5).CR(5.15).CDR(5.15).CSTSH(5).CSTSR(5).                YHS00180
 2 CSTSZ(5).NZ.NR.MFR.MP.BADLEE.MTEST.FLUX(15)                            YHS00200
   COMMON/CONSTC/CA.CB.A2.B2.BA2.UA1.CAA.CUU.CE.CP.CTF(5.15).             YHS00220
 1 CUA(15).CUB(15).TDCA.TDCB.A1U.A2U.UA2.UA3.U2.UA5.UA6.B2BA2.            YHS00240
 2 CUA3UU.CADBA2.CBDBA2                                                   YHS00260
   COMMON/CCREPM/CDTSH(5).CDTSR(5).CDTSZ(5).CDSTRH(5).CDSTRR(5).          YHS00420
 1 CDSTRZ(5).S1(5).S2(5).S3(5).CP3.CSTSHB(5.15).CSTSRB(5.15).             YHS00440
 2 CSTSZB(5.15).SHCB(5.15).SRCB(5.15).SZCB(5.15).CN(5).CSE(5).            YHS00460
 3 CSH(5).CSR(5).CSZ(5)                                                   YHS00480
   COMMON/CSWLM/CSWW(5).CSWI(5).CSW(5).CSWH(5).CSWR(5).CSWZ(5).           YHS00500
 1 CUSWA(15).CUSWB(15).CTSW(5).CSWB(5.15)                                 YHS00520
   COMMON/MIX1/FDHE(5).FDRE(5).FDZE(5).FDCPB.UCPA(15).UCPB(15).           YHS00540
 1 PL(15).CUEA(15).CUEB(15).FUBB(15).BOLE(15).CUAB(15).CUBB(15).          YHS00560
 2 UCPAB(15).UCPBB(15).CUEAB(15).CUEBB(15).CUSWAB(15).CUSWBB(15).         YHS00580
 3 CTSWB(15).CSWB2(5.15).BU.GF.PNB(5.15).FNTSW(5.15).CE3.CW3.             YHS00600
 4 TCE3.TCW3.TCP3.C3.FW3.TFE.TFP.TFW.FCPZB(5.15).FCPRB(5.15).             YHS00620
 5 FCPHB(5.15).CCPHB(5.15).CCPRB(5.15).CCPZB(5.15).FSWUBB(15).            YHS00640
 6 FCPBB(15).FUEB(15).FUEBB(15).FERH(5).FERR(5).FERZ(5).FCPZ(5.15)        YHS00660
 7 .FCPR(5.15).FCPH(5.15).CCPH(5.15).CCPR(5.15).CCPZ(5.15).               YHS00680
 8 FSWUB(15).FCPB(15).FTRH(5).FTRR(5).FTRZ(5).CTRH(5).CTRR(5).            YHS00700
 9 CTRZ(5).CERH(5).CERR(5).CERZ(5)                                        YHS00720
  DIMENSION SSW(5).SI1(5).SI2(5).UW(5) .TCK(5.15).P1T(5).PS(5)
 1 .P2T(5).P3T(5).FFLUX(15)
  TIMES=TIME*3600.
  DO 51 I=1.NR
  TCK(I.K)=(CTF(I.K)-32.)*5./9.
   CNB=(CSTSHB(I.K)+CSTSRB(I.K)+CSTSZB(I.K))/3.
   PS(I)=1.
```

POOR ORIGINAL

733 329

```
        P=(1.214E-2)*TCK(I,K)
        P1T(I)=EXP(-(P-6.070)**2)
        P2T(I)=EXP(-(P-7.284)**2)
        P3T(I)=EXP(-(P-8.498)**2)
   51   CONTINUE
       IF(NCSW .EQ. 1) GO TO 20
       IF(NCSW .EQ. 2) GO TO 21
       IF(NCSW .EQ. 3) GO TO 22
       IF(NCSW .EQ. 4) GO TO 23
       IF(NCSW .EQ. 5) GO TO 24
       IF(NCSW .EQ. 10) GO TO 40
   20   CONTINUE
C***** CLAD SWELLING FROM LIFE-1
       DO 60 I=1,NR
       TC=TCK(I,K
        FF=4.028-(3.712E-2)*TC+(1.0145E-4)*(TC**2)-(7.879E-8)*(TC**3)      DRU19560
       CSWW(I)=(4.5E-37)*((FLUX(K)*TIMES)**1.5)*FF
   60  CONTINUE
       GO TO 50
   21   CONTINUE
C***** ANL MODEL 1
       DO 61 I=1,NR
       P1=(FLUX(K)*TIMES)**1.63354
        CSWW(I)=(1.20078E-39)*P1*P1T(I)*PS(I)
   61  CONTINUE
       GO TO 50
   22  CONTINUE
C***** ANL MODEL 4
       DO 62 I=1,NR
       P1=(FLUX(K)*TIMES)**1.6877368
        CPP    =(9.71574E-41)*P1*P1T(I)
        CSWW(I)=CPP*PS(I)
   62  CONTINUE
        GO TO 50
   23   CONTINUE
C***** ANL MODEL 5
       DO 63 I=1,NR
       P1=(FLUX(K)*TIMES)**1.6877368
        CSWW(I)=(9.71574E-41)*P1*P2T(I)*PS(I)
   63  CONTINUE
         GO TO 50
   24   CONTINUE
C***** ANL MODEL 6
       DO 64 I=1,NR
       P1=(FLUX(K)*TIMES)**1.6877368
        CSWW(I)=(9.71574E-41)*P1*P3T(I)*PS(I)
   64  CONTINUE
         GO TO 50
   40  CONTINUE
C****** CLAD SW MODEL FROM WASHINGTON                                       YHS00300
       DO 65 I=1,NR
        TC=TCK(I,K)                                                         YHS00340
        T2=TC**2                                                            YHS00360
        T3=TC**3                                                            YHS00380
        T4=TC**4                                                            YHS00400
       TC2=-(1.24156E-3)*T2                                                 YHS00420
       TC3=(1.37215E-6)*T3                                                  YHS00440
       TC4=(-6.14E-10)*T4                                                   YHS00460
       CSWP=-88.5499+0.531072*TC+TC2+TC3+TC4
        CSWP=     EXP(CSWP)*0.01
```

```
      TC2=-(3.81081E-4)*T2                                        YHS00520
      TC3=(5.51979E-7)*T3                                         YHS00540
      TC4=-(3.26491E-10)*T4                                       YHS00560
      CSWT=-16.7382+0.130532*TC+TC2+TC3+TC4                       YHS00580
      CSWT=EXP(CSWT)                                              YHS00600
      CAL=-1.12+(6289E-3)*TC                                      YHS00620
      P1=FFLUX(K)*TIMES/(1.E22)                                   YHS00640
      P2=EXP(CAL*(CSWT-P1))                                       YHS00660
      P3=EXP(CAL*CSWT)                                            YHS00680
      P4=(1.+P2)/(1.+P3)                                          YHS00700
      P4=ALOG(P4)                                                 YHS00720
65    CSWW(I)=CSWP*(P1+P4/CAL)
     GO TO 50
 50   CONTINUE
      DO 9 I=1,NR                                                 DRU19520
     CSW(I)=CSWW(I)-CSWB(I,K)
9     CSWB2(I,K)=CSWW(I)
     SI=0.
     DO 10 I=1,NR
     R2=CR(I,K)**2
      GG=CSW(I)*CR(I,K)*CDR(I,K)*0.5
     AI=SI+GG
      SI=SI+CSW(I)*CR(I,K)*CDR(I,K)
     SI1(I)=UA3*AI/R2
 10  SI2(I)=(UA1/3.)*AI/R2
      SI1B=UA3*SI/B2
      SI2B=(UA1/3.)*SI/B2
     SIB=SI1B+SI2B
      DO 11 I=1,NR                                                DRU20000
      R2=CR(I,K)**2                                               DRU20040
      SWH2=CBDBA2*(1.+A2/R2)*SIB
     CSWH(I)=SWH2+SI1(I)+SI2(I)-CUA3UU*CSW(I)
     CSWR(I)=-(SI1(I)+SI2(I))+CBDBA2*(1.-A2/R2)*SIB
     CSWZ(I)=UA5*CBDBA2*SIB-(CUA3UU*CSW(I))
      CSTSH(I )=CSTSH(I)+CSWH(I)                                  DRU20180
      CSTSR(I )=CSTSR(I)+CSWR(I)                                  DRU20200
     UU1=(CR(I,K)/(U2     ))*(SI1(I)+SI2(I))
      UU2=CBDBA2/2.*(CP(I,K)/A1U+(A2/CUU)/CR(I,K))*SIU
 11       UW(I)=UU1+UU2                                           DRU20260
      SIBC=SIB                                                    DRU20400
      S=0.                                                        DRU20420
      DO 102 I=1,NR                                               DRU20420
      S=S+CR(I,K)*CSW(I)*CDR(I,K)                                 DRU20440
102       SSW(I)=S                                                DRU20460
     RETURN                                                       DRU20800
     END                                                          DRU20820
     SUBROUTINE READ  (CTR,DTIMEL,DPFCK,MPFC,CIPFC,FJMX,NJULE,RCC,
    1 FSQ1,FSQ2,TFSQ1,TFSQ2,NFSW,NCSW,FTSWB,SPFC,FPFC,SPO,TCLOSE,
    2  DCL,DFL,REOPEN,MSHP,TGRM,TGGM,AVCV,FPDEN,FFLUX)
      COMMON/FCBV/ACB(15),BCB(15),AFB(15),BFB(15),FTIME,ET,EIT,RF1,   YHS00100
    1 RF2,DPO,MF,MG,JF,MPRINT,RV1,RV2,MPUNCH,MBOLE,TCLB,TFLB,RRES(15) YHS00120
    2,VOLM,VOLU,VOL,AVETK,GAS,AC(15),BC(15),AF(15),BF(15),FL(15)      YHS00140
      COMMON/COMFC/J,K,TIME,DTIME,FR(5,15),FDR(5,15),FSTSH(5),        YHS00160
    1 FSTSR(5),FSTSZ(5),CR(5,15),CDR(5,15),CSTSH(5),CSTSR(5),         YHS00180
    2 CSTSZ(5),NZ,NR,MFR,MP,BADLEF,MTEST,FLUX(15)                     YHS00200
      COMMON/CONSTC/CA,CB,A2,B2,BA2,UA1,CAA,CUU,CE,CP,CTF(5,15),      YHS00220
    1 CUA(15),CUB(15),TDCA,TDCB,A1U,A2U,UA2,UA3,U2,UA5,UA5,B2BA2,     YHS00240
    2 CUA3UU,CADBA2,CBDBA2                                            YHS00260
      COMMON/CONSTF/FA,FB,FA2,FB2,FBA2,FE,FP,FU2,FUA1,FUA2,FUA3,      YHS00280
    1 FUA5,FUA6,FTF(5,15),TDFA,TDFB,FDEB,FUB(15),FAA,FUU,FBBA2,       YHS00300
```

```
 2 FBA22,FBB26,FUA3UU,U1,U3,FADBA2,FBOBA2,FAIU                              YHS00320
   COMMON/FCREPM/FC3,FDTSH(5),FDTSR(5),FDTSZ(5),FS1(5),FS2(5),              YHS00340
 1 FS3(5),FDSTRH(5),FDSTRR(5),FDSTRZ(5),FSTSHB(5,15),FSTSRB(5,15),         YHS00360
 2 FSTSZB(5,15),SHB(5,15),SRB(5,15),SZB(5,15),PN(5),SE(5),SH(5),           YHS00380
 3 SR(5),SZ(5),FMX                                                           YHS00400
   COMMON/CCREPM/CDTSH(5),CDTSR(5),CDTSZ(5),CDSTRH(5),CDSTRR(5),            YHS00420
 1 CDSTRZ(5),S1(5),S2(5),S3(5),CP3,CSTSHB(5,15),CSTSRB(5,15),              YHS00440
 2 CSTSZB(5,15),SHCB(5,15),SRCB(5,15),SZCB(5,15),CN(5),CSE(5),             YHS00460
 3 CSH(5),CSR(5),CSZ(5)                                                      YHS00480
   COMMON/CSWLM/CSWW(5),CSWI(5),CSW(5),CSWH(5),CSWR(5),CSWZ(5),             YHS00500
 1 CUSWA(15),CUSWB(15),CTSW(5),CSWB(5,15)                                   YHS00520
   COMMON/MIX1/FDHE(5),FDRE(5),FDZE(5),FDCPB,UCPA(15),UCPB(15),             YHS00540
 1 PL(15),CUEA(15),CUEB(15),FUBB(15),BOLE(15),CUAB(15),CUBB(15),           YHS00560
 2 UCPAB(15),UCPBB(15),CUEAB(15),CUEBB(15),CUSWAB(15),CUSWBB(15),          YHS00580
 3 CTSWB(15),CSWB2(5,15),BU,GF,PNB(5,15),FNTSW(5,15),CE3,CW3,               YHS00600
 4 TCE3,TCW3,TCP3,C3,FW3,TFE,TFP,TFW,FCPZB(5,15),FCPRB(5,15),               YHS00620
 5 FCPHB(5,15),CCPHB(5,15),CCPRB(5,15),CCPZB(5,15),FSWUBB(15),              YHS00640
 6 FCPBB(15),FUEB(15),FUEBB(15),FERH(5),FERR(5),FERZ(5),FCPZ(5,15)         YHS00660
 7 ,FCPR(5,15),FCPH(5,15),CCPH(5,15),CCPR(5,15),CCPZ(5,15),                 YHS00680
 8 FSWUB(15),FCPB(15),FTRH(5),FTRR(5),FTRZ(5),CTRH(5),CTRR(5),              YHS00700
 9 CTRZ(5),CERH(5),CERR(5),CERZ(5)                                           YHS00720
   COMMON/MIX2/DPGAS,PGAS,FPO,FDPO,FPI,FDPI,PFC(15),DPFC,CPO,CPI,           YHS00740
 1 FDSWUB,FDSWH(5),FDSWR(5),FDSWZ(5),FDSW(5,15),CDPI,CDPO,CDCHE(5)         YHS00760
 2 ,CDCRE(5),CDCZE(5),DUEA,DUEB,TDCA1,TDCA2,TDFB1,TDFB2,DP1,DP2,            YHS00780
 3 FTSW(5,15)                                                                YHS00800
   DIMENSION DPFCK(15),MPFC(15),NBOLE(15),FTSWB(5,15),REOPEN(15),
 1 FFLUX(15)
  READ 51, TIME,FTIME, ET,EIT ,JF,MPRINT,RF1,RF2,RV1,RV2,MPUNCH,
 1 J,MSHP
  READ 52, NR,NZ,MFR,MG,MP,MF,DPO,CPO,CDPO,PGAS,CTR,DTIMEL
  NZ1=NZ-1
  READ  55, NFSW,NCSW,CIPFC,FJMX ,SPFC,FPFL,SPD
  READ  54 ,RCC,FSQ1,FSQ2,TFSQ1,TFSQ2,TCLOSE,DFL,DCL
  READ  10, (REOPEN(K),K=1,NZ1)
  READ  14,(DPFCK(K),K=1,NZ1)
  READ  11,(PFC(K),K=1,NZ1)
  READ  12,(MPFC(K),K=1,NZ1),(NBOLE(K),K=1,NZ1)
   READ  13,(RRES(K),K=1,NZ1)
  READ 6,(AFB(K),K=1,NZ1)
  READ 6,(BFB(K),K=1,NZ1)
  READ 6,(ACB(K),K=1,NZ)
  READ 6,(BCB(K),K=1,NZ)
  READ 5,        TFLB,TCLB,AVCV,FPDEN,TGRM,TGGM
   READ(5,7) (PL(K),K=1,NZ)
   READ(5,6) (FLUX(K),K=1,NZ)
  READ 6,(FFLUX(K),K=1,NZ)
   READ(5,7) ((FTF(I,K),I=1,MFR),K=1,NZ1)
   READ(5,4) ((CTF(I,K),I=1,NR),K=1,NZ)                                      DRU07360
   READ(5,2) ((FSTSHB(I,K),I=1,MFR),K=1,NZ1)
   READ(5,2) ((FSTSRB(I,K),I=1,MFR),K=1,NZ1)
   READ(5,2) ((FSTSZB(I,K),I=1,MFR),K=1,NZ1)
  READ (5,2)((FNTSW(I,K),I=1,MFR),K=1,NZ1)
  READ(5,2) ((FTSWB(I,K),I=1,MFR),K=1,NZ1)
  READ (5,2) ((FCPHB(I,K),I=1,MFR),K=1,NZ1)
  READ (5,2) ((FCPRB(I,K),I=1,MFR),K=1,NZ1)
  READ (5,2) ((FCPZB(I,K),I=1,MFR),K=1,NZ1)
   READ(5,4) ((CSTSHB(I,K),I=1,NR),K=1,NZ)                                   DRU07440
   READ(5,4) ((CSTSRB(I,K),I=1,NR),K=1,NZ)
   READ(5,4) ((CSTSZB(I,K),I=1,NR),K=1,NZ)
   READ(5,3) ((CSWB(I,K),I=1,NR),K=1,NZ)
```

```
      READ (5.3) ((CCPHB(I.K).I=1.NR).K=1.NZ)
      READ (5.3) ((CCPRB(I.K).I=1.NR).K=1.NZ)
      READ (5.3) ((CCPZB(I.K).I=1.NR).K=1.NZ)
      READ(5.6) (FSWUBB(K).K=1.NZ1)
      READ(5.6) ( FCPBB(K).K=1.NZ1)
      READ(5.6) ( FUEBB(K).K=1.NZ1)
       READ(5.6)(CUEAB(K).K=1.NZ)
       READ (5.6)(CUEBB(K).K=1.NZ)
       READ (5.6)(CUAB(K).K=1.NZ)
       READ(5.6)(CUBB(K).K=1.NZ)
       READ(5.6)(UCPAB(K).K=1.NZ)
       READ(5.6)(UCPBB(K).K=1.NZ)
       READ(5.6)(CUSWAB(K).K=1.NZ)
       READ(5.6)(CUSWBB(K).K=1.NZ)
       READ(5.6)(FUBB(K).K=1.NZ1)
 61   FORMAT(4F8.1.I8.I5.4F5.2.2I5.I2      )
 52   FORMAT(6I2.5E12.4.F4.1)
  55  FORMAT(2I5.F10.3.E15.4.3F10.2)
  54  FORMAT(E10.3.4F5.1.      F10.2.2E12.4)
  2   FORMAT(4E15.7)
   3   FORMAT(6E13.7)
   4  FORMAT(6F10.2)
  5   FORMAT(2F10.2.2F5.3.2E15.8)
  6   FORMAT(5E15.7)
  7   FORMAT(8F10.2)
  10  FORMAT(13F4.1)
  11  FORMAT(8F10.3)
  12  FORMAT(26I3)
  13  FORMAT(13F6.4)
  14  FORMAT(8F10.5)
       RETURN                                                            DRO07800
       END                                                               DRO07820
      SUBROUTINE FWRITE(FDTS            )                                DRO07840
       COMMON/COMFC/J.K.TIME.DTIME.FR(5.15).FDR(5.15).FSTSH(5).          YHS00160
     1 FSTSR(5).FSTSZ(5).CR(5.15).CDR(5.15).CSTSH(5).CSTSR(5).           YHS00180
     2 CSTSZ(5).NZ.NR.MFR.MP.BACLEE.MTEST.FLUX(15)                       YHS00200
       COMMON/CONSTF/FA.FB.FA2.FB2.FBA2.FE.FP.FU2.FUA1.FUA2.FUA3.        YHS00280
     1 FUA5.FUA6.FTF(5.15).TDFA.TDFB.FDEB.FUB(15).FAA.FUU.FBBA2.         YHS00300
     2 FBA22.FBB26.FUA3UU.U1.U3.FADBA2.FBDBA2.FA1U                       YHS00320
       COMMON/FCREPM/FC3.FDTSH(5).FDTSR(5).FDTSZ(5).FS1(5).FS2(5).       YHS00340
     1 FS3(5).FDSTRH(5).FDSTRR(5).FDSTRZ(5).FSTSHB(5.15).FSTSRB(5.15).   YHS00360
     2 FSTSZB(5.15).SHB(5.15).SRB(5.15).SZB(5.15).PN(5).SE(5).SH(5).     YHS00380
     3 SR(5).SZ(5).FMX                                                   YHS00400
       COMMON/MIX1/FDHE(5).FDRE(5).FDZE(5).FDCPB.UCPA(15).UCPB(15).      YHS00540
     1 PL(15).CUEA(15).CUEB(15).FUBB(15).BOLE(15).CUAB(15).CUBB(15).     YHS00560
     2 UCPAB(15).UCPBB(15).CUEAB(15).CUEBB(15).CUSWAB(15).CUSWBB(15).    YHS00580
     3 CTSWB(15).CSWB2(5.15).BU.GF.PNB(5.15).FNTSW(5.15).CE3.CW3.        YHS00600
     4 TCE3.TCW3.TCP3.C3.FW3.TFE.TFP.TFW.FCPZB(5.15).FCPRB(5.15).        YHS00620
     5 FCPHB(5.15).CCPHB(5.15).CCPRB(5.15).CCPZB(5.15).FSWUBB(15).       YHS00640
     6 FCPBB(15).FUEB(15).FUEBB(15).FERH(5).FERR(5).FERZ(5).FCPZ(5.15)   YHS00660
     7 .FCPR(5.15).FCPH(5.15).CCPH(5.15).CCPR(5.15).CCPZ(5.15).          YHS00680
     8 FSWUB(15).FCPB(15).FTRH(5).FTRR(5).FTRZ(5).CTRH(5).CTRR(5).       YHS00700
     9 CTRZ(5).CERH(5).CERR(5).CERZ(5)                                   YHS00720
       COMMON/MIX2/DPGAS.PGAS.FPO.FDPO.FPI.FDPI.PFC(15).DPFC.CPO.CPI.    YHS00740
     1 FDSWUB.FDSWH(5).FDSWR(5).FDSWZ(5).FDSW(5.15).CDPI.CDPO.CDCHE(5)   YHS00760
     2 .CDCRE(5).CDCZE(5).DUEA.DUEB.TDCA1.TDCA2.TDFB1.TDFB2.DP1.DP2.     YHS00780
     3 FTSW(5.15)                                                        YHS00800
       DIMENSION FDTS(5)
       WRITE(6.20)                                                       DRO08180
       IF(K .GT. 1) GO TO 18                                             DRO08200
```

```
      PRINT 17,  J,TIME,DTIME                                        DRU08220
18    CONTINUE                                                       DRU08260
     PRINT 19,K,BU
      WRITE(6,10)                                                    DRU08320
     PRINT 15, (PN(I),I=1,MFR),(SE(I),I=1,MFR)
     PRINT 16,(SH(I),I=1,MFR),(SR(I),I=1,MFR),(SZ(I),I=1,MFR)
      PRINT 1,    (FSTSH(I),I=1,MFR),(FSTSR(I),I=1,MFR),
    1 (FSTSZ(I),I=1,MFR)
      PRINT 2,    (FDTSH(I),I=1,MFR),(FDTSR(I),I=1,MFR),
    1  (FDTS (I),I=1,MFR)
      PRINT 4,( FDHE(I),I=1,MFR),(FDRE(I),I=1,MFR)
      PRINT 5,(FDSWH(I),I=1,MFR),(FDSWR(I),I=1,MFR)
     PRINT 8,(FTRH(I),I=1,MFR),(FTRR(I),I=1,MFR),(FTRZ(I),I=1,MFR)
     PRINT 7,(FERH(I),I=1,MFR),(FERR(I),I=1,MFR),(FERZ(I),I=1,MFR)
     PRINT 6,(FCPH(I,K),I=1,MFR),(FCPR(I,K),I=1,MFR),
    1  (FCPZ(I,K),I=1,MFR)
      PRINT 9,(FDSTRH(I),I=1,MFR),(FDSTRR(I),I=1,MFR),
    1  (FDSTRZ(I),I=1,MFR)
      PRINT 11,   (FDSW(I,K),I=1,MFR),(FNTSW(I,K),I=1,MFR),
    1 (FTSW(I,K),I=1,MFR)
     PRINT 12, FCPB(K),FSWUB(K),FUEB(K),FUB(K)
      PRINT 13, FDCPB,FDSWUB,FDEB,TDFB
1     FORMAT(2X,'FSTSH ',4F9.1 ,2X,'FSTSR ',4F9.1 ,2X,'FSTSZ ',4F9.1 ) D
2     FORMAT(2X,'FDTSH ',4F9.1 ,2X,'FDTSR ',4F9.1 ,2X,'FDTS  ',4F9.1 ) DRU08420
4     FORMAT(2X,'FDHE  ',4F9.1 ,2X,'FDRE  ',4F9.1)
5     FORMAT(2X,'FDSWH ',4F9.1 ,2X,'FDSWR ',4F9.1 ,/)
 6   FORMAT(2X,'FTCPH ', 4E9.2 ,2X,'FTCPR ',4E9.2 ,2X,'FTCPZ ',
    1 4E9.2 )
 7   FORMAT(2X,'FTEH  ',4F9.5 ,2X,'FTER  ',4F9.5 ,2X,'FTEZ  ',4F9.5 )
 8   FORMAT(2X,'FTRH  ',4F9.5 ,2X,'FTRR  ',4F9.5 ,2X,'FTRZ  ',4F9.5 )
 9    FORMAT(2X,'FDCPH ',4E9.2 ,2X,'FDCPR ',4E9.2 ,2X,'FDCPZ ',4E9.2 ) DRU08580
10    FORMAT(' FUEL REGION',/)                                       DRU08340
11    FORMAT(2X,'FNDSW ',4E9.2 ,2X,'FNTSW  ',4E9.2  ,2X,'FTSW',4E9.2)
 12  FORMAT(2X,'FCPB',E11.3,2X,'FSWUB',E11.3,2X,'FUEB',E11.3,2X,
    1 'FUB',E11.3)
 13   FORMAT(2X,'FDCPB',E10.2,2X,'FDSWB',E11.3,2X,'FDEB',F11.3,2X,
    1 'TDFB',1PE14.6,/)
20    FORMAT('----------------------------------------------------')DRU08680
 15  FORMAT(2X,'PN    ',4F9.1 ,2X,'SE    ',4F9.1 )
 16   FORMAT(2X,'SH    ',4F9.1 ,2X,'SR    ',4F9.1 ,2X,'SZ    ',4F9.1 )
17    FORMAT(' J=',I5,'  TIME=',F10.2,'  DTIME=',F6.2)               DRU08240
 19  FORMAT(' K=',I2,'     BU % =',F5.2,/)
      RETURN                                                         DRU08700
      END                                                            DRU08720
     SUBROUTINE CWRITE(CDTS         )                                DRU08740
      COMMON/COMFC/J,K,TIME,DTIME,FR(5,15),FDR(5,15),FSTSH(5),       YHS00160
    1 FSTSR(5),FSTSZ(5),CR(5,15),CDR(5,15),CSTSH(5),CSTSR(5),        YHS00180
    2 CSTSZ(5),NZ,NR,MFR,MP,BAQLEE,MTEST,FLUX(15)                    YHS00200
      COMMON/CONSTC/CA,CB,A2,B2,BA2,UA1,CAA,CUU,CE,CP,CTF(5,15),     YHS00220
    1 CUA(15),CUB(15),TDCA,TDCB,A1U,A2U,UA2,UA3,U2,UA5,UA6,B2BA2,    YHS00240
    2 CUA3UU,CADBA2,CBDBA2                                           YHS00260
      COMMON/CCREPM/CDTSH(5),CDTSR(5),CDTSZ(5),CDSTRH(5),CDSTRR(5),  YHS00420
    1 CDSTRZ(5),S1(5),S2(5),S3(5),CP3,CSTSHB(5,15),CSTSRB(5,15),     YHS00440
    2 CSTSZB(5,15),SHCB(5,15),SRCB(5,15),SZCB(5,15),CN(5),CSE(5),    YHS00460
    3 CSH(5),CSR(5),CSZ(5)                                           YHS00480
      COMMON/CSWLM/CSWW(5),CSWI(5),CSW(5),CSWH(5),CSWR(5),CSWZ(5),   YHS00500
    1 CUSWA(15),CUSWB(15),CTSW(5),CSWB(5,15)                         YHS00520
      COMMON/MIX1/FDHE(5),FDRE(5),FDZE(5),FDCPB,UCPA(15),UCPB(15),   YHS00540
    1 PL(15),CUEA(15),CUEB(15),FUBB(15),BOLE(15),CUAB(15),CUBB(15),  YHS00560
    2 UCPAB(15),UCPBB(15),CUEAB(15),CUEBB(15),CUSWAB(15),CUSWBB(15), YHS00580
```

```
  3 CTSWB(15),CSWB2(5,15),BU,GF,PNB(5,15),FNTSW(5,15),CE3,CW3,           YHS00600
  4 TCE3,TCW3,TCP3,C3,FW3,TFE,TFP,TFW,FCPZB(5,15),FCPRB(5,15),           YHS00620
  5 FCPHB(5,15),CCPHB(5,15),CCPRB(5,15),CCPZB(5,15),FSWUBB(15),          HS00640
  6 FCPBB(15),FUEB(15),FUEBB(15),FERH(5),FERR(5),FERZ(5),FCPZ(5,15)      HS00660
  7 ,FCPR(5,15),FCPH(5,15),CCPH(5,15),CCPR(5,15),CCPZ(5,15),             HS00680
  8 FSWUB(15),FCPB(15),FTRH(5),FTRR(5),FTRZ(5),CTRH(5),CTRR(5),          HS00700
  9 CTRZ(5),CERH(5),CERR(5),CERZ(5)                                       YHS00720
    COMMON/MIX2/DPGAS,PGAS,FPO,FDPO,FPI,FDPI,PFC(15),DPFC,CPO,CPI,       YHS00740
  1 FDSWUB,FDSWH(5),FDSWR(5),FDSWZ(5),FDSW(5,15),CDPI,CDPL,CDCHE(5)      YHS00760
  2 ,CDCRE(5),CDCZE(5),DUEA,DUEB,TDCA1,TDCA2,TDFB1,TDFB2,DP1,DP2,        YHS00780
  3 FTSW(5,15)                                                             YHS00800
   DIMENSION CDTS(5)
    IF(K .EQ. NZ) GO TO 2                                                  DR009120
    WRITE(6,1)                                                              DR009140
    GO TO 4                                                                 DR009180
 2  PRINT 5,K
    WRITE(6,3)                                                              DR009240
 4  CONTINUE                                                                DR009280
   PRINT 10,(CN(I),I=1,NR),(CSE(I),I=1,NR)
    PRINT 11,(CSH(I),I=1,NR),(CSR(I),I=1,NR),(CSZ(I),I=1,NR)
   PRINT 12,(CSTSH(I),I=1,NR),(CSTSR(I),I=1,NR),(CSTSZ(I),I=1,NR)
   PRINT 13 ,(CDTSH(I),I=1,NR),(CDTSR(I),I=1,NR),(CDTS (I),I=1,NR)
    PRINT 14, ( CDCHE(I),I=1,NR),(CDCRE(I),I=1,NR)
   PRINT 15,(CSWH(I),I=1,NR),(CSWR(I),I=1,NR)
   PRINT 16,(CTRH(I),I=1,NR),(CTRR(I),I=1,NR),(CTRZ(I),I=1,NR)
   PRINT 17,(CERH(I),I=1,NR),(CERR(I),I=1,NR),(CERZ(I),I=1,NR)
   PRINT 18,(CCPH(I,K),I=1,NR),(CCPR(I,K),I=1,NR),(CCPZ(I,K),I=1,NR)
   PRINT 19,(CDSTRH(I),I=1,NR),(CDSTRR(I),I=1,NR),(CDSTRZ(I),I=1,NR)
   PRINT 20,(CSWW(I),I=1,NR),(CSW(I),I=1,NR)
   PRINT 21, UCPA(K),UCPB(K),CUSWA(K),CUSWB(K),CUFA(K),CUEB(K),
  1 CUA(K),CUB(K),TDCA
1   FORMAT(' CLADDING REGION',/)                                          DR009160
 3  FORMAT(' CLADDING(PLENUM REGION)',/)                                  DR009260
5   FORMAT(' K=',I2,/)                                                     DR009220
10  FORMAT(2X,'CN     ',3F9.1,11X,'CSE    ',3F9.1)
11  FORMAT(2X,'CSH    ',3F9.1,11X,'CSR    ',3F9.1,11X,'CSZ    ',3F9.1)
12  FORMAT(2X,'CSTSH  ',3F9.1,11X,'CSTSR  ',3F9.1,11X,'CSTSZ  ',3F9.1)
13  FORMAT(2X,'CDTSH  ',3F9.4,11X,'CDTSR  ',3F9.4,11X,'CDTS   ',3F9.4)
14  FORMAT(2X,'CDHE   ',3F9.4,11X,'CDRE   ',3F9.4)
15  FORMAT(2X,'CDSWH  ',3E12.4, 2X,'CDSWR  ',3E12.4,/)
16  FORMAT(2X,'CTRH   ',3E9.2,11X,'CTRR   ',3E9.2,11X,'CTRZ   ',3E9.2)
17  FORMAT(2X,'CTEH   ',3E11.3,5X,'CTER   ',3E11.3,5X,'CTEZ   ',3E11.3)
18  FORMAT(2X,'CTCPH  ',3E11.3,5X,'CTCPR  ',3E11.3,5X,'CTCPZ  ',3E11.3)
19  FORMAT(2X,'CDCPH  ',3E11.3,5X,'CDCPR  ',3E11.3,5X,'CDCPZ  ',3F11.3)
20  FORMAT(2X,'CTSW',3E11.3,6X,' CDSW',3E10.2)
21  FORMAT(2X,'UCPA,UCPB',2E9.2 ,' USWA,USWB',2E9.2 ,' UCA,UEB',
  1 2E9.2 ,' CLA,CUB',2E9.2 , ' TDCA',1PE13.6,/)
    RETURN                                                                  DR010180
    END                                                                     DR010200
   SUBROUTINE FUBCWP(FS1B,FS2B,FS3B,S1B                )
    COMMON/COMFC/J,K,TIME,DTIME,FR(5,15),FDR(5,15),FSTSH(5),              YHS00160
  1 FSTSR(5),FSTSZ(5),CR(5,15),CDR(5,15),CSTSH(5),CSTSR(5),              YHS00180
  2 CSTSZ(5),NZ,NR,MFR,MP,BADLEE,MTEST,FLUX(15)                           YHS00200
    COMMON/CONSTF/FA,FB,FA2,FB2,FBA2,FE,FP,FU2,FUA1,FUA2,FUA3,            YHS00280
  1 FUA5,FUA6,FTF(5,15),TDFA,TDFB,FDEB,FUB(15),FAA,FUU,F3BA2,            YHS00300
  2 FBA22,FBB26,FUA3UU,U1,U3,FADBA2,FBDBA2,FA1U                          YHS00320
    COMMON/FCREPM/FC3,FDTSH(5),FDTSR(5),FDTSZ(5),FS1(5),FS2(5),           YHS00340
  1 FS3(5),FDSTRH(5),FDSTRR(5),FDSTRZ(5),FSTSHB(5,15),FSTSRB(5,15),      YHS00360
  2 FSTSZB(5,15),SHB(5,15),SRB(5,15),SZB(5,15),PN(5),SE(5),SH(5),        YHS00380
  3 SR(5),SZ(5),FMX                                                       YHS00400
```



733 335

```
      COMMON/MIX1/FDHE(5),FDRE(5),FDZE(5),FDCPB,UCPA(15),UCPB(15),        YHS00540
     1 PL(15),CUEA(15),CUEB(15),FUBB(15),BOLE(15),CUAB(15),CUBB(15),      YHS00560
     2 UCPAB(15),UCPBB(15),CUEAB(15),CUEBB(15),CUSWAB(15),CUSWBB(15),     YHS00580
     3 CTSWB(15),CSWB2(5,15),BU,GF,PNB(5,15),FNTSW(5,15),CE3,CW3,         YHS00600
     4 TCE3,TCW3,TCP3,C3,FW3,TFE,TFP,TFW,FCPZB(5,15),FCPRB(5,15),         YHS00620
     5 FCPHB(5,15),CCPHB(5,15),CCPRB(5,15),CCPZB(5,15),FSWUBB(15),        YHS00640
     6 FCPBB(15),FUEB(15),FUEBB(15),FERH(5),FERR(5),FERZ(5),FCPZ(5,15)    YHS00660
     7 ,FCPR(5,15),FCPH(5,15),CCPH(5,15),CCPR(5,15),CCPZ(5,15),           YHS00680
     8 FSWUB(15),FCPB(15),FTRH(5),FTRR(5),FTRZ(5),CTRH(5),CTRR(5),        YHS00700
     9 CTRZ(5),CERH(5),CERR(5),CERZ(5)                                    YHS00720
      COMMON/MIX2/DPGAS,PGAS,FPO,FDPO,FPI,FDPI,PFC(15),DPFC,CPO,CPI,      YHS00740
     1 FDSWUB,FDSWH(5),FDSWR(5),FDSWZ(5),FDSW(5,15),CDPI,CDPO,CDCHE(5)    YHS00760
     2 ,CDCRE(5),CDCZE(5),DUEA,DUEB,TDCA1,TDCA2,TDFB1,TDFB2,DP1,DP2,      YHS00780
     3 FTSW(5,15)                                                         YHS00800
C******* PRESSURE EFFECTS
      FDI= FDPI
      FDO= FDPO
      FU1=U1*(FDI -FDO )
      FU5=FDO *FB/2./FAIU
      FU3=U3*(FDI -FDO )
       FDEB=FU1-FU5+FU3
      FUEB(K)=FUEBB(K)+FDEB
C******* CREEP EFFECTS
       FCORT=FUA1/FBA2
       FS1B=FS1B*FCORT
       FS2B=FS2B*FCORT
       FS3B=FS3B*2.*FUU
       UF1=FB*(FS1B+FS2B)/FU2
       UFF2=FB2/2./FBA2                                                   DR015440
       UFF1=FB/(FAA+FUU)+FA2/(FUU*FB)                                     DR015460
       UF2=UFF2*UFF1*(FS1B+FS2B-FS3B)
       FDCPB=UF1+UF2
      FCPB(K)=FCPBB(K)+FDCPB
C******* SWELLING EFFECTS
       UA2B=FA2/FUU/FB
      FDSWUB=(FB*S1B/FU2+F3A22*(FB/FA1U+UA2B)*S1B)
      FSWUB(K)=FSWUBB(K)+FDSWUB
       TDFB=FDEB+FDCPB+FDSWUB-FP*FC3*(FB-FA)/FE
       FUB(K)=FUBB(K)+TDFB
       RETURN                                                             DR015560
       END                                                                DR015580
      SUBROUTINE FPE (FGVP2,DPFCK,MPFC              )
       COMMON/COMFC/J,K,TIME,DTIME,FR(5,15),FDR(5,15),FSTSH(5),           YHS00160
     1 FSTSR(5),FSTSZ(5),CR(5,15),CDR(5,15),CSTSH(5),CSTSR(5),            YHS00180
     2 CSTSZ(5),NZ,N3,MFR,MP,BADLEE,MTEST,FLUX(15)                        YHS00200
       COMMON/CONSTF/FA,FB,FA2,FB2,FBA2,FE,FP,FU2,FUA1,FUA2,FUA3,         YHS00280
     1 FUA5,FUA6,FTF(5,15),TDFA,TDFB,FDEB,FUB(15),FAA,FUU,FBEA2,          YHS00300
     2 FBA22,FBB26,FUA3UU,U1,U3,FADBA2,FBDBA2,FAIU                        YHS00320
       COMMON/MIX1/FDHE(5),FDRE(5),FDZE(5),FDCPB,UCPA(15),UCPB(15),       YHS00540
     1 PL(15),CUEA(15),CUEB(15),FUBB(15),BOLE(15),CUAB(15),CUBB(15),      YHS00560
     2 UCPAB(15),UCPBB(15),CUEAB(15),CUEBB(15),CUSWAB(15),CUSWBB(15),     YHS00580
     3 CTSWB(15),CSWB2(5,15),BU,GF,PNB(5,15),FNTSW(5,15),CE3,CW3,         YHS00600
     4 TCE3,TCW3,TCP3,C3,FW3,TFE,TFP,TFW,FCPZB(5,15),FC RB(5,15),         YHS00620
     5 FCPHB(5,15),CCPHB(5,15),CCPRB(5,15),CCPZB(5,15), SWUBB(15),        YHS00640
     6 FCPBB(15),FUEB(15),FUEBB(15),FERH(5),FERR(5),FERZ(5),FCPZ(5,15)    YHS00660
     7 ,FCPR(5,15),FCPH(5,15),CCPH(5,15),CCPR(5,15),CCPZ(5,15),           YHS00680
     8 FSWUB(15),FCPB(15),FTRH(5),FTRR(5),FTRZ(5),CTRH(5),CTRR(5),        YHS00700
     9 CTRZ(5),CERH(5),CERR(5),CERZ(5)                                    YHS00720
       COMMON/MIX2/DPGAS,PGAS,FPO,FDPO,FPI,FDPI,PFC(15),DPFC,CPO,CPI,     YHS00740
     1 FDSWUB,FDSWH(5),FDSWR(5),FDSWZ(5),FDSW(5,15),CDPI,CDPO,CDCHE(5)    YHS00760
```



733 336

```
   2 .CDCRE(5),CDCZE(5),DUEA,DUEB,TDCA1,TDCA2,TDFB1,TDFB2,DP1,DP2,     YHS00780
   3 FTSW(5,15)                                                         YHS00800
     DIMENSION FGVP2(5,15),DPFCK(15),MPFC(15)
     IF(BOLE(K).EQ. 2.) GO TO 400
403  FPO=PGAS                                                           DRO12720
     FPI=PGAS                                                           DRO12740
    FDPO=DPGAS                                                          DRO12760
    FDPI=DPGAS                                                          DRO12780
     GO TO 401                                                          DRO12800
400  CONTINUE                                                           DRO12820
     IF(TIME .EQ. DTIME .AND. MP .EQ. 1) GO TO 402                      DRO12840
     IF(MPFC(K) .EQ. 1 .AND. MP.EQ.1) PFC(K)=PGAS
     IF(MPFC(K) .EQ. 1 .AND. MP.EQ.1)  DPFCK(K)=DPGAS
    IF(MP .EQ. 1) PFC(K)=PFC(K)+DPFCK(K)
     FPO=PFC(K)                                                         DRO12900
     FPI=PGAS                                                           DRO12920
    FDPO=DPFCK(K)
    FDPI=DPGAS                                                          DRO12960
     GO TO 401                                                          DRO12980
402  PFC(K)=PGAS                                                        DRO13080
     DPFCK(K)=PGAS
     DPFC=PGAS                                                          DRO13100
    GO TO 403
401  CONTINUE                                                           DRO13120
    FDI= FDPI
    FDO= FDPO
     DO 523 I=1,MFR                                                     DRO13140
     R2=FR(I,K)**2                                                      DRO13160
      BR2=FB2/R2                                                        DRO13180
      AR2=FA2/R2                                                        DRO13200
     FDHE(I)=(FADBA2   )*(1.+BR2)*FDI -(FBDBA2   )*(1.+AR2)*FDO         DRO1
     FDRE(I)=(FADBA2   )*(1.-BR2)*FDI -(FBDBA2   )*(1.-AR2)*FDO
523  FDZE(I)=(2. *FP/FBA2)*(FA2*FDI -FB2*FDO )
     DO 666 I=1,MFR                                                     DRO13620
     FSTSH(I)=FSTSH(I)+FDHE(I)
     FSTSR(I)=FSTSR(I)+FDRE(I)
666  CONTINUE                                                           DRO13740
     RETURN                                                             DRO13760
     END                                                                DRO13780
    SUBROUTINE CGP(DPFCK          )
     COMMON/COMFC/J,K,TIME,DTIME,FR(5,15),FDR(5,15),FSTSH(5),
   1 FSTSR(5),FSTSZ(5),CR(5,15),CDR(5,15),CSTSH(5),CSTSR(5),
   2 CSTSZ(5),NZ,NR,MFR,MP,BADLEE,MTEST,FLUX(15)
     COMMON/CONSTC/CA,CB,A2,B2,BA2,UA1,CAA,CUU,CF,CP,CTF(5,15),         YHS00220
   1 CUA(15),CUB(15),TDCA,TDCB,A1U,A2U,UA2,UA3,U2,UA5,UA6,B2BA2,        YHS00240
   2 CUA3UU,CADBA2,CBDBA2                                               YHS00260
     COMMON/MIX1/FDHE(5),FDRE(5),FDZE(5),FDCPB,UCPA(15),UCPB(15),       YHS00540
   1 PL(15),CUEA(15),CUEB(15),FUBB(15),BOLE(15),CUAB(15),CUBB(15),      YHS00560
   2 UCPAB(15),UCPBB(15),CUEAB(15),CUEBB(15),CUSWAB(15),CUSWBB(15),     YHS00580
   3 CTSWB(15),CSWB2(5,15),BU,GF,PNB(5,15),FNTSW(5,15),CE3,CW3,         YHS00600
   4 TCE3,TCW3,TCP3,C3,FW3,TFE,TFP,TFW,FCPZB(5,15),FCPRB(5,15),         YHS00620
   5 FCPHB(5,15),CCPHB(5,15),CCPRB(5,15),CCPZB(5,15),FSWUBB(15),        YHS00640
   6 FCPBB(15),FUEB(15),FUEBB(15),FERH(5),FERR(5),FERZ(5),FCPZ(5,15)    YHS00660
   7 ,FCPR(5,15),FCPH(5,15),CCPH(5,15),CCPR(5,15),CCPZ(5,15),           YHS00680
   8 FSWUB(15),FCPB(15),FTRH(5),FTRR(5),FTRZ(5),CTRH(5),CTRR(5),        YHS00700
   9 CTRZ(5),CERH(5),CERR(5),CERZ(5)                                    YHS00720
     COMMON/MIX2/DPGAS,PGAS,FPO,FDPO,FPI,FDPI,PFC(15),DPFC,CPO,CPI,     YHS00740
   1 FDSWUB,FDSWH(5),FDSWR(5),FDSWZ(5),FDSW(5,15),CDPI,CDPO,CDCHE(5)    YHS00760
   2 ,CDCRE(5),CDCZE(5),DUEA,DUEB,TDCA1,TDCA2,TDFB1,TDFB2,DP1,DP2,     YHS00780
   3 FTSW(5,15)                                                         YHS00800
```





733 337

```
      DIMENSION DPFCK(15)
     IF(K .EQ. NZ) GO TO 50                                              DR021120
      IF(BOLE(K).EQ. 2.) GO TO 400                                       DR021140
 50   CPI=PGAS                                                           DR021160
     CDPI=DPGAS                                                          DR021180
      GO TO 401                                                          DR021200
400   CONTINUE                                                           DR021220
      IF(TIME .EQ. DTIME .AND. MP .EQ. 1) GO TO 402                      DR021240
      CPI=PFC(K)                                                         DR021260
     CDPI=DPFCK(K)                                                       DR021280
      GO TO 401                                                          DR021300
402   CPI=PGAS                                                           DR021320
     CDPI=PGAS                                                           DR021340
 401  CONTINUE                                                           DR021360
     CDI= CDPI
     CDO= CDPO
      DO 130 I=1,NR
      R2=CR(.    .**2                                                    DR021500
      BR2=B2/                                                            DR021520
      AR2=A2/                                                            DR021540
     CDCHE(I)=      A2*(1.+BR2)*CDI   -CBDBA2*(1.+AR2)*CDO
      CDCRE(I)=CADBA2*(1.-BR2)*CDI  -CBDBA2*(1.-AR2)*CDO
130  CDCZE(I)=2.*CP*(A2*CDI -B2*CDO )/BA2
      DO 77 I=1,NR                                                       DR021820
      CSTSH(I)=CSTSH(I   )+CDCHE(I)                                      DR021840
      CSTSR(I)=CSTSR(I   )+CDCRE(I)                                      DR021860
77    CONTINUE                                                           DR021900
     RETURN                                                              DR021920
     END                                                                 DR021940
     SUBROUTINE CBCWP(DUFA,DUFB,S1B,S2B,S3B,S1BC     )
      COMMON/CONFC/J,K,TIME,DTIME,FR(5,15),FDR(5,15),FSTSH(5),           YHS00160
    1 FSTSR(5),FSTSZ(5),CR(5,15),CDR(5,15),CSTSH(5),CSTSR(5),            YHS00180
    2 CSTSZ(5),NZ,NR,MFR,MP,BADLEE,MTEST,FLUX(15)                        YHS00200
      COMMON/CONSTC/CA,CB,A2,B2,BA2,UA1,CAA,COU,CF,CP,CTF(5,15),         YHS00220
    1 CUA(15),CUB(15),TDCA,TDCB,A1U,A2U,UA2,UA3,U2,UA5,UA6,B2BA2,        YHS00240
    2 CUA3UU,CADBA2,CBDBA2                                               YHS00260
      COMMON/CCREPM/CDTSH(5),CDTSR(5),CDTSZ(5),CDSTRH(5),CDSTRR(5),      YHS00420
    1 CDSTRZ(5),S1(5),S2(5),S3(5),CP3,CSTSHB(5,15),CSTSRB(5,15),         YHS00440
    2 CSTSZB(5,15),SHCB(5,15),SRCB(5,15),SZCB(5,15),CN(5),CSF(5),        YHS00460
    3 CSH(5),CSR(5),CSZ(5)                                               YHS00480
      COMMON/CSWLM/CSWW(5),CSW1(5),CSW(5),CSWH(5),CSWR(5),CSWZ(5),       YHS00500
    1 CUSWA(15),CUSWB(15),CTSW(5),CSWB(5,15)                             YHS00520
      COMMON/MIX1/FDHE(5),FDRE(5),FDZE(5),FDCPB,UCPA(15),UCPB(15),       YHS00540
    1 PL(15),CUEA(15),CUEB(15),FUBB(15),BOLE(15),CUAB(15),CUBB(15),      YHS00560
    2 UCPAB(15),UCPBB(15),CUEAB(15),CUEBB(15),CUSWAB(15),CUSWBB(15),     YHS00580
    3 CTSWB(15),CSWB2(5,15),DU,GF,PNB(5,15),FNTSW(5,15),CE3,CW3,         YHS00600
    4 TCE3,TCW3,TCP3,C3,FW3,TFE,TFP,TFW,FCPZB(5,15),FCPRB(5,15),         YHS00620
    5 FCPHB(5,15),CCPHB(5,15),CCPRB(5,15),CCPZB(5,15),FSWUBB(15),        YHS00640
    6 FCPBB(15),FUEB(15),FUEBB(15),FERH(5),FERR(5),FERZ(5),FCPZ(5,15)    YHS00660
    7 ,FCPR(5,15),FCPH(5,15),CCPH(5,15),CCPR(5,15),CCPZ(5,15),           YHS00680
    8 FSWUB(15),FCPB(15),FTRH(5),FTRR(5),FTRZ(5),CTRH(5),CTRR(5),        YHS00700
    9 CTRZ(5),CERH(5),CERR(5),CERZ(5)                                    YHS00720
      COMMON/MIX2/DPGAS,PGAS,FPO,FDPO,FPI,FDPI,PFC(15),DPFC,CPO,CPI,     YHS00740
    1 FDSWUB,FDSWH(5),FDSWR(5),FDSWZ(5),FDSW(5,15),CDPI,CDPO,CDCHE(5)    YHS00760
    2 ,CDCRE(5),CDCZE(5),DUEA,DUEB,TDCA1,TDCA2,TDFB1,TDFB2,DP1,DP2,      YHS00780
    3 FTSW(5,15)                                                         YHS00800
C*******CLADDING BOUNDARY DISPLACEMENT                                    DR018700
C***** CREEP EFFECTS
      DG=UA1/B2                                                          DR018720
      DI2=DG*S1B
```

```
      DI3=DG*S2B
      DI4=(2.*CUU)*S3B
      UF1=CB*(DI2+DI3)/(2.*CUU)                                         DR018800
      UFF1=CB/(CAA+CUU)+(A2/(CB*CUU))                                   DR018820
      UFF2=(B2/(B2-A2))/2.                                              DR018840
      UF2=UFF1*UFF2*(DI2+DI3-DI4)                                       DR018860
      DUFB    =UF1+UF2 .                                                DR018880
      DGP1=1./(CAA+CUU)                                                 DR018940
      DGP2=1./CUU                                                       DR018960
      DUFA=CA*B2*(DGP1+DGP2)*(DI2+DI3-DI4)/(2.*BA2.                     DR018980
      UCPA(K)=  DUFA+UCPAB(K)                                           DR019040
      UCPB(K)=  DUFB+UCPBB(K)                                           DR019050
C***** SWELLING EFFECTS
      DUSWA=(CBDBA2*CA/2.)*(1./A1U+1./CUU)*SIBC
      DUSWB=(CB/U2)*SIBC+(CBDBA2/2.)*(CB/A1U+A2/CUU/CB)*SIBC
         CUSWA(K)= +DUSWA+CUSWAB(K)                                     DR020600
         CUSWB(K)= +DUSWB+CUSWBB(K)                                     DR020620
C***** PRESSURE EFFECTS
     CDI= CDPI
     CDO= CDPO
      PP1=A2*(CDI -CDO )/2./BA2/(CAA+CUU)
      PP2=CDO /2./(CAA+CUU)
      PP3=A2*B2*(CDI -CDO )/BA2/2./CUU
      DUEA=(PP1-PP2)*CA+PP3/CA
       DUEB=(PP1-PP2)*CB+PP3/CB
      CUEA(K)=  DUEA+CUEAB(K)                                           DR004860
      CUEB(K)=  DUEB+CUEBB(K)                                           DR004880
      TDCA=DUFA+DUSWA+DUEA
     TDCB=DUFB+DUSWB+DUEB-CP*CP3*(CB-CA)/CE
      CUA(K)=CUAB(K)+TDCA
      CUB(K)=CUBB(K)+TDCB
      RETURN                                                            DR019120
     END                                                                DR019140
     SUBROUTINE PPRCI( DPFCK,MPFC            )                          YHS00160
      COMMON/COMFC/J,K,TIME,DTIME,FR(5,15),FDR(5,15),FSTSH(5),          YHS00180
    1 FSTSR(5),FSTSZ(5),CR(5,15),CDR(5,15),CSTSH(5),CSTSR(5),           YHS00200
    2 CSTSZ(5),NZ,NR,MFR,MP,BADLEE,MTEST,FLUX(15)                       YHS00220
      COMMON/CONSTC/CA,CB,A2,B2,BA2,UA1,CAA,CUU,CE,CP,CTF(5,15),        YHS00240
    1 CUA(15),CUB(15),TDCA,TDCB,A1U,A2U,UA2,UA3,U2,UA5,UA6,B2BA2,       YHS00260
    2 CUA3UU,CADBA2,CBDBA2                                              YHS00280
      COMMON/CONSTF/FA,FB,FA2,FB2,FBA2,FE,FP,FU2,FUA1,FUA2,FUA3,        YHS00300
    1 FUA5,FUA6,FTF(5,15),TDFA,TDFB,FDEB,FUB(15),FAA,FUU,FBBA2,         YHS00320
    2 FBA22,FBB26,FUA3UU,U1,U3,FADBA2,FBDBA2,FA1U                       YHS00740
      COMMON/MIX2/DPGAS,PGAS,FPO,FDPO,FPI,FDPI,PFC(15),DPFC,CPO,CPI,    YHS00760
    1 FDSWUB,FDSWH(5),FDSWR(5),FDSWZ(5),FDSW(5,15),CDPI,CDPO,CDCHE(5)   YHS00780
    2 ,CDCRE(5),CDCZE(5),DUEA,DUEB,TDCA1,TDCA2,TDFB1,TDFB2,DP1,DP2,     YHS00800
    3 FTSW(5,15)
      DIMENSION DPFCK(15),MPFC(15)
      DPFC=DPFCK(K)
      IF(MP .NE. 1) GO TO 993                                           DR022200
     PFC(K)=PFC(K)-DPFC
      DP1=DPFC
      IF(TIME .EQ. DTIME) DP1=PGAS                                      DR022240
      P1=DP1                                                            DR022260
      TDCAT=(TDCA+TDFB)/2.                                              DR022280
      DDP=DP1*(TDCAT-TDCA)/TDCA                                         DR022300
      DP2=DP1+DDP                                                       DR022320
      DPFC=DP2                                                          DR022340
      PFC(K)=PFC(K)+DP2
      IF(TIME .EQ. DTIME) PFC(K)=DP2                                    DR022380
```

286

733 339

POOR ORIGINAL

```
      MP=MP+1                                                           DR022400
      IF(MPFC(K) .EQ. 2) GO TO 994
      MPFC(K)=MPFC(K)+1
994   CONTINUE
      TDCA1=TDCA                                                        DR022420
      TDFB1=TDFB                                                        DR022440
      GO TO 999                                                         DR022460
993   PFC(K)=PFC(K)-DPFC                                                DR022480
      TDCA2=TDCA                                                        DR022500
      TDFB2=TDFB                                                        DR022520
      DP2=DPFC                                                          DR022560
      AP=(TDCA2-TDCA1)/(TDFB2-TDFB1)                                    DR022580
      BP=TDCA2-AP*TDFB2                                                 DR022600
      Y0=BP/(1.-AP)                                                     DR022620
      X0=Y0                                                             DR022640
      PL2=(X0-TDFB2)**2+(Y0-TDCA2)**2                                   DR022660
      PL2=PL2**0.5                                                      DR022680
      P12=(TDFB1-TDFB2)**2+(TDCA1-TDCA2)**2                             DR022700
      P12=P12**0.5                                                      DR022720
      ALP=P12/PL2                                                       DR022740
      IF(TDFB1 .GT. TDCA1 .AND. TDFB2 .GT. TDCA2) GO TO 10              DR022760
      IF(TDFB1 .LT. TDCA1 .AND. TDFB2 .LT. TDCA2) GO TO 13              DR022780
      DPFC=DP2+(DP1-DP2)/ALP                                            DR022800
      GO TO 16                                                          DR022820
 10   IF(DP2 .LT. DP1) GO TO 11                                         DR022840
      DPFC=DP2+(DP2-DP1)/ALP                                            DR022860
      GO TO 16                                                          DR022880
 11   DPFC=DP2+(DP1-DP2)/ALP                                            DR022900
      GO TO 16                                                          DR022920
 13   IF(DP2 .LT. DP1) GO TO 14                                         DR022940
      DPFC=DP2+(DP1-DP2)/ALP                                            DR022960
      GO TO 16                                                          DR022980
 14   DPFC=DP2+(DP2-DP1)/ALP                                            DR023000
 16   CONTINUE                                                          DR023020
      DP1=DP2                                                           DR023040
      PFC(K)=PFC(K)+DPFC                                                DR023060
      TDCA1=TDCA2                                                       DR023080
      TDFB1=TDFB2                                                       DR023100
      MP=MP+1                                                           DR023120
999   CONTINUE                                                          DR023200
      DPFCK(K)=DPFC
      RETURN                                                            DR023220
      END                                                               DR023240
      SUBROUTINE PUNCH (CTR,DTIMEL,DPFCK,MPFC,CIPFC,FJMX,NBOLE,RCC,
     1 FSQ1,FSQ2,TFSQ1,TFSQ2,NFSW,NCSW,FTSWB,SPFC,FPFC,SPC,ICLOSE,
     2  DCL,DFL,REOPEN,MSHP,TGRM,TGGM,AVCV,FPDEN,FFLUX)
      COMMON/FCBV/ACB(15),BCB(15),AFB(15),BFB(15),FTIME,ET,EIT,RF1,     YHS00100
     1 RF2,DPO,MF,MG,JF,MPRINT,RV1,RV2,MPUNCH,MBOLE,TCLB,TFLB,RRES(15)  YHS00120
     2,VOLM,VOLU,VOL,AVETK,GAS,AC(15),BC(15),AF(15),BF(15),FL(15)      YHS0014
      COMMON/COMFC/J,K,TIME,DTIME,FR(5,15),FDR(5,15),FSTSH(5),          YHS00160
     1 FSTSR(5),FSTSZ(5),CR(5,15),CDR(5,15),CSTSH(5),CSTSR(5),          YHS00180
     2 CSTSZ(5),NZ,NR,MFR,MP,BAOLEE,MTEST,FLUX(15)                      YHS00200
      COMMON/CONSTC/CA,CB,A2,B2,BA2,UA1,CAA,CUU,CE,CP,CTF(5,15),        YHS00220
     1 CUA(15),CUB(15),TDCA,TDCB,A1U,A2U,UA2,UA3,U2,UA5,UA6,B2BA2,      YHS00240
     2 CUA3UU,CADBA2,CBDBA2                                             YHS00260
      COMMON/CONSTF/FA,FB,FA2,FB2,FBA2,FE,FP,FU2,FUA1,FUA2,FUA3,        YHS00280
     1 FUA5,FUA6,FTF(5,15),TDFA,TDFB,FDEB,FUB(15),FAA,FUU,FBBA2,        YHS00300
     2 FBA22,FBB26,FUA3UU,U1,U3,FADBA2,FBDBA2,FAIU                      YHS00320
      COMMON/FCREPM/FC3,FDTSH(5),FDTSR(5),FDTSZ(5),FS1(5),FS2(5),       YHS00340
     1 FS3(5),FDSTRH(5),FDSTRR(5),FDSTRZ(5),FSTSHB(5,15),FSTSRB(5,15),  YHS00360
```



POOR ORIGINAL

733 340

```
2 FSTSZB(5,15),SHB(5,15),SRB(5,15),SZB(5,15),PN(5),SE(5),SH(5),
3 SR(5),SZ(5),FMX
  COMMON/CCREPM/CDTSH(5),CDTSR(5),CDTSZ(5),CDSTRH(5),CDSTRR(5),
1 CDSTRZ(5),S1(5),S2(5),S3(5),CP3,CSTSHB(5,15),CSTSRB(5,15),
2 CSTSZB(5,15),SHCB(5,15),SRCB(5,15),SZCB(5,15),CN(5),CSE(5),
3 CSH(5),CSR(5),CSZ(5)
  COMMON/CSWLM/CSWW(5),CSWI(5),CSW(5),CSWH(5),CSWR(5),CSWZ(5),
1 CUSWA(15),CUSWB(15),CTSW(5),CSWB(5,15)
  COMMON/MIX1/FDHE(5),FDRE(5),FDZE(5),FDCPB,UCPA(15),UCPB(15),
1 PL(15),CUEA(15),CUEB(15),FUBB(15),BOLE(15),CUAB(15),CUBB(15),
2 UCPAB(15),UCPBB(15),CUEAB(15),CUEBB(15),CUSWAB(15),CUSWBB(15),
3 CTSWB(15),CSWB2(5,15),BU,GF,PNB(5,15),FNTSW(5,15),CE3,CW3,
4 TCE3,TCW3,TCP3,C3,FW3,TFE,TFP,TFW,FCPZB(5,15),FCPRB(5,15),
5 FCPHB(5,15),CCPHB(5,15),CCPRB(5,15),CCPZB(5,15),FSWUBB(15),
6 FCPBB(15),FUEB(15),FUEBB(15),FERH(5),FERR(5),FERZ(5),FCPZ(5,15)
7 ,FCPR(5,15),FCPH(5,15),CCPH(5,15),CCPR(5,15),CCPZ(5,15),
8 FSWUB(15),FCPB(15),FTRH(5),FTRR(5),FTRZ(5),CTRH(5),CTRR(5),
9 CTRZ(5),CERH(5),CERR(5),CERZ(5)
  COMMON/MIX2/DPGAS,PGAS,FPO,FDPO,FPI,FDPI,PFC(15),DPFC,CPO,CPI,
1 FDSWUB,FDSWH(5),FDSWR(5),FDSWZ(5),FDSW(5,15),CDPI,CDPO,CDCHE(5)
2 ,CDCRE(5),CDCZE(5),DUEA,DUEB,TDCA1,TDCA2,TDFB1,TDFB2,DP1,DP2,
3 FTSW(5,15)
  DIMENSION DPFCK(15),MPFC(15),NBOLE(15),FTSWB(5,15),REOPEN(15),
1 FFLUX(15)
 NZ1=NZ-1
  GO TO 1000
 PUNCH 70,TIME,FTIME, ET, EIT,JF,MPRINT,RF1,RF2,RV1,RV2,MPC CH,
1 J,MSHP
 PUNCH 75,NR,NZ,MFR,MG,MP..,DPO,CPO,CDPO,PGAS,CTR,DTIMEL
 PUNCH 76, NFSW,NCSW,C..FC,FJMX ,SPFC,FPFC,SPC
 PUNCH 54 ,RCC,FSQ1,FSQ2,TFSQ1,TFSQ2,TCLOSE,DFL,DCL
 PUNCH 10, (REOPEN(K),K=1,NZ1)
 PUNCH 14,(DPFCK(K),K=1,NZ1)
 PUNCH 11,(PFC(K),K=1,NZ1)
 PUNCH 12,(MPFC(K),K=1,NZ1),(NBOLE(K),K=1,NZ1)
 PUNCH  13,(RRES(K),K=1,NZ1)
 PUNCH 72,(AFB(K),K=1,NZ1)
 PUNCH 72, (BFB(K),K=1,NZ1)
 PUNCH 72, (ACB(K),K=1,NZ)
 PUNCH 72, (BCB(K),K=1,NZ)
 PUNCH 5,      TFLB,TCLB,AVCV,FPDEN,TGRM,TGGM
 PUNCH 7 ,  (PL(K),K=1,NZ)
 PUNCH    72,(FLUX(K),K=1,NZ)
 PUNCH   72, (FFLUX(K),K=1,NZ)
 PUNCH 7 ,  ((FTF(I,K),I=1,MFR),K=1,NZ1)
 PUNCH 74,  ((CTF(I,K),I=1,NR),K=1,NZ)
 PUNCH  2,  ((FSTSHB(I,K),I=1,MFR),K=1,NZ1)
 PUNCH  2,  ((FSTSRB(I,K),I=1,MFR),K=1,NZ1)
 PUNCH  2,  ((FSTSZB(I,K),I=1,MFR),K=1,NZ1)
 PUNCH  2,((FNTSW(I,K),I=1,MFR),K=1,NZ1)
 PUNCH  2, ((FTSWB(I,K),I=1,MFR),K=1,NZ1)
 PUNCH  2   ,((FCPHB(I,K),I=1,MFR),K=1,NZ1)
 PUNCH  2,  ((FCPRB(I,K),I=1,MFR),K=1,NZ1)
 PUNC.  2,  ((FCPZB(I,K),I=1,MFR),K=1,NZ1)
 PUNCH 74,  ((CSTSHB(I,K),I=1,NR),K=1,NZ)
 PUNCH 74,  ((CSTSRB(I,K),I=1,NR),K=1,NZ)
 PUNCH 74,  ((CSTSZB(I,K),I=1,NR),K=1,NZ)
 PUNCH 73,  ((CSWB(I,K),I=1,NR),K=1,NZ)
 PUNCH 73  ,((CCPHB(I,K),I=1,NR),K=1,NZ)
 PUNCH 73  ,((CCPRB(I,K),I=1,NR),K=1,NZ)
```





733 341

```
      PUNCH 73   ,((CCPZB(I,K),I=1,NR),K=1,NZ)
      PUNCH 72, (FSWUBB(K),K=1,NZ1)
      PUNCH 72, ( FCPBB(K),K=1,NZ1)
      PUNCH 72, ( FUEBB(K),K=1,NZ1)
      PUNCH 72, (CUEAB(K),K=1,NZ)
      PUNCH 72,  (CUEBB(K),K=1,NZ)
      PUNCH 72,  (CUAB(K),K=1,NZ)
      PUNCH 72, (CUBB(K),K=1,NZ)
      PUNCH 72, (UCPAB(K),K=1,NZ)
      PUNCH 72, (UCPBB(K),K=1,NZ)
      PUNCH 72, (CUSWAB(K),K=1,NZ)
      PUNCH 72, (CUSWBB(K),K=1,NZ)
      PUNCH 72, (FUBB(K),K=1,NZ1)
 70   FORMAT(4F8.1,I8,I5,4F5.2,2I5,I2       )
 75   FORMAT(6I2,5E12.4, F4.1)
 76   FORMAT(2I5,F10.3,E15.4,3F10.2)
 54   FORMAT(E10.3,4F5.1,     F10.2,2E12.4)
 10   FORMAT(13F4.1)
 14   FORMAT(8F10.5)
 11   FORMAT(8F10.3)
 12   FORMAT(26I3)
 13   FORMAT(13F6.4)
 72    FORMAT(5E15.7)
 5    FORMAT(2F10.2,2F5.3,2E15.8)
 7    FORMAT(8F10.2)
 74    FORMAT(6F10.2)
 2    FORMAT(4E15.7)
 73    FORMAT(6E13.7)
1000    NZ1=NZ-1
      RETURN
      END
```

UNITED STATES
NUCLEAR REGULATORY COMMISSION
WASHINGTON, D. C. 20555

OFFICIAL BUSINESS
PENALTY FOR PRIVATE USE, $300

POSTAGE AND FEES PAID
UNITED STATES NUCLEAR
REGULATORY COMMISSION

U.S.MAIL

POOR
ORIGINAL

733 343